Case No. 84739

IN THE SUPREME COURT OF THE STATE OF NEVADA

ADAM SULLIVAN, P.E., NEVADA STATE ENGINEER, et al.

Appellants,

vs.

LINCOLN COUNTY WATER DISTRICT, et al.

JOINT APPENDIX

VOLUME 14 OF 49

USGS
science for a changing world

National Water-Quality Assessment Program

Maps of Estimated Nitrate and Arsenic Concentrations for Basin-Fill Aquifers of the Southwestern United States

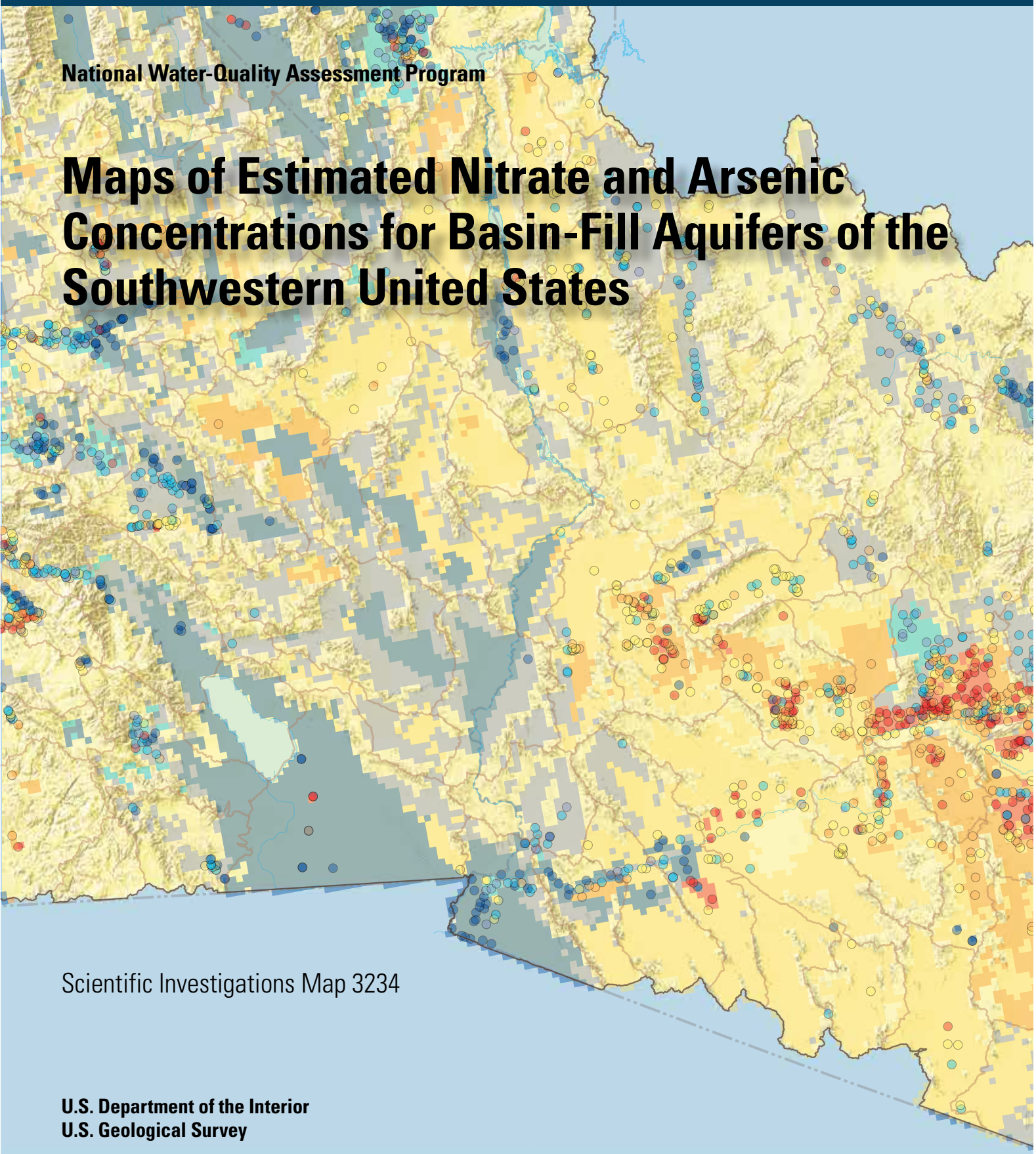

Scientific Investigations Map 3234

U.S. Department of the Interior
U.S. Geological Survey

Cover art: Observed and predicted nitrate concentrations in basin-fill aquifers of the Southwest Principal Aquifers study area.

Maps of Estimated Nitrate and Arsenic Concentrations for Basin-Fill Aquifers of the Southwestern United States

By Kimberly R. Beisner, David W. Anning, Angela P. Paul, Tim S. McKinney, Jena M. Huntington, Laura M. Bexfield, and Susan A. Thiros

National Water-Quality Assessment Program

Scientific Investigations Map 3234

U.S. Department of the Interior
U.S. Geological Survey

U.S. Department of the Interior
KEN SALAZAR, Secretary

U.S. Geological Survey
Marcia K. McNutt, Director

U.S. Geological Survey, Reston, Virginia: 2012

Suggested citation:
Beisner, K.R., Anning, D.W., Paul, A.P., McKinney, T.S., Huntington, J.M., Bexfield, L.M., and Thiros, S.A., 2012, Maps of estimated nitrate and arsenic concentrations in basin-fill aquifers of the southwestern United States: U.S. Geological Survey Scientific Investigations Map 3234, pamphlet 8 p., 2 sheets.

Contents

Figures

Plates

Tables

Vertical coordinate information is referenced to the North American Vertical Datum of 1988 (NAVD 88).

Horizontal coordinate information is referenced to the North American Datum of 1983 (NAD 83).

Maps of Estimated Nitrate and Arsenic Concentrations for Basin-Fill Aquifers of the Southwestern United States

By Kimberly R. Beisner, David W. Anning, Angela P. Paul, Tim S. McKinney, Jena M. Huntington, Laura M. Bexfield, and Susan A. Thiros

Abstract

Human-health concerns and economic considerations associated with meeting drinking-water standards motivated a study of the vulnerability of basin-fill aquifers to nitrate contamination and arsenic enrichment in the southwestern United States. Statistical models were developed by using the random forest classifier algorithm to predict concentrations of nitrate and arsenic across a model grid representing about 190,600 square miles of basin-fill aquifers in parts of Arizona, California, Colorado, Nevada, New Mexico, and Utah. The statistical models, referred to as classifiers, reflect natural and human-related factors that affect aquifer vulnerability to contamination and relate nitrate and arsenic concentrations to explanatory variables representing local- and basin-scale measures of source and aquifer susceptibility conditions. Geochemical variables were not used in concentration predictions because they were not available for the entire study area. The models were calibrated to assess model accuracy on the basis of measured values.

Only 2 percent of the area underlain by basin-fill aquifers in the study area was predicted to equal or exceed the U.S. Environmental Protection Agency drinking-water standard for nitrate as N (10 milligrams per liter), whereas 43 percent of the area was predicted to equal or exceed the standard for arsenic (10 micrograms per liter). Areas predicted to equal or exceed the drinking-water standard for nitrate include basins in central Arizona near Phoenix; the San Joaquin Valley, the Santa Ana Inland, and San Jacinto Basins of California; and the San Luis Valley of Colorado. Much of the area predicted to equal or exceed the drinking-water standard for arsenic is within a belt of basins along the western portion of the Basin and Range Physiographic Province that includes almost all of Nevada and parts of California and Arizona. Predicted nitrate and arsenic concentrations are substantially lower than the drinking-water standards in much of the study area—about 93 percent of the area underlain by basin-fill aquifers was less than one-half the standard for nitrate as N (5.0 milligrams per liter), and 50 percent was less than one-half the standard for arsenic (5.0 micrograms per liter). The predicted concentrations and the improved understanding of the susceptibility and vulnerability of southwestern basin-fill aquifers to nitrate contamination and arsenic enrichment can be used by water managers as a qualitative tool to assess and protect the quality of groundwater resources in the Southwest.

Introduction

The National Water-Quality Assessment (NAWQA) Program of the U.S. Geological Survey (USGS) is performing a regional analysis of water quality in the principal aquifer systems across the United States (Lapham and others, 2005). The Southwest Principal Aquifers (SWPA) study is developing a better understanding of the susceptibility and vulnerability of basin-fill aquifers in the Southwest to groundwater contamination by synthesizing baseline knowledge of groundwater-quality conditions in 16 basins previously studied by the NAWQA Program (fig. 1).

About 46.6 million people live in the SWPA study area (Oak Ridge National Laboratory, 2005), mostly in urban areas, but also in rural agricultural communities that cultivate about 14.4 million acres of cropland (U.S. Geological Survey, 2003). Other rural areas contain small communities with mining, retirement, or tourism/recreational-based economies. Because of the generally limited availability of surface-water supplies in the arid to semiarid climate, cultural and economic activities in the region are dependent on high-quality groundwater supplies. In the year 2000, about 33.7 million acre-feet (acre-ft) of surface water was diverted from streams, and about 23.0 million acre-ft of groundwater was withdrawn from basin-fill aquifers in the SWPA study area (U.S. Geological Survey, 2004). Irrigation and public-supply groundwater withdrawals from basin-fill aquifers in the study area were about 18.0 million acre-ft and 4.1 million acre-ft, respectively, and together account for about one quarter of the total withdrawals from all aquifers in the United States (Maupin and Barber, 2005).

Basin-fill aquifers underlie about half (190,600 square miles (mi^2)) of the 409,000 mi^2 SWPA study area (fig. 1) and are the primary groundwater supply for most cities and agricultural communities. In several areas, these aquifers provide base flow to streams that support important aquatic and riparian habitats. Basin-fill aquifers primarily consist of sand and gravel deposits that partly fill faulted basins and are bounded by consolidated rock mountains.

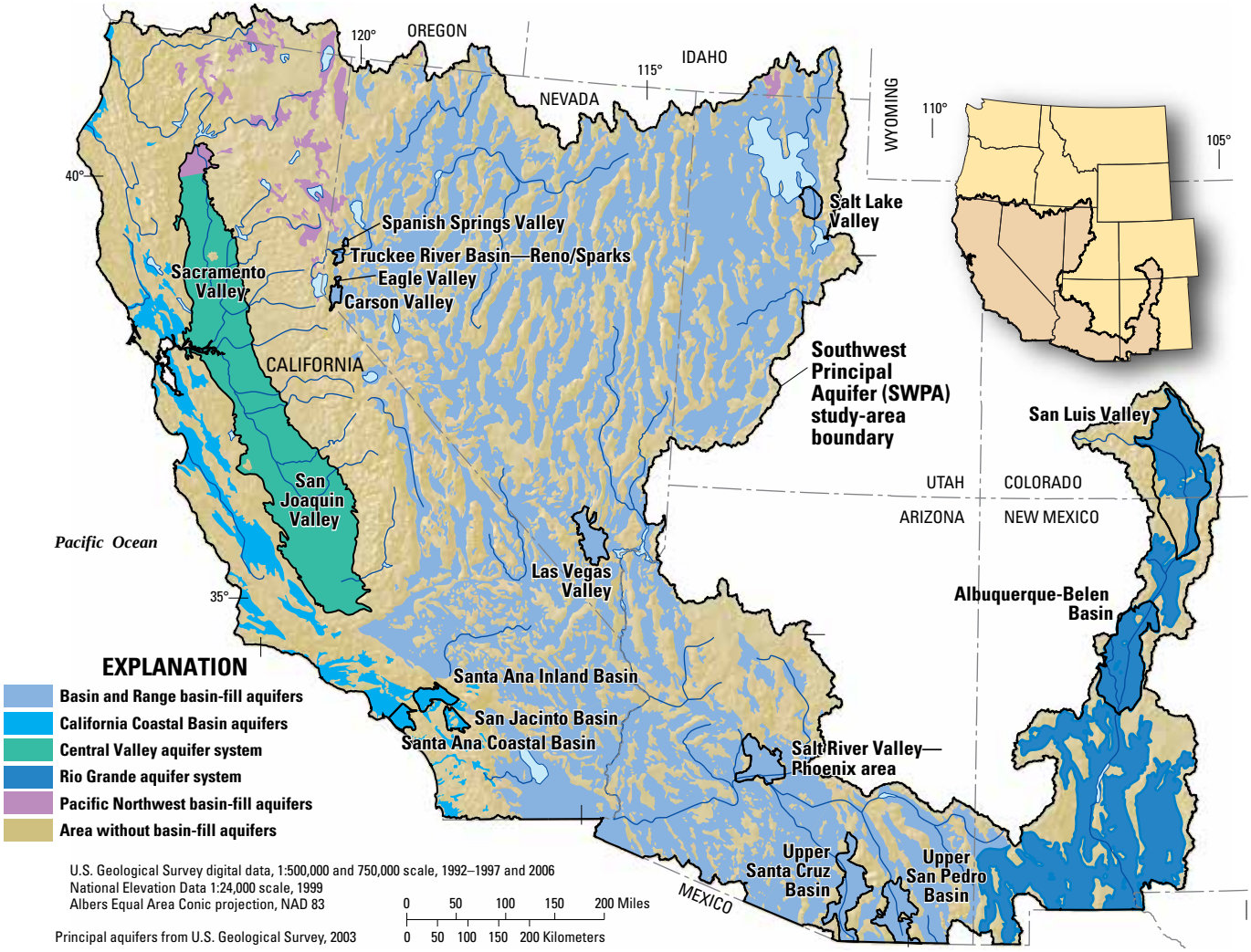

Figure 1. The principal aquifers and locations of basins previously studied by the National Water-Quality Assessment Program in the Southwest Principal Aquifers study area.

Similarities in the hydrogeology, land- and water-use practices, and water-quality issues allow for regional analysis of the vulnerability of basin-fill aquifers to contamination in the SWPA study area. Published studies have summarized current knowledge about the water quality of groundwater systems of basin-fill aquifers in the 16 basins previously studied by NAWQA (Thiros and others, 2010) and developed conceptual models of the primary natural and human-related factors commonly affecting groundwater quality in basin-fill aquifers on a regional scale (Bexfield and others, 2011).

Nitrate and arsenic concentrations are known to be elevated in many areas of the west; however, the contributing factors are distinct for each constituent. The motivation for study of nitrate and arsenic concentrations in basin-fill aquifers in the SWPA study area arose from concerns about human-health issues and economic costs associated with the protection and treatment of drinking water with respect to these constituents, as well as the potential for contaminant concentrations to increase over time and degrade the quality of groundwater in the aquifers as development progresses.

The U.S. Environmental Protection Agency (USEPA) regulates nitrate in drinking water because of the potential for elevated nitrate to restrict oxygen transport in the blood of infants in a condition known as acquired methemoglobinemia or blue-baby syndrome (U.S. Environmental Protection Agency, 2012). Recent concern also has arisen over transformation of nitrate within the human body into *N*-nitroso compounds, which are known carcinogens (Ward and others, 2005). The current nitrate as N standard of 10 milligrams per liter (mg/L) is the maximum allowable concentration of nitrate in drinking water delivered to the consumer by a public-supply system.

Arsenic has been recognized as a toxic element for centuries and is a human-health concern because elevated concentrations can contribute to a wide variety of adverse health effects, including skin damage and circulatory problems. In addition, arsenic in drinking water can lead to several types

of cancers, including bladder, lung, skin, and possibly kidney and liver (National Research Council, 2001). On the basis of a review of available scientific research on health effects of arsenic, long-term consumption of drinking water in excess of 5 micrograms per liter (µg/L) has been linked with an increased human-health risk (National Research Council, 2001). In light of the risk level, the USEPA lowered the drinking-water standard for arsenic from 50 µg/L to 10 µg/L, effective in 2006, as a compromise between the risk to individuals and the expense to water suppliers (U.S. Environmental Protection Agency, 2012).

This report summarizes statistical models developed by Anning and others (2012) that relate concentrations of nitrate and arsenic in basin-fill aquifers of the SWPA study area to selected natural and human-related factors representing contaminant sources and aquifer susceptibility conditions. Statistical models allow the understanding of nitrate and arsenic concentrations to be expanded from discrete observations to broader spatial predictions. Specifically, this report presents the spatial and statistical distribution of nitrate (plate 1) and arsenic (plate 2) concentrations in basin-fill aquifers across the SWPA study area as determined by using predictions from statistical models.

Approach and Methods

Statistical models used in this investigation were constructed by using the random forest classifier algorithm (Breiman, 2001) and are hereafter called 'classifiers.' In short, the classifiers "learn" the relations between known nitrate and arsenic concentrations and known environmental conditions associated with the aquifer. These relations take the form of complex decision trees and are used with known spatially-distributed environmental-condition data to predict concentrations in areas where observed concentration data are unavailable.

The concentration data used for training the classifiers were from 6,234 well samples stored in the USGS National Water Information System (NWIS; U.S. Geological Survey, 2010). These data were partitioned into six concentration groups for nitrate and seven concentration groups for arsenic. The break points between concentration classes were 0.50, 1.0, 2.0, 5.0, and 10 mg/L for nitrate and 1.0, 2.0, 3.0, 5.0, 10, and 25 µg/L for arsenic. The environmental conditions represented in the classifiers were from several existing geospatial datasets and included factors such as nitrogen loading rates, geologic characteristics, soil conditions, land use, water use, and other hydrologic conditions. Anning and others (2012) developed exploratory models with geochemical conditions that were found not to greatly improve the accuracy of the predictions. The environmental factors considered in the statistical model are related to geochemical conditions and likely account for much of the variability without the need for direct use of geochemical data. Additionally, geochemical data were not available for the entire study area.

Classifier and Predicted Concentration Results

The random forest classifiers provided a context to evaluate the spatial distribution of nitrate and arsenic within the upper 200 ft of basin-fill aquifers in the study area and to assess the vulnerability of aquifers throughout the SWPA study area to nitrate contamination and arsenic enrichment. Predicted nitrate and arsenic concentrations are discussed in this report for the upper 200 ft of the aquifer primarily because regression analysis on observed data showed that, at the regional scale, systematic concentration variations with depth were not found in the aquifers.

The classifiers were successfully trained to relations between observed nitrate and arsenic concentrations and important factors affecting them. This enabled the extrapolation of predicted nitrate and arsenic concentrations from areas where concentrations were measured into areas where data were unavailable. The nitrate and arsenic classifiers were found to be generally consistent with, and provided additional information and detail for, the conceptual models for natural and human-related factors affecting these constituents as described in Bexfield and others (2011).

Classifier Goodness-of-Fit and Prediction Uncertainty

The classifiers for nitrate and for arsenic performed well for assessing the vulnerability of basin-fill aquifers in the SWPA study area to contamination by these constituents. The classifiers generally produced unbiased predictions, and misclassification errors for each classifier were generally low, given the spatial variability within individual model grid cells. For each explanatory variable, the range of values in the study area was well represented by nitrate and arsenic observations, and there were no environmental conditions poorly represented by the dataset used to train the classifiers. In addition, analysis of the misclassification errors indicated that there were no environmental conditions where the classifier tended to overpredict or underpredict concentrations. Analysis of the misclassifications indicated that the models were unbiased spatially and unbiased across the distribution of values for the explanatory variables.

The ability of the model to predict concentrations across the study area within plus or minus one concentration class was 72 percent for nitrate and 70 percent for arsenic. Misclassification errors were generally symmetric about the correct (true) class; 29 percent of nitrate and 34 percent of arsenic observations were misclassified into lower concentration classes than the true class, and 29 percent of nitrate and 31 percent of arsenic observations were misclassified into higher concentration classes (fig. 2).

Nitrate

While the training observations indicate nitrate concentrations were equal to or exceeded 10 mg/L in 11 percent of the groundwater samples, use of the prediction classifier to extrapolate concentrations across the SWPA study area (plate 1) revealed that only about 2 percent of the study area underlain by basin-fill aquifers is likely to exceed this concentration, and 93 percent of the area could have groundwater with less than 5.0 mg/L of nitrate as N (fig. 3). These differences in the distribution of observed and predicted nitrate concentrations are expected and result from the fact that the prediction dataset represents the full extent of basin-fill aquifers in the SWPA study area, whereas the training dataset represents a subset of those aquifers where observations were available. Generally, samples of groundwater were collected from areas where groundwater resources have been developed. The measured and predicted concentration datasets have somewhat different but overlapping distributions of source and aquifer-susceptibility variables that affect nitrate in groundwater.

Relative background concentrations of nitrate in groundwater in undeveloped land-use settings were determined to be less than 2.0 mg/L for most biotic communities overlaying basin-fill aquifers, except for the Semidesert Grassland, Mojave Desertscrub, Sonoran Desertscrub-Arizona Uplands, and Sonoran Desertscrub-Lower Colorado River Valley communities generally located in southern Arizona. In these four biotic communities, concentrations were estimated to be less than 5.0 mg/L but greater than 2.0 mg/L. Nitrate concentrations greater than these relative background concentrations are largely found in areas with agricultural or urban land development.

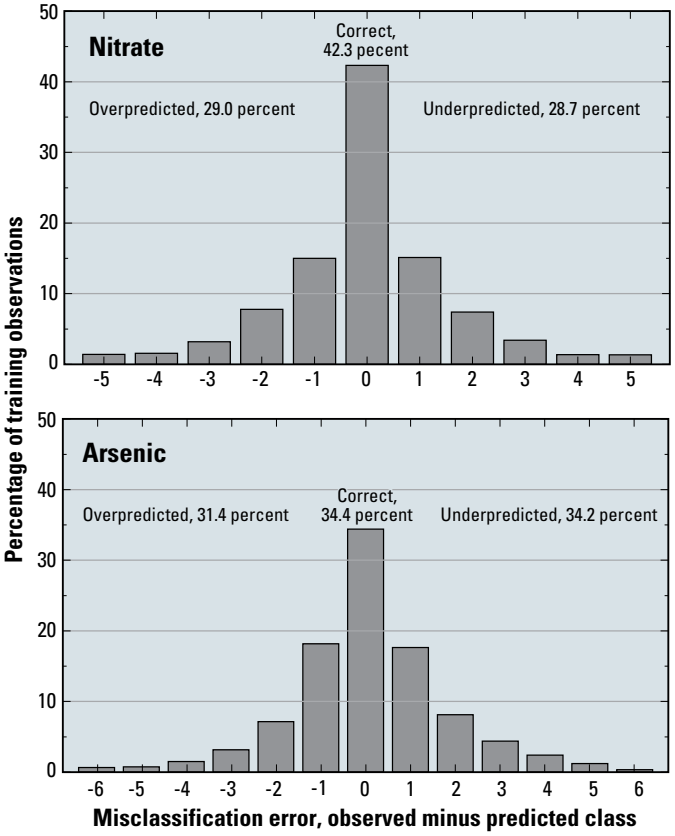

Figure 2. Statistical distribution of misclassification errors for the random forest prediction classifiers of basin-fill aquifers of the Southwest Principal Aquifers study area for nitrate and arsenic concentrations.

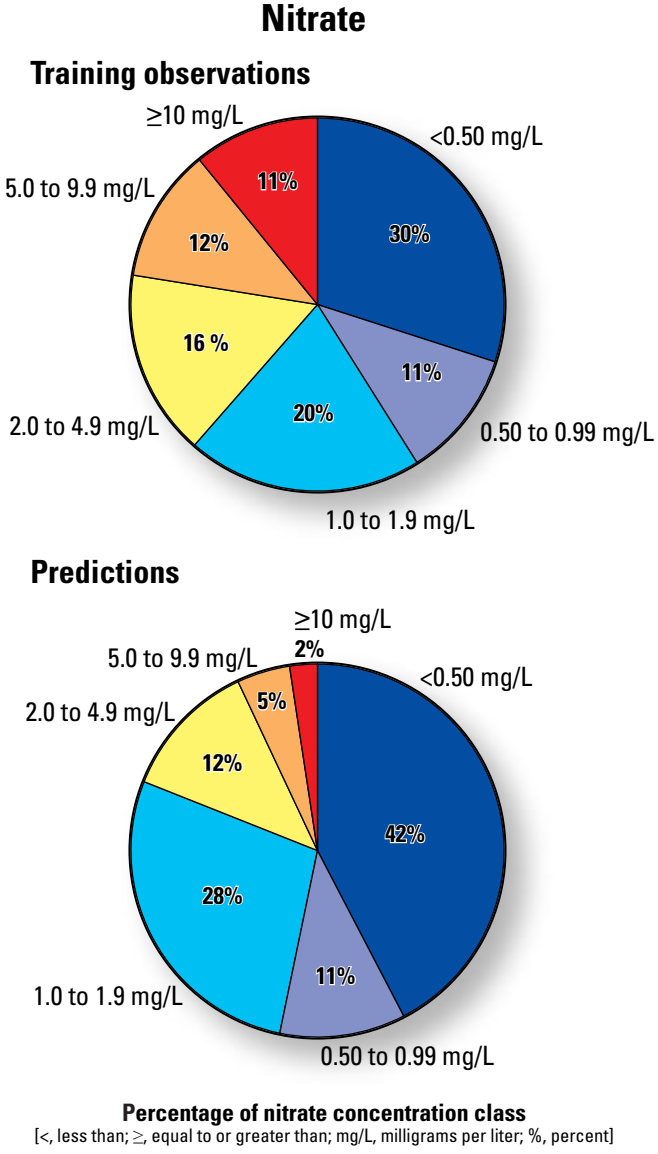

Figure 3. Percentage of nitrate concentration class for training observations and predictions.

Concentrations of nitrate in the basin-fill aquifers were predicted to exceed relative background concentrations in about 34 percent of areas having more than 5-percent agricultural or urban land. Exceedance of relative background concentrations increased with the amount of agricultural or urban development. Nitrate concentrations in basin-fill aquifers underlying land where greater than half the area has been developed for agricultural or urban uses are predicted to equal or exceed 10

mg/L in 15 percent of that area, which increases to 48 percent for areas entirely used for agricultural or urban related activities. Predicted concentrations generally decreased along groundwater-flow paths from the basin margin to the basin lowlands. Nearly all wetland areas in the basin lowlands have concentrations less than 0.50 mg/L, regardless of the amount of land development. These low concentrations could result from denitrification, a microbially facilitated process where nitrate is converted to nitrogen gas, although other explanations are possible (Anning and others, 2012).

A further understanding of conditions that render the basin-fill aquifers in the SWPA study area vulnerable to nitrate contamination was gained from an analysis of the correlations between the predicted concentrations and the explanatory variables (table 1), as well as correlations between observed nitrate and other constituent concentrations in the training dataset, which are described in detail in Anning and others (2012). These univariate correlations indicated that areas are more likely to have higher concentrations and, therefore, are generally more vulnerable to nitrate contamination, where one or more of the following conditions is found:

- Land is used for agricultural or urban purposes, especially where fertilizers are used or where there are livestock.

Table 1. Relation between predicted nitrate and arsenic concentrations and explanatory variables representing conditions for basin-fill aquifers in the Southwest Principal Aquifers study area.

[Positive values of Kendall's tau indicate that higher concentrations are associated with greater values of the explanatory variable and lower concentrations are associated with lesser values of the explanatory variable. Negative values of Kendall's tau indicate that the opposite relation exists between concentration and the explanatory variable. Small p-values (<0.001) indicate the Kendall's tau correlation between the nitrate or arsenic concentration and a given explanatory variable is statistically significant. **Abbreviations:** —, constituent not tested in classifier; <, less than]

Variable group	Explanatory variable	Represented area	Kendall's tau test on predicted nitrate concentration		Kendall's tau test on predicted arsenic concentration	
			tau	p-value	tau	p-value
Source variables						
Nitrogen loading	Atmospheric deposition	Grid cell	–0.06	<0.001	—	—
	Farm fertilizer	Grid cell	0.06	<0.001	—	—
	Non-farm fertilizer	Grid cell	0.05	<0.001	—	—
	Confined manure	Grid cell	0.06	<0.001	—	—
	Unconfined manure	Grid cell	0.03	<0.001	—	—
	Total nitrogen	Grid cell	0.01	<0.001	—	—
Land use	Septic/sewer ratio	Grid cell	–0.02	<0.001	–0.07	<0.001
	Local population	Grid cell	0.09	<0.001	–0.16	<0.001
	Local population density	Grid cell	0.09	<0.001	–0.16	<0.001
	Basin population	Basin average	0.08	<0.001	–0.18	<0.001
	Basin population density	Basin average	0.10	<0.001	–0.20	<0.001
	Local urban land	Grid cell	0.08	<0.001	–0.15	<0.001
	Local agricultural land	Grid cell	0.04	<0.001	–0.11	<0.001
	Basin urban land	Basin average	0.08	<0.001	–0.21	<0.001
	Basin agricultural land	Basin average	0.02	<0.001	–0.20	<0.001
	Basin rangeland	Basin average	0.00	0.551	0.29	<0.001
	Basin other land cover	Basin average	–0.11	<0.001	–0.26	<0.001
Geologic sources	Carbonate rocks	Contributing area	-0.15	<0.001	–0.07	<0.001
	Crystalline rocks	Contributing area	0.18	<0.001	0.04	<0.001
	Clastic sedimentary rocks	Contributing area	–0.10	<0.001	–0.16	<0.001
	Mafic volcanic rocks	Contributing area	0.08	<0.001	0.16	<0.001
	Felsic and silicic volcanic rocks	Contributing area	–0.11	<0.001	0.04	<0.001
	Intermediate composition volcanic rocks	Contributing area	0.05	<0.001	0.11	<0.001
	Undifferentiated volcanic rocks	Contributing area	0.00	0.855	–0.07	<0.001
	Distance to carbonate rocks	Grid cell	0.11	<0.001	0.07	<0.001
	Distance to crystalline rocks	Grid cell	–0.11	<0.001	–0.02	<0.001
	Distantce to clastic sedimentary rocks	Grid cell	0.03	<0.001	0.14	<0.001
	Distance to mafic volcanic rocks	Grid cell	–0.10	<0.001	–0.19	<0.001
	Distance to felsic and silicic volcanic rocks	Grid cell	0.07	<0.001	–0.06	<0.001
	Distance to intermediate composition volcanic rocks	Grid cell	–0.02	<0.001	–0.12	<0.001
	Distance to undifferentiated volcanic rocks	Grid cell	0.01	0.006	0.03	<0.001
	Soil and rock equivalent uranium-238	Grid cell	—	—	0.14	<0.001

Table 1. Relation between predicted nitrate and arsenic concentrations and explanatory variables representing conditions for basin-fill aquifers in the Southwest Principal Aquifers study area.—Continued

[Positive values of Kendall's tau indicate that higher concentrations are associated with greater values of the explanatory variable and lower concentrations are associated with lesser values of the explanatory variable. Negative values of Kendall's tau indicate that the opposite relation exists between concentration and the explanatory variable. Small p-values (<0.001) indicate the Kendall's tau correlation between the nitrate or arsenic concentration and a given explanatory variable is statistically significant. **Abbreviations:** —, constituent not tested in classifier; <, less than]

Variable group	Explanatory variable	Represented area	Kendall's tau test on predicted nitrate concentration		Kendall's tau test on predicted arsenic concentration	
			tau	p-value	tau	p-value
Aquifer susceptibility variables						
Flow path	Land-surface slope	Grid cell	0.05	<0.001	–0.12	<0.001
	Land-surface elevation	Grid cell	–0.17	<0.001	–0.10	<0.001
	Land-surface elevation percentile	Grid cell	0.15	<0.001	–0.16	<0.001
	Basin elevation	Basin average	–0.20	<0.001	–0.07	<0.001
	Distance to basin margin	Grid cell	–0.02	<0.001	0.08	<0.001
Soil properties	Seasonally high water depth	Grid cell	0.25	<0.001	–0.03	<0.001
	Hydric	Grid cell	–0.22	<0.001	0.04	<0.001
	Hydrologic group A[1]	Grid cell	–0.13	<0.001	0.14	<0.001
	Hydrologic group B[2]	Grid cell	0.20	<0.001	–0.04	<0.001
	Hydrologic group C[3]	Grid cell	–0.01	<0.001	–0.11	<0.001
	Hydrologic group D[4]	Grid cell	–0.20	<0.001	0.00	0.806
	Permeability	Grid cell	–0.07	<0.001	0.16	<0.001
	Organic material	Grid cell	0.00	0.695	–0.15	<0.001
	Clay	Grid cell	–0.02	<0.001	–0.07	<0.001
	Silt	Grid cell	–0.13	<0.001	–0.09	<0.001
	Sand	Grid cell	0.12	<0.001	0.09	<0.001
Water use and hydroclimatic	Water-resources development index	Basin average	0.04	<0.001	–0.20	<0.001
	Groundwater use, irrigated agriculture	Grid cell	0.05	<0.001	–0.11	<0.001
	Surface-water use, irrigated agriculture	Grid cell	0.04	<0.001	–0.11	<0.001
	Groundwater use, public water supply	Grid cell	0.03	<0.001	–0.06	<0.001
	Surface-water use, public water supply	Grid cell	0.03	<0.001	–0.05	<0.001
	Recharge, contributing area	Contributing area	0.00	0.938	–0.37	<0.001
	Recharge, basin	Basin average	0.02	<0.001	–0.37	<0.001
	Potential evapotranspiration	Grid cell	0.23	<0.001	0.13	<0.001
	Mean air temperature	Grid cell	0.23	<0.001	0.13	<0.001

[1] Hydrologic Group A—Sand, loamy sand, or sandy loam types of soils. Low runoff potential and high infiltration rates even when thoroughly wetted. Consists chiefly of deep, well to excessively drained sands or gravels and has a high rate of water transmission.

[2] Hydrologic Group B—Silt loam or loam types of soils. Moderate infiltration rate when thoroughly wetted and consists chiefly of moderately deep to deep, moderately well to well drained soils with moderately fine to moderately coarse textures.

[3] Hydrologic Group C—Sandy clay loam type of soil. Low infiltration rates when thoroughly wetted and consists chiefly of soils with a layer that impedes downward movement of water and soils with moderately fine to fine structure.

[4] Hydrologic Group D—Clay loam, silty clay loam, sandy clay, silty clay, or clay types of soils. Highest runoff potential and very low infiltration rates when thoroughly wetted. Consists chiefly of clay soils with a high swelling potential, soils with a permanent high water table, soils with a claypan or clay layer at or near the surface, and shallow soils over nearly impervious material.

- Nitrogen is fixed by natural vegetation, such as legumes in the Sonoran Desert.
- Soils are present that have textures favorable to water infiltration, lack hydric conditions, or lack organic material.
- High water-use from groundwater or surface-water supplies for agricultural purposes or public-water supply.
- Natural recharge is low in the drainage area contributing flow to the groundwater basin.
- Mean air temperatures and potential evapotranspiration are high.
- Bedrock surrounding the basin-fill aquifer has an abundance of crystalline, mafic volcanic, and intermediate composition volcanic rock, which likely produces geochemical conditions favorable to nitrate persistence.

Arsenic

While the training observations indicated arsenic concentrations equal or exceed 10 µg/L in 25 percent of the groundwater samples, use of the prediction classifier to extrapolate concentrations across the SWPA study area (plate 2) revealed 43 percent of the area underlain by basin-fill aquifers is likely to exceed this concentration, whereas 50 percent of the area could have concentrations less than 5.0 µg/L (fig. 4). Such differences in the distributions of observed and predicted arsenic concentrations are expected and result from the fact that the prediction dataset represents the full extent of basin-fill aquifers in the SWPA study area, whereas the training dataset represents a subset of those aquifers where observations were available, and each dataset has somewhat different but overlapping distributions of source and aquifer-susceptibility variables that affect arsenic in groundwater.

The largest area where arsenic concentrations in groundwater were predicted to be equal to or greater than the drinking-water standard of 10 µg/L was in the Basin and Range basin-fill aquifers (fig. 1, plate 2). Spatially, the Basin and Range basin-fill aquifers compose about 73 percent of the regional study area, and much of the area is undeveloped or used as open rangeland. Distribution patterns with depth obtained from the random forest classifiers support the conceptual-model findings indicating that arsenic concentrations can exceed 10 µg/L at various depths within aquifers throughout the SWPA study area (Bexfield and others, 2011).

Within a given basin, predicted concentrations generally increased along groundwater-flow paths from the upper basin margins to the basin lowlands, with greater concentrations associated with basin-fill sediments derived from surrounding mountains predominately composed of volcanic or crystalline bedrock. Basins surrounded by carbonate rocks generally contained groundwater with lower predicted concentrations of arsenic. Although areas developed for agricultural or urban use had lower observed and predicted arsenic concentrations compared to minimally developed areas, this is thought to be largely an artifact of the hydrogeologic nature of the developed areas. Generally, the more developed areas have higher rates of natural recharge because of the availability of water resources and possibly greater flushing rates of solutes out of the basin either to rivers or the ocean. In contrast, basins with lower rates of natural recharge, and likely correspondingly lower flushing rates of solutes, tend to be less developed and generally located in areas with relatively high potential evapotranspiration rates.

A further understanding of conditions that render the basin-fill aquifers in the SWPA study area vulnerable to arsenic enrichment was gained from an analysis of the correlations between the predicted concentrations and the explanatory variables (table 1), as well as correlations between observed arsenic and other constituent concentrations in the training dataset, which are described in detail in Anning and others (2012). These univariate correlations indicated that higher arsenic concentrations are more likely to be found in areas where the following conditions exist:

- Basins are surrounded by mafic volcanic bedrock, felsic/silicic volcanic bedrock, or crystalline bedrock.
- Long groundwater-flow paths.
- There is a general lack of groundwater flushing as indicated by low rates of natural recharge, high potential evapotranspiration rates, and minimal or altogether absent groundwater flow out of the basin.
- Geochemical conditions favor the release of arsenic from aquifer substrates to surrounding groundwater.

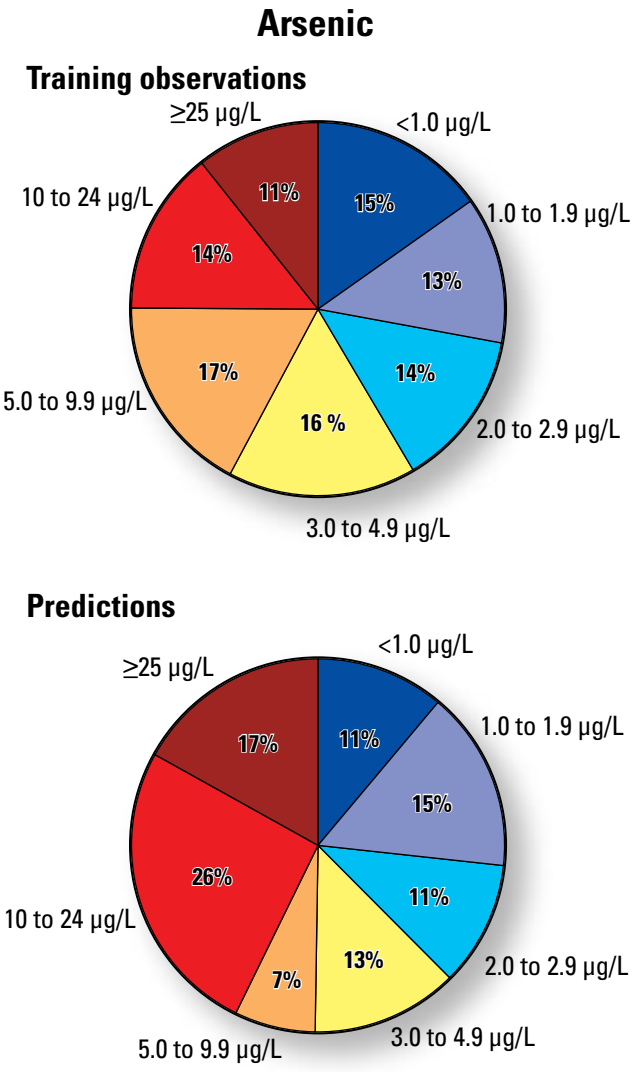

Figure 4. Percentage of arsenic concentration class for training observations and predictions.

Relevance and Implications

Areas predicted to exceed the nitrate drinking-water standard are generally developed, especially for irrigated agriculture, but are also located in more urbanized locations such as Phoenix, Arizona, and Modesto and suburbs east of Los Angeles, California. While population densities are generally much lower in agricultural areas than in urban areas, high nitrate concentrations underlying agricultural landscapes could be problematic with respect to public supply for large populations if those lands are eventually converted to urban uses. For the areas affected by high nitrate concentrations in agricultural land-use settings, fertilizer and livestock manure are significant sources and are typically mitigated with best management practices. Large tracks of land in the Sonoran Desert with nitrate concentrations between 2.0 and 5.0 mg/L, however, appear to be affected by natural nitrogen fixation by legumes and present a more challenging condition for nitrogen management.

Arsenic in groundwater is derived primarily from natural sources, namely the basin-fill sediments and the parent bedrock from which the sediments were derived. Whereas most of the area predicted to have arsenic concentrations equal to or greater than the current drinking-water standard of 10 µg/L is sparsely populated, major population centers are not necessarily unaffected. Areas within or adjacent to the metropolitan areas of Albuquerque, Bakersfield, Phoenix, Reno, Sacramento, Salt Lake City, and Stockton have measured and predicted arsenic concentrations above the drinking-water standard, which could affect future groundwater development as these cities grow.

As population centers in the west continue to grow, areas that are currently undeveloped are sought for alternative public-water supplies. Currently available groundwater data are generally focused on areas where wells already exist for groundwater development. The statistical model and associated reconnaissance scale maps of predictions (plates 1 and 2) for nitrate and arsenic concentrations are representative of the entire basin-fill groundwater resource available in the Southwest. The maps are based on statistical models that do not include geochemical data, and can help inform future management strategies as well as identify the need for additional locally relevant information in areas of interest.

References Cited

Anning, D.W., Paul, A.P., McKinney, T.S., Huntington, J.M., Bexfield, L.M., and Thiros, S.A., 2012, Predicted nitrate and arsenic concentrations in basin-fill aquifers of the southwestern United States: U.S. Geological Survey Scientific Investigations Report 2012–5065, 78 p., available at *http://pubs.usgs.gov/sir/2012/5065/pdf/sir20125065.pdf.*

Bexfield, L.M., Thiros, S.A., Anning, D.W., Huntington, J.M., and McKinney, T.S., 2011, Effects of natural and human factors on groundwater quality of basin-fill aquifers in the Southwestern United States—Conceptual models for selected contaminants: U.S. Geological Survey Scientific Investigations Report 2011–5020, 90 p., available at *http://pubs.usgs.gov/sir/2011/5020/pdf/sir20115020.pdf.*

Breiman, Leo, 2001, Random Forests: Machine Learning v. 45, no. 1, p. 5–32, available at *http://www.springerlink.com/content/u0p06167n6173512/.*

Lapham, W.W., Hamilton, P.A., and Myers, D.N., 2005, National Water-Quality Assessment Program—Cycle II regional assessments of aquifers: U.S. Geological Survey Fact Sheet 2005–3013, available at *http://pubs.usgs.gov/fs/2005/3013/.*

Maupin, M.A., and Barber, N.L., 2005, Estimated withdrawals from principal aquifers in the United States, 2000: U.S. Geological Survey Circular 1279, 46 p., available at *http://pubs.usgs.gov/circ/2005/1279/.*

National Research Council, 2001, Arsenic in drinking water—2001 update: National Academy Press, Washington D.C., 244 p.

Oak Ridge National Laboratory, 2005, LandScan™ Global Population Database, accessed September 2006, at *http://www.ornl.gov/landscan/.*

Thiros, S.A., Bexfield, L.M., Anning, D.W., and Huntington, J.M., 2010, Conceptual understanding and groundwater quality of selected basin-fill aquifers in the Southwestern United States: U.S. Geological Professional Paper 1781, 288 p., available at *http://pubs.usgs.gov/pp/1781/.*

U.S. Environmental Protection Agency, 2012, National primary drinking water regulations, accessed May 2012 at *http://www.epa.gov/safewater/contaminants/index.html.*

U.S. Geological Survey, 2003, Principal aquifers, in National Atlas of the United States of America, 1 sheet, accessed May 6, 2008 at *http://nationalatlas.gov/mld/aquifrp.html.*

U.S. Geological Survey, 2004, Estimated use of water in the United States: county-level data for 2000, available at *http://water.usgs.gov/watuse/data/2000/index.html.*

U.S. Geological Survey, 2010, National Water Information System (NWIS), accessed January 2010 at *http://waterdata.usgs.gov/nwis.*

Ward, M. H., DeKok, T.M., Levallois, Patrick, Brender, Jean, Gulis, Gabriel, Nolan, B.T., and VanDerslice, James, 2005, Workgroup Report: Drinking-water nitrate and health—recent findings and research needs: Environmental Health Perspectives, v. 113, no. 11, p. 1607–1614.

SE ROA 34192

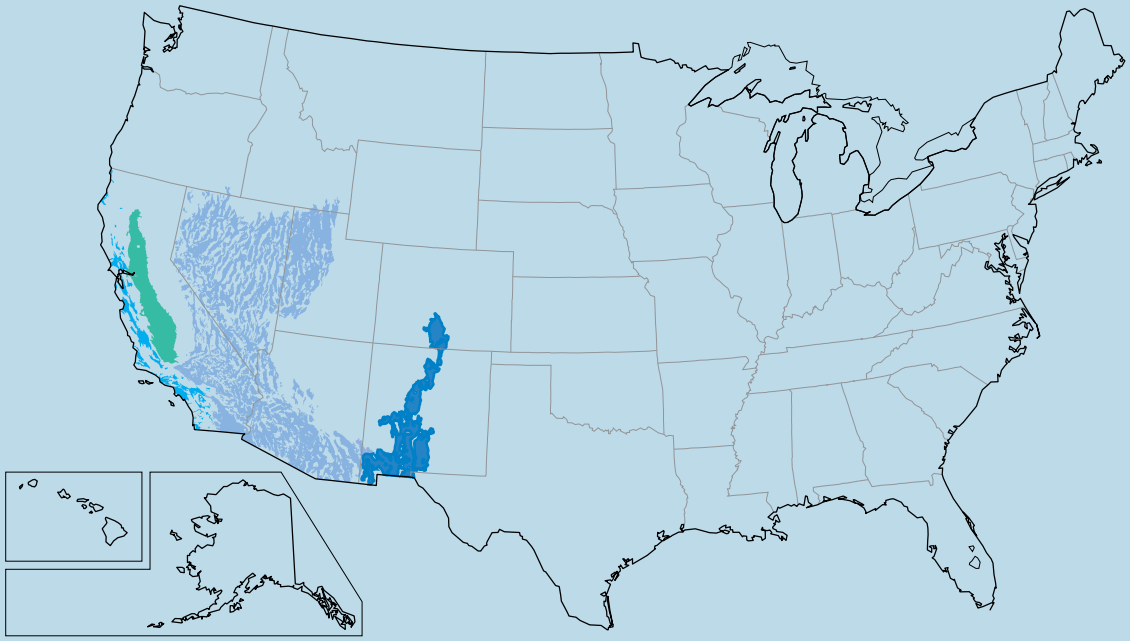

Southwest Principal Aquifers—Includes (from left to right) California Coastal Basin aquifers, Central Valley aquifer system, Basin and Range basin-fill aquifers, and Rio Grande aquifer system

Printed on recycled paper

Introduction

The U.S. Geological Survey (USGS) and the Bureau of Land Management (BLM) initiated a cooperative study through the Southern Nevada Public Land Management Act (Bureau of Land Management, 1998) to install six wells in the carbonate-rock and basin-fill aquifers of Clark County, Nevada, in areas of sparse groundwater data. This map uses water levels from these new wells, water levels from existing wells, and altitudes of spring discharge points to update a regional potentiometric map of the carbonate-rock aquifer and provide evidence to interpret the direction of regional groundwater flow. This potentiometric surface map is accompanied by drilling and borehole geophysical logs, well-construction information, lithology, water chemistry, and water levels from the newly drilled wells.

Carbonate-Rock Aquifer and Regional Groundwater Flow

The carbonate-rock aquifer in Clark County consists of thick sequences of Paleozoic-age limestone and dolomite with thinner beds of shale, sandstone, and quartzite that are deformed and extended. Mountain blocks of carbonate rock, separated by intermountain basins, thicken westward from the Muddy Mountains toward the Las Vegas and Sheep Ranges (Dettinger and others, 1995; Prudic and others, 1995; Harrill and Prudic, 1998; Heilweil and Brooks, 2011). Groundwater in the aquifer flows through fractures and faults associated with regional deformation and through small-scale brittle fractures.

The aquifer is primarily recharged through fractures in high-precipitation areas that are in high-altitude mountain ranges near groundwater divides. Regional discharge is from springs and riparian areas at low altitudes in major drainage basins. Discharge from springs at the regional scale is generally constant and less transient than from springs discharging from more localized flow systems (Toth, 1963). Active groundwater withdrawals (or pumping) can affect local spring discharge, producing fluctuations not characteristic of discharge from natural regional springs.

Parts of three groundwater flow systems compose the carbonate-rock aquifer in Clark County: (1) the Colorado System, (2) Death Valley System, and (3) Mesquite Valley System (Harrill and others, 1988). In Clark County, groundwater flow in the Colorado System is principally to the southeast, discharging at the headwaters to the Muddy River. Flow in the Death Valley System is principally to the west, discharging to springs in Amargosa Valley and Death Valley (Faunt and others, 2010). Localized flow in the Mesquite Valley System discharges by evapotranspiration from phreatophytes and evaporation on the valley playa (Glancy, 1968).

Groundwater flow directions and gradients are presented on potentiometric maps by Bedinger and Harrill (2010) and Brooks and others (2014). Both studies used available groundwater levels, spring altitudes, and discharge data to classify groundwater and springs as regional or local. Bedinger and Harrill (2010) generalized hydrogeologic and geologic characteristics as proxy data to define regional hydraulic heads, which are described as water levels that are (1) lower than the water table in areas of recharge, (2) above the altitude of intermediate and regional discharge areas, and (3) below the altitude of non-discharging dry playas.

Brooks and others (2014) developed a regional-scale numerical groundwater flow model to evaluate groundwater availability in the Great Basin. The published potentiometric contours, representative of the carbonate-rock aquifer, were based on water-level observations from wells completed in basin fill and carbonate rock. These studies were conducted at a regional scale and included relatively few direct observations from wells in Clark County, which are completed in carbonate rock.

Selected Existing Hydrogeologic Data

Water levels, water chemistry, lithology, and construction data from monitoring wells were compiled from the USGS National Water Information System (NWIS) database (U.S. Geological Survey, 2016) and from Thomas and others (1996), and compared to information obtained from the six new wells. Sites near production wells were excluded from this selection because of the potential for pumping related drawdown to affect water levels, and monitoring wells were excluded if screened across multiple intervals. Wells were selected if they were screened in the carbonate-rock aquifer or in the basin-fill aquifer at depths greater than 500 feet. It is assumed that basin-fill wells at this depth are in hydraulic connection with the carbonate-rock aquifer (Prudic and others, 1995). In Clark County, 24 wells completed in carbonate rock, 28 wells completed in deep basin-fill deposits, and 5 springs were selected from the USGS NWIS database (table 1) and included in this report.

Table 1. Existing monitoring wells representative of the carbonate-rock and basin-fill aquifers in Clark County, Nevada.

[ID, identifier; USGS, U.S. Geological Survey; NWIS, National Water Information System; mm/dd/yyyy, month/day/year; NGVD 29, National Geodetic Vertical Datum of 1929; CR, carbonate rock; BF, basin fill; —, no data]

Map ID	USGS site ID	USGS NWIS site name	Site type	Well depth (feet)	Hole depth (feet)	Contributing aquifer	Date of water-level measurement (mm/dd/yyyy)	Water level, in feet below land surface	Water-level altitude, in feet above mean sea level (NGVD 29)
1	361816115241301	212 S19 E59 18AAC 1	Well	542	542	CR	09/01/1964	417.00	3,484
2	363500115400001	161 S16 E56 16 1 Indian Springs Sewage Co	Well	550	590	CR	06/01/1963	54.00	3,146
3	362846114495501	216 S17 E64 09DDCD1 CRYSTAL 2	Well	565	565	CR	08/21/2000	254.94	1,815
4	364741114532801	210 S13 E63 26AAAA1 USGS-MX CE-DT-5	Well	628	628	CR	08/13/1999	349.81	1,820
5	360016115361501	163 S22 E57 29DABC1 USBLM NDOT 01	Well	660	660	CR	09/07/2010	306.15	3,917
6	364743114533101	210 S13 E63 23DDDC1 USGS-MX CE-DT-4	Well	669	669	CR	10/15/2015	356.27	1,819
7	363212115240301	212 S16 E58 23DDD 1 USFWS SBH-1	Well	720	720	CR	05/28/2015	575.20	2,891
8	362531114524201	216 S18 E64 07BB 1 WELL (REPORT R50)	Well	793	793	CR	11/29/1956	226.40	1,819
9	355829115150601	212 S23 E60 03DBCB1 TORTOISE CENTER	Well	800	800	CR	03/19/1990	555.00	2,150
10	361736114531601	215 S19 E63 13DCAA1 EBM-3	Well	900	1,241	CR	02/20/2004	578.73	1,810
11	363308114553001	217 S16 E63 09DDAB1 USBLM SHV-1	Well	920	920	CR	10/01/2015	833.69	1,815
12	363332115244001	212 S16 E58 14A 1 USFWS DR-1	Well	930	960	CR	05/28/2015	813.40	2,760
13	364604114471301	219 S13 E64 35DCAD1 USGS-MX CE-DT-6	Well	937	937	CR	11/01/2002	456.00	1,819
14	364830115512601	160 S13 E55 19 1 TW- 3	Well	1,127	1,860	CR	08/25/2015	1,103.00	2,381
15	363407115215301	212 S16 E59 08 2 USGS - Cow Camp	Well	1,403	1,403	CR	07/29/2015	1,330.30	2,856
16	362507114572701	216 S18 E63 05AADB1	Well	1,979	2,007	CR	03/01/2002	755.00	1,811
17	360946115421401	162 S20 E56 33CCAA1 TROUT CANYON 01	Well	718.5	720	CR	01/05/2015	467.30	4,794
18	364451114585001	210 S14 E62 01ADBD1 CSVM-5	Well	1,780	1,783	CR	09/20/2011	1,081.20	2,048
19	362700114564401	216 S17 E63 21DCCC1 HV-1	Well	2,480	2,480	CR	06/20/2000	882.00	1,820
20	361811115404401	212 S19 E56 15ABBD1	Well	660	660	CR	01/26/1981	214.40	8,500
21	364738114534001	210 S13 E63 26AABD1 CSV-RW-2	Well	710	720	CR	09/14/2011	383.40	1,819
22	364728114531001	210 S13 E63 25BDBB1 CSVM-1	Well	1,040	1,060	CR	09/21/2011	341.90	1,819
23	364529114492401	219 S13HE64 33DBBC1 UMVM-1	Well	1,200	1,200	CR	04/22/2003	247.00	1,831
24	363943114552301	210 S15 E63 03BBCC1 CSVM-2	Well	1,400	1,425	CR	09/20/2011	750.70	1,822
25	360201115204701	212 S22 E59 15DAAB1	Well	532	532	BF	03/14/1990	267.21	2,823
26	363201115333801	211 S16 E57 28B 1 Hwy95 Cons 1	Well	550	550	BF	04/22/1963	98.00	3,083
27	360247115224401	212 S22 E59 09CBDB1 HUMANE	Well	570	570	BF	01/21/2009	354.80	2,898
28	363452115405101	161 S16 E56 08BAAC1 USAF Well 3	Well	600	600	BF	07/29/2015	68.00	3,062
29	363447115404601	161 S16 E56 08BAAD1 USAF Well 106-2	Well	604	604	BF	07/29/2015	63.15	3,067
30	363255115515801	161 S16 E54 24BCBA1 Army 2	Well	627	658	BF	08/17/2015	495.20	3,318
31	355015115102601	166 S24 E61 20DDAC1 HIDDEN VALLEY	Well	640	640	BF	12/03/1956	605.00	2,423
32	354454115205401	164A S25 E59 27AACA1 JAIRPORT	Well	650	650	BF	12/11/2008	280.90	2,499
33	361136115101401	212 S23 E61 03BCC 1 Sky Harbor Airport	Well	650	650	BF	04/18/2011	215.36	2,160
34	360941115104801	212 S20 E61 32CDC 1	Well	665	665	BF	04/18/2011	18.47	2,077
35	355923115174201	212 S22 E60 32CB 1	Well	700	700	BF	08/06/1979	460.00	2,420
36	360826115020001	212 S21 E62 10ACAA1 Nevada Power Company	Well	715	715	BF	04/20/2011	21.94	1,683
37	364601114514301	210 S13 E64 31DADA1 USGS CSV-1	Well	765	765	BF	07/31/2009	346.91	1,813
38	361939115154801	212 S19 E60 04DAB 2 NV Division of Forestry	Well	780	780	BF	04/21/2011	77.51	2,376
39	364127114553001	210 S14 E63 28AACD1 USGS CSV-3	Well	780	780	BF	09/20/2011	594.00	1,820
40	355947115163501	212 S22 E60 33BB 1	Well	785	785	BF	12/10/1976	585.00	2,120
41	360931115083802	212 S21 E61 03ABB 2	Well	807	807	BF	04/18/2011	9.08	2,005
42	361843115161001	212 S19 E60 09BCC 1	Well	830	830	BF	04/28/2011	155.76	2,354
43	361233115021501	212 S20 E62 15BBAB1 USAF Nellis 12 (C)	Well	1,000	1,000	BF	04/27/2011	124.71	1,691
44	361346115115901	212 S20 E61 06CBDD1 CNLV Desert Aire	Well	1,000	1,000	BF	04/27/2011	60.72	2,150
45	361400115040901	212 S20 E62 05CAAA1 CNLV Wilshire	Well	1,000	1,000	BF	10/01/2015	62.56	1,806
46	361303115140301	212 S20 E60 11CAAA1 LVVWD W028	Well	1,003	1,003	BF	01/18/2007	202.05	2,085
47	361232115061001	212 S20 E61 13ABDB1 CNLV Diana Terrace	Well	1,230	1,230	BF	10/01/2015	11.83	1,845
48	361626115090701	212 S19 E61 21DDB 1 CNLV Regional Park 1	Well	1,300	1,300	BF	09/01/2015	40.72	2,119
49	360809115252601	212 S21 E58 12DDDD1 RED ROCK WASH	Well	503	503	BF	11/07/2008	400.54	3,288
50	364014114315301	220 S14 E67 31DACD1	Well	387	620	BF	03/19/1987	116.00	1,574
51	364912114041201	222 S13 E71 09BDCA1 PS27	Well	1,450	1,493	BF	07/08/1994	84.00	1,573
52	364044114165201	222 S14 E69 33ABC 1 D & HA	Well	880	880	BF	03/10/1985	37.26	1,341
53	362239114263501	215 S18 E67 12DDAD1 ROGERS SPRING	Spring	—	—	CR	—	—	1,576
54	362321114252601	215 S18 E68 07ABBA1 BLUE POINT SPRING	Spring	—	—	CR	—	—	1,562
55	09419625	CORN CK SPGS AT NATIONAL FISH & WILDLIFE HDQRS, NV	Spring	—	—	CR	—	—	2,930
56	09415910	PEDERSON SPGS NR MOAPA, NV	Spring	—	—	CR	—	—	1,811
57	362450115442001	161 S18 E55 01DACC1 COLD CREEK SPRING	Spring	—	—	CR	—	—	6,324

Drilling, Borehole Geophysical Logs, Lithology, and Well Construction

Groundwater monitoring wells were installed at six locations in Clark County. Criteria for selecting drill sites included (1) the carbonate-rock aquifer was relatively close to the surface, (2) there were no nearby groundwater withdrawals, and (3) access for drilling equipment was possible on existing roads.

Drilling techniques were dependent upon borehole advancement rate and lithology. Mud rotary drilling was predominantly used when drilling through unconsolidated material consisting mostly of sand, gravel, and cobbles. At all sites, the drill penetration rate through unconsolidated material was relatively consistent and progressed rapidly with this technique. When penetration rate slowed in denser rock units, air-hammer drilling was used. A change in drilling method allowed for consistent downward progress and limited drill time and cost.

Spontaneous potential (SP), natural gamma, caliper, and resistivity (borehole, 16- and 64-inch normal) wireline geophysical logs were obtained at each newly drilled borehole. The SP logs measure the voltage between the borehole and an electrode at the surface and are used to identify permeability changes and boundaries between formations at depth. Natural gamma logs show formation radiation intensity, which is generally higher for clay-rich rocks and sediments that tend to emit elevated levels of radiation from natural decay of uranium and thorium to potassium-40. Caliper logs measure borehole diameter and can indicate the presence of fractures along the borehole wall. Resistivity logs record the electrical resistivity of the formation and can indicate higher-porosity transmissive zones. These logs are used together to provide information on the subsurface geology.

Drill cuttings (chips of broken geologic material brought to the surface by drilling fluids) were washed and analyzed. These cuttings, borehole geophysical data, and observations made during drilling provide an indication of the subsurface geologic characteristics at each new drill site. Borehole geophysical logs, drill penetration rate, and subsurface lithology are presented with the study area map.

Wells were constructed of steel or polyvinyl chloride (PVC) well casing ranging from 4.5 to 6.625 inches in diameter. Vertically slotted screens were installed in water-bearing zones interpreted from borehole geophysics. A summary of well-construction information for each of the newly drilled wells is shown in table 2.

Table 2. Summary of well construction information for newly drilled wells in Clark County, Nevada.

[USGS, U.S. Geological Survey; NWIS, National Water Information System; ID, identifier; NDWR, Nevada Division of Water Resources; OD, outside dimension; DCR, depth to consolidated rock; WP, water production; gpm, amount of water pumped from well in gallons per minute; SCH, schedule; PVC, polyvinyl chloride; CR, carbonate rock; BF, basin fill; MR, mud rotary; AH, air hammer; >, greater than; —, no data; NA, not applicable]

Well name	USGS NWIS site ID	Map ID	NDWR log ID	Hole depth (feet)	Well depth (feet)	Diameter of casing (OD), in inches	Screened interval depth: From (feet)	Screened interval depth: To (feet)	Casing material	DCR (feet)	Aquifer completion	Drilling method	Well test data: WP (gpm)	Well test data: Time (hours)
BW-01	364204114454501	A	109838	1,928	1,926	4.500	1,786	1,926	SCH 80 PVC	595	CR	MR/AH	3 to 5	24
LSC-01	362454115270201	B	112697	905	890	6.625	336 808	417 889	SCH 40 steel	65	CR	MR	150	6
LSC-01 (nested)		B	—	—	210	2.250	190	210	SCH 80 PVC	—	BF	MR	0 (dry)	0 (dry)
RB-01	362135114285401	C	113526	975	973	6.000	810	952	SCH 40 steel	755	CR	MR/AH	>150	3
BUFPKTS-01	362352114414501	D	114409	1,200	1,198	4.500	988	1,198	SCH 40 steel	221	CR	MR	20	10
IVPH-01	354849115225001	E	115275	1,295	1,290	4.500	1,065	1,275	SCH 40 steel	38	CR	MR/AH	30	10
JM-01	362901115220001	F	121811	1,103	1,080	4.500	200 780	300 1,080	SCH 40 steel SCH 40 steel	NA	BF	MR	50 to 75	50

Table 3. Total dissolved solids and concentrations of major ions in water samples collected from new wells in Clark County, Nevada.

[mm/dd/yyyy, month/day/year; mg/L, milligrams per liter; <, less than; CR, carbonate rock; BF, basin fill]

Well name	Date (mm/dd/yyyy)	Total dissolved solids (mg/L)	Calcium (mg/L)	Magnesium (mg/L)	Sodium (mg/L)	Potassium (mg/L)	Chloride (mg/L)	Sulfate (mg/L)	Carbonate (mg/L)	Bicarbonate (mg/L)	Principal contributing aquifer
BW-01	04/30/2010	616	60.8	24.4	101	11.0	56.3	195	< 1.0	264	CR
LSC-01	06/14/2012	249	45.1	28.2	5.0	1.46	2.90	21.4	< 1.0	246	CR
RB-01	04/09/2014	2,980	399	135	272	18.5	312	1,570	< 1.0	145	CR
BUFPKTS-01	04/10/2014	234	7.6	4.8	72.4	5.68	17.9	20.6	8.4	166	CR
IVPH-01	04/11/2014	499	67.1	38.2	53.9	3.33	105	86.4	< 1.0	210	CR
JM-01	03/14/2013	283	35.7	28.5	33.4	1.82	5.85	19.0	< 1.0	299	BF

Water Chemistry

Water-quality samples for major-ion chemistry and the stable isotopes of water (deuterium, δ^2H, and oxygen, $\delta^{18}O$) were collected at each new well site, and results of analysis were compared to existing values from springs and wells near the drill sites. Total dissolved solids (TDS) and concentrations of calcium (Ca), magnesium (Mg), sodium (Na), potassium (K), chloride (Cl), sulfate (SO_4), carbonate (CO_3), and bicarbonate (HCO_3) were measured by the USGS National Water Quality Laboratory (NWQL), in Denver, Colorado (table 3). Deuterium (δ^2H) and oxygen ($\delta^{18}O$) isotopes were analyzed by the USGS Radiogenic Isotope Facility in Denver, Colorado (table 4).

Standard three-well-casing volumes were purged from each well, and water samples were collected with a submersible pump except at two sites (wells IVPH–01 and BUFPKTS–01) where samples were obtained through bailing. A 20-foot-long bailer was used to purge water from the well and collect a representative water sample.

Table 4. Isotopic ratios of deuterium (δ^2H) and oxygen ($\delta^{18}O$) in water samples collected from new wells drilled in Clark County, Nevada.

[δ^2H, deuterium (^2H) to protium (^1H) isotopic ratio relative to VSMOW; $\delta^{18}O$, oxygen-18 to oxygen-16 isotopic ratio relative to VSMOW; VSMOW, Vienna Standard Mean Ocean Water; ‰, per mil (parts per thousand)]

Well name	δ^2H (‰)	$\delta^{18}O$ (‰)
BW-01	–97.49	–12.89
LSC-01	–103.00	–13.98
RB-01	–91.70	–12.38
BUFPKTS-01	–82.50	–11.26
IVPH-01	–92.30	–12.71
JM-01	–95.67	–13.01

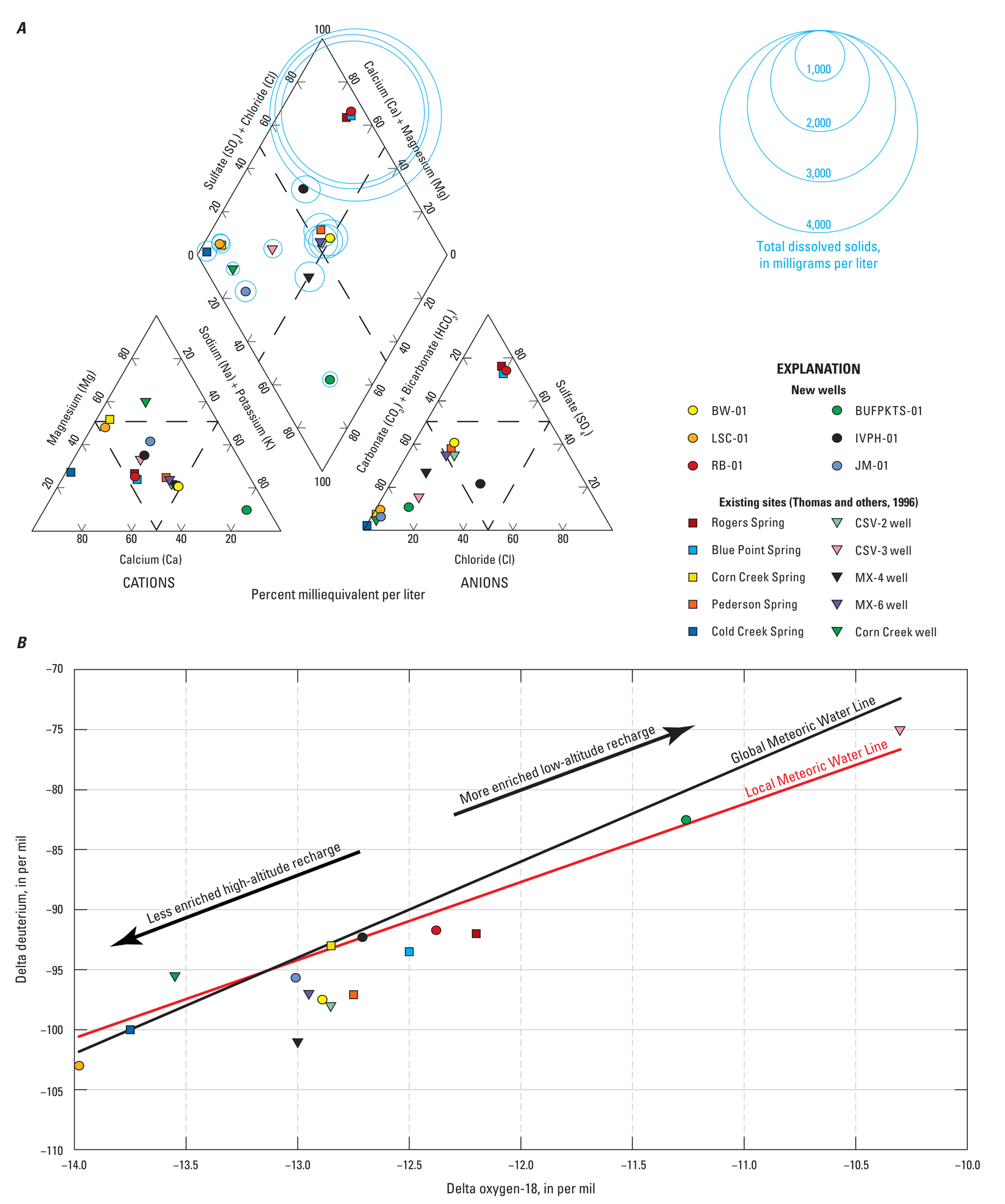

Figure 1. *A*, Total dissolved solids and major-ion concentrations in water samples collected from wells and springs associated with regional groundwater flow, and *B*, isotopic ratios of delta deuterium (δ^2H) and delta oxygen-18 ($\delta^{18}O$) in samples collected from new and reference wells and springs in Clark County, Nevada (Global Meteoric Water Line [$\delta^2H = 8\times\delta^{18}O + 10$; Craig, 1961], and Local Meteoric Water Line [$\delta^2H = 6.5\times\delta^{18}O - 9.7$; Friedman and others, 1992]).

Major-ion chemistry is important to an understanding of the migration of water through a groundwater flow system. A Piper diagram (fig. 1*A*) can be used to evaluate the chemical characteristics of groundwater and the effects of chemical processes occurring between minerals and water. Groundwater samples from newly drilled wells show similar major-ion chemistry to previously sampled wells and springs (Thomas and others, 1996) that are assumed to represent groundwater from the regional carbonate-rock aquifer.

Isotopic ratios of δ^2H and $\delta^{18}O$ in water samples collected from wells drilled for this study and in samples previously collected from wells and springs, are compared to the Global Meteoric Water Line (GMWL) and a Local Meteoric Water Line (LMWL) on figure 1*B*. This plot provides a comparison of recharge from low-altitude and high-altitude precipitation sources to waters from previously published data (Thomas and others, 1996).

Water-Level Information

Water levels from newly drilled wells were measured periodically from 2009 to 2015 and stored in the USGS NWIS database (https://waterdata.usgs.gov/nwis). These data were quality assured, which included evaluating measurements for temporal irregularity and adjustments due to known borehole deviation. Water levels were relatively stable throughout the duration of this project except for well BW-01, which experienced a decline of approximately 3 feet from January 2010 to May 2013, and a subsequent recovery of approximately 1 foot from June 2013 to June 2014.

Variations in borehole direction during drilling (drift) are common and can require corrections to water-level measurements. Borehole drift was monitored, and deviation was measured where drift was detected during the drilling of all new wells. The borehole at well BUFPKTS–01 was the only site that needed correction because borehole drift occurred above the depth of the static water level. The water level for this well was corrected using the equation from Elliott and Fenelon (2010):

$$V_d = \left(M_d - M_{top}\right)\times\left(\frac{\Delta V_{int}}{\Delta M_{int}}\right) + V_{top} \quad (1)$$

$$V_d = M_d \times 0.993 - 3.45 \quad (2)$$

where

V_d is the corrected vertical depth,
M_d is the measured depth,
M_{top} is the measured depth to the top of the correction interval,
ΔV_{int} is the difference in the true vertical depth between the top and bottom of the correction interval,
ΔM_{int} is the difference in the measured top and bottom of the correction interval, and
V_{top} is the corrected vertical depth to the top of the interval over which the correction applies.

Regional Potentiometric Surface

Groundwater levels from the six wells drilled for this project and wells fitting the criteria described in the section "Selected Existing Hydrogeologic Data," were compiled and used to construct a groundwater-level map representing the regional potentiometric surface of the upper carbonate-rock aquifer in Clark County, Nevada, in 2009–2015. Data used to construct the potentiometric surface are published separately as a USGS data release (Wilson, 2019). This map is similar to the regional potentiometric surface shown on previous maps by Bedinger and Harrill (2010) and Brooks and others (2014). In general, the potentiometric surface on this map follows the overlying land-surface topography. Higher topographic altitudes typically have higher groundwater altitudes, hydraulic gradients generally are steep near mountain ranges and low (flatten) in basins, and water-level contours parallel and intersect surface-water features.

Area on map	Description
A	In the Las Vegas and Sheep Ranges, and the Spring Mountains, mountain block recharge contributes to and directs regional groundwater flow in Clark County.
B	Water-level contours generally indicate groundwater flow to the east, terminating at discharge points along the Las Vegas Wash in Las Vegas Valley, and the Muddy River near Moapa Valley.
C	A low water-level gradient near Moapa Valley indicates slow groundwater movement toward the Muddy River and Lake Mead.
D	A low water-level gradient in northeast Clark County indicates that groundwater in this area flows toward the Virgin River.

Summary and Conclusions

During 2009 and 2015, the U.S. Geological Survey in cooperation with the Bureau of Land Management installed six new wells in Clark County, Nevada. The wells were installed to address the spatial gaps of wells completed in the carbonate-rock aquifer. This map describes new and existing water-level and hydrologic data used to (1) develop a potentiometric map, and (2) provide additional supporting evidence for the direction of regional groundwater flow in the upper carbonate-rock aquifer in Clark County. Results from this study indicate that the Spring Mountains and the Las Vegas and Sheep Ranges provide primary recharge to the groundwater system in western Clark County. Additionally, potentiometric contours indicate eastward groundwater flow in much of Clark County that terminates at springs along Las Vegas Wash, the Muddy River, and the Virgin River. Previous maps by Bedinger and Harrill (2010) and Brooks and others (2014) show similar water-surface altitudes and gradients. This study introduces new water-level measurement sites that cover data gaps and support previous regional water-surface interpretations. Additionally, comparison of lithologic descriptions, geophysical logs, and groundwater chemistry from the six wells drilled during this study to existing data, substantiates that water levels in the new wells represent the regional carbonate-rock aquifer.

Well JM-01 (362901115220001)

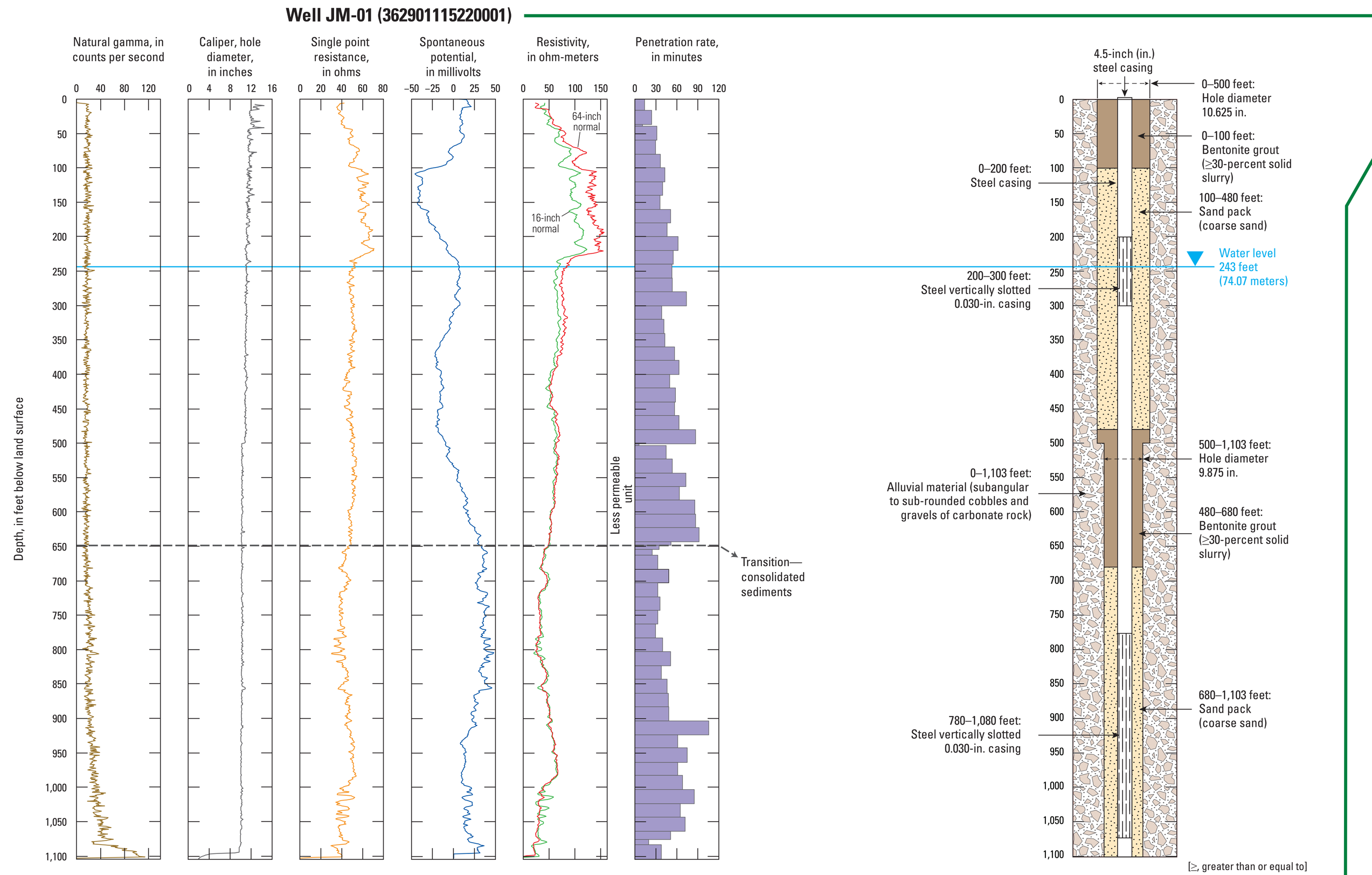

Well LSC-01 (362454115270201)

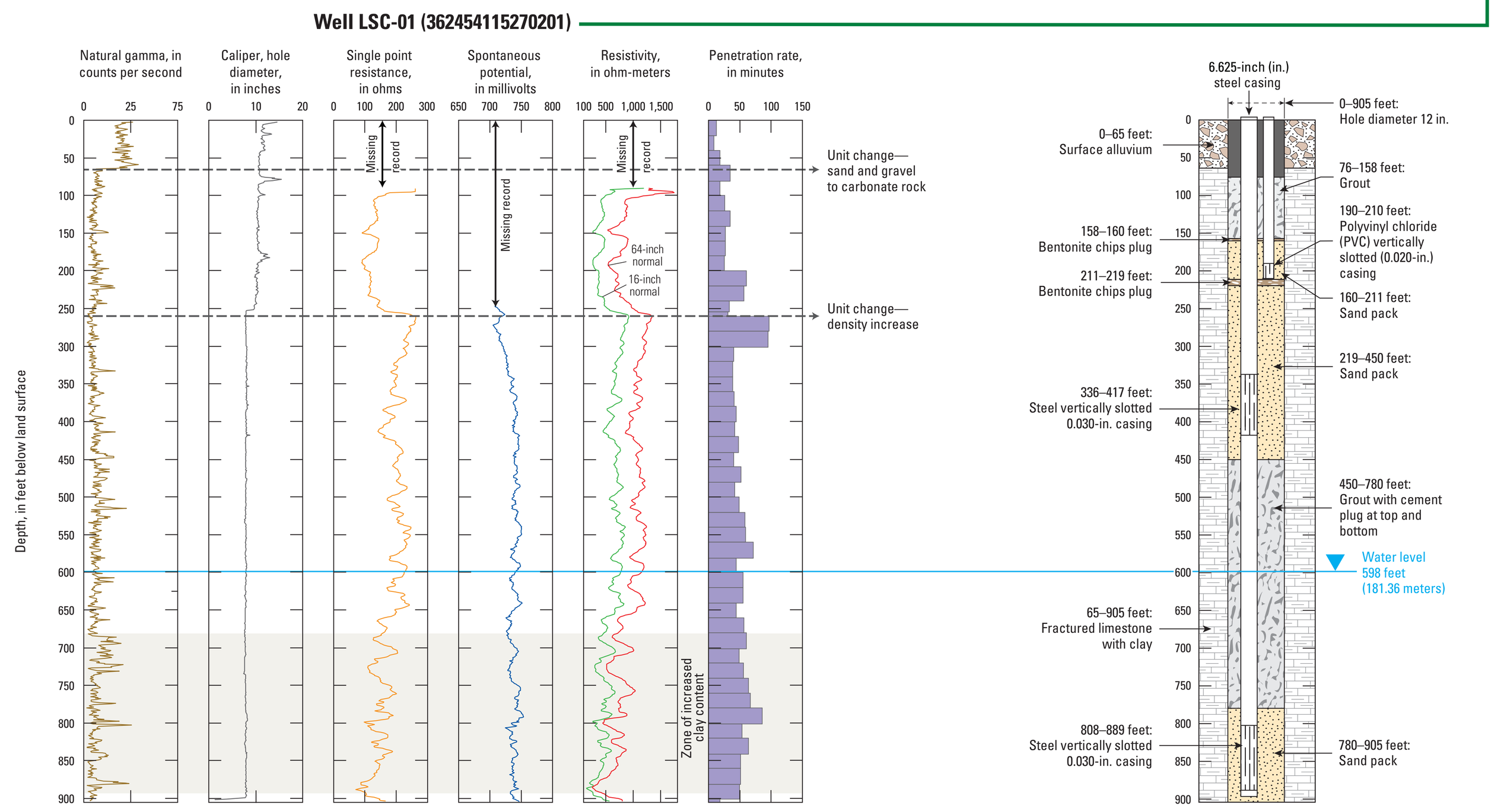

References Cited

Bedinger, M.S., and Harrill, J.R., 2010, Appendix 1: Regional potential for interbasin flow of groundwater, *in* Belcher, W.R., and Sweetkind, D.S., eds., Death Valley regional groundwater flow system, Nevada and California—Hydrogeologic framework and transient groundwater flow model: U.S. Geological Survey Professional Paper 1711, p. 345–364, https://pubs.usgs.gov/pp/1711/.

Brooks, L.E., Masbruch, M.D., Sweetkind, D.S., and Buto, S.G., 2014, Steady-state numerical groundwater flow model of the Great Basin carbonate and alluvial aquifer system: U.S. Geological Survey Scientific Investigations Report 2014–5213, 124 p., https://pubs.usgs.gov/sir/2014/5213/.

Bureau of Land Management, 1998, Southern Nevada Public Land Management Act of 1998—Public Law 105–263: Bureau of Land Management, https://www.gpo.gov/fdsys/pkg/PLAW-105publ263/pdf/PLAW-105publ263.pdf.

Craig, H., 1961, Isotopic variations in meteoric waters: Science, v. 133, no. 3465, p. 1702–1703, http://www.jstor.org/stable/1708089?origin=JSTOR-pdf.

Dettinger, M.D., Harrill, J.R., Schmidt, D.L., and Hess, J.W., 1995, Distribution of carbonate-rock aquifers and the potential for their development, southern Nevada and adjacent parts of California, Arizona, and Utah: U.S. Geological Survey Water-Resources Investigations Report 91–4146, 100 p., 2 pl., https://pubs.er.usgs.gov/publication/wri914146.

Elliott, P.E., and Fenelon, J.M., 2010, Database of groundwater levels and hydrograph descriptions for the Nevada Test Site area, Nye County, Nevada (ver. 9.0, February 2019): U.S. Geological Survey Data Series 533, 13 p., https://doi.org/10.3133/ds533.

Faunt, C.C., D'Agnese, F.A., and O'Brien, G.M., 2010, Hydrology, chap. D *in* Belcher, W.R., and Sweetkind, D.S., eds., Death Valley regional groundwater flow system, Nevada and California—Hydrogeologic framework and transient groundwater flow model: U.S. Geological Survey Professional Paper 1711, p. 133–159, https://pubs.usgs.gov/pp/1711/.

Friedman, I., Smith, G.I., Gleason, J.D., Warden, A., and Harris, J.M., 1992, Stable isotope composition of waters in southeastern California—1. Modern precipitation: Journal of Geophysical Research—Atmospheres, v. 97, no. D5, p. 5795–5812, https://agupubs.onlinelibrary.wiley.com/doi/abs/10.1029/92JD00184.

Glancy, P.A., 1968, Water-resources appraisal of Mesquite–Ivanpah Valley area, Nevada and California: Nevada Department of Conservation and Natural Resources, Groundwater Resources Reconnaissance Series Report 46, 57 p.

Harrill, J.R., Gates, J.S., and Thomas, J.M., 1988, Major ground-water flow systems in the Great Basin region of Nevada, Utah, and adjacent states: U.S. Geological Survey Hydrologic Investigations Atlas HA-694-C, 2 sheets, scale 1:1,000,000, https://doi.org/10.3133/ha694C.

Harrill, J.R., and Prudic, D.E., 1998, Aquifer systems in the Great Basin region of Nevada, Utah, and adjacent states—Summary report: U.S. Geological Survey Professional Paper 1409–A, 66 p., https://pubs.usgs.gov/pp/1409a/report.pdf.

Heilweil, V.M., and Brooks, L.E., eds., 2011, Conceptual model of the Great Basin carbonate and alluvial aquifer system: U.S. Geological Survey Scientific Investigations Report 2010–5193, 191 p., https://pubs.usgs.gov/sir/2010/5193/.

Prudic, D.E., Harrill, J.R., and Burbey, T.J., 1995, Conceptual evaluation of regional ground-water flow in the carbonate-rock province of the Great Basin, Nevada, Utah, and adjacent states: U.S. Geological Survey Professional Paper 1409–D, 102 p., https://pubs.er.usgs.gov/publication/pp1409D.

Schaefer, D.H., Thiros, S.A., and Rosen, M.R., 2005, Ground-water quality in the carbonate-rock aquifer of the Great Basin, Nevada and Utah, 2003: U.S. Geological Survey Scientific Investigations Report 2005–5232, 41 p., https://pubs.usgs.gov/sir/2005/5232/.

Thomas, J.M., Welch, A.H., and Dettinger, M.D., 1996, Geochemistry and isotope hydrology of representative aquifers in the Great Basin region of Nevada, Utah, and adjacent states: U.S. Geological Survey Professional Paper 1409–C, 100 p., https://pubs.er.usgs.gov/publication/pp1409C.

Toth, J., 1963, A theoretical analysis of groundwater flow in small drainage basins: Journal of Geophysical Research, v. 68, no. 16, p. 4795–4812, https://agupubs.onlinelibrary.wiley.com/doi/10.1029/JZ068i016p04795.

U.S. Geological Survey (USGS), 2016, USGS water data for the Nation: U.S. Geological Survey National Water Information System database, accessed January 2016, at https://doi.org/10.5066/F7P55KJN.

Wilson, J.W., 2019, Supplemental data for drilling, construction, water chemistry, water levels, and regional potentiometric surface of the upper carbonate-rock aquifer in Clark County, Nevada, 2009–2015: U.S. Geological Survey data release, https://doi.org/10.5066/P9K73T7Q.

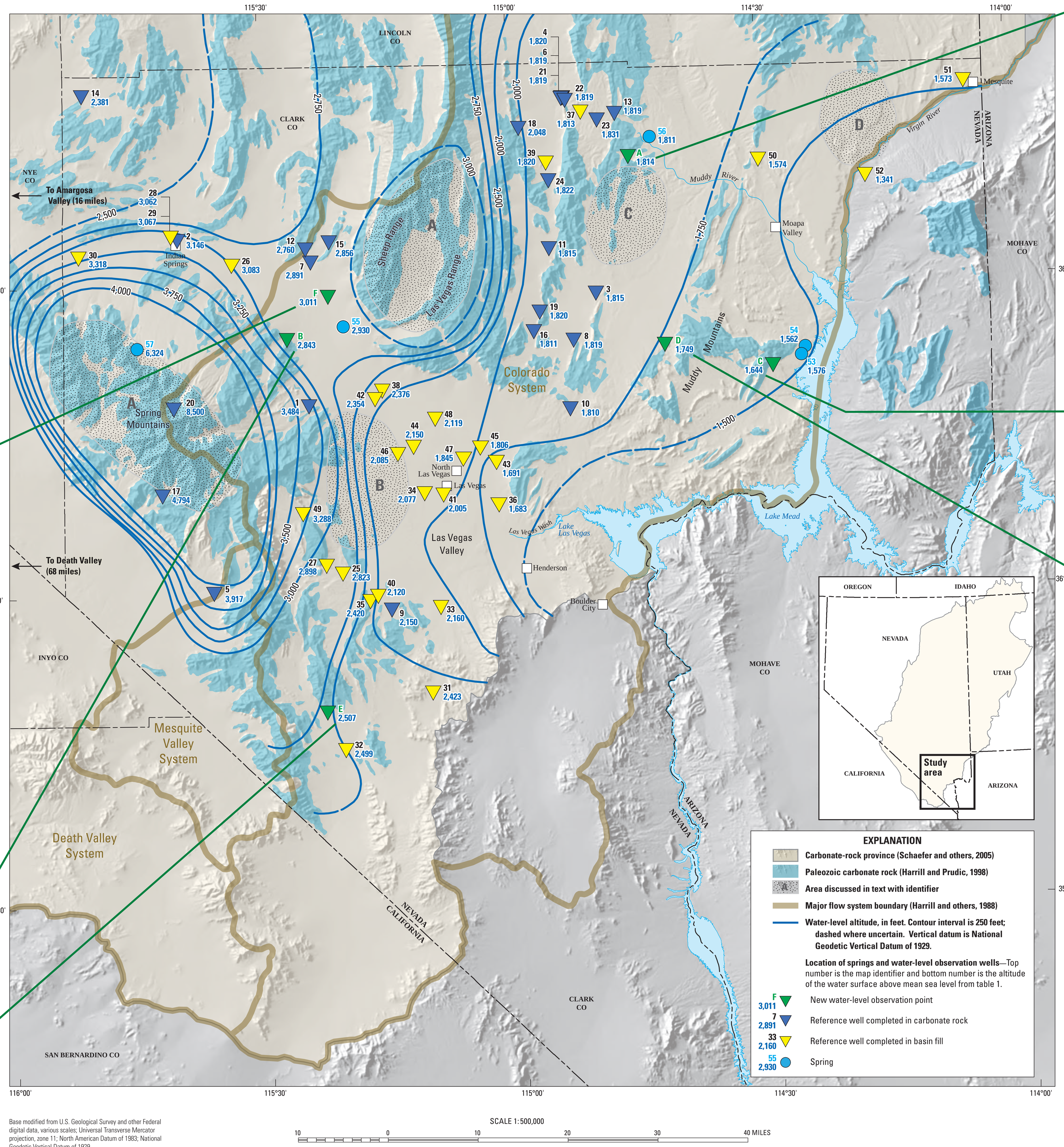

Well IVPH-01 (354849115225001)

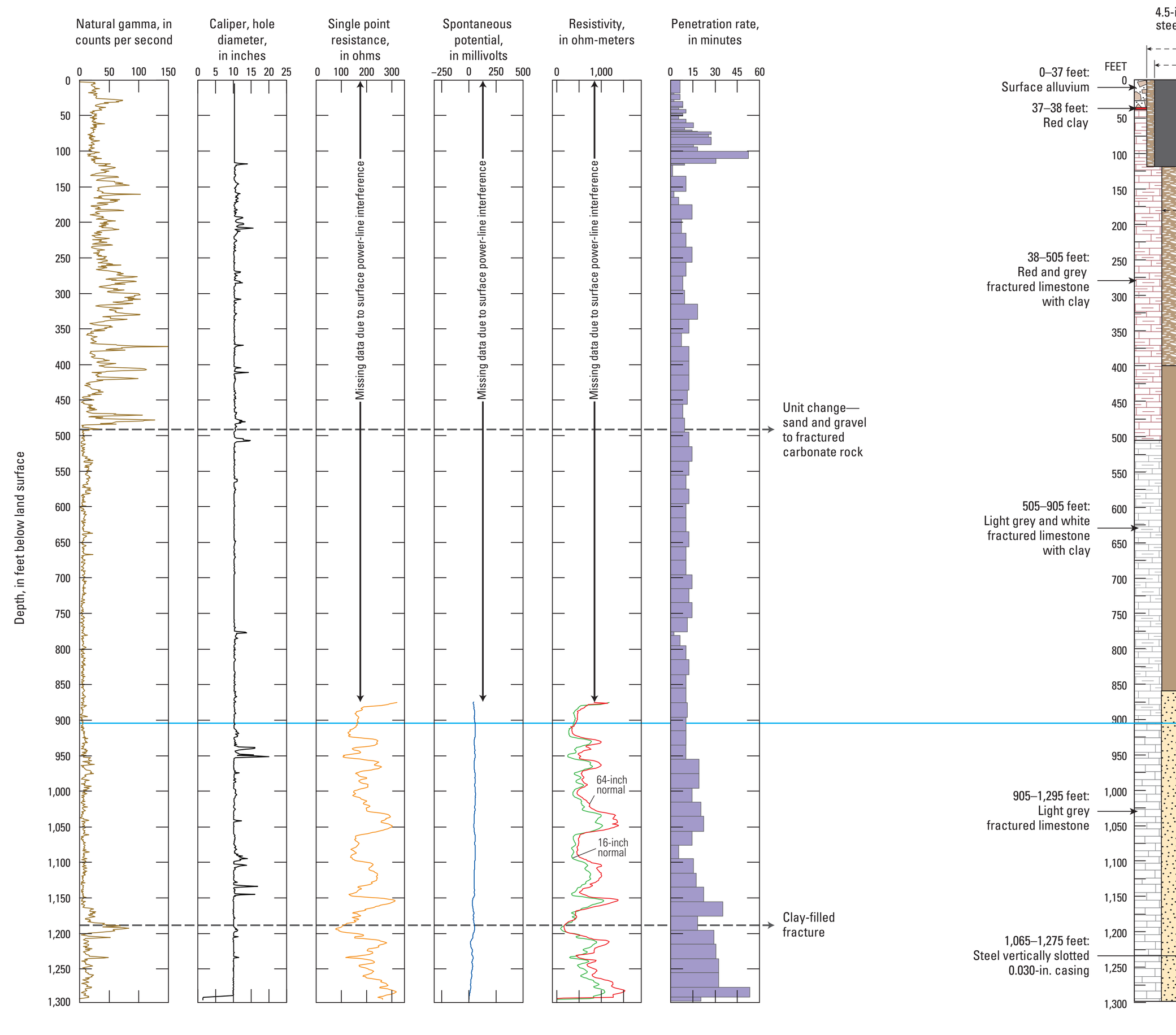

Well BW-01 (364204114454501)

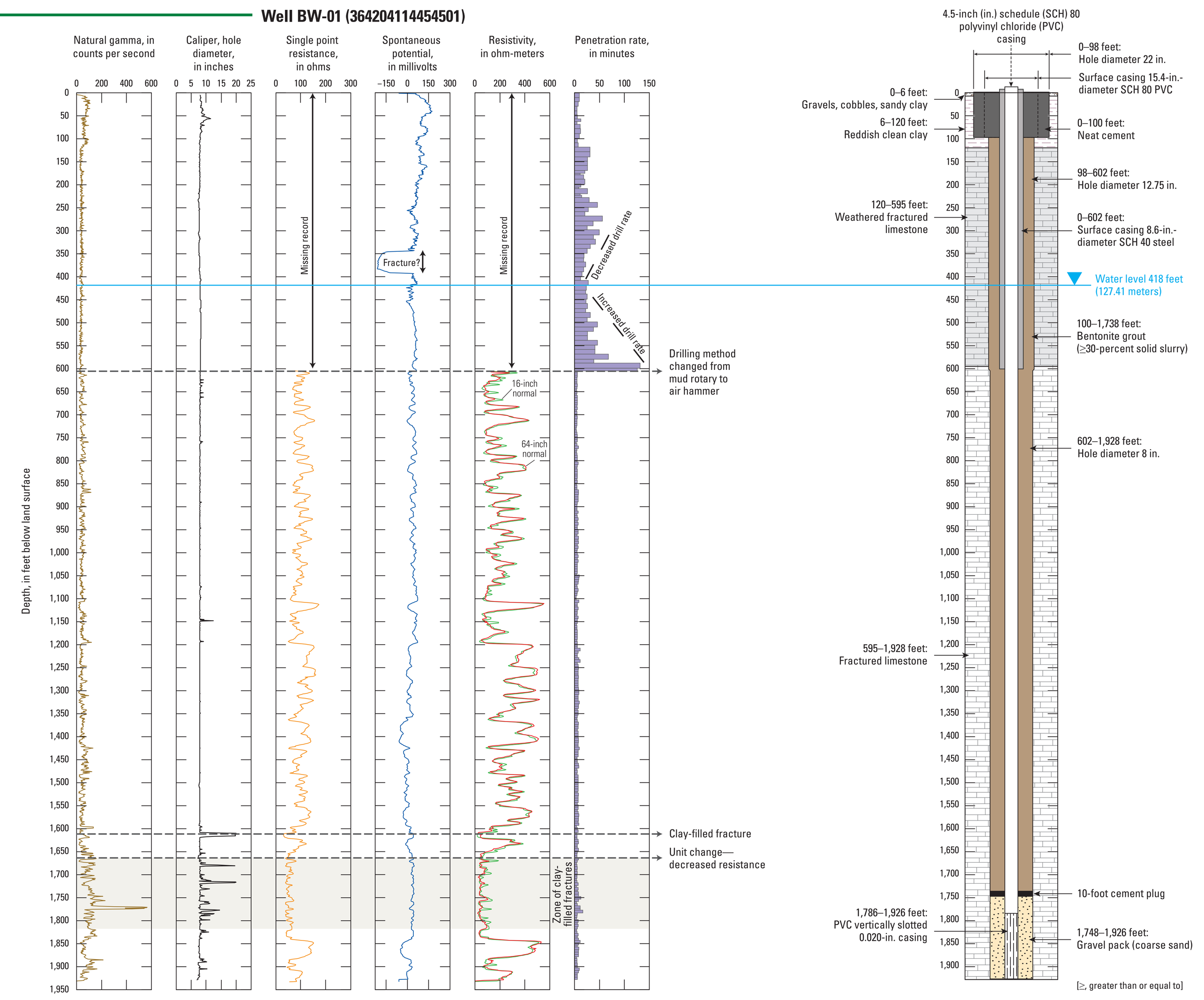

Well RB-01 (362135114285401)

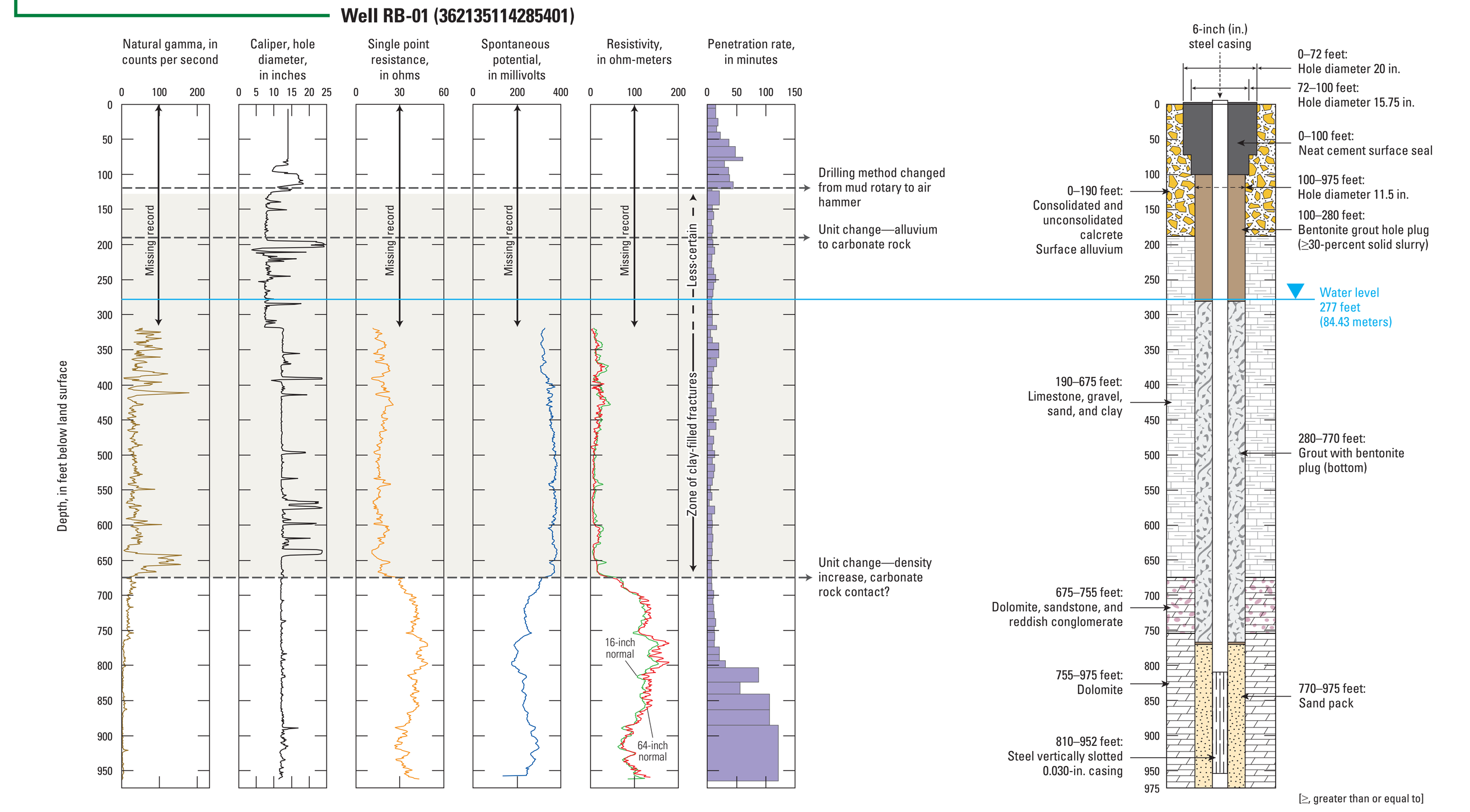

Well BUFPKTS-01 (362352114414501)

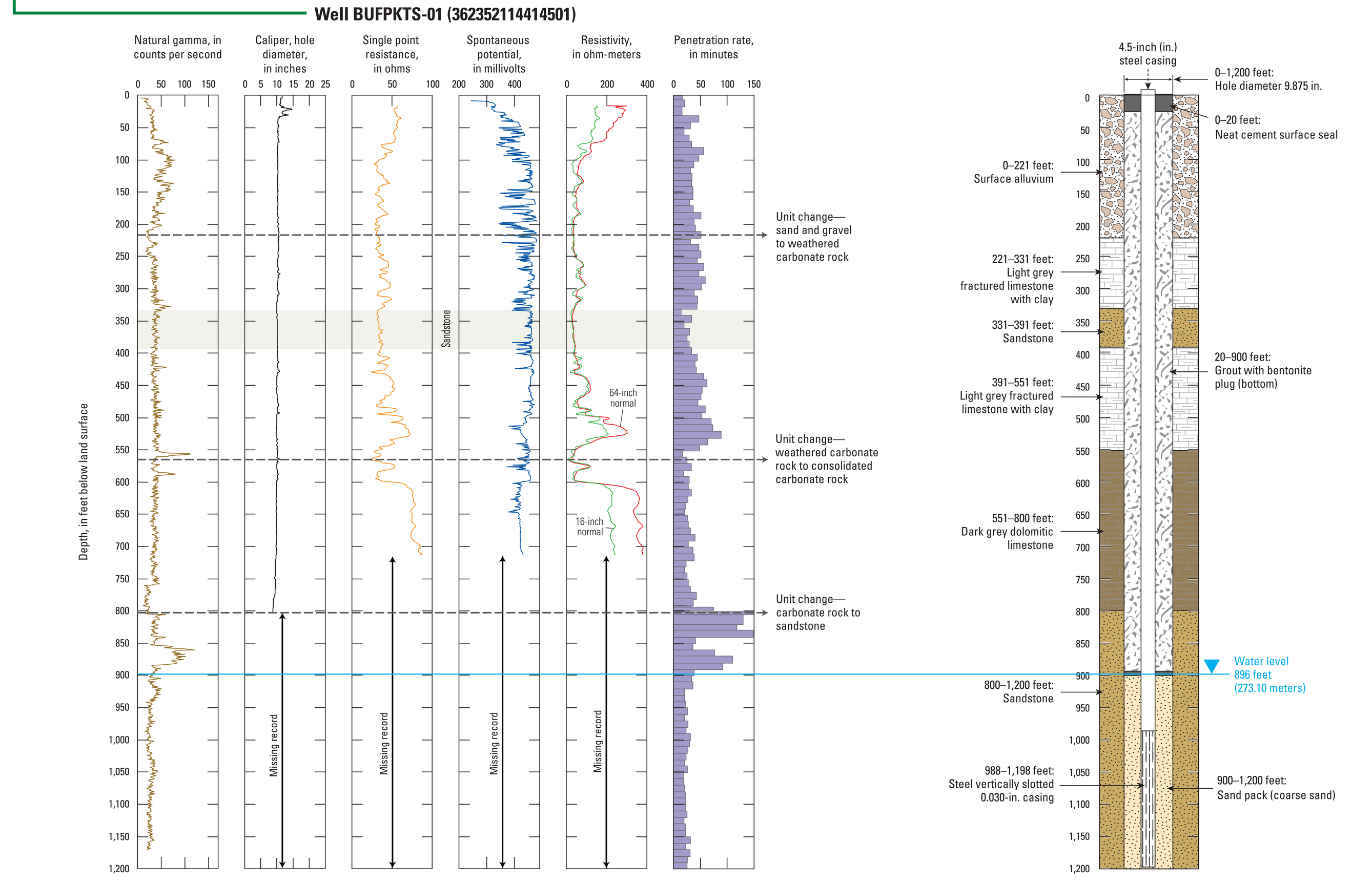

Drilling, Construction, Water Chemistry, Water Levels, and Regional Potentiometric Surface of the Upper Carbonate-Rock Aquifer in Clark County, Nevada, 2009–2015

By
Jon W. Wilson
2019

ISSN 2329-132X (online)
https://doi.org/10.3133/sim3434

Digital files available at https://doi.org/10.3133/sim3434 or https://pubs.usgs.gov/sim/3434/.

Suggested citation: Wilson, J.W., 2019, Drilling, construction, water chemistry, water levels, and regional potentiometric surface of the upper carbonate-rock aquifer in Clark County, Nevada, 2009–2015: U.S. Geological Survey Scientific Investigations Map 3434, scale 1:500,000, https://doi.org/10.3133/sim3434.

University of Nevada, Reno

Nevada Bureau of Mines and Geology

Nevada Bureau of Mines and Geology Report 56

Geology and Geophysics of White Pine and Lincoln Counties, Nevada, and Adjacent Parts of Nevada and Utah: The Geologic Framework of Regional Groundwater Flow Systems

Peter D. Rowley, Gary L. Dixon, Edward A. Mankinen, Keith T. Pari, Darcy K. McPhee, Edwin H. McKee, Andrew G. Burns, James M. Watrus, E. Bartlett Ekren, William G. Patrick, and Judith M. Brandt

NEVADA BUREAU OF MINES AND GEOLOGY
REPORT 56

Geology and Geophysics of White Pine and Lincoln Counties, Nevada, and Adjacent Parts of Nevada and Utah: The Geologic Framework of Regional Groundwater Flow Systems

Peter D. Rowley[1], Gary L. Dixon[2], Edward A. Mankinen[3], Keith T. Pari[4], Darcy K. McPhee[3], Edwin H. McKee[3], Andrew G. Burns[4], James M. Watrus[4], E. Bartlett Ekren[5],William G. Patrick[4], and Judith M. Brandt[4]

[1]Geologic Mapping, Inc., New Harmony, Utah
[2]Southwest Geology LLC, Blackfoot, Idaho
[3]U.S. Geological Survey, Menlo Park, California
[4]Southern Nevada Water Authority, Las Vegas, Nevada
[5]Private consultant, White Sulphur Springs, Montana

2017

SOUTHERN NEVADA WATER AUTHORITY
Resources & Facilities Department
Water Resources Division
♦ snwa.com

SOUTHERN NEVADA WATER AUTHORITY

This report is dedicated to Gary L. Dixon, who died at age 73 from cancer on January 14, 2017 as the manuscript was being reviewed and edited. Gary, a great field geologist, led the 20-year study presented here through the strength of his competence and personality. He began the study when he was a Geologist with the U.S. Geological Survey. After retirement, he continued with it as a consulting geologist. Perhaps more important to his coauthors and many others, we loved Gary and can attribute major parts of our careers to mentorship by him and to collaboration with him. To his wife, Wendy Dixon, and his children, Chris Dixon and Natalie Dixon Pique, he was a loving husband and father and a loyal friend to them and most others he met. His passions were geology, golf, and supporting Wendy's equally extraordinary career with the U.S. Department of Energy. All of us miss him.

CONTENTS

FIGURES

PLATES

ABSTRACT

This report describes the geologic framework of a >65,000 km^2 area that straddles the Nevada-Utah border. The studied region includes most of White Pine and Lincoln counties and adjacent counties in eastern Nevada, as well as parts of Tooele, Juab, Millard, Beaver, and Iron counties in western Utah. This study represents more than a 20-year effort by the Southern Nevada Water Authority (SNWA) to understand the groundwater resources of this part of the Great Basin. This first step, which includes a compilation of all the information on the geologic and geophysical setting, was necessary for hydrological and biological investigations. To understand the geologic framework, we compiled all known geologic mapping at a scale of 1:250,000, and constructed 25 geologic cross sections at the same scale. We also present new geophysical data, consisting of gravity surveys and audiomagnetotelluric (AMT) profiles, plus assembly of available aeromagnetic data, contracted from the U.S. Geological Survey (USGS), as well as additional AMT profiles by the SNWA. This report focuses on two large regional groundwater flow systems: the White River and Great Salt Lake Desert systems. Although the map boundaries presented here bound these aforementioned flow systems, the maps, cross sections, and text are intended to serve as a modern multidisciplinary regional geological and geophysical review, comparable to many old county reports in Nevada and Utah.

Many of the oldest exposed rocks are thick marine quartzites and other clastic rocks deposited in Neoproterozoic and Early Cambrian time. In the Middle Cambrian through late Permian time, there was a shift in sedimentation to ~10 km thick marine carbonates that represent the great carbonate aquifer. In Late Devonian to late Mississippian time, east-verging thrust faults and folds of the Antler orogeny affected the area just northwest of the study area, resulting in clastic sedimentation, including the Chainman Shale that was deposited in a foreland basin east of the Antler Highland. These clastic confining rocks are intertongued with the carbonates. Mesozoic to lower Cenozoic rocks consist mostly of continental clastic deposits, now significantly removed by erosion except in the southern part of the study area. These rocks were deposited, in part, during east-verging thrusting and folding of the Sevier orogeny of Middle Jurassic through early Paleocene. Large frontal thrusts formed in the extreme south as well as east of the study area, but most of the area is referred to as the orogenic hinterland (highland) of small thrusts that was the source of clastic sedimentation eastward.

Eocene to lower Miocene, subduction-related, calc-alkaline volcanic rocks, mostly ash-flow tuffs, were erupted from east-trending igneous belts that young to the south. These deposits are locally thick in the south but are older in the north and therefore have been mostly removed by erosion. The igneous belts are prominent on aeromagnetic maps. From lower Miocene to the present, east-west regional Basin and Range extension affected most of the study area. The Great Basin formed as large, north-striking, high-angle normal faults resulted in alternating ranges and basins. Thick clastic, continental basin-fill deposits were deposited in the basins from erosion of the ranges, and relatively small-volume bimodal (basalt and high-silica rhyolite) volcanic rocks were simultaneously deposited. Gravity-inversion data show that the basin-fill deposits are in many places 3 km thick, and they are the most important aquifer in the area. The east-west extension led to less extensive northeast- or northwest-striking transfer faults and east-striking transverse zones. Also secondary to the north-striking high-angle faults are low-angle, non-rooted, normal attenuation/denudation faults that formed as the tops of the ranges slid into adjacent basins during uplift of the ranges along the large high-angle normal faults. The present topography formed from ~10 Ma to the present, during the most active part of Basin and Range extension.

INTRODUCTION

This report describes the geology and geophysics of a >65,000 km^2 area in east-central to southeastern Nevada and adjacent parts of western Utah. We compiled geologic maps at a scale of 1:250,000 from all available published and unpublished maps, supplemented by site studies and local new geologic mapping in all parts of the area, especially in the south. Based on these compiled maps, we constructed 25 new geologic cross sections at the same scale. We also compiled and interpreted new geophysical data from the U.S. Geological Survey (USGS), including primarily gravity readings and audiomagnetotelluric (AMT) profiles, and available but re-gridded aeromagnetic data.

This report is an update of the many valuable geologic reports originally done in the 1960s through 1980s for all counties in Nevada. Such geologic reports, authored by geologists of the USGS in cooperation with geologists of the Nevada Bureau of Mines and Geology (NBMG), contained 1:250,000-scale geologic maps. At about the same time, the USGS published a series of 1x2-degree (1:250,000 scale) geologic-map sheets, but only two of these reached as far west as western Utah and none were done in Nevada. The Utah Geological Survey (UGS) also had a program at the same time of scattered county reports that included reconnaissance geologic maps. With few exceptions, all these older maps and reports lacked geophysics and cross sections, and most are now partly obsolete. In the last two decades, however, the UGS has issued modern 0.5- x 1-degree geologic-map sheets (1:100,000-scale), with cross sections, that span most of the state, including some of the Utah part of the study area.

BACKGROUND

In the early 1990s, the Southern Nevada Water Authority (SNWA), which is the research arm that supplies culinary water to the city of Las Vegas through Las Vegas Valley Water District, became interested in the availability and amounts of groundwater resources in upstate Nevada. Las Vegas at the time was the fastest growing city in the U.S., and its culinary water came primarily from the surface water in Lake Mead, with some supplementary groundwater from Las Vegas basin. By then they had secured groundwater rights and applications for additional rights in selected upstate groundwater basins. The basins of interest are, from north to south, Snake Valley, Spring Valley, Cave Valley, Dry Lake Valley, Delamar Valley, and Coyote Spring Valley. SNWA recognized that understanding the hydrology and the water resources of these basins required a three-dimensional geologic framework of these basins and adjacent basins that may or may not be hydraulically connected. They eventually selected the large study area outlined in red on figure 1.

The SNWA contracted with USGS geologists from the Las Vegas office to develop geologic maps across the study area. These geologists included some of the authors of this report. Detailed (1:24,000 scale) geologic maps were prepared of problem areas and parts of the southern basins, concentrating on likely groundwater flow paths as well as boundaries between basins so as to test their hydraulic connections with each other. The sheer size of the area required that the scale be at 1:250,000. Geologic maps commonly include geologic cross sections at the same scale that are constructed based on surface observations. However, geologic maps that focus on mineral or groundwater resources need more accurate assessments of the subsurface geology via geophysical methods and well data. The SNWA contracted for new gravity surveys, new AMT profiles, and analysis of available aeromagnetic data with the USGS office in Menlo Park, California. These data were used to prepare the geologic cross sections of this report.

The southern part of the White River regional groundwater flow system (figure 2) was compiled first. The geologic map and some hydrogeologic implications of this area, about 22,000 km^2 in size and almost entirely in Nevada, were published at 1:250,000 scale by Page et al. (2005a). Related geophysical studies, primarily gravity data, were reported by Phelps et al. (2000) and Scheirer (2005).

More recently we extended the study area northward to encompass the entire White River

flow system and adjacent parts of other flow systems. The White River system extends about 430 km from north to south. Dixon et al. (2007a) released the first summary of the geology, geophysics, and hydrogeology of the flow systems, including parts of the adjacent Great Salt Lake Desert regional groundwater flow system (figure 2) in Nevada and Utah. This is the same scale (1:250,000) and area as that of the present report. Dixon et al. (2007a) included summaries and analysis of the USGS gravity and AMT studies. This regional framework study, along with hydrology reports by SNWA and analyses of all springs in the study area (Southern Nevada Water Authority, 2006), were presented at hearings of the Nevada State Engineer. The full geophysical reports were published by Mankinen et al. (2006, 2007, 2008), McPhee et al. (2005, 2006a and b, 2007, 2008), Scheirer et al. (2006), and Scheirer and Andreason (2008).

We next extended studies of similar scope farther northeast, concentrating in Snake and Hamlin valleys but also in more eastern Utah parts of the Great Salt Lake Desert flow system (figure 2). This flow system is about 240 km from north to south. The published topics consisted of water chemistry (Acheampong et al., 2009), surface water and springs (Kistinger et al., 2009), gravity and aeromagnetic studies (Mankinen and McKee, 2009, 2011), AMT profiles (McPhee et al., 2009), and geology and limited hydrology (Rowley et al. 2009). The geologic map and profiles of the study area covered almost 16,000 km^2 (plate 1 of Rowley et al., 2009) at 1:250,000 scale, most of it northeast of the present study area.

This northeastward expansion of the study allowed greater understanding of the Great Salt Lake Desert flow system. It was followed by further updating of the geology, geophysics, and hydrogeology of the primary study area, with an emphasis on the project basins of Spring, Cave, Dry Lake, and Delamar valleys. The result was the geologic and geophysical framework analysis of Rowley et al. (2011), of the same area as that of Dixon et al. (2007a). This unpublished analysis was presented at new (late 2011) hearings of the Nevada State Engineer. Other primary components of the hearings testimony included the hydrologic analysis (Burns and Drici, 2011) and all AMT profiles (Pari and Baird, 2011). We also incorporated the results of the various geological, geophysical, hydrogeological, and hydrological investigations into an Environmental Impact Statement (Southern Nevada Water Authority, 2011; Bureau of Land Management, 2012), which included an updated analysis of all significant springs in the study area. The current report covers the same study area of both Dixon et al (2007a) and Rowley et al. (2011). Although updated by new data and interpretations, the current report stresses the geology and geophysics but limits the discussion of hydrologic conclusions. Mankinen et al. (2016) and Rowley et al. (2016) provided early summaries of the current report. We suggest that this overall multi-year effort is how a modern groundwater analysis should be fashioned.

STUDY AREA

The study area is within the Great Basin physiographic province, primarily characterized by north-trending basins and ranges that formed by north-striking normal faults. This topography consists of a number of closed and partially closed basins, typical of the Great Basin region, where surface-water flow is generally restricted to each individual basin. Exceptions to closed surface-water basins occur near the Great Basin boundary, where a few basins have surface water exiting to the Colorado River. These exceptions include basins containing the Virgin River, Muddy River, and Las Vegas Wash (figure 1), as well as basins containing the ancestral White River and Meadow Valley Wash.

During wetter periods of Pleistocene time, the latest of which was about 10,000 to 15,000 years before the present (Reheis et al., 2014), ancestral lakes formed and grew in many closed basins. Some of these lakes filled and overtopped individual basins, one by one, and thus integrated multiple basins. For instance, the White River and its tributaries integrated several basins and eventually flowed southward through much of the southwestern part of the map area (Tschanz and Pampeyan, 1970). During this time, the White River joined other streams that flowed southward to join the Colorado River near present-day Lake Mead, at the southern edge of the study area.

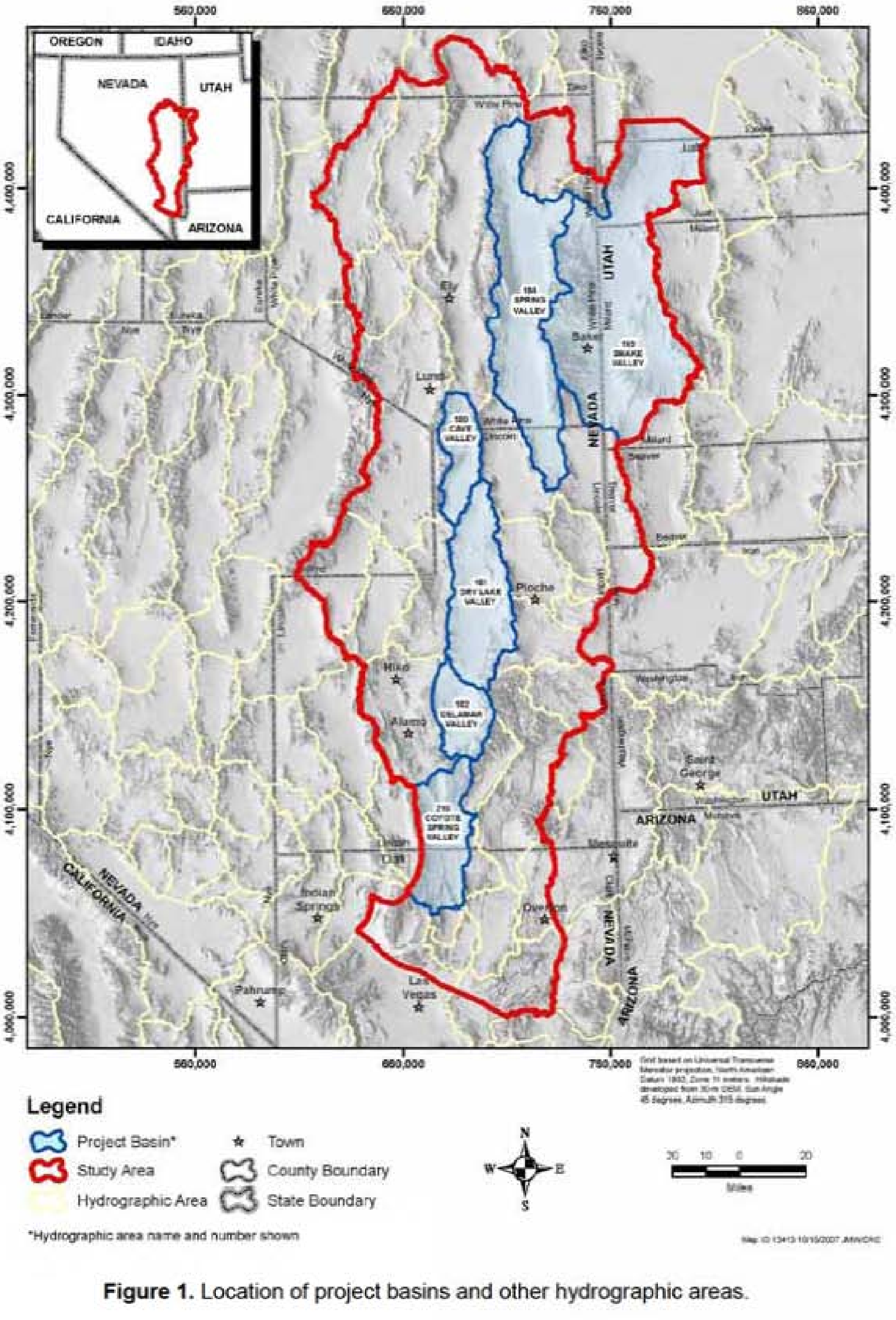

Figure 1. Location of project basins and other hydrographic areas.

Presently, the descendant drainages of the White River are discontinuously dispersed and intermittent over most of its course and as far south as Moapa, Nevada.

Despite the intermittent nature of surface water, groundwater occurs at different depths beneath all of the map area. The groundwater exists in aquifers within and between a number of groundwater basins, and it flows through these aquifers in a large number of defined regional groundwater flow systems. These flow systems may include a dozen or more closed or integrated topographic basins that are interconnected in the subsurface. These regional flow systems are defined by evidence that their groundwater flow paths pass beneath topographic divides and continue beneath some adjacent basins and ranges (Eakin, 1966; Winograd and Thordarson, 1975; Harrill et al., 1988; Harrill and Prudic, 1998).

The White River and part of the Great Salt Lake Desert regional groundwater flow systems are shown with respect to the study area, which is portrayed by the red line in figure 2. The White River flow system (Eakin, 1966), as referred to here, was called the Colorado flow system by Harrill and Prudic (1998) and Heilweil and Brooks (2011) (see also Belcher, 2004). The Meadow Valley flow system was considered a subset of the Colorado flow system, and therefore can be considered part of the White River system (figure 2). The various flow systems were defined by Eakin (1966), Harrill et al. (1988), and Harrill and Prudic (1998). Groundwater flow in the White River flow system is southward to the Colorado River, whereas flow in the Great Salt Lake Desert flow system is northward to the Great Salt Lake Desert. Parts of adjacent flow systems are included within this study because their basins may be in hydraulic connection with those of the White River and Great Salt Lake Desert systems. In other words, the entire broader region (figure 1) needed study because of the potential hydraulic continuity or discontinuity between basins due to geologic influences. In addition, we compiled the regional geology and made cross sections at a constant scale (1:250,000) over an even larger area, whose limits are demarcated by the thick black line outside the edge of the study area in figure 2. This was done to assess the broader geologic framework in order to determine the best model area and to provide additional data should the boundaries of the model area later change. Later the sections, map, and discussion were revised to an area that was trimmed to the current size.

The primary regional aquifers in the flow systems consist of Paleozoic carbonate rocks, volcanic rocks (notably Tertiary ash-flow tuffs), and Miocene to Holocene basin-fill sediments. The primary regional aquitards within the flow systems are Proterozoic to Cambrian schist, quartzite, slate, and shale, Mississippian shale, Mesozoic clastic sedimentary rocks, and Jurassic to Tertiary plutonic rocks.

FRACTURE FLOW

In addition to influencing the present topography, Basin and Range extension controls groundwater flow. This is because the direction of groundwater flow is generally enhanced along (parallel to), and the direction guided by, high-angle normal faults. More specifically, groundwater flows along and through rock fractures associated with these high-angle faults (Rowley et al., 2012; see discussion below). Conversely, groundwater flow across faults is commonly retarded. Extensional (normal) faults are more important than contractional (reverse) faults in allowing flow along them, because normal faults tend to stay open. This concept is especially important in understanding the groundwater hydrology of the study area in the Great Basin region because normal faults are abundant. Therefore, geologic mapping and identification of faults provides a first approximation of groundwater flow in the study area. This manner of groundwater movement is known as "fracture flow" or "fracture-dominated flow" (Caine et al., 1996). Knowledge about fracture flow has accumulated for many decades, because it plays an important role in the study of isolation of radioactive waste in underground repositories, groundwater transport of radionuclides, cleanup of toxic waste, exploitation of geothermal and petroleum reservoirs, and of course movement of groundwater (e.g., Rowley and Dixon, 2004).

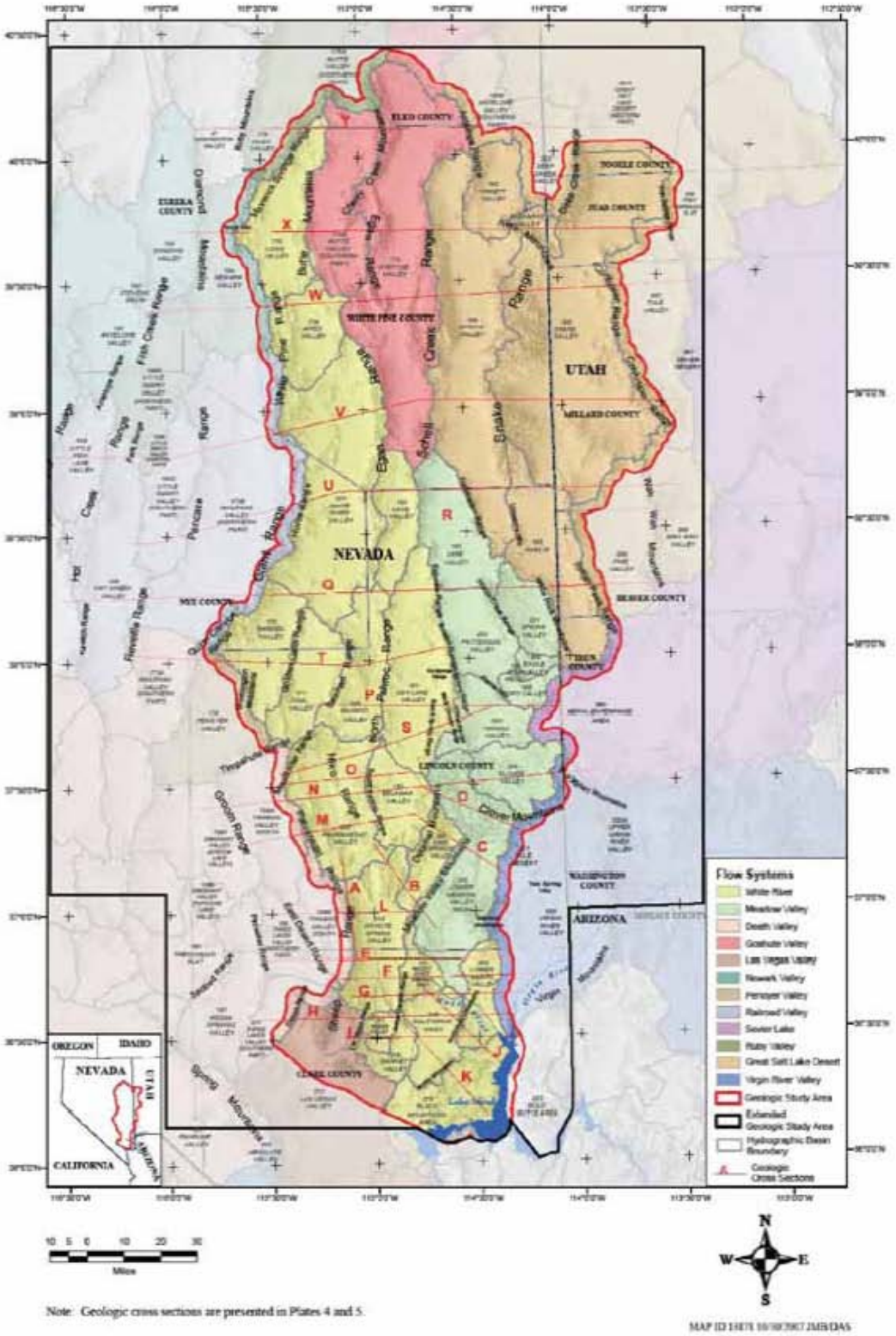

Note: Geologic cross sections are presented in Plates 4 and 5.

Figure 2. Hydrographic areas, ranges, and flow systems in the study area.

Much of what we know about fracture flow began with U.S. Department of Energy-funded studies, primarily by the USGS, on the Nevada Test Site (NTS), to trace movement of contaminated groundwater resulting from hundreds of above- and below-ground nuclear tests (Winograd and Thordarson, 1968, 1975; Laczniak et al., 1996; Leahy and Lyttle, 1998; Rowley and Dixon, 2004). These studies began in the 1950s and resulted in publications on the geology, detailed geologic mapping of the entire NTS, and conclusions from well tests and other hydrologic data. The studies resulted in the discovery of the large (north-south length about 300 km) Death Valley regional groundwater flow system (Harrill et al., 1988; Dettinger, 1992; Dettinger et al., 1995; Burbey, 1997; Laczniak et al., 1996; Harrill and Prudic, 1998; Slate et al., 1999; D'Agnese et al., 2002; Workman et al., 2002a and b; Belcher, 2004). In this flow system, recharge originated in the broad, high mountains of central Nevada, and flow terminated as spring discharge in Ash Meadows, Oasis Valley, and Death Valley. Among the numerous reports that resulted, the words structural "barriers" and "conduits" were introduced (Winograd and Thordarson, 1968, p. 35) to describe faults and other fractures that respectively create dams to groundwater flow across them and exhibit high transmissivities along them.

A greater understanding of the role of faults in groundwater flow came from the studies of Caine et al. (1996), Sibson (1996), and Caine and Forster (1999). In particular, Caine et al. (1996) proposed that a central "core zone" of a fault commonly contains fine-grained gouge that inhibits flow across it, whereas on either side of the core zone, a "damage zone" consists of fractures parallel to the core zone that provide increased secondary permeability along them (figure 3). Where the damage zones are in carbonate rocks, solution of the carbonate rocks along the fractures can create still larger groundwater flow paths.

All known springs of significance, whether cold or hot, in the study area rise along faults (Kistinger et al., 2009; Southern Nevada Water Authority, 2011; Bureau of Land Management, 2012). Many of the active springs have active spring mounds, generally of calcium carbonate. Pleistocene spring mounds for springs that are no longer active occur locally, as in the Ute railroad stop in the California Wash area. Feeders for ancient springs and for spring mounds that have been eroded away are locally expressed as calcite veins or dikes, as in the Wildcat Wash area of the southeastern Meadow Valley Mountains (Page and Pampeyan, 1996) and in other areas (Schmidt, 1994; Schmidt and Dixon, 1995).

Because of its importance in understanding movement of groundwater in the study area, expanded discussions of fracture flow were given in Rowley and Dixon (2004), Page et al. (2005a), and Rowley et al. (2009, 2011). The concept is also used to site production water wells along faults, as documented in the Mesquite basin of southeastern Nevada (Dixon and Katzer, 2002; Johnson et al., 2002) and in the Sand Hollow well field east of St. George of southwestern Utah (Rowley et al., 2004). Bhark et al. (2006) demonstrated conduit flow when they injected tracers down wells in a fault zone on the NTS, then detected those tracers 69 hours later in a pumped (1900 lpm) well 180 m down gradient (south) on the same fault. Pumping this well also lowered the water level in a well 9.6 km north of it on the same fault, yet pumping had no effect (barrier flow) on wells east and west of the fault. In a study of interference (drawdown of water levels) in springs and monitoring wells by pumping wells 0.8 and 1.3 km away on the same fault zone south of New Harmony, Utah, Rowley et al. (2012) documented conduit flow, and on wells east and west of that fault, a lack of interference indicated barrier flow.

TECHNICAL APPROACH

In this investigation we combined and reviewed published and unpublished geologic information from dozens of references, which was supplemental with geologic fieldwork by the authors. In addition, we evaluated borehole information from oil and gas test wells, monitor wells such as those drilled during the U.S. Air Force's MX missile-siting program of the early 1980s, and borehole information from exploratory test wells and monitor wells constructed by SNWA in support of the project. Geophysical studies concentrated on gravity surveys and AMT profiles

performed by the USGS under contract from SNWA and on AMT profiles by SNWA. These geophysical studies provided many of the details on the geometry and location of many normal faults and on thickness of basin fill.

Based on the evaluation of the compiled and new data, we compiled the geologic maps (plates 1 and 2) and constructed new geologic cross sections (plates 3 and 4). Because of the complexity of the geology of the study area, the maps and cross sections represented works in progress, and we periodically updated them as new data became available.

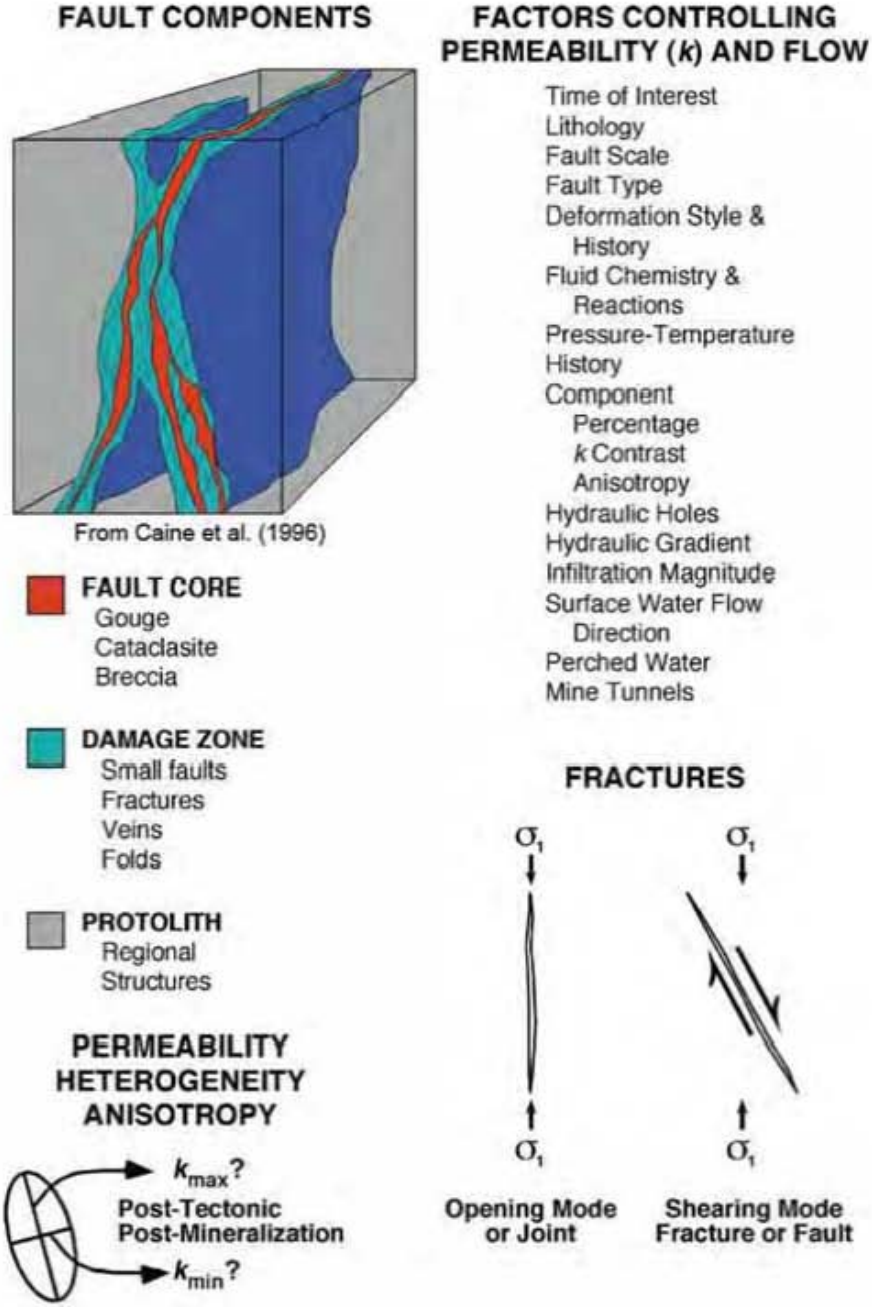

Figure 3. Conceptualization of fault components and factors controlling permeability and groundwater flow (after Caine et al., 2010).

PREPARATION OF GEOLOGIC MAPS AND SECTIONS

The geology of the southern part of the study area (figure 4) has been discussed by Page et al. (2005a). In their report, the geology for this area was compiled as a digital map at 1:250,000 scale; most of their map is included in plate 2. To the west of this area, digital geologic and tectonic maps were also published at 1:250,000 scale (Workman et al., 2002a and b), and some of this mapping was included in southwestern parts of plates 1 and 2. These previous geologic maps included significant new and unpublished geologic mapping. The geology of the northeastern part of the study area, and of some adjacent basins east of this northeastern area were compiled at 1:250,000 scale and discussed by Rowley et al. (2009, plate 1).

For the geologic maps (plates 1 and 2) and the Description of Map Units, much of the Nevada geology was compiled from county 1:250,000-scale geologic maps and the Nevada 1:500,000-scale state geologic map (Stewart and Carlson, 1978). From west to east and north to south, the Nevada counties covered by these maps are southern Elko County (Roberts et al., 1967), eastern Nye County (Cornwall, 1972; Kleinhampl and Ziony, 1985), White Pine County (Hose and Blake, 1976), Lincoln County (Tschanz and Pampeyan, 1970), and Clark County (Longwell et al., 1965). Most of the Utah geology was compiled from four 1:100,000-scale maps (Hintze and Davis, 2002a and b; Rowley et al., 2006 and 2008; Biek et al., 2009), two 1:250,000-scale maps (Morris, 1987; Steven et al., 1990), and the Utah 1:500,000-scale state geologic map (Hintze, 1980a). Summary reports on the geology of Millard County (Hintze and Davis, 2003) and the geology of Utah (Hintze, 1988 and 2005; Hintze and Kowallis, 2009) were also valuable. Both the Nevada and Utah state geologic maps were digitized and re-released as digital files, but not updated with respect to maps and reports published since their original release dates of 1978 and 1980, respectively. These new 1:500,000-scale digital files were compiled by Hess and Johnson (1997), Raines et al. (2003), and Crafford (2007) for Nevada and by Hintze et al. (2000) for Utah.

Most of the regional geologic maps (figure 4) were published decades ago. A significant part of the entire study area was compiled by Terrascan Group, Inc. (Howard, 1978), but in most places this compilation included the same county maps without updating them. As part of the USGS Basin and Range Carbonate-Rock Aquifer System study (BARCAS; Welch et al., 2007; Sweetkind et al., 2007b), Sweetkind et al. (2007a) compiled a 1:500,000-scale, digital geologic map of a large area that includes all but the eastern edge of the area of plate 1. However, their map was compiled from Stewart and Carlson (1978), Hintze (1980a), Hintze et al. (2000), and Raines et al. (2003), from which all faults were removed. To that file, Sweetkind et al. (2007a) added some gravity interpretations, dotted "geophysically determined faults," and some sketched faults. Two diagrammatic cross sections accompanied this map, but neither matched the topography, geology, or geophysics of their map. As part of the BARCAS study, Watt and Ponce (2007) and Wallace et al. (2007) provided geophysical data for east-central Nevada and west-central Utah, but their maps were at 1:750,000 scale.

Hurlow (2014) published a major Utah Geological Survey summary report on the hydrology and hydrogeology of a large area of Utah that focused on Snake Valley, Hamlin Valley, Tule Valley, and Fish Springs Flat and also included adjacent areas in Utah and Nevada. It followed several years of drilling, geochemistry, and monitoring of the groundwater resources of the Utah part of their study area. They found that water levels in Snake Valley have been falling since 1980, due largely to increasing irrigation pumping in Utah and partly to decreases in annual precipitation (see also Hurlow and Inkenbrandt, 2016). The report of Hurlow (2014) included a geologic map and cross sections at 1:250,000 scale that cover most of the northeastern part of our plate 1 area. It also included a study of the geophysics, primarily the collection of new gravity stations in the area and the analysis of these data to determine depth to basement in the valleys. The maps, cross sections, and geophysics provided an important framework for their hydrogeologic conclusions.

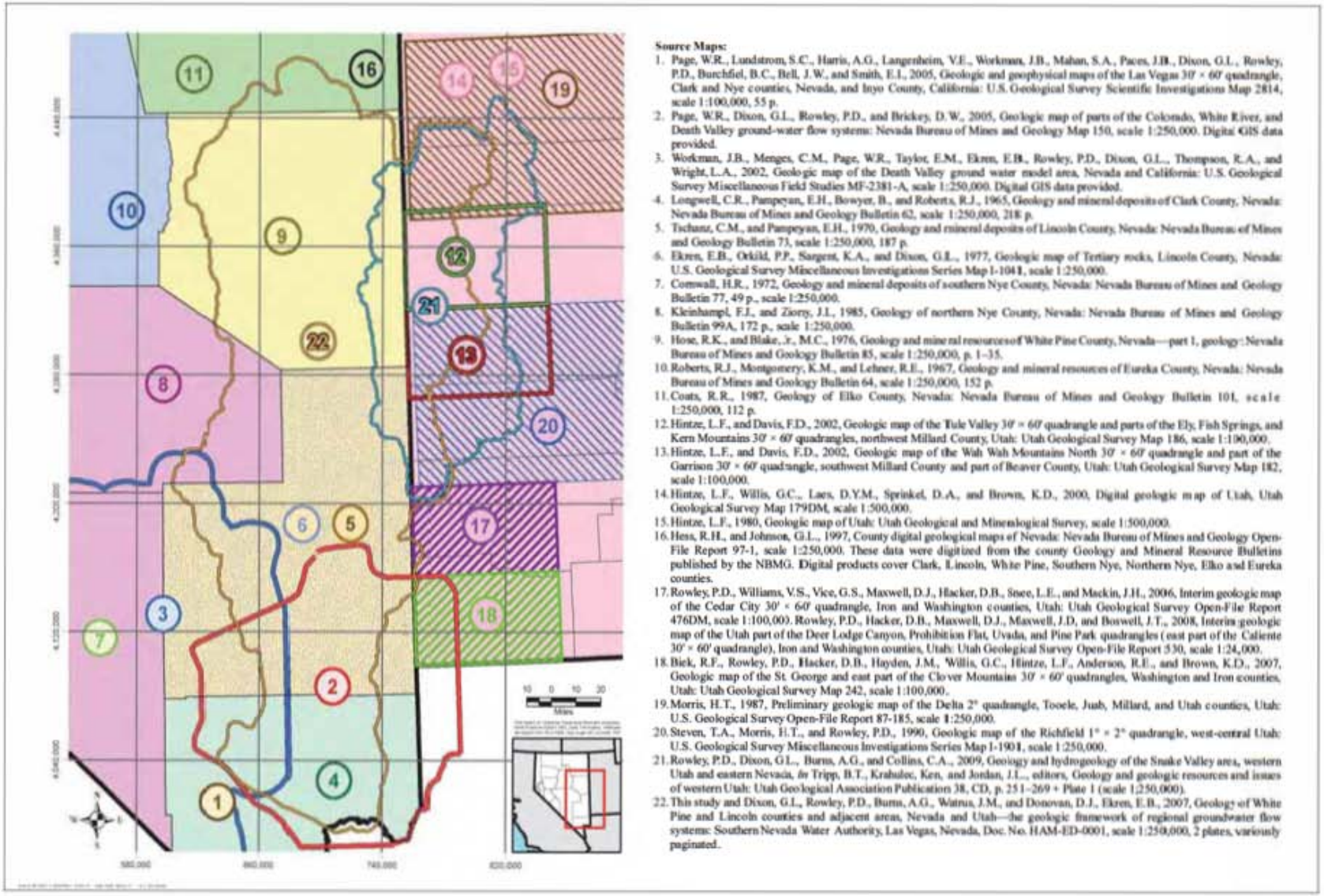

Source Maps:

1. Page, W.R., Lundstrom, S.C., Harris, A.G., Langenheim, V.E., Workman, J.B., Mahan, S.A., Paces, J.B., Dixon, G.L., Rowley, P.D., Burchfiel, B.C., Bell, J.W., and Smith, E.I., 2005, Geologic and geophysical maps of the Las Vegas 30' × 60' quadrangle, Clark and Nye counties, Nevada, and Inyo County, California: U.S. Geological Survey Scientific Investigations Map 2814, scale 1:100,000, 55 p.
2. Page, W.R., Dixon, G.L., Rowley, P.D., and Brickey, D.W., 2005, Geologic map of parts of the Colorado, White River, and Death Valley ground-water flow systems: Nevada Bureau of Mines and Geology Map 150, scale 1:250,000. Digital GIS data provided.
3. Workman, J.B., Menges, C.M., Page, W.R., Taylor, E.M., Ekren, E.B., Rowley, P.D., Dixon, G.L., Thompson, R.A., and Wright, L.A., 2002, Geologic map of the Death Valley ground water model area, Nevada and California: U.S. Geological Survey Miscellaneous Field Studies MF-2381-A, scale 1:250,000. Digital GIS data provided.
4. Longwell, C.R., Pampeyan, E.H., Bowyer, B., and Roberts, R.J., 1965, Geology and mineral deposits of Clark County, Nevada: Nevada Bureau of Mines and Geology Bulletin 62, scale 1:250,000, 218 p.
5. Tschanz, C.M., and Pampeyan, E.H., 1970, Geology and mineral deposits of Lincoln County, Nevada: Nevada Bureau of Mines and Geology Bulletin 73, scale 1:250,000, 187 p.
6. Ekren, E.B., Orkild, P.P., Sargent, K.A., and Dixon, G.L., 1977, Geologic map of Tertiary rocks, Lincoln County, Nevada: U.S. Geological Survey Miscellaneous Investigations Series Map I-1041, scale 1:250,000.
7. Cornwall, H.R., 1972, Geology and mineral deposits of southern Nye County, Nevada: Nevada Bureau of Mines and Geology Bulletin 77, 49 p., scale 1:250,000.
8. Kleinhampl, F.J., and Ziony, J.I., 1985, Geology of northern Nye County, Nevada: Nevada Bureau of Mines and Geology Bulletin 99A, 172 p., scale 1:250,000.
9. Hose, R.K., and Blake, Jr., M.C., 1976, Geology and mineral resources of White Pine County, Nevada—part 1, geology: Nevada Bureau of Mines and Geology Bulletin 85, scale 1:250,000, p. 1–35.
10. Roberts, R.J., Montgomery, K.M., and Lehner, R.E., 1967, Geology and mineral resources of Eureka County, Nevada: Nevada Bureau of Mines and Geology Bulletin 64, scale 1:250,000, 152 p.
11. Coats, R.R., 1987, Geology of Elko County, Nevada: Nevada Bureau of Mines and Geology Bulletin 101, scale 1:250,000, 112 p.
12. Hintze, L.F., and Davis, F.D., 2002, Geologic map of the Tule Valley 30' × 60' quadrangle and parts of the Ely, Fish Springs, and Kern Mountains 30' × 60' quadrangles, northwest Millard County, Utah: Utah Geological Survey Map 186, scale 1:100,000.
13. Hintze, L.F., and Davis, F.D., 2002, Geologic map of the Wah Wah Mountains North 30' × 60' quadrangle and part of the Garrison 30' × 60' quadrangle, southwest Millard County and part of Beaver County, Utah: Utah Geological Survey Map 182, scale 1:100,000.
14. Hintze, L.F., Willis, G.C., Laes, D.Y.M., Sprinkel, D.A., and Brown, K.D., 2000, Digital geologic map of Utah, Utah Geological Survey Map 179DM, scale 1:500,000.
15. Hintze, L.F., 1980, Geologic map of Utah: Utah Geological and Mineralogical Survey, scale 1:500,000.
16. Hess, R.H., and Johnson, G.L., 1997, County digital geological maps of Nevada: Nevada Bureau of Mines and Geology Open-File Report 97-1, scale 1:250,000. These data were digitized from the county Geology and Mineral Resource Bulletins published by the NBMG. Digital products cover Clark, Lincoln, White Pine, Southern Nye, Northern Nye, Elko and Eureka counties.
17. Rowley, P.D., Williams, V.S., Vice, G.S., Maxwell, D.J., Hacker, D.B., Snee, L.E., and Mackin, J.H., 2006, Interim geologic map of the Cedar City 30' × 60' quadrangle, Iron and Washington counties, Utah: Utah Geological Survey Open-File Report 476DM, scale 1:100,000. Rowley, P.D., Hacker, D.B., Maxwell, D.J., Maxwell, J.D, and Boswell, J.T., 2008, Interim geologic map of the Utah part of the Deer Lodge Canyon, Prohibition Flat, Uvada, and Pine Park quadrangles (east part of the Caliente 30' × 60' quadrangle), Iron and Washington counties, Utah: Utah Geological Survey Open-File Report 530, scale 1:24,000.
18. Biek, R.F., Rowley, P.D., Hacker, D.B., Hayden, J.M., Willis, G.C., Hintze, L.F., Anderson, R.E., and Brown, K.D., 2007, Geologic map of the St. George and east part of the Clover Mountains 30' × 60' quadrangles, Washington and Iron counties, Utah: Utah Geological Survey Map 242, scale 1:100,000.
19. Morris, H.T., 1987, Preliminary geologic map of the Delta 2° quadrangle, Tooele, Juab, Millard, and Utah counties, Utah: U.S. Geological Survey Open-File Report 87-185, scale 1:250,000.
20. Steven, T.A., Morris, H.T., and Rowley, P.D., 1990, Geologic map of the Richfield 1° × 2° quadrangle, west-central Utah: U.S. Geological Survey Miscellaneous Investigations Series Map I-1901, scale 1:250,000.
21. Rowley, P.D., Dixon, G.L., Burns, A.G., and Collins, C.A., 2009, Geology and hydrogeology of the Snake Valley area, western Utah and eastern Nevada, *in* Tripp, B.T., Krahulec, Ken, and Jordan, J.L., editors, Geology and geologic resources and issues of western Utah: Utah Geological Association Publication 38, CD, p. 251–269 + Plate 1 (scale 1:250,000).
22. This study and Dixon, G.L., Rowley, P.D., Burns, A.G., Watrus, J.M., and Donovan, D.J., Ekren, E.B., 2007, Geology of White Pine and Lincoln counties and adjacent areas, Nevada and Utah—the geologic framework of regional groundwater flow systems: Southern Nevada Water Authority, Las Vegas, Nevada, Doc. No. HAM-ED-0001, scale 1:250,000, 2 plates, variously paginated.

Figure 4. Previous large-scale mapping used to evaluate geology and to create the geologic and hydrogeologic maps of plates 1 and 2.

The plates and text of our report incorporate all known revisions and reinterpretations of previously published reports and geologic maps that were deemed necessary. Large-scale (less detailed) geologic maps used in the creation of plates 1 and 2 are indexed in figure 4. Many more small-scale (more detailed) maps were used in the creation of plates 1 and 2. These are cited in the text. In addition, plates 1 and 2 include some new, unpublished geologic mapping and field observations.

The compilation of the geology in this 65,000 km^2 area required many name changes to specific geologic units throughout this large study area. Map scale required some lumping of units with others. New names or new correlations required other changes. In many places, facies changes resulted in major changes in the lithology of a specific unit, and in other places, different formation names were used essentially for the same unit. In some instances, a specific unit thinned in certain areas and was included as a member of another unit or as an inconsequential bed within another unit. An example is the Mississippian Chainman Shale, which is a major shale confining unit in the north, as in White Pine County (Hose and Blake, 1976), but a generally inconsequential shale bed included within other units in the southern map area, as in Clark County (Longwell et al., 1965). During compilation of the geologic map, separate stratigraphic columns were used for different counties, along with a stratigraphic column for units in western Utah. Correlations between specific geologic units are commonly given in the literature, and these correlations were generally used to associate units of the same or similar age in different parts of the map area. An example is the correlation of the Devonian Guilmette Formation with the Devils Gate Limestone (Hose and Blake, 1976).

During map compilation, a hard copy of the available digital file—generally the county map—was modified by hand, then digitized. Before this compilation, all available new geologic data about the area were accumulated, assimilated, and evaluated. The new data included reports, different concepts, detailed or regional maps, geophysics, and well logs. Several new interpretations conflicted with older interpretations, some resulting from more accurate placement of contacts or faults. Decisions on the final linework were based on what appeared to be scientifically the most reasonable alternative and depended primarily on the judgment and experience of the authors.

The geologic maps (plates 1 and 2) includes many new geologic cross sections (plates 3 and 4) that trend mostly east-west so as to be perpendicular to most structures. In addition, geologic cross sections were drawn through many springs in the study area (Volume 3 of Southern Nevada Water Authority, 2008). The cross sections on plates 3 and 4 are roughly evenly spaced across the study area, at the same scale as the map, and at locations chosen to best show specific geologic and structural relationships important to the interpretation of the hydrogeology. Few of the reports and maps used to compile the geologic maps had associated geologic cross sections, so the cross sections in our report are based on our interpretations of the county geologic maps along with all other available maps and reports of the study area. The geologic map by Terrascan Group, Inc. (Howard, 1978), however, presented associated cross sections that were used to help interpret some of the cross sections in our report. In addition, the geologic map of Elko County (Coats, 1987) was used to help interpret cross section Y–Y' (plate 3), along the northern edge of the study area. The cross sections of Page et al. (2006) aided in constructing the cross sections in the southern part of the study area. The cross section of Smith et al. (1991) was useful in constructing cross section X–X' (plate 3) near the northern margin of the study area.

Unlike our compiled geologic maps, most of the cross sections are newly authored for this report. The first step in the construction of cross sections is to satisfy the three-dimensional geometry of the rocks at depth based on the types, attitudes, and thicknesses of rocks and structures on the surface. Without additional data, subsurface geometries are relatively unconstrained in cross sections constructed from the surface geology alone. Therefore, geophysics and well logs, when located near the line of sections, are valuable. Aeromagnetic and gravity geophysical data were widely available for much of the area, but well

logs, AMT profiles, and publicly available seismic reflection profiles are rare. When subsurface data is unavailable, analogies are made with areas in other parts of the Great Basin, where seismic and drill-log data provide insight to the geometries of rocks and structures at depth. As with the compilation of geologic maps, the judgment and experience of the authors is also important.

All cross sections incorporated lithologic information from available oil- and water-well logs. Oil-well logs in Nevada are available online from the Nevada Bureau of Mines and Geology (NBMG) (data from 1907 to 2011) and related publications (Garside et al., 1988; Hess, 2001, 2004; Hess et al., 2011). Oil-well logs in Utah were obtained from the Utah Division of Oil, Gas, and Mining website (2006, 2011). Water-well logs in Utah were obtained from the Utah Division of Water Rights website (2006).

Geophysical studies, notably gravity maps (Saltus, 1988a and b; Cook et al., 1989; Ponce, 1992; Saltus and Jachens, 1995; Ponce et al., 1996), aeromagnetic maps (Hildenbrand and Kucks, 1988a and b), and seismic reflection sections (Allmendinger et al., 1983; Hauser et al., 1987; Alam, 1990; Alam and Pilger, 1991) were used to aid in the interpretation of geologic cross sections. Gravity maps and AMT profiles were completed by the USGS as part of USGS/SNWA joint funding agreements (Mankinen et al., 2006, 2007, 2008, and 2016; McPhee et al., 2005, 2006a and b, 2007, 2008, and 2009; Mankinen and McKee, 2009 and 2011; Scheirer, 2005; Scheirer et al., 2006; Scheirer and Andreason, 2008). The gravity data were converted to depth-to-basement data and were used to aid in constructing the cross sections.

GEOLOGY

OVERVIEW

The study area (figure 2) is in the Great Basin subprovince of the Basin and Range physiographic province (Fenneman, 1931). The Basin and Range Province is made up of mostly parallel north-trending mountain ranges separated by parallel northerly trending alluvial basins (valleys). The ranges and basins formed because the region was affected by regional extension since the Miocene (e.g., Hamilton and Myers, 1966; Stewart, 1971, 1980a and b; Christiansen and Yeats, 1992). This ongoing east-west extension has resulted in north-striking normal faulting and the development of the north-trending basins and ranges.

Defining regional flow systems and determining directions and amounts of groundwater flow requires an understanding of the stratigraphy and structural geology of the study area. The study area (plates 1 and 2) is characterized by a thick stratigraphic sequence of Proterozoic to Holocene rocks that have been structurally deformed during several tectonic episodes. The thick sequence includes three major assemblages that are important aquifers:

- Carbonate aquifer of Paleozoic age
- Volcanic rocks of Tertiary age
- Basin-fill sediments of Tertiary to Quaternary age.

Along with the aquifers are moderate to thick confining units or low-permeability units, including:

- Archean to Proterozoic metamorphic and igneous rocks
- Neoproterozoic to Lower Cambrian quartzite and shale
- Shale, sandstone, and conglomerate of Mississippian age
- Triassic to Cretaceous shale, siltstone, and sandstone
- Mesozoic and Cenozoic plutons.

Three tectonic episodes, plus an intervening episode of extensive volcanism, have affected the hydrogeology of the region. The oldest tectonic episode is the Antler deformation (Late Devonian to Late Mississippian). This episode included east-verging thrust sheets. The second tectonic episode was the Sevier deformation (Jurassic through early Cenozoic) that resulted in east-verging thrust sheets in which Paleozoic carbonate rocks were placed over younger rocks.

In Eocene to early Miocene time, volcanism resulted in the development of thick deposits of ash-flow tuff and related lava flows, including many scattered calderas that were the sources of the tuffs. The caldera margins formed new groundwater flow paths and barriers.

The third tectonic episode is the Miocene to Holocene Basin and Range deformation that shaped the current topography of the Great Basin. Basin and Range extensional faulting produced graben and horst topography, resulting in deep basins and relatively high mountain ranges, generally oriented north-south. The mountain ranges provided areas of groundwater recharge, and accumulations of alluvial fill within the basins provided areas of aquifer storage and avenues of groundwater flow. Normal faults may provide hydrogeologic barriers to groundwater flow (Caine et al., 1996; Caine and Forster, 1999). But more commonly, these normal faults provide conduits to groundwater flow, especially north or south directed flow. These north-south conduits may act as barriers to east or west flow (Caine, et al., 1996).

STRATIGRAPHY

The age of the rocks in the study area is summarized in a geologic time scale chart (figure 5). The oldest rocks are Paleoproterozoic (early Proterozoic) and Neoproterozoic (late Proterozoic) metamorphic and igneous units. These rocks are overlain by thick sequences of Neoproterozoic quartzite and subordinate shale, which are locally metamorphosed to slate and schist. The Neoproterozoic rocks transition conformably upward into rocks of similar type and thickness, though less metamorphosed, that are Neoproterozoic to Early Cambrian. During Middle

Cambrian time, carbonate deposition initiated, and thick sequences of marine limestone and dolomite were deposited until the Permian. These rocks make up the carbonate aquifer of Nevada and adjacent parts of Utah and range in thickness between 1500 and 9000 m throughout this area (Harrill and Prudic, 1998).

Locally, marine sandstone and shale interfinger with the carbonates. These units generally do not form significant impediments to regional groundwater flow, with the exception of the Late Mississippian Chainman Shale and related shale and sandstone. This unit locally exceeds 600 m in thickness, and in all but the southern part of the study area, this unit divides the carbonate aquifer into two distinct aquifers, the lower and upper carbonate aquifers. The Chainman Shale and related clastic units were derived from erosion of a structural highland, the Antler Highland, in and northwest of the study area. The highland, made up in large part of the Roberts Mountain allochthon, was produced by the Antler orogeny.

Mesozoic rocks in the study area consist of generally thin (mostly <600 m except in the extreme southern part of the area) deposits of nonmarine clastic rocks that have mostly been removed by erosion. Mesozoic and older rocks were deformed during the Sevier deformational event (DeCelles, 2004). At this time, the study area was a highland as part of the hinterland of the Sevier thrust belt, and regional erosion removed most Mesozoic rocks.

Plutons of Late Jurassic to Paleocene age were intruded during Sevier deformation. These plutons were likely associated with extrusive volcanic units that have since been eroded. Mesozoic plutons commonly led to significant mineralization in the study area.

Middle Tertiary (Eocene to lower Miocene) time marked the continuation of calc-alkaline intrusion and resulting volcanism, the terminal product of relatively rapid subduction beneath western North America that began in the Triassic (Lipman et al., 1972; Hamilton, 1995; Dickinson, 2009; Humphreys, 2009; Schellart et al., 2010). Above individual source plutons, vent deposits included andesitic and dacitic lava flows and volcanic mudflow breccia that locally exceeded several hundred meters of thickness. Caldera deposits consist of dacitic to rhyolitic ash-flow tuffs, which are at least several hundred meters thick within individual calderas. Farther outward from the vents above the plutons, lava flows are sparse because they do not flow more than a few kilometers from their source vents; outflow ash-flow tuffs, on the other hand, traveled as far as 160 km from their source caldera, so accumulated to aggregate thicknesses exceeding 300 m in most of the study area (e.g., Cook, 1965).

Starting at about 20 Ma (lower Miocene), subduction ceased or slowed and extensional deformation increased in the Great Basin (Christiansen and Lipman, 1972; Christiansen and Yeats, 1992; Rowley and Dixon, 2001; Schellart et al., 2010). Basin and Range deformation, characterized by steeply dipping normal faulting, began to form alternating mountain ranges and valley basins. The main pulse of this basin and range faulting began about 10 Ma, during which time the present topography formed. As valleys formed, they were filled by debris eroded from the adjacent mountain ranges, creating basin-fill deposits.

Individual rock units, structures, basins, and ranges are described in the following sections. Thicknesses of most units are from the county reports. The relationships between geologic units in the different areas of the map can be determined from figures 6 to 9. These figures illustrate geologic columns for Lincoln (figure 6), White Pine (figure 7), and Clark counties (figure 8), Nevada, and western Utah (figure 9). The Utah area consists of western Iron, Beaver, Millard, and Juab counties and the southwestern corner of Tooele County.

Precambrian Rocks

Proterozoic Rocks

The oldest rocks are in and adjacent to the southern part of the study area in the Beaver Dam Mountains, Mormon Mountains, Virgin Mountains, northeastern Spring Mountains, and the Desert Range (plate 2) (Tschanz and Pampeyan, 1970; Longwell et al., 1965). These rocks are Paleoproterozoic crystalline

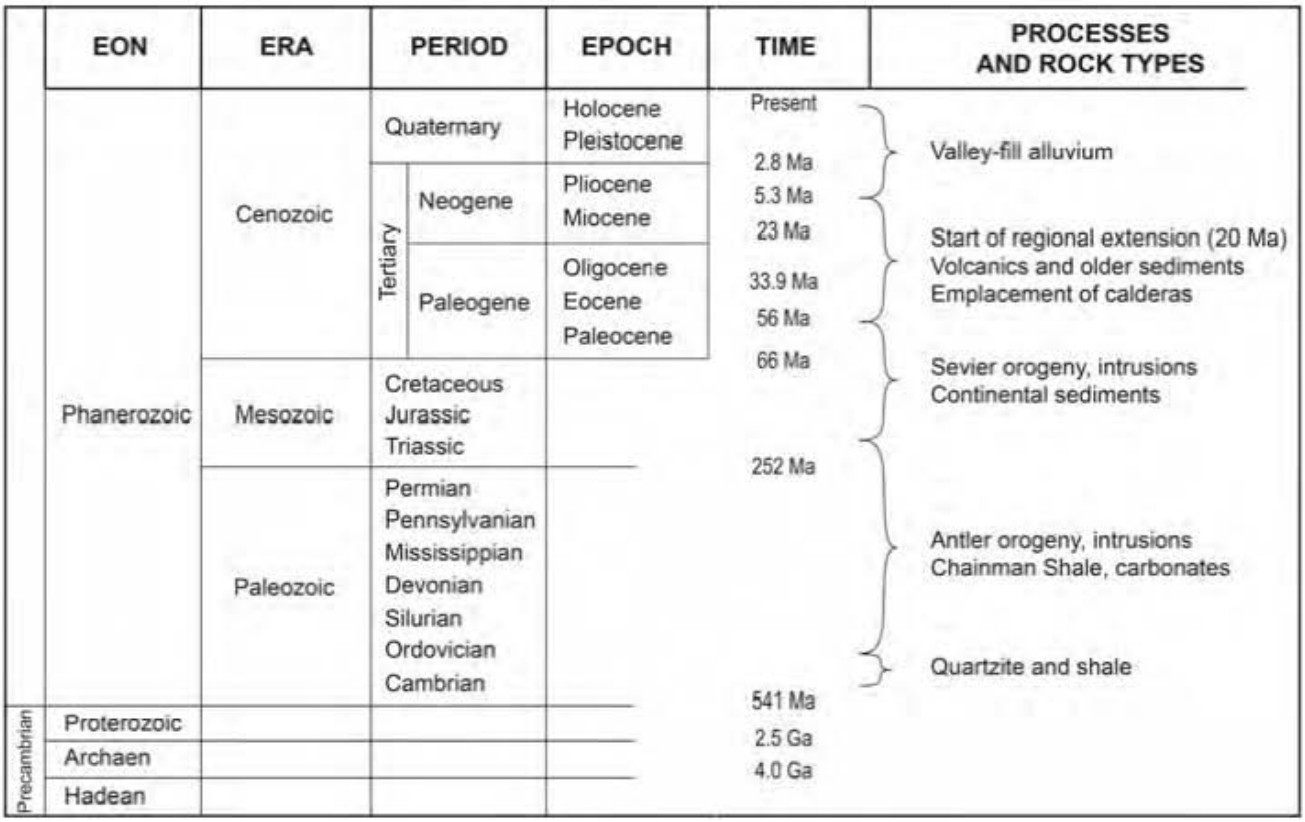

Figure 5. Geologic time scale, including rock type and tectonic events. (after Walker et al., 2013)

metamorphic rocks (Page et al., 2005a) that have been mapped in this report as Precambrian rocks (p€). Over most of the study area, however, the oldest rocks are Neoproterozoic to Lower Cambrian quartzite. These Neoproterozoic to Cambrian units appear to be the initial deposits of the Cordilleran miogeocline, a western belt of offshore carbonate-shelf and intertidal deposits (Page et al., 2005a). These units were deposited in shallow marine waters along a passive continental margin of western North America (Stewart and Poole, 1974; Stewart, 1976). No Mesoproterozoic rocks or pre-Proterozoic rocks are exposed in the study area.

In White Pine County and adjacent Utah, the principal Neoproterozoic unit is the McCoy Creek Group (figure 7). The assemblage consists of well-bedded, resistant feldspathic quartzite and subordinate slate and argillite more than 2700 m thick in the Schell Creek Range (plate 1) and about 2300 m thick in the Deep Creek Range, Utah. The metamorphic grade of these units is low to moderate, locally producing schist. The unit is mapped in the Deep Creek Range with the underlying Trout Creek group (figure 9), also of Neoproterozoic age and similar in appearance. The Trout Creek group is estimated at 3500 m thick (Hintze and Kowallis, 2009) and of higher metamorphic grade. Link et al. (1993) concluded that, based on fossils, both of these sequences range in age from 780 to 560 Ma and that the upper part of the McCoy Creek Group may correlate with the Johnnie Formation of southern Nevada, which is as much as 1200 m thick. In Lincoln County and at least in parts of White Pine County, the basal units of the overlying Prospect Mountain Quartzite are considered to be partly Neoproterozoic. The McCoy Creek and Trout Creek units are mapped in the study area as Precambrian rocks (p€).

Paleozoic Rocks

Cambrian Rocks

The Prospect Mountain Quartzite (Cambrian to Precambrian sedimentary rocks, €p€s) overlies

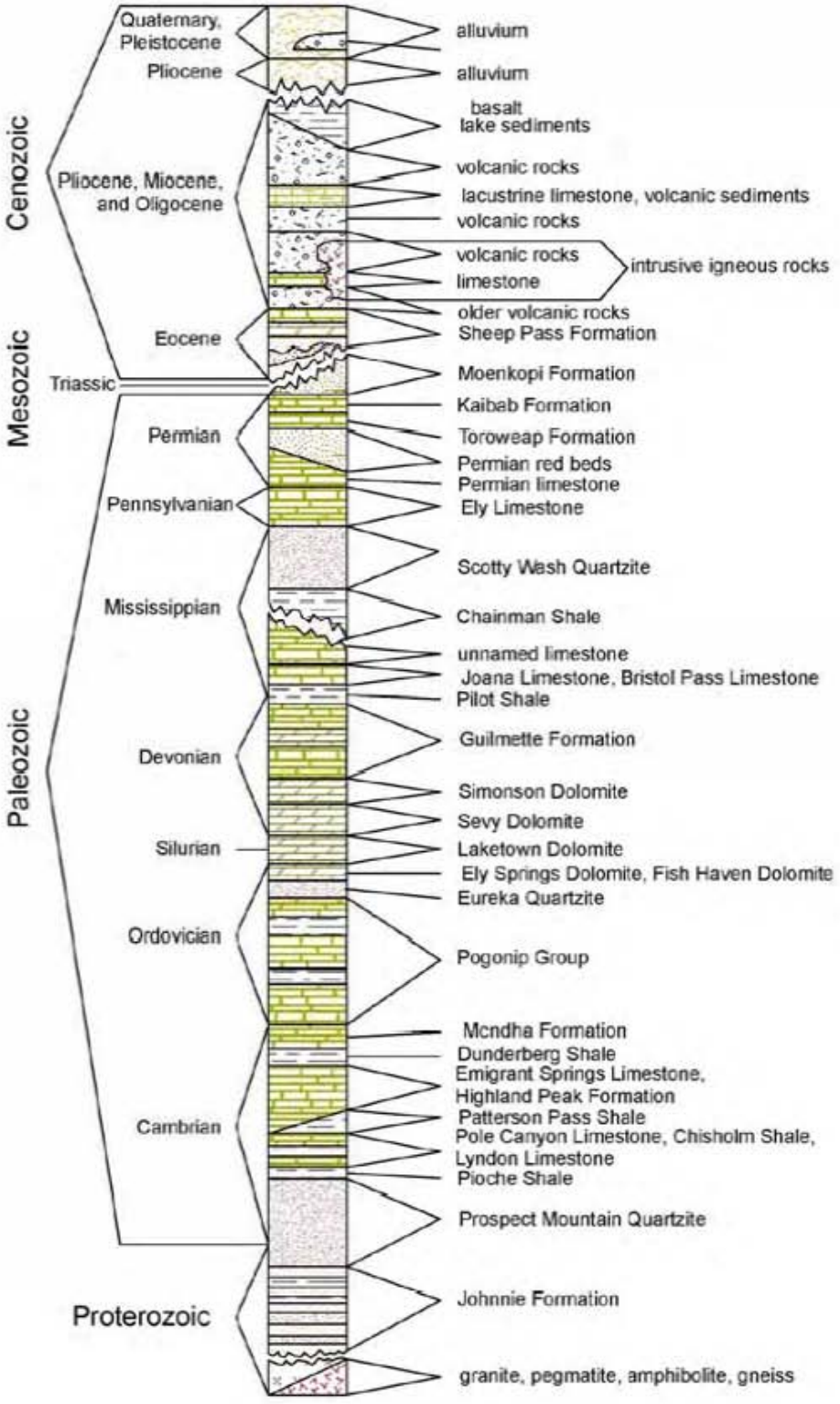

Figure 6. Geologic units of Lincoln County, Nevada (from Tschanz and Pampeyan, 1970). Vertical scale shows relative thickness of units.

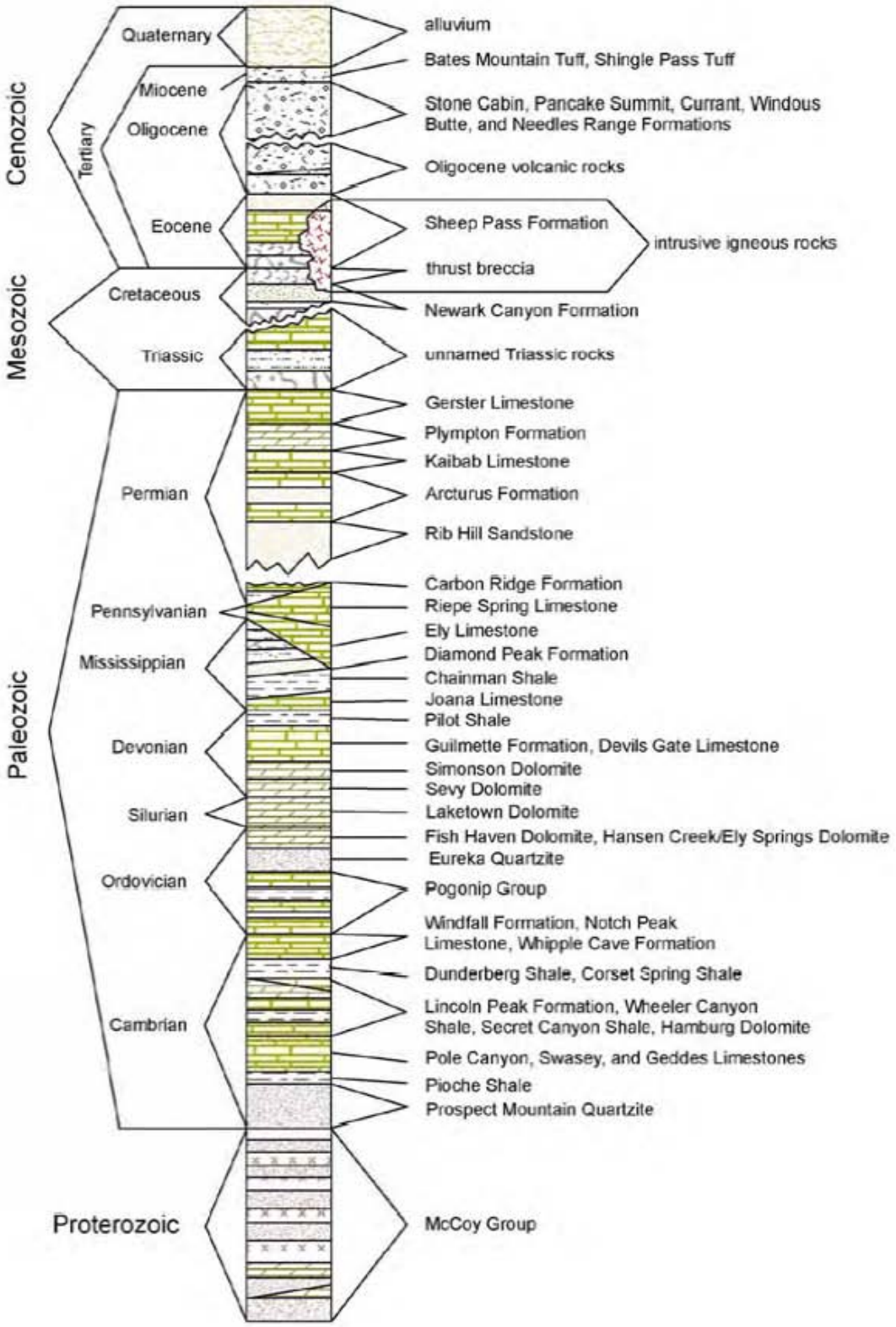

Figure 7. Geologic Units of White Pine County, Nevada (from Hose and Blake, 1976). Vertical scale shows relative thickness of units.

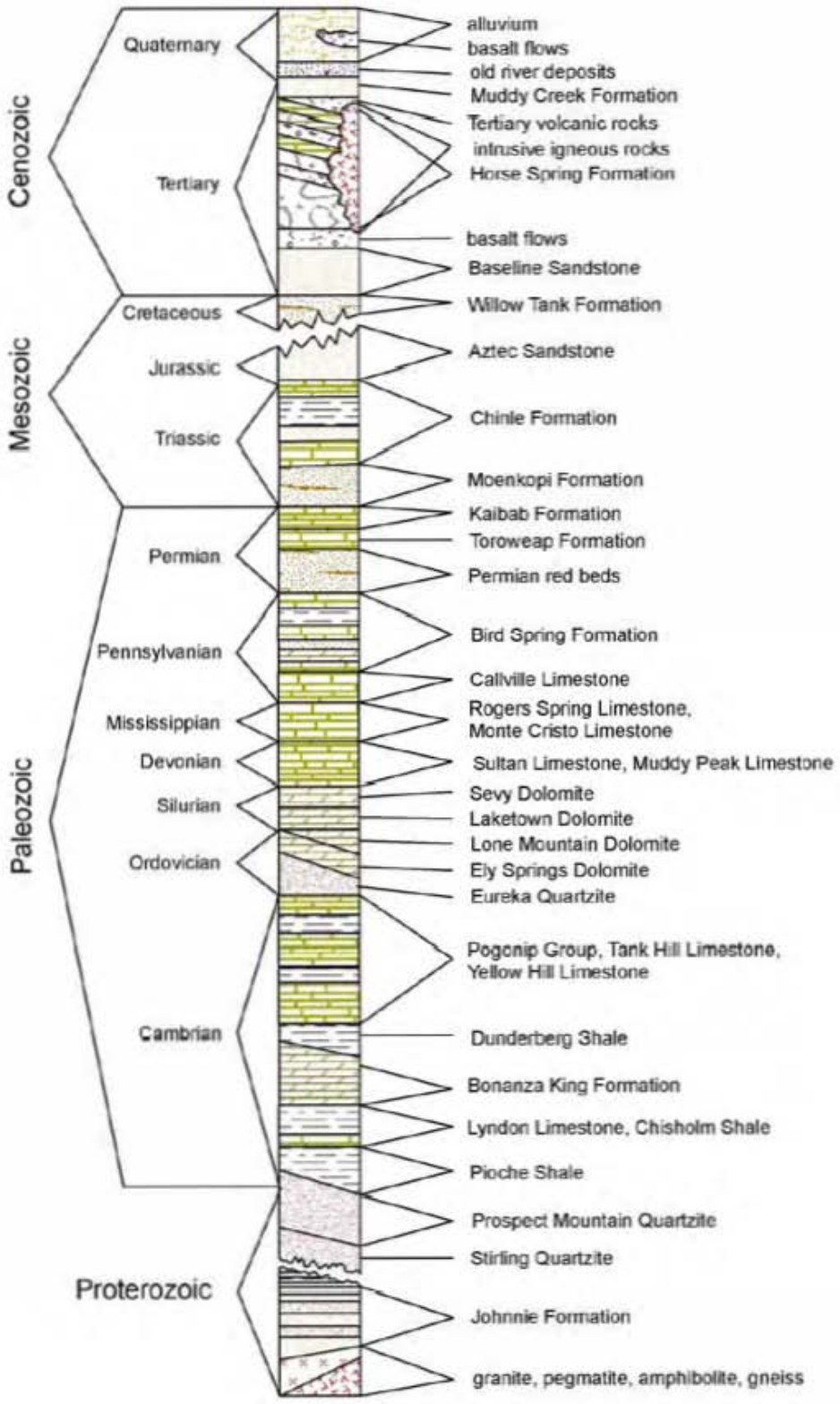

Figure 8. Geologic units of Clark County, Nevada (from Longwell et al., 1965). Vertical scale shows relative thickness of units.

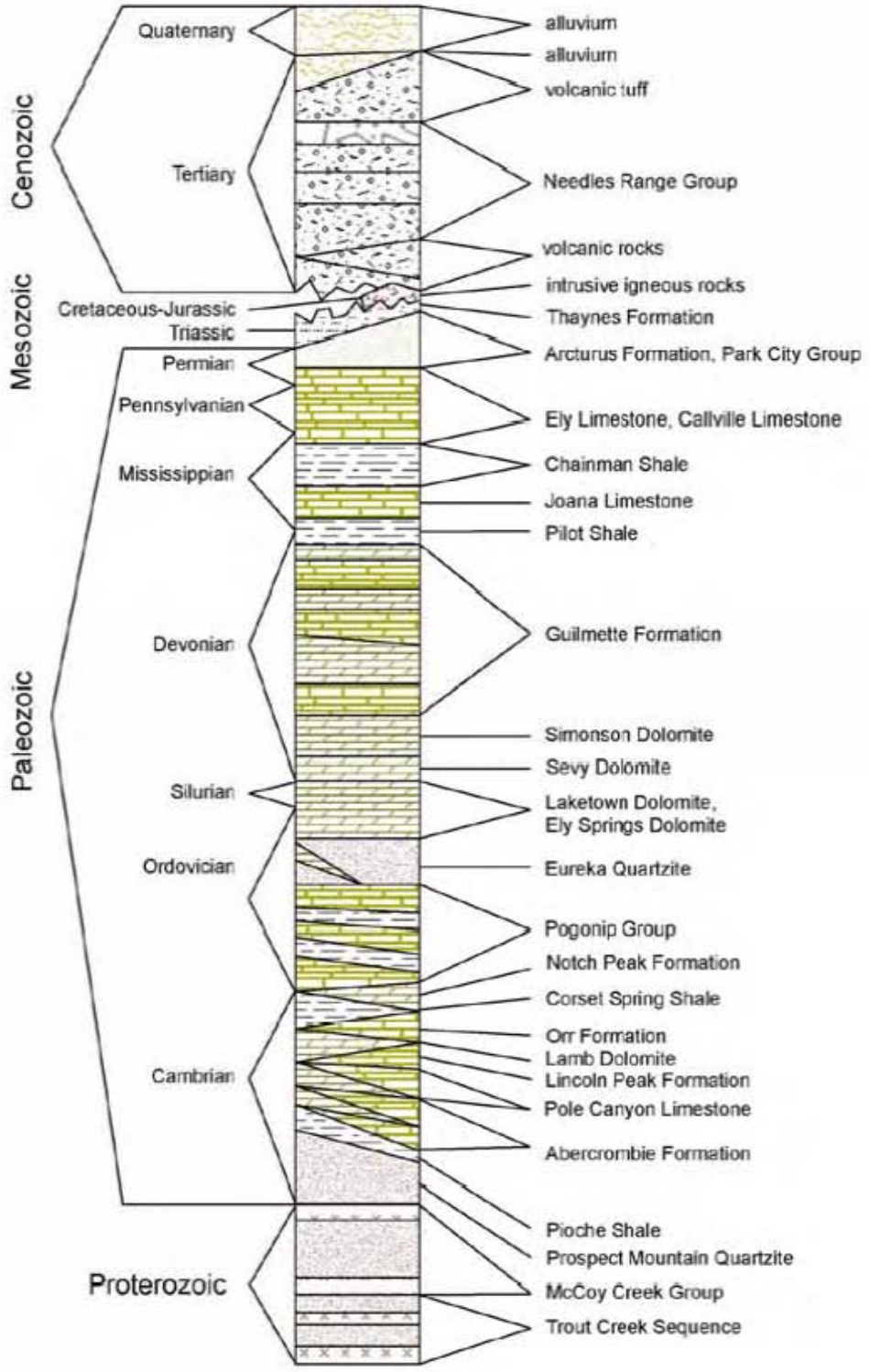

Figure 9. Geologic units of western Utah (after Hintze and Kowallis, 2009, Charts 45 and 46). Vertical scale shows relative thickness of units.

the McCoy Creek Group in White Pine County (figure 7). The Prospect Mountain Quartzite consists of well-bedded, resistant quartzite and subordinate shale, commonly weakly metamorphosed. It has been generally considered to be Early Cambrian, although it is not well characterized by age or correlation from place to place, and at least in the southern part of the study area is partly Neoproterozoic. In the study area, complete sections are uncommon, but the unit ranges from 900 to about 2400 m thick (Tschanz and Pampeyan, 1970). Thickness decreases southward to just 100 m in the Mormon Mountains. The Prospect Mountain Quartzite in the southern half of the study area is correlated with three units mapped in and west of the southern part of the study area: the Stirling Quartzite (Neoproterozoic and Early Cambrian), the Wood Canyon Formation (Early Cambrian), and the Zabriskie Quartzite (Early Cambrian) (Stewart, 1970, 1974, and 1984; Rowley et al., 1994).

In the southern part of the study area, the Stirling Quartzite is at least 600 m thick and the base is not exposed. Link et al. (1993) considered the Stirling Quartzite to postdate the Neoproterozoic McCoy Creek Group. In the Desert Range and above the Gass Peak thrust in the Las Vegas Range, the Wood Canyon Formation, a quartzite, is 300 to 900 m thick.

Above the Prospect Mountain Quartzite are, from base to top, the Pioche Shale (Lower and Middle Cambrian, 60 to 300 m thick), Lyndon Limestone (Middle Cambrian, 45 to 120 m thick), and Chisholm Shale (Middle Cambrian, 30 to 100 thick) are present. These three units are combined in many places with the Prospect Mountain Quartzite, as €p€s in White Pine County. These rocks are partly correlative with the Carrara Formation at the NTS and in portions of Clark County.

Cambrian carbonate rocks range in thickness from almost 1500 m over most of the study area to about 2300 m just southwest of the study area. The map unit is mostly middle Cambrian labeled €m. In the southern half of the study area, the most widespread and best studied of the Cambrian carbonate rocks is the Highland Peak Formation, consisting of Middle and Late Cambrian, well-bedded limestone and dolomite about 1400 m thick (Tschanz and Pampeyan, 1970). To the west, in the Groom mining district, it is 1645 m thick.

In the northern part of the study area, the Cambrian carbonate rocks consist of many named units of generally similar lithology, total thickness, and age (Hose and Blake, 1976). Just to the northwest, in the Eureka area, these were originally named, from base to top, the Eldorado dolomite, the Geddes Limestone, the Secret Canyon Shale, and the Hamburg dolomite (Roberts et al., 1967). In the Snake Range, these are, from base to top, the Pole Canyon Limestone, the Lincoln Peak Formation, and the Johns Wash Limestone. These latter names are now preferred in the northwestern part of the study area and areas to the west. In the Cherry Creek Range and extending into western Utah, the units making up the entire sequence of Middle Cambrian carbonate rocks are, from base to top, the Dome Formation, Swasey Limestone, Wheeler Shale, Marjum Limestone, Weeks Limestone, Trippe Limestone, Wah Wah Summit Formation, Orr Formation, and others (Hose and Blake, 1976; Hintze and Davis, 2003). The overall Middle Cambrian carbonate sequence is roughly equivalent to the Bonanza King Formation to the south (Longwell et al., 1965). See figures 6 to 9 for geologic sections in different areas of the maps.

Above the Middle Cambrian carbonate section in Nevada is an Upper Cambrian to Lower Ordovician(?) sequence that includes a lower unit, the Dunderberg Shale, and an unnamed upper unit of limestone and dolomite (Tschanz and Pampeyan, 1970). The rocks are mapped as an upper part of the Cambrian section (€u); in some cross sections, the map unit is combined with €m as Cambrian carbonate rocks, undivided (€c). In White Pine County and in Utah, the €u limestone unit has been variously referred to as the Windfall Formation, Orr Formation, Notch Peak Limestone, and Whipple Cave Formation. In the southern part of the study area, the €u limestone unit is the Nopah limestone. See figures 6 to 9 for geologic sections. The Dunderberg Shale generally is about 90 m thick over most of the study area, but it is as much as 420 m thick in the southern Ruby Mountains (Hose and Blake, 1976). The overlying limestone ranges in thickness from 120 to 1200 m, generally thickest on the western side of the study area (Tschanz and Pampeyan, 1970).

Ordovician to Devonian Rocks

Ordovician to Silurian rocks in the study area are shown as a lower unit (Middle and Lower Ordovician, symbol Ol) and an upper unit (Silurian and Upper Ordovician, symbol SOu). The lower unit consists in ascending order of the Pogonip Group and the Eureka Quartzite. The Pogonip Group consists of interbedded thick-bedded limestone, sandy to silty limestone, conglomerate, and shale, generally about 600 to 1070 m thick in the study area. The Eureka Quartzite is a distinctive white, resistant, brittle, vitreous, fine- to medium-grained quartzite that thins southward from 180 to 240 m thick in the Confusion Range to 60 m in southern Lincoln County (Hose and Blake, 1976; Tschanz and Pampeyan, 1970). The Eureka Quartzite is a major marker bed throughout most of the study area (plates 1 and 2). Just northwest of the study area, the lower unit includes the Vinini and Valmy Formations.

The upper unit (SOu) is comprised of, in ascending order, the Hanson Creek Formation, Ely Springs Dolomite, Fish Haven Dolomite, and Laketown Dolomite. The Ely Springs Dolomite is a poorly resistant, gray to dark-gray carbonate unit that occurs over most of the area of plate 1 in Lincoln County (Tschanz and Pampeyan, 1970). The Ely Springs Dolomite in Lincoln County overlaps into northern Nye and Eureka counties, where it is locally called the Hanson Creek Formation, a dark dolomite and/or limestone unit that thins southward from 150 to 30 m (Tschanz and Pampeyan, 1970; Kleinhampl and Ziony, 1985). In White Pine County, the Ely Springs Dolomite is called the Fish Haven Dolomite and ranges between 60 and 260 m thick. The Silurian Laketown Dolomite is lithologically similar to the Ely Springs Dolomite and Fish Haven Dolomite and ranges between 180 and 560 m thick. Where the Ely Springs Dolomite and Laketown Dolomite are thin in Lincoln and Clark counties, they are included with unit Ol.

In Eureka and Nye counties, the Laketown Dolomite is underlain by, and partly equivalent in age to, the Lone Mountain formation. This unit consists of reef limestone and dolomite that is not present farther east in Lincoln and White Pine counties (Kleinhampl and Ziony, 1985). In Nye County, these units, particularly the Lone Mountain formation, overlie and interfinger with the Roberts Mountain Formation. The Roberts Mountain Formation is a western facies of deep-water sediments and is comprised of shaley limestone, dolomite, and shale with a thickness of 150 to 580 m (Kleinhampl and Ziony, 1985).

Devonian carbonate rocks in eastern Nevada formed on a shallow-water marine carbonate platform. These rocks have been mapped as, in ascending order, the Sevy Dolomite, Simonson Dolomite, and Guilmette Formation. Where combined, they are mapped as undivided Devonian rocks (Du) or, when local Silurian rocks are included, as undivided Devonian and Silurian sedimentary rocks (DS). In the southern part of the study area, the DS map unit includes the Muddy Peak Limestone (Upper and Middle(?) Devonian). However, in most places the two mapped formations are the Sevy and Simonson Dolomites (Ds) and Guilmette Formation (Dg). Sandberg et al. (1997) redefined the upper part of the Simonson Dolomite in Nevada, or the lower part of the Guilmette Formation in Utah (Hintze and Kowallis, 2009), as the Fox Mountain formation. The Sevy Dolomite is a resistant, gray dolomite, commonly argillaceous and with a sandstone unit near the top. This dolomite increases in thickness southward across the study area from about 140 m in the Snake Range to 400 m in the Limestone Hills and southward (Tschanz and Pampeyan, 1970). This thickness decreases south of the Pahranagat Range, and the unit disappears south of the Delamar Mountains. The Simonson Dolomite is resistant, dark- and light-gray dolomite about 270 to 370 m thick over most of the study area, but it thins to less than 210 m in the southeastern part of the study area, continuing to decrease in thickness farther south. The Simonson Dolomite is about 150 m thick in the Snake Range (Tschanz and Pampeyan, 1970), although both the Simonson and Sevy Dolomites were locally reduced in thickness by faulting. The Fox Mountain formation consists of thin (generally 30 to 45 m), gray limestone except for dolomite in its upper part.

The Guilmette Formation (Dg) is a mostly resistant, fossiliferous limestone and dolomite, with biostromes and bioherms, and commonly

sandy with minor sandstone layers. The unit ranges in thickness from about 300 to 1070 m and appears to decrease in thickness in all directions from its thickest occurrences in north-central Lincoln County (Tschanz and Pampeyan, 1970; Hose and Blake, 1976). The middle part of the Guilmette Formation consists of the Alamo Breccia Member, which is as thick as 90 m northwest of Alamo, Nevada. It was formed by the cataclysmic Alamo bolide impact event (Warme et al., 2008). In Clark County, the Guilmette map unit includes the Sultan Limestone, which is made up of a lower dolomite unit and an upper limestone unit with a thickness of 550 m (Longwell et al., 1965). The Sultan Limestone is equivalent to the Muddy Peak Limestone in the Muddy Mountains.

In Eureka County and northern Nye County, the rocks of the Sevy, Simonson, and lower Guilmette units are called the Nevada formation (Dn), which is about 750 m thick. This map unit locally includes the Cockalorum Wash formation. In Eureka and northern Nye counties, the upper Guilmette Formation is called the Devils Gate Limestone (Dd), which is about 600 m thick (Roberts et al., 1967; Hose and Blake, 1976; Kleinhampl and Ziony, 1985).

Mississippian to Lower Permian Rocks

In White Pine County, a distinctive sequence of clastic rocks consists, in ascending order, of the Pilot Shale, Joana Limestone, Chainman Shale (Mc), and Diamond Peak Formation (Md). In Lincoln County, only the Pilot Shale is recognized (Tschanz and Pampeyan, 1970). These map units represent products of the Antler deformation, which took place in Late Devonian to Late Mississippian time and resulted in the Antler Highland located along the western side and northwest of the study area (Roberts et al., 1967; Kleinhampl and Ziony, 1985). The basin of deposition of these units was to the east of the highland (Poole and Sandberg, 1977 and 1991; Larson and Langenheim, 1979, figures 7 and 8). Where these four units are thin, they are categorized on the maps as Mississippian to Devonian rocks (MDd). But in most places, Chainman Shale and Diamond Peak Formation are mapped separately and Pilot Shale and Joana Limestone are combined as unit MD. The Late Devonian to Early Mississippian Pilot Shale is a poorly resistant, gray, thin-bedded dolomitic siltstone and limestone containing little shale. This unit is generally 30 to 120 m thick, but locally, in northern White Pine County and western Utah, it is 150 to 270 m thick (Hose and Blake, 1976; Tschanz and Pampeyan, 1970; Hintze and Davis, 2002a and b). The Joana Limestone (Lower Mississippian) is a mostly resistant, bluish-gray limestone, and is 30 to 300 m thick.

The Monte Cristo Group of southern Nevada, which is Upper and Lower Mississippian, is considered equivalent to the Joana Limestone. The Monte Cristo Group overlies the Sultan Limestone. The Monte Cristo Group is a dark-gray to light-gray limestone containing abundant chert and is about 230 m thick. In the Muddy Mountains, the Mississippian Rogers Spring Limestone has a similar lithology and is considered to be equivalent in age to the Monte Cristo Group (Longwell et al., 1965). The general equivalent of the Chainman Shale southwest of the study area is the Eleana Formation (Mississippian and Upper Devonian), which is at least 1000 m thick (Workman et al., 2002a). The Monte Cristo Group, Rogers Spring Limestone, and Eleana Formation are included with the MD map unit. The map unit also includes local units Mercury Limestone and Bristol Pass Limestone (both mostly in White Pine County), Webb Formation (Elko County), Ochre Mountain Limestone (Utah), and West Range Limestone (Upper Devonian) in northern Lincoln County, Nevada.

The Upper Mississippian Chainman Shale is a soft, black, impermeable shale that is between 60 and 600 m thick. This unit is mapped as unit Mc over the northern part of the study area, but the Chainman is thin to the south, where it is included within a sequence of more permeable carbonate rocks. It is a regional confining unit (called the "upper aquitard") separating the lower carbonate aquifer from the upper carbonate aquifer over all except the southern part of the study area. Paleotopography during deposition and post-depositional erosion resulted in substantial variations in Chainman thickness. The unit was mapped (Hintze and Davis, 2002a) in the

Confusion Range with a thicknesses greater than 600 m. A similar thickness is reported from an oil-well log in Lake Valley (Hess, 2004). Although these two locations are distal from the source area, they represent localized depositional basins.

In the northwestern part of the study area, the Upper Mississippian Diamond Peak Formation is mapped as unit Md above the Chainman Shale. The Diamond Peak Formation is a poorly resistant, gray siltstone, claystone, sandstone, and conglomerate that ranges in thickness from 180 to 760 m (Hose and Blake, 1976; Kleinhampl and Ziony, 1985). The unit thins and pinches out eastward in north-central White Pine County. The Diamond Peak Formation is derived from erosion of the Antler Highland and is generally included in the upper aquitard with the Chainman Shale. The Diamond Peak Formation is generally equivalent to the Scotty Wash Quartzite in the southern part of the study area. The Scotty Wash Quartzite is made up of interbedded sandstone, shale, and local limestone of limited extent. The Scotty Wash Quartzite is included with the Md map unit.

The Mississippian to Permian Ely Limestone, which is predominately Pennsylvanian in age, underlies much of the study area. Here it is mapped as Pennsylvanian rocks (IP). In the Utah part of the study area, the Ely Limestone is 560 to 600 m thick (Hintze and Davis, 2002a and b). The map unit is called the Wildcat Peak Formation in the northwestern part of the study area and the Callville Limestone in the southern and eastern part of the study area. The Ely Limestone is overlain by a Lower Permian limestone of similar lithology in northern White Pine County (Hose and Blake, 1976). All units are resistant, gray limestone sequences that collectively range in thickness from 600 to 900 m thick. The overlying Lower Permian limestone is called the Riepe Spring Limestone. Where both the Ely and Riepe Spring Limestones are mapped together in the northern part of the study area, they are shown as Permian and Pennsylvanian rocks, undivided (PIP). The rocks in the PIP unit are unnamed in Lincoln County and range from 1100 to more than 1500 m thick (Tschanz and Pampeyan, 1970). The Ely and Riepe Spring Limestones are overlain by, and partly equivalent to, the Carbon Ridge Formation, a Lower Permian, nonresistant, thin-bedded limestone and shale that is 420 to 700 m thick. The Carbon Ridge Formation is locally mapped separately in the northwestern part of the study area as Pc, or where thinner is included within the PIP map unit.

The Bird Spring Formation is an Upper Mississippian to Lower Permian limestone in the southern part of the study area that is roughly equivalent in age to the combined Ely Limestone, Riepe Spring Limestone, and Carbon Ridge Formation of White Pine County (Longwell et al., 1965; Tschanz and Pampeyan, 1970). The Bird Spring is a sequence of limestone beds with sandstone and dolomitic limestone layers. The formation is as much as 2400 m thick in the Spring Mountains and Las Vegas Range (Page et al., 2005b) and at least 1650 m thick in the Meadow Valley Mountains (Pampeyan, 1993). The Bird Spring Formation is included in the PIP map unit, as is the Brock Canyon Formation in the northwestern part of the study area and the Oquirrh Group (Lower Permian and Pennsylvanian) in the northeastern part of the study area.

The Lower Permian Rib Hill Sandstone (Pr) overlies the Carbon Ridge Formation in the northwestern part of the study area (Hose and Blake, 1976). The Rib Hill Sandstone is a nonresistant sandstone and dolomite 150 to 420 m thick. In northern White Pine County and adjacent parts of Utah, the Lower Permian Arcturus Formation (Pa) is the name for a sequence of poorly resistant, gray limestone, sandstone, and siltstone that is 820 to 1040 m thick (Hose and Blake, 1976). In the northwestern part of the study area, the Arcturus Formation overlies the Rib Hill Sandstone. Where the two are combined in the mapping, they are shown as unit Par. In Elko County, this map unit includes the Pequop Formation, a fusilinid-bearing limestone as much as 1160 m thick (Coats, 1987). In the southern part of the study area, the Par map unit is about 400 m thick (Longwell et al., 1965) and includes a redbed sequence, and in the southeastern part of the study area, the map unit includes the Queantoweap Sandstone.

Park City Group

The Park City Group (Pp) is a distinctive, resistant, light-gray Lower Permian limestone and dolomite sequence that is exposed only locally. The scattered nature of the outcrops suggests that the unit was originally fairly extensive in the study area but has been partly removed by erosion over most of its original extent. In White Pine County and adjacent western Utah, the group is made up, from base to top, of the Kaibab Limestone, Plympton Formation, and Gerster Limestone. The Kaibab Limestone is 15 to 180 m thick, the Plympton Formation is 210 to 275 m thick, and the Gerster Limestone is as thick as 335 m (Hose and Blake, 1976). These rocks are not observed in Eureka or Nye counties.

In Lincoln County and east of the study area in Utah, the east platform part of the sequence consists of the Toroweap Formation, the Kaibab Limestone, and locally the Plympton Formation (Tschanz and Pampeyan, 1970). In Lincoln County, these units have a combined thickness of between 75 and 140 m. The Toroweap Formation is a cherty, thin-bedded, shaley limestone, and the Kaibab Limestone is a cherty, sandy, light-gray limestone. The Kaibab Limestone and Toroweap Formation in Clark County have a maximum combined thickness of 400 m in the Muddy Mountains (Bohannon, 1983). In Clark County, their lithology is dominated by cherty limestone, sandstone, and red shale, with local gypsum beds (Bohannon, 1983; Page et al., 2005b).

Mesozoic Rocks

Mesozoic rocks in eastern Nevada and western Nevada were deposited locally or have been largely removed by erosion (e.g., Long, 2012). However, they are exposed in some ranges and are widespread east and south of the study area. Most of these rocks are continental clastic rocks deposited in fluvial, lacustrine, eolian, and marginal marine environments (Hintze and Davis, 2003; Long, 2012). The Thaynes Formation (Lower Triassic) is a nonresistant, gray, thin-bedded claystone and limestone that is locally about 580 m thick in western Utah in the northeastern part of the study area (Hintze and Davis, 2002a). The overlying Moenkopi Formation (Lower Triassic) is a mostly nonresistant, red and gray, thin-bedded siltstone, limestone, sandstone, and shale, commonly gypsiferous, and locally about 600 m thick in western Utah. The Thaynes and Moenkopi Formations are mostly thin in the Nevada portion of plate 1 and are not separated on this map. In White Pine County, these thin rocks are considered to be the Thaynes Formation. In Clark and southeast Lincoln counties, however, the Moenkopi Formation is about 600 m thick and of similar lithology to that in Utah, with gypsum beds in the upper part of the Formation (Page et al., 2005b); the Thaynes Formation is not present here.

The Upper Triassic Chinle Formation includes a basal unit, the Shinarump Conglomerate Member, which is a resistant gray sandstone and conglomerate that ranges from 3 to 75 m thick. The balance of the formation is of soft, variegated mudstone and siltstone that is widely exposed above the Moenkopi Formation in the southern part of the study area (Bohannon, 1983; Page et al., 2005b). This mudstone and siltstone have been measured to be about 300 to 1000 m thick within the study area. The Luning Formation (Upper Triassic) is locally exposed northwest of the area. All Triassic rocks have been combined as Triassic sedimentary rocks (Ŧs).

Jurassic sedimentary rocks (Js) are exposed in the southern part of the study area (plate 2). These rocks are dominated by the Lower Jurassic Aztec Sandstone, a brick-red, buff, and light-gray, fine- to medium-grained eolian sandstone containing large-scale (10+ m) cross beds. The Aztec Sandstone is 180 to 1100 m thick. The equivalent Navajo Sandstone is about 600 m thick in the southeastern part of the study area. It is here underlain by the Moenave (lower) and Kayenta (upper) Formations, both of Early Jurassic age and mostly made up of fine-grained sandstone and siltstone of eolian and fluvial origin, with a combined thickness of 150 to 900 m. The Navajo Sandstone is here overlain by the Temple Cap (lower) and Carmel (upper) Formations, both of Middle Jurassic age and made up of sandstone, limestone, siltstone, and shale of mostly marginal marine origin and with a combined thickness of

about 280 m. The map unit also includes the Dunlap Formation (Lower Jurassic) in the northwestern part of the study area.

Cretaceous synorogenic sedimentary rocks (Ks) are present but uncommon in the study area. Most of this area was a highland undergoing erosion at that time (Hintze and Davis, 2003). The Lower Cretaceous Newark Canyon Formation occurs in the northwestern part of the study area as a poorly exposed, reddish-brown to gray, fresh-water limestone, siltstone, conglomerate, and sandstone from 430 to 550 m thick (Hose and Blake, 1976). Upper Cretaceous sedimentary rocks, shed east from erosion of Sevier highlands in and north of the study area, are thin and patchy in the map area but extensive and thick to the east and south. Upper Cretaceous through Paleocene fault breccias, primarily from thrust faults related to Sevier deformation, are locally exposed in the study area.

In Clark County, Cretaceous sedimentary units include from older to younger the Willow Tank Formation (Lower Cretaceous) and the Baseline Sandstone. The Willow Tank Formation is 90 to 140 m thick and consists of a basal conglomerate and overlying fine-grained sediments, including bentonitic clay, and is primarily restricted to the Muddy Mountains. The Baseline Sandstone consists of about 900 to 1500 m of gray and red, well-bedded sandstone and conglomerate. In the southeastern (Utah) part of the study area, the Upper Cretaceous Cedar Mountain Formation and overlying Iron Springs Formation consist of mudstone, shale, sandstone, and conglomerate about 900 m thick.

Plutonic rocks related to the Middle Jurassic through Paleocene Sevier deformational event are exposed locally throughout the study area (Maldonado et al., 1988). Much of the southern Snake Range is intruded by a Middle and Upper Jurassic batholith (Miller et al., 1999a), and Jurassic quartz monzonite and diabase have been identified in the House Range and in the Burbank Hills, respectively, both in Utah near the eastern edge of the study area (Hintze and Davis, 2002a and b, and 2003). Other quartz monzonite to granodiorite plutons, mostly of Middle Jurassic age, form a north-trending belt along the eastern edge of White Pine County, Nevada, extending from the southern Snake Range to the Clifton Hills of western Utah. A north-trending plutonic belt of Cretaceous age is exposed in eastern White Pine County, Nevada, extending into the Deep Creek Range of western Utah and including the main mass of the large Kern Mountains granite batholith of apparent Cretaceous and Eocene age (Best et al., 1974; Miller et al., 1999a). On the geologic maps, these plutonic rocks are shown as Jurassic (Ji), Cretaceous (Ki), Tertiary to Cretaceous (TKi), or Tertiary (Ti) intrusive rocks. Geophysical data show that the batholith extends eastward, downthrown beneath Snake Valley and buried by basin-fill sediments (Mankinen and McKee, 2009).East rending strings of small Lower Cretaceous plutons are present in the Eureka and Ely areas (plate 1).

Cenozoic Rocks

Cenozoic rocks in the study area belong to three main sequences: (1) locally exposed, mostly thin, older continental sedimentary rocks; (2) generally voluminous, calc-alkaline volcanic rocks and their source plutons; and (3) rocks that formed during regional extension, namely thin bimodal-composition (basalt and high-silica rhyolite) lava flows and locally thick basin-fill sediments. On the geologic maps, most of these rocks are separated into several rock types based on age, following the mapping strategy of Ekren et al. (1977). Basalts are mapped as Quaternary to late Tertiary basaltic rocks (QTb). Basin-fill sedimentary rocks and surficial sediments are mapped as Quaternary to late Tertiary alluvium (QTa). Locally thin basalts intertongued with basin-fill sediments are included in QTa.

Latest Cretaceous (?) to Miocene Sedimentary Rocks

The oldest Cenozoic sedimentary rocks (Ts_1) are thin and poorly exposed in the study area but are more common in eastern Clark County and southwestern Utah. These units were deposited with, or unconformably deposited on, rocks deposited and deformed during the Sevier orogeny. In eastern Nevada, the principal Ts_1 unit is the Sheep Pass Formation of Eocene to Oligocene age

(Hose and Blake, 1976; Druschke et al., 2009). The Sheep Pass Formation occupies a 40,000 km^2 basin extending south from Ely and Eureka, Nevada, to Penoyer and northern Pahranagat valleys (Vandervoort and Schmitt, 1990; Fouch et al., 1991; Druschke et al., 2009). The unit is mostly nonresistant, gray conglomerate, sandstone, mudstone, and limestone, with a thickness of 180 to 900 m.

In Utah, just southeast of the study area, the mostly resistant Grapevine Wash Formation and overlying Claron Formation are included within the Ts_1 map unit. The Grapevine Wash Formation, poorly constrained in age as Late Cretaceous to early Tertiary but considered by Hintze et al. (1994a) to postdate Sevier deformation, consists of as much as 600 m of gray, tan, and red conglomerate and sandstone. The Claron Formation, also poorly constrained in age but likely Eocene and Paleocene (Biek et al., 2015), is sandstone, limestone, and conglomerate as much as 600 m thick.

Similar sedimentary rocks (Ts_2, Ts_3, and Ts_4) of various names and ages, from Oligocene to Miocene, are exposed in the study area. These include the Gilmore Gulch Formation of about 30 Ma (Ts_2), exposed in the northwestern part of the area. The Horse Spring Formation, about 12 to 20 Ma, and the red sandstone unit, 11 to 12 Ma, that overlies it are mapped as Ts_4 in the southern part of the study area (Bohannon, 1983 and 1984). The Horse Spring Formation consists of conglomerate, sandstone, siltstone, claystone, limestone, dolomite, tuff, and gypsum as much as 3000 m thick.

Tertiary Volcanic Rocks

Volcanic rocks make up the primary Cenozoic rock type in the study area. The older (Eocene to lower Miocene) sequence of calc-alkaline arc rocks consists of andesite to low-silica rhyolite that are mapped as different units separated by rock type and age. Tertiary plutonic rocks, which are the sources for the volcanic rocks, are mapped as unit Ti whether of calc-alkaline or bimodal origin. The calc-alkaline sequence is made up largely of regional ash-flow tuff sheets derived from widely scattered calderas. The oldest tuffs are mapped as Tt_1 (Eocene and Oligocene) that predate the Needles Range Group (about 32 Ma). The next younger group of tuffs, consisting mostly of the Needles Range Group, is mapped as Tt_2 (Oligocene), from about 32 Ma to 27 Ma. The younger aged tuffs are part of the Isom Formation. The next younger tuffs are mapped as Tt_3 (Oligocene and Miocene), ranging in age from that of the Shingle Pass Tuff (about 27 Ma) to the youngest calc-alkaline tuffs (about 18 Ma). Individual calderas are filled with thick intracaldera ash-flow tuffs that are at least several hundred meters thick. Their outflow sheets are typically thin; generally less than 300 m, but the aggregate thickness of all of these tuffs is at least 1000 m in the southern half of the study area. Isopach (thickness) maps of most tuffs in the study area were given by Sweetkind and du Bray (2008).

The outflow tuffs are interspersed with locally distributed but thick central stratovolcano deposits made up of lava flows and volcanic mudflow breccia generally deposited above their source plutons. Where these calc-alkaline flows and breccia are largely andesite, they are mapped as Ta_1, Ta_2, Ta_3, and Ta_4 based on ages that correspond to those of the related ash-flow tuffs. Unit Ta_4 is made up of post-18 Ma andesitic (calc-alkaline) flows that are exposed in the southern part of the study area. Where calc-alkaline flows and breccia are predominately low-silica rhyolite, they are mapped as Tr_1, Tr_2, and Tr_3 based on ages that correspond to those of the tuffs (e.g., Tr_1: >32 Ma, Tr_2:32–27 Ma, and Tr_3: 27–18 Ma).

In the Great Basin, vents—notably calderas—for Tertiary calc-alkaline arc volcanic rocks comprise a generally east-trending igneous belt that youngs from north to south (Ekren et al., 1976 and 1977; Stewart and Carlson, 1976; Stewart et al., 1977; Rowley, 1998; Rowley and Dixon, 2001). These magmatic belts, as well as other belts in the southern Basin and Range that become young to the north, represent removal (Humphreys, 1995, 2009) or rollback (Dickinson, 2006, 2009, 2013) of parts of the subducted Farallon slab beneath the Great Basin. The igneous belts are partly controlled by transverse zones and are underlain by batholiths whose cupolas provide the vents for the volcanic rocks. The oldest volcanic rocks in the study area

belong to the Ely-Tintic igneous belt (belt names from Rowley, 1998) in the northern part of the study area. The ages of vents in this belt are ~38 Ma and locally older (Eocene) along the northern margin of the area, and 36 Ma farther south (Rowley, 1998). An east-trending gap in vent areas, with a 50–100 km north-south width, occurs south of Ely and Preston, Nevada, and a volcanic plain of thin outflow tuffs underlies the gap (Gans et al., 1989). The axis of the next igneous belt to the south, the Pioche-Marysvale igneous belt, is south of Pioche, Nevada. The volcanic centers here are 32–31 Ma on the northern side of the belt and 28–27 Ma along the southern part. About 20 km south of the Pioche-Marysvale belt is the Delamar-Iron Springs igneous belt, of ~24 Ma along its northern side and 16 Ma along its southern side. Its southern edge is just south of the latitude of Pahranagat Valley, Nevada.

In the Ely-Tintic igneous belt, the 35 Ma Kalamazoo ash-flow tuff is the most voluminous volcanic unit, which was deposited as an east-trending 145-km-long and 40-km-wide elongate tuff sequence (Gans et al., 1989). Its caldera source has not been found but Gans et al. (1989) suggested that it may be buried beneath northern Spring Valley, which is near the center of the area of deposition of the Kalamazoo tuff. Gravity data (Gravity Data section, Geophysics chapter) do not support this hypothesis but rather suggest that the caldera may be buried beneath southern Tippett Valley. Other ash-flow tuffs and lava flows underlie and overlie the Kalamazoo tuff, and the overall thickness of the volcanic rocks in the igneous belt is about 150 to 450 m. Plutons ranging in age from 45 to 30 Ma, are scattered throughout the belt; most of these represent source areas of volcanic rocks that have since been removed by erosion. One of these plutons (Best et al., 1974) is the composite-age Kern Mountains pluton. This and other Eocene to Oligocene plutons and batholiths in the northern Snake Range, Kern Mountains, and Deep Creek Range represent initial calc-alkaline magmatism beneath these ranges (Miller et al., 1999a) that later were uplifted during Basin and Range extension.

In the Pioche-Marysvale belt, volcanic rocks are thicker and more widespread than in the Ely-Tintic belt: calderas are more abundant and larger, and the volcanic rocks are somewhat younger and thus less eroded. Most volcanic rocks are regional ash-flow tuffs from calderas, but lava flows and mudflow breccia erupted from volcanoes in and along the margins of calderas or from isolated volcanoes such as the Seaman Range volcanic center. The largest vent area in the belt is the Indian Peak caldera complex (Best et al., 1989a and 2013a) in the southeastern part of the study area. It erupted ash-flow tuffs and related rocks of the Needles Range Group (Oligocene, about 32 to 27 Ma) and the Isom Formation (27 to 26 Ma). This may be the largest caldera complex in the world; ash-flow tuffs from this complex are spread over an area of about 320 km east-west by 240 km north-south.

Intracaldera megabreccia deposits result from landsliding of the outside wall of a caldera margin into a caldera following rapid eruption of huge ash-flow tuff sheets and the resulting collapse of the caldera floor to fill the erupted parts of the underlying magma chamber (Rowley et al., 1995, 2001; Best et al., 2013a). These megabreccia deposits (Tmb) are mapped only in the Indian Peak caldera complex (plate 1) and cross section Q–Q' (plate 3). Megabreccia deposits (Tmb) are also mapped in and west of the southern Sheep Range (plate 2, plate 4 - cross section H–H'); however, these deposits do not include significant volcanic rocks but instead result from large gravity slides off the Sheep Range.

A cluster of smaller calderas west of the Indian Peak caldera complex also belongs to the Pioche-Marysvale igneous belt (e.g., Dixon et al., 1972, Ekren et al, 1972, 1973a and b, and 1974; Snyder et al., 1972; Quinlivan et al., 1974; Sargent and Roggensack, 1984). Some of these calderas produced regional ash-flow tuffs, from oldest to youngest and generally from north to south respectively, known as the Stone Cabin Tuff (35.3 Ma), Pancake Summit Tuff (34.8 Ma), Windous Butte Formation (31.3 Ma), tuff of Hot Creek Canyon (29.7 Ma), Monotony Tuff (27.3 Ma), tuff of Orange Lichen Creek (26.8 Ma), Shingle Pass Tuff (26.7 to 26 Ma), tuff of Lunar Cuesta (25.4 Ma), tuff of Goblin Knobs (25.4 Ma), tuff of Big Ten Peak (25 Ma), Pahranagat tuff (22.6 Ma), and Fraction Tuff (18.3 Ma) (Best et al., 1989b, 1993, and 2013b; Ekren et al., 2012). This cluster of

calderas has been referred to as the "central Nevada caldera complex" (Best et al., 1993 and 2013b; Scott et al., 1995a). However, we note that this feature is not a classic caldera complex because it has not all subsided following tuff eruptions but instead consists of individual calderas separated by Phanerozoic sedimentary rocks. Within calderas in the study area, intracaldera ash-flow tuffs and subordinate lava flows and mudflow breccia are several hundred meters thick and are underlain by intracaldera source plutons. Outside the calderas, the thickness of volcanic rocks in the belt in the area is about 450 to 900 m, but locally more. A few plutons of the same age range, likely representing sources for volcanic rocks that have been removed by erosion, occur in the Grant Range and many other parts of the study area.

In the Delamar-Iron Springs igneous belt, at the southern edge of the study area, the largest igneous centers are the Caliente and Kane Springs Wash caldera complexes (plate 2). The Caliente caldera complex erupted ash-flow tuffs that were deposited over an area extending 240 km by 160 km in the east-west and north-south directions, respectively. The complex was active for at least ~10 myr. (Rowley et al., 1995). The regional ash-flow tuffs derived from it include the Swett (23.7 Ma) and Bauers (22.8 Ma) Tuff Members of the Condor Canyon Formation, Racer Canyon Tuff (18.7 Ma), Hiko Tuff (18.3 Ma), tuff of Tepee Rocks (17.8 Ma), tuff of Dow Mountain (17.4 Ma), tuff of Acklin Canyon (17.1 Ma), tuff of Rainbow Canyon (15.6 Ma), Ox Valley Tuff (13.5 Ma), and probably the Leach Canyon Formation (23.8 Ma) (Hintze et al., 1994a; Rowley et al., 1995; Scott and Swadley, 1995; Snee and Rowley, 2000; Best et al., 2013a). The Kane Springs Wash caldera complex, just to the south, erupted the tuff of Narrow Canyon (15.8 Ma), tuff of Boulder Canyon (15.1 Ma), and Kane Wash Tuff (14.7 to 14.4 Ma) (Scott et al., 1995a and 1996; Scott and Swadley, 1995). The total thickness of volcanic rocks in the igneous belt generally does not exceed 300 m outside the caldera complexes.

The middle Miocene to Quaternary bimodal sequence, which postdates the calc-alkaline sequence, is made up of small basalt lava flows and cinder cones as well as small high-silica rhyolite volcanic domes, lava flows, ash-flow tuffs, and ash-fall tuffs. The basalts are categorized on the geologic maps as unit QTb, rhyolite domes and flows as Tr_4, and tuffs as Tt_4. All the volcanic rocks derived from the Kane Springs Wash caldera complex, and those that postdate the tuff of Tepee Rocks (Rowley et al., 1995) from the Caliente caldera complex, are included within the bimodal assemblage. The tectonic environment during bimodal magmatism was severe east-west extension, with the direction of principal maximum compressive stress generally oriented vertically, creating an environment of north-south normal faults. Bimodal magmatism coincided with Basin and Range extension, in which the present topography was created and previous tectonic features and topography were deformed and obscured.

Miocene to Holocene Sediments

With the start of Basin and Range deformation at ~20 Ma, north-striking normal faults created the present ranges and basins. Erosion of the uplifted ranges resulted in basin-fill sediments that accumulated to thicknesses of locally more than 3000 m in down-faulted basins. In most places, the basin-fill sediments are unnamed. These units are referred to here as middle Miocene to Holocene alluvium (QTa) and are mostly aquifers, especially where fractured by faulting.

Coeval bimodal volcanic rocks were either high-silica rhyolite or basalt lava flows and tuffs. Their distribution is sporadic (plates 1 and 2) and their thickness is rarely more than a kilometer, except for their source volcanic domes or cinder cones. Where thin (roughly 10 m), they may be combined in the cross sections with the older, much thicker calc-alkaline volcanic rocks or with thick interbedded basin-fill sediments.

The basin-fill sediments (QTa) were largely deposited by streams in closed basins. In general, coarse-grained materials accumulated around the edges of the mountain fronts, whereas finer materials accumulated toward the center of the basins. In some basin interiors, fine-grained sediments accumulated in ephemeral playa lakes. The largest lakes were pluvial lakes of Pleistocene age, including the latest Pleistocene Bonneville

and Lahontan lakes that had water depths of as much as 300 m, resulting in deposition of clay and saline sediments in many basins (Mifflin and Wheat, 1979; Currey, 1982; Currey et al., 1984; Reheis et al., 2014). These lakes, however, were short lived and produced fine-grained materials that rarely exceeded 10 m in thickness. The Bonneville lake left behind spectacular shorelines in some northeast parts of the study area, including the high Bonneville shoreline that formed about 18,000 years ago and the lower Provo shoreline that formed between 16,500 and 15,000 years ago (Reheis et al., 2014). Quaternary basin-fill deposits are mostly thin (a couple hundred meters) and overlie Pliocene and Miocene basin-fill sediments that may be thousands of meters thick, depending on the throw of the normal faults that produced the basins. Data from boreholes in Snake Valley indicate at least 100 m of Tertiary evaporites within the deepest part of the basin.

The concept that extensional basins contain coarse-grained sediments on their margins and fine-grained sediments in their interiors may be valid for periods of time that are geologically short (thousands of years) but is invalid for longer periods (tens of thousands of years) because of the vagaries of the sizes of storms that deposit sediments, of climate changes, of integration of some basins, and of timing of the deformation of basin-bounding versus intra-basin faults. Basin margins may become basin centers and vice versa, over 10 myr. Therefore, in practice, the stratigraphy of basin-fill sediments is characterized by a complex intertonguing of beds of all lithologies. Intra-basin faults commonly produced horsts of soft basin-fill sediments that were then eroded away by streams and redeposited as younger basin-fill sediments. Plate 1 includes thin surficial deposits in and on the flanks of the ranges, including stream deposits, landslides, and spring deposits. However, these deposits are not individually separated in this report or on the maps because of their limited extent.

In some places the basin-fill sediments have local names that were categorized as QTa on the geologic maps, for example, the 11–5 Ma Muddy Creek Formation (Bohannon, 1984) in southern Lincoln and Clark counties (southeastern part of plate 2). The Muddy Creek Formation consists of locally gypsiferous shale, siltstone, and fine-grained sandstone. Another named unit is the ~10–2 Ma Panaca Formation, located in the central part of the study area (Meadow Valley, southeastern part of plate 1), which consists of sandstone, siltstone, shale, and conglomerate (Rowley and Shroba, 1991). Other units of similar lithology to the Panaca Formation are the Horse Camp Formation in the northwestern part of the area (Brown and Schmitt, 1991) and the Salt Lake Formation northeast of the area. All these units are generally more than 300 m thick and locally more than 1500 m thick.

STRUCTURAL GEOLOGY

Three Phanerozoic tectonic events affected the study area: (1) Late Devonian to Late Mississippian Antler orogeny, (2) Late Jurassic to early Tertiary Sevier orogeny, and (3) late Cenozoic Basin and Range extension. Between the Sevier and Basin and Range deformation during the middle Cenozoic, eastern Nevada was characterized by mild extension (Hamilton, 1995; Rowley, 1998; Miller et al., 1999a; Rowley and Dixon, 2001), voluminous calc-alkaline volcanism, and initiation of east-trending transverse zones. These events profoundly affected the topography of the study area.

Antler Orogeny

The Late Devonian to Late Mississippian Antler orogeny affected the northwestern part of the study area, generating a north-trending highland (Larson and Langenheim, 1979; Carpenter et al., 1994; Poole and Sandberg, 1977, 1991; Dickinson, 2006). This event formed folds and thrusts of the Roberts Mountain allochthon, which was at least 2500 m thick and passed through Eureka, Nevada (Carpenter et al., 1994; Saucier, 1997), just northwest of the study area. The thrusts transported deeper-water sedimentary rocks eastward as much as 160 km. The effect to the study area consisted of coarse synorogenic siliceous clastic detritus shed from the highland into the foreland basin to the east, transitioning to shale farther east. The main synorogenic rock units that resulted were the Chainman Shale and

Diamond Peak Formation, and farther south the Scotty Wash Quartzite.

Sevier Orogeny

The second structural event in the Phanerozoic, the Middle Jurassic to early Tertiary Sevier orogeny, resulted in generally north- to north-northeast-striking, east-verging folds and thrust faults. Scattered Middle Jurassic to lower Tertiary plutons were emplaced in many mountain ranges of the study area. Eastward-directed overthrusts emplaced Neoproterozoic to middle Paleozoic rocks over Paleozoic to Jurassic rocks (Armstrong, 1968). At least six frontal thrusts are exposed in the Las Vegas area, each with displacements ranging from several to 30 km (Page et al., 2005b). Minimum shortening estimates in southern Nevada are at least 35 to 72 km (Stewart, 1980b; Burchfiel et al., 1974). East of the study area, at least four major frontal thrust systems are well exposed, with total shortening of at least 210 km (DeCelles, 2004; DeCelles and Coogan, 2006). Except for the southern part of the study area, most of the study area is considered to be the hinterland of the deformation. In other words, Sevier deformation thickened the crust and created Late Cretaceous to early Tertiary highlands (hinterlands) that in turn shed most clastic debris to the east (Vandervoort and Schmitt, 1990; Druschke et al., 2009; DeCelles, 2004; DeCelles and Coogan, 2006; Long, 2012; Long et al., 2014 and 2015). However, some of the Las Vegas area thrusts, including the Gass Peak thrust, have been projected northward into the hinterland in the central and northern part of the study area, including the Timpahute Range, Worthington Mountains, Golden Gate Range, Grant Range, Pancake Range, and Newark Valley (Vandervoort and Schmitt, 1990; Dobbs et al., 1994; Taylor et al., 1991 and 2000). Taylor et al. (1993 and 2000), Long (2012), and Greene (2014) referred to this region as the central Nevada thrust belt, and considered it to be a fold-thrust belt of relatively small displacement within the overall hinterland. In contrast to the small east-verging thrusts in the hinterland, Lewis et al. (1999) and Gebelin et al. (2015) suggested some west-verging Sevier thrusts in the northern Snake Range and the Deep Creek Range.

East of the central Nevada thrust belt, a north-trending belt of high-grade metamorphic rocks is exposed, with its axis passing along the Snake Range. The rocks contain Jurassic, Cretaceous, and lower Tertiary components and notably yield Late Cretaceous cooling ages. The belt is interpreted to represent a crustal welt of tectonic shortening that spawned the frontal Sevier thrusts to the east (Coney and Harms, 1984; Miller and Gans, 1989, DeCelles, 2004).

Small east-verging thrusts have been mapped in the Confusion Range (e.g., Hintze and Davis, 2002a and b). Most workers, including us, consider these thrusts to represent mostly minor movement along bedding planes in weak beds during tight folding of Sevier age (e.g., Hintze and Davis, 2003). Anderson (1983), however, interpreted the faults to have formed by gravity sliding into the axis of a synclinorium. A broad uplifted area east of the Confusion Range, in the House Range and Sevier Desert, known as the Sevier arch or Sevier culmination, was similarly considered to be an area of minor thrusting (Hintze and Davis, 2003). Therefore, the Confusion Range and Sevier arch make up the eastern part of the hinterland. DeCelles (2004) and DeCelles and Coogan (2006), in an extensive, long-term review of Sevier-age thrusts in the west, projected some of their major thrusts beneath the Sevier arch. More recently, Greene and Herring (2013) have taken this theme significantly further by drawing cross sections through the Confusion Range that show significant thrusts in the subsurface. Although they agree with the previous mapping in the Confusion Range that indicates only minor thrusts, they concluded on the basis of their analysis and cross sections that the Confusion Range may be a western part of the Sevier frontal thrust belt yet exposed well east of the Sevier arch. Any proof of major thrusts beneath the Confusion Range must await future seismic studies or deep drilling. Some of their inferred thrusts are beneath the level of our cross sections. Greene (2014) expanded on these interpretations to give the regional implications of the thrusts in and beneath the Confusion Range. He named these thrusts and folds the western Utah thrust belt, comparable to the central Nevada thrust belt, and both containing relatively small-displacement thrusts and folds within the hinterland. These two

small belts were suggested to each have roughly 10 km of horizontal shortening (Greene, 2014). Sevier-type deformation is shown schematically on figure 10, and the Sevier-age Glendale/Muddy Mountain thrust in the Muddy Mountains of the southern part of the study area is shown on figure 11.

Middle Cenozoic Volcanism

Middle Cenozoic time was characterized by voluminous calc-alkaline arc magmatism (Rowley, 1998; Miller et al., 1999a; Rowley and Dixon, 2001). This was the terminal product of subduction beneath western North America that began in the Triassic (Lipman et al., 1972; Hamilton, 1995; Dickinson, 2009; Humphreys, 2009). This last episode of subduction was low angle, so the subducted slab extended as far east beneath western North America as Colorado, generating arc magmas along the way. The tectonic environment during calc-alkaline magmatism was generally one of mild east-west extension in the

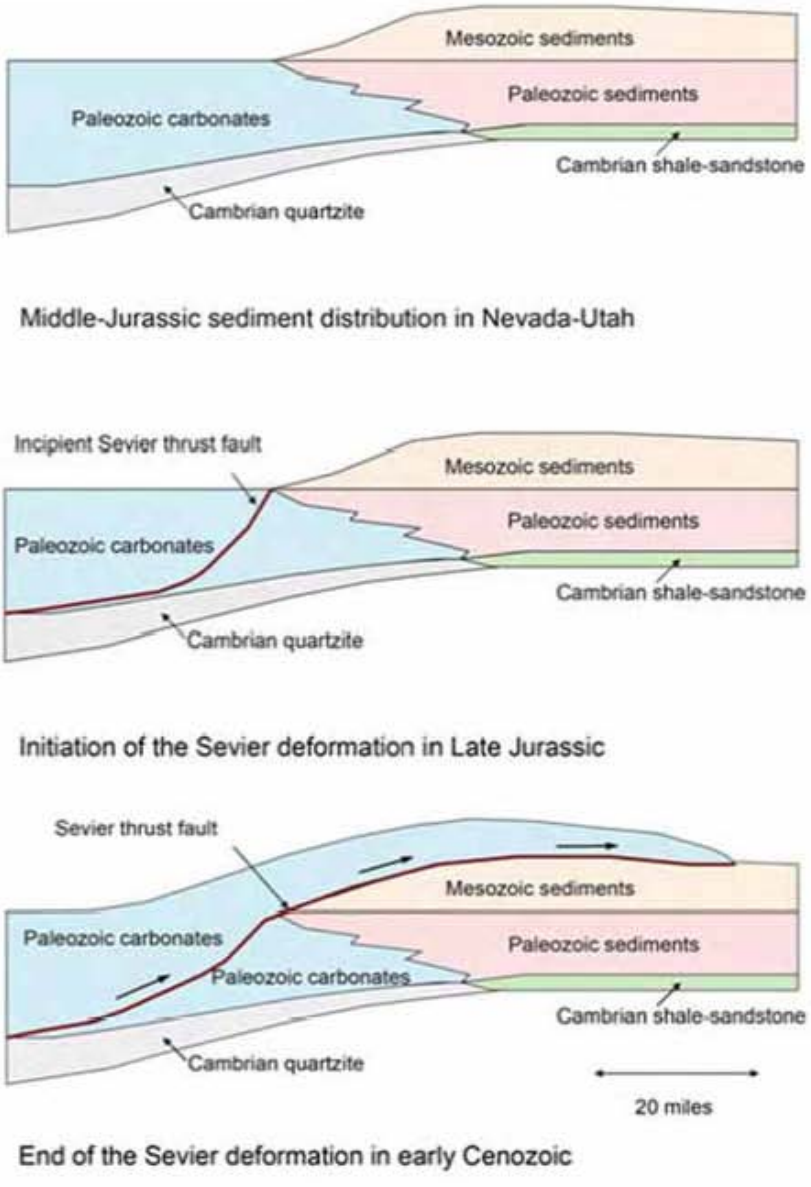

Figure 10. Schematic diagram of Sevier thrust sheets, illustrating the movement of Paleozoic carbonates over cratonic sediments.

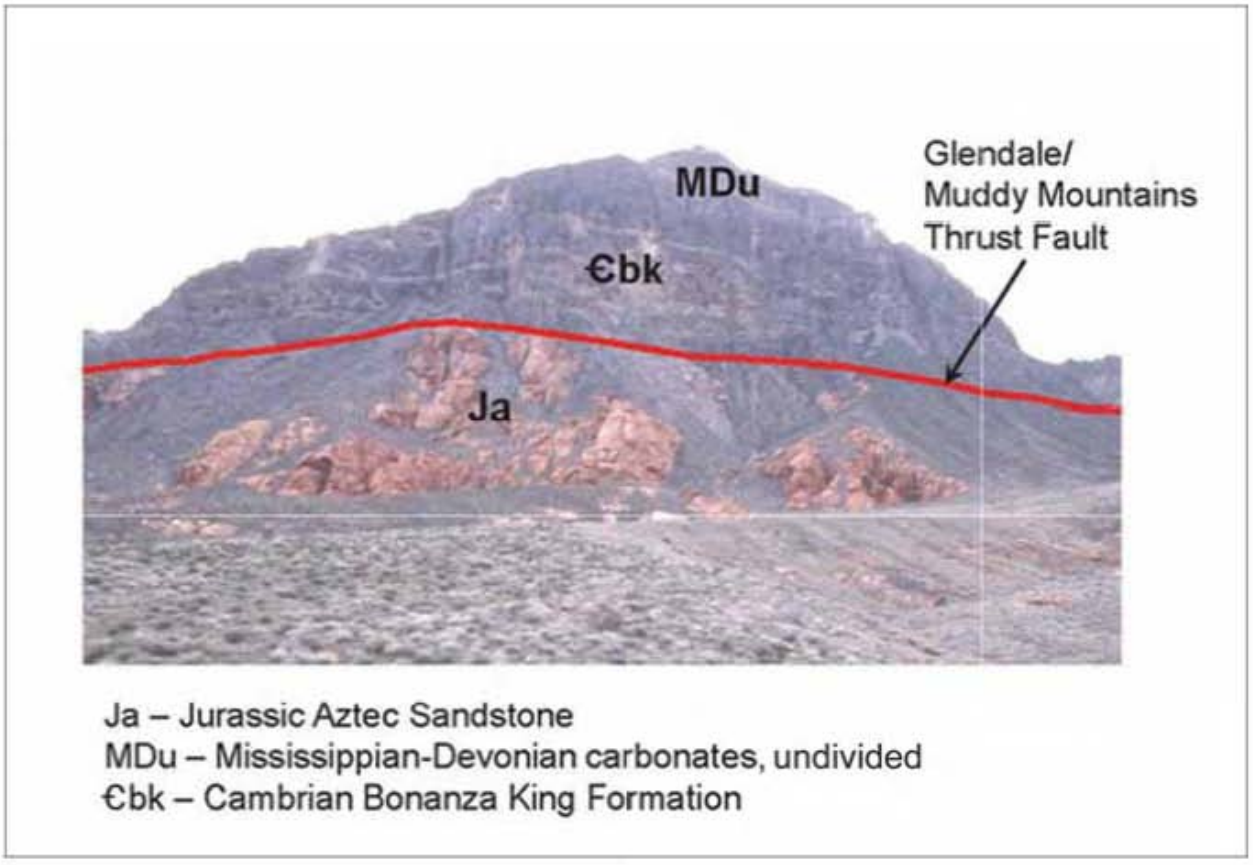

Figure 11. Paleozoic carbonates thrust over Jurassic Aztec Sandstone in the Muddy Mountains near Muddy Peak.

Great Basin. The direction of principal maximum compressive stress was generally north-south, creating an environment of strike-slip and oblique-slip faults (Anderson, 1981, 1983, 1989, 2013; Anderson and Barnhard, 1993; Anderson et al, 2013; Rowley, 1998).

In the Great Basin, the mostly east-trending igneous belts are made up of volcanic vents, including calderas, and underlying source batholiths, resulting in a topography almost 90 degrees different from the present topography, with generally east-trending highlands that resulted from thermal expansion by the underlying batholith and from near-vent volcanism. These highlands presumably alternated with plains north and south of the highland, where outflow tuffs accumulated after erupting from calderas in the highlands. Lava flows, unlike ash-flow tuffs, are not deposited far from their vents so they accumulated to great thicknesses in the higher axes of the belts. Nonetheless, at that time most of the Great Basin was a high upland (Vandervoort and Schmitt, 1990; Dilek and Moores, 1999; Henry, 2008; Henry et al., 2012; Best et al., 2009; Long, 2012), analogous to the Altiplano of the modern Andes and thus termed by DeCelles (2004) as the Nevadaplano. The upland was a holdover from crustal thickening caused by Sevier crustal shortening in the hinterland west of the frontal thrusts of the Sevier deformational event. The Nevadaplano extended from the eastern part of what is now the Sierra Nevada to the frontal Sevier thrust faults that surfaced along the eastern edge of the Great Basin. The Nevadaplano had a north-trending east-west drainage divide in eastern to central Nevada (Henry, 2008; Henry et al., 2012; Long, 2012).

East-Trending Transverse Zones

East-striking folds and faults and alignments of plutons, volcanic vents, geophysical anomalies, hot springs, hydrothermally altered rocks, mineral deposits, and local basins and ranges have been noted in the Great Basin for years, primarily by geologists of the mining industry. Ekren et al. (1976, 1977), Rowley et al. (1978), and Stewart et al. (1977) called these alignments "lineaments" with an origin similar to transform faults in the ocean basins. Ekren et al. (1976) suggested that the lineaments began to form in the Cretaceous, if not earlier, and continued to be active throughout both Tertiary calc-alkaline magmatism and Basin and Range deformation. Like transform faults, these lineaments seem to represent boundaries between areas to the north and south that had different amounts, rates, and types of structural deformation. Rowley (1998) and Rowley and Dixon (2001) referred to them as transverse zones, and we follow their terminology here. They are poorly known and have been mapped in detail only locally, so they are projected with limited evidence between the areas where they are known. Therefore, transverse zones are delineated as speculative zones of potential disruption on plates 1 and 2.

Transverse zones bound parts of most igneous belts in the Great Basin. They also define the northern and southern sides of the Caliente caldera complex, representing structures by which this caldera spread east and west to a degree much more profound than most other caldera complexes in the Great Basin. Some transverse zones seem to be discontinuous along strike. The Sand Pass transverse zone (Rowley, 1998; Rowley and Dixon, 2001), which bounds the northern and southern side of the Kern Mountains, is buried beneath surficial sediments in Snake Valley, absent through the carbonate bedrock of the northern Confusion Range and western Middle Range (plate 1), and exposed again in the carbonate bedrock and basin-fill sediments of the central and eastern Middle Range and of Sand Pass (Rowley et al., 2009, plate 1). Farther east, east-trending features are absent in the Drum Mountains and Thomas Range (Rowley et al., 2009, plate 1), but they are prominent east of the Thomas Range most of the way to and east of the Wasatch front in central Utah (Stoeser, 1993; Rowley, 1998; Rowley and Dixon, 2001).

Basin and Range Extension

Ongoing Basin and Range extension began at ~20 Ma. It is characterized by east-west extension accommodated primarily by north-striking normal faults. Early phases of this deformation locally produced north-striking basins and ranges due partly to broad warping (Rowley et al., 1981; Liberty et al., 1994), but these basins and ranges were not necessarily in the same locations as they are today. The present topography was produced later, during the main pulse of extension that began after 10 Ma for most parts of the Great Basin. The north-south orientation of axes of some basins and ranges, which formed during main-phase (post-10 Ma) extension, may be 10 km or more east or west of axes produced during early (20 to 10 Ma) extension (Rowley et al., 1981; Liberty et al., 1994; Rowley, 1998). Some parts of the older basins were uplifted as part of the new ranges and some parts of the older ranges were downthrown as part of the new basins. An example is the presence of Miocene lacustrine limestones and associated clastics in the North Pahroc and Pahranagat ranges (Tschanz and Pampeyan, 1970) that were originally deposited in one or more older extensional basins.

Most structures shown on plates 1 and 2 formed during Basin and Range extension. Therefore, the maps illustrate many types of structures that have combined over mostly the last 20 Ma to produce a dynamic and continuing regional pattern of extensional deformation. Such deformation, in the experience of the authors, is typical of most other parts of the Great Basin but is not commonly portrayed at such a regional scale in a single report. Although faults exposed in basin fill and bedrock were faithfully reproduced from previously published maps, we applied geophysics and well logs to show buried (dotted) faults in the basins, thereby adding to the overall framework by showing structures not previously published. The resulting complex pattern thus consists of (1) the primary, mostly north-striking high-angle normal faults, (2) low-angle normal attenuation/denudation or detachment faults, (3)

northwest- or northeast-striking oblique-slip transfer faults, and (4) east-striking transverse zones. All are the result of east-west extension. We interpret that most of the total deformation was produced by fault type #1 (i.e., the steeply dipping normal faults) some of which had dip-slip movement of more than 3000 m; only some of the other fault types locally included such large displacements. We present the larger faults that are responsible for large-magnitude displacement, most of which bound the ranges, on plates 1 and 2 as regional faults, whereas lesser faults are shown as subsidiary faults. Movement on the high-angle normal faults caused the dominant topography of alternating north-trending ranges and valleys, which are mostly made up respectively of complex horsts and grabens (Stewart, 1971, 1980).

Of the four types of normal faults, the attenuation/denudation faults (fault type #2) shown on plates 1 and 2 are non-rooted faults that represent failure by gravity as the ranges went up along the large high-angle normal faults and the rising tops of these ranges failed along weak beds. Some of these attenuation/denudation faults may be considered gravity slides, as in the southwestern Sheep Range/Desert Range (Guth, 1980) and in the Mormon Mountains (Carpenter and Carpenter, 1994a). The Snake Range décollement is a regional fault in the Pioche Shale that is covered below in greater detail because of its controversial nature; we consider it to be an attenuation/denudation fault.

Fault type #3, transfer faults, are those that transfer east-west strain into both normal and strike-slip movement because the faults strike mostly northeast or northwest. A synonym for transfer faults that we have previously applied (e.g., Rowley et al., 2016) are "accommodation" faults. However, Faulds and Varga (1998) have defined this fault more narrowly as a belt of intermeshing, oppositely-dipping normal faults. The northwest-striking transfer faults tend to have right-lateral movement under east-west extension, in addition to some component of vertical movement, whereas the northeasterly-striking transfer zones tend to have left-lateral movement in addition to some component of vertical movement. Examples of transfer zones include the northeast-striking, left-lateral Pahranagat shear zone (PSZ) at the southern end of Pahranagat and Delamar valleys (Ekren et al., 1977). The eastern and western ends of some of these northeast-striking faults merge with north-striking dip-slip normal faults. Another transfer zone is the north-northeast-striking, left-lateral Kane Spring fault zone that separates the Delamar Range from the Meadow Valley Mountains. Others are the west-northwest-striking, right-lateral Las Vegas Valley shear zone, which passes eastward into the east-northeast-striking, left-lateral Lake Mead fault zone (e.g., Anderson and Beard, 2010).

Fault type #4, the east-striking transverse zones, separate broad masses of rock, both north and south of the zone, that were pulled apart in east and west directions at different rates or amounts, or by different expressions of deformation—including folding—north and south of the transverse zone (Ekren, et al., 1976, 1977; Rowley et al., 1978; Rowley, 1998; Rowley and Dixon, 2001). Transverse zones are long lived (probably several million years) and deep seated, so along strike they may pass beneath rocks that appear to exhibit no surface expression, although such an absence of structures may reflect older mapping that we compiled. Most faults in transverse zones tend to be strike-slip or oblique-slip. Compilation of transverse zones in the Great Basin (Rowley, 1998; Rowley and Dixon, 2001) suggests that that their strike-slip component most commonly is left lateral but it seems likely, given their long-lived nature and their origin as transform structures, that both right-lateral and left-lateral motions may be present on the same fault or on different strands of the same transverse zone. Examples of transverse zones, from north to south, include the Sand Pass transverse zone, which is clearly present at Sand Pass, separating the Fish Springs Range on the north from the House Range on the south (see Rowley et al., 2009, Plate 1), as well as many but not all areas along strike extending well to the east (Stoeser, 1993). West of Sand Pass, its presence across the Middle Range and northern Confusion Range is expressed only by several easterly-striking faults, but its expression is much more profound farther west in the Kern Mountains, where it bounds both sides of this unusual east-trending range. The Blue Ribbon transverse zone farther south is well expressed east

of the study area (Rowley et al., 1978), not expressed by published mapping across the Indian Peak caldera complex, well expressed between the Fairview Range and Bristol Range (Ekren and Page, 1995; Page and Ekren, 1995), and moderately to well-expressed to the western edge of the study area, and, indeed, to the western edge of the Great Basin, where Ekren et al. (1976) called it the Warm Springs lineament (Rowley, 1998; Rowley and Dixon, 2001). The Timpahute transverse zone farther south is well expressed across the entire map area, as well as far to the east and west (Ekren et al., 1976, 1977; Rowley, 1998; Rowley and Dixon, 2001). Transverse zones are not well known, and few persons besides the authors have mapped any parts of them in detail. Most of the transfer faults and transverse zones may represent activation of older structures.

The main (post-10 Ma) episode of Basin and Range deformation continued from the late Miocene through the Pliocene and Quaternary. Except for the attenuation/denudation faults, all the different types of faults that were active during this regional extension had some Pleistocene and/or Holocene movement. Age relationships of faults shown on plates 1 and 2 suggest that Pleistocene and Holocene motion can be considered the latest tectonic adjustment to east-west extension that is now at the same or a greater level of deformation as earlier, throughout the study area. In other words, the primary current deformation regime is regional extension—with ranges going up and the basins moving down along normal faults—along with many domains involving strike-slip and oblique-slip motion.

In northern parts of the study area, many low-angle faults previously mapped as thrust faults (e.g., Hazzard and Turner, 1957; Misch, 1960; Nelson, 1966; Drewes, 1967) have since been interpreted as Cenozoic low-angle normal faults. The workers who mapped them as thrusts correctly noted that most of them partly followed weak shale beds and placed younger rocks on top of older rocks, in contrast to Sevier thrust faults that are exposed to the east. The first workers to publish on the significance of the younger on older relationships were Scott (1965) and Moores et al. (1968) from detailed geologic mapping in the Grant and White Pine ranges, as well as Armstrong (1963, 1972) from regional studies over much of the study area. They and other geologists also recognized that the rocks above these faults were not thickened and compressed, as above thrust faults, but instead were stretched and attenuated. Therefore, they must represent Cenozoic expressions of structural extension. Although most rocks deformed by the faults are of Paleozoic age, the mapping and regional studies confirmed that the faults postdated Sevier deformation and most likely represented Basin and Range deformation. These geologists suggested that the low-angle faults formed during and after rapid Basin and Range uplift of the ranges, in which the tops of the uplifted blocks were structurally stripped (or attenuated or denuded) by low-angle faults that verged into the adjacent low areas, much like large gravity slides. They called them attenuation or denudation faults. Most formed during the Basin and Range deformation. Nonetheless, compilation of the county maps of the area (Hose and Blake, 1976; Kleinhampl and Ziony, 1985) showed the low-angle faults as thrusts, even though these authors (especially Kleinhampl and Ziony) had misgivings and clearly recognized that at least some of these faults were due to Cenozoic extension. Later, Lund et al. (1991), Lund and Beard (1992), Francis and Walker (2002), Walker and Francis (2002), Long (2014), and Long and Walker (2015) remapped part of the northern Grant Range, confirming that most of the low-angle faults are brittle attenuation faults that continue beneath parts of Railroad Valley to the west, and whose interpretation has implications for finding oil occurrences in the large Railroad Valley oil field. The faults here largely follow weak beds of the Chainman Shale.

Low-angle normal faults in the Schell Creek and Snake Ranges have been studied in great detail, and are generally correlated with each other and referred to as the Snake Range décollement (Misch, 1960). This assumed single fault horizon, which largely follows weak beds of the Pioche Shale, juxtaposed Middle Cambrian carbonates and some younger rocks over Lower and Middle Cambrian and older rocks. The oldest of these rocks are in the Hendrys Creek area on the eastern flank of the northern Snake Range, where metamorphosed muscovite-bearing quartzite and

schist of the Neoproterozoic McCoy Creek Group are exposed (Lewis et al., 1999; Gebelin et al., 2015). Drewes (1967) mapped the décollement east of the crest of the Schell Creek Range. Whitebread (1969) mapped it in detail over a large part of the southern Snake Range that includes Great Basin National Park (GBNP). Hose and Blake (1976) extended the décollement (shown as a thrust) in reconnaissance over the Snake, Schell Creek, Egan, Cherry Creek, Antelope, and southwestern Deep Creek ranges. These workers emphasized that younger rocks were emplaced over older rocks, which is opposite of the thrust-fault geometry. Misch (1960) and Drewes (1967) considered the structure to be a thrust anyway, whereas Whitebread (1969) and Hose and Blake (1976) were equivocal on the age or origin of the faults.

An important advance was made by Coney (1974), who studied small-scale structures in the hanging wall of the décollement in the Snake and Schell Creek ranges and found that upper-plate rocks on the eastern side of the Schell Creek Range and both the eastern and western sides of the Snake Range moved down the flanks of the ranges, whether to the east or the west; he considered the faults to be Tertiary denudation faults comparable to gravity slides that moved downslope along much the same (Lower Cambrian) planes of weakness. Therefore these large faults were not necessarily all the same fault, whose hanging wall moved eastward, as many others suggested. Gebelin et al. (2015) appeared to have confirmed Coney's conclusions by a study of samples collected from the footwall metamorphic rocks of the décollement from both the western side of the northern Snake Range (north of the latitude of Sacramento Pass) and 16 km to the east from the eastern side (Hendrys Creek) of the Snake Range. Gebelin et al. found that footwall rocks on the western flank indicated movement of the hanging wall to the west, whereas footwall rocks on the eastern flank indicated movement of the hanging wall to the east. Yet despite his remark (p. 154) that "quartzite from the two areas did not experience the same type of deformation," Gebelin et al. (2015) seemed to have discarded his own relative-movement data from the western side, preferring instead to join most previous workers in advocating that the décollement was a single large structure whose upper plate moved east. Following a comprehensive study of the décollement, Miller et al. (1983) and Gans et al. (1985, 1989) reinterpreted the fault as an Eocene to Miocene low-angle surface in which the rocks above it were extended by brittle mechanisms, whereas the rocks below were extended a similar amount by ductile mechanisms, then later the surface was exhumed during uplift of the area as a metamorphic core complex. They suggested that relative movement along the décollement was minor because the surface represented a ductile-brittle transition zone that originally formed at about 6 km depth.

Bartley and Wernicke (1984) interpreted the Snake Range décollement differently, using a model based on work by Wernicke et al. (1985) from a study of the Mormon Mountains of southern Nevada. Bartley and Wernicke (1984, p. 652) suggested that the décollement was a major low-angle detachment fault with 60 km of eastward displacement of the upper plate relative to its underlying footwall. A detachment fault is a low-angle normal fault whose use may be applied in such a non-genetic way, but more commonly the term is used for a low-angle normal fault due to extension above a rising metamorphic core complex. This hypothesis was later accepted by numerous other geologists (Allmendinger et al., 1983; Lee, 1995; Lewis et al., 1999; Kirby and Hurlow, 2005; Sweetkind et al., 2007a and b; Wallace et al., 2007). In contrast, Gans and Miller (1985, p. 411; Gebelin et al., 2015) pointed out that the fault plane occupies the same stratigraphic position (top of the Pioche Shale) and does not "cut downsection to the east," so they therefore proposed that it could not have "a large amount of translation" and more likely represents "decoupling along the stratigraphic horizon in the Pioche Shale."

After more field work, Miller et al. (1999a) concluded that, whereas the décollement had an older (late Eocene and early Oligocene) history, most displacement on it was early Miocene and younger, coinciding with Basin and Range deformation. Gebelin et al. (2015) also emphasized the possibility of early (Eocene)

deformation on the décollement based on $^{40}Ar/^{39}Ar$ ages (49–45 Ma) in footwall rocks from the eastern flank of the northern Snake Range, yet plutonism and volcanism of this same age occurs throughout the Ely-Tintic igneous belt, and such magmatism has no bearing on low-angle faults elsewhere. Ruksznis and Miller (2014) re-emphasized that most uplift and deroofing of the northern Snake Range and Kern Mountains was post-21 Ma, synchronous with Basin and Range deformation. Yet Norman and Gans (2014) noted $^{40}Ar/^{39}Ar$ ages of 40–35 Ma for two low-angle normal faults in the central Schell Creek Range. In their summary report of all field work on the origin of the décollement, Miller et al. (1999a) recanted some of their earlier theories and presented several alternative origins. Among them was adoption of a rolling-hinge model (Lee, 1995) for a metamorphic core complex, by which the hanging wall of the décollement had been translated primarily eastward about 11 to 14 km, although they acknowledged that movement on the décollement on the western side of the Snake Range was westward, as had been recognized by Coney (1974). Their core complex consisted only of the Deep Creek Range, Kern Mountains, and Snake Range. Then, in their final concluding paragraph, Miller et al. (1999a, p. 902) also proposed that the décollement may not be a normal fault at all but instead a "highly complex structural boundary developed above a rising and extending mass of hot crystalline rocks."

Most regional summaries of the geology of the Great Basin list the Snake Range as a metamorphic core complex (e.g., Dickinson, 2006), following the conclusions of Miller et al. (1983). In a summary of world-wide core complexes, Whitney et al. (2013, p. 277, figures 2 and 3) was one of the latest to make this conclusion. Among such advocates, Greene (2014, p. 163–165) in particular had difficulty reconciling thrusting in the Confusion Range with a detachment dipping eastward beneath Snake Valley and the Confusion Range and presumably carrying the Confusion Range in its hanging wall, as most workers have suggested. In the eastern Great Basin, not all high mountain ranges that contain flat faults (e.g., Deep Creek, Antelope, Cherry Creek, Snake, Egan, Schell Creek, and Grant ranges and Mineral, Tushar, Pine Valley, and Morman mountains) are core complexes. In other words, it is likely that most large ranges in the Basin and Range Province contain low-angle normal faults, whether as detachments related to core complexes or as non-rooted (gravity driven) denudation/attenuation faults related to structural uplift along large, high-angle range-front normal faults. In fact, in places where these high mountain ranges consist mostly of Tertiary volcanic rocks, huge gravity slides of the same or greater areal extent as the so-called Snake Range décollement may form as sector collapses of volcanic fields prior to basin and range deformation, as in the Pine Valley Mountains of southwestern Utah (Hacker, 1998; Hacker et al., 2002) and the Tushar Mountains/Markagunt Plateau of south-central Utah (Biek et al., 2014, 2015; Hacker et al., 2014). Most such denudation/attenuation faults and giant gravity slides fail along weak shale beds.

GEOPHYSICS

OVERVIEW

To interpret the subsurface of the study area, SNWA contracted with the USGS Geophysical Unit at Menlo Park, California, to collect and analyze geophysical data in the area. This was done in a series of cooperative agreements between SNWA and USGS between 2003 and 2010. The primary studies used gravity, aeromagnetic, ground magnetic, and audiomagnetotelluric (AMT) methods. Particular attention was given to a series of basins that covered an area of about 60,000 km^2 in eastern Nevada and western Utah. These data were combined with those previously obtained, mostly by the USGS, in adjacent ranges over an area of about 155,000 km^2 (figure 12). The analysis defined the overall shape and thickness of basins, identified buried faults that may be either barriers or conduits to groundwater flow, speculated on interbasin flow, helped characterize aquifers, and allowed us to better understand the overall geology. Discussions below will concentrate on both the larger region as well as selected areas for more detailed study.

GRAVITY, AEROMAGNETIC, AND GROUND MAGNETIC STUDIES

Collection of Data

Gravity Data

Gravity data for the region were obtained from Ponce (1997), Bankey et al. (1998), Scheirer (2005), Kucks et al. (2006), Mankinen et al. (2006, 2007, 2008), Scheirer and Andreasen (2008), and Mankinen and McKee (2007, 2009, 2011). These were supplemented with unpublished USGS data obtained from the Basin and Range Carbonate Aquifer Study (BARCAS) project (Sweetkind et al., 2007a and b; Watt and Ponce, 2007). All data were reduced using standard gravity corrections (Blakely, 1995) and were referenced to the International Gravity Standardization Net 1971 (ISGN 71) gravity datum (Morelli, 1974) to produce the complete Bouguer anomaly. A regional isostatic field was calculated using an Airy-Heiskanen (Heiskanen and Vening Meinesz, 1958) model for local compensation of topographic loads (Jachens and Roberts, 1981; Simpson et al., 1986). This model assumes a crustal thickness of 25 km, a crustal density of 2670 kg/m^3, and a 400 kg/m^3 density contrast between the crust and mantle. This regional isostatic field was subtracted from the Bouguer anomaly, thus removing long-wavelength variations in the gravity field that are inversely related to topography. The resulting isostatic residual gravity anomaly, therefore, is a reflection of local density distributions within middle to upper crustal levels.

Because gravity data for the study area were obtained by many different observers at different times, we examined the composite dataset to remove duplicate and inconsistent entries. To test for possible errors, we first compared reported station elevations with elevations interpolated from 10 and 30 m DEMs, using the procedure of D. Plouff (written commun., 2005). Large elevation differences indicate possible errors in station location or elevation, and each station identified was examined individually to determine the cause of the discrepancy. Some errors occurred because of imprecise locations (e.g., lack of significant digits in published reports) and could be corrected with a high degree of confidence. If the source of the discrepancy could not be determined and corrected, the station was omitted from the data set. The revised data set was gridded at a spacing of 0.5 km using a minimum curvature algorithm of Webring (1981), resulting in the isostatic gravity map shown in figure 13. Anomalies reflect local density variations in the middle and upper crust. Gravity lows (cool colors) generally indicate sedimentary material within valleys; gravity highs (warm colors) generally reflect denser basement rocks in mountain ranges.

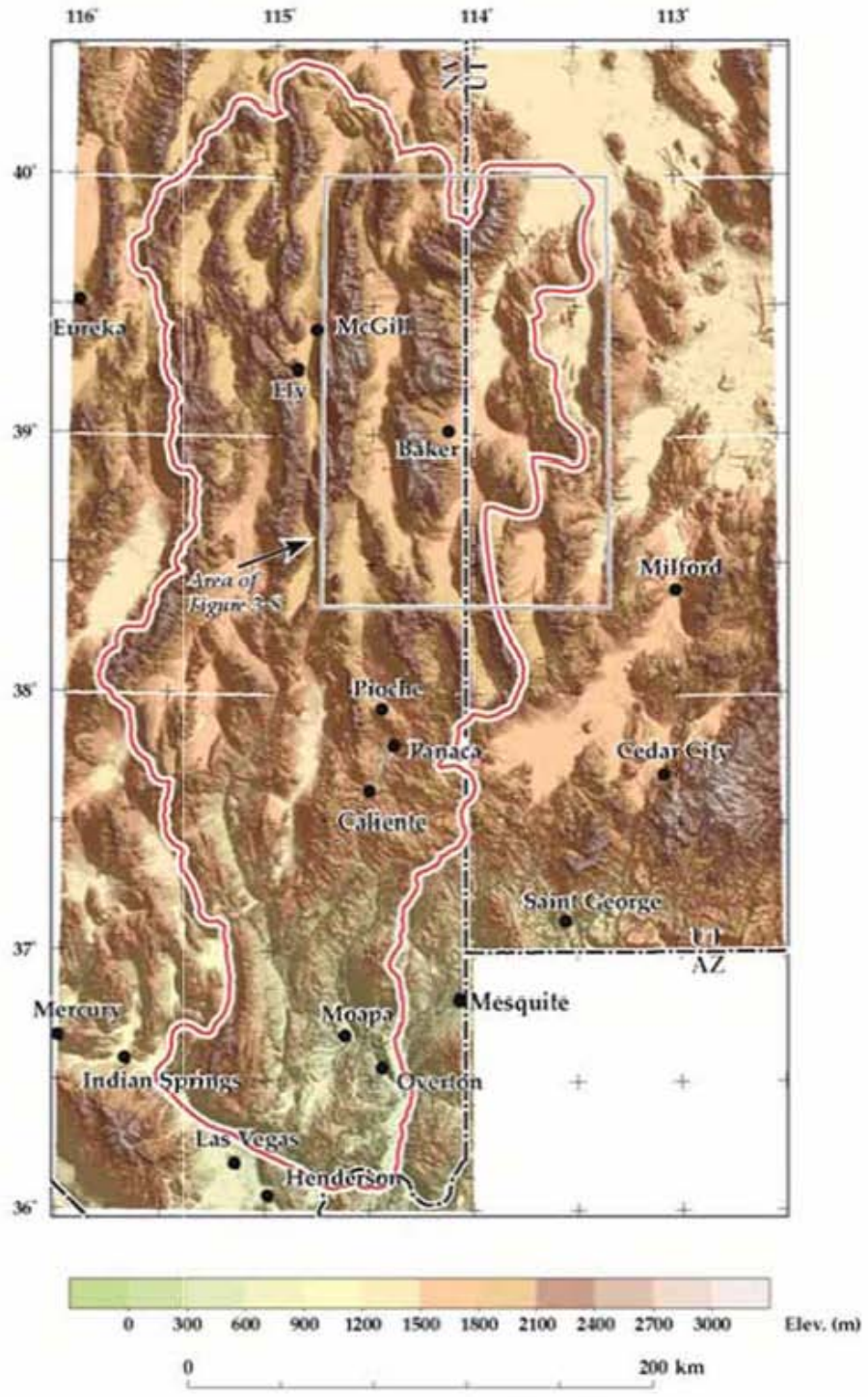

Figure 12. Shaded-relief map of eastern Nevada and western Utah. Red line bounds study area.

Aeromagnetic Data

Aeromagnetic surveys of the Great Basin were presented by Zietz et al. (1976, 1978), Mabey et al. (1978), Hildenbrand et al. (1983), Hildenbrand and Kucks (1988a and b), and Bankey et al. (1998). Flight-line spacing ranged between 3.2 and 1.6 km in Utah, and between 8 and 1.6 km over most of Nevada. Because aeromagnetic survey specifications are often widely disparate for a variety of reasons, a collaborative effort was undertaken by the Geological Survey of Canada, the Consejo de Recursons Minerales de Mexico, and the USGS to upgrade all available data from Canada, Mexico, and the United States. The data were reprocessed, gridded at a spacing of 1 km, converted from level to drape, and merged into a coherent representation of the data as if they had all been flown at a constant 305 m above terrain. Results are available as a digital magnetic anomaly database and map for North America (North American Magnetic Anomaly Group [NAMAG], 2002). Aeromagnetic data shown in figure 14 were extracted from this map and re-gridded to a 0.5 km spacing. A recent compilation of aeromagnetic data for Nevada also is available from Kucks et al. (2006).

Ground Magnetic Data

Ground magnetic data were obtained from selected traverses using a portable cesium-vapor magnetometer integrated with a differential GPS receiver. The GPS receiver has an accuracy of less than 1 m horizontally and 1–2 m vertically. The magnetometer was mounted on a non-magnetic aluminum frame and towed behind a vehicle at speeds of as much as 60 km/hr. (Tilden et al., 2006). Measurements were taken at one-second intervals while operating the instrument in continuous mode. A stationary base-station magnetometer to record diurnal variations was not employed because of the short duration of the traverses.

Processing of Data

Geophysical data can be enhanced in a number of ways to better characterize causative sources of their anomalies (e.g., Blakely, 1995). Derivative gravity and magnetic maps used here are intended to de-emphasize surface and near-surface features. The deep-seated crustal structures thus identified reveal major tectonic domains that form the structural underpinnings of the region. Boundaries between these crustal blocks may represent zones of weakness that could later influence the emplacement of intrusions or potentially localized mineral deposits, regional groundwater flow, hydrothermal activity, and young tectonic activity.

Upward Continuation

The gravity anomalies shown in figure 13 were analytically upward-continued by 3 km (Hildenbrand, 1983) to de-emphasize surface and near-surface features and to enhance the contribution from deeper sources, resulting in figure 15. This figure also shows "maxspots," which are discussed below in Horizontal Gradients.

Magnetic Potential

The aeromagnetic data of the study area were analyzed by transforming them to their magnetic potential (the "pseudogravity" transform of Baranov, 1957; Blakely, 1995), shown in figure 16. This procedure generally helps to isolate broad magnetic features that may be masked by high-amplitude shallow magnetic sources, reduces anomaly asymmetry, and roughly centers the anomalies over their sources. Because the pseudogravity transform converts a magnetic anomaly into one that would be observed if the magnetic distribution of the body were replaced by an identical density distribution, interpretation of their sources is simplified by allowing the use of gravity techniques, as described below.

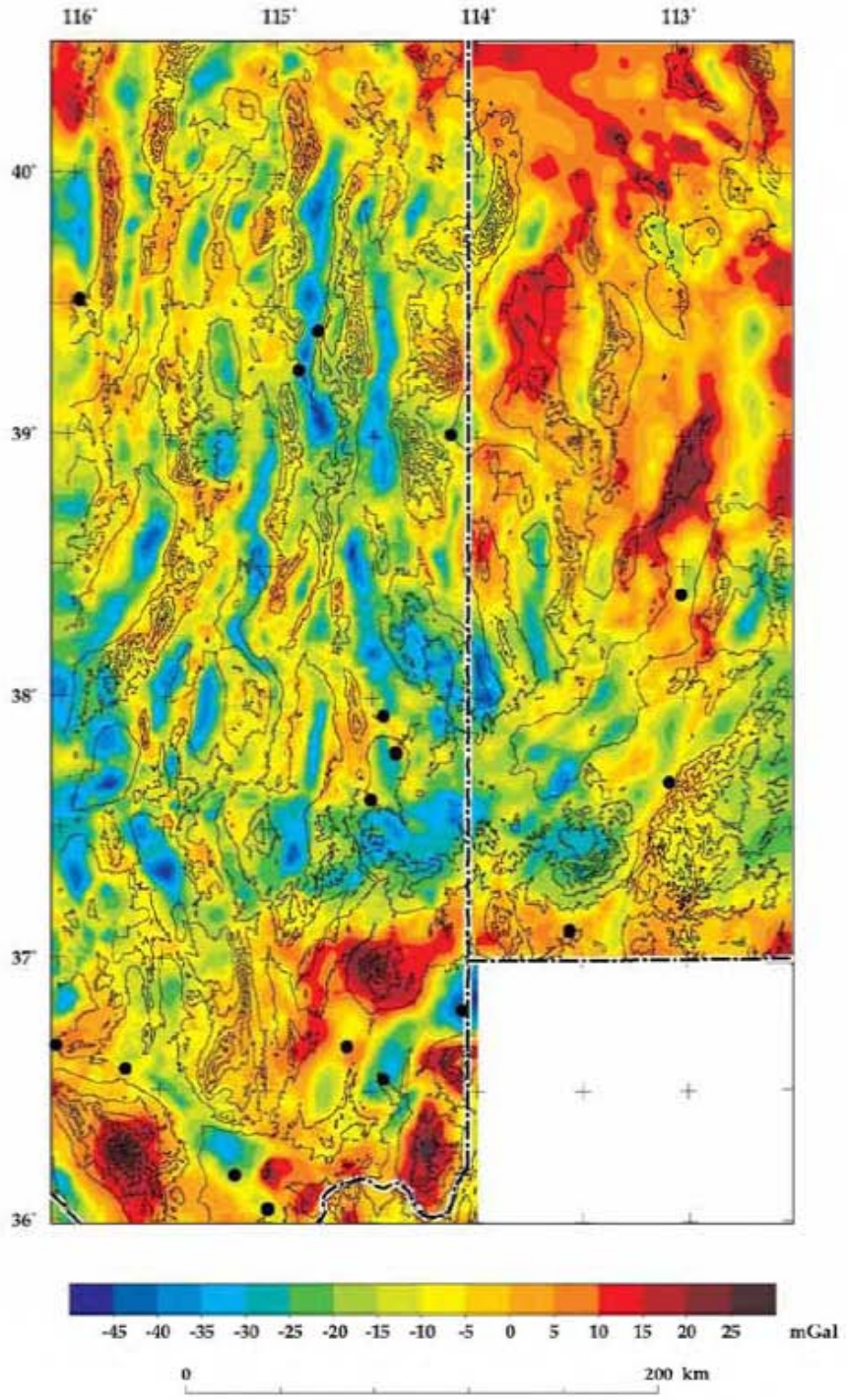

Figure 13. Isostatic-gravity field in eastern Nevada and western Utah. Black dots are towns. Topographic contour interval is 400 m.

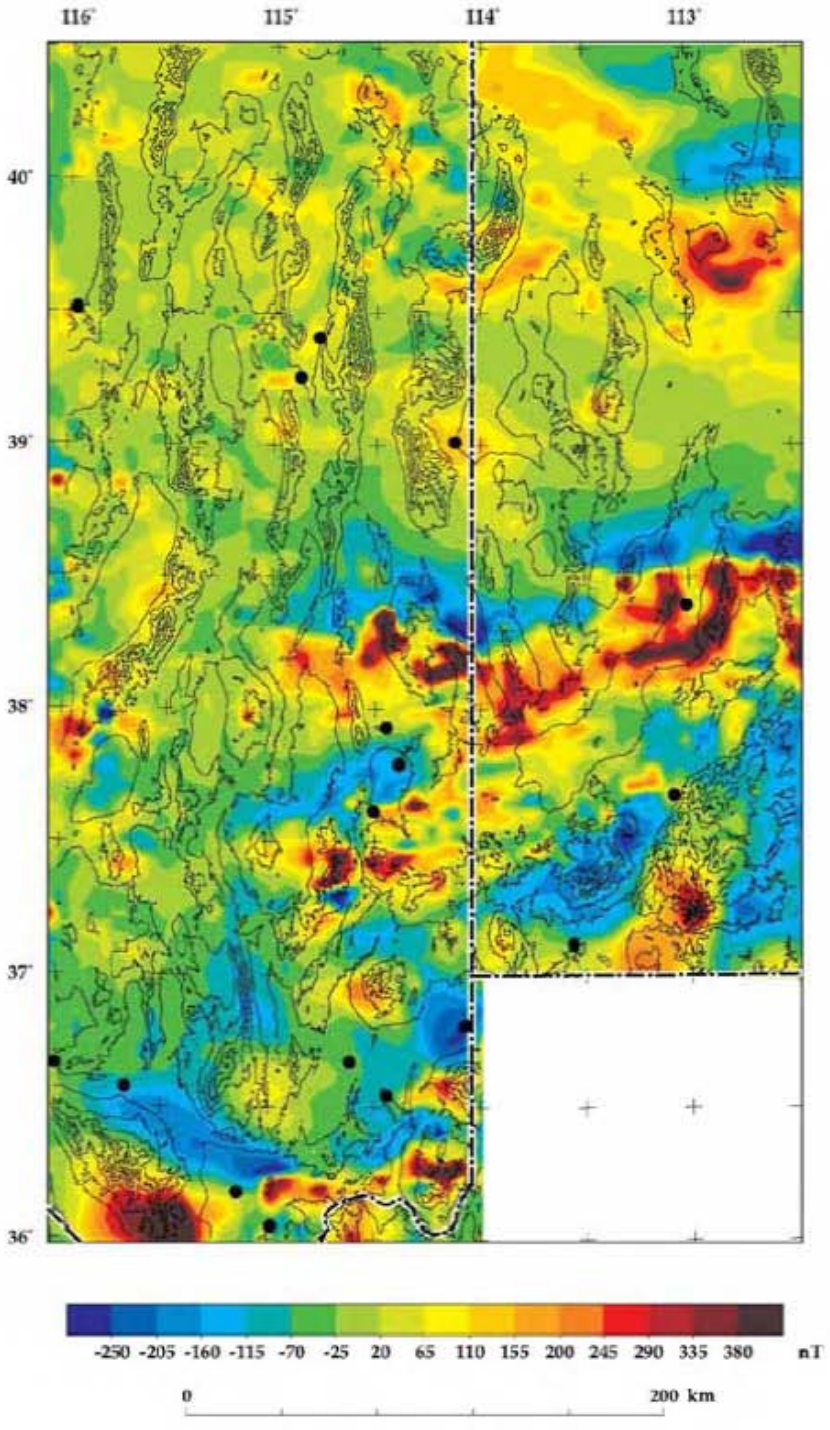

Figure 14. Aeromagnetic map of eastern Nevada and western Utah. Black dots are towns. Topographic contour interval is 400 m.

Horizontal Gradients

Horizontal gradients can be calculated for the long-wavelength gravity anomalies identified by the upward-continued data (e.g., Cordell, 1979; Blakely, 1995) and by the magnetic potential (Cordell and Grauch, 1985). When calculated for two-dimensional data grids, horizontal gradients will place narrow ridges over significant contrasts in gravity (figure 15) and magnetic potential (figure 16). The method of Blakely and Simpson (1986) was used to calculate the maximum values of these horizontal gradients of the upward-continued data or "maxspots," the locations of which tend to overlie the edges of causative bodies with abrupt, near-vertical contacts. These maxima identify contrasts that can help delineate deep-seated crustal structures, primarily faults that separate major tectonic domains. Figures 15 and 16 show the results of upward continuation, with calculation of maxima (small dots or maxspots) that in most places shown are faults but in some places could be caldera margins or intrusive contacts. For non-vertical contacts between geologic units of contrasting properties, maximum values of the horizontal gradients will be displaced down-dip and away from the edges of the body.

Gravity Inversion

The isostatic gravity field (figure 13) generally reflects a pronounced contrast between dense pre-Cenozoic rocks and significantly less dense overlying volcanic and sedimentary rocks. Because of this relationship, the gravity inversion method derived by Jachens and Moring (1990) can be used to separate the isostatic residual anomaly into pre-Cenozoic basement and young basin fill, and thereby provide an estimate of the thickness of Cenozoic volcanic rocks and sedimentary basin fill. Subvolcanic Cenozoic intrusions are included here as part of the basement because their physical properties are similar to most of the older rocks and differ greatly from those of the volcanic and basin-fill sequences. The method first separates gravity observations on pre-Cenozoic rocks from those on Cenozoic deposits. A modified version of the method (B.A. Chuchel, USGS, unpublished data, 2005) allows basement gravity values to be approximated by correcting the isostatic gravity anomaly at sites where depth to basement is known from deep boreholes or inferred from seismic data (e.g., Gans et al., 1985). At locations where wells did not penetrate the full thickness of the basin-fill, the maximum depths reached were used as minimum constraints in an iterative process. Constraints on the inversion process, shown in figure 17, are gravity measurements on pre-Cenozoic rocks and available well data. Information on oil and gas wells for Nevada and Utah is available at Hess (2004) and http://ogm.utah.gov/oilgas/, respectively. Additional data were obtained from Utah geothermal wells (Hintze and Davis, 2003), selected USGS test wells (Berger et al., 1987; Schaefer et al., 1989), test-well data from the MX-missile siting study in Utah (Mason et al., 1985), and SNWA test wells.

The accuracy of thickness estimates derived by the gravity inversion technique depends on the assumed density-depth relation of the Cenozoic volcanic and sedimentary rocks and on the initial density assigned to the basement rocks. Density of basement rocks is assumed to be 2670 kg/m^3, and density-depth values are from Jachens and Moring (1990). These values have been shown to be widely applicable throughout the Great Basin (Saltus and Jachens, 1995; Blakely et al., 1998, 2000; Mankinen et al., 2003). Isostatic gravity (figure 13) and the digital geology of Nevada and Utah were converted to a 2-km grid before performing the inversion. Results were then re-gridded at a spacing of 0.5 km. The result, as given in figure 18, is the depth to pre-Cenozoic basement. Deepest blue colors denote all depths greater than 3 km. The basin-thickness estimates calculated by Hurlow (2014) from gravity are somewhat greater than the more conservative estimates given here, because of slightly different assumptions.

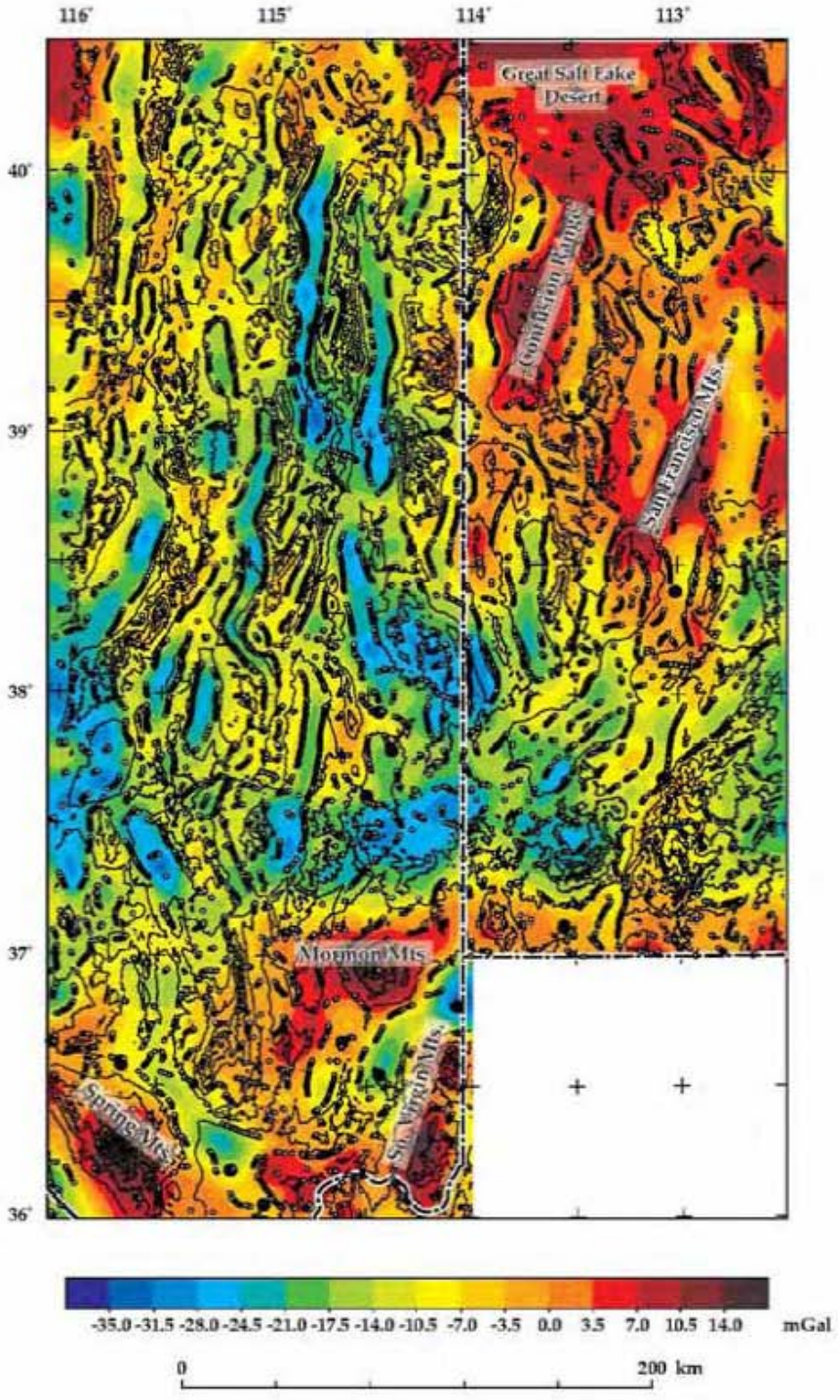

Figure 15. Isostatic gravity anomalies upward-continued by 3 km. Small dots are maxima in the horizontal gradient.

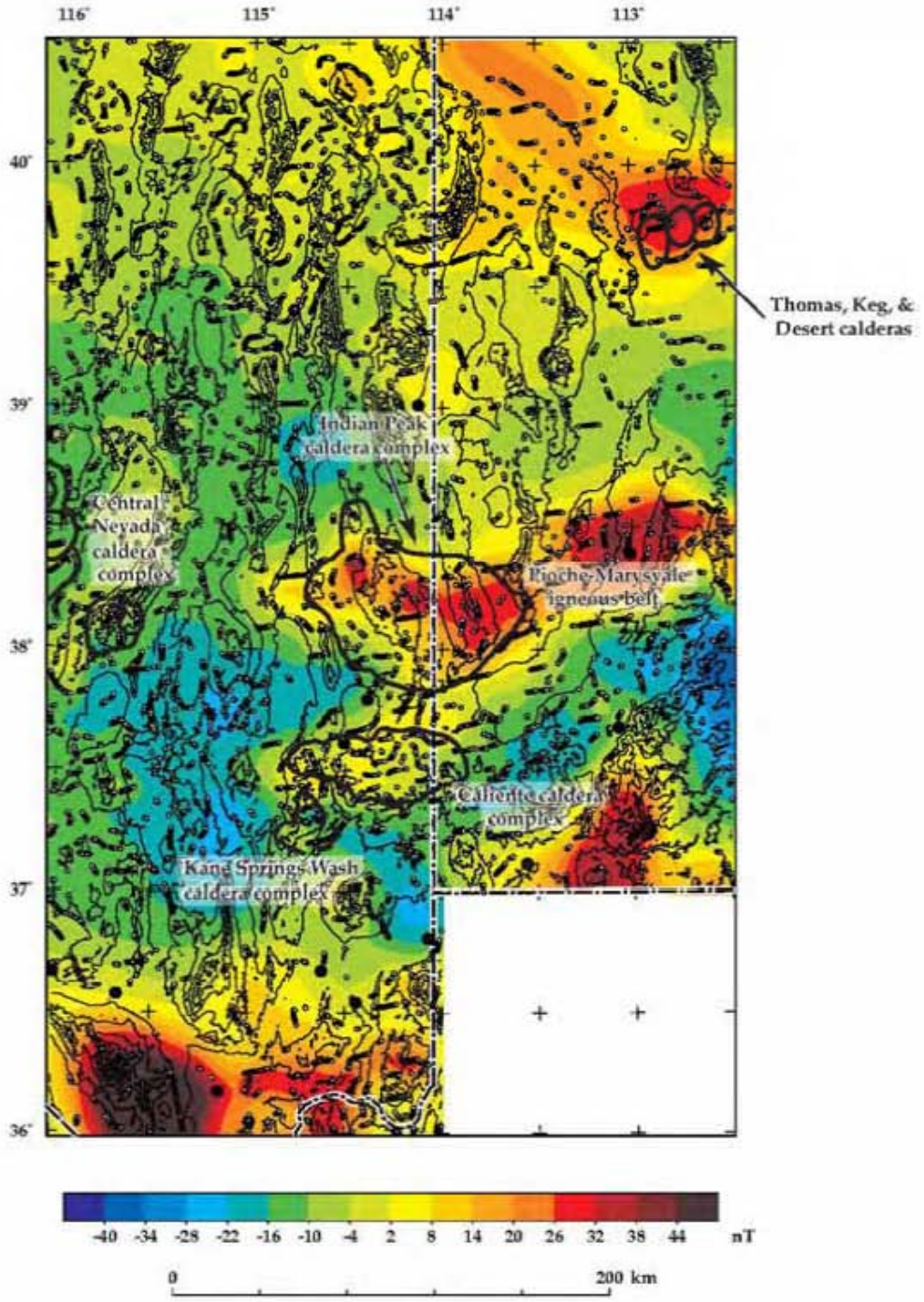

Figure 16. Aeromagnetic data transformed to their magnetic potential ("pseudogravity"). Small dots are maxima in the horizontal gradient. Heavy lines are calderas.

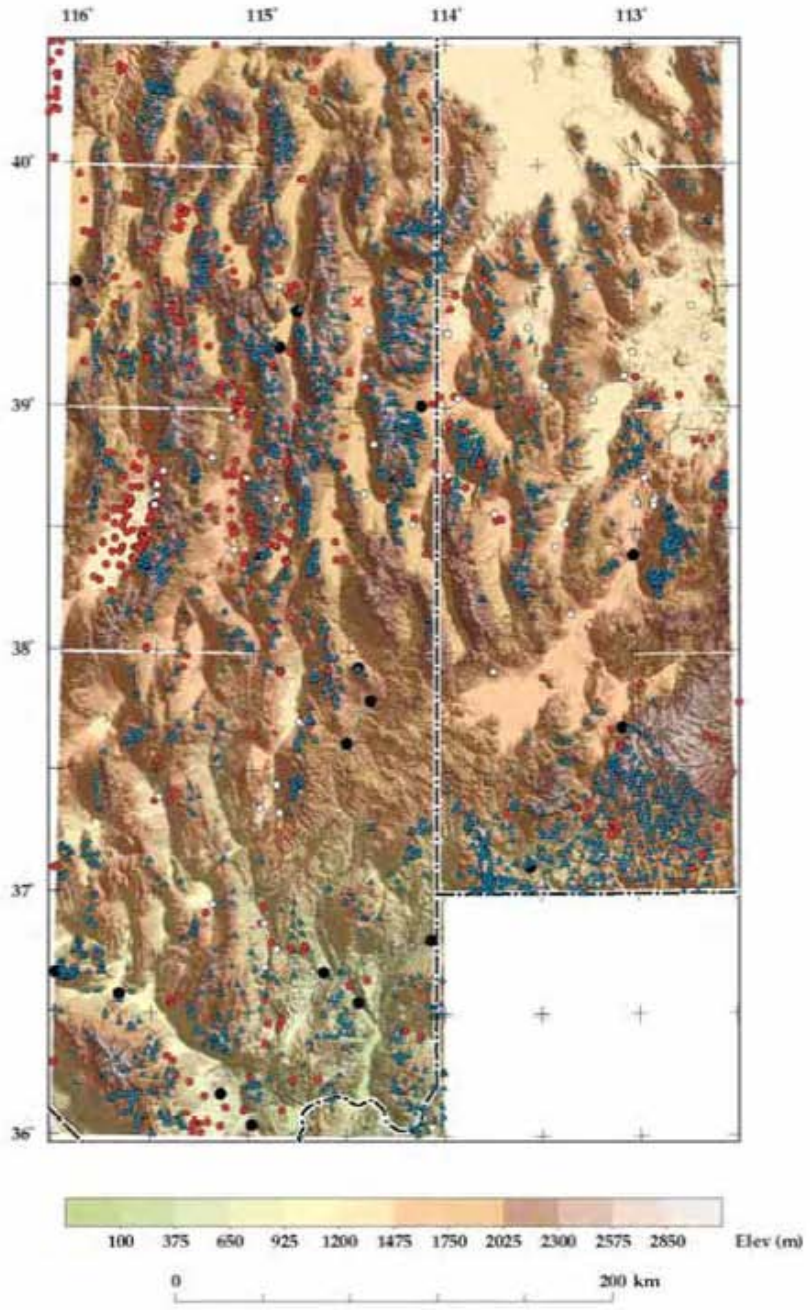

Figure 17. Constraints for the gravity inversion method. Red dots are wells spudded into or reaching pre-Cenozoic basement; white dots are wells providing minimum depth constraints; triangles are gravity observations on pre-Cenozoic basement rocks; red "x" is a pre-Cenozoic basement pick from a seismic survey (Gans et al., 1985).

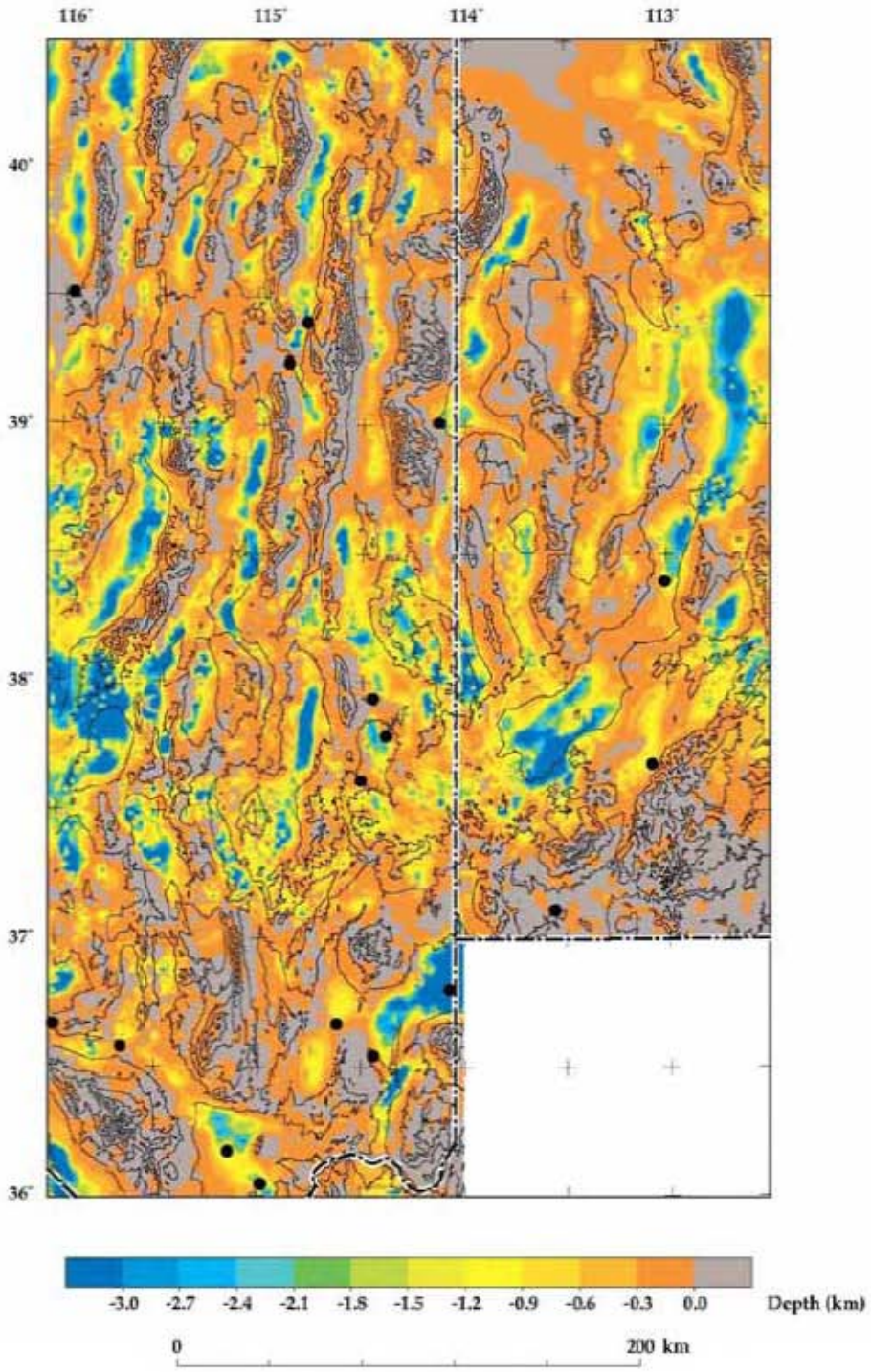

Figure 18. Depth to pre-Cenozoic basement in eastern Nevada and western Utah.

Interpretation

Regional Geophysics

Figures 13 through 18 provide geophysical data for the area shown in figure 12. The following section discusses geophysical observations, and interpretations, from across this region. Figure 13 displays the pronounced contrast between dense pre-Cenozoic rocks and significantly less dense overlying strata. Most gravity geophysicists refer to pre-Cenozoic rocks as "basement," even though that is not to mean that they are Precambrian. The Cenozoic rocks above such "basement" consist of calc-alkaline and high-silica rhyolite (bimodal) volcanic rocks and overlying basin-fill and surficial sedimentary rocks and sediments. In most cases, volcanic rocks and these sedimentary rocks cannot be distinguished by gravity data. However, Cenozoic basaltic rocks are dense and have the same higher anomalies as pre-Cenozoic rocks, but basalts are rare or thin in the general area except along the eastern edge of figure 13 south of 40°N, in the Sevier and Black Rock deserts. The pre-Cenozoic rocks underlie most ranges, which therefore are shown in shades of red, orange, and yellow (warm colors), whereas Cenozoic volcanic rocks and basin-fill sedimentary rocks most commonly underlie the valleys and basins, which are shown in blue and green (cool colors). Figure 13 has an obvious north-south linear pattern, reflecting Basin and Range deformation that produced alternating basins (grabens) and ranges (horsts). Deep basins, in dark blue, are particularly noticeable as Steptoe Valley, containing McGill and Ely (figure 12), and Spring Valley to the east. In some places, however, the Cenozoic volcanic rocks make up volcanic fields that are commonly exposed in the ranges or in calderas that typically span north-south basins and ranges. Examples of calderas (subcircular and blue) that show up particularly well are the Indian Peak caldera complex north and east of Pioche, and the Caliente caldera complex south and southeast of Caliente (figure 12). East of the Caliente caldera complex in Utah, another subcircular area in blue and green consists of calc-alkaline volcanic rocks and laccoliths exposed in the Bull Valley Mountains and Pine Valley Mountains.

There is a marked contrast in the magnitude of gravity anomalies between eastern Nevada and western Utah. This is especially true in the northern half of the area of figure 13, where ranges and even most parts of the Great Salt Lake Desert show up as strong positive anomalies, in red. These anomalies include the large red anomaly northeast of Baker (figure 12) that underlies the Confusion and Conger ranges, narrow parts that extend northward and northeastward of these ranges that underlie the Fish Springs, Thomas, and Dugway ranges, and narrow parts that extend from them southeast of Baker that underlie the Burbank Hills and Mountain Home Range. Most of these positive anomalies are caused by carbonate rocks, especially dolomite with a density of 2.8 g/cm^3, which constitutes about 80 percent of the Middle Cambrian through Permian stratigraphic sequence in these areas (Mankinen et al., 2016). Ranges with Pennsylvanian to Permian outcrops have a greater thickness of carbonate rocks than those that have only the lower part (e.g., Silurian, Ordovician, and Cambrian) of the carbonate rock sequence at the surface. We would therefore expect that ranges that have the most complete, and hence thickest, section of carbonate strata would produce the highest gravity anomalies. This interpretation is supported by the observations in figures 13 and 15, where gravity anomalies are much stronger over the Confusion Range (~7 km of carbonate rock) than over the northern House Range (~3.5 km of carbonate rock) to the east and the southern Snake Range (southeast of Baker) to the west. About a 1 to 2 km thick sequence of quartzose rocks (densities about 2.6 g/cm^3) of the Neoproterozoic to Lower Cambrian McCoy Creek Group and Prospect Mountain Quartzite underlies much of the carbonate rock. The northern and central Snake Range, as well as the Kern Mountains and southern Deep Creek Range farther north, are cored by this quartzite and intruded by granite plutons, so here the anomalies are of much smaller amplitude (yellow).

The ranges north of Milford, Utah (figure 12, shown in bright red on figure 13) represents the San Francisco and Cricket mountains, to the south and north respectively. The San Francisco Mountains are underlain by Tertiary volcanic rocks and Neoproterozoic quartzite, whereas the Cricket

Mountains are underlain by ~2 km of Cambrian carbonate rocks. These rocks in both ranges, however, are interpreted to be underlain by large frontal Sevier thrusts that likely contain repeated sections of Paleozoic carbonates (DeCelles and Coogan, 2006), resulting in significant positive anomalies. Similar explanations are applied in the southwestern part of figure 13, where strong positive anomalies underlie the Mormon Mountains, the Meadow Valley Mountains and Arrow Canyon Range (west of Moapa, red finger on figure 13), and the Spring Mountains (far to the southwest). Here, the exposed rocks are middle and upper Paleozoic, but these areas are underlain by the large frontal Sevier thrusts of the Las Vegas area (Page et al., 2005a). The two red bullseyes south of Mesquite and southeast of Overton, however, are interpreted to be due to denser high-grade metamorphic Paleoproterozoic rocks (Page et al., 2005b; Beard et al., 2007).

The aeromagnetic map (figure 14) shows areas of high magnetization with warm colors and areas of low magnetization with cool colors. Unlike the gravity map (figure 13), a lack of north-south texture indicates that the main causes of magnetic anomalies are unrelated to the episode of Basin and Range deformation. Instead, most high (red) anomalies are due to calc-alkaline and lesser bimodal intrusions, most of which are arranged in three east- to east-northeast-trending igneous belts that span all or parts of the study area. These belts represent the main eruptive centers in the area. High magnetic anomalies in the southern part of the area (mostly southern Nevada), however, appear to be caused by Paleoproterozoic high-grade metamorphic or igneous rocks (Page et al., 2005b; Langenheim et al., 2010). Anderson (1981) and Anderson and Barnhard (1993) formerly called this same southern area an "amagmatic corridor" because of its lack of Cenozoic igneous rocks.

The three igneous belts become younger from north to south (Stewart et al., 1977; Christiansen and Yeats, 1992; Rowley, 1998; Rowley and Dixon, 2001), and in the southern Basin and Range, igneous belts are younger from south to north (Anderson, 1989; Humphreys. 2009). The igneous belts, from north to south, are the (1) Ely-Tintic igneous belt (39° to 40° N latitude) that extends at least as far west as Ely; (2) Pioche-Marysvale igneous belt that extends 100 km into Nevada (mostly south of 38° 30' N at the eastern end but both north and south of 38° N at the western end); and (3) the Delamar-Iron Springs igneous belt that also extends well into Nevada (north and south of 38° N at the eastern end but north of 37° N at the western end) (Rowley, 1998; Rowley and Dixon, 2001). The Ely-Tintic belt is less pronounced than the Pioche-Marysvale belt probably because it is older and more eroded. The Delamar-Iron Springs belt is less pronounced than the Pioche-Marysvale belt probably because many of the source plutons are high-silica granite (bimodal). The margins of some of these igneous belts are bounded by transverse zones that were active both during and subsequent to the calc-alkaline magmatism (Rowley, 1998; Rowley and Dixon, 2001). Between these belts, cool colors show basins with the same trend that contain the eruptive and sedimentary products of these centers. One such area, in the southwestern part of figure 14 north of Las Vegas, trends west-northwest; it is a basin controlled by the Las Vegas Valley shear zone, which is a transfer fault created by oblique-slip (right-lateral and normal) motion during Basin and Range deformation.

Figure 15 presents upward-continued gravity data, which provide emphasis on deeper causes of the anomalies. When compared with the anomalies of figure 13, the positive anomalies are larger. This supports the interpretation that most range-front fault contacts between the carbonate rocks that probably cause the anomalies and the basin fill on either side must be dipping toward the basin. The lines of maxspots that are the most continuous are ones where confidence is greatest that these are maxima. The locations of the maxspots suggest that most of these contacts are faults. For example, the maxspots on both sides of Steptoe and Spring Valleys agree with reconnaissance mapping of these valleys that faults bound the valley margins. Therefore, we infer that the maxspots define grabens. Similarly, the maxspots along the western side of the Confusion Range support our conclusion that this is a good fault zone that separates the range from eastern Snake Valley, although some workers have argued

otherwise. We are also confident that the western side of Snake Valley is a large fault zone, yet here the maxspots are not as continuous, probably because the gravity contrast across the fault is not as large as that on the eastern side of Snake Valley.

Figure 16 shows aeromagnetic data that have been transformed to pseudogravity in order to emphasize sources of magnetism, after which maxspots were drawn. In comparison with figure 14, the anomalies are broader and more diffuse, probably reflecting more accurately the intrusive sources of many of the anomalies, some of which are batholiths. Many of the maxspots may reflect intrusive contacts. As in figure 14, three main areas dominate the magnetic potential of the region. In the northeast part of the overall area, ash-flow tuffs and intrusions are associated with the Thomas, Keg, and Desert calderas (Shawe, 1972) in the Ely-Tintic igneous belt. The central area contains the ash-flow tuffs and intrusive rocks of the Indian Peak caldera complex (Best et al., 1989a). This complex makes up the western part of the east-trending Pioche-Marysvale igneous belt (Rowley, 1998; Rowley and Dixon, 2001), which continues eastward to the Marysvale volcanic field (Steven et al., 1984, 1990). The southern area contains thick intracaldera ash-flow tuffs of the Caliente and Kane Springs Wash caldera complexes (Rowley et al., 1995; Scott et al., 1995a), which are the western part of the east-trending Delamar-Iron Springs igneous belt.

For purposes of hydrology, an important type of geophysical data is the calculation of gravity inversion. This allows determinations of thickness of Cenozoic volcanic and sedimentary rocks above the geophysical "basement." Figure 17 gives the constraints used for this calculation. In general, in areas where there is good basement depth control from outcrops and drill holes that encountered pre-Cenozoic rocks, the inversion uncertainties are approximately 300 m (e.g., Jachens and Moring, 1990; Hildenbrand et al., 2006). Figure 18 presents the map of the results, from which depth to basement data were used directly to draw our cross sections. This determination is especially useful in estimating thickness of basin-fill deposits within structural basins, which are the primary aquifers in the area. Volcanic rocks, whose densities are similar to sedimentary basin-fill deposits, cannot be distinguished from the sedimentary rocks. Unlike the sedimentary deposits, which were deposited during or after structural development of the basins, most of the volcanic rocks predate the development of basins related to regional extension, so they are commonly exposed in the adjacent ranges. Therefore, this exposed volcanic thickness can be subtracted from the depth-to-basement thickness to determine the sedimentary basin-fill component.

Figure 18 shows that most of the major valleys have basin-fill (including the volcanic rocks) ranging from 1 to 3 km thick. Deeper (thicker) areas extend to about 6 km in Cave Valley (see also Scheirer, 2005) south-southwest of Ely, to 7 km beneath the Sevier Desert near the eastern edge of the figure 18, and to 7 km beneath Railroad Valley and Sand Spring Valley near the western edge of the figure, where several of the central Nevada calderas contribute to the thickness. The deepest basins are beneath the Escalante Desert (i.e., a depth of 9 km) west of Cedar City and the Virgin River depression/Mesquite basin (i.e., a depth of 8 km). Part of the Virgin River depression in Arizona may be as deep as 10 km (Langenheim et al., 2000).

Geophysics of Spring and Snake Valleys

The Spring and Snake valley areas (figure 19) were investigated in greater detail to better understand the aquifers as well as their interconnection, recharge, and groundwater flow. Figure 20 presents their isostatic gravity and aeromagnetic anomalies, with maxspots (small dots) added for each so as to utilize fully the horizontal gradients of the data. Solid lines in the figure are interpreted as major gravity and magnetic lineaments, whereas light blue lines are locations of ground-magnetic traverses. Maxspots are calculated for only vertical or nearly vertical density or magnetic contrasts, so low-angle faults, including thrusts, that have been suggested for the area will not be visible by this method. Some parts of the analysis were given by Mankinen et al. (2006 and 2007), Mankinen and McKee (2009), and Rowley et al. (2009) for not only the area of figure 19 but also areas in Utah farther east and south.

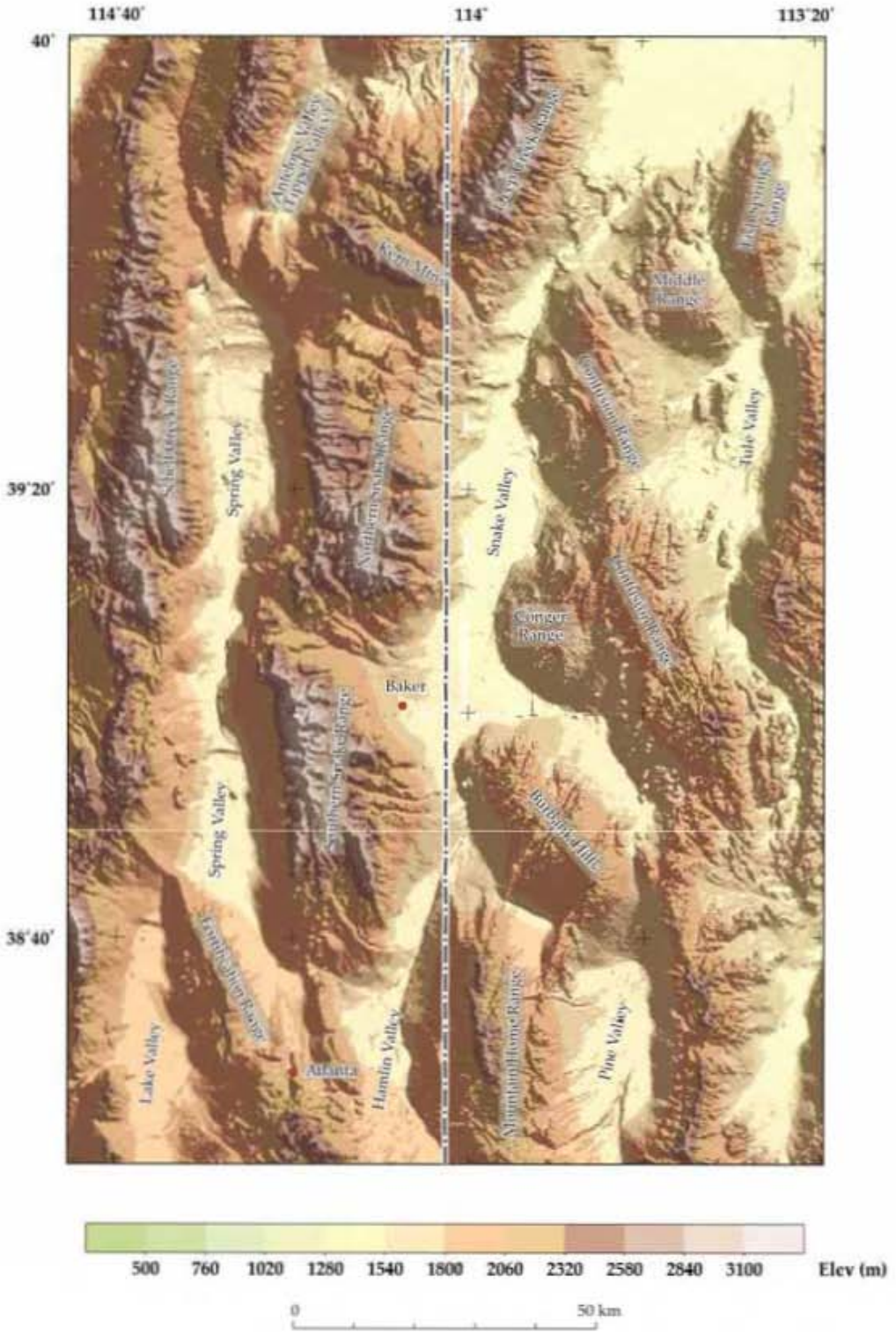

Figure 19. Shaded relief map of the Spring and Snake valley region.

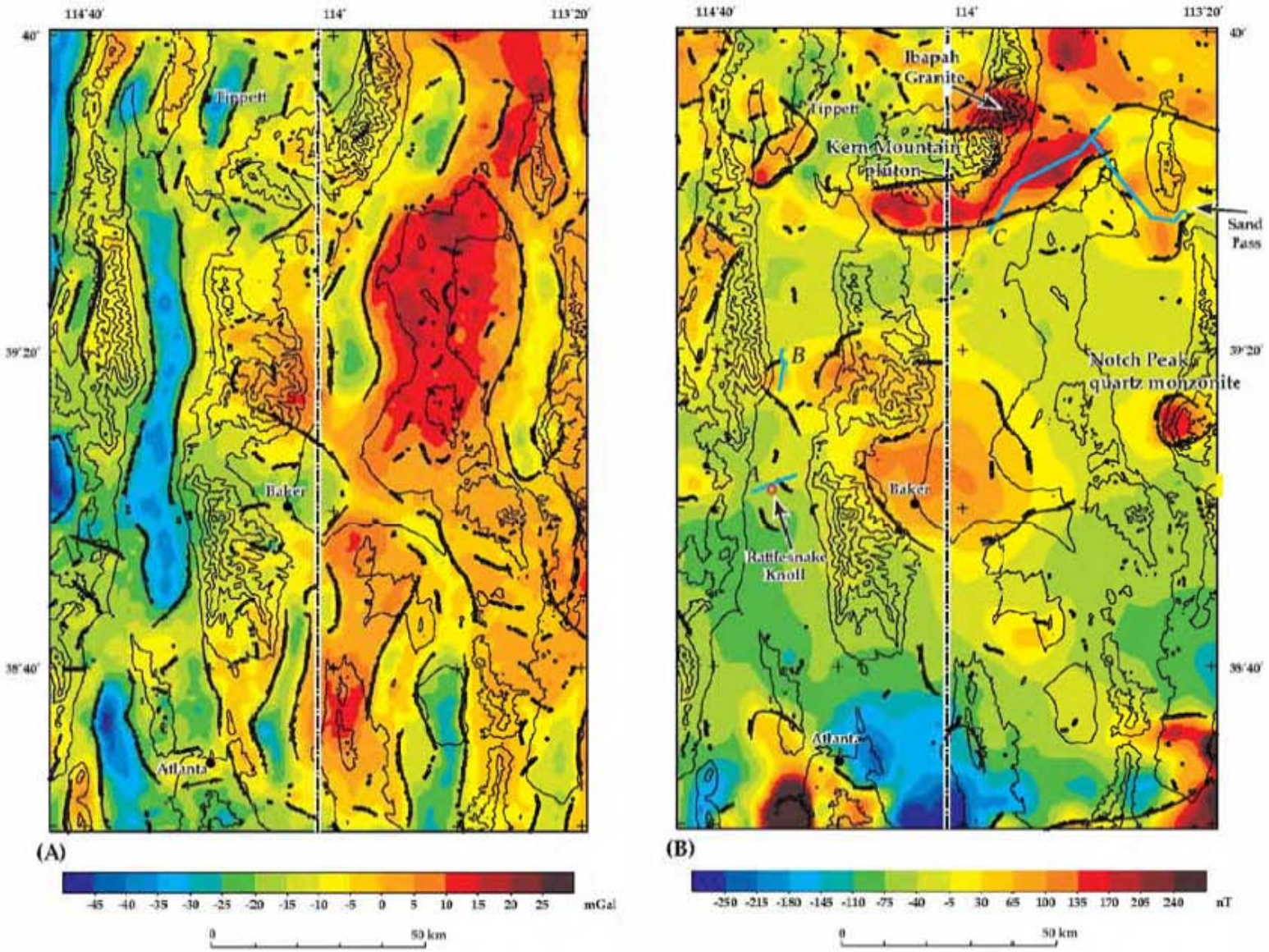

Figure 20. Isostatic gravity (A) and reduced-to-pole aeromagnetic (B) anomalies in the Spring and Snake valley area.

Figure 20a provides isostatic gravity data that delineate alternating basins and ranges by their different densities. The deepest basins (figure 18) are Spring Valley, northern Lake Valley, and—at the western edge of the figure—Steptoe Valley. Although the Snake and Hamlin valleys appear continuous and uninterrupted on the ground, Hamlin Valley is of lesser depth. Tule Valley, which separates the Confusion Range from the House Range to the east, is shallow, generally less than 1 km. All basins have deeper interior parts, or holes, reflecting local areas of deeper subsidence, largely due to concealed interior grabens.

Specifics on basin depth in Spring Valley comes from depth-to-pre-Cenozoic-basement analyses reported by Mankinen et al. (2006 and 2007) that were more detailed than given in figure 18. They showed that the volcanic rocks and basin-fill sediments in Spring Valley have a maximum thickness of almost 4 km in the northern part (west of the Antelope Range) but elsewhere are generally 1.5 to 2 km thick, and locally 3 km thick. Two geophysical sub-basins in Spring Valley are separated by an intra-valley bedrock ridge that is entirely buried to a depth of about 0.4 km by basin-fill alluvium, extending between the northern Fortification Range and the southwestern Snake Range. The southern sub-basin, west of the Limestone Hills, has a maximum depth of 1.6 km. Tippett Valley, east of the Antelope Range, has a general depth of more than 3 km but locally is 5 to 5.5 km depth. Steptoe and Hamlin valleys have a maximum depth of 3 to 3.5 km except that Steptoe Valley gets to about 4 km at its northern end. The deepest part of Snake Valley is at a depth of about 4 km, but the rest of the valley is considerably less.

South of the area of figure 19, detailed depth-to-pre-Cenozoic-basement analyses of the Cave, Dry Lake, and Delamar valleys were summarized by Mankinen et al. (2008). They found that southern Cave Valley extends down to 3 to 5 km, northern Dry Lake Valley has a maximum depth of 2 km, southern Dry Lake Valley has a maximum depth of 3 to 5 km and perhaps locally to 6.5 km, and southern Delamar Valley has a maximum depth of 2 to 3 km (figure 18, plate 1). Still farther south, Coyote Spring Valley northwest of Moapa was studied by Phelps et al. (2000), who found two deeper parts of the basin, at about 1 km deep each, just west of the Meadow Valley Mountains and north and northeast of the Arrow Canyon Range (Dixon et al., 2007a; figure 18, plate 2).

Most maxspots in figure 20a represent high-angle normal faults that have been verified by geologic mapping or are concealed and inferred by mapping. The faults shown by maxspots should be considered but a small expression of the faults in the area, for many faults juxtapose rocks of similar densities so would not be shown. The maxspots demonstrate, as also indicated by mapping, that most basins are grabens and most ranges are horsts. In the center of figure 20a, maxspots show a northwest-striking fault that crosses the state border. This is the Sacramento Pass fault, which cuts across the Snake Range closely following the highway. This fault, which is mapped on plate 1, has Pleistocene or younger displacement at its southeastern end. The maxspots do not continue northwest all the way to Spring Valley, but the gravity anomaly continues farther northwest, and northeast-trending audiomagnetotelluric (AMT) profile SNV13 farther northwest images that fault (see AMT Profile SVN13).

Greene and Herring (2013) and Greene (2014) proposed that the Confusion Range is part of an east-vergent Sevier fold-thrust system with about 10 km of horizontal shortening. They acknowledged that this area is part of the hinterland of the Sevier and Black Rock frontal thrust systems, which accommodated a minimum of ~220 km shortening (DeCelles and Coogan, 2006). Yet the interpretation of Greene and Herring (2013) and Greene (2014) suggests much greater thrust deformation than previously proposed (e.g., Hintze and Davis, 2002a and b, 2003) and is not supported by any drilling or seismic work. In other words, their new thrusts are not exposed and are hypothesized to be at great depth in the subsurface. If valid, their proposal would entail significant thickening of the stratigraphic sequence. The gravity data of figure 20a are unable to support such thickening. The gravity anomalies given in figures 13 and 20a can be accounted for by the geology as previously mapped and interpreted, and they argue against the

deep thrusts proposed by Greene and Herring (2013) and Greene (2014).

Aeromagnetic data from the Spring and Snake valley region were extracted from figure 14, reduced to the magnetic pole, and shown as figure 20b. The reduced-to-pole technique eliminates asymmetry of most anomalies and shifts their positions laterally so that they are more nearly centered over the bodies that cause them. Although one of the largest plutons in the region forms the core of the Kern Mountains, it is expressed by a weak magnetic anomaly (green). The main part of this composite pluton (the two-mica Tungstonia Granite of Best et al., 1974) is atypical of Great Basin plutons in that it has a weak magnetic signature and apparently lacks a coherent remanent magnetization (Hudson and Geissman, 1982). More clearly expressed (yellow and red) is an east-trending belt of volcanic rocks and intrusions that extend from the southern edge of the Kern Mountains into Snake Valley. Hagstrum and Gans (1989) described one of these intrusions as a Tertiary hornblende dacite pluton, containing significant Fe-Ti oxides and thus presumably more typical of Great Basin plutons. Other small plutons, mapped as Tertiary or Cretaceous in the northernmost Snake Range could be larger at depth. These plutons could also have caused the red east-trending anomaly that continues into Snake Valley, beneath basin-fill sediments. Maxspots on the northern and southern sides of the red anomaly may be intrusive contacts. The Ibapah granite (Miller et al., 1999a) of the southern Deep Creek Range clearly has a magnetic signature (red) that is typical of Great Basin plutons and also resembles the anomalies beneath Snake Valley basin fill, suggesting that the Snake Valley anomalies are down faulted Ibapah granite.

Other plutons are apparent in figure 20b. The sharp positive anomaly beneath the Notch Peak quartz monzonite (Hintze and Davis, 2003) is obvious in the southern House Range, and its maxspots are probably intrusive contacts. Even stronger positive anomalies apparent at the southern edge of the figure represent intracaldera intrusions in the Indian Peak caldera complex. The western of these anomalies may have led to the mineral deposits in the Atlanta mining district (figure 19). A large subdued anomaly in the middle of figure 20b doubtless represents one or more plutons that are exposed in the area and mapped as Jurassic to Tertiary (Grauch et al., 1988). The largest of these exposed plutons is just north of Sacramento Pass, near the center of the strongest part of the anomaly. The overall anomaly is ringed by maxima (maxspots) that are suggestive of intrusive contacts except for the southern part of the southwesternmost one, which may be due to the Sacramento Pass fault. Subdued anomalies on either side of the northern Fish Springs Range represent a buried pluton that has been intersected during drilling in the adjacent Fish Springs mining district (Staargaard, 2009; Rowley et al., 2009). The western of these anomalies continues northwest to the edge of the area covered by the figure.

Four ground magnetic traverses, shown by blue lines in figure 20b, were done in Spring and Snake valleys. Profile A is along U.S Highway 50 adjacent to Rattlesnake Knoll, which consists of bedded volcanic breccia that has been mined for fluorspar. Rattlesnake Knoll protrudes into the middle of Spring Valley and is interpreted to represent a buried east-trending bedrock ridge (see also AMT profile POD 54010,) at about 600 m depth that crosses the graben (Mankinen et al 2007). Profile B, farther north, was designed to investigate a subdued magnetic high in Spring Valley, which we conclude is caused by calc-alkaline volcanic rocks within the fill at a depth of 400 m (Mankinen et al., 2007).

Profile C crossed Snake Valley to investigate the origin and depth of the strong anomalies, probably plutons. Mankinen and McKee (2009) interpreted the source to be at a depth of about 800 m near the southwestern end of the traverse, and at a depth of 200–500 m near the northeast end of the traverse. Profile D traversed from Snake Valley at the northwest along a road between the Middle Range and Fish Springs Range to Sand Pass (Mankinen and McKee, 2009). From the northwest end, it passed along basaltic rocks at the surface and depth, then crossed a sharper positive anomaly interpreted to be a buried pluton at the northern end of Tule Valley, and then crossed a small positive anomaly at Sand Pass interpreted to be a buried part of a pluton found by Chidsey (1978).

AUDIOMAGNETOTELLURIC STUDIES

Collection and Processing of Data

Audiomagnetotelluric (AMT) technology detects variations in shallow (<300 m) subsurface electrical resistivity. The results are presented as a two-dimensional cross section model along a linear profile perpendicular to geologic structures. The technology is a valuable tool to map subsurface faults and the lithology of shallow parts of basins (McPhee et al., 2006a, b, 2007, 2008, 2009; Pari and Baird, 2011).

AMT uses the magnetotelluric (MT) method, a technique that applies the earth's natural electromagnetic fields as an energy source to investigate the electrical resistivity structure of the subsurface (Telford et al., 1990; Vozoff, 1991). Within the earth's upper crust, the resistivity of geologic units is largely dependent on their fluid content, porosity, density, fractures, and conductive mineral content (Keller, 1987). Saline fluids within pore spaces and fracture openings can reduce bulk resistivity by several orders of magnitude relative to dry rock. Resistivity can also be lowered by the presence of conductive clay minerals, graphite, and metallic sulfide minerals. Tables of electrical resistivity for a variety of rocks, minerals, and geologic environments may be found in Keller (1987) and Palacky (1987). For example, marine shale, mudstone, Pleistocene lake beds, and clay-rich alluvium are normally conductive, with values of a few tens of ohm-m (ohm-meters). Fault zones can appear as low-resistivity (i.e., high conductivity) units of less than 100 ohm-m when they are composed of rocks fractured enough to host fluids and clay alteration minerals (Eberhart-Phillips et al., 1995). Carbonate and clastic rocks are moderately to highly resistive, having values of hundreds to thousands of ohm-m depending on their fluid content, porosity, fractures, and impurities. Unaltered, metamorphic, and nongraphitic rocks are moderately to highly resistive. Unaltered, unfractured igneous rocks normally are resistive and have values greater than 500 ohm-m.

Using the same principles as the MT method, the AMT method estimates the electrical resistivity of the earth over depth ranges of a few meters to about one kilometer, depending upon site conditions, using a high-frequency range (Zonge and Hughes, 1991; McPhee et al., 2006a), whereas MT typically uses a lower frequency range. In areas where the resistivity distribution does not change rapidly from station to station, resistivity soundings provide a good estimate of the resistivity layering beneath the site.

Interpretation

AMT profiling was done in the Spring, Snake, Cave, Dry Lake, and Delamar valleys to define the faults, interpret the stratigraphy, and aid in siting drill-hole locations. Most profiles were oriented east-west, perpendicular to mapped and inferred faults. Initially, the data in the profiles were collected by the USGS through a cooperative agreement with SNWA and largely interpreted by SNWA. Later profiles were collected by Layne Geosciences (2009), working for SNWA, and interpreted by SNWA. More recent profiles were entirely collected and interpreted by SNWA. Except for the profiles in Snake Valley, we show the location of each profile plotted on a geologic map, below which is the 2D inversion model with its interpretation. The vertical scale to the right of the model gives resistivity, in ohm-m. We use the words resistivity and conductivity to describe the anomalies, but the reader should remember that they have opposite meanings: low resistivity is the same as high conductivity, and high resistivity is the same as low conductivity. All except the profiles in Snake Valley and one in Spring Valley are described in greater detail by Pari and Baird (2011). Those profiles that were collected and first published by the USGS are noted. The profiles within each valley are described from north to south.

Spring Valley

The most AMT profiles (i.e., 26) were done in Spring Valley. All profiles were interpreted by SNWA and all but one are discussed by Pari and Baird (2011). Only nine of the analyzed profiles are presented here, from north to south, as shown in figure 21. Four of these were collected and first published by the USGS, as noted below. Of the rest,

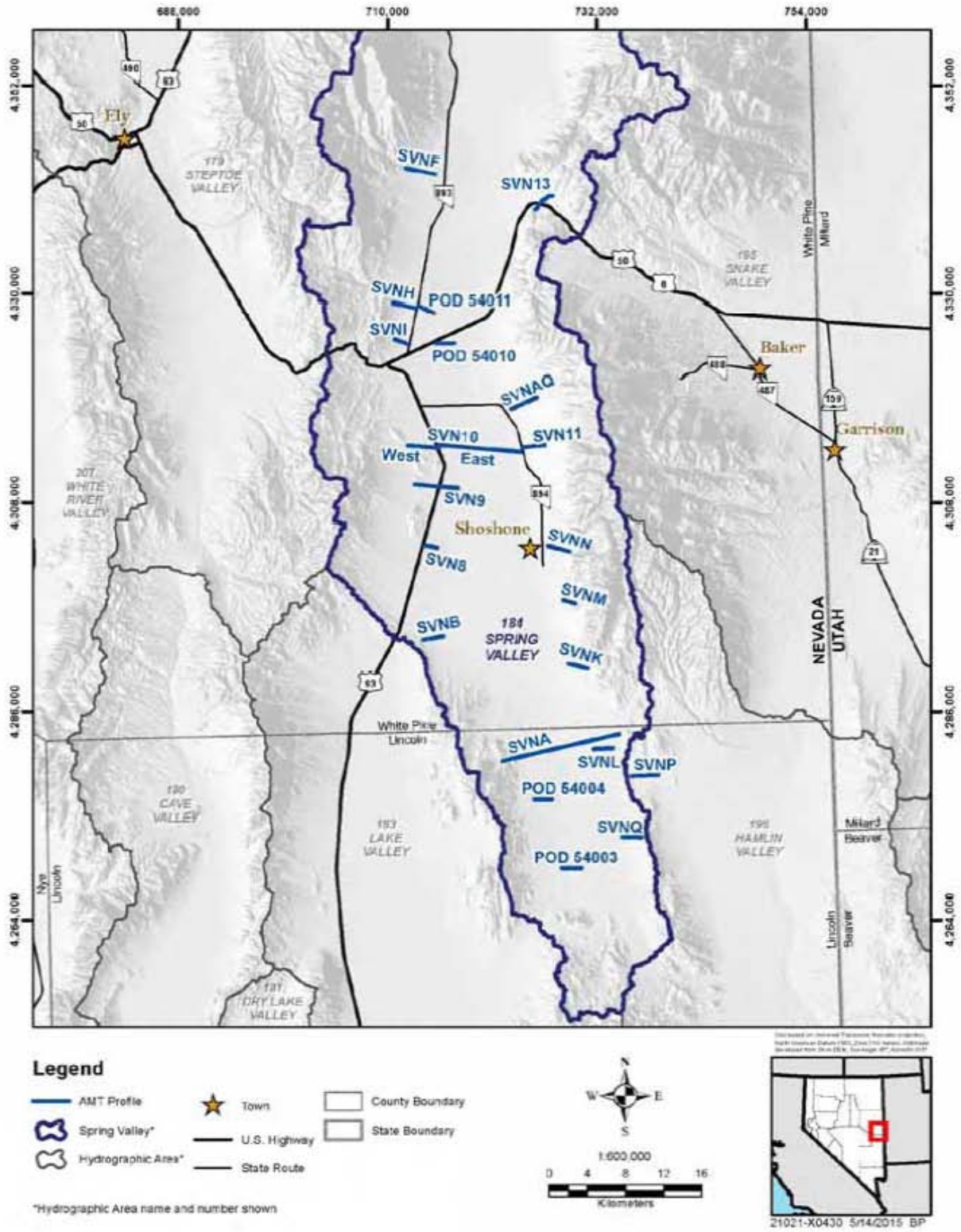

Figure 21. Map of Spring Valley area showing locations of AMT profiles.

profile SVN13 was collected and interpreted by SNWA, whereas the rest were collected by Layne Geosciences (2009) and interpreted by SNWA.

AMT Profile SVN13

Profile SNV13 (figure 22) was designed to extend northeastward for 2.3 km so as to cross and confirm a large concealed, northwest-striking oblique-slip fault mapped through Sacramento Pass at the eastern edge of Spring Valley (plate 1; also Dixon et al., 2007a, and Rowley et al., 2009). The fault shows up as a large resistivity contrast at about the 0.6 to 0.7 km mark in the profile; this clear, broad anomaly is characteristic of large oblique-slip or strike-slip faults, such as in parts of Dry Lake Valley (AMT Profile DLV50) and the Pahranagat shear zone in southern Delamar Valley (AMT Profile DELA5 and AMT Profile DELA1), which strikes northeast and has left-lateral offset. Such faults are heavily fractured and commonly carry groundwater, and other parts of the high-conductivity anomaly may owe to hydrothermal clays and gouge in the fault zone. The strike of the fault suggests that the strike-slip component is right lateral, as is commonly the case with northwest-striking faults subject to east-west Basin and Range extension in the Great Basin. The fault entirely crosses the pass and the Snake Range, from Spring Valley to Snake Valley. It passes into or cuts down-to-the-east normal faults that displace Snake Valley downward, relative to the Snake Range, near Baker. Smaller faults are apparent in the profile: (1) a concealed relatively small down-to-the-southwest fault near the left edge of the profile, and (2) a concealed fault that crosses the profile southwest of Rock Spring and results in a significant resistivity contrast near the right side of the profile. This latter fault may be the same one that is exposed eastward on the geologic map and that separates Ordovician from Precambrian bedrock. It was considered by Hose and Blake (1976) to be relatively low angle, although the profile suggests that this fault is relatively high angle, and it is shown as such in the profile interpretation.

AMT Profile POD 54010

Profile POD 54010 (figure 23) was completed near the center of Spring Valley, just south of U.S. Highway 6/U.S. Highway 50 and north and east of Rattlesnake Knoll, a small hill of volcanic breccia that protrudes from the basin fill (see also the ground magnetic profile described in Geophysics of Spring and Snake Valleys). The profile is about 2.0 km long and passes through the location of a Point of Diversion (POD) application of SNWA. Station S5 was not used in the modeling process due to poor data quality from an unknown noise source. The profile defines a deep graben east of Rattlesnake Knoll. The fault block at and just east of Rattlesnake Knoll is relatively shallow, for it is underlain by high-resistivity bedrock. The high-conductivity basin-fill rocks in the upper part of this shallower block and in the graben to the east are probably playa lake beds and/or beds containing significant groundwater.

AMT Profile SVN10 West

Profile SVN10 West (figure 24) was completed in western Spring Valley, about 10 km south of U.S. Highway 6/U.S. Highway 50 and mostly west of U.S. Highway 93, on the northern side of a horst block of carbonate rocks protruding from the basin fill. The profile, about 3.2 km long, was sited to identify faults in the large normal fault zone that defines the eastern side of the Schell Creek Range. Shallow and deep resistivity contrasts are interpreted as faults. The carbonates show high resistivity, and the eastern faults bound high conductivity rocks that probably are lake beds and/or large amounts of groundwater.

AMT Profile SVN10 East

Profile SVN10 East (figure 25) extends for 8.5 km east of U.S. Highway 93 across the main graben of Spring Valley, now occupied by a playa and formerly occupied by Pleistocene Lake Bonneville. In conjunction with Profile SVN10 West, the profile gives a good overview of the fault complexity of the basin in the vicinity of SNWA's Point of Diversion (POD). Stations S5, S6, S13, and S15 through S19 were not used in the

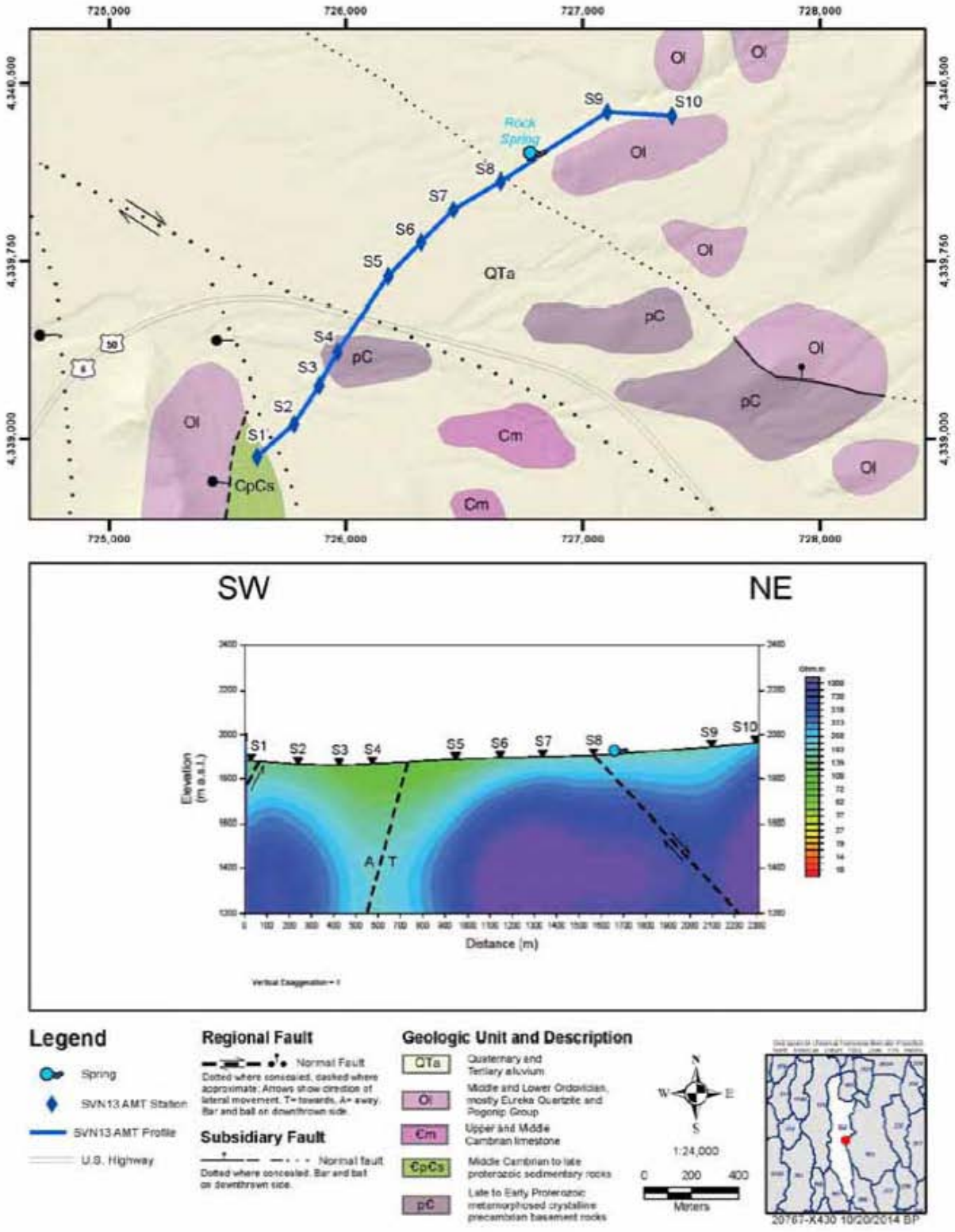

Figure 22. Geologic map and 2D model of AMT profile SVN13.

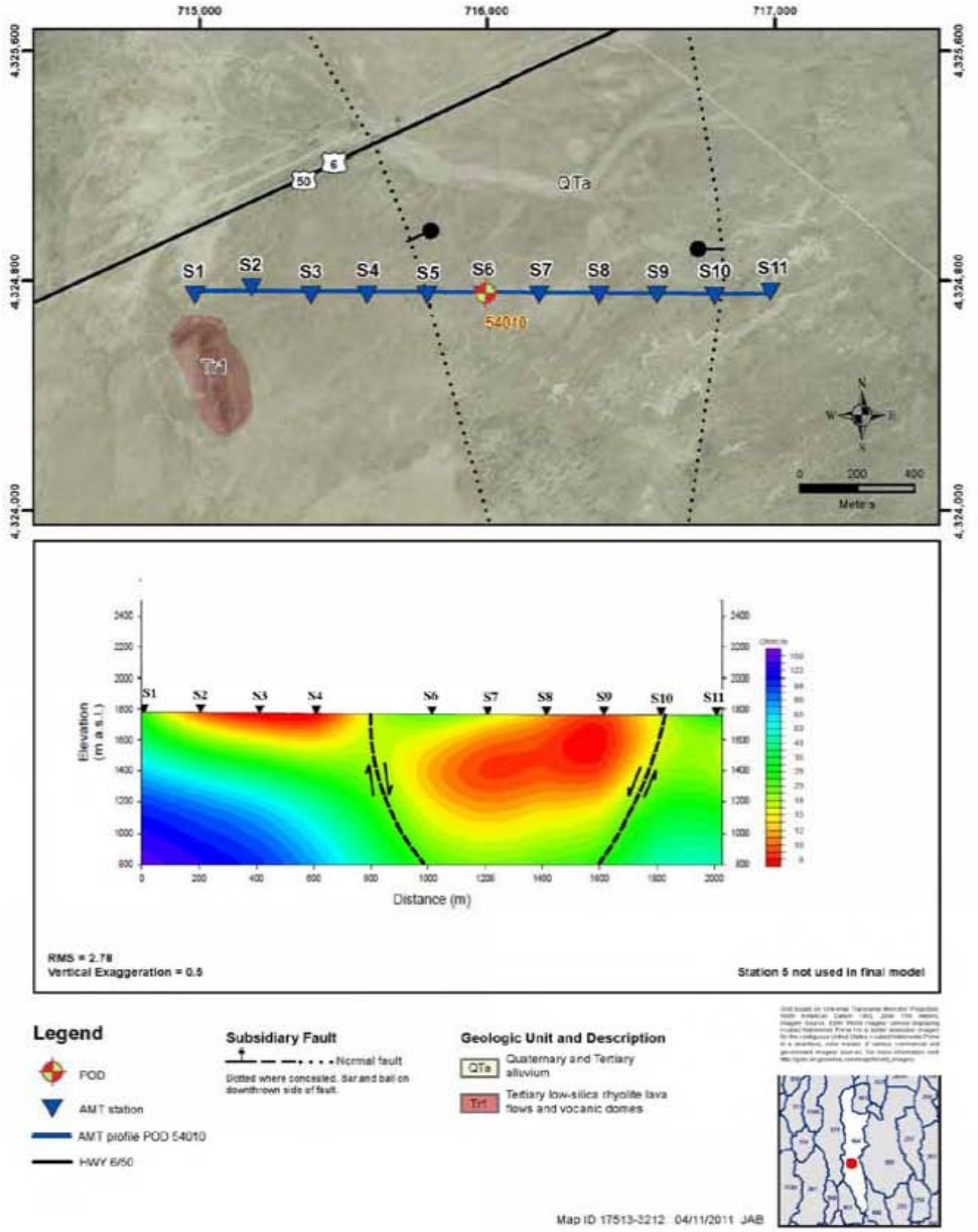

Figure 23. Geologic map and 2D model of AMT profile of area of POD54010.

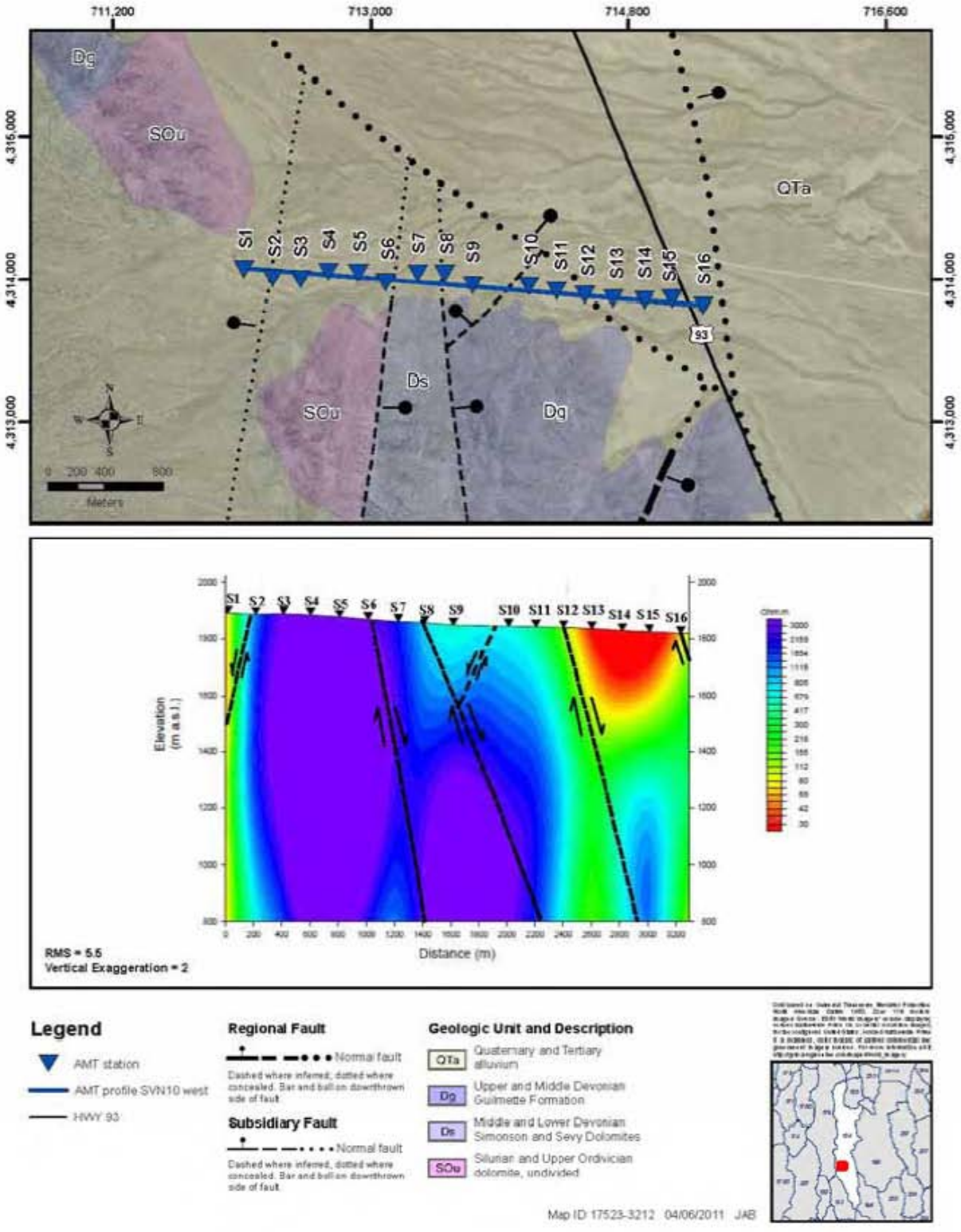

Figure 24. Geologic map and 2D model of AMT profile SVN10 West.

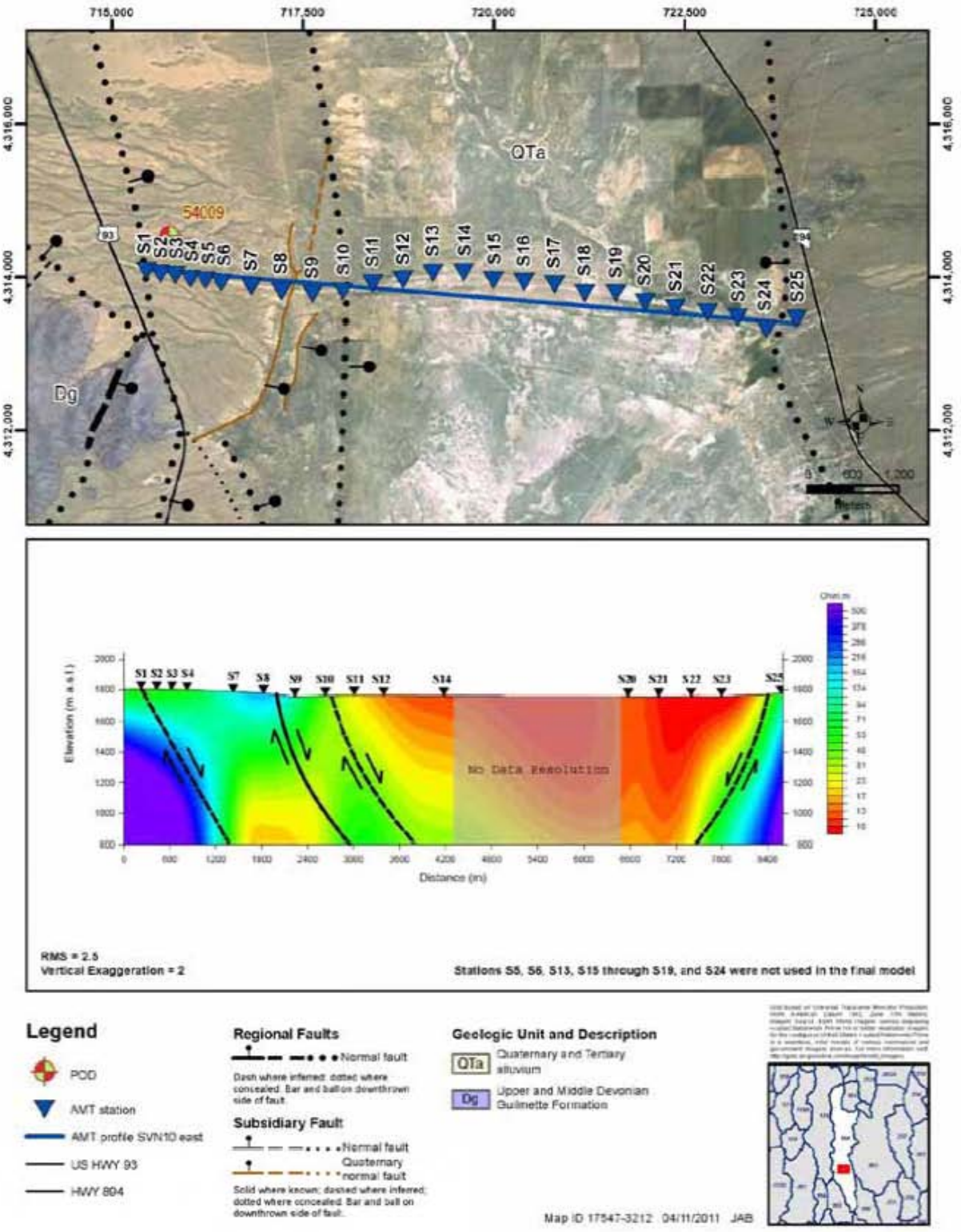

Figure 25. Geologic map and 2D model of AMT profile SVN10 East.

modeling process due to poor data quality from an unknown noise source. The fault near station S8 is a mapped fault that has Quaternary displacement. This fault, the fault east of it, and the fault at station S25 control several springs. The high-conductivity rocks between stations S10 and S25 are probably saline playa-lake deposits with significant groundwater, as are being deposited today.

AMT Profile SVN9

Profile SVN9 (figure 26) extends for 4.8 km, in western Spring Valley across the fault zone that raised the Schell Creek Range to the west. Stations S19, S21, and S24 were not included in the model due to poor data quality caused by an unknown noise source. At station S23, a large down-to-the-east fault is well displayed by the resistivity data, and its displacement is confirmed by several mapped Quaternary faults that control several springs. Lake beds and/or a low groundwater level are suggested by the anomalies east of station S14.

AMT Profile SVNN

Profile SVNN (figure 27) was completed for 2.5 km across down-to-the-west normal faults on the eastern side of Spring Valley that accommodated uplift the western Snake Range (McPhee et al., 2008). The main range-front fault passes through station S12, with highly resistive bedrock in the footwall (eastern side), and the smaller fault at station S3 is interpreted to be an intra-basin fault. Swallow Spring, near station S10, may be the cause of the higher conductivity anomaly there. The spring is perhaps controlled by a fracture or small fault related to the main fault at station S12. Alternatively, the more conductive rocks here represent finer grained beds within the basin-fill sediments. Test well SPR7007X, near station S6, was drilled by SNWA to a depth of 317 m, entirely in Quaternary and Tertiary basin-fill sediments, which here consist of coarse sand and gravel of quartzite clasts derived from erosion of the adjacent Snake Range.

AMT Profile SVNA

Profile SVNA (figure 28) extends for 12.7 km, entirely across the southern sub-basin of Spring Valley, from the Fortification Range on the west to the Limestone Hills on the east (McPhee et al., 2005, 2006a and b). The profile identified 14 faults, providing a typical example of the fault complexity of the various basins studied in the study area. Monitor well 184W508M, near station S11, was drilled by SNWA to a depth of 360 m, encountering only 27 m of basin-fill alluvium, then 332 m of nonwelded to moderately welded ash-flow tuff, which makes up the adjacent part of the Fortification Range. The higher-conductivity anomalies in the basin fill may represent groundwater and/or lake beds.

AMT Profile SVNL

Profile SVNL (figure 29) is 2.0 km long, located just south of the eastern part of Profile SVNA (McPhee et al., 2007). It was sited to identify faults between volcanic and carbonate rocks and to help interpret SNWA Test Well 184W101, which was drilled to a depth of 536 m, entirely in carbonates. At depth, beneath stations S5 to S6, the large resistivity contrast of the bedrock units juxtaposed by the fault are typical of ash-flow tuff versus carbonate rocks, with the high-conductivity bed west of the fault interpreted to be a permeable ash-fall tuff interbedded within the ash-flow tuff.

AMT Profile SVNP

Profile SVNP (figure 30) extends for 2.8 km through The Troughs, a cattle tank in a low pass through the Limestone Hills (McPhee et al., 2008). The profile was sited to provide more information on mapped faults in the area, which might provide eastward groundwater flow through the pass, from Spring Valley to Snake Valley. The high conductivity rocks beneath station S10 may be the fault itself. The basin-fill sediments farther west have higher conductivity at depth, probably reflecting

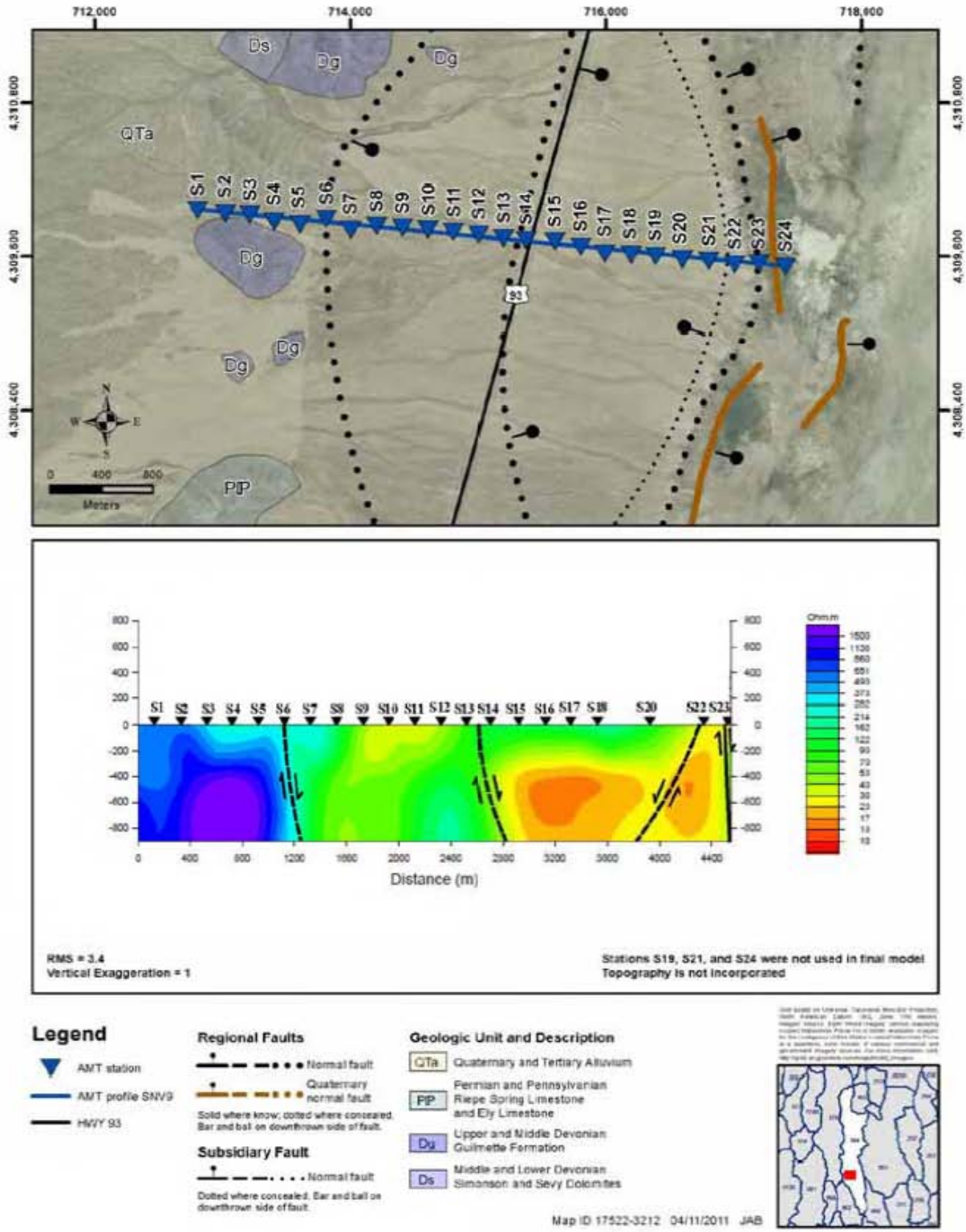

Figure 26. Geologic map and 2D model of AMT profile SVN9.

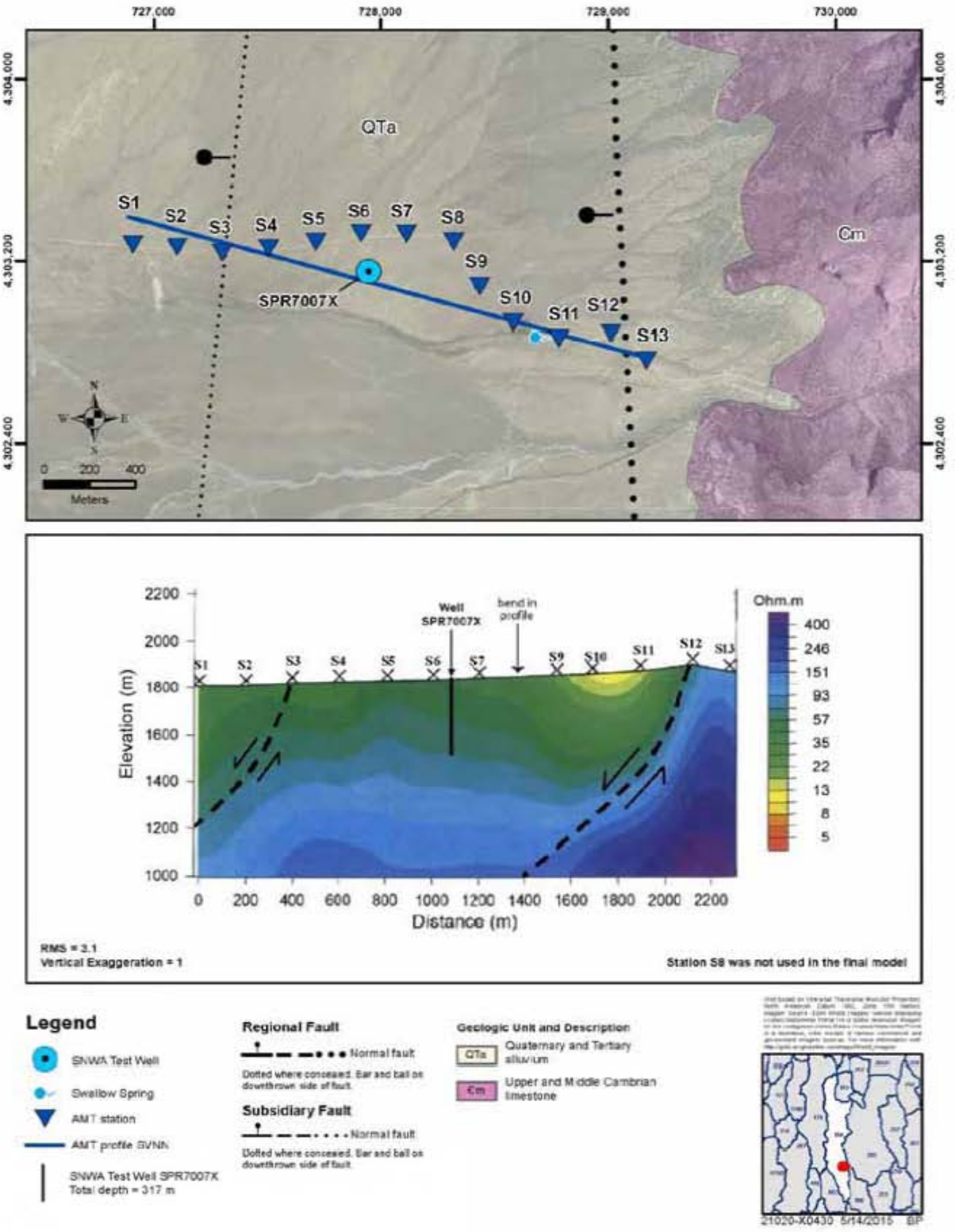

Figure 27. Geologic map and 2D model of AMT profile SVNN.

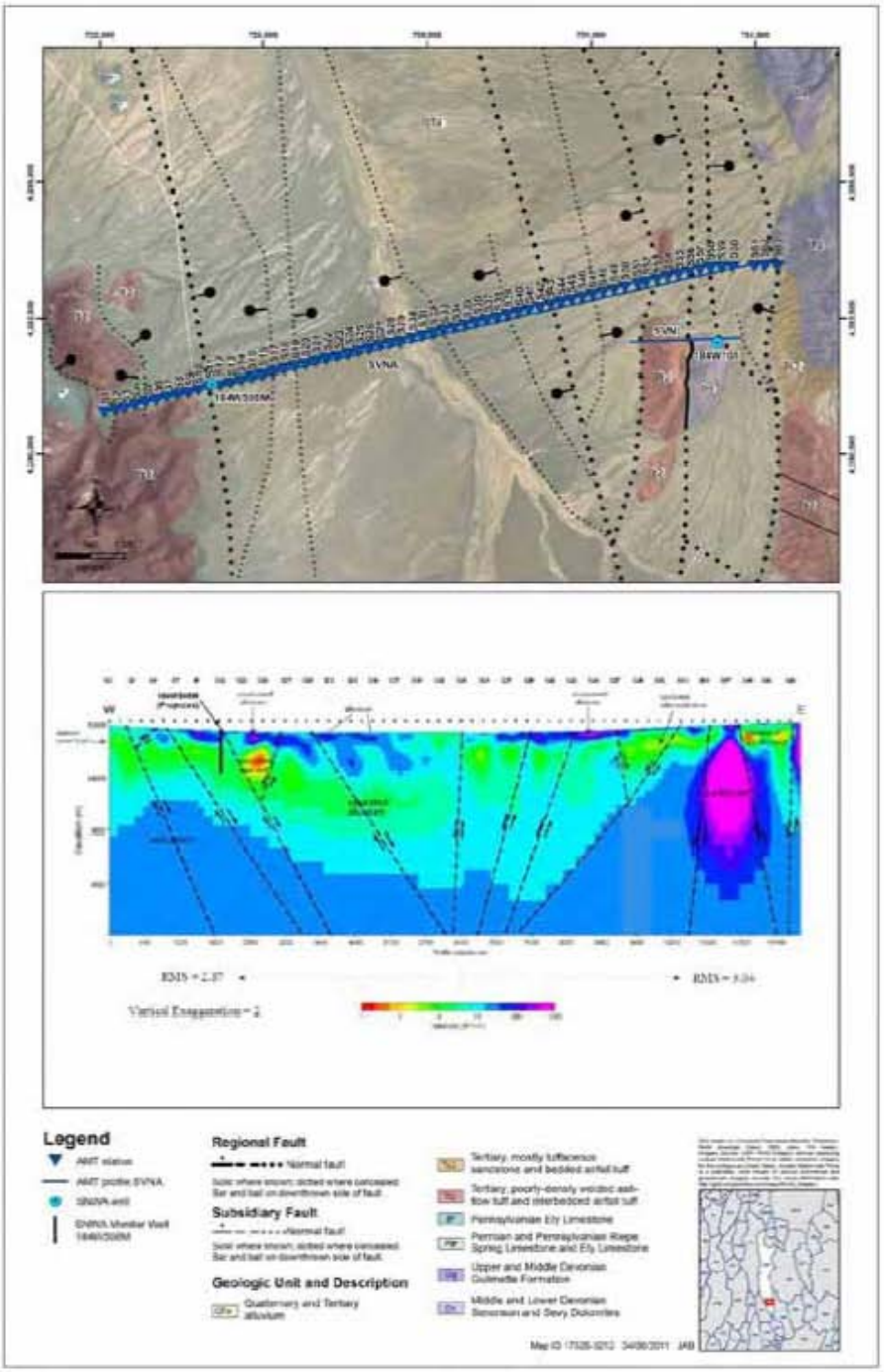

Figure 28. Geologic map and 2D model of AMT profile SVNA.

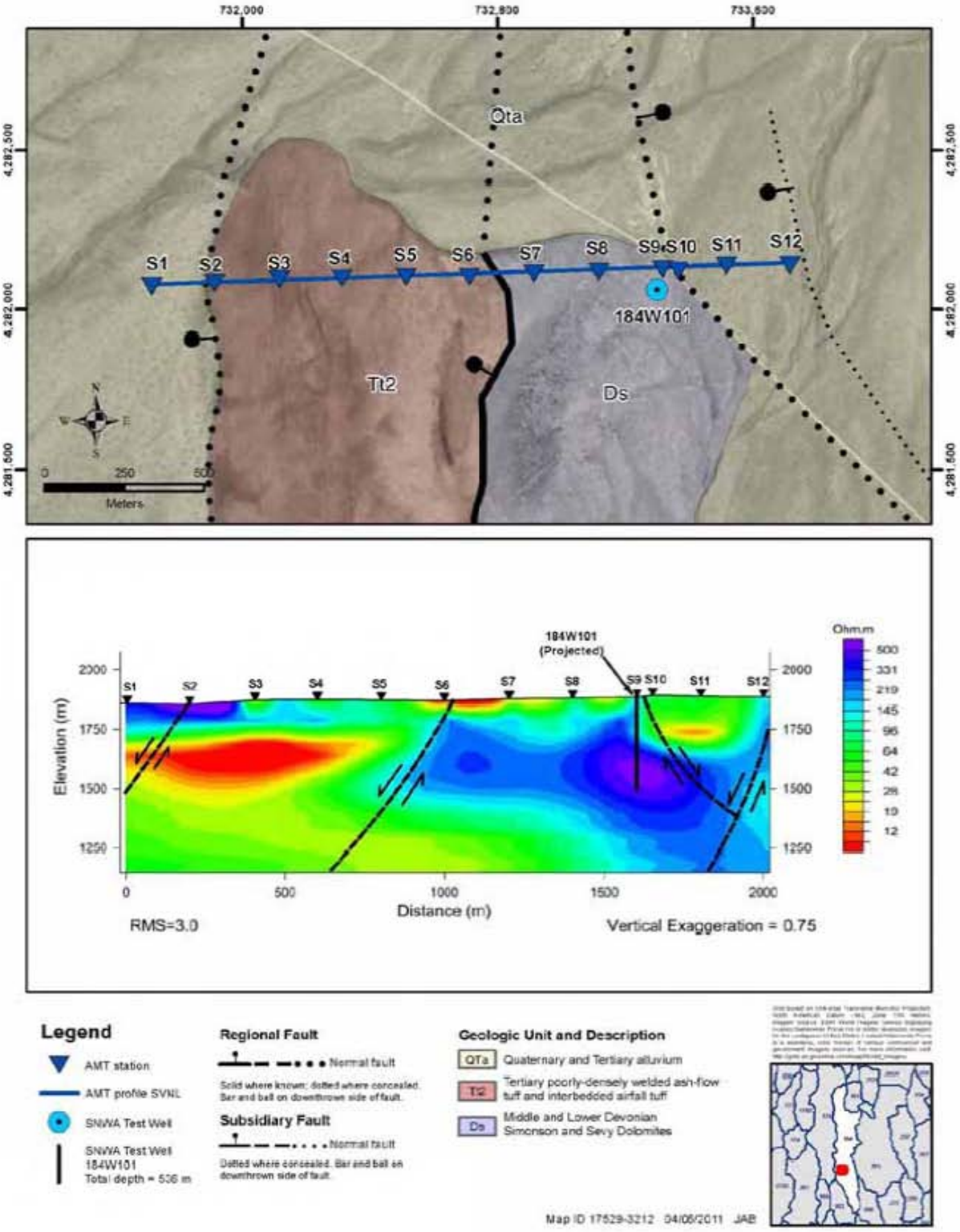

Figure 29. Geologic map and 2D model of AMT profile SVNL.

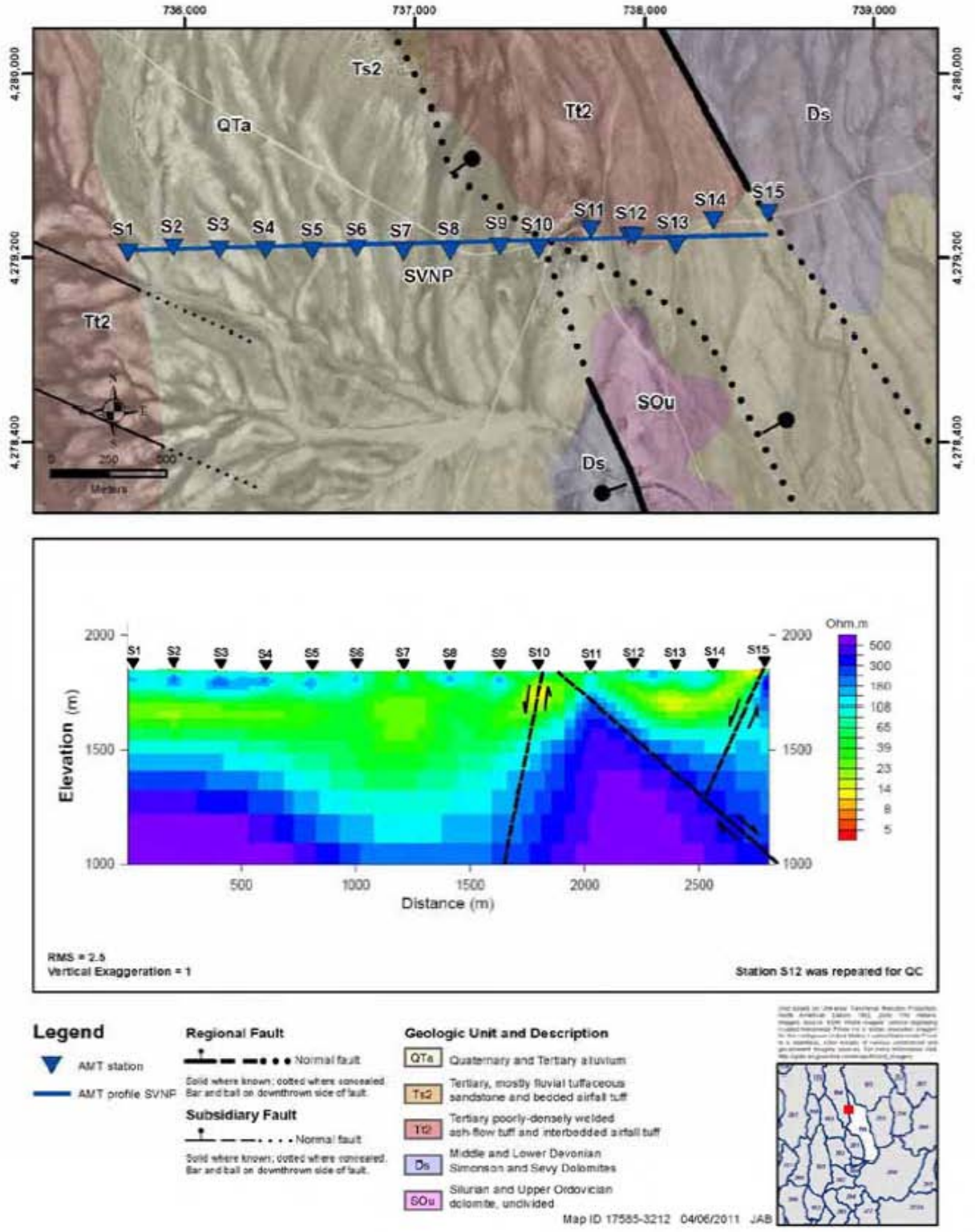

Figure 30. Geologic map and 2D model of AMT profile SVNP.

groundwater beneath a water table. The higher conductivity rocks east of S10 may represent a permeable bed within the volcanic section, perhaps ash-fall tuff.

Snake Valley

Four AMT profiles were done on the Nevada (western) side of Snake Valley. All were completed by the USGS (McPhee et al., 2007) and in part interpreted by SNWA and republished (McPhee et al., 2009). Locations and geologic setting of all of them are given on figure 31, from McPhee et al. (2009, figure 1). The profiles were intended to identify the location of the main range-front faults that raise the eastern Snake Range with respect to Snake Valley. Two of these profiles are given below.

AMT Profile SNK1

Profile SNK1 (figure 32) extends for 4.6 km from limestone bedrock at the range front, just east of which is a large range-front fault (McPhee et al., 2009, figure 3A). Farther east, the profile crosses a broad graben. A small north-south power line crosses the middle of the graben, resulting in minor model resolution in this part of the profile. Farther east, the profile continues across the eastern part of the graben, then past a narrow horst of limestone, the eastern bounding fault of which is the main range-front fault that separates the Snake Range from Snake Valley. High-conductivity rocks in the basin fill just east of this fault probably are saline playa lake beds at depth in the valley.

AMT Profile SNK4

Profile SNK4 (figure 33) extends for nearly 5.0 km from limestone bedrock at the range front eastward across basin-fill sediments to determine the fault control for springs at and near Big Springs (McPhee et al., 2009, figure 6A). Some of these faults have Pleistocene, or possibly Holocene, displacement that may be traced for kilometers as low scarps in Pleistocene alluvial fans. At the western end of the profile, basin-fill sediments are thin, then at about station 12, the large range-front fault is crossed, and higher conductivity basin-fill deposits are present to the east. Yet low-conductivity sediments occur at the surface, probably representing sediments above the water table. The basin fill is hardly uniform in appearance along the profile, requiring an interpretation of at least four more faults. The fault shown between stations 21 and 22 is interpreted to be the concealed southern part of the exposed Pleistocene fault scarp that controls Big Spring itself, about 2 km to the north. The most highly conductive rocks east of this fault is likely fine-grained lake sediments, charged with groundwater. The faults interpreted at stations 38 and 45 are considered to be the controls for, respectively, North Little Springs and South Little Springs, about 1 km north of the profile.

Cave Valley

Only one AMT profile was completed in Cave Valley. It is on the eastern side of southern Cave Valley, starting at the western part of Sidehill Pass at the edge of the Schell Creek Range (figure 34).

AMT Profile CVE

Profile CVE (figure 35) has a length of 3.4 km, as collected and interpreted by McPhee et al. (2005, 2006a and b). It is also discussed by Dixon et al. (2007a) and Pari and Baird (2011). The profile images the western range-front fault of the Schell Creek Range and shows conductive basin-fill sediments west of this fault. The lower conductivity beds at the surface are above the water table. A case could be made for several small faults west of the big fault, but the evidence is not clear. SNWA well 180W504M, drilled south of the profile and east of the main fault, penetrated basin-fill sediments to a depth of 150 m, then passed into carbonate rocks to a total depth of 272 m. Sidehill Pass Federal No. 18-13, drilled just north of the map of figure 35 and west of the big fault, penetrated 1550 m of basin-fill sediments before passing into the Mississippian Joana Limestone, then continued to a total depth of 2000 m (Hess, 2004).

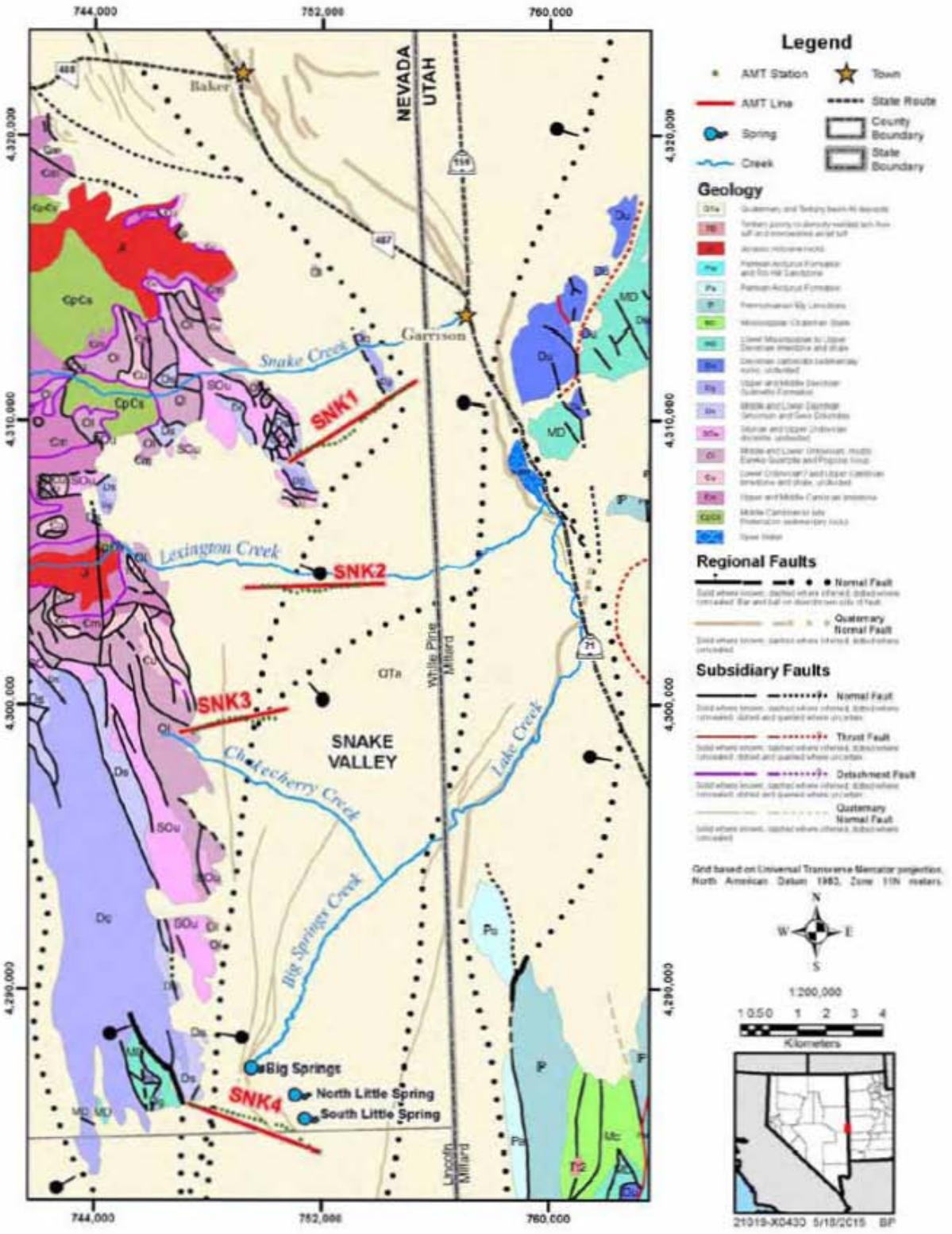

Figure 31. Map of Snake Valley area showing locations of AMT profiles.

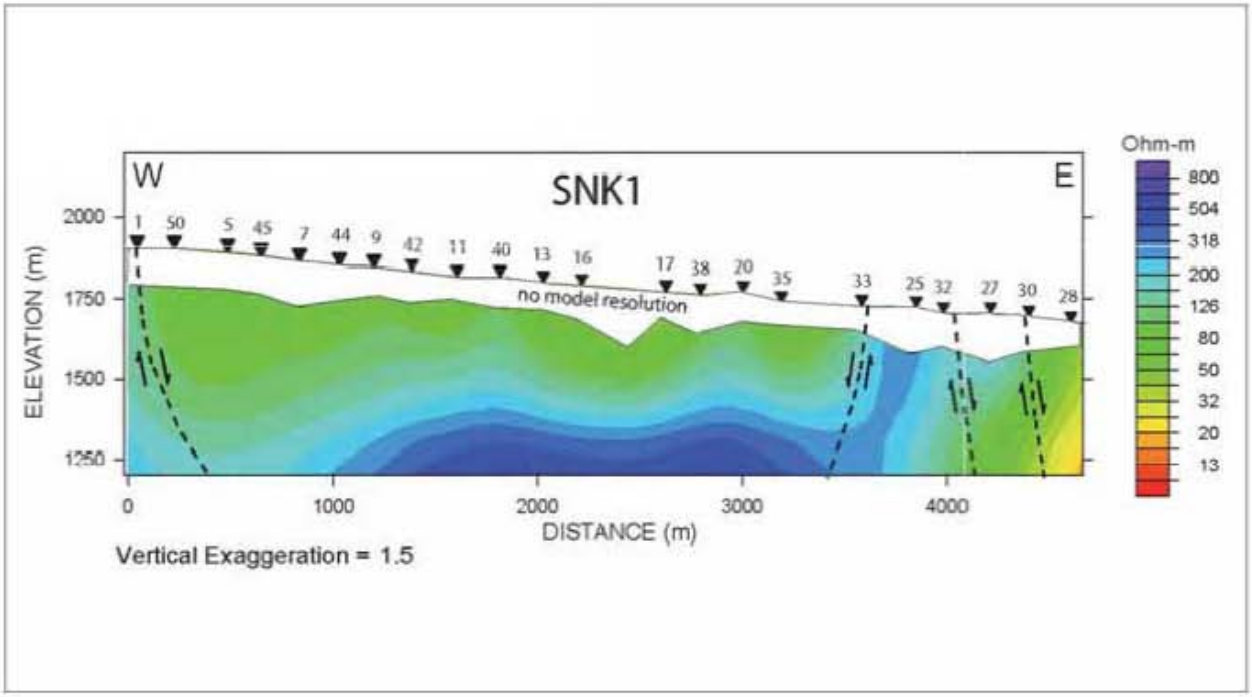

Figure 32. 2D model of AMT profile SNK1.

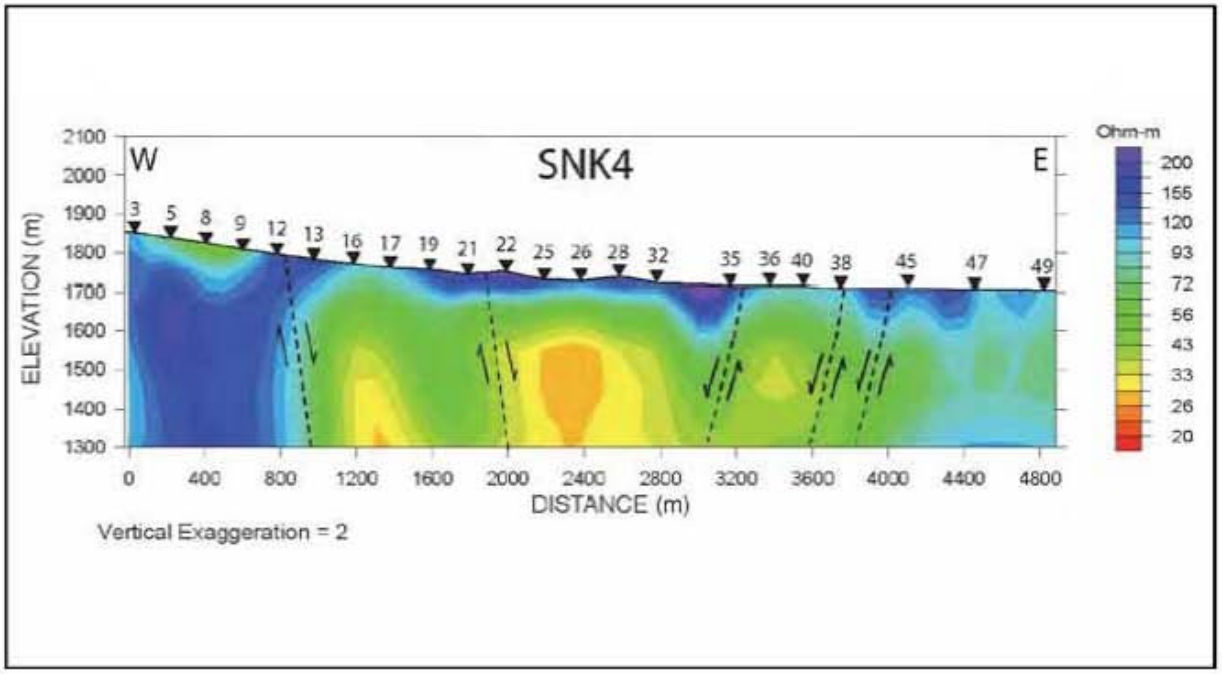

Figure 33. 2D model of AMT profile SNK4.

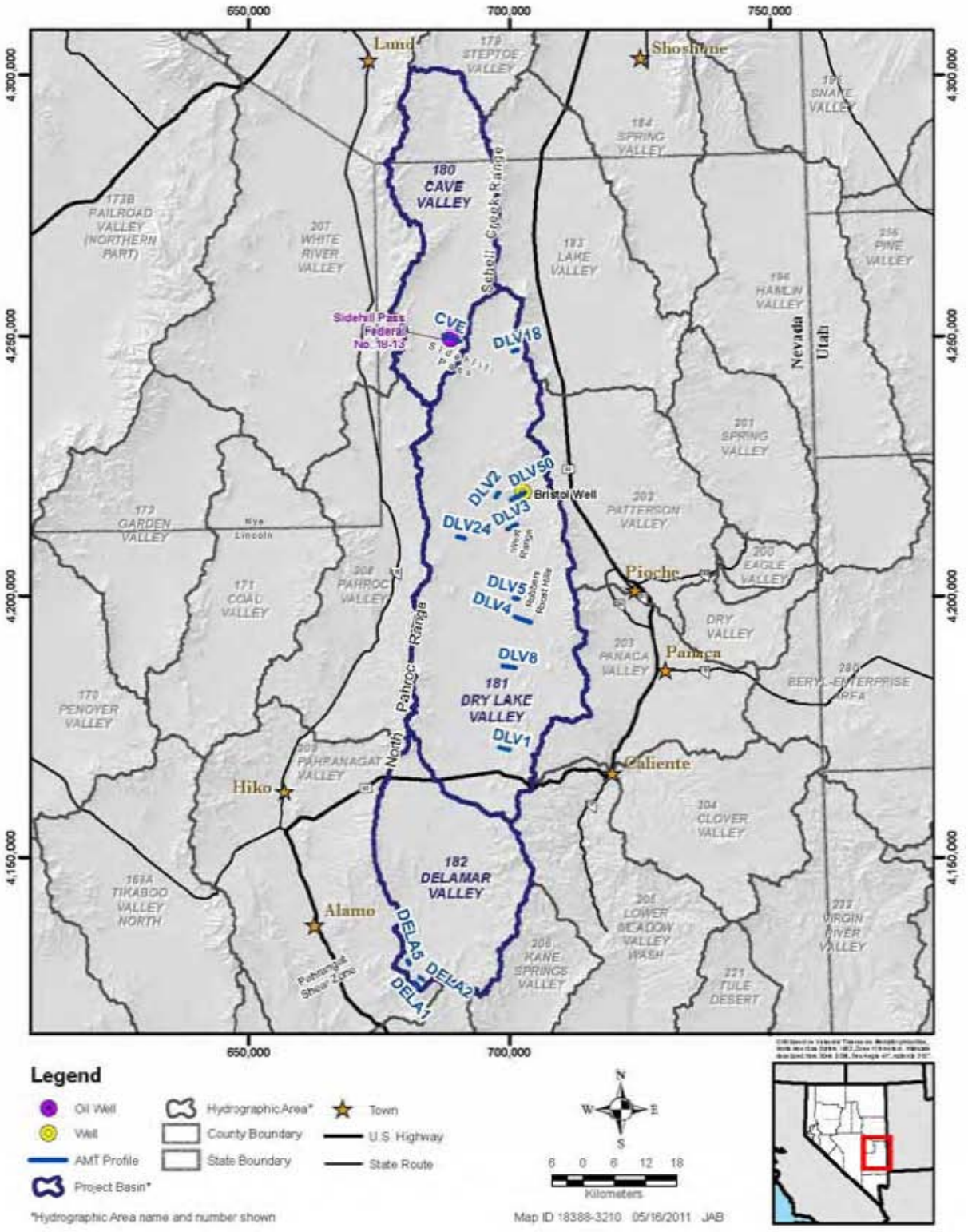

Figure 34. Map of Cave, Dry Lake, and Delamar valleys, showing locations of AMT profiles.

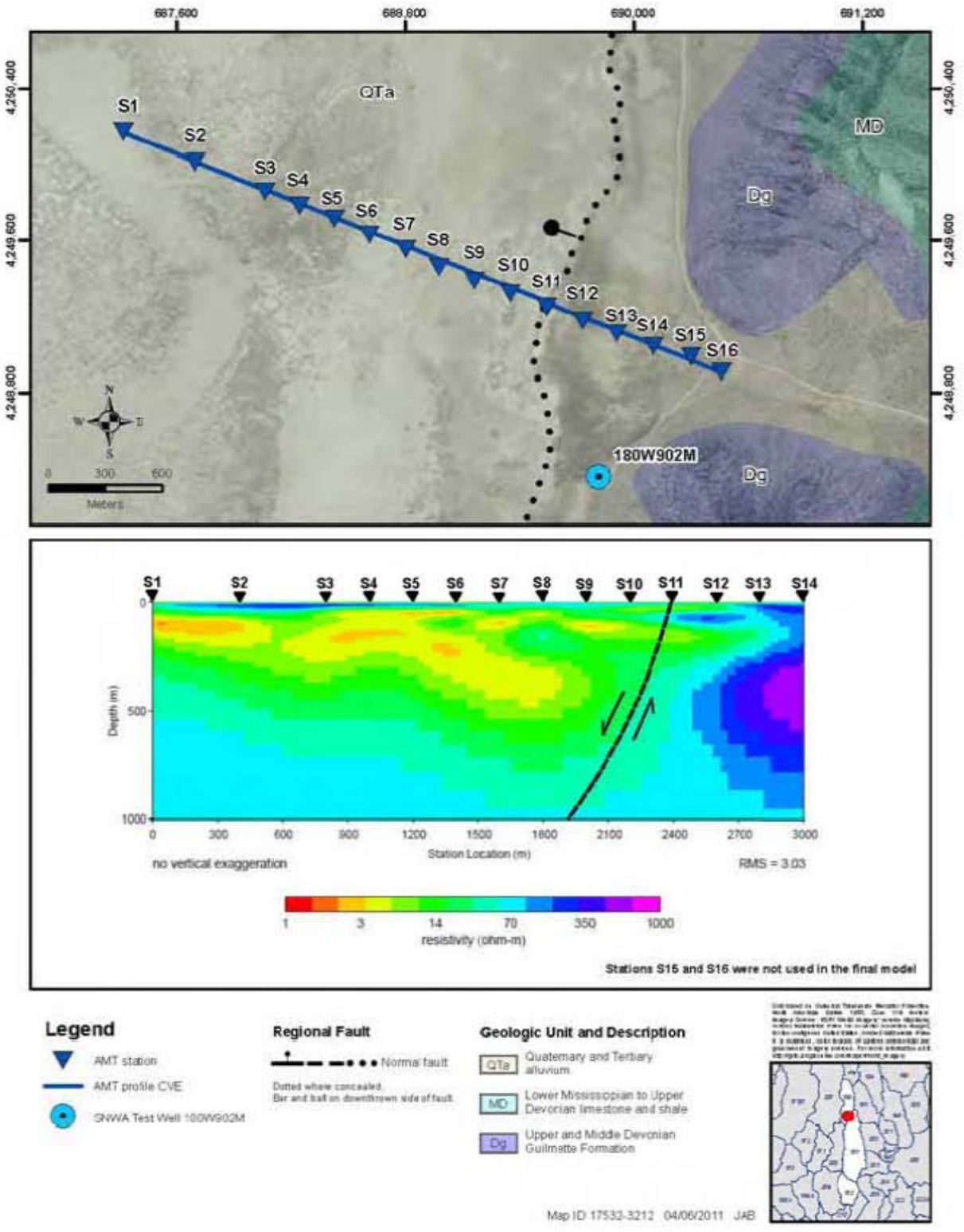

Figure 35. Geologic map and 2D model of AMT profile CVE.

Dry Lake Valley

Dry Lake Valley, whose northern end is locally called Muleshoe Valley and is east of southern Cave Valley, continues south to where it appears to pass uninterrupted into Delamar Valley. Northern Dry Lake (Muleshoe) Valley is relatively shallow and is separated from the southern, deeper, main part of Dry Lake Valley by a series of uplifted fault blocks that span much of the valley and formed along the generally east-striking Blue Ribbon transverse zone (Rowley, 1998; Rowley and Dixon, 2001). The southern end of Dry Lake Valley is separated from northern Delamar Valley by a similar series of uplifted fault blocks of the generally east-striking Timpahute transverse zone, but these blocks are not exposed and are covered by thin basin-fill sediments. Dry Lake Valley was the focus of nine AMT profiles, seven by the USGS (McPhee et al., 2008) and two by SNWA. All profiles are described by Pari and Baird (2011). Only five of them are discussed here (figure 34).

AMT Profile DLV50

Profile DLV50 (figure 36) extends for 3.2 km along a northeast trend so as to cross several faults along the eastern side of the West Range and west of Bristol Well. Bristol Well served the traveler along an east-west wagon trail and road that allowed access from Lake Valley on the east, across Dry Lake Valley, to White River Valley on the west. The West Range is a structurally complex area in the northeastern part of the main part of Dry Lake Valley just west of the northern Bristol Range. These areas were mapped in detail by Page and Ekren (1995). The profile was collected and interpreted by SNWA; stations S1 through S3 were omitted from the profile due to poor data quality. Three faults were imaged by the remaining part of the profile, all interpreted to be oblique-slip faults with right-lateral and normal displacement. As with other faults in the Great Basin that have a significant component of strike slip, the faults are broad and their resistivity contrasts are large. The high conductivity that marks the faults is probably a function of large amounts of groundwater flow, plus fault gouge and hydrothermal clay, along the faults. The higher conductivity beds between S8 and S14 probably are lake beds and/or high groundwater.

AMT Profile DLV3

Profile DLV3 (figure 37) extends for 2.1 km from the western side of the West Range into the main part of Dry Lake Valley. The data were collected by McPhee et al. (2008) and interpreted by SNWA. Three down-to-the-west normal faults that accommodated development of Dry Lake Valley are imaged. The western of these cuts Pleistocene and Holocene basin-fill sediments. Interpretation of the AMT data indicates that the eastern of these is relatively small, the middle fault is the main fault, and the western fault has significant displacement, only the latest of which is demonstrated by the mapped fault scarp. Inner-basin lake deposits, probably containing groundwater, are indicated at depth beneath stations S3 and S7.

AMT Profile DLV24

Profile DLV24 (figure 38), which has a length of 1.4 km, was collected by McPhee et al. (2008) and interpreted by SNWA. The profile extends basinward from the eastern part of the North Pahroc Range (Ekren and Page, 1995). Three buried faults are imaged, the western of which Ekren and Page (1995) interpreted to be an oblique-slip fault based on their mapping. The two faults farther east form a graben containing probable high-conductivity lake beds and/or permeable sediments containing groundwater. The low-conductivity material at the eastern end of the profile suggests that a block of Paleozoic carbonates has been brought up from depth, although this is based only on station S8, one data point.

AMT Profile DLV4

Profile DLV4 (figure 39) extends westward 3.2 km from the western edge of the Burnt Springs Range so as to look at the concealed normal faults in this part of eastern Dry Lake Valley. The data were collected by McPhee et al. (2008) and interpreted by SNWA. The profile

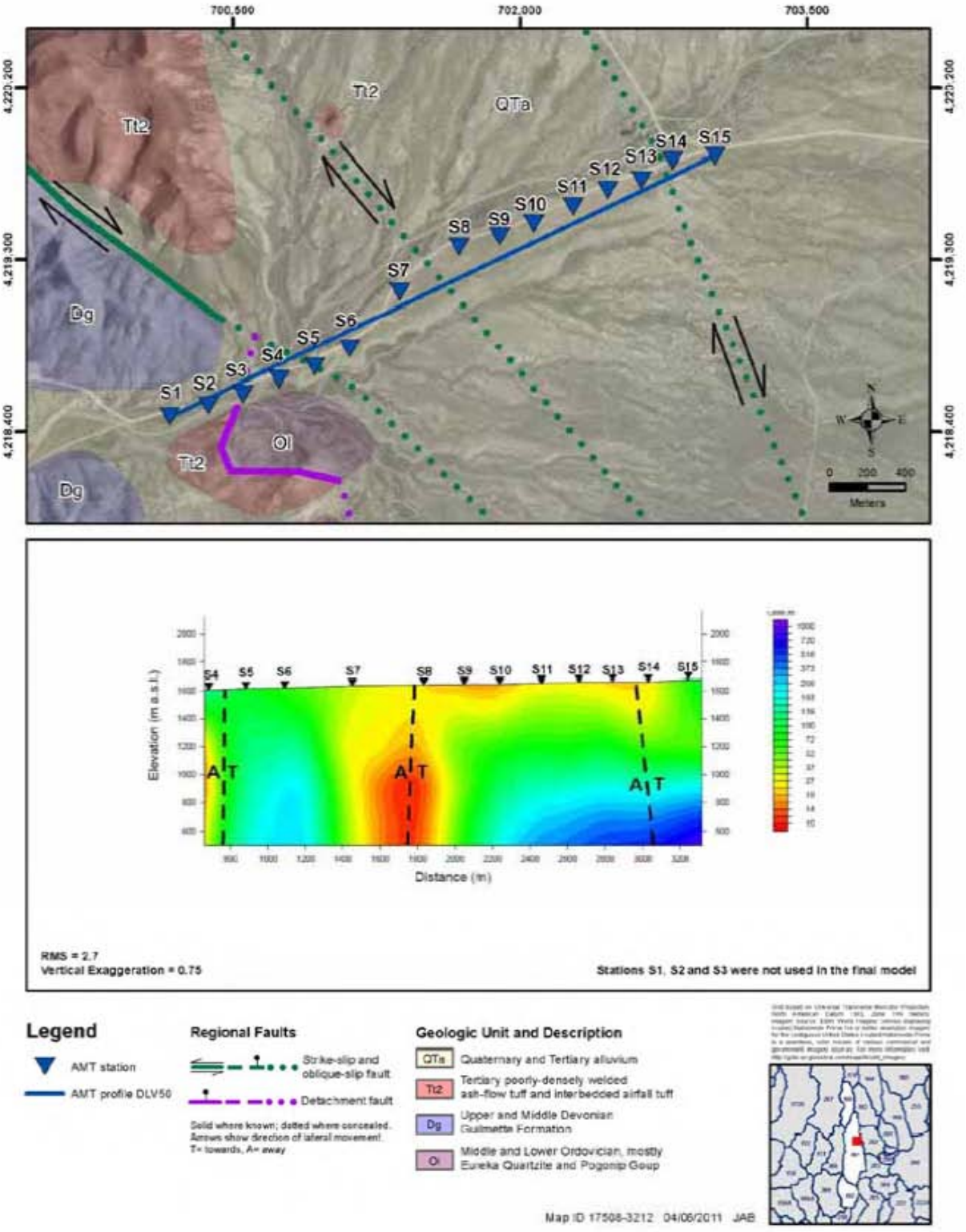

Figure 36. Geologic map and 2D model of AMT profile DLV50.

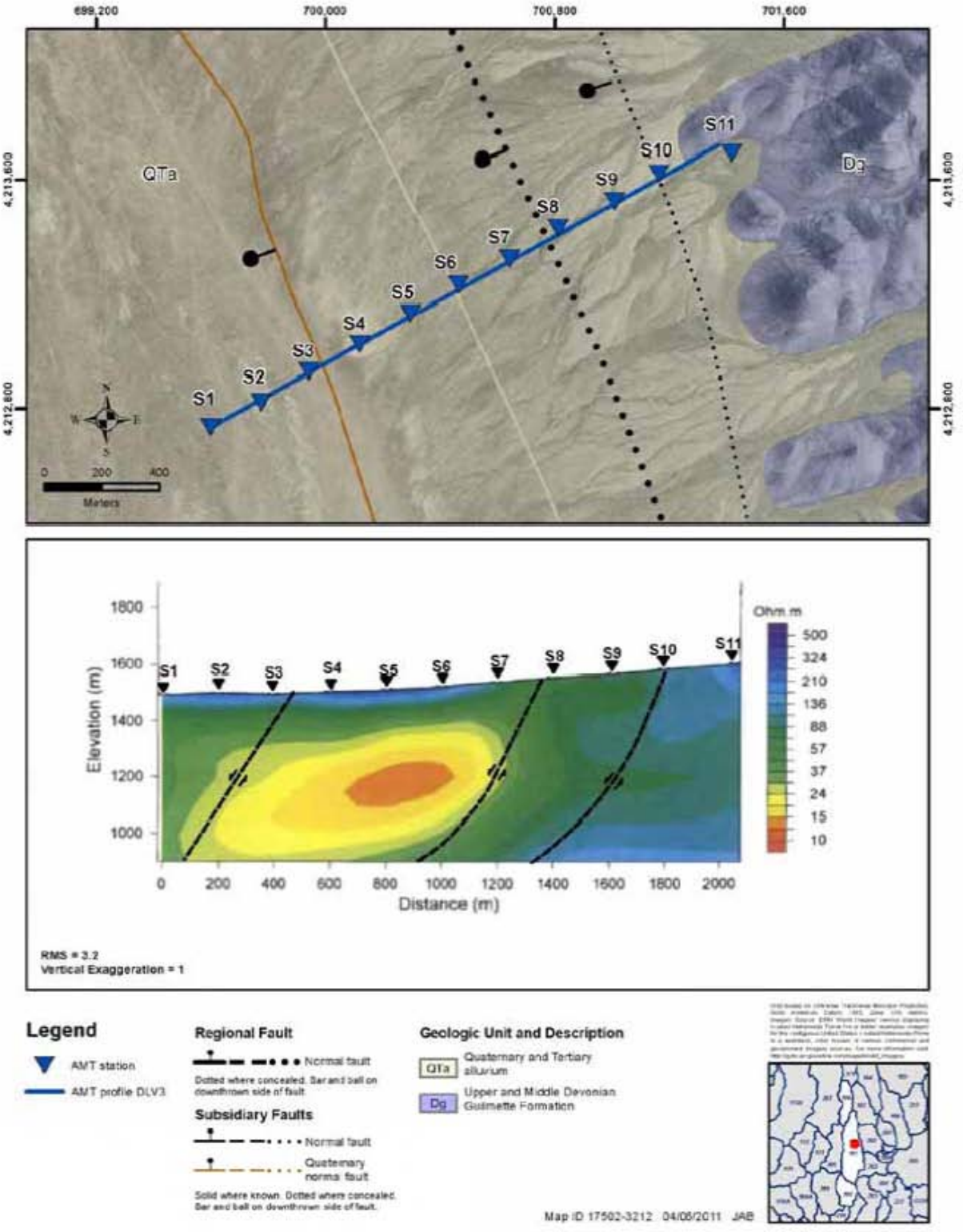

Figure 37. Geologic map and 2D model of AMT profile DLV3.

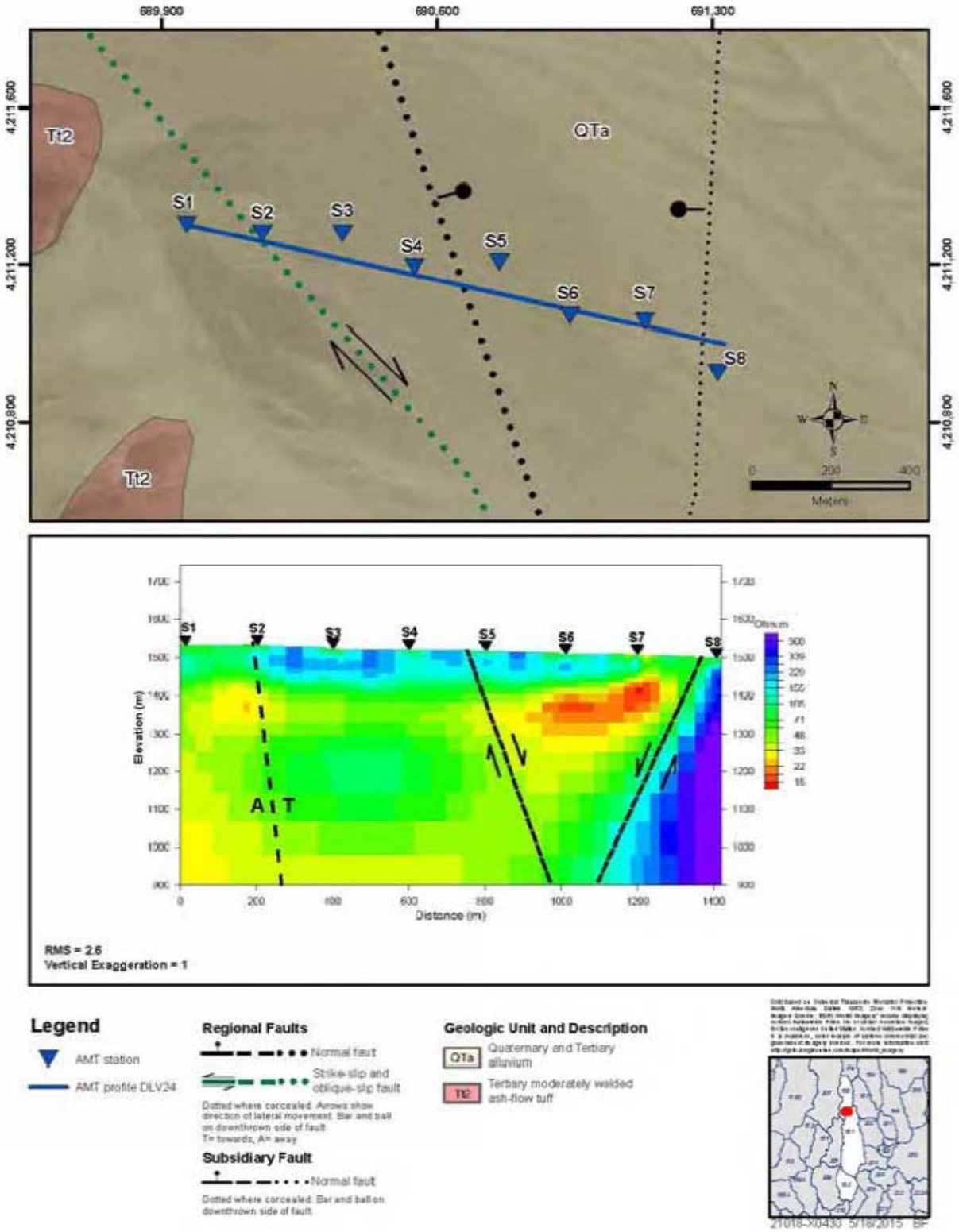

Figure 38. Geologic map and 2D model of AMT profile DLV24.

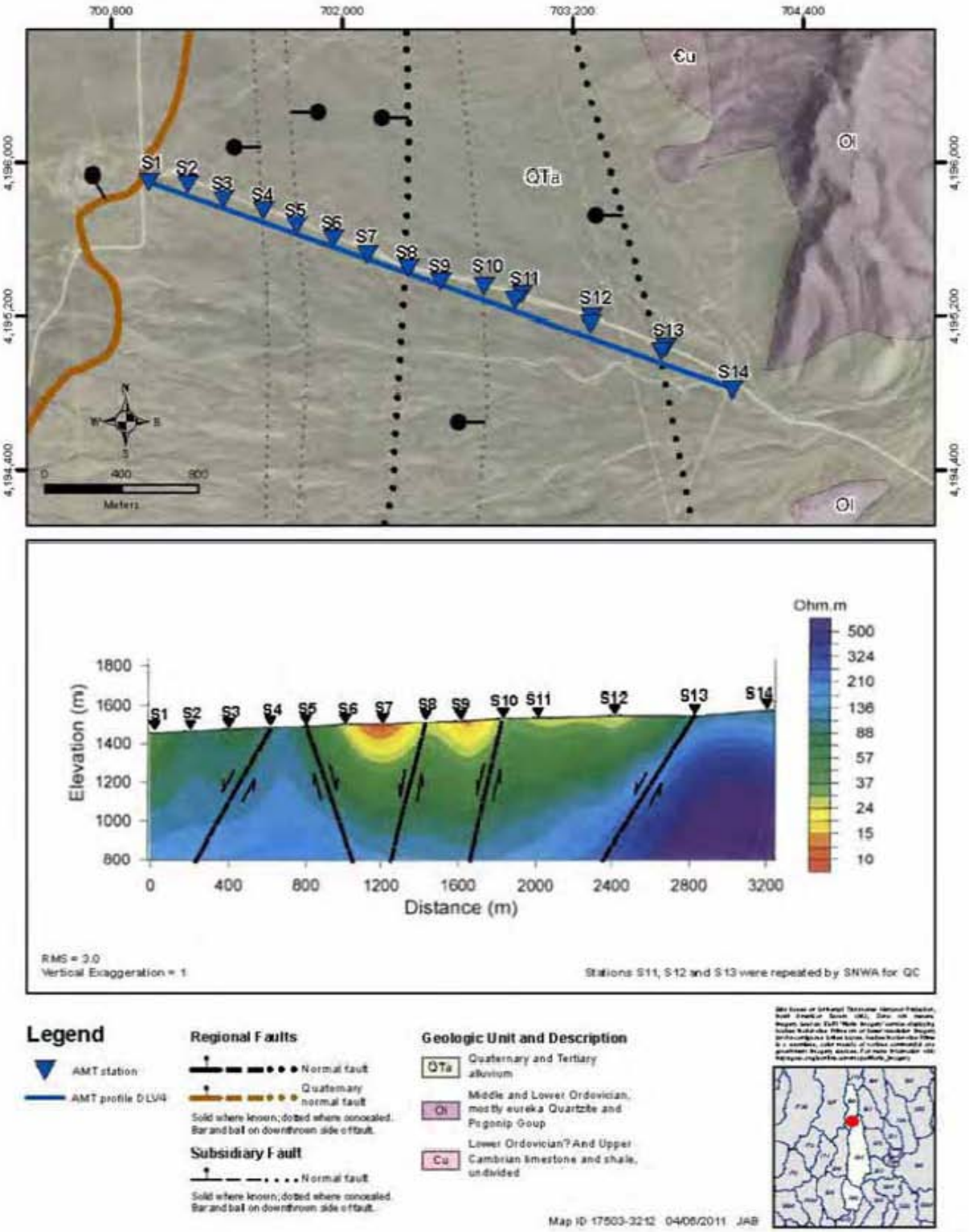

Figure 39. Geologic map and 2D model of AMT profile DLV4.

reveals the complexity of concealed normal faults in Dry Lake Valley. Only the westernmost of these faults was mapped, displacing Quaternary deposits, although the profile did not cross it. The profile allows interpretation of the buried faults and the most likely locations of high-conductivity lake beds. These AMT data demonstrate a horst block in the western part of the profile and show that the eastern fault is the main fault.

AMT Profile DLV8

Profile DLV8 (figure 40), farther south from the western edge of the Burnt Springs Range into eastern Dry Lake Valley, has a length of 2.5 km. The data were collected by McPhee et al. (2008) and interpreted by SNWA. They show that the mapped fault, which has Quaternary displacement, has significant older displacement. About 10 km north of the profile, large historic open fissures (Swadley, 1995) formed by movement along this Quaternary fault, and surface water pours into these cracks during each rainstorm. The main fault, however, is the eastern buried one. The highly conductive material probably represents gouge and groundwater in the Quaternary fault and its fissures as well as groundwater and lake clays in the basin-fill sediments.

Delamar Valley

Three northwest-trending AMT profiles were done in southwestern Delamar Valley to look at two large northeast-striking, oblique-slip (left lateral and normal) faults of the Pahranagat shear zone (Ekren et al., 1977; Scott et al., 1993). These faults pass into north-striking normal faults at both of their ends, so the Pahranagat shear zone can be considered a transfer fault that allowed east, west, northeast, and southwest movement during east-west extension. In other words, the slip in this overall arrangement of faults is largely strike-slip along the northeast-striking faults and is largely dip-slip along the north-striking faults. It is likely that considerable groundwater is moving southwestward along these two faults. All profiles were collected by McPhee et al. (2008) and interpreted by SNWA; all are discussed by Pari and Beard (2011). Only two of the profiles are described here (figure 34).

AMT Profile DELA5

Profile DELA5 (figure 41) has a length of 0.7 km so as to cross the Delamar Lake fault of the Pahranagat shear zone. The map shows that the profile runs along the southwestern side of Delamar Lake, a playa lake that is generally dry except after rain. The profile shows a wide, steeply southeast-dipping fault zone marked by highly conductive material that likely represents hydrothermal clay, fault gouge, and groundwater. South of the fault zone, lake clays are the more highly conductive material at depth; lower conductivity rocks at the surface are sediments above the water table.

AMT Profile DELA1

Profile DELA1 (figure 42) has a length of 1.2 km, extending northwestward from the southern Delamar Mountains to cross the Maynard Lake fault, the largest of the faults of the Pahranagat shear zone. The spectacular resistivity contrasts clearly demonstrate a large subvertical strike-slip fault carrying a great deal of groundwater southwestward. Interestingly, the axis of the fault has less conductivity than the rocks on either side. This axis probably represents fault gouge in the central core zone of the fault, which has less permeability than the fractures on either side of the axis in the outer damage zones of the fault.

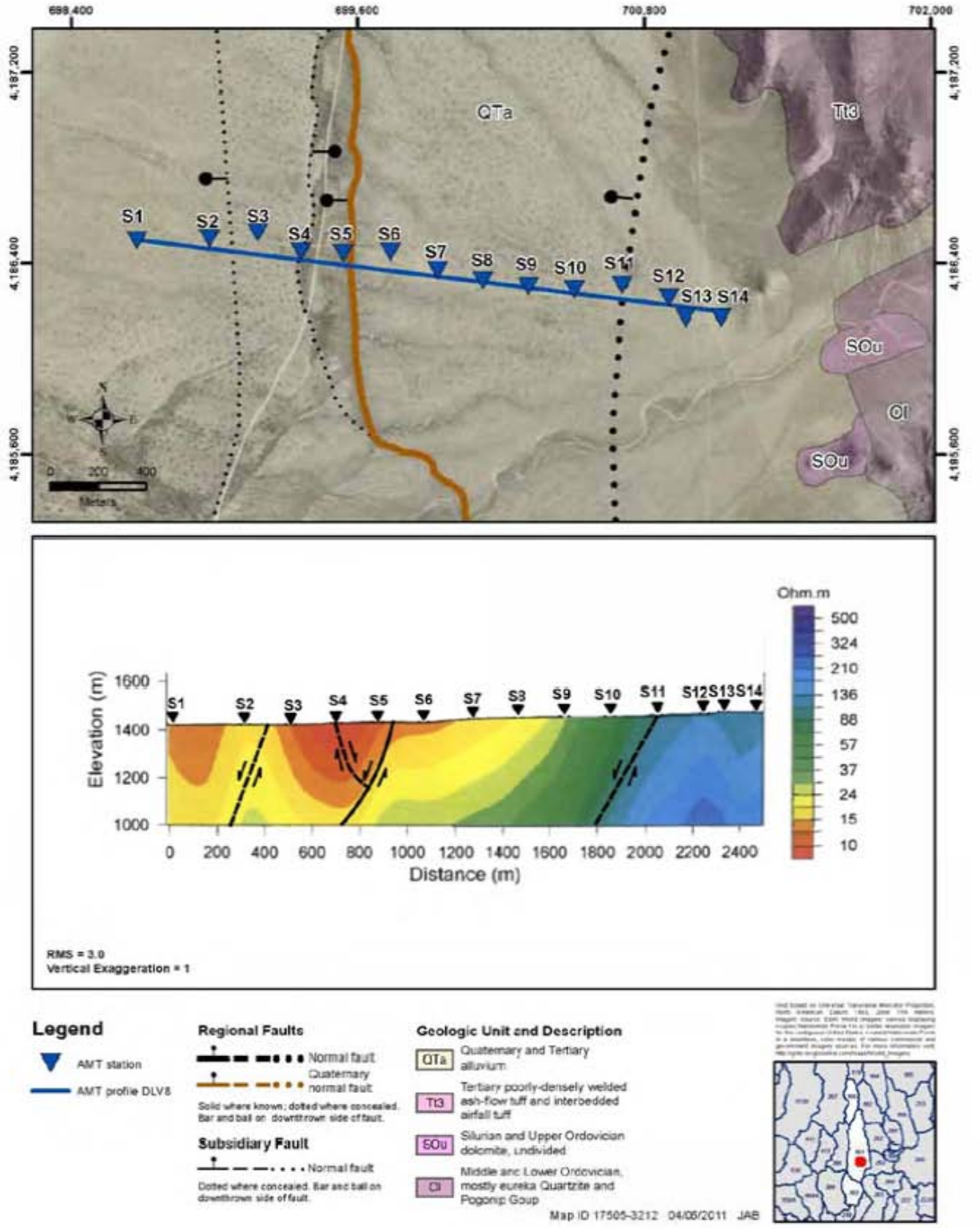

Figure 40. Geologic map and 2D model of AMT profile DLV8.

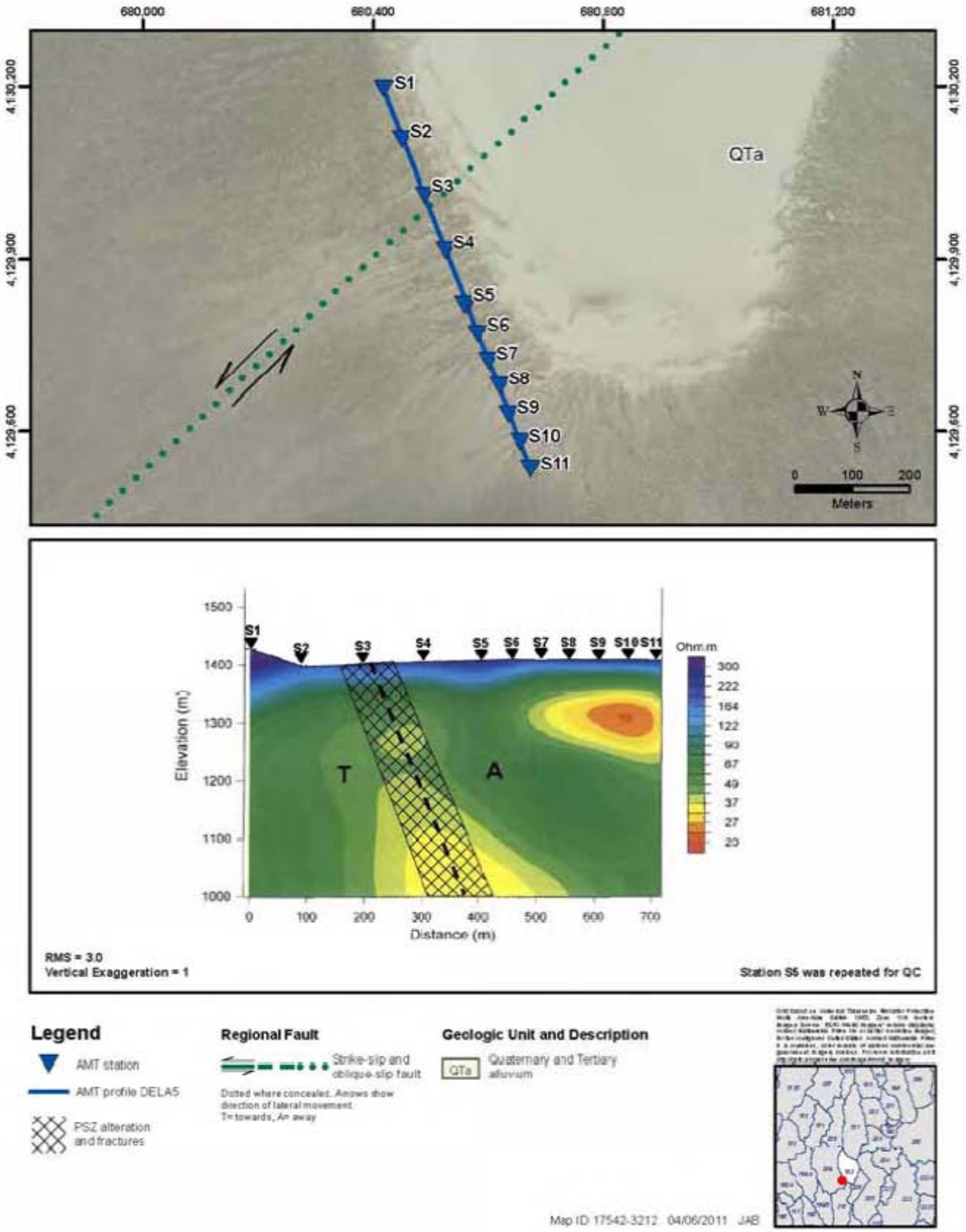

Figure 41. Geologic map and 2D model of AMT profile DELA5.

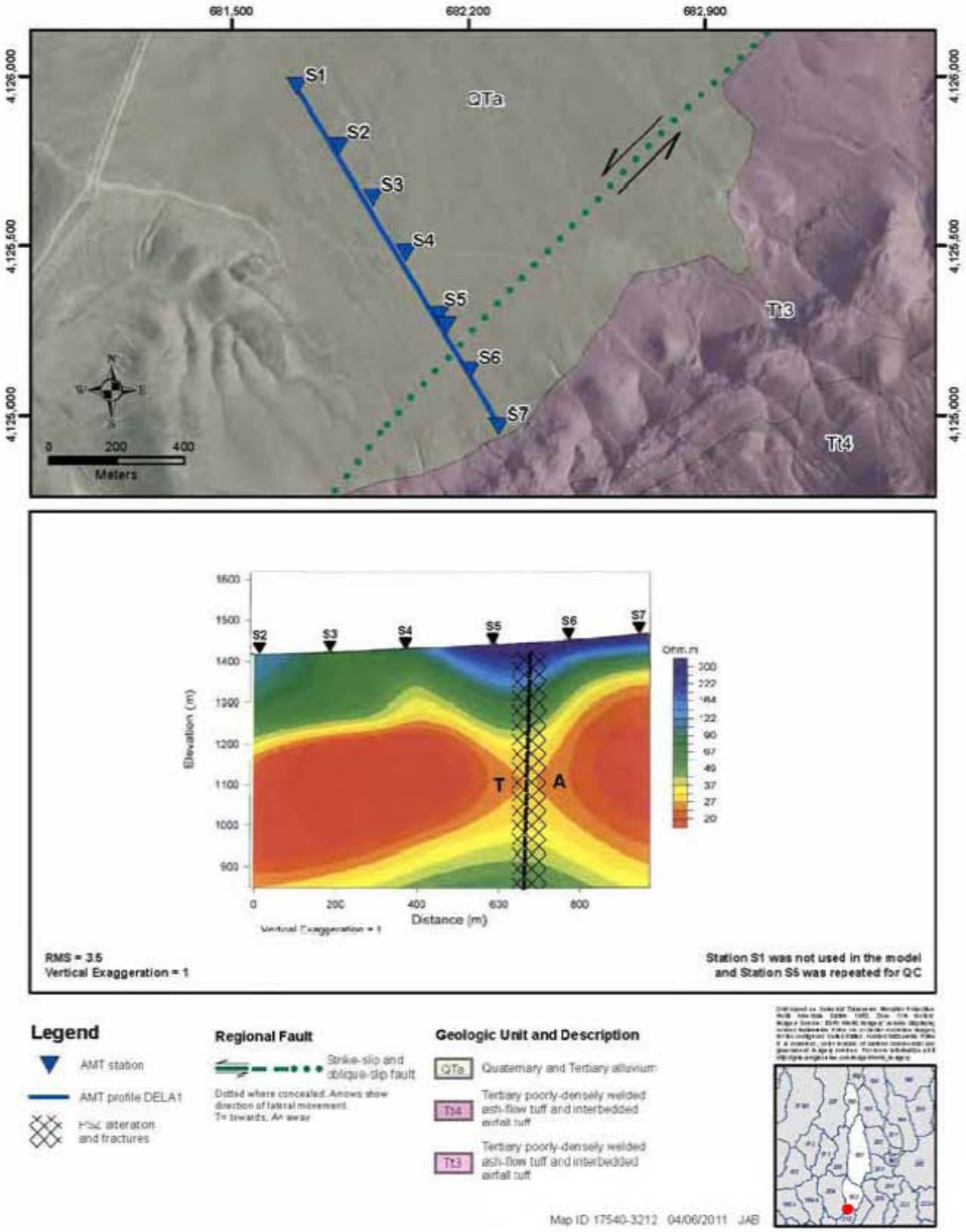

Figure 42. Geologic map and 2D model of AMT profile DELA1.

DESCRIPTIONS OF BASINS AND RANGES

Knowledge of the structure, stratigraphy, and geometry of individual basins and ranges in the study area (figure 2) was needed in order to understand the potential for interbasin groundwater flow. Specific flow pathways are controlled by topographic and geologic features, whose accurate geologic mapping and analysis are critical to interpreting flow routes between basins. This section also updates the discussion of individual basins and ranges provided by the old county reports. Mountain ranges adjacent to the basins are described in more detail than the valleys due to their greater exposure of pre-Quaternary geologic units. Because of this, the discussion below is organized by ranges, and the adjacent basins are discussed within these sections going from north to south and west to east, starting in the northwestern part of the study area.

RUBY MOUNTAINS, BALD MOUNTAIN, AND BUCK MOUNTAIN

The Ruby Mountains, just west of the study area, form a horst in which large amounts of vertical uplift resulted in detachment or attenuation faults along the margins. The range is considered a metamorphic core complex formed during major uplift (Howard et al., 1979; Wright and Snoke, 1993; Howard et al., 2011). Most rocks in the range dip east and are early Paleozoic in age. The Ruby Mountains is cored by a Jurassic to Miocene batholith and Precambrian to Lower Cambrian rocks.

Bald Mountain consists of east-dipping lower Paleozoic rocks cored by Jurassic intrusions that formed major deposits of gold, silver, and other metals (Hitchborn et al., 1996). Bald Mountain joins Buck Mountain, a horst of subhorizontal middle Paleozoic rocks. Low-angle Tertiary attenuation faults separate Paleozoic units in many places, from Bald Mountain to Buck Mountain, and several Sevier thrust faults of small displacement were also noted (Nutt, 2000; Nutt and Hart, 2004).

Ruby Valley is a deep graben bounded by the Ruby Mountains to the west, Maverick Springs Range (see Maverick Springs Range below) to the east, and Bald Mountain to the south (figure 2). This graben is locally ~1500 m deep. On the western side of the Ruby Mountains and Bald Mountain is Huntington Valley, a graben that is several hundred meters deep. This valley is bounded on the west by the Diamond Mountains. Newark Valley is bounded by the Diamond Mountains to the west and by Bald and Buck mountains to the east. This valley is another graben with locally more than 1500 m of valley fill (plate 3, cross section X–X'); it is further described in Butte Mountains and White Pine Range. Seismic profiles reveal Sevier thrusts beneath the basin-fill deposits (Dobbs et al., 1994). These thrusts, which are well exposed just to the west, south of the town of Eureka, are part of the east-verging thrusts and folds of the central Nevada thrust belt, within the Sevier hinterland (Greene, 2014).

MAVERICK SPRINGS RANGE

The Maverick Springs Range of northern White Pine County, Nevada, is a low, northeast-trending range of mostly east-dipping upper Paleozoic rocks uplifted along a normal fault on the western side. The range bounds the southeastern edge of Ruby Valley. The eastern side of the Maverick Springs Range is bounded by a normal fault, down to the east, that separates it from Long Valley to the east. The northern end of the Maverick Springs Range is cored by a Tertiary pluton (plate 3, cross section Y–Y') that continues north into Elko County, Nevada, as a broad series of hills, floored by cupolas of a Tertiary stock or batholith. The southern half of the Maverick Springs Range becomes Alligator Ridge, which joins Buck Mountain to the south, although geologically separated from Buck Mountain by a down-to-the-west normal fault. Alligator Ridge is the site of a major gold deposit (Nutt, 2000). Tertiary attenuation faults and a small Sevier thrust fault have been mapped on Alligator Ridge (Nutt, 2000; Nutt and Hart, 2004).

Long Valley, at the northwestern part of the study area, is narrow and shallow (i.e., thin basin-fill sediments) at its northern end but it widens and

deepens to at least 1000 m of basin-fill sediments to the south. The fault zone that bounds the western side of the Maverick Springs Range in Ruby Valley passes south through Mooney Basin (between the southern Maverick Springs Range and the Bald Mountain-Buck Mountain ridge).

BUTTE MOUNTAINS AND WHITE PINE RANGE

The Butte Mountains are located east of Long Valley, to the west of central and southern Butte Valley. The Butte Mountains are a 60-km-long, north-trending horst of east-dipping to anticlinally folded, upper Paleozoic sedimentary rocks (Hose and Blake, 1976; Otto, 2008; Douglass, 1960; Pekarek, 1988). Several Sevier thrust faults of small displacement were mapped by Howard (1978) and Otto (2008). The small thrusts are due to tight harmonic folding (Otto, 2008). Southward, the Butte Mountains joins the eastern side of the north-trending, 80-km-long White Pine Range across a low range of hills of upper Paleozoic carbonate rocks and Tertiary volcanic rocks. The southern end of the Butte Mountains also joins with several repeated fault ridges of the Egan Range (see Northern Egan Range) to the east across a similarly low range of volcanic hills that forms the southern end of Butte Valley.

The northern White Pine Range is comprised of a low, broad series of horsts and grabens (Gans, 2000a). One of the grabens becomes Long Valley to the north, and the eastern horst becomes the Butte Mountains to the north. The northern White Pine Range is underlain largely by upper Paleozoic rocks, but middle Paleozoic rocks underlie some of the horsts (Lumsden et al., 2002) and Tertiary volcanic rocks underlie some of the grabens (plate 3, cross section W–W'). The middle Paleozoic rocks include repeated fault blocks containing the Chainman Shale. The southern end of the White Pine Range has considerable elevation (up to 3500 m) and is made up mostly of east-dipping, lower to middle Paleozoic rocks. The range here has a large eastward bulge, the White River caldera, which includes an underlying resurgent dome that undoubtedly is responsible for the high relief of the range (plate 3, cross section V–V'). The north-trending axis of the caldera contains a narrow, north-striking graben. West of the caldera, the rocks include Cambrian to Precambrian siliciclastic rocks intruded by a Tertiary pluton. Locally the Paleozoic rocks are cut by late Cenozoic attenuation/denudation faults (Moores et al., 1968; Francis and Walker, 2002; Walker and Francis, 2002), and Gans (2000a) mapped one small east-verging Sevier thrust.

Butte Valley, east of the Butte Mountains, is a graben similar to Long Valley. Butte Valley contains upper Paleozoic rocks at a shallow depth, with overlying Tertiary volcanic rocks in the southern part of the valley. The valley fill is a maximum of about 1200 m thick, in turn overlying less than 300 m of Tertiary volcanic rocks. A narrow horst is within the northern end of Butte Valley (plate 3, cross section Y–Y').

Jakes Valley, south of the Butte Mountains, may be as deep as 2000 m (plate 3, cross section W–W'), with Tertiary volcanic rocks and upper Paleozoic carbonate rocks beneath about 1500 m of basin-fill sediments. West of the White Pine Range, Newark Valley is a shallow graben, narrowing and becoming shallower to the south, as described in Ruby Mountains, Bald Mountain, and Buck Mountain. West of the southern end of the White Pine Range, Newark Valley opens out southward into Railroad Valley, a broad deep graben. East of the axis of the White River caldera, the White Pine Range is dropped down along many down-to-the-east normal faults that also accommodated development of White River Valley to the east. Although relatively shallow at this latitude, near Preston and Lund, Nevada, White River Valley widens and becomes a deep, broad graben to the south, with a depth of more than 1500 m (see next section).

HORSE, GRANT, AND QUINN CANYON RANGES

At the southern side of the White River caldera in northern Nye County, Nevada, the east-striking, oblique-slip (left lateral and normal) Currant Summit fault zone (Moores et al., 1968; Williams and Taylor, 2002), part of the Pritchards Station transverse zone (Ekren et al., 1976; Rowley, 1998; Rowley and Dixon, 2001), structurally separates the White Pine Range to the north from

the small, 30-km-long, north-trending Horse Range to the south. Another east-striking, oblique-slip (left-lateral and normal) fault zone, called the Stone Cabin fault zone by Moores et al. (1968), passes through the Horse Range about 15 km south of the Pritchards Station transverse zone and continues west to terminate the northern end of the Grant Range; this is the eastern part of the Pancake Range transverse zone (Ekren et al., 1976; Rowley, 1998; Rowley and Dixon, 2001). The Horse Range (Moores et al., 1968) consists of east-dipping, lower to middle Paleozoic sedimentary rocks (plate 3, cross section U–U'). The Horse Range is uplifted on its western side against thick, east-dipping volcanic rocks and basin-fill sediments to the west. The basin-fill sediments fill Horse Camp Basin (Moores et al., 1968; Brown and Schmitt, 1991), and the volcanic rocks form the eastern flank of the northern Grant Range and underlie the basin.

The Grant Range is 60-km-long, increasing in width southward. It, in turn, passes into the high, broad Quinn Canyon Range to the south, which is 24 km north-south by 32 km east-west. These ranges are bounded on the west by the deep graben of Railroad Valley, whereas the Horse and Grant ranges are bounded on the east by the large, deep graben of White River Valley. The Grant Range is underlain mostly by east-dipping Cambrian through Permian carbonate rocks (Lumsden et al., 2002), with Tertiary ash-flow tuffs on the eastern flank (Scott, 1965). In addition to the large north-striking, high-angle normal faults that control the range, the northern part of the range is cut by many late Cenozoic, low-angle attenuation/denudation faults (Scott, 1965; Moores et al., 1968; Lund et al., 1991; Lund and Beard, 1992; Francis and Walker, 2002; Walker and Francis, 2002). These low-angle faults continue south into the northern Quinn Canyon Range, north into the White Pine Range, and west into Railroad Valley. They also have been mapped as far east as the Schell Creek Range. Commonly the faults follow the Chainman Shale (Francis and Walker, 2002; Walker and Francis, 2002). In the Grant Range, the attenuation faults were preceded by east-verging Sevier thrust faults of the central Nevada thrust belt (Bartley et al., 1988; Fryxell, 1988; Bartley and Gleason, 1990; Taylor et al., 1993, 2000; Ekren et al., 2012). Composite Upper Cretaceous and Tertiary plutons, including the Troy Peak granite, were intruded into the Paleozoic rocks in the southwestern part of the Grant Range (Armstrong, 1970; Fryxell, 1988) (plate 3, cross section Q–Q'). Low-angle Tertiary attenuation/denudation faults dip into Railroad Valley from both sides, especially from the Grant Range on the east (Lund et al., 1991). Many subsurface attenuation/denudation faults were detected during widespread exploration for oil in Railroad Valley (Lund et al., 1991; Blank, 1993; Schalla and Johnson, 1994; French and Schalla, 1998; Ehni and Faulds, 2002). The carbonate rocks plunge generally northward in the range, so Cambrian and Precambrian siliciclastic rocks and the Tertiary intrusive rocks form the core of the southern Grant Range.

The Quinn Canyon Range, south of the Grant Range, is bordered by Garden Valley to the east, the southern end of Railroad Valley to the north and northwest, and Penoyer Valley (Sand Spring Valley) to the south. Garden Valley is a narrow graben several hundred meters deep, between the Quinn Canyon and Golden Gate ranges (plate 3, cross sections T–T' and Q–Q'). The Quinn Canyon Range is almost entirely underlain by all or parts of several eastern calderas of the newly discovered Monotony Valley caldera complex (Ekren et al., 2012), the source of the Monotony Tuff (27 Ma) and Shingle Pass Tuff (26 Ma). It is the eastern part of a cluster of calderas that continues west and northwest (Dixon et al., 1972; Ekren et al., 1972, 1973a and b, 1974; Snyder et al., 1972; Quinlivan et al., 1974). This cluster of calderas is what Best et al. (1993, 2013b) and Scott et al. (1995a) called the central Nevada caldera complex. This feature is not, however, a true caldera complex because not all of it has subsided as a caldera; instead, individual calderas are separated by pre-caldera rocks, so it might better be considered a cluster of adjacent calderas. The southeastern end of the Quinn Canyon Range and the southern edge of the Monotony Valley caldera complex is in Lincoln County. The caldera complex underlies Penoyer Valley (Sand Spring Valley), which makes up the single-basin Penoyer Valley flow system (Harrill et al., 1988).

Gravity surveys on the eastern side of White River Valley (Scheirer, 2005) suggest that the valley consists of thick basin-fill sediments and volcanic and carbonate rocks. We interpret that the White River Valley contains at least 1500 m of valley fill (Dixon et al., 2007a and c) (plate 3, cross sections Q–Q' and U–U'). The valley narrows southward east of the Seaman Range (here called Pahroc Valley) as the ephemeral White River was incised into Pleistocene basin-fill sediments during canyon cutting following drainage integration with the Colorado River (Dixon, 2007) (plate 3, cross section T–T').

Springs are abundant in White River Valley, especially in the center of the valley and near Nevada Highway 318, which is just west of the eastern side of the valley. Those in the center of the valley are warm and hot springs, some of which supply lakes that together were grouped and set aside as the Wayne Kirch Wildlife Management Area, managed by the Nevada Department of Wildlife. As far as we can tell, virtually all springs in White River Valley come up along north-trending normal faults, many of them with Quaternary displacement. Hydrologic data and geologic cross sections of most springs in White River Valley are discussed in Volume 3 of Southern Nevada Water Authority (2008), including Hot Creek Spring in the Wayne Kirch Wildlife Management Area.

WORTHINGTON MOUNTAINS AND TIMPAHUTE RANGE

The northern end of the narrow, 25 km-long, north-trending Worthington Mountains is just southeast of the Quinn Canyon Range. The Worthington Mountains define the northeastern side of Penoyer Valley and the western side of southern Garden Valley. The Worthington Mountains consists mostly of west-dipping Ordovician through Mississippian rocks that are uplifted along a north-striking fault on the eastern side of the range. The range contains the east-verging Freiburg thrust, which placed Ordovician rocks on Ordovician and Devonian rocks during Sevier deformation (Taylor et al., 2000). The thrust is part of the central Nevada thrust belt (Greene, 2014).

The Worthington Mountains extend southward into the east-trending Timpahute Range, which separates the southeastern side of Penoyer Valley from northern Tikaboo Valley. The Timpahute Range is underlain by Upper Cambrian through Permian sedimentary rocks, unconformably overlain by Tertiary volcanic rocks. The Paleozoic rocks are cut by several Sevier thrusts, the lowest of which places Devonian rocks over Devonian through Permian rocks. The uppermost thrust places Cambrian through Ordovician rocks above younger rocks (Taylor et al., 1994). The western end of the range includes the Tempiute mining district of tungsten and silver, associated with two Tertiary granite stocks. The range is heavily broken by north-south normal faults and synchronous east-west faults. The east-west faults, which define the southern margin of the range, are part of the Timpahute transverse zone, which also controls the northern side of the Caliente caldera complex.

Garden Valley, east of the Worthington Mountains, terminates southward against the eastern Timpahute Range. Garden Valley is a graben containing about 1000 m of basin-fill sediment (plate 3, cross section T–T'). Penoyer Valley is bounded on the east by a range-front fault and on the south by the east-west Timpahute transverse zone. Penoyer Valley probably contains about 1000 m meters of basin-fill sediments.

GOLDEN GATE RANGE, MOUNT IRISH, AND PAHRANAGAT RANGE

The north-trending Golden Gate Range is 60 km long and consists of low faulted hills that pass southward into the Mount Irish Range, a 15-km by 15-km range bounded by east-striking faults. The Mount Irish Range is the northernmost part of the larger, 60-km-long Pahranagat Range, which continues southward into the 80-km-long Sheep Range. The northern end of the Golden Gate Range, located in Nye County, Nevada, forms the western side of White River Valley and the eastern side of Garden Valley. The main part of this range forms the boundary between Garden and Coal valleys in Nye and Lincoln counties. In Nye County, the Golden Gate Range consists of Devonian through Pennsylvanian rocks overlain by

Tertiary volcanic rocks. Here and farther south, the range is a west-tilted horst; the main controlling normal fault is on the eastern side. In Lincoln County, the rocks of the Golden Gate Range are Devonian to Pennsylvanian sedimentary deposits, of which Ordovician through Devonian rocks are thrust over Devonian to Mississippian rocks (Armstrong, 1991) (plate 3, cross section T–T').

The Mount Irish Range is a stubby, east-trending block that is the eastern continuation of the Timpahute Range and is controlled by east-striking, oblique-slip faults of the Timpahute transverse zone. The Mount Irish Range is made up of Ordovician through Mississippian rocks containing the same thrusts, including the Gass Peak thrust, that occur in the Timpahute Range (plate 3, cross sections O–O' and S–S') (Taylor et al., 1994 and 2000). The Mount Irish block closes the southern end of Coal Valley.

The Pahranagat Range, including a separate parallel structural block along the eastern side that is called the East Pahranagat Range, is bounded by deep (thick basin-fill sediments) Tikaboo Valley on the west and shallow Pahranagat Valley (Tingley et al., 2010) on the east. The Pahranagat Range (Page et al., 2005a; Jayko, 1990 and 2007) is a horst bounded on both sides by major normal faults (plate 3, cross sections M–M' and N–N'). In the north, the range dips gently west but in the south it is a syncline. The east-verging Sevier-related Gass Peak thrust strikes the length of the range, placing Middle Cambrian to Devonian rocks on Devonian to Mississippian rocks. The East Pahranagat Range locally consists of an overturned fold of Devonian to Pennsylvanian rocks. Tertiary volcanic rocks unconformably overlie the folded and thrust-faulted Paleozoic rocks and are thickest where downfaulted into a graben between the Pahranagat Range and East Pahranagat Range. At their southern ends, the Pahranagat and East Pahranagat Ranges are separated from the northern Sheep Range by a series of east-northeast-striking splays of the predominantly left-lateral Pahranagat shear zone (PSZ) (Ekren et al., 1977; Johnson, M. 2007a). The southern splay of the PSZ is the Maynard Lake fault zone (plate 4, cross section A–A') (Tschanz and Pampeyan, 1970; Jayko, 1990 and 2007). The western part of this fault is interpreted to join the main north-south normal fault that defines the western side of the Sheep Range, and the eastern part of the fault is interpreted to join the main north-south normal fault that defines the western side of the Delamar Mountains. In this interpretation, the Maynard Lake zone—like the others of the PSZ—is a transfer fault that transfers east-west extension (pulling apart) into left-lateral shear. In this scenario, in those places where faults strike north, all east-west extension is taken up by normal movement down the dip of the fault plane, and where faults strike northeast, east-west pulling apart is taken up by mostly left-lateral movement.

Pahranagat Valley (see also North Pahroc, South Pahroc, and Hiko Ranges), between the East Pahranagat Range on the west and the Hiko Range on the east, is a remarkably well-watered valley containing the agricultural communities of Hiko and Alamo, Nevada, and two large lakes that are the home of the Pahranagat National Wildlife Refuge (U.S. Fish and Wildlife Service). Structurally, the valley is a shallow graben (plate 3, cross sections S–S', O–O', N–N', and M–M'). Several large regional springs, including Hiko and Crystal springs and Ash Spring, are controlled by normal faults (Dixon and Van Liew, 2007; Volume 3 of Southern Nevada Water Authority, 2008).

SHEEP RANGE, LAS VEGAS RANGE, AND ELBOW RANGE

The northern Sheep Range is a narrow and high mountain range that consists of Cambrian and Ordovician sedimentary rocks forming the leading edge of the Gass Peak thrust fault of the main Sevier frontal thrust belt (plate 4, cross section L–L'; Page et al., 2005a; see also Greene, 2014). The southern Sheep Range consists of mostly Cambrian and Ordovician carbonate rocks that dip eastward (plate 4, cross sections E–E', F–F', G–G', and H–H') (Guth, 1980). The entire range is a large tilt block uplifted along major north-striking, normal faults on its western side. The thrust transported Neoproterozoic to Cambrian quartzite and Cambrian to Devonian carbonate rocks eastward over Cambrian to Mississippian rocks. Within the Sheep Range, north-striking normal faults are abundant, but some cross-faults

that strike east to east-northeast also have been mapped.

Quaternary normal faults define much of the eastern side of the range (Dohrenwend et al., 1996). Pleistocene basalt has locally been injected into some of these eastern faults.

A small, north-trending range lies east of the northwestern arm of Coyote Spring Valley and west of Pahranagat Wash, U.S. Highway 93, and northeastern Coyote Spring Valley. The small range is considered part of the northern Sheep Range but is separated from the high Sheep Range to the west by northwestern Coyote Spring Valley. The northern end of this small range terminates against the Maynard Lake fault zone of the PSZ. This small Basin and Range tilt block consists largely of east-dipping volcanic rocks (Jayko, 1990 and 2007) that rest unconformably on Pennsylvanian and Permian carbonate rocks. North-striking normal faults within, west, and east of the small range pass into the Maynard Lake fault zone and transfer their normal slip to oblique slip. The buried north-striking trace of the Gass Peak thrust fault passes beneath the normal faults near the western side of the small range.

The Las Vegas Range northwest of Apex is defined by the Gass Peak thrust, which transported rocks as old as the Cambrian Wood Canyon Formation eastward over Mississippian, Pennsylvanian, and Permian carbonate rocks of the Bird Spring Formation (plate 4, cross sections F–F', G–G', H–H', and I–I') (Maldonado and Schmidt, 1991). Most of the range is made up of folded Bird Spring limestone, with the Gass Peak thrust exposed along its western side (Maldonado and Schmidt, 1991; Page, 1998). The small Elbow Range, which bounds the Las Vegas Range on the northeast, is made up of thrusted and folded Bird Spring Formation (Page and Pampeyan, 1996) that has been uplifted as a horst (plate 4, cross sections E–E' and F–F'). The southern ends of the Sheep Range and Las Vegas Range, and continuing east, of the Arrow Canyon Range (see Arrow Canyon Range), Dry Lake Range, and Muddy Mountains (see North Muddy Mountains, Muddy Mountains, and Dry Lake Range) terminate against the west-northwest-striking, oblique-slip (right-lateral and normal) Las Vegas Valley Shear Zone (LVVSZ), which defines the northern side of the Las Vegas basin (Workman et al., 2002a and b; Page et al., 2005a and b; Beard et al., 2007; Anderson and Beard, 2010).

CHERRY CREEK RANGE

The high Cherry Creek Range is in northern White Pine and southern Elko counties. The range is a large horst of gently to moderately west-dipping Precambrian through Permian sedimentary rocks. Normal faults separate it from Butte Valley on the west and from Steptoe Valley on the east; the bigger fault is on the east. A thin sliver of bedrock cored by a Tertiary intrusion connects the Cherry Creek Range with the northern Egan Range. A northeast-striking oblique-slip fault, left-lateral and down-to-the-west, cuts through the southern end of this sliver.

NORTHERN EGAN RANGE

Like the Cherry Creek Range to the north, the Egan Range is a high, north-trending west-tilted horst of Precambrian through Permian rocks, unconformably overlain by Tertiary volcanic rocks. The major normal fault zone that uplifted the Egan Range is along the eastern side. The vertical displacement along this fault is at least 3000 m. The range continues southward for 110 km in White Pine County, then another 60 km in Lincoln County. In the northern end of the range, the rocks dip westward and are intruded by Tertiary stocks. The Snake Range décollement is present here as a thin skin of Paleozoic rocks at the crest of the range and along its western slope (plate 3, cross section X–X'). The décollement is a Tertiary denudation/attenuation fault that transported rocks as old as Middle Cambrian eastward and placed them on top of older rocks. Butte Valley is to the west and Steptoe Valley is to the east of the northern Egan Range.

About 30 km south of the northern end of the Egan Range, the range becomes considerably wider and lower as the Butte Mountains join it from the west and Butte Valley closes. Here, the range is broken into a series of horsts and grabens (plate 3, cross section W–W'). The downthrown areas on the western side of the Egan Range are underlain by Tertiary volcanic rocks that form low ridges and

hills that connect with the southeastern Butte Mountains. The towns of Ely and Ruth, Nevada, are located in this broad, low, heavily faulted part of the Egan Range, in areas called Copper Flat and Smith Valley. A major mining district, the Robinson district, was developed on a series of east-trending ore deposits of copper, molybdenum, lead, zinc, silver, and gold associated with a middle Cretaceous pluton. Barren Eocene rhyolite plutons and volcanic rocks also are present in the area and extend to Ely on the eastern side of the Egan Range adjacent to Steptoe Valley (Brokaw and Shawe, 1965; Brokaw and Heidrick, 1966; Brokaw and Barosh, 1968; Brokaw, 1967, Brokaw et al., 1973; Jones, 1996; Gans et al., 2001; Tingley et al., 2010). Southwest of the mining district, a series of low hills extends southwest to the White River caldera of the White Pine Range. These hills provide the southeastern margin of Jakes Valley and the north-northwestern margin of White River Valley (figure 2).

South of the Robinson mining district, the Egan Range continues southward for almost 50 km to the latitude of Lund as a single, high horst of east-dipping Cambrian through Permian rocks that together are more than 10 km thick (plate 3, cross section V–V') (Kellogg, 1963 and 1964; Taylor et al., 1991). Patches of volcanic rocks overlie the Paleozoic rocks on the eastern edge of the range. Several small plutons also are exposed. Major faults of the horst separate the Egan Range from the White River Valley to the west and southern Steptoe Valley to the east. Steptoe Valley is a deep graben containing as much as 2500 m of basin-fill sediments. Thus, it is one of the deepest grabens in the central Great Basin.

SOUTHERN EGAN RANGE

At the latitude of Lund, Nevada, a narrow ridge of Cambrian to Permian rocks extends southeastward from the main part of the Egan Range to the Schell Creek Range. This ridge, at Bullwhack Summit, forms the southern end of Steptoe Valley and the northern end of Cave Valley. The Egan and Schell Creek Ranges continue southward, with Cave Valley between them. Along the western side of Cave Valley (plate 3, cross section U–U'), the Egan Range is a complexly faulted horst of east-dipping Cambrian to Permian rocks, overlain by Tertiary volcanic rocks. White River Valley is west of the Egan Range. Southward, halfway down Cave Valley, at a latitude about 30 km south of Lund, a northeast-striking oblique-slip fault passes through the Egan Range at Shingle Pass (plate 3, cross section R–R') then crosses Cave Valley to join the western range-front fault of the Schell Creek Range. Farther south, the Egan Range remains an east-tilted horst of Cambrian through Tertiary rocks, then bends southeast to join the southern end of the Schell Creek Range. Prominent springs occur along the western range-front fault of the entire Egan Range, as well as along many faults in eastern White River Valley. Cave Valley terminates where the Egan and Schell Creek ranges join each other in a complex of north-northeast- and north-northwest-striking normal and oblique-slip faults. Farther south, the combined Egan and Schell Creek ranges become a low, narrow, north-northwest-striking horst of faulted Paleozoic sedimentary rocks and Tertiary volcanic rocks (plate 3, cross section Q–Q') that topographically continues southward to the northern end of the North Pahroc Range.

Cave Valley consists of two distinct but connected portions, separated by the oblique-slip fault at Shingle Pass. One of these portions, northern Cave Valley, is a narrow graben containing mostly east-dipping Cambrian rocks at shallow depth overlain by relatively thin volcanic rocks and in turn basin-fill sediments (plate 3, cross section U–U'). Gravity data (Scheirer, 2005) and oil test well logs (Hess, 2004) indicate that the base of the combined basin-fill sediments and volcanic rocks is about 1000 m below the valley floor of northern Cave Valley.

Shingle Pass is formed by the intersection of several major faults, but primarily it is defined by the northeast-striking, oblique-slip (left lateral and normal) fault zone. At the western end of Shingle Pass, this fault zone cuts through upper Paleozoic limestone on its northern side and lower Paleozoic limestone on its southern side.

Southern Cave Valley, in Lincoln County, is as narrow as about 3 km wide at its northern end. The narrowing is due to a northeast-trending tilt block bounded on the northwest by the fault at Shingle

Pass and striking northeast across most of Cave Valley. The block is buried but continues in the subsurface to the northeast to the large north-trending range-front fault zone that uplifts the Schell Creek Range (plate 3, cross section R–R'). To the southwest, the tilt block swings into the main north-trending part of the Egan Range, which continues to the south. The tilt block consists of southeast-dipping Cambrian through Mississippian rocks that includes the Mississippian Chainman Shale, which is buried along the southeastern edge of the block. These relationships are supported by oil-test-well drilling, gravity surveys, seismic surveys and AMT profiles (Hess, 2004; McPhee et al., 2005, 2006a and b; Mankinen et al., 2006; Scheirer, 2005). Southern Cave Valley generally contains less than 1000 m of basin-fill sediments and volcanic rocks. In a narrow, central, north-trending axial part of the valley, however, these Cenozoic rocks are 2000 m or more thick. McPhee et al. (2005 and 2007) provided information on faults on the eastern side of the basin based on AMT profiles.

At the southern end of Cave Valley, a series of north-northwest-striking right-lateral oblique-slip faults and north-northeast-striking, left-lateral oblique-slip faults forms the boundary between southern Cave Valley, northern Pahroc Valley, and northern Dry Lake Valley. The range-front, oblique-slip fault (left-lateral and normal) zone that defines the western side of the southern Schell Creek Range juxtaposes Devonian dolomite against intrusive rocks. Two other north-northeast-striking faults west of the range-front fault cut through upper Paleozoic limestone, largely overlain by a relatively thin veneer of Tertiary ash-flow tuffs, in the block that defines the southern end of Cave Valley east of the eastern range-front fault of the Egan Range.

SEAMAN RANGE

The 55-km-long, intensely faulted Seaman Range, located in Nye and Lincoln counties, is a horst that trends north and northwest and joins the Golden Gate Range at the northern end of both ranges (see Golden Gate Range, Mount Irish, and Pahranagat Range). Coal Valley, between the two ranges, is a graben containing about 1000 m of basin-fill sediments (plate 3, cross section T–T'). The valley is bounded on the south by the Timpahute Range. At its northern end, the Seaman Range is low and bounds the southern end of the White River Valley. In Nye County, the Seaman Range is made up of Devonian to Pennsylvanian sedimentary rocks, overlain unconformably by Tertiary volcanic rocks (du Bray and Hurtubise, 1994). In Lincoln County, the Seaman Range is made up of gently west-dipping Ordovician to Pennsylvanian rocks that are unconformably overlain by Tertiary volcanic rocks. The Tertiary volcanic rocks include the dacitic to rhyolitic Seaman volcanic center of flows, subordinate tuffs, and a central plug (Ekren et al., 1977; Hurtubise and du Bray, 1992; du Bray, 1993; du Bray and Hurtubise, 1994).

NORTH PAHROC, SOUTH PAHROC, AND HIKO RANGES

The North Pahroc Range extends south for 60 km from the junction with the southern Egan and Schell Creek ranges. It is separated from the smaller South Pahroc Range by an east-trending belt of faulted rocks of low relief formed by the east-striking Timpahute transverse zone. This zone of faulted rocks is also the boundary between Dry Lake Valley to the north and Delamar Valley to the south. The Seaman (see Seaman Range) and the North Pahroc ranges are separated by Pahroc Valley but the ranges join together at their southern ends. The Hiko Range continues south of this intersection. The Hiko Range is a small range parallel to and west of the South Pahroc Range and east of northern Pahranagat Valley. The South Pahroc Range is south of the North Pahroc Range and forms the western boundary of Delamar Valley. The South Pahroc Range connects with the Hiko Range at their southern ends to form the eastern boundary of southern Pahranagat Valley. The ephemeral channel of the White River is present along the western side of the North Pahroc Range. The channel is deeply incised through Tertiary volcanic rocks at White River Narrows (Cook, 1965; du Bray, 1995; Dixon, 2007) then enters the Pahranagat Valley north of the town of Hiko, where the ephemeral channel is called Pahranagat Wash. Pahranagat Valley (see Golden Gate Range,

Mount Irish, and Pahranagat Range) is a shallow graben west of the Hiko Range that contains volcanic and Paleozoic bedrock (plate 3, cross sections S–S', O–O', and N–N'). The large springs, including Crystal Spring (Dixon and Van Liew, 2007; Johnson, M., 2007b), in eastern Pahranagat Valley, are controlled by the range-front faults that define the western side of the Hiko Range.

The North Pahroc, South Pahroc, and Hiko ranges are complex horsts. The North Pahroc Range consists of upper Paleozoic rocks overlain by Tertiary volcanic rocks. These rocks dip west off major faults along the eastern and western sides of the range (Scott et al., 1994 and 1995b; Scott and Swadley, 1992; Swadley et al., 1994a). The South Pahroc Range is a series of west-tilted blocks of volcanic rocks. The main faults are on the eastern side of the range (Swadley and Scott, 1991; Scott et al., 1993). The Hiko Range consists of Devonian rocks and overlying volcanic rocks that dip east off the normal fault that separates the range from the floor of Pahranagat Valley. The South Pahroc and Pahranagat ranges terminate to the south against the east-northeast-trending PSZ, which also truncates Pahranagat and Delamar valleys.

Dry Lake Valley is a deep graben (plate 3, cross sections T–T', P–P', and S–S'), bounded in part by Quaternary faults and located east of the southern Schell Creek Range and North Pahroc Range. The valley contains, in most places, 1000–1500 m of basin-fill sediments (Swadley, 1995; Mankinen et al., 2006; Dixon and Rowley, 2007b) but locally along the axis of the graben as much as 3000 m of sediments and underlying downfaulted volcanic rocks (Scheirer, 2005). Delamar Valley, just south of Dry Lake Valley, is a southward-deepening graben with a general maximum thickness of more than 1000 m of basin-fill sediments east of the South Pahroc Range (Mankinen et al., 2006; Dixon and Rowley, 2007b) but locally as much as 1500 m of sediments and underlying downfaulted volcanic rocks (Scheirer, 2005). AMT profiles show some details of the faults in Dry Lake and Delamar valleys.

The basin boundary between Dry Lake Valley and Delamar Valley is so low as to be imperceptible to a person standing on the ground. Here US 93 runs east-west along the boundary, traversing what appears to be a continuous north-trending valley. Bedrock made up of east-striking fault blocks of Tertiary ash-flow tuffs and lava flows are exposed along the basin boundary both west (Scott and Swadley, 1992; Scott et al., 1995b; Swadley et al., 1994a) and east (Swadley and Rowley, 1994) of the valley, and regional tectonic studies (Rowley, 1998; Rowley and Dixon, 2001) indicate that the buried Timpahute transverse zone passes beneath the valley at US 93 and is exposed to the east and west of the valley. A depth-to-basement map shows that the thickness of basin-fill sediments and volcanic rocks along the basin boundary is from 750 to 2000 m thick. This thickness at the basin boundary, as well as continuation through the basin boundary between Dry Lake Valley and Delamar Valley of north-striking normal faults that bound the ranges on either side of the combined valleys, indicate that any basin boundary is indeed superficial.

The southern end of Delamar Valley is structurally complicated. It is defined by the northeast- trending PSZ (Ekren et al., 1977; Scott et al., 1993; Johnson, M., 2007b), which has at least 5 parallel, left-lateral faults, spread across a width of about 16 km. Three of these faults enter southern Delamar Valley, where they pass into a north-striking normal fault. In addition, other north-striking normal faults, some feeding into faults of the shear zone, define the east and west sides of Delamar Valley; some continue southward into Coyote Spring Valley. Two of the fault zones of the PSZ that enter southern Delamar Valley are the Delamar Lake fault to the north and the Maynard Lake fault to the south. The Maynard Lake fault continues southwestward to define the southern end of Pahranagat Valley and the Pahranagat Range and the northern end of the Sheep Range, then the fault enters Tikaboo Valley. AMT profiles made across both faults in southern Delamar Valley show that both are large subvertical faults. Near Maynard Lake, some of the fractures in the fault zone served as vents for late Cenozoic basalt lava flows. The fault creates a natural dam that impounds southern Pahranagat Lake, in the southern end of Pahranagat Valley. The lake is fed by springs that issue from the western range-front fault of the southern Hiko Range.

SCHELL CREEK RANGE

The northern end of the Schell Creek Range is just south of the northern border of White Pine County. The range continues south for 190 km, mostly as a high, narrow, north-striking horst. Steptoe and Cave valleys are on the west, and Spring Valley, northern Lake Valley, and northern Dry Lake Valley (Muleshoe Valley) are on the east. The northern part of the Schell Creek Range is made up of a west-dipping sequence of Neoproterozoic through Permian rocks (Lumsden et al., 2002), with overlying Tertiary volcanic rocks along the faulted western flank of the range (plate 3, cross section X–X'). Small Tertiary intrusions are exposed locally along the range. The main bounding normal fault, likely with thousands of meters of vertical throw, is on the eastern side of the range. The Snake Range décollement is locally exposed at the crest of the Schell Creek Range. This denudation/attenuation fault transported Middle Cambrian and younger rocks both westward and eastward over Lower Cambrian and older rock. About 15 km northeast of Ely, two north-northeast-striking, high-angle normal faults form a graben, Duck Creek Valley, within the range (plate 3, cross section W–W'). The southern half of the Schell Creek Range along Cave Valley contains a narrow, heavily faulted sequence of Neoproterozoic through Tertiary rocks that dips east. Here the dominant fault is on the western flank of the range. West of the Geyser Ranch (Johnson, M., 2007a) (plate 3, cross section U–U'), the rocks are mostly Neoproterozoic and Cambrian quartzite (Van Loenen, 1987), but farther south the rocks are dropped down along an east-trending fault at Patterson Pass and are mostly of middle to upper Paleozoic and Tertiary age (plate 3, cross section R–R'). Where the Schell Creek Range joins the Egan Range, a Tertiary pluton has mineralized adjacent carbonate rocks at the Silver King Mine (plate 3, cross section Q–Q').

Spring Valley, discussed in Snake Range and Limestone Hills, is a broad, deep graben. On the southwestern side of Spring Valley, a thin ridge of gently northeast-dipping Pennsylvanian and Permian carbonate rocks extends southeast from the central Schell Creek Range to the Fortification Range. Here, the low pass traversed by US 93 is called Lake Valley Summit. Spring Valley continues southeast on the eastern side of the Fortification Range. South of the thin carbonate ridge is Lake Valley (Johnson, M., 2007a), between the Schell Creek Range and the Fortification Range. Lake Valley contains at least 600 m of basin-fill sediments throughout its 90 km length but locally the sediments may be much thicker (plate 3, cross sections U–U', R–R', and Q–Q') (Scheirer, 2005). The Schell Creek Range forms the northwestern boundary of Lake Valley for about 30 km southward until it bends south-southwest to join the Egan Range.

Northern Dry Lake Valley, also known as Muleshoe Valley, lies east of the southern Schell Creek Range. This valley contains about 1000 m of basin-fill sediments (plate 3, cross section Q–Q'), and gravity surveys (Scheirer, 2005) indicate that locally more than 2000 m of basin-fill sediments plus underlying downfaulted volcanic rocks underlie the valley. A seismic profile crosses the valley.

FAIRVIEW, BRISTOL, WEST, ELY SPRINGS, HIGHLAND, BLACK CANYON, BURNT SPRING, AND CHIEF RANGES, AND PIOCHE HILLS

From north to south, the Fairview, Bristol, Highland, and Chief ranges are a 90-km-long group of north-trending, heavily faulted ranges of mostly east-dipping rocks. These in-line horsts and tilt blocks lie west of Lake and Panaca (Meadow) valleys. From north to south, the West, Ely Springs, Black Canyon, and Burnt Spring ranges are small horsts along the western side of the Bristol, Highland, and Chief ranges. Northern Dry Lake (Muleshoe) Valley is west of the Fairview Range, and the rest of Dry Lake Valley is west of the West, Ely Springs, Black Canyon, and Burnt Spring ranges. The Pioche Hills, which extend southeast from the eastern side of the southern Bristol Range, separates Lake Valley on the north from Panaca (Meadow) Valley on the south. All the ranges are uplifted along normal and oblique-slip (left-lateral and right-lateral, normal) faults.

The Fairview Range touches the Schell Creek Range across Muleshoe Pass, through which runs

the range-front faults for both the Schell Creek and Fairview Ranges. The Fairview Range is a horst made up of Devonian to Pennsylvanian rocks at both the northern and southern ends of the range (Best et al, 1998). The central part of the range consists of the western lobe of the Indian Peak caldera complex. The low passes between the Fairview Range and the Bristol Range and between Muleshoe Valley and the main part of Dry Lake Valley are cut by numerous east-striking faults of the Blue Ribbon transverse zone (Ekren and Page, 1995: Page and Ekren, 1995), which crosses the entire Great Basin at about this latitude (Rowley, 1998; Rowley and Dixon, 2001).

The Bristol Range is a horst that consists mostly of an east-dipping sequence of Cambrian carbonate rocks. The range is cored by a Tertiary pluton on the northern end that is associated with silver deposits of the Jackrabbit and Bristol districts. A low angle, west-dipping denudation or gravity-slide fault that placed Devonian rocks on Cambrian rocks is exposed in the northwestern part of the range (Page and Ekren, 1995). The Highland Range, which is the southward continuation of the Bristol Range, consists of east-dipping Cambrian carbonate rocks, underlain by Neoproterozoic and Cambrian quartzite. A moderately west-dipping, down-to-the-west fault on the western side of the range, apparently the breakaway part of the Highland detachment fault, placed the younger carbonate rocks on the apparently older quartzite. The Chief Range, south of the Highland Range, is made up of east-dipping Neoproterozoic and Cambrian quartzite that is unconformably overlain by Tertiary volcanic rocks and cut by a Tertiary pluton that controls the small Chief gold district (Rowley et al., 1992, 1994). The faults that lift the range on the western side consist of an oblique-slip fault (right lateral and normal) and the west-dipping Highland detachment fault.

The small West Range, to the west of the northern Bristol Range, consists of Devonian sedimentary rocks and Tertiary volcanic rocks on which Devonian rocks are emplaced along a low-angle fault that can be interpreted as a denudation fault or a gravity-slide plane (plate 3, cross section T–T') (Page and Ekren, 1995). The Ely Springs Range, south of the West Range and northwest of the Highland Range, consists of Cambrian through Silurian rocks, overlain by Tertiary volcanic rocks. The Black Canyon Range, south of the Ely Springs Range and southwest of the Highland Range, consists of Cambrian sedimentary rocks and Tertiary volcanic rocks (plate 3, cross section P–P'). The Burnt Springs Range, southwest of the Black Canyon Range, is made up of Cambrian sedimentary rocks unconformably overlain by Tertiary volcanic rocks (plate 3, cross section S–S').

The Pioche Hills consists of Cambrian sedimentary rocks unconformably overlain to the northeast by Tertiary volcanic rocks (Dixon and Rowley, 2007c). The hills contain the major Pioche lead-zinc- silver mining district, which is controlled by its proximity to the margin of the Indian Peak caldera complex (Best et al., 1989a and b). The margin includes caldera-collapse megabreccia and caldera ring dikes. Panaca (Meadow) Valley, south of the Pioche Hills, is probably at least 1500 m deep (plate 3, cross section P–P') and is filled with Pliocene to upper Miocene basin-fill sediments of the Panaca Formation (Rowley and Shroba, 1991).

DELAMAR MOUNTAINS

The Delamar Mountains extend southward for 60 km from the Burnt Springs Range, forming the western side of Delamar Valley and continuing to Coyote Spring Valley. The boundary between the Delamar and Burnt Spring ranges is the northern caldera wall of the Caliente caldera complex, here controlled by the east-trending Timpahute transverse zone (Ekren et al., 1976; Swadley and Rowley, 1994; Rowley, 1998). The eastern side of the northern Delamar Mountains is bounded by perennial, south-flowing Meadow Valley Wash, which drains Panaca (Meadow) Valley, passes south through Caliente, Nevada, and then creates Rainbow Canyon that separates the Delamar Mountains from the Clover Mountains to the east (Dixon and Rowley, 2007a and c; Tingley et al., 2010). The stream becomes ephemeral at the southern end of Rainbow Canyon, but in the Pleistocene it was part of through-flowing drainage that joined the Muddy River at Glendale, Nevada, and from there to the Colorado River. The eastern side of the southern Delamar Mountains is

Kane Springs Valley, to the east of which are the Meadow Valley Mountains.

The Delamar Mountains consist of east-dipping Neoproterozoic to Cambrian rocks and Tertiary volcanic rocks. The range, however, is dominated by Tertiary caldera complexes. The western end of the 24 to 12 Ma Caliente caldera complex is in the northern part of the range, and the 16 to 14 Ma Kane Springs Wash caldera complex is in the central part of the range (plate 3, cross sections N–N', D–D', and C–C') (Scott et al., 1990a and b, 1991a and b, 1995a, and 1996; Swadley et al, 1994b; Harding et al., 1995; Rowley et al., 1995; Rowley and Dixon, 2001; Dixon et al., 2007b). The main bounding fault of the Delamar Mountains is the down-to-the-west normal fault on the western side (Page et al., 1990; Scott et al., 1990b), and this is joined from the southwest by several splays of the left-lateral and normal PSZ (Ekren et al., 1977). In Kane Springs Valley, the bounding fault is the oblique (left-lateral and normal down-to-the-west) Kane Springs Wash fault zone (Scott et al., 1991a; Swadley et al., 1994b).

MEADOW VALLEY MOUNTAINS

The Meadow Valley Mountains constitutes a narrow, generally low, north-northeast-trending range about 60 km long. The northern 50 km of the range consists mostly of outflow ash-flow tuffs and part of the Kane Springs Wash caldera complex (plate 3, cross section C–C') (Scott et al., 1991a; Scott and Harding, 2006). The southern end of the Meadow Valley Mountains, just east of Coyote Spring Valley, is made up of mostly thrust-faulted and normally faulted Paleozoic rocks (plate 3, cross sections C–C'; plate 4, cross sections B–B', E–E', and F–F') (Pampeyan, 1993; Las Vegas Valley Water District, 2001). The Meadow Valley Mountains are separated from the Delamar Mountains on the west by Kane Springs Valley, a shallow valley underlain along the eastern side by the oblique-slip (normal, left-lateral) Kane Springs Wash fault zone (Swadley et al., 1994b; Harding et al., 1995; Scott et al., 1996). The broad, deep valley of Meadow Valley Wash lies east of the Meadow Valley Mountains and west of the Mormon Mountains (Schmidt, 1994; Dixon and Rowley, 2007a).

ARROW CANYON RANGE

The Arrow Canyon Range is a sharp, narrow, north-trending range consisting of a syncline of Cambrian to Mississippian carbonate rocks. It is uplifted along its western side by normal faults of the Arrow Canyon Range fault zone (plate 4, cross section I–I') (Schmidt and Dixon, 1995; Page and Pampeyan, 1996; Page, 1992, 1998). The trace of the north-striking Dry Lake thrust, which carries Cambrian rocks over Silurian through Permian carbonate rocks, is exposed and projected north just east of the range (Page and Dixon, 1992; Schmidt and Dixon, 1995; Las Vegas Valley Water District, 2001). East of the Dry Lake thrust, the Silurian through Permian rocks form a series of low, unnamed, north-trending hills. These hills are controlled by north-striking normal faults, along some of which are Pleistocene carbonate spring-mound deposits that indicate that the faults formerly carried significant groundwater (Schmidt and Dixon, 1995).

Coyote Spring Valley is west of the Arrow Canyon Range and Meadow Valley Mountains. A gravity survey by Phelps et al. (2000), as discussed by Dixon et al. (2007a), indicates that most of the valley is underlain by thin basin-fill sediments, generally less than 300 m thick (plate 4, cross sections E–E', F–F', G–G', and L–L'), but that two deep (maximum depth at least 1000 m), north-trending sub-basins occur just west of the southern Meadow Valley Mountains and northern Arrow Canyon Range. The generally shallow (maximum depth about 500 m) Table Mountain basin lies just east of the northern Arrow Canyon Range (Page, 1992).

Pahranagat Wash drains Coyote Spring Valley, then continues between the Arrow Canyon Range and the Meadow Valley Mountains to join the Muddy River near Muddy River Springs. Pahranagat Wash is currently an intermittent stream but was perennial after White River Valley was integrated with the Colorado River, at least ten thousand years ago. It is well known that southeast-flowing groundwater beneath Pahranagat Wash is the principal source of the many large springs in

the Muddy River Springs area, which currently create the surface flow in the perennial part of the Muddy River below the springs (Schmidt and Dixon, 1995; Donovan et al., 2004; Buqo, 2007; Donovan, 2007; Johnson, J., 2007). The details of the groundwater flow to Muddy River Springs were determined in part from the geologic mapping by Page (1992), Page and Pampeyan (1996), Schmidt et al. (1996), Williams et al. (1997c), and Donovan et al. (2004), and the geophysics of Scheirer et al. (2006). The mapping recognized that, following stream integration during the late Pleistocene, ancestral Pahranagat Wash flowed southeast—as it does now—through Table Mountain basin, which contains well exposed basin-fill sediments of the Muddy Creek Formation and younger Holocene to late Miocene deposits. Many of these younger sediments were deposited by spring discharge. From Table Mountain basin, the ancestral river continued southeast, parallel to and south of Nevada Highway 168, through an unnamed ridge of north-trending, east-dipping, Paleozoic carbonates. The ridge is the southward continuation of the southeastern prong of the Meadow Valley Mountains. Among other southeastern tributaries, the ancestral stream cut spectacular Arrow Canyon (Page, 1992), which is currently dry. At Muddy River Springs, the dry Pahranagat Wash becomes the Muddy River.

Additional geologic mapping by the USGS and SNWA showed that the bedrock ridge continues, although locally buried, for 30 km south of Arrow Canyon to become the Dry Lake Range (plates 2 and 4, cross sections F–F', G–G', H–H', and I–I'). The bedrock ridge is uplifted on both sides by north-trending basin and range faults, the largest being on the western side. These faults, plus others that parallel them on the east, served as groundwater conduits that carried groundwater southward, forming several upper Pleistocene spring mounds north of I-15 and west of the railway stop of Ute. Calcite veins as wide as 2 m, exposed in Wildcat Wash in the unnamed bedrock ridge, represent feeders for groundwater discharge along faults and fractures of the ancestral White River groundwater flow system (Page and Pampeyan, 1996). Within the bedrock ridge, east-trending faults are abundant, including some that control Arrow Canyon and Battleship Wash just to the south. In addition, mapping suggests that a west- northwest-striking fault zone, probably with right-lateral motion, formed a broad canyon now followed by Highway 168 that was probably the result of another large ancestral stream that carried surface water, with groundwater beneath it. Virtually all springs in the Muddy River springs complex are controlled by fault intersections of east-, north-, and northwest-trending faults. Locally the faults created abrupt Pleistocene scarps, some of which failed as landslides (Donovan et al., 2004). White, post-Muddy Creek Formation (Pliocene) sediments were deposited by spring discharge east-southeast of Muddy River springs, in upper Moapa Valley. The new mapping indicated that west- to northwest-striking faults appear to control nearly the entire course of the Muddy River between Muddy River Springs and Logandale, including the course of the river through the North Muddy Mountains (at Jackman Narrows). As described in North Muddy Mountains, Muddy Mountains, and Dry Lake Range, north-northwest-striking faults probably controlled the course of the Muddy River from Logandale to Overton, as well as the Overton Arm of Lake Mead. Some of the faults suggested by new mapping between Table Mountain basin and Lake Mead are buried by surficial sediments. To test the likelihood of faults in these areas, Scheirer and Andreasen (2008) interpreted gravity data that they collected along traverses oriented perpendicular to buried parts of some of the possible faults. The gravity data supported faults beneath Pahranagat Wash in Table Mountain basin (gravity line 2 of Scheirer and Andreasen, 2008), along Nevada 168 in Table Mountain basin (gravity lines 1 and 2) and perhaps north of Muddy River springs (gravity line 3), perhaps at Muddy River springs (gravity line 3), beneath the Muddy River south of Moapa (gravity line 4se), and perhaps in three places near Overton (gravity line 12).

FORTIFICATION RANGE, WILSON CREEK RANGE, AND WHITE ROCK MOUNTAINS

The Fortification Range is a narrow, locally high, north-northwest-trending range about 30 km

long. The range is a horst bounded on both sides by normal faults. Northern Lake Valley is on the west, and the southern end of Spring Valley is on the east. The northern half of the Fortification Range is a series of faulted, upper Paleozoic carbonate rocks including, at the northern end, a narrow, low, north-northwest-trending, northeast-dipping cuesta that joins the eastern side of the Schell Creek Range. The northern Fortification Range is complexly faulted and contains repeated sections of the Chainman Shale beneath the surface.

The southern half of the Fortification Range consists of east-dipping volcanic rocks (Loucks et al., 1989), part of which we interpret to be intracaldera rocks of the Indian Peak caldera complex. The Fortification Range connects at its southern end with the broad Wilson Creek Range beyond a low pass. This pass, at the mining town of Atlanta, Nevada, is partly underlain by an east-striking normal fault.

The Wilson Creek Range is a complexly faulted, north-northwest-trending range that forks southward, with the continuation of the Wilson Creek Range on the west and with the White Rock Mountains on the east. A small central valley (graben), named Spring Valley, separates the two ranges. This valley is called "little" Spring Valley in this report to distinguish it from the much larger Spring Valley to the north. The Wilson Creek Range and White Rock Mountains are each about 55 km long and consist entirely of intracaldera volcanic rocks, probably floored by an unexposed intracaldera (resurgent) intrusion of the Indian Peak caldera complex (Willis et al., 1987; Best et al., 1989c). The western side of the Wilson Creek Range is bounded by its main normal fault. The valleys to the west of the range are northern Lake and Patterson (southern Lake) valleys. The southern half of northern Lake Valley and all of Patterson Valley are within the Indian Peak caldera. The White Rock Mountains are a horst, with its main fault on the eastern side. The southern ends of the Wilson Creek Range and White Rock Mountains pass into a series of mostly unnamed, generally low fault blocks of intracaldera volcanic rocks (Best, 1987; Keith et al., 1994; Best and Williams, 1997; Williams et al., 1997a). These fault blocks continue southward for 15 km to the southern wall of the Indian Peak caldera. The fault blocks of the southern end of the White Rock Mountains extend eastward to join the southern Needle Range (Indian Peak Range) (Best et al., 1987a, b, and c), thereby closing off Hamlin Valley east of the White Rock Mountains. More fault blocks extend southward another 25 km as outflow volcanic rocks to the Clover Mountains, which is underlain by the Caliente caldera complex. Panaca Summit, traversed by Nevada State Route (SR) 319 and 15 km east of Panaca, is a pass through these hills of outflow volcanic rocks.

CLOVER MOUNTAINS AND BULL VALLEY MOUNTAINS

The Clover Mountains, Bull Valley Mountains, and northern Delamar Mountains represent a poorly defined, broad, east-trending, 100 km-long series of low mountains made up of heavily faulted volcanic rocks. North-south Rainbow Canyon, at the western edge of the mountain mass, is a narrow erosional cut made by Meadow Valley Wash. The northern part of the Delamar Mountains is west of Rainbow Canyon. The Clover Mountains extends from Rainbow Canyon for about 50 km to the Utah/Nevada border on the east, and from the Panaca (Meadow) Valley on the north about 40 km to the Tule Desert on the south. The Bull Valley Mountains extends another 30 km eastward from the Utah/Nevada border and is about 30 km north to south. The entire east-trending mountain mass passes into north-trending ranges on all sides. The mountain mass gets its unusual easterly trend partly because it is cored by the 80-km by 30-km Caliente caldera complex (Ekren et al., 1977; Rowley et al., 1992, 1995), mostly in Nevada but partly in Utah, and one of the largest calderas in the United States. The caldera complex is floored by an inferred intracaldera intrusion of batholithic dimensions, but it is exposed in few places (plate 3, cross sections N–N' and D–D'). The caldera complex is unusually long lived, from 24 to 12 Ma.

Another reason for the easterly trend of the mountain mass is that the east-elongated Caliente caldera complex is bounded on the north and south by east-trending transverse zones, the Timpahute on the north and the Helene on the south (Rowley, 1998). The zones here consist of oblique-slip

(normal and left-lateral) faults. Locally, the transverse zones are caldera margins. These transverse zones facilitated differential east-west growth (spreading) of the caldera, driven by east-west extension and caldera eruptions. Rowley and Anderson (1996) referred to the complex as a syntectonic caldera. Hudson et al. (1998) called the mountain mass the Caliente-Enterprise zone. They found from paleomagnetic data that Tertiary calc-alkaline igneous rocks within this belt have undergone vertical-axis counterclockwise rotation due to the mass being bounded by left-lateral shears that were active largely during Basin and Range extension. The northern of these shears corresponds to the Timpahute transverse zone, and the southern corresponds to the Helene transverse zone. Petronis et al. (2014) provided additional data in Utah that confirmed most of the conclusions of Hudson et al. Petronis et al. found that the zone extends eastward to the Colorado Plateau, where the rocks are not rotated. Furthermore, the northern side of the zone represents, and owes its rotation to, a place where the generally north-south Colorado Plateau–Great Basin boundary swings abruptly to trend west, so that east-west extension is pulling on an east-west boundary. South of the caldera complex, the Clover Mountains is underlain by Paleozoic carbonate rocks cut by a Sevier thrust fault and many high-angle normal faults, but these rocks are blanketed by a thick cover of outflow ash-flow tuff, and the area is remote and poorly studied and mapped.

Anderson et al. (2013) interpreted that the Caliente-Enterprise zone formed from southerly ductile flow of middle- to lower-crustal material, and they questioned whether plate tectonics is the most logical driving force for such flow. However, in the latest of many analyses of GPS data in the Great Basin, Hammond et al. (2014) confirmed generally east-west extension and resulting shear across the central Great Basin, with maximum strain rates at the eastern and western margins of the Great Basin, all consistent with known Pacific/North American relative plate motions.

MORMON MOUNTAINS

The Mormon Mountains are a nearly circular range, about 30 km across, east of lower Meadow Valley Wash. The Mormon Mountains represent a dome of mostly Cambrian to Permian rocks, underlain by Paleoproterozoic crystalline metamorphic rocks. East-verging Sevier thrust faults placed Cambrian rocks above Cambrian to Mississippian rocks. The range subsequently underwent major uplift, and it now is underlain by prominent positive aeromagnetic and gravity anomalies. Wernicke et al. (1985) interpreted the range to contain west-verging detachment faults that resulted from late Tertiary extension above a metamorphic core complex. Wernicke et al. (1985) suggested that these detachment faults followed thrust faults within the mountains. Anderson and Barnhard (1993) disputed the detachment hypothesis, and they instead emphasized footwall deformation along normal and oblique-slip, generally high-angle faults that flatten upward and formed during the major domal uplift. Carpenter and Carpenter (1994a) also disputed the detachment hypothesis, partly on seismic data unavailable to Wernicke and colleagues. Carpenter and Carpenter (1994a and b) argued for Tertiary extension along high-angle normal faults and explained Wernicke's low-angle structures as representing gravity slides. Walker et al. (2007) discussed data that supported the gravity-slide concept. These interpretations based on the findings since 1985 have been largely adopted by Page et al. (2005a), Scheirer et al. (2006), Anderson et al. (2010), and this report.

The broad valley of Meadow Valley Wash, to the west and northwest of the Mormon Mountains, is underlain by three geophysical sub-basins, the northern two of which contain basin-fill sediments and underlying volcanic rocks as thick as 2000 m, whereas the southern geophysical basin contains basin-fill and volcanic rocks as thick as 3000 m (Scheirer et al., 2006). Well logs suggest that the component of basin-fill sediments in these sub-basins is as much as 900 m (plate 4, cross section E–E'). Northwest of the Mormon Mountains, two buried thrust faults have been hypothesized (plate 3, cross section C–C'). Southwest of the Mormon Mountains, buried Paleozoic carbonate rocks may be present beneath Meadow Valley Wash (plate 4, cross section B–B'). A band of hills continuing southward from the Mormon Mountains is underlain by Paleozoic

sedimentary rocks that are cut by Sevier thrust faults, including the Glendale/Muddy Mountains thrust (plate 4, cross sections E–E' and F–F').

NORTH MUDDY MOUNTAINS, MUDDY MOUNTAINS, AND DRY LAKE RANGE

The southeastern corner of the study area contains the North Muddy Mountains and, to the south, the Muddy Mountains (plate 4, cross sections H–H', I–I', and K–K') (Bohannon, 1983). The North Muddy Mountains separates the California Wash area on the west from the Mesquite basin (Virgin River Valley) on the east. The Muddy Mountains occupy the northern side of Lake Mead. West of the Muddy Mountains, the study area includes the small Dry Lake Range east of Apex. This range is made up mostly of Bird Spring carbonate rocks. A narrow arm of bedrock extending west from Apex connects with the southern Arrow Canyon Range/Las Vegas Range. A thin finger of Quaternary sediments at Apex, just west of the Dry Lake Range, most probably was a pathway for Tertiary and Quaternary basin-fill sediments entering the Las Vegas Valley in the southwestern corner of the study area. The finger also is along the trace of the north-northeast-striking Dry Lake thrust (Page and Dixon, 1992). Basin-fill sediments to the northeast along the I-15 corridor (California Wash area) belong to an east-tilted half graben that reaches depths of 3000 to 4000 m (Langenheim et al., 2001, 2010; Scheirer et al., 2006). The California Wash area does not appear to have been connected with the Las Vegas basin because, based on limited mapping in the area, the basin sediments are not correlated with those in the Las Vegas Valley.

In the Muddy Mountains and North Muddy Mountains, high-angle normal faults strike north-northeast (Bohannon, 1983; Beard et al., 2007), and the east-west gap between the two ranges, now occupied by Tertiary and Quaternary basin-fill sediments, is also likely underlain by fractures of the same strike. The northern Muddy Mountains and North Muddy Mountains contain significant Jurassic sedimentary rocks (Bohannon, 1983; Beard et al., 2007), including the Aztec Formation. The northwestern side of the North Muddy Mountains is made up of upper Paleozoic carbonate rocks (Eichhubl et al., 2004; dePolo and Taylor, 2012). East-striking faults define the northern Muddy Mountains. These faults include the northeast-verging Glendale/Muddy Mountains thrust (Bohannon, 1983; Carpenter and Carpenter, 1994b; Beard et al., 2007). Bohannon interpreted this structure as the northern continuation of the Keystone thrust zone, which has been displaced approximately 60 km right laterally by the LVVSZ (see Sheep Range, Las Vegas Range, and Elbow Range). As with the Keystone/Glendale/Muddy Mountains thrust zone, the Dry Lake thrust just west of the Keystone/Glendale/Muddy Mountains thrust has been displaced the same amount by the same shear zone; its southern equivalent is the Deer Creek thrust in the Spring Mountains. Farther east in the North Muddy Mountains, the Summit/Willow Tank thrust is exposed (plate 4, cross section J–J') (Bohannon, 1983, 1984, and 1992; Carpenter and Carpenter, 1994b; Beard et al., 2007). At the southeastern end of the Muddy Mountains and northern side of Lake Mead, the LVVSZ passes eastward into the northeast-striking, oblique-slip (left-lateral and normal) Lake Mead fault zone, both part of Quaternary and late Tertiary east-west extension in the area (Anderson and Barnhard, 1993; Castor et al., 2000; Workman et al., 2002a and b; Anderson, 2003; Duebendorfer, 2003; Page et al., 2005a and b; Beard et al., 2007, 2010; Langenheim et al., 2010; Anderson, 2013).

Lower Moapa Valley, in the southeastern edge of the study area and northwest of where the Muddy and Virgin rivers enter the Overton Arm of Lake Mead, is clearly an area of groundwater discharge (Harrill et al., 1988). Surficial sediments, dominated by Quaternary and Pliocene river deposits of the ancestral and present Virgin and Muddy rivers, and resistant calcretes underlie the valley and Mormon Mesa (Williams, 1996 and 1997; Williams et al., 1997b and c). The surficial deposits are underlain by Pliocene and upper Miocene basin-fill deposits making up the southwestern end of Mesquite basin (Billingsley and Workman, 2000; Dixon and Katzer, 2002; Johnson et al., 2002). Surficial and basin-fill sediments are lumped as the QTa unit in plates 2 and 4, respectively, but in this area most basin-fill sediments are represented by the Horse Spring and

Muddy Creek Formations, which are exposed as low hills west of the river lowlands at Logandale and Overton. The Black Mountains and Gold Butte areas, respectively southwest and east of Lake Mead, contain Proterozoic metamorphic rocks that extend northeastward to the southwestern Virgin Mountains. Numerous fault zones have been mapped here and in the north Muddy Mountains (Beard et al., 2007; Anderson, 2003). These faults include northeast-striking faults of the Lake Mead fault zone (e.g., Anderson and Beard, 2010) that are discharge points for Rogers and Blue Point springs in the Lake Mead National Recreation Area.

Although not distinguished on the maps from Tertiary basin-fill deposits, deposits of the ancestral and present-day Virgin and Muddy rivers are likely to be many tens of meters thick, inasmuch as both rivers have been carrying and depositing sediments since at least the Pliocene. Permeability in the deposits is probably considerably greater than i n the underlying finer-grained Muddy Creek Formation but probably not in the coarser Horse Springs Formation. A large northwest-striking, down-to-the-northeast, normal fault is interpreted to partly control the axis of the basin and the linear nature of Overton arm of Lake Mead. Gravity line 12 (Scheirer and Andreasen, 2008) imaged three density contrasts that might represent splays of the fault, even though density contrasts would be expected to be small between different beds in the underlying basin sediments. This fault downthrows river deposits on the northeast against Muddy Creek Formation on the southwest. Southwest of that fault, the poorly exposed Muddy Creek Formation may be dropped down against the Horse Spring Formation by a queried normal fault. These rock units, as well as underlying Mesozoic rocks west of them, dip northeast into the basin.

ANTELOPE RANGE

The Antelope Range, in northeastern White Pine County, Nevada, is a relatively small, low range of faulted, Tertiary volcanic rocks that unconformably overlie west-dipping Silurian to Permian sedimentary rocks, dominantly carbonate rocks. It is a horst between the narrow, northern part of Spring Valley on the west, and Tippett Valley (Antelope Valley) on the east. At its northern end, Spring Valley contains about 600 m of basin-fill sediments. Tippett Valley contains at least 300 m of basin-fill sediments, with thick volcanic rocks beneath these sediments. Geophysical data, however, indicate that the depth to the pre-volcanic rocks locally is as much as 5500 m.

Gans et al. (1989) and Sweetkind et al. (2007a) speculatively showed the caldera source of the largest ash-flow tuff in the area, the 35 Ma Kalamazoo tuff, to be buried beneath northern Spring Valley just south of the Antelope Range and southwest of the Red Hills. Detailed gravity data were collected and analyzed by Mankinen and McKee (2011) of the USGS, through a cooperative agreement with SNWA. The gravity anomalies and depth-to-basement data do not support a caldera there, but suggest alternative caldera sites within Tippett Valley (see Kern Mountains and Adjacent Small Ranges).

DEEP CREEK RANGE

The Deep Creek Range is a high (about 3650 m altitude), north-trending range about 60 km long just east of the Nevada-Utah border and northeast of the Kern Mountains. The Deep Creek Range is a horst bounded by north-striking normal faults on either side that separate it from Deep Creek Valley to the west and northern Snake Valley and the Great Salt Lake Desert to the east. The fault on the eastern side of the Deep Creek Range appears to be the main normal fault controlling the range, and has vertical displacement of at least 3000 m, based on the height of the range and the Precambrian and plutonic rocks on its crest. Some of that displacement is Holocene (Black et al., 2003). The normal fault on the western side is also significant, for it drops Deep Creek Valley, which contains as much as 1500 m of basin-fill sediments.

Geologic mapping of the Deep Creek Range began with Nolan's (1935) classic report on the Gold Hill mining district at the northern end of the range. Here, Jurassic, Eocene, and Miocene plutons formed gold, tungsten, arsenic, silver, lead, copper, and zinc deposits in limestone of mostly Pennsylvanian and Mississippian age (Nolan, 1935; Robinson, 1993). Nolan mapped many east-striking faults that he called "transverse faults" and

recognized that they cut the range in many places. Rocks in the northern part of the mountains dip east and range from Neoproterozoic to Cambrian quartzite on the east to Devonian dolomite on the west. In the central part of the range, another Tertiary pluton, the Ibapah granite of 39 Ma (Rodgers, 1987; Miller et al., 1999a) spans the width of the range. The southern part of the range consists of highly deformed Neoproterozoic quartzite and schist of the McCoy Creek and Trout Creek groups. These Precambrian units have a combined thickness estimated at 6000 m (Nutt et al., 1990; Hintze and Kowallis, 2009). West of the southern part of the range, Paleozoic sedimentary rocks dip westward. These rocks range from Neoproterozoic and Cambrian quartzite through Cambrian and Devonian carbonate rocks and Mississippian Chainman Shale. They are cut by many low- to high-angle faults subparallel to the north-northeast-striking beds. The faults include low-angle faults (Miller et al., 1999a) that probably represent attenuation deroofing of the Deep Creek Range during its uplift.

KERN MOUNTAINS AND ADJACENT SMALL RANGES

The Kern Mountains is a 27-km-long, east-trending range that was structurally controlled by the Sand Pass transverse zone. East-striking faults occur on both the northern and southern sides of the range (Rowley, 1998; Rowley and Dixon, 2001). The granite core of the Kern Mountains is made up of three separate plutons. These plutons are all biotite-bearing. The largest pluton also contains primary muscovite. The plutons range in age from 75 to 35 Ma (Best et al., 1974; Ahlborn, 1977; Miller et al., 1999a). A separate, shallow Tertiary pluton erupted lava flows on the southeastern side of the range (Gans et al., 1989). The batholith that underlies the Kern Mountains is considered by Miller et al. (1999a) to represent part of an underlying core complex that formed the Snake and Deep Creek ranges and their attenuation/denudation faults. The Red Hills, a small north-trending range south of the western end of the Kern Mountains, consists mostly of complexly faulted and mineralized Paleozoic rocks. A narrow east-draining valley, Pleasant Valley, separates the Kern Mountains and the Deep Creek Range to the north. This valley may have as much as 1000 m of valley fill (plate 3, cross section X–X'). A broad unnamed valley between the Kern Mountains and the Snake Range contains white, coarse-grained, basin-fill sediments at its eastern end but these rocks appear to be relatively thin.

SNAKE RANGE AND LIMESTONE HILLS

The Snake Range is a broad, high, north-trending range. It contains Wheeler Peak, within Great Basin National Park (GBNP). The range is about 100 km long, nearly all of it in White Pine County, but with the low southern end in Lincoln County. The range is a complexly faulted horst, bounded on both sides by major high-angle normal fault zones. South of the Snake Range, the Limestone Hills are a narrow, low, heavily-faulted east-tilted low horst of mostly Devonian carbonate rocks about 30 km long.

Except for the southern end, the Snake Range is cored by Neoproterozoic to Cambrian quartzite that is intruded by a massive composite batholith formed apparently by multiple episodes of intrusion in Middle and Late Jurassic and Tertiary time (Whitebread, 1969; Miller et al., 1994, 1995, 1999a and b; Gans et al., 1999a and b; Lee et al., 1999a, b, and c; Miller and Gans, 1999; Gans, 2000b). The range was uplifted along its high-angle faults and the roof stretched apart so that its rocks failed along bedding planes in the Pioche Shale and moved in opposite directions down the flanks of the range as a non-rooted, gravity-driven structure best known as the Snake Range décollement (see Basin and Range Extension). The décollement places complexly faulted Middle Cambrian carbonate and younger rocks over a lower plate of Middle Cambrian carbonate rocks, Lower Cambrian clastic rocks, and older rocks. Most development of the décollement was synchronous with Basin and Range extension (Miller et al., 1999a; Gans, 2000a). The décollement is exposed on the top and both sides of the northern half of the range (Tingley et al., 2010; Ruksznis and Miller, 2014) (plate 3, cross section W–W'). East of the range, the décollement has been interpreted to have been imaged by

seismic profiles (Allmendinger et al., 1983 and 1985; Hauser et al., 1987; Miller et al., 1999a) as it passes eastward beneath the surface of Snake Valley. Allmendinger et al. (1983) and Kirby and Hurlow (2005) suggested that the eastern frontal fault of the Snake Range, separating the range from Snake Valley, is the low-angle Snake Range décollement itself. Geophysics (Mankinen and McKee, 2009; McPhee et al., 2009) and the straight range front argue instead for our interpretation of a high-angle normal fault that bounds the eastern side of the range (plates 1 and 6). Rodgers (1987), Alam (1990), Smith et al. (1991), Alam and Pilger (1991), McGrew (1993), and Miller et al. (1999a, figure 10) also showed such a high-angle normal fault that is younger than, and thus cuts, the décollement (plate 3, cross section W–W'). They considered, however, that this fault had "minor" displacement (Miller et al., 1999a, p. 891). Geophysics and well data argue otherwise.

The central part of the Snake Range is narrower and becomes progressively lower southward, and décollement faults are not exposed. Where U.S. Highway 6/U.S. Highway 50 crosses the range at Sacramento Pass, north-striking, east-dipping listric normal faults drop down to the east Miocene basin-fill sediments that are about 2000 m thick (Gans et al., 1989; Miller et al., 1994, 1995, and 1999a). The area south of Sacramento Pass includes GBNP (Sweetkind, 2007a and b), the centerpiece of which is Wheeler Peak, which at 13,065 ft (3982 m) is the second highest mountain peak in Nevada. The northern part of the Park was geologically mapped by Whitebread (1969) at 1:48,000 scale. In his mapping, he recognized the Snake Range décollement, which he left unnamed but referred to it not as a thrust but as a low-angle fault that placed younger rocks on older rocks. He considered all faults in the area to be of low angle and of the same structural event, although it is not clear whether he considered them of Sevier or Tertiary age. This mapping was compiled at 1:250,000 scale by Hose and Blake (1976). Following comprehensive detailed mapping in mostly the northern Snake Range (Miller et al., 1994, 1995, and 1999b; Gans et al., 1999a and b; Lee et al., 1999a, b, and c; Miller and Gans, 1999), Miller et al. (1999a) summarized the geology of the Snake Range décollement. Miller and her colleagues continued their mapping southward to include the entire Park, resulting in an unpublished, unauthored, and unreviewed digital 1:24,000-scale draft geologic map of the park, on file in 2008 with the National Park Service (NPS). It compiled—with some modifications—and expanded the mapping of Whitebread. Because the emphasis of their project was the Snake Range décollement, their mapping—as with Whitebread (1969)—of surficial (Quaternary) and basin-fill (Quaternary to Miocene) deposits was cursory and inadequate, and large-displacement, high-angle, basin and range normal faults that define both sides of the range and uplift the range, and also are abundant within the range, were not recognized. Updating the geology of the Snake Range on plate 1 required examination of 1:40,000-scale aerial photos and Google Earth images as well as limited field work and a review of more recent publications, including those on young and active high-angle faults in the area (Black et al., 2003; dePolo et al., 2009). Many previously unrecognized high-angle, generally north-trending, normal faults, some cutting Quaternary and Pliocene surficial and basin-fill deposits, were added to the maps. The two broad, north-striking range-front fault zones that define the western and eastern sides of the Snake Range include many of these Quaternary faults. Cumulative vertical displacement along these two great fault zones was thousands of meters. These two fault zones led to the deroofing (denudation) of the range along faults of the Snake Range décollement.

The southern end of the Snake Range is a low series of tilt-block cuestas of Devonian and Mississippian sedimentary rocks faulted against Tertiary volcanic rocks (plate 3, cross section U–U'). These tilt blocks become progressively lower in elevation to the south, and the eastern tilt blocks plunge beneath the valley fill. The western tilt blocks continue southward to become the Limestone Hills, which consists mostly of east-dipping Devonian carbonate rocks bounded by normal faults on the western and eastern sides. The Limestone Hills continues southward into the Wilson Creek Range (see Fortification Range, Wilson Creek Range, and White Rock Mountains). The southern end of the Limestone Hills forms part of the northern wall of the Indian Peak caldera

complex. Here the Atlanta silver-gold mining district is in Silurian to Ordovician carbonate rocks along the east-striking caldera margin.

Spring Valley, west of the Snake Range, is a 160-km-long, broad, deep graben containing about 2000 m of basin-fill sediments and defined by normal faults of at least 3000 m of vertical displacement (McPhee et al., 2005, 2006a and b; Mankinen et al., 2006; Dixon and Rowley, 2007d; Mankinen, 2007; McPhee, 2007) (plate 3, cross sections X–X', W–W', V–V', and U–U'). Details on the faults bounding and within the valley are given by isostatic residual gravity and maxspots and depth to pre-Cenozoic basement. About 25 AMT profiles in the valley locate range-front and subsidiary faults and provide estimates of depth to bedrock (Pari and Baird, 2011).

Spring Valley is made up of at least two geophysical sub-basins, as indicated by gravity data. The northern of these is about 145 km long. It is structurally deepest at its northern end, west of the Antelope Range, where it is a separate small basin. The southern end of the northern geophysical sub-basin is near the northeastern end of the Fortification Range, where depth-to-basement data show a shallow buried east-west bedrock ridge connecting the northern Fortification Range with the southern Snake Range. Near the central part of this northern geophysical sub-basin, just south of where US 6/50 crosses Spring Valley, Rattlesnake Knoll protrudes above the valley. This Knoll, investigated by Mankinen et al. (2006), may be the surface expression of another, narrower, buried east-west ridge. The southern geophysical sub-basin is about 30 km long, between the Fortification Range and the Limestone Hills. It is part of the same surface-drainage basin as the northern geophysical sub-basin, with surface flow northward into the low part of the northern sub-basin.

Snake Valley, east of the Snake Range, is a 150 km-long, broad, deep graben that passes southward into Hamlin Valley (Rowley et al., 2009, plate 1). The main graben-bounding faults, which also define the ranges on either side of Snake Valley, are interpreted to be high-angle normal faults (cross sections in our plate 1). These faults locally (cross section W–W') drop down the Snake Range décollement, which cut the Cambrian units beneath the basin fill of Snake Valley and perhaps from there pass beneath the western part of the Confusion Range.

As noted above, not all previous workers subscribed to the view that Snake Valley is a graben. In fact, even fewer workers interpreted a high-angle normal fault on the eastern side of Snake Valley as on the western side. Allmendinger et al. (1983), Miller et al. (1983, 1999a), Hauser et al. (1987), Smith et al. (1991), McGrew (1993), and Kirby and Hurlow (2005) suggested that the Confusion and related ranges represent the hanging wall of the Snake Range décollement, with no range-front normal fault defining the western side of Snake Valley. One possible reason for this misinterpretation is because Consortium for Continental Reflection Profiling (COCORP) data did not image any fault here. Yet, as Derik Howard (Southern Nevada Water Authority, personal commun., 2009) and A.G. Green (Swiss Federal Institute of Technology, 2009 "Pitfalls in high-resolution seismic methods," online at http://www.aug.geophys.ethz.ch/methods/seismic/seismic_pitfalls.html) noted that high-angle faults are notorious for not being imaged or poorly imaged by seismic data.

By itself, the presence of linear range fronts on both sides of Snake Valley argues for high-angle faults. The only place where the linear front is interrupted is east of where Sacramento Pass crosses the Snake Range. Here a westward embayment in the range front is underlain by a small basin containing deformed, west-dipping Miocene basin-fill sediments at least 2000 m thick (Miller et al., 1995 and 1999a). These sediments are cut by listric normal faults (Miller et al., 1995). A suggestion that these listric faults feed into the décollement at depth (Miller et al., 1995 and 1999a) does not explain the origin of the basin itself. Instead, a basin containing a great thickness of sediments requires a graben created by high-angle listric faults with significant vertical displacement, as elsewhere along the eastern flank of the Snake Range. Abundant northwest-striking Quaternary faults and a parallel youthful range front on the southwestern side of the Miocene basin argue that these northwest-striking faults control one side of the graben and continue across

the range through Sacramento Pass. Other Quaternary faults, most of them trending northerly, have been mapped throughout the length and width of Snake Valley (plate 1). Clearly Snake Valley is a deep, complex graben bounded by mostly high-angle faults, and that the interior part of the valley itself and its basin-fill sediments are cut by innumerable smaller faults of the same age and origin. Gravity data (Mankinen and McKee, 2009), including max spots that locally define some faults, and AMT profiles that image faults themselves (McPhee et al., 2009; Asch and Sweetkind, 2010, 2011), support this picture.

Basin-fill sediments beneath Snake Valley are locally more than 2000 m thick, with local holes in the basin containing thicker (3000 m) basin-fill and volcanic rocks (plate 3, cross sections X–X', W–W', and V–V') (Allmendinger et al., 1983; Saltus and Jachens, 1995; Davis, 2005; Kirby and Hurlow, 2005). Seismic sections (Alam, 1990; Alam and Pilger, 1991) and logs of oil wells in Snake Valley support these thicknesses (Herring et al., 1998). Logs of five test wells are particularly instructive: (1) Baker Creek no. 12-1 (TD=1459 m), 5 km east-northeast of Baker, indicated that basin-fill sediments and presumed Tertiary volcanic rocks extend to 1400 m depth (Hess, 2004); (2) Shell Oil Baker Creek Unit 1 (TD=1286 m), 10 km northeast of Baker, encountered basin-fill deposits that extend to a depth of more than 1100 m, if not 1250 m (Utah Division of Oil, Gas, and Mining, 2006, 2011); (3) Balcron Cobra State no. 12-36 (TD=1148 m), 50 km north-northeast of Baker, penetrated 562 m of basin-fill sediments, then 245 m of possible basal Tertiary sedimentary rocks (but more likely older basin-fill sedimentary rocks) (Herring, 1998a); (4) EREC Mamba Federal no. 31-22 (TD=993 m), 45 km north-northeast of Baker, penetrated 853 m of basin-fill sediments, underlain by Chainman Shale (Herring, 1998b); and (5) Amarada-Hess Federal no. 1-28 (TD=2372 m), 35 km north-northeast of Baker, penetrated at least 300 m of basin-fill sediments (the rocks between 300 and 1394 m below the surface were considered "undetermined") (Schalla, 1998; Hintze and Davis, 2002b). Additional information on thicknesses is given from gravity data and AMT profiles.

As with Spring Valley west of Snake Valley and other valleys east of Snake Valley, surficial sediments in northern Snake Valley are dominated by deposits of late Pleistocene lakes, notably LakeBonneville (Currey, 1982; Reheis et al., 2014). Bonneville shorelines reach as far south as the Baker area, with an elevation of about 1560 m, and the older Provo shorelines reach as far south as the Gandy area, with an elevation of about 1462 m (Currey, 1982).

Hamlin Valley, southeast of the Snake Range and south of, and tributary to, Snake Valley is about 90 km long. Like Snake Valley, it is a deep graben bounded by high-angle normal faults (plate 1, cross sections Q–Q', U–U'; see also Rowley et al., 2009, plate 1). Gravity data indicate that the maximum thickness of basin-fill deposits and underlying volcanic rocks beneath Hamlin Valley is about 3000 m (Mankinen and McKee, 2009). The Valley in most places contains at least 1200 m of basin-fill sediments. Five east-west and one north-south, oil company seismic profiles in southern Snake Valley and northern Hamlin Valley (Alam, 1990; Alam and Pilger, 1991) support this conclusion. Of these profiles, the northern east-west profile, which crosses the valley about 19 km south of Baker, found a thickness of basin-fill sediments of about 1000 m. The southern east-west profile, which crosses the valley east of the southern Limestone Hills, found a thickness of basin-fill sediments of about 2000 m. Both profiles discriminated volcanic rocks beneath the sediments.

The five profiles are tied to two oil-test boreholes, the Outlaw Federal no. 1 and the Fletcher no. 1. These and two other wells provide additional information on thicknesses: (1) Outlaw Federal no. 1 (TD=3962 m), near the eastern side of Snake Valley and the northern end of the Mountain Home Range, about 27 km south-southeast of Baker, spudded in, then went through, about 400 m of Arcturus Formation (Alam, 1990, figure 8); (2) Fletcher no. 1 (TD=2280 m), near the center of Hamlin Valley 54 km south of Baker, went through 1950 m of basin-fill sediments underlain by volcanic rocks to its total depth (Alam, 1990, figure 9; Hess, 2004); (3) Hamlin Wash no. 18-1 (TD=1216 m), located 3 km north of the

Fletcher well, penetrated 790 m of basin-fill sediments, then 180 m of volcanic rocks (Hess, 2004); and (4) Hamlin Wash no. 19-1 (TD=2127 m), located near Hamlin Wash no. 18-1, penetrated 1070 m of basin-fill sediments, then about 180 km of volcanic rocks (Hess, 2004). About 15 km south of the Fletcher well, the buried northern margin of the Indian Peak caldera complex is projected across Hamlin Valley. The southern half of Hamlin Valley contains a presumed similar thickness of basin-fill sediments as shown by the Fletcher and Hamlin Wash wells, but these sediments are underlain instead by intracaldera volcanic and intrusive rocks.

Many springs in Snake and Hamlin valleys (USGS, 2008) owe their presence to normal faults, which allow groundwater to move to the surface from the underlying water table. Big Springs occurs on the southeastern flank of the Snake Range at the edge of northwestern Hamlin Valley.

CONFUSION RANGE, CONGER RANGE, BURBANK HILLS, AND TUNNEL SPRING MOUNTAINS

The Confusion Range and small ranges of similar rocks form the entire eastern (Utah) side of Snake Valley. The area includes hills (Middle Range) connected to and east of the northern end of the Confusion Range. The Confusion Range proper is 95 km long, with a general northerly trend. The Conger Range is a 25-km-long, southwest-diverging fork in the southern Confusion Range and is located northeast of the small communities of Baker, Nevada, and Garrison, Utah. The Burbank Hills is a 25-km-long range south of the Conger Range and southeast of Baker and Garrison. The Burbank Hills is separated from the Conger Range by a northwest-trending valley known as the Ferguson Desert. The Tunnel Spring Mountains is a narrow, 30-km-long range southeast of the Burbank Hills and east of northern Pine Valley. Tule Valley is east of the Confusion Range. Northern Pine Valley connects with the southeastern end of the Ferguson Desert.

All of these ranges consist almost entirely of north-striking, folded, thrusted, and attenuated, middle to upper Paleozoic rocks and Triassic rocks that together form a synclinorium, in other words a combination of synclines and anticlines that overall appear as a broad syncline (plates 1 and 3, cross sections W–W' and V–V') (Hose, 1977; Hintze and Davis, 2002a and b, and 2003). The Mississippian Chainman Shale, 300 to 600 m thick in the area, is repeated and thus exposed on both sides of and beneath all these ranges because it is deformed into north-striking folds (Hintze and Davis, 2002a and b, and 2003). Tertiary regional ash-flow tuffs formerly covered most of the area to a thickness of as much as 150 m, but erosion has left only patches of these tuffs, notably the Oligocene Needles Range Group, derived from the Indian Peak caldera complex (Best et al., 1989a and b). Normal faults cut all these ranges, but most are of small displacement so individual stratigraphic units are remarkably coherent and continuous over this large area. The most significant normal fault is the northerly-trending fault zone that defines the eastern side of Snake Valley. Normal faults that separate the Confusion Range from Tule Valley have moderate vertical offset.

Greene and Herring (2013) and Greene (2014) suggested that Sevier thrusting in the Confusion Range is much more significant than previously reported, yet they agreed that exposed thrusts are in general correct as portrayed by previous mappers. Therefore, their proposed new thrusts, as shown in their new cross sections, exist only in the subsurface and have no support by existing drilling or seismic sections. Some of their proposed thrusts are beneath the depth of our cross sections. Greene (2014) called the thrusts in the Confusion Range the western Utah thrust belt, which he considered to be one of several small belts in the Sevier hinterland west of the large frontal Sevier thrust belt.

Tule Valley is an internally drained, north-trending valley that is about 100 km long. It joins the Great Salt Lake Desert to the north and the Wah Wah Valley to the south over low passes of about 1525 m elevation. The Valley is a graben, with a maximum thickness of basin fill suggested by Davis (2005) to be 2000 m based on a seismic profile published by Allmendinger et al. (1985). Gravity data, however, indicate that the maximum thickness of basin-fill deposits and volcanic rocks beneath Tule Valley are about 1200 m (Mankinen

and McKee, 2009). The surface of Tule Valley is dominated by deposits of Pleistocene pluvial Lake Bonneville (Sack, 1990), including Bonneville shorelines (elevation 1564 to 1583 m) and Provo shorelines (elevation 1460 to 1470 m) (Currey, 1982). Tule Valley contains several warm springs (Stephens, 1977), with temperatures between 75°F and 88°F (24°C and 31°C; Blackett and Wakefield, 2004), that are aligned along north-south normal faults (Stephens, 1977; Sack, 1990).

The Ferguson Desert, about 30 km long, connects Snake Valley with Pine Valley. Gravity data indicate that the Ferguson Desert is shallow, and as much as 1000 m of basin-fill deposits is shown on plate 3, cross section V–V'. A water well in the center of the upper Ferguson Desert penetrated only 158 m of basin-fill sediments before intersecting limestone bedrock (Hood and Rush, 1965, p. 19). The western part of the Ferguson Desert is cut by many north-northeast-trending normal faults and is underlain at shallow depth by the Chainman Shale. Pine Valley is an internally drained, north-trending valley about 80 km long. The basin is a graben underlain by basin-fill sediments and underlying volcanic rocks that have a maximum thickness of about 3000 m (Mankinen and McKee, 2009).

NEEDLE RANGE AND WAH WAH MOUNTAINS

The Needle Range, just east of the Nevada-Utah state line, is about 80 km long and consists of two subranges, the Mountain Home Range to the north and the Indian Peak Range to the south. The Mountain Home Range merges with the Burbank Hills to the north. Hamlin Valley, to the west, separates the Needle Range from the southern Snake Range, Limestone Hills, and White Rock Mountains to the west. To the east of the Needle Range is Pine Valley and to the south is the Escalante Desert. The Wah Wah Mountains are a parallel tilt block of similar length to, and located east of, the Needle Range, east of the study area. The Wah Wah Mountains are the southward continuation of the Confusion Range. Wah Wah Valley is east of the Wah Wah Mountains and west of the San Francisco Mountains.

The northern part of the Needle Range consists of folded, middle to upper Paleozoic rocks (Hintze and Davis, 2002b). Locally, lower Paleozoic carbonate rocks are thrust over upper Paleozoic carbonate rocks (Best et al., 1987a and b). Most of the Needle Range, however, consists of east-dipping outflow ash-flow tuffs derived primarily from the Indian Peak caldera complex. The southeastern caldera margin passes through much of the southern part of the range (Williams et al., 1997a). The Needle Range is a faulted horst, with the main normal fault separating Hamlin Valley from the Needle Range (plate 1, cross sections U–U' and Q–Q'). The basin-fill sediments in the southern half of Hamlin Valley are underlain by the Indian Peak caldera complex (plate 3, cross section Q–Q'). A significant normal fault separates the eastern side of the Needle Range from Pine Valley.

The northern Wah Wah Mountains, like the southern Confusion Range just to the north, consist of gently folded and locally thrusted, lower to middle Paleozoic carbonate rocks. These structures and those in the Needle Range are part of Greene's (2014) western Utah thrust belt. Farther south, east-dipping Neoproterozoic to Cambrian quartzite and overlying Cambrian carbonate rocks form most of the range (Hintze and Davis, 2002b; Rowley et al., 2009, plate 1). An oil well drilled by Hunt Oil Company in the southern Wah Wah Mountains was spudded in the Prospect Mountain Quartzite and penetrated 3800 m of rocks, including several thrust zones (Erskine, 2001). Other thrust faults that place lower Paleozoic rocks over middle and upper Paleozoic rocks are well exposed and unconformably overlain by east-dipping, Tertiary ash-flow tuffs (Abbott et al., 1983). Near the southern end of the range, other Sevier thrusts place Cambrian rocks above the Jurassic Navajo Sandstone (Best et al., 1987c; Hintze et al., 1994b). The thrusts in the southern Wah Wah Mountains are part of the main Sevier frontal thrust belt. The southeastern part of the Indian Peak caldera complex cuts the southwestern end of the Wah Wah Mountains (Williams et al., 1997a). As with the Needle Range, the dominant structure controlling the range is a normal fault zone on the western margin, beneath Pine Valley. The southern ends of both the Needle Range and

the Wah Wah Mountains merge with each other (Best et al., 1987c) and, still farther southwest, merge with the White Rock Mountains. These southern range margins form the northern margin of the Escalante Desert and the southern margin of the Indian Peak caldera complex (Best, 1987).

Wah Wah Valley is an internally drained valley about 50 km long. At its southern end, a low pass at an elevation of about 1700 m separates the valley from the Escalante Desert to the south. At the northern end of Wah Wah Valley, an even lower pass separates the valley from the Sevier Desert to the north. The thickness of basin-fill sediments in Wah Wah Valley is not well known. From comparison of gravity data with well logs in and near the valley, Stephens (1977) estimated the maximum thickness of basin-fill sediments to be 730 m. Mankinen and McKee (2009) applied a modern gravity survey to calculate a more likely maximum thickness of basin-fill and volcanic deposits beneath the valley to be about 2000 m. Bonneville and Provo shorelines are mapped in the northern half of Wah Wah Valley (Currey, 1982).

FISH SPRINGS AND HOUSE RANGES

The 30-km-long Fish Springs Range extends south from the Great Salt Lake Desert. The southward continuation of the Fish Springs Range is the 100-km-long House Range. The two ranges form the eastern boundary of Tule Valley. The Fish Springs Range is a highly faulted but generally gently west-dipping horst consisting of Middle Cambrian to Middle Devonian carbonate rocks that rest on Lower Cambrian siliciclastic rocks (plate 3, cross section X–X') (Kepper, 1960; Hintze, 1980a and b; Morris, 1987; Hintze et al., 2000; Hintze and Kowallis, 2009). The range is bounded by large normal faults on its western and eastern sides, with the main fault being the one on the eastern side. This fault is still active and has components of Holocene and Pleistocene movement (Oviatt, 1991; Black et al., 2003). East-striking, oblique-slip faults have been mapped throughout the range (Hintze, 1980a and b). Some of them partly control the Fish Springs zinc-lead-silver-tungsten mining district on the northwestern side of the range (Oliveira, 1975; Christiansen, 1977). A newly discovered, buried Eocene quartz monzonite pluton also controls this district (Puchlik, 2009). A concentrated series of east-striking faults occurs at Sand Pass, which separates the southern end of the Fish Springs Range from the northern end of the House Range. This east-trending fault zone is part of the Sand Pass transverse zone, which extends intermittently as far to the east as the Wasatch front and as far to the west as the Kern Mountains (Stoeser, 1993; Rowley, 1998; Rowley and Dixon, 2001). At Sand Pass, the transverse zone contains small intrusions (Chidsey, 1978) and causes profound structural differences (the rocks have opposite dips and the main fault is on opposite sides) between the two ranges north and south of it, as in some other transverse zones (Faulds and Varga, 1998).

The high House Range is a tilted horst, bounded on the western side by a major normal fault beneath eastern Tule Valley and on the eastern side by a fault of lesser displacement. The faults uplift the range and tilt it several degrees east (Hintze and Davis, 2002a; Rowley et al., 2009, plate 1). Like the main bounding fault zone of the Fish Springs Range, the main fault zone of the House Range is an active fault zone of large displacement that includes Holocene and Pleistocene movement (Sack, 1990; Black et al., 2003), but this fault zone is on the western side of the House Range. The range, famous among paleontologists for its trilobites, consists mostly of Cambrian strata, which include clastic sedimentary rocks at the western base of the range and carbonate rocks above. The central part of the range is intruded by the Notch Peak quartz monzonite pluton of Jurassic age.

Fish Springs Flat is a 50-km-long, north-trending valley east of the Fish Springs Range and northern House Range. It drains northward into the Dugway Proving Ground part of the Great Salt Lake Desert (Clark et al., 2007, 2008). The south end of Fish Springs Flat is marked by a low pass at about 1550 m that separates it from northern Whirlwind Valley. Whirlwind Valley drains southward into Sevier Lake. Fish Springs Flat is a complex graben bounded on the west by the major late Miocene to Pleistocene Fish Springs fault zone that was reactivated in the Holocene, and on the east by faults that raise the Black Rock Hills,

Thomas Range, Drum Mountains, and Little Drum Mountains. The northern end of Fish Springs Flat contains the large Fish Springs spring complex, managed by the USFWS as the Fish Springs National Wildlife Refuge. Although the groundwater that discharges from Fish Springs is part of the north-flowing Great Salt Lake Desert flow system, the source of this water is controversial, as discussed by Rowley and others (2009, 2016), Hurlow (2014), and Gardner and Heilweil (2014). All springs are controlled by the Fish Springs fault zone. The thickness of basin-fill sediments and underlying volcanic rocks beneath Fish Springs Flat is about 1000 m (Mankinen and McKee, 2009) (plate 3, cross section X–X'). At the surface of Fish Springs Flat and the flanks of its bounding ranges, deposits of late Pleistocene pluvial Lake Bonneville are well exposed, including the Bonneville shoreline (elevation 1583 to 1591 m) and Provo shoreline (elevation 1471 to 1476 m) (Currey, 1982; Oviatt, 1991).

CONCLUSIONS

This report describes the results of a long-term study of the three-dimensional geologic framework of a large part of the Great Basin of Nevada and Utah so as to identify and understand two regional groundwater flow systems as well as adjacent flow systems that might interact with the subject flow systems.

GEOLOGIC FRAMEWORK

In the Neoproterozoic and Early Cambrian, thick quartzite and other clastic rocks were deposited in Eastern Nevada and adjacent parts of Utah. These rocks represent the initial deposits of the Cordilleran miogeocline, and were deposited in shallow marine water along the western passive continental margin of North America. Middle Cambrian through Lower Permian rocks record a shift in deposition to mostly carbonate sedimentation. Predominately limestone and dolomite strata, with a thickness of 10,000 m or locally more, are known as the great carbonate aquifer. All these rocks can be grouped into two facies that are gradational over time and place: (1) a western facies of the Cordilleran miogeocline, now exposed over most of the study area, that represents a Neoproterozoic through Devonian offshore carbonate shelf and intertidal environment of deposition and an overlying Mississippian to Permian carbonate platform; and (2) a thinner eastern facies that includes cratonic platform rocks (Colorado Plateau) in the extreme southeastern part of the study area that are mostly shallow marine but locally are near-shore through continental sediments.

In Late Devonian to Late Mississippian time, thrust faults and folds of the Antler orogeny transported deeper-marine rocks eastward to approximately the longitude of Eureka, Nevada, and created a highland there. Clastic sediments, which included the Chainman Shale, were deposited in a marine foreland basin east of the Antler Highland. Carbonate deposition resumed by Late Mississippian time and continued through the Pennsylvanian and into the Permian.

Triassic, Jurassic, and Cretaceous rocks in the study area are mostly continental clastic units deposited only in the eastern part of the area. In fact, the entire study area was characterized by erosion during and after deposition of these units. Thus, Jurassic, and Cretaceous strata are variably dispersed and have a collective thickness of less than several thousand meters, although thicker in the extreme southeastern part of the study area. From Middle Jurassic through the early Paleocene, thrust faults, folds, and intrusions of the Sevier orogenic belt were emplaced. The thrusts transported western facies rocks eastward onto thinner eastern, more cratonic facies. A series of large frontal thrusts are well exposed throughout the southern part of the area. Most thrusts strike north-northeast and therefore pass east of the northern part of the study area. The central and northern parts of the area are referred to as the hinterland of the thrusts, characterized by minor thrusting and folding. The deformation created a highland over most of the area that shed clastic sediment eastward.

During and following the waning stages of the Sevier deformation in the Paleocene, erosional stripping of the Sevier highland that included the northern two-thirds of the study area led to sedimentation east of the study area. Only the post-deformational Sheep Pass Formation in mostly White Pine County and the Claron Formation just southeast of the area remain as sediment patches unconformably deposited on the older thrusted and folded structures. These sedimentary rocks, as well as the deeply eroded underlying Paleozoic and Mesozoic rocks, were then inundated by voluminous Eocene to Miocene calc-alkaline, subduction-related arc volcanic rocks. Most of these rocks are ash-flow tuff, derived from many scattered calderas in and near the area, but andesitic to dacitic lava flows and volcanic mudflow breccia from stratovolcanoes in the area were also deposited. Depositional thickness of overall outflow ash-flow tuffs and flows ranged from about 300 to 2000 m thick over most of the area, but intracaldera tuffs are thicker. Intrusions, the ultimate sources of the volcanic rocks, are abundant. The eruptive centers, including the intrusive sources, for these rocks formed three east-trending igneous belts, as

supported by aeromagnetic data. The belts become younger from north to south, so most depositional products from the northern belt have been removed by erosion. The locations and types of post-Sevier, pre-extension faults that deformed the lower to middle Tertiary sedimentary and volcanic rocks are uncertain but doubtless included oblique-slip, high-angle faults and were part of an upland remaining from Sevier times. East-trending transverse zones, which began to form in the Mesozoic, deformed the calc-alkaline rocks and continued active throughout the Cenozoic, including today.

By early Miocene, at roughly 20 Ma in and east of the study area, subduction ceased and east-west regional extension began. The Basin and Range extension was predominantly characterized by north-striking high-angle normal faults. The map pattern, however, demonstrates that additional structures also accommodated the deformation, namely low-angle attenuation/denudation normal faults of various strikes, mostly northwesterly-striking right-lateral and northeasterly-striking left-lateral oblique-slip transfer faults, and east-striking transverse zones. As the rocks were extended east-west, all these structures had their own part in the deformation and left their trademark features. The high-angle normal faults resulted in the north-trending ranges that were uplifted on one side as tilt blocks or more commonly on both sides as horsts, and adjacent north-trending basins went down as tilt blocks or grabens. Isostatic residual gravity data, in conjunction with horizontal gradients (maxspots) calculated from gravity and magnetic data provide evidence that all major basins and ranges are bounded by high-angle normal faults. The low-angle attenuation/denudation faults are non-rooted, gravity-driven structures that resulted from sliding of the flanks and tops of the rising ranges into the adjacent valley, generally along weak shale beds, notably the Pioche Shale and Chainman Shale. The northwest- and northeast-striking transfer faults, where strike-slip motion is greater the closer the strike of the fault is to east-west, in places pass along strike into north-striking high-angle normal faults, where the motion is largely dip slip. The transverse zones are a type of transform zone, by which broad east-trending masses of rock north and south of each transverse zone moved at different amounts and rates or along different structures, with respect to the other side of the zone, in response to regional east-west compression (during the Sevier event) or east-west extension (during the Basin and Range event). Transverse zones are considered to be deep high-angle structures and so may not be always expressed at the surface in all places along the strike of the zone.

The basins and ranges that were produced early (20 to 10 Ma) during Basin and Range extension are not necessarily in the same places as the current basins and ranges. The current basins and ranges seemed to have started to form at about 10 Ma based on information from in and east of the study area. At this time, extensional deformation appears to have intensified and the present topography began to form. The rising ranges were stripped by erosion and the subsiding basins were again filled by erosional debris. The resulting basin-fill sediments accumulated to many kilometers thick. Bimodal (basalt and rhyolite) volcanic rocks, generally thin, are locally intertongued with the basin-fill sediments. The sedimentary basin fill is the primary current aquifer in the study area, as elsewhere in the Great Basin. Gravity geophysical data converted to depth-to-pre-Cenozoic basement by the gravity-inversion method provide accurate information on basin depths. Including thin calc-alkaline volcanic rocks that underlie the basin-fill sediments that cannot be geophysically separated from basin-fill sediments, thicknesses of Cenozoic rocks are locally more than 6 km thick in some basins. Most of this depth, relative to the pre-Cenozoic bedrock ("basement") in the adjacent ranges, can be ascribed to offset along multiple high-angle normal faults. All Basin and Range structures, whether high-angle normal faults, low-angle normal faults, transfer faults, or transverse zones, show Quaternary displacement in the study area or nearby.

Geologic maps at 1:250,000 scale cannot do justice to the actual fault complexity of the study area, for thousands of real faults cannot be shown. AMT profiles, as presented here, determined the fault architecture of parts of some basins and of their range-bounding faults, most of which were

buried by young basin-fill and surficial sediments. All of the AMT profiles shown in the geophysics chapter, and especially several of the longer profiles, demonstrate this detailed complexity. Examples are Profiles SVN10 West and East (figure 24 and figure 25) across central Spring Valley, Profile SVNA (figure 28) across southern Spring Valley, and Profile SNK4 (figure 34) across southern Snake Valley. We consider these profiles to typify the level of fault complexity across most basins and ranges in the study area. The profiles also distinguish many regional from subsidiary (smaller) faults. These same AMT profiles provide information on the lithology of basin-fill sediments versus underlying bedrock and as such allow information on the size of these faults as well as their location.

Some of the transfer faults were crossed by AMT profiles, showing that many of these faults are comparable in size and extent of deformation to the regional range-front high-angle normal faults. Examples are Profile SVN13 (figure 22) at Sacramento Pass across the Snake Range, Profile DLV50 (figure 36) in eastern Dry Lake Valley, and Profiles DELA5 and DELA1 (figure 41 and figure 42) that cross different strands of the PSZ in southern Delamar Valley. AMT profiles across some of the Quaternary faults show that some of these faults have large displacements, perhaps a conclusion not anticipated considering that the scarps in Pleistocene and Holocene sediments are rarely higher than 3 m. Examples of large faults that have Quaternary displacement are Profiles DLV3 (figure 37) and DLV8 (figure 40) in Dry Lake Valley. Clearly these faults have been active for a longer time than just Quaternary.

HYDROGEOLOGIC IMPLICATIONS

Understanding the regional hydrology of areas making up many thousands of square kilometers and in complex geologic terrains requires major investments in time and finances. SNWA's investment in time has been almost 30 years. The first step in this major investigation was to accumulate geologic information, leading next to putting together the three-dimensional geologic and geophysical framework of the area of interest. This framework is the subject of the present report. Such a framework allowed synchronous and later hydrologic and biologic investigations to proceed. Of these, the hydrologic studies enabled predictions of amounts and quality of groundwater, directions of groundwater flow, sources of recharge of groundwater, and best sites for extraction of groundwater. Data and conclusions on these topics, however, are found in unpublished reports by SNWA that were intended for presentations at public hearings of the Nevada State Engineer. Yet published hydrologic studies in much the same area, using their own geologic frameworks, were done independently during the last decade by the UGS (e.g., Hurlow, 2014; Hurlow and Inkenbrandt, 2016) and the USGS (e.g., Welch et al., 2007; Heilweil and Brooks, 2011; Masbruch et al., 2014, 2016). Perhaps not unexpectedly, the major hydrologic conclusions from the studies of all three organizations are remarkably similar, with some exceptions noted by Rowley et al. (2016). Regardless of the relatively small differences in the major conclusions, their similarity demonstrates the value of different groups independently working on the same complex problem by applying similar long-term efforts. The investigations by the three organizations is continuing. For example, hydrologists and biologists at the SNWA, UGS, and USGS continue their monitoring, and the UGS and USGS periodically issue new published hydrologic reports.

Major hydrologic conclusions given in many SNWA reports are not covered here because they require the supporting data, including maps of water levels, monitoring of water levels, precipitation values, recorded annual well discharges, water chemistry, cross sections and analyses of the controls and discharges of major springs, water budgets, aquifer tests such as pumped volumes and other hydraulic data, etc. However, speaking only of hydrogeologic conclusions resulting from our framework study, several items stand out, although the discovery of many of these must be credited also to previous work, especially on the Death Valley regional groundwater flow system and other work on the NTS that all current authors participated in. First, as documented in the Introduction, the governing concept in determining groundwater flow through

regional flow systems in the Great Basin is fracture flow along normal faults and their parallel fault-caused joints. It seems undeniable that the flow of the main volumes of groundwater is along these faults and their related joints. Therefore the geologic mapping of faulted terranes provides the first approximation of groundwater flow directions and locations.

Many of the hydrographic areas (basins) in the study area are closed basins. The first approximation as to whether groundwater moves beneath topographic divides to another basin, therefore determination of what basins make up a groundwater flow system (e.g., Harrill et al., 1988), and what the likely groundwater pathways are, derives largely from the topography, maps of water levels, and hydraulic heads observed. However, geologic mapping of the faults and the relative positions of aquifers and confining units making up the boundaries of basins will allow a more accurate interpretation of whether flow paths are likely, unlikely, or permissible across any particular part of basin boundaries. Such an exercise was part of the overall study (Dixon et al., 2007a; Rowley et al., 2011, 2016) and those by the UGS and USGS. Accurate geologic maps are essential in making assessments of flow paths beneath basin boundaries.

Each succeeding episode of deposition of rocks and their deformation had increasingly greater effects on the hydrogeology of the study area. Most of the hydrogeologic effects for Paleozoic events, including the Antler orogeny in the Devonian and Mississippian, resulted from deposition of the various sedimentary units that would become important aquifers and aquitards in the study area. The greatest of these bedrock aquifers is the Cambrian to Permian carbonate aquifer. In these rocks, groundwater dissolution resulted in even larger and more interconnected conduits. And an interruption in this carbonate deposition by Antler clastic sedimentation resulted in perhaps the most important confining unit in the northern part of the study area, the Chainman Shale. After the Permian, deposition of clastic continental sedimentary rocks dominated throughout the Mesozoic, resulting primarily in confining units or low-permeability sedimentary rocks. Yet most of these Mesozoic rocks were stripped away during Sevier deformation, so such Mesozoic rocks have little bearing on water resources over most parts of the study area. Although Sevier thrust faults are large and relatively abundant in the south, they are relatively small and sparse elsewhere in the study area. Either way, individual thrusts seem to have had negligible effects to groundwater flow, and they created barriers when the thrusts carried confining units onto the carbonate sequences.

During the Eocene, Oligocene, and early Miocene, emplacement of calderas, with associated caldera ring-fault walls and intracaldera intrusions, created areas of low permeability. Aeromagnetic data help to define calderas and plutons, which formed east-trending highlands that erupted thick sequences of volcanic rocks. Yet the calc-alkaline ash-flow tuffs derived from the calderas--whether filling the calderas or spread outside their source calderas--formed significant although thin aquifers in many places. Some other calc-alkaline volcanic rocks, such as mudflows that tend to be confining units and may be sandwiched between valley fill above and carbonate rocks below, may reduce the interconnection between the carbonate aquifer and the valley fill in some basins. Such relationships would explain some carbonate aquifers that are under artesian pressure or at least have a piezometric head higher than that of basin fill. Some springs may result from this. During Mesozoic to late Cenozoic, east-west transverse zones developed. These zones may provide potential conduits or barriers to groundwater flow, although their hydraulic significance is generally unknown.

From middle Miocene to the present time, extensional tectonics resulted in the dominant north-south high-angle faults of the Great Basin. This deformational regime and the rocks deposited as a result of it had by far the greatest effect on groundwater resources and their movement. The north-striking structures are excellent conduits to north or south groundwater flow. Gouge in the core zone of these faults acted as partial to complete barriers, however, to east or west flow. There is significant evidence, as well as simple logic, that indicates that large faults have a greater influence on flow than smaller faults, and therefore plates 1 and 2 show both sizes, with the clear suggestion that the bigger ones are more important in

hydrologic assessments. During Basin and Range tectonism, all rocks became fractured, but brittle units such as carbonate rocks, ash-flow tuffs, basalt and rhyolite flows, and locally some quartzite units became shattered throughout and thus are local or regional aquifers. The most important and most extensive aquifer in the study area is the basin-fill aquifer. Depth-to-basement calculations based on gravity data provide the information needed to assess the size of this aquifer in any one place.

Concealed normal faults, whether defining the edges of most basins or within basins, can be located by gravity (maxspots) and AMT data. Upward-continued gravity and aeromagnetic maxspots and some AMT profiles can determine which way the fault or caldera wall dips. Of the two types of geophysics, AMT profiles also provide information on depths to groundwater in some parts of basins. AMT profiles are sufficiently detailed to allow siting of wells on faults, which are the best places to locate production and monitoring wells. Ideally, the best location would be a range-front fault of a large range with abundant recharge, near the mouth of a perennial creek that carries some of that recharge. The objective to site a well is to drill the downthrown side of a high-angle normal fault, the larger the better, to intersect the fault beneath the water table. If the dip of this fault is not known but the direction of throw (and the depth to the water table) is, one can assume an average dip of 60 degrees, then position the drill rig with respect to the fault accordingly.

Virtually all significant springs in the study area arise along faults. That includes warm and hot springs, most of which represent rapid vertical rise along faulted "channels" of water heated by the geothermal gradient. Springs provide the surface expression of fracture flow, and mapping of springs gives valuable information on water tables, local permeability, and availability of groundwater. Fault and fracture pathways for groundwater commonly leave behind calcite growths, in places expressed as spring mounds or, where older and more deeply eroded, as calcite veins.

This long-term study combined simultaneous and closely coordinated studies of cutting-edge geology, geophysics, and hydrology. We suggest that it is a model for future hydrological analyses elsewhere in the increasingly thirsty western United States.

ACKNOWLEDGMENTS

This report is the culmination of more than two decades of work by the authors, including several interim reports. Nearly all reports were funded by the Southern Nevada Water Authority. Our work involved, with our grateful appreciation, collaboration with many colleagues, only some of whom are mentioned below. We received hydrologic, geologic, and geophysical data, expertise, and advice from Ken Albright, Zane Marshall, Casey Collins, Jim Prieur, Gavin Kistinger, Frank Baird, Steve Acheampong, and Dave Donovan of SNWA, from Jim Faulds of NBMG, from private consultants Terry Katzer of Reno, Farrel Lytle of Pioche, and Frank D'Agnese of Tucson, from Hugh Hurlow, Lucy Jordan, and Paul Inkenbrandt of the Utah Geological Survey, from Ric Page, Randy Laczniak, Mel Kuntz, Jim Harrill, Vicki Langenheim, Tom Hildenbrand, Bob Jachens, Rick Blakely, Marith Reheis, Vic Heilweil, Phil Gardner, Bruce Chuchel, Louise Pellerin, Jonathan Caine, Jeremy Workman, Dave Prudic, and Don Sweetkind of the USGS, from Dan Netcher, Mark Henderson, and Dawna Ferris of the Bureau of Land Management, and from Bill Van Liew of the National Park Service. Word processing was accomplished through the help of Yvonne Honore, Donna Lewis, and Cheri Walker. Mel Kuntz, Emeritus Geologist of the USGS, Denver, did a thorough technical review of the entire text and plates. We thank Andrew Zuza, Jim Faulds, Rachel Micander, Jennifer Vlcan, and Jack Hursh of NBMG for their detailed and valuable technical reviews of, and editorial comments on, the text, sections, and maps.

DESCRIPTION OF MAP UNITS

QTa – Surficial and basin-fill deposits (Holocene to lower Miocene) — Unconsolidated to moderately consolidated, locally tuffaceous beds of sand, gravel, silt, and minor limestone deposited mostly by streams and small playa lakes. Generally thin, but where unit fills basin-range-fault-bounded basins, may be significantly more than 1500 meters thick and forms the upper valley-fill aquifer. Some basin-fill deposits bear local names, including the Muddy Creek Formation (southern part of plate 2), Panaca Formation (southern part of plate 1), Horse Camp Formation (northwestern part of plate 1), and Salt Lake Formation (northeastern part of plate 1).

QTb – Basalt lava flows (Holocene to lower Miocene) — Resistant, thin basalt lava flows and cinder cones. The mafic end of the bimodal volcanic sequence that is synchronous with basin-range extensional faulting.

Ts_4 – Sedimentary rocks, unit 4 (Miocene) — Moderately to well consolidated, mostly fluvial sandstone, conglomerate, and minor lacustrine limestone. Primarily the Horse Spring Formation (11 to 20 Ma), a basal basin-fill sedimentary unit that is locally thick (1000+ meters) in the southern part of plate 2.

Ts_3 – Sedimentary rocks, unit 3 (Miocene and Oligocene) — Moderately to well consolidated, thin, mostly fluvial, tuffaceous sandstone and bedded ash-fall tuff.

Ts_2 – Sedimentary rocks, unit 2 (Oligocene) — Moderately to well consolidated, thin, mostly fluvial, tuffaceous sandstone and conglomerate. Includes the Gilmore Gulch Formation, with an age of about 30 Ma, in the northwestern part of plate 1.

Ts_1 – Sedimentary rocks, unit 1 (Oligocene to Upper Cretaceous?) — Moderately to well consolidated, mostly fluvial sandstone, conglomerate, and minor lacustrine limestone. Primarily the Sheep Pass Formation, but just southeast of plate 1, includes the Paleocene and Upper Cretaceous(?) Grapevine Wash Formation and the Eocene and Paleocene Claron Formation. Includes the Fowkes Formation and White Sage Formation in the northeastern part of plate 1. In most places, unit is overlain by volcanic rocks.

Tv – Volcanic rocks, undivided (Miocene to Eocene) — Unit shown only in cross sections. May be several thousand meters thick in many places. In calderas and near other source vents, unit may be many thousands of meters thick. On plates 1 and 2, unit is separated into several rock types based on age, following the mapping strategy of Ekren et al. (1977). Locally includes QTb where too thin to show.

Tt_4 – Ash-flow tuff and interbedded ash-fall tuff, unit 4 (Miocene) — Poorly to densely welded, bimodal high-silica rhyolite and locally peralkaline ash-flow tuff and related ash-fall tuffs. Includes the tuff of Honeycomb Rock (12.0 Ma), Ox Valley Tuff (14.0 Ma), tuff of Etna (14.0 Ma), tuff of Rainbow Canyon (15.6 Ma), tuff of Acklin Canyon (17.1 Ma), and tuff of Dow Mountain (17.4 Ma), derived from the Caliente caldera complex. Includes the Kane Wash Tuff (14.4 to 14.7 Ma), the tuff of Boulder Canyon (15.1 Ma), and the tuff of Narrow Canyon (15.8 Ma), derived from the Kane Springs Wash caldera complex.

Tt_3 – Ash-flow tuff and interbedded ash-fall tuff, unit 3 (Miocene to Oligocene) — Poorly to densely welded, calc-alka line, low-silica rhyolite to da cite ash-flow tuff and related ash-fall tuffs. Includes the tuff of Teepee Rocks (17.8 Ma), Hiko Tuff (18.3 Ma), Racer Canyon Tuff (18.7 Ma), and both Bauers Tuff Member (22.8 Ma) and Swett Tuff Member (23.7 Ma) of the Condor Canyon Formation, all derived from the Caliente caldera complex. Also includes the Harmony Hills Tuff (22.0 Ma), probably derived from the eastern Bull Valley Mountains; the Leach Canyon Formation (23.8 Ma), probably derived from the Caliente caldera complex; the Bates Mountain Tuff (22.8 Ma), derived from Lander County, Nevada; and the tuff of Saulsbury Wash (21.6 Ma), the Pahranagat Formation (22.6 Ma), the tuff of White Blotch Spring (24 to 25 Ma), the tuff of Kiln Canyon (24.1 to 25.1 Ma), the tuff of Lunar Cuesta (24.6 Ma), the

tuff of the Quinn Canyon Range, and the Shingle Pass Tuff (26.4), all derived from central Nevada, including the Monotony Valley caldera complex; and the tuff of Bald Mountain (about 25 Ma), derived from the Bald Mountain caldera in the Groom Range.

Tt_2 – Ash-flow tuff and interbedded ash-fall tuff, unit 2 (Oligocene) — poorly to densely welded, calc-alkaline, low-silica rhyolite to dacite and trachydacite ash-flow tuff and related ash-fall tuffs. Includes the Isom Formation (about 27 Ma), probably derived from the Indian Peak caldera complex; the outflow Monotony Tuff (27.3 Ma), the intra caldera tuff of Goblin Knobs (27.3 Ma), and the tuff of Hot Creek Canyon (30.0 Ma), all probably derived from the Monotony Valley caldera complex; the outflow Windous Butte Formation (31.4 Ma) and intracaldera tuff of Williams Ridge and Morey Peak (31.3 Ma), derived from the Williams Ridge caldera of central Nevada; and the Needles Range Group (27 to 32 Ma), derived from the Indian Peak caldera complex.

Tt_1 – Ash-flow tuff and interbedded ash-fall tuff, unit 1 (Oligocene to Eocene) — Poorly to densely welded, calc-alkaline, low-silica rhyolite to da cite and trachydacite ash-flow tuff and related ash-fall tuffs. Deposited in the northern part of plate 1. Includes the Pancake Summit Tuff (33.7 Ma), derived from the Broken Back caldera west of Eureka; the Stone Cabin Formation (35.4 Ma), derived from an unknown caldera in or near northern Railroad Valley; and the Kalamazoo tuff (35 Ma), derived from an unknown caldera source probably in the northern Schell Creek Range or beneath adjacent northern Spring Valley or Antelope Valley. In Utah, includes the Tunnel Spring Tuff (35.4 Ma).

Tr_4 – Rhyolite lava flows, unit 4 (Miocene) — High-silica rhyolite lava flows and volcanic domes, mostly in and near the Caliente and Kane Springs Wash caldera complexes.

Tr_3 – Rhyolite lava flows, unit 3 (Miocene to Oligocene) — Low-silica rhyolite lava flows and volcanic domes, mostly in and near the Indian Peak, Caliente, and other caldera complexes.

Tr_2 – Rhyolite lava flows, unit 2 (Oligocene) — Low-silica rhyolite lava flows and volcanic domes, mostly in central Nevada and the Indian Peak caldera complex.

Tr_1 – Rhyolite lava flows, unit 1 (Oligocene to Eocene) — Low-silica rhyolite lava flows and volcanic domes, exposed in the northern part of plate 1.

Ta_4 – Intermediate-composition lava flows, unit 4 (Miocene) — Andesitic and locally dacitic lava flows, flow breccia, and mudflow breccia. Includes andesite of the Hamblin-Cleopatra volcano (11.5 to 14.2 Ma) in the Lake Mead area.

Ta_3 – Intermediate-composition lava flows, unit 3 (Miocene to Oligocene) — Andesitic and locally dacitic lava flows, flow breccia, and mudflow breccia. Includes andesite between the Racer Canyon Tuff and Condor Canyon Formation just southeast of plate 2, between the Caliente and Kane Springs Wash caldera complexes, and in and near the Indian Peak caldera complex.

Ta_2 – Intermediate-composition lava flows, unit 2 (Oligocene) — Andesitic and locally dacitic lava flows, flow breccia, and mudflow breccia. Includes andesite in and near the Indian Peak caldera complex and in the southern Egan Range.

Ta_1 – Intermediate-composition lava flows, unit 1 (Oligocene to Eocene) — Andesitic and locally dacitic lava flows, flow breccia, and mudflow breccia. Exposed in the northern part of plate 1. In the northeastern part of plate 1 includes thin ash-flow tuffs, notably the Kalamazoo tuff. In Utah, includes the Horn Silver Andesite.

Tmb – Megabreccia (Miocene to Oligocene) — Masses of mostly Paleozoic sedimentary rocks and intertongued volcanic breccia deposited within calderas from landsliding of the oversteepened caldera margins following caldera subsidence as a result of rapid eruptions of ash-flow tuff. Includes rocks in the Indian Peak caldera complex, Caliente

caldera complex, and calderas in central Nevada. Also includes gravity slides west of the Sheep Range and Beaver Dam Mountains.

Ti – Intrusive rocks (Miocene to Paleocene) — Mostly silicic, calc-alkaline plutons.

TKi – Intrusive rocks (Miocene to Cretaceous) — Mostly silicic, calc-alkaline plutons.

Ki – Intrusive rocks (Upper Cretaceous) — Mostly silicic, calc-alkaline plutons that accompanied Sevier deformation.

Ks – Sedimentary rocks, undivided (Upper and Lower Cretaceous) — Sevier-age, mostly thin, fluvial synorogenic clastic deposits, including the Baseline Sandstone (Upper and Lower Cretaceous) and Willow Tank Formation (Upper Cretaceous) in the southern part of plate 2; the Iron Springs Formation (Upper Cretaceous), Cedar Mountain Formation (Upper Cretaceous), and Dakota Sandstone (Upper Cretaceous) east of plate 2; and the Newark Canyon Formation (Paleocene? to Lower Cretaceous?) in the northern part of plate 1.

Ji – Intrusive rocks (Jurassic) — Mostly silicic, calc-alkaline plutons that accompanied Sevier deformation.

Js – Sedimentary rocks, undivided (Jurassic) — Includes, in the southeastern part of plate 2, the mostly marine Carmel and underlying Temple Cap Formations (Middle Jurassic). Also in the southeastern part of plate 2, includes the eolian Navajo Sandstone and mostly fluvial Kayenta and Moenave Formations, all Lower Jurassic. Mostly clastic units. In the southern part of plate 2, the Aztec Sandstone is the equivalent of the Navajo Sandstone. Includes the Dunlap Formation (Lower Jurassic) in the northwestern part of plate 1.

Ꝛs – Sedimentary rocks, undivided (Triassic) — Includes, in the southeastern part of plate 2, the mostly fluvial Chinle Formation (Upper Triassic) and mostly fluvial Moenkopi Formation (Middle? and Lower Triassic). Includes the Luning Formation (Upper Triassic) in the northwestern part of plate 1. In the northeastern part of plate 1, includes the Thaynes Formation (Lower Triassic). The majority of these rocks are clastic.

Pzu – Sedimentary rocks, undivided (Paleozoic) — Shown on plate 3, where rocks in the hanging wall of the Snake Range decollement are buried by younger rocks.

Pp – Park City Group, undivided (Upper and Lower Permian) — From top to base, consists of the Gerster Limestone (Upper Permian), Plympton Formation (Upper and Lower Permian), Kaibab Limestone (Lower Permian), and Toroweap Formation (Lower Permian). These make up the top of the upper carbonate aquifer.

Par – Arcturus Formation and Rib Hill Sandstone, undivided (Lower Permian) — Included within the upper carbonate aquifer. Includes the Pequop Formation in Elko County, a redbed unit in the southern part of plate 2, and the Queantoweap Sandstone in the southeastern part of plate 2.

Pa – Arcturus Formation (Lower Permian) — Predominantly carbonate rocks in the northern part of plate 1, thickening eastward.

Pr – Rib Hill Sandstone (Lower Permian) — Nonresistant sandstone and dolomite only in the northwestern part of plate 1.

PIP – Riepe Spring Limestone and Ely Limestone, undivided (Lower Permian to Pennsylvanian) — Mapped only in the northern part of plate 1. The Riepe Spring Limestone (Lower Permian) is exposed in the northwestern part of plate 1. Includes the Brock Canyon Formation (Permian and/or Pennsylvanian) in the northwestern part of plate 1; the Oquirrh Group (Lower Permian and Pennsylvanian) in the northeastern part of plate 1; and the Bird Spring Formation (Lower Permian to Upper Mississippian) in Clark County, Nevada, and the Pakoon formation (Lower Permian) in Utah.

IP – Ely Limestone (Pennsylvanian) — May include Missippian rocks at its base. Mapped mostly in the central and northern part of plate 1,

thickening eastward. Includes the Wildcat Peak Formation in the northwestern part of plate 1 and the Callville Limestone in the southern and eastern part of plate 2.

MDd – Diamond Peak Formation, Chainman Shale, Joana Limestone, and Pilot Shale, undivided (Upper Mississippian to Upper Devonian).

Md – Diamond Peak Formation (Upper Mississippian) — Only in the northwestern part of plate 1. This is a clastic unit derived from erosion of the Antler highland, including the Roberts Mountain thrust formed during the Antler deformational event. Includes the Scotty Wash Quartzite in the southwestern part of plate 2.

Mc – Chainman Shale (Upper Mississippian) — A clastic confining unit that has a similar origin to the Diamond Peak Formation. The two make up the upper aquitard in the northern half of plate 1. Thus for this part of the map area, it separates the upper from the lower carbonate aquifer; in the area of plate 2, the Chainman Shale is thin and does not constitute a significant regional aquitard.

MD – Joana Limestone and Pilot Shale, undivided (Lower Mississippian to Upper Devonian) — The Joana Limestone (Lower Mississippian) and Pilot Shale (Lower Mississippian and Upper Devonian) make up the top of the lower carbonate aquifer in the northern half of plate 1. Includes local Lower Mississippian units Mercury Limestone and Bristol Pass Limestone. Includes the Rogers Spring Limestone (Lower Mississippian) and Monte Cristo Limestone (Upper and Lower Mississippian) in the southern part of plate 2; the Eleana Formation (Mississippian and Upper Devonian) in the western part of plate 2; the Webb Formation (Lower Mississippian) in Elko County; the Ochre Mountain Limestone and underlying Woodman Formation (Lower Mississippian) in the eastern part of plate 1; and the West Range Limestone (Upper Devonian) in northern Lincoln County. May include, at the top, thin deposits of the Chainman Shale.

DЄ – Carbonate and clastic rocks, undivided (Devonian to Upper Cambrian).

DS – Sedimentary rocks, undivided (Devonian to Silurian).

Du – Carbonate sedimentary rocks, undivided (Devonian) — Includes the Woodruff Formation (Upper and Middle Devonian) in Elko County; and the Muddy Peak Limestone (Upper and Middle? Devonian) in the southern part of plate 2.

Dd – Devils Gate Formation (Upper to Middle Devonian) — The western equivalent of the Guilmette Formation.

Dg – Guilmette Formation (Upper to Middle Devonian) — Mapped throughout, except in the western part of plate 1. Includes the Sultan Limestone in Clark County.

Dn – Nevada formation (Middle to Lower Devonian) — The western equivalent of the Simonson and Sevy Dolomites. Includes the Cockalorum Wash formation, also in the western part of plate 1.

Ds – Simonson Dolomite (Middle to Lower Devonian) and Sevy Dolomite, undivided (Lower Devonian) — Mapped in all but the western part of plate 1.

SO – Sedimentary rocks, undivided (Silurian to Ordovician) — Unit shown only on the cross sections.

SOu – Dolomite, upper part, undivided (Silurian to Upper Ordovician) — Includes the Laketown Dolomite (Silurian), Fish Haven Dolomite (Upper Ordovician), Ely Springs Dolomite (Upper Ordovician), and Hanson Creek Formation (Upper Ordovician). Includes the Roberts Mountains Formation and the Lone Mountain Dolomite in the northwestern part of plate 1.

Ol – Dolomite, lower part, undivided (Middle to Lower Ordovician) — Mostly the Eureka Quartzite (Middle Ordovician) and the Pogonip Group (Middle and Lower Ordovician). Includes

the Vinini Formation and Valmy Formation in the northwestern part of plate 1. Includes the Laketown Dolomite and Ely Springs Dolomite where thin in Clark and Lincoln counties. In Utah, includes the Crystal Peak Dolomite, Watson Ranch Quartzite, and Fillmore formations and the House Limestone.

€c – Carbonate sedimentary rocks, undivided (Cambrian) — Unit shown only on the cross sections.

€u – Limestone and shale, upper part, undivided (Lower Ordovician? to Upper Cambrian) — Includes the Notch Peak Formation, Orr Formation, Windfall Formation, Nopah Formation, Dunderberg Shale, and Corset Spring Shale. In the extreme southwestern part of plate 2, includes the Emigrant Formation (Upper and Middle Cambrian).

€m – Limestone and shale, middle part, undivided (Upper to Middle Cambrian) — Mostly the Highland Peak Formation and its southwestern equivalent, the Bonanza King Formation. In Nevada, includes local units known as the Pole Canyon Limestone, Lincoln Peak Formation, Patterson Pass Shale, Hamburg formation, Secret Canyon Shale, Geddes Limestone, and Eldorado formation. Includes the Muav Limestone in eastern Clark County. In Utah, includes the Wah Wah Summit Formation, Trippe Limestone, Pierson Cove Formation, Eye of Needle Limestone, Swasey Limestone, Whirlwind Formation, Dome Limestone, Chisholm Shale, and Howell Limestone. This unit is a thick limestone sequence that marks the base of the lower carbonate aquifer.

€p€s – Lower part (Middle Cambrian to Neoproterozoic) — Chisholm Shale (Middle Cambrian), Lyndon Limestone (Middle Cambrian), Pioche Shale (Middle and Lower Cambrian), Carrara Formation (Middle and Lower Cambrian), Stella Lake Quartzite (Lower Cambrian), Prospect Mountain Quartzite (Lower Cambrian and Neoproterozoic), and Johnnie Formation (Neoproterozoic). The Prospect Mountain Quartzite, in turn, has been subdivided into the Zabriskie Quartzite (Lower Cambrian), Wood Canyon Formation (Lower Cambrian), and Stirling Quartzite (Lower Cambrian and Neoproterozoic). Locally includes the Reed Dolomite (Lower Cambrian) and underlying Wyman formation (Lower Cambrian?) in the southwestern part of plate 2.

p€ – Metamorphosed and crystalline basement rocks (Neoproterozoic to Paleoproterozoic) — Throughout most of plates 1 and 2, consists of meta morphosed quartzite of Neoproterozoic age, namely the McCoy Creek Group and, in Utah, also the underlying Trout Creek group. Locally, in the southern part of plate 2, includes crystalline basement rocks.

REFERENCES

Abbott, J.T., Best, M.G., and Morris, H.T., 1983, Geologic map of the Pine Grove-Blawn Mountain area, Beaver County, Utah: U.S. Geological Survey Miscellaneous Investigations Series Map I-1479, scale 1:24,000.

Acheampong, S.Y., Farnham, I.M., and Watrus, J.M., 2009, Geochemical characterization of ground water and surface water of Snake Valley and the surrounding areas in Utah, *in* Tripp, B.T., Krahulec, K., and Jordan, J.L., editors, Geology and geologic resources and issues of western Utah: Utah Geological Association Publication 38, p. 325–344.

Ahlborn, R.C., 1977, Mesozoic-Cenozoic structural development of the Kern Mountains, eastern Nevada-western Utah [M.S. thesis]: Brigham Young University Geology Studies, v. 24, Pt. 2, p. 117–131.

Alam, A.H.M.S, 1990, Crustal extension in the southern Snake Range and vicinity, Nevada-Utah: An integrated geological and geophysical study [Ph.D. dissertation]: Louisiana State University, 126 p.

Alam, A.H.M.S., and Pilger, Jr., R.H., 1991, An integrated geologic and geophysical study of the structure and stratigraphy of the Cenozoic extensional Hamlin Valley, Nevada-Utah, *in* Raines, G.L., Lisle, R.E., Schafer, R.W., and Wilkinson, W.H., editors, Geology and ore deposits of the Great Basin: Geological Society of Nevada, Symposium Proceedings, April 1–5, 1990, v. 1, p. 93–100.

Allmendinger, R.W., Sharp, J., VonTish, D., Oliver, J., and Kaufman, S., 1985, A COCORP crustal-scale seismic profile of the Cordilleran hingeline, eastern Basin and Range province, *in* Gries, R.R., and Dyer, R.C., editors, Seismic exploration of the Rocky Mountain region: Denver, Rocky Mountain Association of Geologists and Denver Geophysical Society, p. 23–30.

Allmendinger, R.W., Sharp, J.W., Von Tish, D., Serpa, L., Brown, L., Kaufman, S., Oliver, J., and Smith, R.B., 1983, Cenozoic and Mesozoic structure of the eastern Basin and Range province, Utah, from COCORP seismic-reflection data: Geology, v. 11, no. 9, p. 532–536.

Anderson, R.E., 1981, Structural ties between the Great Basin and Sonoran Desert sections of the Basin and Range province, *in* Howard, K.A., Carr, M.D., and Miller, D.M., editors, Tectonic framework of the Mohave Sonoran Desert, California and Arizona: U.S. Geological Survey Open-File Report 81-503, p. 4–6.

Anderson, R.E., 1983, Cenozoic structural history of selected areas in the eastern Great Basin, Nevada-Utah: U.S. Geological Survey Open-File Report 83-504, 47 p.

Anderson, R.E., 1989, Tectonic evolution of the Intermontane System, Basin and Range, Colorado Plateau, and High Lava Plains, *in* Pakiser, L.C., and Mooney, W.D., editors, Geophysical framework of the continental United States: Geological Society of America Memoir 172, p. 163–176.

Anderson, R.E., 2003, Geologic map of the Callville Bay quadrangle, Clark County, Nevada and Mohave County, Arizona: Nevada Bureau of Mines and Geology Map 139, scale 1:24,000.

Anderson, R.E., 2013, On the importance of non-uniform tilt, strike slip, and hydrogeology in shaping the Neogene tectonics of the eastern Lake Mead area, *in* Anderson, R.E., editor, Neogene deformation between central Utah and the Mojave Desert: Geological Society of America Special Paper 499, p. 69–94.

Anderson, R.E., and Barnhard, T.P., 1993, Aspects of three-dimensional strain at the margin of the extensional orogen, Virgin River depression area, Nevada, Utah, and Arizona: Geological Society of America Bulletin, v. 105, p. 1019–1052.

Anderson, R.E., and Beard, L.S., 2010, Geology of the Lake Mead region—an overview, *in* Umhoefer, P.J., Beard, L.S., and Lamb, M.A., editors, Miocene tectonics of the Lake Mead region, central Basin and Range: Geological Society of America Special Paper 463, p. 1–28.

Anderson, R.E., Beard, L.S., Mankinen, E.A., and Hillhouse, J.W., 2013, Analysis of Neogene deformation between Beaver, Utah, and Barstow, California—suggestions for altering the extensional paradigm, *in* Anderson, R.E., editor, Neogene deformation between central Utah and the Mojave Desert: Geological Society of America Special Paper 499, p.1–67.

Anderson, R.E., Felger, T.J., Diehl, S.F., Page, W.R., and Workman, J.B., 2010, Integration of tectonic, sedimentary, and geohydrologic processes leading to a small-scale extension model for the Mormon Mountains area north of Lake Mead, Lincoln County, Nevada, *in* Umhoefer, P.J., Beard, L.S., and Lamb, M.A., editors, Miocene tectonics of the Lake Mead region, central Basin and Range:

Geological Society of America Special Paper 463, p. 395–426.

Armstrong, P.A., 1991, Displacement and deformation associated with lateral thrust propagation—an example from the Golden Gate Range, southern Nevada [M.S. thesis]: University of Utah, Salt Lake City, 162 p.

Armstrong, R.L., 1963, Geochronology and geology of the eastern Great Basin in Nevada and Utah: New Haven, Connecticut, unpublished Ph.D. thesis, Yale University, 202 p + illustrations.

Armstrong, R.L., 1968, Sevier orogenic belt in Nevada and Utah: Geological Society of America Bulletin, v. 79, no. 4, p. 429–458.

Armstrong, R.L., 1970, Geochronology of Tertiary igneous rocks, eastern Basin and Range province, western Utah, eastern Nevada, and vicinity, U.S.A.: Geochimica et Cosmochimica Acta, v. 34, no. 2, p. 203–232.

Armstrong, R.L., 1972, Low-angle (denudation) faults, hinterland of the Sevier orogenic belt, eastern Nevada and western Utah: Geological Society of America Bulletin, v. 83, no. 6, p. 1729–1754.

Asch, T.H., and Sweetkind, D.S., 2010, Geophysical characterization of range-front faults, Snake Valley, Nevada: U.S. Geological Survey Open-File Report 2010-1016, 39 p.

Asch, T.H., and Sweetkind, D.S., 2011, Audiomagnetotelluric characterization of range-front faults, Snake Range, Nevada: Geophysics, v. 76, p. B1–B7.

Bankey, V., Grauch, V.J.S., and Kucks, R.P., 1998, Utah aeromagnetic and gravity maps and data, a web site for distribution of data: U.S. Geological Survey Open-File Report 98-761. [http://pubs.usgs.gov/of/1998/ofr-98-0761/]

Baranov, V., 1957, A new method for interpretation of aeromagnetic maps—Pseudo-gravimetric anomalies: Geophysics, v. 22, p. 359–383.

Bartley, J.M., and Gleason, Gayle, 1990, Tertiary normal faults superimposed on Mesozoic thrusts, Quinn Canyon and Grant ranges, Nye County, Nevada, *in* Wernicke, B.P., editor, Basin and Range extensional tectonics near the latitude of Las Vegas, Nevada: Geological Society of America Memoir 176, p. 195–212.

Bartley, J.M., and Wernicke, B.P., 1984, The Snake Range décollement interpreted as a major extensional shear zone: Tectonics, v. 3, no. 6, p. 647–657.

Bartley, J.M., Axen, G.J., Taylor, W.J., and Fryxell, J.E., 1988, Cenozoic tectonics of a transect through eastern Nevada near 38° N latitude, *in* Weide, D.L., and Faber, M.L., editors, This extended land—geological journeys in the southern Basin and Range: Geological Society of America, Cordilleran Section, Field trip guidebook, p. 1–20.

Beard, L.S., Anderson, R.E., Block, D.L., Bohannon, R.G., Brady, R.J., Castor, S.B., Duebendorfer, E.M., Faulds, J.E., Felger, T.J., Howard, K.A., Kuntz, M.A., and Williams, V.S., 2007, Preliminary geologic map of the Lake Mead 30′×60′ quadrangle, Clark County, Nevada, and Mohave County, Arizona: U.S. Geological Survey Open-File-Report 2007-1010, 109 p., 3 plates, scale 1:100,000. [http://pubs.usgs.gov/of/2007/1010/].

Beard, L.S., Campagna, D.J., and Anderson, R.E., 2010, Geometry and kinematics of the eastern Lake Mead fault system in the Virgin Mountains, Nevada and Arizona, *in* Umhoefer, P.J., Beard, L.S., and Lamb, M.A., editors, Miocene tectonics of the Lake Mead region, central Basin and Range: Geological Society of America Special Paper 463, p. 243–274.

Belcher, W.R., editor, 2004, Death Valley regional ground-water flow system, Nevada and California—hydrogeologic framework and transient ground-water flow model: U.S. Geological Survey Scientific Investigations Report 2004–5205, 408 p.

Berger, D.L., Kilroy, K.C., and Schaefer, D.H., 1987, Geophysical logs and hydrologic data for eight wells in Coyote Spring Valley area, Clark and Lincoln Counties, Nevada: U.S. Geological Survey Open-File Report 87-679, 59 p.

Best, M.G., 1987, Geologic map and sections of the area between Hamlin Valley and Escalante Desert, Iron County, Utah: U.S. Geological Survey Miscellaneous Investigations Series Map I-1774, scale 1:50,000.

Best, M.G., and Williams, V.S., 1997, Geologic map of the Rose Valley quadrangle, Lincoln County, Nevada: U.S. Geological Survey Geologic Quadrangle Map GQ-1765, scale 1:24,000.

Best, M.G., Armstrong, R.L., Graustein, W.C., Embree, G.F., and Ahlborn, R.C., 1974, Mica granites of the Kern Mountains pluton, eastern White Pine County, Nevada: Remobilized basement of the Cordilleran miogeosyncline?: Geological Society of America Bulletin, v. 85, p. 1277–1286.

Best, M.G., Barr, D.L., Christiansen, E.H., Gromme, S., Deino, A.L., and Tingey, D.G., 2009, The Great Basin aliplano during the middle Cenozoic ignimbrite flareup—insights from volcanic rocks:

International Geology Review, v. 51, p. 589–633.
Best, M.G., Christiansen, E.H., and Blank, Jr., R.H., 1989a, Oligocene caldera complex and calc-alkaline tuffs and lavas of the Indian Peak volcanic field, Nevada and Utah: Geological Society of America Bulletin, v. 101, p. 1076–1090.
Best, M.G., Christiansen, E.H., Deino, A.L., Grommé, C.S., McKee, E.H., and Noble, D.C., 1989b, Eocene through Miocene volcanism in the Great Basin of the western United States, *in* Chapin, C.E., and Zidek, J., editors, Field excursions to volcanic terranes in the western United States, Volume II: Cascades and Intermountain West: New Mexico Bureau of Mines and Mineral Resources Memoir 47, p. 91–133.
Best, M.G., Christiansen, E.H., Deino, A.L., Gromme, C.S., Hart, G.L., and Tingey, D.G., 2013a, The 31–18 Ma Indian Peak-Caliente ignimbrite field and calderas, southwestern Great Basin, U.S.A.—Multicyclic super-eruptions: Geosphere, v. 9, p. 1–87.
Best, M.G., Grant, S.K., Hintze, L.F., Cleary, J.G., Hutsinpiller, A., and Saunders, D.M., 1987a, Geologic map of the Indian Peak (southern Needle) Range, Beaver and Iron Counties, Utah: U.S. Geological Survey Miscellaneous Investigations Series Map I-1795, scale 1:50,000.
Best, M.G., Gromme, Sherman, Deino, A.L., Christiansen, E.H., Hart, G.L., and Tingey, D.G., 2013b, The 36–18 Ma central Nevada ignimbrite field and calderas, Great Basin, USA—Multicyclic super-eruptions: Geosphere, v. 9, p. 1–75.
Best, M.G., Hintze, L.F., Deino, A.L., and Maughan, L.L., 1998, Geologic map of the Fairview Range and Grassy Mountain, Lincoln County, Nevada: Nevada Bureau of Mines and Geology Map 114, scale 1:24,000, 2 sheets.
Best, M.G., Hintze, L.F., and Holmes, R.D., 1987b, Geologic map of the southern Mountain Home and northern Indian Peak Ranges (central Needle Range), Beaver County, Utah: U.S. Geological Survey Miscellaneous Investigations Series Map I-1796, scale 1:50,000.
Best, M.G., Morris, H.T., Kopf, R.W., and Keith, J.D., 1987c, Geologic map of the southern Pine Valley area, Beaver and Iron Counties, Utah: U.S. Geological Survey Miscellaneous Investigations Series Map I-1794, scale 1:50,000.
Best, M.G., Scott, R.B., Rowley, P.D., Swadley, WC, Anderson, R.E., Grommé, C.S., Harding, A.E., Deino, A.L., Christiansen, E.H., Tingey, D.G., and Sullivan, K.R., 1993, Oligocene-Miocene caldera complexes, ash-flow sheets, and tectonism in the central and southeastern Great Basin, *in* Lahren, M.M., Texler, Jr., J.H., and Spinosa, C., editors, Crustal evolution of the Great Basin and Sierra Nevada—Field trip guidebook: Geological Society of America, Cordilleran and Rocky Mountain sections meeting, p. 285–311.
Best, M.G., Toth, M.I., Kowallis, J.B., Willis, J.B., and Best, V.C., 1989c, Geologic map of the northern White Rock Mountains-Hamlin Valley area, Beaver County, Utah, and Lincoln County, Nevada: U.S. Geological Survey Miscellaneous Investigations Series Map I-1881, scale 1:50,000.
Bhark, E., Kelly, V., Pickens, J., Ruskauff, G., Gable, C., Reimus, P., and Vesselinov, V., 2006, Well ER-6-1 tracer test analysis: Yucca Flat, Nevada Test Site, Nye County, Nevada: Stoller-Navarro, 177 p.
Biek, R.F., Hacker, D.B., and Rowley, P.D., 2014, New constraints on the extent, age, and emplacement history of the early Miocene Markagunt Megabreccia, southwest Utah—one of the World's largest subaerial gravity slides, *in* MacLean, J.S., Biek, R.F., and Huntoon, J.E., editors, Geology of Utah's far south: Utah Geological Association Publication 43, CD, p. 565–598.
Biek, R.F., Rowley, P.D., Anderson, J.J., Maldonado, Florian, Moore, D.W., Eaton, J.G., Hereford, Richard, and Matyjasik, Basia, 2015, Geologic map of the Panguitch 30'x60' quadrangle, Garfield, Iron, and Kane Counties, Utah: Utah Geological Survey Map 270, CD, scale 1:65,000.
Biek, R.F., Rowley, P.D., Hayden, J.M., Hacker, D.B., Willis, G.C., Hintze, L.F., Anderson, R.E., and Brown, K.D., 2009, Geologic map of the St. George and east part of the Clover Mountains 30'×60' quadrangles, Washington and Iron Counties, Utah: Utah Geological Survey Map 242, 109 p.
Billingsley, G.H., and Workman, J.B., 2000, Geologic map of the Littlefield 30'×60' quadrangle, Mohave County, northwestern Arizona: U.S. Geological Survey Geologic Investigations Series Map I-2628, scale 1:100,000.
Black, B.D., Hecker, S., Hylland, M.D., Christenson, G.L., and McDonald, G.N., 2003, Quaternary fault and fold database and map of Utah: Utah Geological Survey Map 193DM, scale 1:500,000. (CD-ROM).
Blackett, R.E., and Wakefield, S., 2004, Geothermal resources of Utah—2004: Utah Geological Survey Open-File Report 431DM, CD-ROM.
Blakely, R.J., 1995, Potential theory in gravity and magnetic applications: Cambridge, U.K., Cambridge University Press, 441 p.

Blakely, R.J., Langenheim, V.E., Ponce, D.A., and Dixon, G.L., 2000, Aeromagnetic survey of the Amargosa Desert, Nevada and California—a tool for understanding near-surface geology and hydrology: U.S. Geological Survey Open-File Report 00-188, 35 p.

Blakely, R.J., Morin, R.L., McKee, E.H., Schmidt, K.M., Langenheim, V.E., and Dixon, G.L., 1998, Three-dimensional model of Paleozoic basement beneath Amargosa Desert and Pahrump Valley, California and Nevada—implications for tectonic evolution and water resources: U.S. Geological Survey Open-File Report 98-496, 27 p.

Blakely, R.J., and Simpson, R.W., 1986, Approximating edges of source bodies from magnetic or gravity anomalies: Geophysics, v. 51, p. 1494–1498.

Blank, H.R., 1993, Basement structure in the Railroad Valley—Grant Range region, east-central Nevada, from interpretation of potential-field anomalies, *in* Scott, R.W., Jr., Detra, P.S., and Berger, B.R., editors, Advances related to United States and international frameworks and exploration technologies: U.S. Geological Survey Bulletin 2039, p. 25–30

Bohannon, R.G., 1983, Geologic map, tectonic map and structure sections of the Muddy and Northern Black Mountains, Clark County, Nevada: U.S. Geological Survey Miscellaneous Investigations Series Map I-1406, scale 1:62,500.

Bohannon, R.G., 1984, Nonmarine sedimentary rocks of Tertiary age in the Lake Mead region, southeastern Nevada and northwestern Arizona: U.S. Geological Survey Professional Paper 1259, 72 p.

Bohannon, R.G., 1992, Geologic map of the Weiser Ridge quadrangle, Clark County, Nevada: U.S. Geological Survey Geologic Quadrangle Map GQ-1714, scale 1:24,000.

Brokaw, A.L., 1967, Geologic map and sections of the Ely quadrangle, White Pine County, Nevada: U.S. Geological Survey Geologic Quadrangle Map GQ-697, scale 1:24,000.

Brokaw, A.L., and Barosh, P.J., 1968, Geologic map and sections of the Riepetown quadrangle, White Pine County, Nevada: U.S. Geological Survey Geologic Quadrangle Map GQ-758, scale 1:24,000.

Brokaw, A.L., and Heidrick, T., 1966, Geologic map and sections of the Giroux Wash quadrangle, White Pine County, Nevada: U.S. Geological Survey Geologic Quadrangle Map GQ-476, scale 1:24,000.

Brokaw, A.L., and Shawe, D.R., 1965, Geologic map and sections of the Ely 3 SW quadrangle, White Pine County, Nevada: U.S. Geological Survey Miscellaneous Geological Investigations Map I-449, scale 1:24,000.

Brokaw, A.L., Bauer, H.L., and Breitrick, R.A., 1973, Geologic map of the Ruth quadrangle, White Pine County, Nevada: U.S. Geological Survey Geologic Quadrangle Map GQ-1085, scale 1:24,000.

Brown, C.L., and Schmitt, J.G., 1991, Horse Camp Formation: Record of Miocene-Pliocene extensional basin development, northern Grant Range, Nevada, *in* Flanigan, Donna M.H., Mike Hansen and T. Edward Flanigan, editors, Geology of White River Valley, the Grant Range, Eastern Railroad Valley and Western Egan Range, Nevada: 1991 Fieldtrip Guidebook, Nevada Petroleum Society, Reno, p. 7–13.

Bureau of Land Management, 2012, Clark, Lincoln, and White Pine Counties Groundwater Development Project Final Environmental Impact Statement, FES 12-33.

Buqo, T., 2007, Carbonate development in the Muddy Springs area, *in* Coache, R., ed., Regional tour of the carbonate system guidebook: Nevada Water Resources Association, Clark County, Nevada, June 18–20, 2007, p. 5–6.

Burbey, T.J., 1997, Hydrogeology and potential for ground-water development, carbonate-rock aquifers, southern Nevada and southeastern California: U.S. Geological Survey Water-Resources Investigations 95–4168, 65 p.

Burchfiel, B.C., Fleck, R.J., Secor, D.T., Vincelette, R.R., and Davis, G.A., 1974, Geology of the Spring Mountains, Nevada: Geological Society of America Bulletin, v. 85, no. 7, p. 1013–1022.

Burns, A.G., and Drici, W., 2011, Hydrology and water resources of Spring, Cave, Dry Lake, and Delamar valleys, Nevada and vicinity: Presentation to the Office of the Nevada State Engineer: Southern Nevada Water Authority, Las Vegas, Nevada.

Caine, J.S., Evans, J.P., and Forster, C.B., 1996, Fault zone architecture and permeability structure: Geology, v. 24, no. 11, p. 1025–1028.

Caine, J.S., and Forster, C.B., 1999, Fault zone architecture and fluid flow: Insights from field data and numerical modeling, *in* Haneberg, W.C., Mozley, P.S., Moore, J.C., and Goodwin, L.B., editors, Faults and subsurface fluid flow in the shallow crust: American Geophysical Union Geophysical Monograph 113, p. 101–127.

Caine, J.S., Manning, A.H., Berger, B.R., Kremer, Y., Guzman, M.A., Eberl, D.D., and Schuller, K., 2010, Characterization of geologic structures and host rock properties relevant to the hydrogeology of the Standard Mine in Elk Basin, Gunnison County, Colorado: U.S. Geological Survey Open-File Report 2010–1008, 56 p.

Carpenter, J.A., and Carpenter, D.G., 1994a, Analysis of Basin-Range and Fold-Thrust Structure, and Reinterpretation of the Mormon Peak Detachment and Similar Features as Gravity Slide Systems: Southern Nevada, Southwest Utah, and Northwest Arizona, *in* Dobbs, S.W., and W.J. Taylor, editors, Structural and Stratigraphic Investigations and Petroleum Potential of Nevada, with Special Emphasis South of the Railroad Valley Producing Trend: Nevada Petroleum Society Conference Volume II, p. 15–52.

Carpenter, J.A., and Carpenter, D.G., 1994b, Fold-Thrust Structure, Synorogenic Rocks, and Structural Analysis of the North Muddy and Muddy Mountains, Clark County Nevada, *in* Dobbs, S.W., and W.J. Taylor, editors, Structural and Stratigraphic Investigations and Petroleum Potential of Nevada, with Special Emphasis South of the Railroad Valley Producing Trend: Nevada Petroleum Society Conference Volume II, p. 65–94.

Carpenter, J.A., Carpenter, D.G., and Dobbs, S.W., 1994, Antler Orogeny: Paleostructural Analysis and Constraints on Plate Tectonic Models with a Global Analogue in Southeast Asia, *in* Dobbs, S.W., and W.J. Taylor, editors, Structural and Stratigraphic Investigations and Petroleum Potential of Nevada, with Special Emphasis South of the Railroad Valley Producing Trend: Nevada Petroleum Society Conference Volume II, p. 187–240.

Castor, S.B., Faulds, J.E., Rowland, S.M., and dePolo, C.M., 2000, Geologic map of the Frenchman Mountain quadrangle, Clark County, Nevada: Nevada Bureau of Mines and Geology Map 127, scale 1:24,000.

Chidsey, Jr., T.C., 1978, Intrusions, alteration, and economic implications in the northern House Range, Utah: Brigham Young University Geology Studies, v. 25, pt. 3, p. 47–65.

Christiansen, W.J., 1977, Geology of the Fish Springs mining district, Juab County, Utah [M.S. thesis]: Salt Lake City, University of Utah, 66 p.

Christiansen, R.L., and Lipman, P.W., 1972, Cenozoic volcanism and plate-tectonic evolution of the western United States: II. Late Cenozoic: Royal Society of London Philosophical Transactions A, v. 271, no. 1213, p. 249–284.

Christiansen, R.L., and Yeats, R.S., 1992, Post-Laramide geology of the U.S. Cordilleran region, *in* Burchfiel, B.C., Lipman, P.W., and Zoback, M.L., editors, The Cordilleran Orogen: Conterminous U.S.: Boulder, Colorado, Geological Society of America, The Geology of North America, v. G-3, p. 261–406.

Clark, D.L., Oviatt, C.G., and Page, David, 2007, Progress Report geologic map of Dugway Proving Ground and adjacent areas, parts of the Wildcat Mountain, Rush Valley, and Fish Springs 30'x60' quadrangles, Tooele County, Utah (Year 1 of 2): Utah Geological Survey Open-File Report 501, scale 1:62,5000.

Clark, D.L., Oviatt, C.G., and Page, David, 2008, Interim geologic map of Dugway Proving Ground and adjacent areas, parts of the Wildcat Mountain, Rush Valley, and Fish Springs 30'x60' quadrangles, Tooele County, Utah (Year 2 of 2): Utah Geological Survey Open-File Report 532, scale 1:75,000.

Coats, R.R., 1987, Geology of Elko County, Nevada: Nevada Bureau of Mines and Geology Bulletin 101, 112 p.

Coney, P.J., 1974, Structural analysis of the Snake Range décollement, east-central Nevada: Geological Society of America Bulletin, v. 85, no. 6, p. 973–978.

Coney, P.J., and Harms, T., 1984, Cordilleran metamorphic core complexes—Cenozoic extensional relics of Mesozoic compression: Geology, v. 12, p. 550–554.

Cook, E.F., 1965, Stratigraphy of Tertiary volcanic rocks in eastern Nevada: Nevada Bureau of Mines and Geology Report 11, 61 p.

Cook, K.L., Bankey, V., Mabey, D.R., and DePangher, M., 1989, Complete Bouguer gravity anomaly map of Utah: Utah Geological and Mineral Survey Map 122, scale 1:500,000.

Cordell, L., 1979, Gravimetric expression of graben faulting in Santa Fe County and the Espanola Basin, *in* Ingersoll, R.V., editor, Guidebook to Santa Fe County, 30th Field Conference: New Mexico Geological Society, p. 59–64.

Cordell, L., and Grauch, V.J.S., 1985, Mapping basement magnetization zones from aeromagnetic data in the San Juan Basin, New Mexico, *in* Hinze, W.J., editor, The utility of regional gravity and magnetic anomaly maps: Society of Exploration Geophysicists, Tulsa, Oklahoma, p. 181–197.

Cornwall, H.R., 1972, Geology and mineral deposits

of southern Nye County, Nevada: Nevada Bureau of Mines and Geology Bulletin 77, 49 p.
Crafford, A.E.J., 2007, Geologic Map of Nevada: U.S. Geological Survey Data Series 249, 1 CD-ROM, 46 p., 1 plate.
Currey, D.R., 1982, Lake Bonneville: Selected features of relevance to neotectonic analysis: U.S. Geological Survey Open-File Report 82-1070, 30 p.
Currey, D.R., Atwood, G., and Mabey, D.R., 1984, Major levels of Great Salt Lake and Lake Bonneville: Utah Geological Survey Map 73, scale 1:750,000.
D'Agnese, F.A., O'Brien, G.M., Faunt, C.C., Belcher, W.R., and San Juan, C., 2002, A three-dimensional numerical model of predevelopment conditions in the Death Valley regional ground-water flow system, Nevada and California: U.S. Geological Survey Water-Resources Investigations Report 02–4102, 114 p.
Davis, F.D., 2005, Water resources of Millard County, Utah: Utah Geological Survey Open-File Report 447, 27 p.
DeCelles, P.G., 2004, Late Jurassic to Eocene evolution of the Cordilleran thrust belt and foreland basin systems, western U.S.A.: American Journal of Science, v. 304, p. 105–168.
DeCelles, P.G., and Coogan, J.C., 2006, Regional structure and kinematic history of the Sevier fold-and-thrust belt, central Utah: Geological Society of America Bulletin, v. 118, p. 841–864.
dePolo, C.M., and Taylor, W.J., 2012, Geologic map of the Ute quadrangle, Clark County, Nevada: Nevada Bureau of Mines and Geology Map 177, scale 1:24,000.
dePolo, C.M., Johnson, G.L., Price, J.G., and Mauldin, J.M., 2009, Quaternary faults in Nevada—Online interactive map: Nevada Bureau of Mines and Geology Open-File Report 09-9, scale 1:1,000,000.
Dettinger, M.D., 1992, Geohydrology of areas being considered for exploratory drilling and development of the carbonate-rock aquifers in southern Nevada—preliminary assessment: U.S. Geological Survey Water-Resources Investigations Report 90–4077, 35 p.
Dettinger, M.D., Harrill, J.R., Schmidt, D.L., and Hess, J.W., 1995, Distribution of carbonate-rock aquifers and the potential for their development, southern Nevada and adjacent parts of California, Arizona, and Utah: U.S. Geological Survey Water-Resources Investigations Report91–4146, 100 p.
Dickinson, W.R., 2006, Geotectonic evolution of the Great Basin: Geosphere, v. 2, p. 353–368.
Dickinson, W.R., 2009, Anatomy and global context of the North American cordillera, *in* Kay, S.M.,Ramos, V.A., and Dickinson, W.R., editors, Backbone of the Americas—shallow subduction, plateau uplift, and ridge and terrane collision: Geological Society of America Memoir 204, p.1–29.
Dickinson, W.R., 2013, Phanerozoic palinspastic reconstruction of Great Basin geotectonics (Nevada-Utah, USA): Geosphere, v. 9, p. 1384–1396.
Dilek, Y., and Moores, E.M., 1999, A Tibetan model for the early Tertiary western United States: Journal of the Geological Society, London, v. 156, p. 929–941.
Dixon, G., 2007, Geology of White River Narrows and Pahroc Valley, *in* Coache, R., editor, Regional tour of the carbonate system guidebook: Nevada Water Resources Association, Clark County, Nevada, June 18-20, 2007, p. 17–18.
Dixon, G.L., and Katzer, T., 2002, Geology and hydrology of the lower Virgin River Valley in Nevada, Arizona, and Utah: Virgin Valley Water District, Mesquite, Nevada, Report VVWD-01, 126 p.
Dixon, G., and Rowley, P., 2007a, Hydrogeology of Caliente and lower Meadow Valley Wash, *in* Coache, R., editor, Regional tour of the carbonate system guidebook: Nevada Water Resources Association, Clark County, Nevada, June 18–20, 2007, p. 65–66.
Dixon, G.L., and Rowley, P.D., 2007b, Hydrogeology of Dry Lake and Delamar valleys, *in* Coache, R., editor, Regional tour of the carbonate system guidebook: Nevada Water Resources Association, Clark County, Nevada, June 18-20, 2007, p. 69–70.
Dixon, G.L., and Rowley, P.D., 2007c, Hydrogeology of Pioche, Panaca and Caliente areas, *in* Coache, R., editor, Regional tour of the carbonate system guidebook: Nevada Water Resources Association, Clark County, Nevada, June 18–20, 2007, p. 63–64.
Dixon, G.L., and Rowley, P.D., 2007d, Hydrogeology of Spring Valley, *in* Coache, R., editor, Regional tour of the carbonate system guidebook: Nevada Water Resources Association, Clark County, Nevada, June 18–20, 2007, p. 35–36.
Dixon, G.L., Donovan, D.J., and Rowley, P.D., 2007b, Geology of Oak Springs Summit, *in* Coache, R., editor, Regional tour of the carbonate system guidebook: Nevada Water Resources Association, Clark County, Nevada, June 18–20, 2007, p. 71–72.
Dixon, G.L., Donovan, D.J., and Rowley, P.D., 2007c,

Hydrogeology of White River Valley, *in* Coache, R., editor, Regional tour of the carbonate system guidebook: Nevada Water Resources Association, Clark County, Nevada, June 18–20, 2007, p. 21–22.

Dixon, G.L., Hedlund, D.C., and Ekren, E.B., 1972, Geologic map of the Pritchards Station quadrangle, Nye County, Nevada: U.S. Geological Survey Miscellaneous Geologic Investigations Map I-728, scale 1:48,000.

Dixon, G.L., Rowley, P.D., Burns, A.G., Watrus, J.M., Donovan, D.J., and Ekren, E.B., 2007a, Geology of White Pine and Lincoln counties and adjacent areas, Nevada and Utah: The geologic framework of regional groundwater flow systems: Southern Nevada Water Authority, Las Vegas, Nevada, Doc. No. HAM-ED-0001, 157 p.

Dixon, G.L., and Van Liew, B., 2007, Hydrogeology of Crystal Springs, *in* Coache, R., editor, Regional tour of the carbonate system guidebook: Nevada Water Resources Association Clark County, Nevada, June 18–20, 2007, p. 13–14.

Dobbs, S.W., Garbee, Jr., J.J., Stuart, C.K., and Nelson, S.L., 1994, Intergrated [sic] Geological and Geophysical Interpretation in the Newark Valley Area, Eureka Fold-and-Thrust Belt, East-Central Nevada, *in* Dobbs, S.W., and Taylor, W.J. editors, Structural and Stratigraphic Investigations and Petroleum Potential of Nevada, with Special Emphasis South of the Railroad Valley Producing Trend: Nevada Petroleum Society Conference Volume II, p. 241–253.

Dohrenwend, J.C., Schell, B.A., Menges, C.M., Moring, B.C., and McKittrick, M.A., 1996, Reconnaissance photogeologic map of young (Quaternary and late Tertiary) faults in Nevada, *in* Singer, D.A., editor, An analysis of Nevada's metal-bearing mineral resources: Nevada Bureau of Mines and Geology Open-File Report 96–2, p. 9-1–9-12.

Donovan, D.J., 2007, Geology of Muddy River Springs, *in* Coache, R., editor, Regional tour of the carbonate system guidebook: Nevada Water Resources Association, Clark County, Nevada, June 18-20, 2007, p. 1–2.

Donovan, D.J., Dixon, G.L., and Rowley, P.D., 2004, Detailed geologic mapping in the Muddy Springs area, Clark County, Nevada [abs.]: Nevada Water Resources Association Annual Conference, Mesquite, Nevada, February 24–26, 2004, p. 23.

Douglass, W. B., Jr., 1960, Geology of the southern Butte Mountains, White Pine County, Nevada, *in* Geology of east central Nevada: Intermountain Association Petroleum Geologists Guidebook, 11th Annual Field Conference, 1960, p. 181–185.

Drewes, Harald, 1967, Geology of the Connors Pass quadrangle, Schell Creek Range, east-central Nevada: U.S. Geological Survey Professional Paper 557, 94 p., scale 1:24,000.

Druschke, P., Hanson, A.D., Wells, M.L., Rasbury, T., Stockli, D.F., and Gehrels, G., 2009, Synconvergent surface-breaking normal faults of Late Cretaceous age within the Sevier hinterland, east-central Nevada: Geology, v. 37, no. 5, p. 447–450.

du Bray, E.A., 1993, The Seaman volcanic center—a rare middle Tertiary stratovolcano in southern Nevada: U.S. Geological Survey Bulletin 2052, 19 p.

du Bray, E.A., 1995, Chemistry and petrology of Oligocene and Miocene ash-flow tuffs of the southeastern Great Basin, Nevada: U.S. Geological Survey Professional Paper 1559, 38 p.

du Bray, E.A., and Hurtubise, D.O., 1994, Geologic map of the Seaman Range, Lincoln and Nye counties, Nevada: U.S. Geological Survey Miscellaneous Investigations Series Map I-2282, scale 1:50,000.

Duebendorfer, E.M., 2003, Geologic map of the Government Wash quadrangle, Clark County, Nevada: Nevada Bureau of Mines and Geology Map 140, scale 1:24,000.

Eakin, T.E., 1966, A regional interbasin groundwater system in the White River area, southeastern Nevada: Water Resources Research, v. 2, no. 2, p. 251–271.

Eberhart-Phillips, D., Stanley, W.D., Rodriguez, B.D., and Lutter, W.J., 1995, Surface seismic and electrical methods to detect fluids related to faulting: Journal of Geophysical Research, v. 100, no. B7, p. 12919–12936.

Ehni, W., and Faulds, J., editors, 2002, Detachment and attenuation in eastern Nevada and its application to petroleum exploration: Nevada Petroleum Society 2002 Field Trip Guidebook, 163 p.

Eichhubl, P., Taylor, W.L., Pollard, D.D., and Aydin, A., 2004, Paleo-fluid flow and deformation in the Aztec Sandstone at the Valley of Fire, Nevada—evidence for the coupling of hydrogeologic, diagenetic, and tectonic processes: Geological Society of America Bulletin, v. 116, p. 1120–1136.

Ekren, E.B., and Page, W.R., 1995, Preliminary geologic map of the Coyote Spring quadrangle, Lincoln County, Nevada: U.S. Geological Survey Open-File Report 95–550, scale 1:24,000.

Ekren, E.B., Bucknam, R.C., Carr, W.J., Dixon, G.L.,

and Quinlivan, W.D., 1976, East-trending structural lineaments in central Nevada: U.S. Geological Survey Professional Paper 986, 16 p.

Ekren, E.B., Hinrichs, E.N., and Dixon, G.L., 1972, Geologic map of The Wall quadrangle, Nye County, Nevada: U.S. Geological Survey Miscellaneous Geologic Investigations Map I-719, scale 1:48,000.

Ekren, E.B., Hinrichs, E.N., Quinlivan, W.D., and Hoover, D.L., 1973a, Geologic map of the Moores Station quadrangle, Nye County, Nevada: U.S. Geological Survey Miscellaneous Geologic Investigations Map I-756, scale 1:48,000.

Ekren, E.B., Orkild, P.P., Sargent, K.A., and Dixon, G.L., 1977, Geologic map of Tertiary rocks, Lincoln County, Nevada: U.S. Geological Survey Miscellaneous Investigations Series Map I-1041, scale 1:250,000.

Ekren, E.B., Quinlivan, W.D., Snyder, R.P., and Kleinhampl, F.J., 1974, Stratigraphy, structure, and geologic history of the Lunar Lake caldera of northern Nye County, Nevada: U.S. Geological Survey Journal of Research, v. 2, no. 5, p. 599–608.

Ekren, E.B., Rogers, C.L., and Dixon, G.L., 1973b, Geologic and bouguer gravity map of the Reveille quadrangle, Nye County, Nevada: U.S. Geological Survey Miscellaneous Geologic Investigations Map I-806, scale 1:48,000.

Ekren, E.B., Rowley, P.D., Dixon, G.L., Page, W.R., Kleinhampl, F.J., Ziony, J.I., Brandt, J.M., and Patrick, B.G. 2012, Geology of the Quinn Canyon Range and vicinity, Nye and Lincoln Counties, Nevada: Southern Nevada Water Authority, Las Vegas, Nevada, Doc. No. HAM-ED-0004, 46 p., scale 1:250,000.

Erskine, M.C., 2001, Structural overlap of passive continental margin stratigraphic packages onto the Colorado Plateau cratonic package in southwestern Utah, *in* Erskine, M.C., Faulds, J.E., Bartley, J.M., and Rowley, P.D., editors, The geologic transition, High Plateaus to Great Basin—a symposium and field guide: The Mackin Volume: Utah Geological Association Publication 30, and American Association of Petroleum Geologists Publication GB78, September 20–22, 2001, p. 365–377.

Faulds, J.E., and Varga, R.J., 1998, The role of accommodation zones and transfer zones in the regional segmentation of extended terranes, *in* Faulds, J.E., and Stewart, J.H., editors, Accommodation zones and transfer zones—the regional segmentation of the Basin and Range province: Geological Society of America Special Paper 323, p. 1–45.

Fenneman, N.M., 1931, Physiography of western United States: New York, McGraw-Hill Book Company, Inc., 534 p.

Fouch, T.D., Lund, K., Schmitt, J.G., Good, S.C., and Hanley, J.H., 1991, Late Cretaceous(?) and Paleogene sedimentary rocks and extensional(?) basins in the region of the Egan and Grant ranges, and White River and Railroad valleys, Nevada: Their relation to Sevier and Laramide contractional basins in the southern Rocky Mountains and Colorado Plateau, *in* Flanigan, Donna M.H., Mike Hansen and T. Edward Flanigan, editors, Geology of White River Valley, the Grant Range, Eastern Railroad Valley and Western Egan Range, Nevada: 1991 Fieldtrip Guidebook, Nevada Petroleum Society Inc., p. 15–28.

Francis, R.D., and Walker, C.T., 2002, Cenozoic detachments and attenuation in east-central Nevada, *in* Ehni, William, and Faulds, James, editors, Detachment and attenuation in eastern Nevada and its application to petroleum exploration: Nevada Petroleum Society 2002 Field Trip Guidebook, p. 73–95.

French, Don E., and Schalla, Robert A., editors, 1998, Hydrocarbon habitat and special geologic problems of the Great Basin: 1998 Field Trip Guidebook, Nevada Petroleum Society, 109 p.

Fryxell, J.E., 1988, Geologic map and descriptions of stratigraphy and structure of the west-central Grant Range, Nye County, Nevada: Geological Society of America Map and Chart Series MCH064, 15 p., scale 1:24,000.

Gans, P.B., 2000a, The northern White Pine Range, *in* Gans, P.B., and Seedorff, E., editors, Geology and ore deposits 2000: The Great Basin and beyond: Geological Society of Nevada, Symposium Proceedings, May 15–18, 2000, p. 83–95.

Gans, P.B., 2000b, The Snake Range metamorphic core complex—Geologic overview of the northern Snake Range, *in* Gans, P.B., and Seedorff, E., editors, Geology and ore deposits 2000: The Great Basin and beyond: Geological Society of Nevada, Symposium Proceedings, May 15–18, 2000, p. 99–117.

Gans, P.B., and Miller, E.L., 1985, Comment on "The Snake Range décollement interpreted as a major extensional shear zone" by John M. Bartley and Brian P. Wernicke: Tectonics, v. 4, no. 4, p. 411–415.

Gans, P.B., Mahood, G.A., and Schermer, E., 1989, Synextensional magmatism in the Basin and Range province: A case study from the eastern

Great Basin: Geological Society of America Special Paper, v. 233, 53 p.

Gans, P.B., Miller, E.L., Huggins, C.C., and Lee, J., 1999b, Geologic map of the Little Horse Canyon quadrangle, Nevada and Utah: Nevada Bureau of Mines and Geology Field Studies Map 20, scale 1:24,000.

Gans, P.B., Miller, E.L., and Lee, J., 1999a, Geologic map of the Spring Mountain quadrangle, Nevada and Utah: Nevada Bureau of Mines and Geology Field Studies Map 18, scale 1:24,000.

Gans, P.B., Miller, E.L., McCarthy, J., and Ouldcott, M.L., 1985, Tertiary extensional faulting and evolving ductile-brittle transition zones in the northern Snake Range and vicinity: New insights from seismic data: Geology, v. 13, p. 189–193.

Gans, P.B., Seedorff, E., Fahey, P.L., Hasler, R.W., Maher, D.J., Jeanne, R.A., and Shaver, S.A., 2001, Rapid Eocene extension in the Robinson district, White Pine County, Nevada: Constraints from $^{40}Ar/^{39}Ar$ dating: Geology, v. 29, no. 6, p. 475–478.

Gardner, P.M., and Heilweil, V.M., 2014, A multiple-tracer approach to understanding regional groundwater flow in the Snake Valley area of the eastern Great Basin, U.S.A.: Applied Geochemistry, v. 45, p. 33–49.

Garside, L.J., Hess, R.H., Fleming, K.L, and Weimer, B.S., 1988, Oil and gas developments in Nevada: Nevada Bureau of Mines and Geology Bulletin 104, 136 p.

Gebelin, A., Teyssier, C., Heizler, M.T., and Mulch, A., 2015, Meteoric water circulation in a rolling-hinge detachment system (northern Snake Range core complex, Nevada): Geological Society of America Bulletin, v. 127, p. 149–161.

Grauch, V.J.S., Blakely, R.J., Blank, H.R., Oliver, H.W., Plouff, D., and Ponce, D.A., 1988, Geophysical delineation of granitic plutons in Nevada: U.S. Geological Survey Open-File Report 88-11, scale 1:1,000,000.

Greene, D.C., 2014, The Confusion Range, west-central Utah—fold-thrust deformation and a western Utah thrust belt in the Sevier hinterland: Geosphere, v. 10, p. 148–169.

Greene, D.C., and Herring, D.M., 2013, Structural architecture of the Confusion Range, west-central Utah—a Sevier fold-thrust belt and frontier petroleum province: Utah Geological Survey Open-File Report 613, CD.

Guth, P.L., 1980, Geology of the Sheep Range, Clark County, Nevada [Ph.D. dissertation]: Massachusetts Institute of Technology, Cambridge, Massachusetts, 189 p.

Hacker, D.B., 1998, Catastrophic gravity sliding and volcanism associated with the growth of laccoliths—examples from early Miocene hypabyssal intrusions of the Iron Axis magmatic province, Pine Valley Mountains, southwest Utah: Kent, Ohio, unpublished Ph.D. thesis, Kent State University, 258 p.

Hacker, D.B., Biek, R.F., and Rowley, P.D., 2014, Catastrophic emplacement of the gigantic Markagunt gravity slide, southwest Utah (USA)—implications for hazards associated with sector collapse of volcanic fields: Geology, v. 42, no. 11, p. 943–946.

Hacker, D.B., Holm, D.K., Rowley, P.D., and Blank, H.R., 2002, Associated Miocene laccoliths, gravity slides, and volcanic rocks, Pine Valley Mountains and Iron Axis region, southwestern Utah, *in* Lund, W.R., editor, Field guide to geologic excursions in southwestern Utah and adjacent areas of Arizona and Nevada, prepared for the Geological Society of America, Rocky Mountain Section Meeting in Cedar City, Utah, May 7–9, 2002: U.S. Geological Survey Open-File Report 02-172, p. 236–283.

Hagstrum, J.T., and Gans, P.B., 1989, Paleomagnetism of the Oligocene Kalamazoo Tuff–Implications for middle Tertiary extension in east-central Nevada: Journal of Geophysical Research, v. 94, p. 1827–1842.

Hamilton, W.B., 1995, Subduction systems and magmatism, *in* Smellie, J.L., editor, Volcanism Associated with Extension at Consuming Plate Margins: Geological Society Special Publication No. 81, p. 3–28.

Hamilton, Warren, and Myers, W.B., 1966, Cenozoic tectonics of the western United States: Reviews of Geophysics, v. 4, p. 509–549.

Hammond, W.C., Blewitt, G., and Kreemer, C., 2014, Steady contemporary deformation of the central Basin and Range province, United States: Journal of Geophysical Research, v. 119, doi:10.1002/2014JB011145, 19 p. (online).

Harding, A.E., Scott, R.B., Mehnert, H.H., and Snee, L.W., 1995, Evidence of the Kane Springs Wash caldera in the Meadow Valley Mountains, southeastern Nevada, *in* Scott, R.B., and Swadley, WC, editors, Geologic studies in the Basin and Range–Colorado Plateau transition in southeastern Nevada, southwestern Utah, and northwestern Arizona, 1992: U.S. Geological Survey Bulletin 2056, p. 135–180.

Harrill, J.R., Gates, J.S., and Thomas, J.M., 1988, Major ground-water flow systems in the Great

Basin region of Nevada, Utah, and adjacent states: U.S. Geological Survey Hydrologic Investigations Atlas HA-694-C, scale 1:1,000,000, 2 sheets.

Harrill, J.R., and Prudic, D.E., 1998, Aquifer systems in the Great Basin region of Nevada, Utah, and adjacent states—summary report: U.S. Geological Survey Professional Paper 1409-A, 66 p.

Hauser, E., Potter, C., Hauge, T., Burgess, S., Burtch, S., Mutschler, J., Allmendinger, R., Brown, L., Kaufman, S., and Oliver, J., 1987, Crustal structure of eastern Nevada from COCORP deep seismic reflection data: Geological Society of America Bulletin, v. 99, p. 833–844.

Hazzard, J.C., and Turner, E.F., 1957, Décollement-type overthrusting in south-central Idaho, northwestern Utah, and northeastern Nevada [abs.]: Geological Society of America Bulletin, v. 68, no. 12, p. 1829.

Heilweil, V.M., and Brooks, L.E., editors, 2011, Conceptual model of the Great Basin carbonate and alluvial aquifer system: U.S. Geological Survey Scientific Investigations Report 2010-5193, 191 p.

Heiskanen, W.A., and Vening Meinesz, F.A., 1958, The earth and its gravity field: New York, McGraw-Hill, 470 p.

Henry, C.D., 2008, Ash-flow tuffs and paleovalleys in northeastern Nevada—Implications for Eocene paleogeography and extension in the Sevier hinterland, northern Great Basin: Geosphere, v. 4, p. 1–35.

Henry, C.D., Hinz, N.H., Faulds, J.E., Colgan, J.P., John, D.A., Brooks, E.R., Cassel, E.J., Garside, L.J., Davis, D.A., and Castor, S.B., 2012, Eocene-early Miocene paleotopography of the Sierra Nevada—Great Basin—Nevadaplano based on widespread ash-flow tuffs and paleovalleys: Geosphere, v. 8, p. 1–27.

Herring, D.M., 1998a, Drilling results for the Balcron Oil #12-36 Cobra State dry hole, Millard County, Utah, *in* French, D.E., and Schalla, R.A., editors, Hydrocarbon habitat and special geologic problems of the Great Basin: 1998 Field Trip Guidebook, Nevada Petroleum Society, p. 88–89.

Herring, D.M., 1998b, Drilling results of the EREC #31-22 Mamba Federal dry hole, Millard County, Utah, *in* French, Don E., and Schalla, Robert A., editors, Hydrocarbon habitat and special geologic problems of the Great Basin: 1998 Field Trip Guidebook, Nevada Petroleum Society, p. 85–86.

Herring, D.M., Greene, D.C., French, D.E., Schalla, R.A., and Taylor, W.J., 1998, 1998 Nevada Petroleum Society Field Trip—Day 3: Ely to Snake Valley, *in* French, D. E., and Schalla, R.A., editors, Hydrocarbon habitat and special geologic problems of the Great Basin: 1998 Field Trip Guidebook, Nevada Petroleum Society, p. 81–101.

Hess, R., 2001, Nevada oil and gas well map: Nevada Bureau of Mines and Geology Open-File Report 2001–07.

Hess, R., 2004, Nevada oil and gas well database (NVOILWEL): Nevada Bureau of Mines and Geology Open-File Report 04–01, 240 p.

Hess, R.H., Henson, M.A., Davis, D.A., Limerick, S.H., Siewe, S.S., and Niles, M., 2011, Oil and gas well information for Nevada—2011 update: Nevada Bureau of Mines and Geology Open-File Report 11-6, 9643 digital files.

Hess, R.H., and Johnson, G.L., 1997, Nevada Bureau of Mines and Geology county digital mapping project: Nevada Bureau of Mines and Geology Open-File Report 97–1, scale 1:250,000.

Hildenbrand, T.G., 1983, FFTFIL—A filtering program based on two-dimensional Fourier analysis: U.S. Geological Survey Open-File Report 83-237, 61 p.

Hildenbrand, T.G., and Kucks, R.P., 1988a, Filtered magnetic anomaly maps of Nevada: Nevada Bureau of Mines and Geology Map 93B, scale 1:1,000,000, 5 sheets.

Hildenbrand, T.G., and Kucks, R.P., 1988b, Total intensity magnetic anomaly map of Nevada: Nevada Bureau of Mines and Geology Map 93A, scale 1:750,000.

Hildenbrand, T.G., Kucks, R.P., and Sweeney, R.E., 1983, Digital colored magnetic-anomaly map of the Basin and Range province: U.S. Geological Survey Open-File Report 83-189, 11 p.

Hildenbrand, T.G., Phelps, G., and Mankinen, E.A., 2006, Inversion of gravity data to define the pre-Cenozoic surface and regional structures possibly influencing groundwater flow in the Rainier Mesa region, Nye County, Nevada: U.S. Geological Survey Open-File Report 2006-1299, 28 p.

Hintze, L.F., 1980a, Geologic map of Utah: Utah Geological and Mineralogical Survey, scale 1:500,000.

Hintze, L.F., 1980b, Preliminary geologic map of the Sand Pass NW quadrangle, Juab County, Utah: U.S. Geological Survey Miscellaneous Field Studies Map MF-1149, scale 1:24,000.

Hintze, L.F., 1988, A field guide to Utah's rocks: Geologic history of Utah: Brigham Young University Geology Studies, Special Publication 7, 202 p.

Hintze, L.F., 2005, Utah's spectacular geology: How it came to be. Provo, Utah, Brigham Young University.

Hintze, L.F., Anderson, R.E., and Embree, G.F., 1994a, Geologic map of the Motoqua and Gunlock quadrangles, Washington County, Utah: U.S. Geological Survey Miscellaneous Investigations Series Map I-2427, scale 1:24,000.

Hintze, L.F., and Davis, F.D., 2002a, Geologic map of the Tule Valley 30′×60′ quadrangle and parts of the Ely, Fish Springs, and Kern Mountains 30′×60′ quadrangles, northwest Millard County, Utah: Utah Geological Survey Map 186, scale 1:100,000, 2 sheets.

Hintze, L.F., and Davis, F.D., 2002b, Geologic map of the Wah Wah Mountains North 30′×60′ quadrangle and part of the Garrison 30′×60′ quadrangle, southwest Millard County and part of Beaver County, Utah: Utah Geological Survey Map 182, scale 1:100,000, 2 sheets.

Hintze, L.F., and Davis, F.D., 2003, Geology of Millard County, Utah: Utah Geological Survey Bulletin 133, 305 p.

Hintze, L.F., Grant, S.K., Weaver, C.L., and Best, M.G., 1994b, Geologic map of the Blue Mountain-Lund area, Beaver and Iron counties, Utah: U.S. Geological Survey Miscellaneous Investigations Map I-2361, scale 1:50,000.

Hintze, L.F., and Kowallis, B.J., 2009, Geologic history of Utah. Provo, Utah, Brigham Young University Geology Studies Special Publication 9, 225 p.

Hintze, L.F., Willis, G.C., Laes, D.Y.M., Sprinkel, D.A., and Brown, K.D., 2000, Digital geologic map of Utah: Utah Geological Survey Map 179DM, scale 1:500,000, 2 sheets.

Hitchborn, A.D., Arbonies, D.G., Peters, S.G., Connors, K.A., Noble, D.C., Larson, L.T., Beebe, J.S., and McKee, E.H., 1996, Geology and gold deposits of the Bald Mountain mining district, White Pine County, Nevada, *in* Coyner, A.R., and Fahey, P.L., editors, Geology and Ore Deposits of the American Cordillera: Geological Society of Nevada Symposium Proceedings, Reno/Sparks, Nevada, April 1995, p. 505–546.

Hood, J.W., and Rush, F.E., 1965, Water-resources appraisal of the Snake Valley area, Utah and Nevada: Nevada Department of Conservation and Natural Resources Water Resources–Reconnaissance Series Report 34, 40 p.

Hose, R.K., 1977, Structural geology of the Confusion Range, west-central Utah: U.S. Geological Survey Professional Paper 971, 9 p.

Hose, R.K., and Blake, Jr., M.C., 1976, Geology and mineral resources of White Pine County, Nevada Part I, Geology: Nevada Bureau of Mines and Geology Bulletin 85, p. 1–35.

Howard, E.L., 1978, Geologic map of the eastern Great Basin, Nevada and Utah: Terrascan Group, Inc., Lakewood, Colorado, scale 1:250,000.

Howard, K.A., Kistler, R.W., Snoke, A.W., and Willden, R., 1979, Geologic map of the Ruby Mountains, Nevada: U.S. Geological Survey Miscellaneous Investigations Series Map I-1136, scale 1:125,000.

Howard, K.A., Wooden, J.L., Barnes, C.G., Premo, W.R., Snoke, A.W., and Lee, S.-Y., 2011, Episodic growth of a Late Cretaceous and Paleogene intrusive complex of pegmatitic leucogranite, Ruby Mountains core complex, Nevada, USA: Geosphere, v. 7, p. 1220–1248.

Hudson, M.R., and Geissman, J.W., 1982, Dispersed paleomagnetic data from the Kern Mountains metamorphic core complex, northeastern Nevada: Eos, Transactions of the American Geophysical Union, v. 63, no. 45, p. 919.

Hudson, M.R., Rosenbaum, J.G., Gromme, C.S., Scott, R.B., and Rowley, P.D., 1998, Paleomagnetic evidence for counterclockwise rotation in a broad sinistral shear zone, Basin and Range province, southeastern Nevada and southwestern Utah, *in* Faulds, J.E., and Stewart, J.H., editors, Accommodation zones and transfer zones—the regional segmentation of the Basin and Range province: Geological Society of America Special Paper 323, p. 149–180.

Humphreys, E.D., 1995, Post-Laramide removal of the Farallon slab, western United States: Geology, v. 23, p. 987–990.

Humphreys, E., 2009, Relation of flat subduction to magmatism and deformation in the western United States, *in* Kay, S.M., Ramos, V.A., and Dickinson, W.R., editors, Backbone of the Americas—shallow subduction, plateau uplift, and ridge and terrane collision: Geological Society of America Memoir 204, p. 85–98.

Hurlow, H., editor, 2014, Hydrogeologic studies and groundwater monitoring in Snake Valley and adjacent hydrographic areas, west-central Utah and east-central Nevada: Utah Geological Survey Bulletin 135, 294 p. (DVD).

Hurlow, H.A., and Inkenbrandt, P.C., 2016, Alanalysis (sic) of groundwater-level records from Snake Valley, western Millard County, Utah, *in* Comer, J.B., Inkenbrandt, P.C., Krahulec, K.A., and Pinnell, M.L., editors, Resources and geology of Utah's West Desert: Utah Geological Association Publication 45, p. 221–246.

Hurtubise, D.O., and du Bray, E.A., 1992, Stratigraphy and structure of the Seaman Range and Fox Mountain, Lincoln, and Nye Counties, Nevada: U.S. Geological Survey Bulletin 1988-B, 31 p.

Jachens, R.C., and Moring, B.C., 1990, Maps of the thickness of Cenozoic deposits and the isostaticresidual gravity over basement for Nevada: U.S. Geological Survey Open-File Report 90-404, 15 p.

Jachens, R.C., and Roberts, C.W., 1981, Documentation of program, ISOCIETYOMP, for computing isostatic residual gravity: U.S. Geological Survey Open-File Report 81-574, 26 p.

Jayko, A.S., 1990, Shallow crustal deformation in the Pahranagat area, southern Nevada, *in* Wernicke, B.P., ed., Basin and Range extensional tectonics near the latitude of Las Vegas, Nevada: Boulder, Colorado, Geological Society of America Memoir 176, p. 213–236.

Jayko, A.S., 2007, Geologic map of the Pahranagat Range 30′×60′ quadrangle, Lincoln and Nye Counties, Nevada: U.S. Geological Survey Scientific Investigations Map 2904, scale 1:100,000. [http://pubs.usgs.gov/sim/2007/2904/].

Johnson, J.A., 2007, Hydrology of Muddy River Springs, *in* Coache, R., editor, Regional tour of the carbonate system guidebook: Nevada Water Resources Association, Clark County, Nevada, June 18–20, 2007, p. 3–4.

Johnson, M., 2007a, Geyser Spring complex hydrology and Lake Valley activities, *in* Coache, R., editor, Regional tour of the carbonate system guidebook: Nevada Water Resources Association, Clark County, Nevada, June 18–20, 2007, p. 59–60.

Johnson, M., 2007b, Hydrogeology of Pahranagat shear zone and surrounding area, *in* Coache, R., editor, Regional tour of the carbonate system guidebook: Nevada Water Resources Association, Reno, Nevada, p. 11–12.

Johnson, M., Dixon, G.L., Rowley, P.D., Katzer, T.C., and Winters, M., 2002, Hydrology and ground-water conditions of the Tertiary Muddy Creek Formation in the lower Virgin River basin of southeastern Nevada and adjacent Arizona and Utah, *in* Lund, W.R., editor, Field guide to geologic excursions in southwestern Utah and adjacent areas of Arizona and Nevada: Utah Geological Survey Open-File Report 02–172, p. 284–315.

Jones, A.E., ed., 1996, Geology and gold deposits of eastern Nevada—1996 Spring Field Trip Guidebook: Geological Society of Nevada Special Publication No. 23, Reno, Nevada, May 3–5, 1996, 166 p.

Keith, J.D., Tingey, D.G., and Best, M.G., 1994, Geologic map of the Rice Mountain quadrangle, Nevada and Utah: Nevada Bureau of Mines and Geology Field Studies Map 7, scale 1:24,000.

Keller, G.V., 1987, Rock and mineral properties, *in* Nabighian, M.N., editor, Electromagnetic methods in applied geophysics: Volume 1, Theory, Tulsa, Oklahoma, Society of Exploration Geophysicists, Investigations in Geophysics no. 3, p. 13–51.

Kellogg, H.E., 1963, Paleozoic stratigraphy of the southern Egan Range, Nevada: Geological Society of America Bulletin, v. 74, p. 685–708.

Kellogg, H.E., 1964, Cenozoic stratigraphy and structure of the southern Egan Range, Nevada: Geological Society of America Bulletin, v. 75, p. 949–968.

Kepper, J.C., 1960, Stratigraphy and structure of the southern half of the Fish Springs Range, Juab County, Utah [M.S. thesis]: University of Washington, Seattle, 92 p.

Kirby, S., and Hurlow, H., 2005, Hydrogeologic setting of the Snake Valley hydrologic basin, Millard County, Utah, and White Pine and Lincoln Counties, Nevada—implications for possible effects of proposed water wells: Utah Geological Survey Report of Investigation 254, 39 p.

Kistinger, G.M., Prieur, J.P., Rowley, P.D., and Dixon, G.L., 2009, Characterization of streams and springs in the Snake Valley area, Utah and Nevada, *in* Tripp, B.T., Krahulec, K., and Jordan, J.L., editors, Geology and geologic resources and issues of western Utah: Utah Geological Association Publication 38, p. 299–323.

Kleinhampl, F.J., and Ziony, J.I., 1985, Geology of northern Nye County, Nevada: Nevada Bureau of Mines and Geology Bulletin 99A, 172 p.

Kucks, R.P., Hill, P.L., and Ponce, D.A., 2006, Nevada magnetic and gravity maps and data—a website for the distribution of data: U.S. Geological Survey Data Series 234 [http://pubs.er.usgs.gov/usgspubs/ds/ds234/].

Laczniak, R.J., Cole, J.C., Sawyer, D.A., and Trudeau, D.A., 1996, Summary of hydrogeologic controls on ground-water flow at the Nevada Test Site, Nye County, Nevada: U.S. Geological Survey Water-Resources Investigations Report 96–4109, 59 p.

Langenheim, V.E., Beard, L.S., and Faulds, J.E., 2010, Implications of geophysical analysis on basin geometry and fault offsets in the northern Colorado River extensional corridor and adjoining Lake Mead region, Nevada and Arizona, *in* Umhoefer, P.J., Beard, L.S., and

Lamb, M.A., editors, Miocene tectonics of the Lake Mead region, central Basin and Range: Geological Society of America Special Paper 463, p. 39–59.

Langenheim, V.E., Glen, J.M., Jachens, R.C., Dixon, G.L., Katzer, T.C., and Morin, R.L., 2000, Geophysical constraints on the Virgin River depression, Nevada, Utah, and Arizona: U.S. Geological Survey Open-File Report 2000-407, 26 p.

Langenheim, V.E., Miller, J.J., Page, W.R., and Grow, J.A., 2001, Thickness and geometry of Cenozoic deposits in California Wash area, Nevada, based on gravity and seismic-reflection data: U.S. Geological Survey Open-File Report 01-393, 26 p.

Larson, E.R., and Langenheim, Jr., R.L., 1979, The Mississippian and Pennsylvanian (Carboniferous) systems in the United States—Nevada: U.S. Geological Survey Professional Paper 1110-BB, p. BB1–BB19.

Las Vegas Valley Water District, 2001, Water resources and ground-water modeling in the White River and Meadow Valley flow systems, Clark, Lincoln, Nye and White Pine counties, Nevada: Las Vegas Valley Water District, Las Vegas, Nevada, 297 p.

Layne Geosciences, 2009, Status report audiomagnetotelluric surveys Spring and Snake valleys, Nevada: Layne Geosciences, Fontana, California, 274 p.

Leahy, P.P., and Lyttle, P.T., 1998, The re-emerging and critical role of geologic understanding in hydrology, *in* Brahana, J.V., Eckstein, Y., Ongley, L.K., Schneider, R., and Moore, J.E., editors, Gambling with groundwater—physical, chemical, and biological aspects of aquifer-stream relations: Proceedings International Association of Hydrogeologists and the American Institute of Hydrologists, Las Vegas, Nevada, September 28–October 2, 1998: The American Institute of Hydrology, p. 19–24.

Lee, J., 1995, Rapid uplift and rotation of mylonitic rocks from beneath a detachment fault—Insights from potassium feldspar $^{40}Ar/^{39}Ar$ thermochronology, northern Snake Range, Nevada: Tectonics, v. 14, p. 54–77.

Lee, J., Gans, P.B., and Miller, E.L., 1999a, Geologic map of the Mormon Jack Pass quadrangle, Nevada: Nevada Bureau of Mines and Geology Field Studies Map 17, scale 1:24,000.

Lee, J., Gans, P.B., and Miller, E.L., 1999b, Geologic map of the Third Butte East quadrangle, Nevada: Nevada Bureau of Mines and Geology Field Studies Map 16, scale 1:24,000.

Lee, J., Miller, E.L., Gans, P.B., and Huggins, C.C., 1999c, Geologic map of the Mount Moriah quadrangle, Nevada: Nevada Bureau of Mines and Geology Field Studies Map 19, scale 1:24,000.

Lewis, C.J., Wernicke, B.P., Selverstone, Jane, and Bartley, J.M., 1999, Deep burial of the footwall of the northern Snake Range décollement, Nevada: Geological Society of America Bulletin, v. 111, p. 39–51.

Liberty, L.M., Heller, P.L., and Smithson, S.B., 1994, Seismic reflection evidence for two-phase development of Tertiary basins from east-central Nevada: Geological Society of America Bulletin, v. 106, p. 1621–1633.

Link, P.K., Christie-Blick, N., Devlin, W.J., Elston, D.P., Horodyski, R.J., Levy, M., Miller, J.M.G., Pearson, R.C., Prave, A., Stewart, J.H., et al., 1993, Middle and Late Proterozoic stratified rocks of the western U.S. Cordillera, Colorado Plateau, and Basin and Range province, *in* Reed, Jr., J.C., editor, Precambrian: Conterminous U.S.: Geological Society of America, The Geology of North America, v. C-2, p. 463–595.

Lipman, P.W., Prostka, H.J., and Christiansen, R.L., 1972, Cenozoic volcanism and plate-tectonic evolution of the western United States. I. Early and middle Cenozoic: Royal Society of London Philosophical Transactions A, v. 271, no. 1213, p. 217–248.

Long, S.P., 2012, Magnitudes and spatial patterns of erosional exhumation in the Sevier hinterland, eastern Nevada and western Utah, USA—Insight from a Paleogene paleogeologic map: Geosphere, v. 8, p. 881–901.

Long, S.P., 2014, Preliminary geologic map of Heath Canyon, central Grant Range, Nye County, Nevada: Nevada Bureau of Mines and Geology Open-File Report 14-6, scale 1:24,000, 4 p.

Long, S.P., and Walker, J.P., 2015, Geometry and kinematics of the Grant Range brittle detachment system, eastern Nevada, U.S.A.: an end-member style of upper-crustal extension: Tectonics, v. 34, TC003918, 26 p., doi: 10.1002/2015TC003918

Long, S.P., Henry, C.D., Muntean, J.L., Edmondo, G.P., and Casel, E.V., 2014, Early Cretaceous constructionof a structural culmination, Eureka, Nevada, U.S.A.—implications for out-of-sequence deformation in the Sevier hinterland: Geosphere, v. 10, p. 564–584.

Long, S.P., Thomson, S.N., Reiners, P.W, and Di Fiori, R.V., 2015, Synorogenic extension localized by upper-crustal thickening—an example from the

Late Cretaceous Nevadaplano: Geology, v. 43, p. 351–354.

Longwell, C.R., Pampeyan, E.H., Bowyer, B., and Roberts, R.J., 1965, Geology and mineral deposits of Clark County, Nevada: Nevada Bureau of Mines and Geology Bulletin 62, 218 p.

Loucks, M.D., Tingey, D.G., Best, M.G., Christiansen, E.H., and Hintze, L.F., 1989, Geologic map of the Fortification Range, Lincoln and White Pine Counties, Nevada: U.S. Geological Survey Miscellaneous Investigations Series Map I-1866, scale 1:50,000.

Lumsden, W.W., Walker, C.T., and Francis, R.D., 2002, The Precambrian and Paleozoic stratigraphy of the White Pine, Grant and Schell Creek Ranges in eastern Nevada—The key to interpreting structures formed by extension and attenuation, *in* Ehni, W., and Faulds, J., editors, Detachment and attenuation in eastern Nevada and its application to petroleum exploration: Nevada Petroleum Society 2002 Field Trip Guidebook, p. 33–72.

Lund, Karen, and Beard, L.S., 1992, Extensional geometry in the northern Grant Range, east central Nevada—implications for oil deposits in Railroad Valley, *in* Thorman, C.H., editor, Application of structural geology to mineral and energy resources of the central and western United States: U.S. Geological Survey Bulletin 2012, p. I1–I9.

Lund, K., Beard, L.S., and Perry, Jr., W.J., 1991, Structures of the northern Grant Range and Railroad Valley, Nye County, Nevada: Implications for oil occurrences, *in* Flanigan, D.M.H., Hansen M., and Flanigan, T.E., editors, Geology of White River Valley, the Grant Range, Eastern Railroad Valley and Western Egan Range, Nevada: 1991 Fieldtrip Guidebook, Nevada Petroleum Society Inc., Reno, p. 1–6.

Mabey, D.R., Zietz, I., Eaton, G.P., and Kleinkopf, M.D., 1978, Regional magnetic patterns in part of the Cordillera in the western United States, *in* Smith, R.B., and Eaton, G.P., editors, Cenozoic tectonics and regional geophysics of the western Cordillera: Geological Society of America Memoir 152, p. 93–106.

Maldonado, F., and Schmidt, D.L., 1991, Geologic map of the southern Sheep Range, Fossil Ridge, and Castle Rock area, Clark County, Nevada: U.S. Geological Survey Miscellaneous Investigations Series Map I-2086, scale 1:24,000.

Maldonado, F., Spengler, R.W., Hanna, W.F., and Dixon, G.L., 1988, Index of granitic rock masses in the State of Nevada: U.S. Geological Survey Bulletin 1831, 81 p.

Mankinen, E.A., 2007, Gravity and magnetic studies of the Spring Valley region, *in* Coache, R., editor, Regional tour of the carbonate system guidebook: Nevada Water Resources Association, Clark County, Nevada, June 18–20, 2007, p. 37–38.

Mankinen, E.A., and McKee, E.H., 2007, Gravity data from Newark Valley, White Pine County, Nevada: U.S. Geological Survey Open-File Report 2007-1306, 18 p.

Mankinen, E.A., and McKee, E.H., 2009, Geophysical setting of western Utah and eastern Nevada between latitudes 37°45' and 40°N, *in* Tripp, B.T., Krahulec, K., and Jordan, J.L., editors, Geology and geologic resources and issues of western Utah: Utah Geological Association Publication 38, p. 271–286.

Mankinen, E.A., and McKee, E.H., 2011, Principle facts for gravity stations collected in 2010 from White Pine and Lincoln Counties, east-central Nevada: U.S. Geological Survey Open-File Report 2011-1084, 24 p.

Mankinen, E.A., Roberts, C.W., McKee, E.H., Chuchel, B.A., and Moring, B.C., 2006, Geophysical Data from the Spring and Snake valleys area, Nevada and Utah: U.S. Geological Survey Open-File Report 2006-1160, 36 p.

Mankinen, E.A., Roberts, C.W., McKee, E.H., Chuchel, B.A., and Moring, R.L., 2007, Geophysical data from Spring Valley to Delamar Valley, east-central Nevada: U.S. Geological Survey Open-File Report 2007-1190, 42 p.

Mankinen, E.A., Rowley, P.D., Dixon, G.L., and McKee, E.H., 2016, Regional geophysics of western Utah and eastern Nevada, with emphasis on the Confusion Range, *in* Comer, J.B., Inkenbrandt, P.C., Krahulec, K.A., and Pinnell, M.L., editors, Resources and geology of Utah's West Desert: Utah Geological Association Publication 45, p. 147–166.

Mankinen, E.A., Chuchel, B.A., and Moring, B.C., 2008, Gravity data from Dry Lake and Delamar Valleys, east-central Nevada: U.S. Geological Survey Open-File Report 2008-1299, 30 p. [http://pubs.usgs.gov/of/2008-1299/].

Masbruch, M.D., Gardner, P.M., and Brooks, L.E., 2014, Hydrology and numerical simulation of groundwater movement and heat transport in Snake Valley and surrounding areas, Juab, Millard, and Beaver counties, Utah, and White Pine and Lincoln counties, Nevada: U.S. Geological Survey Scientific Investigations Report 2014-5103, 108 p.

Masbruch, M.D., Gardner, P.M., and Brooks, L.E., 2016, Numerical simulation of groundwater movement and heat transport in Snake Valley and

surrounding areas, Juab, Millard, and Beaver counties, Utah, and White Pine and Lincoln counties, Nevada, *in* Comer, J.B., Inkenbrandt, P.C., Krahulec, K.A., and Pinnell, M.L., editors, Resources and geology of Utah's West Desert: Utah Geological Association Publication 45, p. 201–220.

Mason, J.L., Atwood, J.W., and Buettner, P.S., 1985, Selected test-well data from the MX-missile siting study, Tooele, Juab, Millard, Beaver, and Iron Counties, Utah: Utah Hydrologic-Data Report 43, U.S. Geological Survey Open-File Report 85-374, 15 p.

McGrew, A.J., 1993, The origin and evolution of the southern Snake Range décollement, east central Nevada: Tectonics, v. 12, no. 1, p. 21–34.

McPhee, D.K., 2007, Audiomagnetotelluric imaging of the Spring Valley region, *in* Coache, R., editor, Regional tour of the carbonate system guidebook: Nevada Water Resources Association, Clark County, Nevada, June 18–20, 2007, p. 39–40.

McPhee, D.K., Chuchel, B.A., and Pellerin, L., 2006b, Audiomagnetotelluric data from Spring, Cave, and Coyote Spring valleys, Nevada: U.S. Geological Survey Open-File Report 2006-1164, 43 p.

McPhee, D.K., Chuchel, B.A., and Pellerin, L., 2007, Audiomagnetotelluric data and two-dimensional models from Spring, Snake, and Three Lakes Valleys, Nevada: U.S. Geological Survey Open-File Report 2007-1181, 47 p. [http://pubs.usgs.gov/of/2007/1181/].

McPhee, D.K., Chuchel, B.A., and Pellerin, L., 2008, Audiomagnetotelluric data and preliminary two-dimensional models from Spring, Dry Lake, and Delamar Valleys, Nevada: U.S. Geological Survey Open-File Report 2008-1301, 59 p.

McPhee, D.K., Pari, K., and Baird, F., 2009, Audiomagnetotelluric investigation of Snake Valley, eastern Nevada and western Utah, *in* Tripp, B.T., Krahulec, K., and Jordan, J.L., editors, Geology and geologic resources and issues of western Utah: Utah Geological Association Publication 38, p. 287–298.

McPhee, D.K., Pellerin, L., Chuchel, B.A., and Dixon, G.L., 2005, Resistivity imaging of Spring Valley, Nevada, using the audiomagnetotelluric method, EOS, Transactions American Geophysical Union, 86(18), Joint Assembly Supplement, Abstract NS23B-06.

McPhee, D.K., Pellerin, L., Chuchel, B.A., Tilden, J.E., and Dixon, G.L., 2006a, Resistivity imaging in eastern Nevada using the audiomagnetotelluric method for hydrogeologic framework studies, *in* Proceedings of the 19th Annual Symposium on the Application of Geophysics to Engineering and Environmental Problems (SAGEEP), Seattle, Washington, April 2–6, 2006, p. 712–718.

Mifflin, M.D., and Wheat, M.M., 1979, Pluvial lakes and estimated pluvial climates of Nevada: Nevada Bureau of Mines and Geology Bulletin 94, 57 p.

Miller, E.L., and Gans, P.B., 1989, Cretaceous crustal structure and metamorphism in the hinterland of the Sevier thrust belt, western U.S. Cordillera: Geology, v. 17, p. 59–62.

Miller, E.L., and Gans, P.B., 1999, Geologic map of The Cove quadrangle, Nevada and Utah: Nevada Bureau of Mines and Geology Field Studies Map 22, scale 1:24,000.

Miller, E.L., Gans, P.B., and Garing, J., 1983, The Snake Range décollement—an exhumed mid-Tertiary ductile-brittle transition: Tectonics, v. 2, no. 3, p. 239–263.

Miller, E.L., Dumitru, T.A., Brown, R.W., and Gans, P.B., 1999a, Rapid Miocene slip on the Snake Range—Deep Creek Range fault system, east-central Nevada: Geological Society of America Bulletin, v. 111, no. 6, p. 886–905.

Miller, E.L., Gans, P.B., and Grier, S.P., 1994, Geologic map of Windy Peak 7.5' quadrangle, WhitePine County, Nevada: U.S. Geological Survey Open-File Report 94–687, scale 1:24,000.

Miller, E.L., Gans, P.B., Grier, S.P., Huggins, C.C., and Lee, J., 1999b, Geologic map of the Old Mans Canyon quadrangle, Nevada: Nevada Bureau of Mines and Geology Field Studies Map 21, scale 1:24,000.

Miller, E.L., Grier, S.P., and Brown, J.L., 1995, Geologic map of the Lehman Caves quadrangle, White Pine County, Nevada: U.S. Geological Survey Geologic Quadrangle Map GQ-1758, scale1:24,000.

Misch, P., 1960, Regional structural reconnaissance in central-northeast Nevada and some adjacent areas—observations and interpretations, *in* Boettcher, J.W., and Sloan, Jr., W.W., editors, Guidebook to the geology of east central Nevada: Intermountain Association of Petroleum Geologists and Eastern Nevada Geological Society, 11th Annual Field Conference, Salt Lake City, Utah, September 8–10, 1960, p. 17–42.

Moores, E.M., Scott, R.B., and Lumsden, W.W., 1968, Tertiary tectonics of White Pine-Grant Range region, east-central Nevada, and some regional implications: Geological Society of America Bulletin, v. 79, no. 12, p. 1703–1726.

Morelli, C., editor, 1974, The international gravity standardization net 1971: International Association

of Geodesy Special Publication 4, 194 p.
Morris, H.T., 1987, Preliminary geologic map of the Delta 2° quadrangle, Tooele, Juab, Millard, and Utah Counties, Utah: U.S. Geological Survey Open-File Report 87–185, scale 1:250,000, 3 sheets.
Nelson, R.B., 1966, Structural development of northernmost Snake Range, Kern Mountains, and Deep Creek Range, Nevada and Utah: American Association of Petroleum Geologists Bulletin, v. 50, no. 5, p. 921–951.
Nolan, T.B., 1935, The Gold Hill mining district, Utah: U.S. Geological Survey Professional Paper 177, 172 p.
Norman, B.W., and Gans, P.B., 2014, Polyphase (Eocene and Miocene) extensional faulting of the central Schell Creek Range, White Pine County, Nevada (abs.): Geological Society of America 2014 Abstracts with Programs, v. 46, no. 6, p. 171.
North American Magnetic Anomaly Group (NAMAG), 2002, Digital data grids for the magnetic anomaly map of North America: U.S. Geological Survey Open-File Report 02-414, 4 p.
Nutt, C.J., 2000, Geologic map of the Alligator Ridge area, including the Buck Mountain East and Mooney Basin Summit quadrangles and parts of the Sunshine Well NE and Long Valley Slough quadrangles, White Pine County, Nevada: U.S. Geological Survey Geologic Investigations Series Map I-2691, scale 1:24,000.
Nutt, C.J., and Hart, K.S., 2004, Geologic map of the Big Bald Mountain quadrangle and part of the Tognini Spring quadrangle, White Pine County, Nevada: Nevada Bureau of Mines and Geology Map 145, scale 1:24,000.
Nutt, C.J., Zimbelman, D.R., Campbell, D.L., Duval, J.S., and Hannigan, B.J., 1990, Chapter C: Mineral resources of the Deep Creek Mountains wilderness study area, Juab and Tooele counties, Utah: U.S. Geological Survey Bulletin 1745-C, 40 p.
Oliveira, M.E., 1975, Geology of the Fish Springs mining district, Fish Springs Range, Utah: Brigham Young University Geology Studies, v. 22, pt. 1, p. 69–104.
Otto, B.R., 2008, Geologic map of the central Butte Range, White Pine County, Nevada: Nevada Bureau of Mines and Geology Map 160, scale 1:48,000.
Oviatt, C.G., 1991, Quaternary geology of Fish Springs Flat, Juab County, Utah: Utah Geological Survey Special Study 77, 16 p.
Page, W.R., 1992, Preliminary geologic map of the Paleozoic rocks in the Arrow Canyon quadrangle, Clark County, Nevada: U.S. Geological Survey Open-File Report 92-681, scale 1:24,000.
Page, W.R., 1998, Geologic map of the Arrow Canyon NW quadrangle, Clark County, Nevada: U.S. Geological Survey Geologic Quadrangle Map GQ-1776, scale 1:24,000.
Page, W.R., and Dixon, G.L., 1992, Northern terminus of Mesozoic Dry Lake thrust fault, Arrow Canyon Range, southeastern Nevada [abs]: Geological Society of America Abstracts with Programs, v. 24, no. 6, p. 56.
Page, W.R., and Ekren, E.B., 1995, Preliminary geologic map of the Bristol Well quadrangle, Lincoln County, Nevada: U.S. Geological Survey Open-File Report 95-580, scale 1:24,000.
Page, W.R., and Pampeyan, E.H., 1996, Preliminary geologic map of the Paleozoic rocks in the Wildcat Wash SE and Wildcat Wash SW quadrangles, Lincoln and Clark Counties, Nevada: U.S. Geological Survey Open-File Report 96-26, scale 1:24,000, 2 sheets.
Page, W.R., Dixon, G.L., Rowley, P.D., and Brickey, D.W., 2005a, Geologic map of parts of the Colorado, White River, and Death Valley groundwater flow systems, Nevada, Utah, and Arizona: Nevada Bureau of Mines and Geology Map 150, scale 1:250,000.
Page, W.R., Lundstrom, S.C., Harris, A.G., Langenheim, V.E., Workman, J.B., Mahan, S.A., Paces, J.B., Dixon, G.L., Rowley, P.D., Burchfiel, B.C., Bell, J.W., and Smith, E.I., 2005b, Geologic and geophysical maps of the Las Vegas 30'×60' quadrangle, Clark and Nye Counties, Nevada, and Inyo County, California: U.S. Geological Survey Scientific Investigations Map 2814, scale 1:100,000, 2 sheets.
Page, W.R., Scheirer, D.S., and Langenheim, V.E., 2006, Geologic cross sections of parts of the Colorado, White River, and Death Valley regional ground-water flow systems, Nevada, Utah, and Arizona: U.S. Geological Survey Open-File Report 2006–1040, Denver, CO, 80225.
Page, W.R., Swadley, WC, and Scott, R.B., 1990, Preliminary geologic map of the Delamar 3 SW quadrangle, Lincoln County, Nevada: U.S. Geological Survey Open-File Report 90–336, scale 1:24,000.
Palacky, G.J., 1987, Resistivity characteristics of geologic targets, *in* Nabighian, M.N., editor, Electromagnetic methods in applied geophysics, Volume 1, Theory: Society of Exploration Geophysics, Tulsa, Oklahoma, Investigations in

Geophysics, no. 3, p. 53–129.
Pampeyan, E.H., 1993, Geologic map of the Meadow Valley Mountains, Lincoln and Clark Counties, Nevada: U.S. Geological Survey Miscellaneous Investigations Series Map I-2173, scale 1:50,000, 2 sheets.
Pari, K.T., and Baird, F.A., 2011, Audiomagnetotelluric investigations in selected basins in White Pine and Lincoln Counties, East-Central Nevada: Southern Nevada Water Authority, Las Vegas, Nevada, Doc. No. RDS-ED-0022, 81 p.
Pekarek, A.H., 1988, Structural geology and petroleum potential of Long Valley, White Pine County, Nevada: Mountain Geologist, v. 25, no. 4, p. 141–180.
Petronis, M.S., Holm, D.K., Geissman, J.W., Hacker, D.B., and Arnold, B.J., 2014, Paleomagnetic results from the eastern Caliente-Enterprise zone, southwestern Utah—implications for initiation of a major Miocene transfer zone: Geosphere, v. 10, p. 534–563.
Phelps, G.A., Jewel, E.B., Langenheim, V.E., and Jachens, R.C., 2000, Principal facts for gravity stations in the vicinity of Coyote Spring Valley, Nevada, with initial gravity modeling results: U.S. Geological Survey Open-File Report 00–420, 22 p.
Ponce, D.A., 1992, Complete Bouguer gravity map of Nevada, Ely sheet: Nevada Bureau of Mines and Geology Map 99, scale 1:250,000.
Ponce, D.A., 1997, Gravity data of Nevada: U.S. Geological Survey Digital Data Series DDS-42, 27 p., CD-ROM.
Ponce, D.A., Morin, R.L., and Robbins, S.L., 1996, Bouguer gravity map of Nevada, Elko sheet: Nevada Bureau of Mines and Geology Map 107, scale 1:250,000.
Poole, F.G., and Sandberg, C.A., 1977, Mississippian paleogeography and tectonics of the western United States, *in* Stewart, J.H., Stevens, C.H., and Fritsche, A.E., editors, Paleozoic paleogeography of the western United States: Society of Economic Paleontologists and Mineralogists, Pacific Section, Pacific Coast Paleogeography Symposium 1, April 22, 1977, p. 67–85.
Poole, F.G., and Sandberg, C.A., 1991, Mississippian paleogeography and conodont biostratigraphy of the western United States, *in* Cooper, J.D., and Stevens, C.H., editors, Paleozoic paleogeography of the western United States—II: Society of Economic Paleontologists and Mineralogists, Pacific Section, Pacific Coast Paleogeography, p. 107–136.
Puchlik, K., 2009, The crypto zinc-indium-copper-molybdenum skarn deposit, western Juab County, Utah: Utah Geological Association Newsletter, v. 41, no. 6, p. 1–2.
Quinlivan, W.D., Rogers, C.L., and Dodge, Jr., H.W., 1974, Geologic map of the Portuguese Mountain quadrangle, Nye County, Nevada: U.S. Geological Survey Miscellaneous Investigations Series Map I-804, scale 1:48,000.
Raines, G.L., Connors, K.A., Moyer, L.A., and Miller, R.J., 2003, Spatial digital database for the geologic map of Nevada. Digital database, Version 3.0: U.S. Geological Survey Open-File Report 03-66.
Reheis, M.C., Adams, K.D., Oviatt, C.G., and Bacon, S.N., 2014, Pluvial lakes in the Great Basin of the western United States—a view from the outcrop: Quaternary Science Reviews, v. 97, p. 1–25.
Roberts, R.J., Montgomery, K.M., and Lehner, R.E., 1967, Geology and mineral resources of Eureka County, Nevada: Nevada Bureau of Mines and Geology Bulletin 64, 152 p., scale 1:250,000, 12 sheets.
Robinson, J.P., 1993, Provisional geologic map of the Gold Hill quadrangle, Tooele County, Utah: Utah Geological Survey Map 140, scale 1:24,000, 3 sheets.
Rodgers, D.W., 1987, Thermal and structural evolution of the southern Deep Creek Range, west central Utah and east central Nevada [Ph.D. dissertation]: Stanford University, California, 149 p.
Rowley, P.D., 1998, Cenozoic transverse zones and igneous belts in the Great Basin, western United States: Their tectonic and economic implications, *in* Faulds, J.E., and Stewart, J.H., editors, Accommodation zones and transfer zones—the regional segmentation of the Basin and Range Province: Geological Society of America Special Paper 323, p. 195–228.
Rowley, P.D., and Anderson, R.E., 1996, The syntectonic caldera—a new caldera type bounded by synchronous linear faults [abs.]: Geological Society of America Abstracts with Programs, v. 28, no. 7, p. A-449.
Rowley, P.D., and Dixon, G.L., 2001, The Cenozoic evolution of the Great Basin area, U.S.A.—new interpretations based on regional geologic mapping, *in* Erskine, M.C., Faulds, J.E., Bartley, J.M., and Rowley, P.D., editors, The geologic transition, High Plateaus to Great Basin—A symposium and field guide: The Mackin Volume: Utah Geological Association Publication 30 and

American Association of Petroleum Geologists Publication GB78, September, 20–22, 2001, p. 169–188.

Rowley, P.D., and Dixon, G.L., 2004, The role of geology in increasing Utah's ground-water resources from faulted terranes—lessons from the Navajo Sandstone, Utah, and the Death Valley flow system, Nevada-California, *in* Spangler, L.E., editor, Ground water in Utah—Resource, protection, and remediation—Field Symposium: Utah Geological Association, Salt Lake City, Utah, September 24–25, 2004, Publication 31, p. 27–41.

Rowley, P.D., and Shroba, R.R., 1991, Geologic map of the Indian Cove quadrangle, Lincoln County, Nevada: U.S. Geological Survey Geologic Quadrangle Map GQ-1701, scale 1:24,000.

Rowley, P.D., Christensen, E.F., Dixon, G.L., Burns, A.G., Watrus, J.M., and Collins, C.A., 2012, Fault derived conduit and barrier groundwater flow at Sawyer Spring, eastern margin of the Pine Valley Mountains, Washington County, Utah, *in* Hylland, M.D., and Harty, K.M., editors, Selected topics in engineering and environmental geology in Utah: Utah Geological Association Publication 41, CD, p. 99–114.

Rowley, P.D., Dixon, G.L., Burns, A.G., and Collins, C.A., 2009, Geology and hydrogeology of the Snake Valley area, western Utah and eastern Nevada, *in* Tripp, B.T., Krahulec, K., and Jordan, J.L., editors, Geology and geologic resources and issues of western Utah: Utah Geological Association Publication 38, p. 251–269.

Rowley, P.D., Dixon, G.L., Burns, A.G., Pari, K.T., Watrus, J.M., and Ekren, E.B., 2011, Geology and geophysics of Spring, Cave, Dry Lake, and Delamar valleys, White Pine and Lincoln counties and adjacent areas, Nevada and Utah: The geologic framework of regional groundwater flow systems: Presentation to the Office of the Nevada State Engineer: Southern Nevada Water Authority, Las Vegas, Nevada.

Rowley, P.D., Dixon, G.L., D'Agnese, F.A., O'Brien, G.M., and Brickey, D.W., 2004, Geology and hydrology of the Sand Hollow reservoir and well field area, Washington County, Utah: Washington County Water Conservancy District Report WCWCD-01, 14 p.

Rowley, P.D., Dixon, G.L., Watrus, J.M., Burns, A.G., Mankinen, E.A., McKee, E.H., Pari, K.T., Ekren, E.B., and Patrick, W.G., 2016, Geology, selected geophysics, and hydrogeology of the White River and parts of the Great Salt Lake Desert regional groundwater flow systems, Utah and Nevada, *in* Comer, J.B., Inkenbrandt, P.C., Krahulec, K.A., and Pinnell, M.L., editors, Resources and geology of Utah's West Desert: Utah Geological Association Publication 45, p. 167–200.

Rowley, P.D., Hacker, D.B., Maxwell, D.J., Maxwell, J.D., and Boswell, J.T., 2008, Interim geologic map of the Utah part of the Deer Lodge Canyon, Prohibition Flat, Uvada, and Pine Park quadrangles (east part of the Caliente 30'×60' quadrangle), Iron and Washington counties, Utah: Utah Geological Survey Open-File Report 530, scale 1:24,000.

Rowley, P.D., Lipman, P.W., Mehnert, H.H., Lindsey, D.A., and Anderson, J.J., 1978, Blue Ribbon lineament, an east-trending structural zone within the Pioche mineral belt of southwestern Utah and eastern Nevada: U.S. Geological Survey Journal of Research, v. 6, no. 2, p. 175–192.

Rowley, P.D., Nealey, L.D., Unruh, D.M., Snee, L.W., Mehnert, H.H., Anderson, R.E., and Grommé, C.S., 1995, Stratigraphy of Miocene ash-flow tuffs in and near the Caliente caldera complex, southeastern Nevada and southwestern Utah, *in* Scott, R.B., and Swadley, WC, editors, Geologic studies in the Basin and Range–Colorado Plateau transition in southeastern Nevada, southwestern Utah, and northwestern Arizona, 1992: U.S. Geological Survey Bulletin 2056, p. 43–88.

Rowley, P.D., Shroba, R.R., Simonds, F.W., Burke, K.J., Axen, G.J., and Olmore, S.D., 1994, Geologic map of the Chief Mountain quadrangle, Lincoln County, Nevada: U.S. Geological Survey Geologic Quadrangle Map GQ-1731, scale 1:24,000.

Rowley, P.D., Snee, L.W., Anderson, R.E., Nealey, L.D., Unruh, D.M., and Ferris, D.E., 2001, Field trip to the Caliente caldera complex, east-striking transverse zones, and nearby mining districts in Nevada-Utah—Implications for petroleum, ground-water, and mineral resources, *in* Erskine, M.C., Faulds, J.E., Bartley, J.M., and Rowley, P.D., editors, The geologic transition, High Plateaus to Great Basin—a symposium and field guide: The Mackin Volume: Utah Geological Association Publication 30 and American Association of Petroleum Geologists Publication GB78, September 20–22, 2001, p. 401–418.

Rowley, P.D, Snee, L.W., Mehnert, H.H., Anderson, R.E., Axen, G.J, Burke, K.J., Simonds, F.W., Shroba, R.R., and Olmore, S.D., 1992, Structural setting of the Chief mining district, eastern Chief Range, Lincoln County, Nevada, *in* Thorman, C.H.,

editor, Application of structural geology to mineral and energy resources of the central and western United States: U.S. Geological Survey Bulletin 2012, p. H1–H17.

Rowley, P.D., Steven, T.A., and Mehnert, H.H., 1981, Origin and structural implications of upper Miocene rhyolites in Kingston Canyon, Piute County, Utah: Geological Society of America Bulletin, Part I, v. 92, p. 590–602.

Rowley, P.D., Williams, V.S., Vice, G.S., Maxwell, D.J., Hacker, D.B., Snee, L.W., and Mackin, J.H., 2006, Interim geologic map of the Cedar City 30'×60' quadrangle, Iron and Washington counties, Utah: Utah Geological Survey Open-File Report 476DM, scale 1:100,000.

Ruksznis, A., and Miller, E.L., 2014, Stratigraphy and age of Cenozoic syn-extensional sedimentary basins, east-central Nevada (abs.): Geological Society of America 2014 Abstracts with Programs, v. 46, no. 5, p. 24.

Sack, D., 1990, Quaternary geologic map of Tule Valley, west-central Utah: Utah Geological and Mineral Survey Map 124, scale 1:100,000.

Saltus, R.W., 1988a, Bouguer gravity anomaly map of Nevada: Nevada Bureau of Mines and Geology Map 94A, scale 1:750,000.

Saltus, R.W., 1988b, Regional, residual, and derivative gravity maps of Nevada: Nevada Bureau of Mines and Geology Map 94B, scale 1:000,000, 4 sheets.

Saltus, R.W., and Jachens, R.C., 1995, Gravity and basin-depth maps of the Basin and Range province, western United States: U.S. Geological Survey Geophysical Investigations Map GP-1012, scale 1:2,500,000.

Sandberg, C.A., Morrow, J.R., and Warme, J.E., 1997, Late Devonian Alamo impact event, global Kellwasser Events, and major eustatic events, eastern Great Basin, Nevada and Utah: Brigham Young University Geology Studies, v. 42, pt. 1, p. 129–160.

Sargent, K.A., and Roggensack, K., 1984, Map showing outcrops of pre-Quaternary ash-flow tuffs and volcaniclastic rocks, Basin and Range province, Nevada: U.S. Geological Survey Water-Resources Investigations Report 83-4119-E, scale 1:500,000, 2 sheets.

Saucier, A.E., 1997, The Antler Thrust System in Northern Nevada, *in* Perry, A.J., and Abbott, E.W., editors, The Roberts Mountains Thrust, Elko and Eureka counties, Nevada: Nevada Petroleum Society, 1997 Field Trip Guidebook, Reno, Nevada, p. 1–16.

Schaefer, D.H., Morris, T.M., and Dettinger, M.D., 1989, Hydrogeologic and geophysical data for selected wells and springs in the Sheep Range, Clark and Lincoln counties, Nevada: U.S. Geological Survey Open-File Report 89-425, 36 p.

Schalla, R.A., 1998, History of recent exploration activity in Snake Valley, *in* French, D.E., and Schalla, R.A., editors, Hydrocarbon habitat and special geologic problems of the Great Basin: 1998 Field Trip Guidebook, Nevada Petroleum Society p. 84–85.

Schalla, R.A., and Johnson, E.H., editors, 1994, Oil fields of the Great Basin: Nevada Petroleum Society, Reno, Nevada, 380 p.

Scheirer, D.S., 2005, Gravity studies of Cave, Dry Lake, and Delamar valleys, east-central Nevada: U.S. Geological Survey Open-File Report 2005-1339, 27 p.

Scheirer, D.S., Page, W.R., and Miller, J.J., 2006, Geophysical studies based on gravity and seismic data of Tule Desert, Meadow Valley Wash, and California Wash basins, southern Nevada: U.S. Geological Survey Open-File Report 2006-1396, 42 p.

Scheirer, D.S., and Andreasen, A.D., 2008, Results of gravity fieldwork conducted in March 2008 in the Moapa Valley region of Clark County, Nevada: U.S. Geological Survey Open-File Report2008-1300, 35 p. [http://pubs.usgs.gov/of/2008/1300/].

Schellart, W.P., Stegman, D.R., Farrington, R.J., Freeman, J., and Moresi, L., 2010, Cenozoic tectonics of western North America controlled by evolving width of Farallon slab: Science, v. 329, no. 5989, p. 316–319.

Schmidt, D.L., 1994, Preliminary geologic map of the Farrier quadrangle, Clark and Lincoln counties, Nevada: U.S. Geological Survey Open-File Report 94-625, scale 1:24,000.

Schmidt, D.L. and Dixon, G.L., 1995, Geology and aquifer system of the Coyote Spring Valley area, southeastern Nevada: U.S. Geological Survey Open-File Report 95-579, 47 p.

Schmidt, D.L., Page, W.R., and Workman, J.B., 1996, Preliminary geologic map of the Moapa West quadrangle, Clark County, Nevada: U.S. Geological Survey Open-File Report 96-521, scale1:24,000.

Scott, R.B., 1965, The Tertiary geology and ignimbrite petrology of the Grant Range, east-central Nevada: Houston, Texas, unpublished Rice University Ph.D. thesis, 116 p.

Scott, R.B., and Harding, A.E., 2006, Geologic map of the Vigo NE quadrangle, Lincoln County, Nevada:

U.S. Geological Survey Scientific Investigations Map 2892, 18 p., scale 1:24,000.

Scott, R.B., and Swadley, WC, 1992, Preliminary geologic map of the Pahroc Summit Pass quadrangle and part of the Hiko SE quadrangle, Lincoln County, Nevada: U.S. Geological Survey Open-File Report 92-613, scale 1:24,000.

Scott, R.B., and Swadley, WC, editors, 1995, Geologic studies in the Basin and Range—Colorado Plateau transition in southeastern Nevada, southwestern Utah, and northwestern Arizona, 1992: U.S. Geological Survey Bulletin 2056, 275 p.

Scott, R.B., Grommé, C.S., Best, M.G., Rosenbaum, J.G., and Hudson, M.R., 1995a, Stratigraphic relationships of Tertiary volcanic rocks in central Lincoln County, southeastern Nevada, *in* Scott, R.B., and Swadley, WC, editors, Geologic studies in the Basin and Range—Colorado Plateau transition in southeastern Nevada, southwestern Utah, and northwestern Arizona, 1992: U.S. Geological Survey Bulletin 2056, p. 7–41.

Scott, R.B., Harding, A.E., Swadley, WC, and Pampeyan, E.H., 1991a, Preliminary geologic map of the Vigo NW quadrangle, Lincoln County, Nevada: U.S. Geological Survey Open-File Report 91-389, scale 1:24,000.

Scott, R.B., Novak, S.W., and Swadley, WC, 1990a, Preliminary geologic map of the Delamar 3 NE quadrangle, Lincoln County, Nevada: U.S. Geological Survey Open-File Report 90-33, scale 1:24,000.

Scott, R.B., Page, W.R., and Swadley, WC, 1990b, Preliminary geologic map of the Delamar 3 NW quadrangle, Lincoln County, Nevada: U.S. Geological Survey Open-File Report 90-405, scale 1:24,000.

Scott, R.B., Rowley, P.D., Snee, L.W., Anderson, R.E., Harding, A.E., Unruh, D.M., Nealey, L.D., Hudson, M.R., Swadley, WC, and Ferris, D.E., 1996, Synchronous Oligocene and Miocene extension and magmatism in the vicinity of caldera complexes in southeastern Nevada: Colorado Geological Survey Open-File Report 96-4, 36 p.

Scott, R.B., Swadley, WC, and Novak, S.W., 1993, Geologic map of the Delamar Lake quadrangle, Lincoln County, Nevada: U.S. Geological Survey Geologic Quadrangle Map GQ-1730, scale 1:24,000.

Scott, R.B., Swadley, WC, Page, W.R., and Novak, S.W., 1991b, Preliminary geologic map of the Gregerson Basin quadrangle, Lincoln County, Nevada: U.S. Geological Survey Open-File Report 90-646, scale 1:24,000.

Scott, R.B., Swadley, WC, and Taylor, W.J., 1994, Preliminary geologic map of the Wheatgrass Spring quadrangle, Lincoln County, Nevada: U.S. Geological Survey Open-File Report 94-175, scale 1:24,000.

Scott, R.B., Swadley, WC, Taylor, W.J., and Harding, A.E., 1995b, Preliminary geologic map of the Deadman Spring quadrangle, Lincoln County, Nevada: U.S. Geological Survey Open-File Report 95-94, scale 1:24,000.

Shawe, D.R., 1972, Reconnaissance geology and mineral potential of Thomas, Keg, and Desert calderas, central Juab Count, Utah: U.S. Geological Survey Professional Paper 800-B, p. B67–B77.

Sibson, R.H., 1996, Structural permeability of fluid-driven fault-fracture meshes: Journal of Structural Geology, v. 18, Issue 8, p. 1031–1042.

Simpson, R.W., Jachens, R.C., Blakely, R.J., and Saltus, R.W., 1986, A new isostatic residual gravity map of the conterminous United States with a discussion on the significance of isostatic residual anomalies: Journal of Geophysical Research, v. 91, p. 8348–8372.

Slate, J.L., Berry, M.E., Rowley, P.D., Fridrich, C.J., Williams, V.S., Morgan, K.S., Workman, J.B., Young, O.D., Dixon, G.L., Williams, V.S., et al., 1999, Digital geologic map of the Nevada Test Site and vicinity, Nye, Lincoln, and Clark counties, Nevada, and Inyo County, California: U.S. Geological Survey Open-File Report 99-554-A, 53 p.

Smith, D.L., Gans, P.B., and Miller, E.L., 1991, Palinspastic restoration of Cenozoic extension in the central and eastern Basin and Range province at latitude 39–40°N, *in* Raines, G.L., Lisle, R.E., Schafer, R.W., and Wilkinson, W.H., editors, Geology and ore deposits of the Great Basin, Geological Society of Nevada, Symposium Proceedings, April 1–5, 1990, v. 1, p. 75–86.

Snee, L.W., and Rowley, P.D., 2000, New $^{40}Ar/^{39}Ar$ dates from the Caliente caldera complex, Nevada-Utah—at least 10 million years of Tertiary volcanism in one of the World's largest caldera complexes: Geological Society of America Abstracts with Programs, v. 32, no. 7, p. A-461.

Snyder, R.P., Ekren, E.B., and Dixon, G.L., 1972, Geologic map of the Lunar Crater quadrangle, Nye County, Nevada: U.S. Geological Survey Miscellaneous Geologic Investigations Map I-700, scale 1:48,000.

Southern Nevada Water Authority, 2006, Documentation of the physical settings of selected

springs in White Pine, Lincoln and Clark counties, Nevada: Technical Report 3, Spring documentation and evaluation, Southern Nevada Water Authority, Las Vegas, Nevada, 156 p + appendices.

Southern Nevada Water Authority, 2008, Baseline characterization report for Clark, Lincoln, and White Pine counties groundwater development project: Southern Nevada Water Authority, Las Vegas, Nevada, 1146 p.

Southern Nevada Water Authority, 2011, Southern Nevada Water Authority Clark, Lincoln, and White Pine counties groundwater development project conceptual plan of development: Southern Nevada Water Authority, Las Vegas, Nevada, 152 p.

Staargaard, C.F., 2009, Geology and exploration at the Crypto zinc-indium-copper-molybdenum skarn, in Tripp, B.T., Krahulec, K, and Jordan, J.L., editors, Geology and geologic resources and issues of western Utah: Utah Geological Association Publication 38, p. 143–156.

Stephens, J.C., 1977, Hydrologic reconnaissance of the Tule Valley drainage basin, Juab and Millard counties, Utah: Utah Department of Natural Resources Technical Publication, no. 56, 37 p.

Steven, T.A., Morris, H.T., and Rowley, P.D., 1990, Geologic map of the Richfield 1°×2° quadrangle, west-central Utah: U.S. Geological Survey Miscellaneous Investigations Series Map I-1901, scale 1:250,000.

Steven, T.A., Rowley, P.D., and Cunningham, C.G., 1984, Calderas of the Marysvale volcanic field, west central Utah: Journal of Geophysical Research, v. 89, p. 8751–8764.

Stewart, J.H., 1970, Upper Precambrian and Lower Cambrian strata in the southern Great Basin, California and Nevada: U.S. Geological Survey Professional Paper 620, 206 p.

Stewart, J.H., 1971, Basin and Range structure—a system of horsts and grabens produced by deep-seated extension: Geological Society of America Bulletin, v. 82, p. 1019–1044.

Stewart, J.H., 1974, Correlation of uppermost Precambrian and lower Cambrian strata from southern to east-central Nevada: U.S. Geological Survey Journal of Research, v. 2, p. 609–618.

Stewart, J.H., 1976, Late Precambrian evolution of North America: Plate tectonics implication: Geology, v. 4, p. 11–15.

Stewart, J.H., 1980a, Regional tilt patterns of late Cenozoic basin-range fault blocks, western United States: Geological Society of America Bulletin, part I, v. 91, p. 460–464.

Stewart, J.H., 1980b, Geology of Nevada—a discussion to accompany the *geologic map of Nevada*: Nevada Bureau of Mines and Geology Special Publication 4, 136 p.

Stewart, J.H., 1984, Stratigraphic sections of lower Cambrian and upper Proterozoic rocks in Nye, Lander, and Lincoln counties, Nevada, and Sonora, Mexico: U.S. Geological Survey Open-File Report 84-691, 53 p.

Stewart, J.H., and Carlson, J.E., 1976, Cenozoic rocks of Nevada—four maps and brief description of distribution, lithology, age, and centers of volcanism: Nevada Bureau of Mines and Geology Map 52, scale 1:1,000,000, 4 sheets.

Stewart, J.H., and Carlson, J.E., 1978, Geologic map of Nevada: U.S. Geological Survey, scale 1:500,000.

Stewart, J.H., Moore, W.J., and Zietz, I., 1977, East-west patterns of Cenozoic igneous rocks, aeromagnetic anomalies, and mineral deposits, Nevada and Utah: Geological Society of America Bulletin, v. 88, p. 67–77.

Stewart, J.H., and Poole, F.G., 1974, Lower Paleozoic and uppermost Precambrian Cordilleran miogeocline, Great Basin, western United States, *in* Dickinson, W.R., editor, Tectonics and sedimentation: Society of Economic Paleontologists and Mineralogists Special Publication No. 22, p. 28–57.

Stoeser, D.B., 1993, Tertiary calderas and regional extension of the east-central part of the Tintic-Deep Creek mineral belt, eastern Great Basin, Utah, *in* Scott, Jr., R.W., Detra, P.S., and Berger, B.R., editors, Advances related to United States and International Mineral Resources: Developing frameworks and exploration technologies: U.S. Geological Survey Bulletin 2039, p. 5-23.

Swadley, WC, 1995, Maps showing modern fissures and quaternary faults in the Dry Lake Valley area, Lincoln County, Nevada: U.S. Geological Survey Miscellaneous Investigations Series Map I-2501, scale 1:50,000.

Swadley, WC, Page, W.R., and Scott, R.B., 1994a, Preliminary geologic map of the Deadman Spring NE quadrangle, Lincoln County, Nevada: U.S. Geological Survey Open-File Report 94-283, scale 1:24,000.

Swadley, WC, Page, W.R., Scott, R.B., and Pampeyan, E.H., 1994b, Geologic map of the Delamar 3 SE quadrangle, Lincoln County, Nevada: U.S. Geological Survey Geologic Quadrangle Map GQ-1754, scale 1:24,000.

Swadley, WC, and Rowley, P.D., 1994, Geologic map

of the Pahroc Spring SE quadrangle, Lincoln County, Nevada: U.S. Geological Survey Geologic Quadrangle Map GQ-1752, scale 1:24,000.

Swadley, WC, and Scott, R.B., 1991, Preliminary geologic map of the Delamar NW quadrangle, Lincoln County, Nevada: U.S. Geological Survey Open-File Report 90-622, scale 1:24,000.

Sweetkind, D.S., 2007b, Geology of Great Basin National Park, *in* Coache, R., editor, Regional tour of the carbonate system guidebook: Nevada Water Resources Association, Clark County, Nevada, June 18–20, 2007, p. 47–48.

Sweetkind, D.S., 2007a, Geology of Snake Range, *in* Coache, R., editor, Regional tour of the carbonate system guidebook: Nevada Water Resources Association, Clark County, Nevada, June 18–20, 2007, p. 43–44.

Sweetkind, D.S., and duBray, E.A., 2008, Compilation of stratigraphic thicknesses for caldera-related tertiary volcanic rocks, east-central Nevada and west-central Utah: U.S. Geological Survey Data Series 271, 40 p.

Sweetkind, D.S., Knochenmus, L.A., Ponce, D.A., Wallace, A.R., Scheirer, D.S., Watt, J.T., and Plume, R.W., 2007b, Hydrogeologic framework, *in* Welch, A.H., Bright, D.J., and Knochenmus, L.A., editors, Water resources of the Basin and Range carbonate-rock aquifer system, White Pine County, Nevada, and adjacent areas in Nevada and Utah: U.S. Geological Survey Scientific Investigations Report 2007-5261, p. 11–36.

Sweetkind, D.S., Knochenmus, L.A., Ponce, D.A., Wallace, A.R., Scheirer, D.S., Watt, J.T., and Plume, R.W., 2007a, Hydrogeologic map and cross sections, White Pine County, Nevada, and adjacent areas in Nevada and Utah, *in* Welch, A.H., Bright, D.J., and Knochenmus, L.A., editors, Water resources of the Basin and Range carbonate-rock aquifer system, White Pine County, Nevada, and adjacent areas in Nevada and Utah: U.S. Geological Survey Scientific Investigations Report 2007-5261, Plate 1, scale 1:500,000.

Taylor, M.E., Poole, F.G., and Cook, H.E., 1991, Summary of Paleozoic stratigraphy in the southern Egan and Schell Creek ranges, east-central Nevada, *in* Flanigan, D.M.H., Hansen, M., and Flanigan, T.E., editors, Geology of White River Valley, the Grant Range, Eastern Railroad Valley and Western Egan Range, Nevada: 1991 Fieldtrip Guidebook, Nevada Petroleum Society Inc., Reno, p. 29–35.

Taylor, W.J., Bartley, J.M., Fryxell, J.E., Schmitt, J.G., and Vandervoort, D.S., 1993, Tectonic style and regional relations of the central Nevada thrust belt, *in* Lahren, M.M., Trexler, J.H., Jr., and Spinosa, C., editors, Crustal evolution of the Great Basin and Sierra Nevada: Geological Society of America Guidebook, Cordilleran/Rocky Mountain Section, Department of Geological Sciences, University of Nevada, Reno, p. 57–96.

Taylor, W.J., Bartley, J.M., Martin, M.W., Geissman, J.W., Walker, J.D., Armstrong, P.A., and Fryxell, J.E., 2000, Relations between hinterland and foreland shortening: Sevier orogeny, central North American Cordillera: Tectonics, v. 19, no. 6, p. 1124–1143.

Taylor, W.J., Dobbs, S.W., Nelson, S.L., and Armstrong, P.A., 1994, Generation of four-way closure through multiple tectonic events: Structures of the Timpahute Range, southern Nevada, *in* Dobbs, S.W., and Taylor, W.J., editors, Structural and stratigraphic investigations and petroleum potential of Nevada, with special emphasis south of the Railroad Valley producing trend: Nevada Petroleum Society Conference Volume II, p. 141–156.

Telford, W.M., Geldart, L.P., and Sheriff, R.E., 1990, Applied geophysics. Second edition: New York, Cambridge University Press.

Tilden, J.E., Ponce, D.A., Glen, J.M.G., Chuchel, B.A., Tushman, K., and Duvall, A., 2006, Gravity, magnetic, and physical property data in the Smoke Creek Desert area, northwest Nevada: U.S. Geological Survey Open-File Report 2006-1197, 33 p.

Tingley, J.V., Pizarro, K.A., Ross, C. and Pearthree, P.A., 2010, A geologic and natural history tour through Nevada and Arizona along U.S. Highway 93, with GPS coordinates: Nevada Bureau of Mines and Geology Special Publication 35 and Arizona Geological Survey Down-to-Earth 19, 175 p.

Tschanz, C.M., and Pampeyan, E.H., 1970, Geology and mineral deposits of Lincoln County, Nevada: Nevada Bureau of Mines and Geology Bulletin 73, 187 p.

U.S. Geological Survey, 2008, A study of the connection among basin-fill aquifers, carbonate-rock aquifers, and surface-water resources in southern Snake Valley, Nevada: U.S. Geological Survey Fact Sheet 2008-3071, 2 p.

Utah Division of Oil, Gas, and Mining, 2006, Online oil and gas information system, well logs, database [Internet], [accessed March 8, 2006], available from http://utstnrogmsg/3.state.ut.us/UTAHRBDMSWe

b/Logs.htm.
Utah Division of Oil, Gas, and Mining, 2011, Online oil and gas information system, well logs database [Internet], [accessed on May 4, 2011], available from http://oilgas.ogm.utah.gov.
Utah Division of Water Rights, 2006, Well drilling database [Internet], [accessed March 8, 2006], available from http://nrwrt1.nr.state.ut.us/cgi/bin/wellview.exe.
Vandervoort, D.S., and Schmitt, J.G., 1990, Cretaceous to early Tertiary paleogeography in the hinterland of the Sevier thrust belt, east-central Nevada: Geology, v. 18, p. 567–570.
Van Loenen, R.E., 1987, Geologic map of the Mount Grafton wilderness study area, Lincoln and White Pine counties, Nevada: U.S. Geological Survey Miscellaneous Field Studies Map MF-1938, scale 1:50,000.
Vozoff, K., 1991, The magnetotelluric method, *in* Nabighian, M.N., editor, Electromagnetic methods in applied geophysics: Volume 2, Application Parts A and B: Society of Exploration Geophysicists, Tulsa, Oklahoma, Investigations in Geophysics, no. 3, p. 641–711.
Walker, C.D., Anders, M.H., and Christie-Blick, N., 2007, Kinematic evidence for downdip movement on the Mormon Peak detachment: Geology, v. 35, no. 3, p. 259–262.
Walker, C.T., and Francis, R.D., 2002, Tectonic styles associated with extension and attenuation in the Grant, Schell Creek, and White Pine Ranges, *in* Ehni, W., and Faulds, J., editors, Detachment and attenuation in eastern Nevada and its application to petroleum exploration: Nevada Petroleum Society 2002 Field Trip Guidebook, p. 97–127.
Walker, J.D., Geissman, J.W., Bowring, S.A., and Babcock, L.E., 2013, The Geological Society of America geologic time scale: Geological Society of America Bulletin, v. 125, p. 259–272.
Wallace, A.R., Watt, J.T., and Ponce, D.A., 2007, Geologic and geophysical basin-by-basin descriptions, *in* Watt, J.T., and Ponce, D.A., editors, Geophysical framework investigations influencing ground-water resources in east-central Nevada and west-central Utah: U.S. Geological Survey Open-File Report 2007-1163, p. 9–28.
Warme, J.E., Morrow, J.R., and Sandberg, C.A., 2008, Devonian carbonate platform of eastern Nevada: Facies, surfaces, cycles, sequences, reefs, and cataclysmic Alamo impact breccia, *in* Duebendorfer, E.M., and Smith, E.I., editors, Field guide to plutons, volcanoes, faults, reefs, dinosaurs, and possible glaciation in selected areas of Arizona, California, and Nevada: Geological Society of America Field Guides, v. 11, p. 215–247.
Watt, J.T., and Ponce, D.A., 2007, Geophysical framework investigations influencing ground-water resources in east-central Nevada and west-central Utah, with a section on geologic and geophysical basin-by-basin descriptions, by Wallace, A.R., Watt, J.T., and Ponce, D.A.: U.S. Geological Survey Open-File Report 2007-1163 [http://pubs.usgs.gov/of/2007/1163/].
Webring, M., 1981, MINC-A gridding program based on minimum curvature: U.S. Geological Survey Open-File Report 81-1224, 43 p.
Welch, A.H., Bright, D.J., and Knochenmus, L.A., editors, 2007, Water resources of the Basin and Range carbonate-rock aquifer system, White Pine County, Nevada, and adjacent areas in Nevada and Utah: U.S. Geological Survey Scientific Investigations Report 2007-5261, 96 p.
Wernicke, B., Walker, J.D., and Beaufait, M.S., 1985, Structural discordance between Neogene detachments and frontal Sevier thrusts, central Mormon Mountains, southern Nevada: Tectonics, v. 4, no. 2, p. 213–246.
Whitebread, D.H., 1969, Geologic map of the Wheeler Peak and Garrison quadrangles, Nevada and Utah: U.S. Geological Survey Miscellaneous Geologic Investigations Map I-578, scale 1:48,000.
Whitney, D.L., Teyssier, C., Rey, P., and Buck, W.R., 2013, Continental and ocean core complexes: Geological Society of America Bulletin, v. 125, p. 273–298.
Williams, N., and Taylor, W.J., 2002, Extensional oblique-slip barrier transfer fault—the Currant Summit fault, east-central Nevada, *in* Ehni, W. and Faulds, J., editors, Detachment and attenuation in eastern Nevada and its application to petroleum exploration: Nevada Petroleum Society 2002 Field Trip Guidebook, p. 149–163.
Williams, V.S., 1996, Preliminary geologic map of the Mesquite quadrangle, Clark and Lincoln counties, Nevada, and Mohave County Arizona: U.S. Geological Survey Open-File Report96-676, scale 1:24,000.
Williams, V.S., 1997, Preliminary geologic map of the Flat Top Mesa quadrangle, Clark and Lincoln counties, Nevada: U.S. Geological Survey unpublished data, scale 1:24:000.
Williams, V.S., Best, M.G., and Keith, J.D., 1997a, Geologic map of the Ursine-Panaca Summit-Deer Lodge area, Lincoln County, Nevada, and Iron

County, Utah: U.S. Geological Survey Miscellaneous Investigations Series Map I-2479, scale 1:50,000.

Williams, V.S., Bohannon, R.G., and Hoover, D.L., 1997b, Geologic map of the Riverside quadrangle, Clark County, Nevada: U.S. Geological Survey Geologic Quadrangle Map GQ-1770, scale 1:24,000.

Williams, V.S., Schmidt, D.L., and Bohannon, R.G., 1997c, Preliminary geologic map of the Moapa East quadrangle, Clark County, Nevada: U.S. Geological Survey Open-File Report 97-449, scale 1:24,000.

Willis, J.B., Best, M.G., Kowallis, B.J., and Best, V.C., 1987, Preliminary geologic map of the northern Wilson Creek Range, Lincoln County, Nevada: U.S. Geological Survey Miscellaneous Field Studies Map MF-1971, scale 1:50,000.

Winograd, I.J., and Thordarson, W., 1968, Structural control of ground-water movement in miogeosynclinal rocks of south-central Nevada, *in* Eckel, E.B., editor, Nevada Test Site: Geological Society of America Memoir 110, p. 35–48.

Winograd, I.J., and Thordarson, W., 1975, Hydrogeologic and hydrochemical framework, south-central Great Basin, Nevada-California, with special reference to the Nevada Test Site: U.S. Geological Survey Professional Paper 712-C, 126 p.

Workman, J.B., Menges, C.M., Page, W.R., Ekren, E.B., Rowley, P.D., and Dixon, G.L., 2002a, Tectonic map of the Death Valley ground-water model area, Nevada and California: U.S. Geological Survey Miscellaneous Field Studies Map MF-2381-B, 58 p., scale 1:250,000.

Workman, J.B., Menges, C.M., Page, W.R., Taylor, E.M., Ekren, E.B., Rowley, P.D., Dixon, G.L., Thompson, R.A., and Wright, L.A., 2002b, Geologic map of the Death Valley ground-water model area, Nevada and California: U.S. Geological Survey Miscellaneous Field Studies MF-2381-A, 26 p., 1:250,000 scale, 2 sheets.

Wright, J.E., and Snoke, A.W., 1993, Tertiary magmatism and mylonitization in the Ruby-East Humboldt metamorphic core complex, northeastern Nevada: U-Pb geochronology and Sr, Nd, and Pb isotope geochemistry: Geological Society of America Bulletin, v. 105, no. 7, p. 935–952.

Zietz, I., Shuey, R., and Kirby, J.R., Jr., 1976, Aeromagnetic map of Utah: U.S. Geological Survey Geophysical Investigations Map GP-907, scale 1:1,000,000.

Zietz, I., Gilbert, F.P., and Kirby, J.R., Jr., 1978, Aeromagnetic map of Nevada: U.S. Geological Survey Geophysical Investigations Map GP-922, scale 1:1,000,000.

Zonge, K.L., and Hughes, L.J., 1991, Controlled source audio-frequency magnetotellurics, *in* Nabighian, M.N., editor, Electromagnetic methods in applied geophysics, Volume 2, Application Parts A and B: Society of Exploration Geophysicists, Tulsa, Oklahoma, Investigations in Geophysics, no. 3, p. 713–809.

Suggested Citation:

Rowley, P.D., Dixon, G. L., Mankinen, E.A., Pari, K.T., McPhee, D.K., McKee, E.H., Burns, A.G., Watrus, J.M., Ekren, E.B., Patrick, W.G, and Brandt, J.M., 2017, Geology and geophysics of White Pine and Lincoln counties, Nevada, and adjacent parts of Nevada and Utah: the geologic framework of regional groundwater flow systems: Nevada Bureau of Mines and Geology Report 56, scale 1:250,000, 4 plates, 146 p.

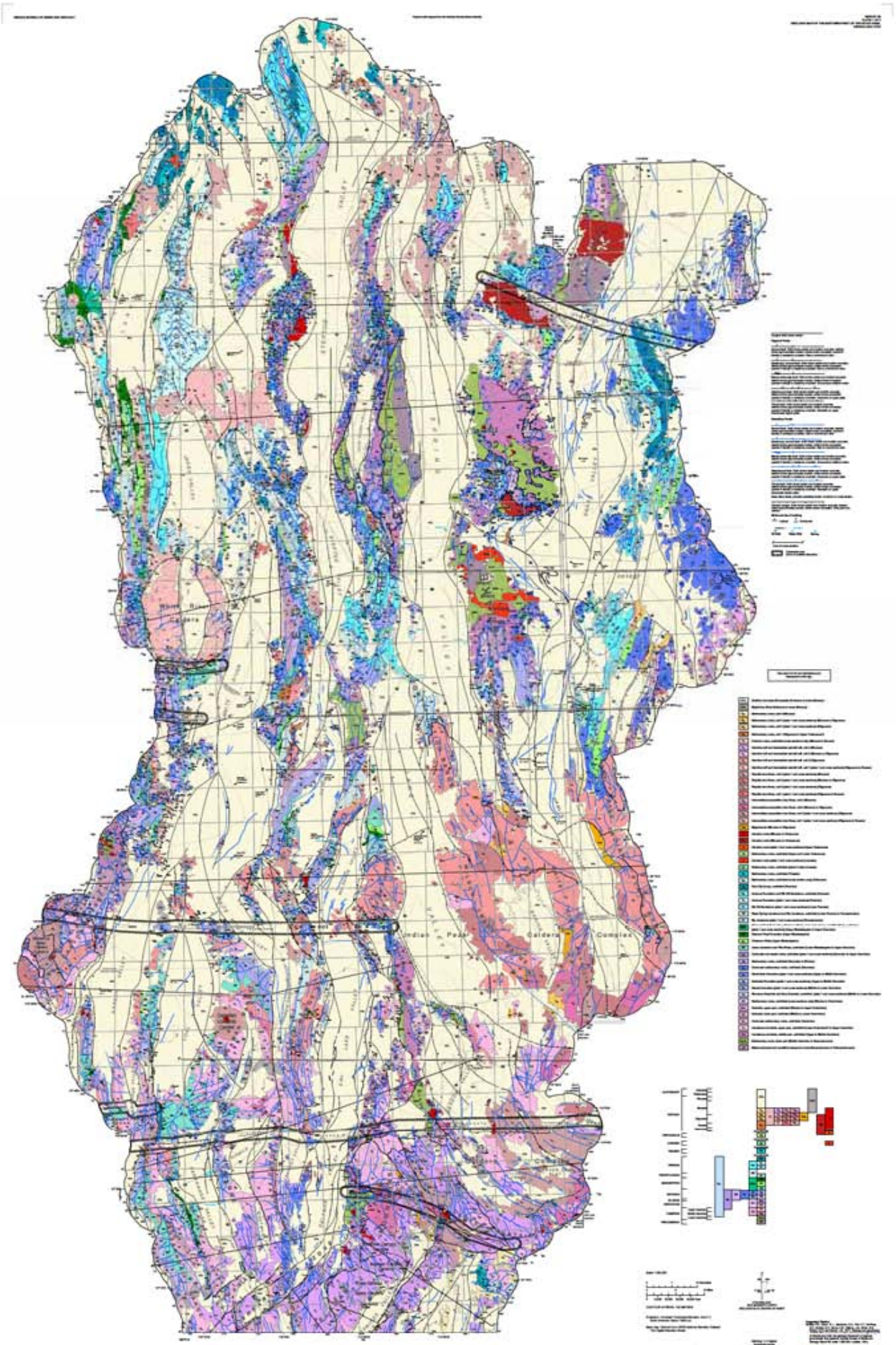

GEOLOGIC MAP OF THE NORTHERN PART OF THE STUDY AREA, NEVADA AND ARIZONA
PLATE 1 of 4

Peter D. Rowley[1], Gary L. Dixon[2], Edward A. Mankinen[3], Keith T. Ariel[4], Darcy K. McPhee[3], Edwin H. McKee[3], Andrew G. Burns[5], James M. Watrus[6], E. Bartlett Ekren[3], William G. Patrick[5], and Judith M. Brandt[6]

[1]Geologic Mapping, Inc., New Harmony, UT, [2]Southwest Geology LLC, Blackfoot, ID, [3]U.S. Geological Survey, Menlo Park, CA
[4]Southern Nevada Water Authority, Las Vegas, NV, [5]Private consultant, White Sulphur Springs, MT

2017

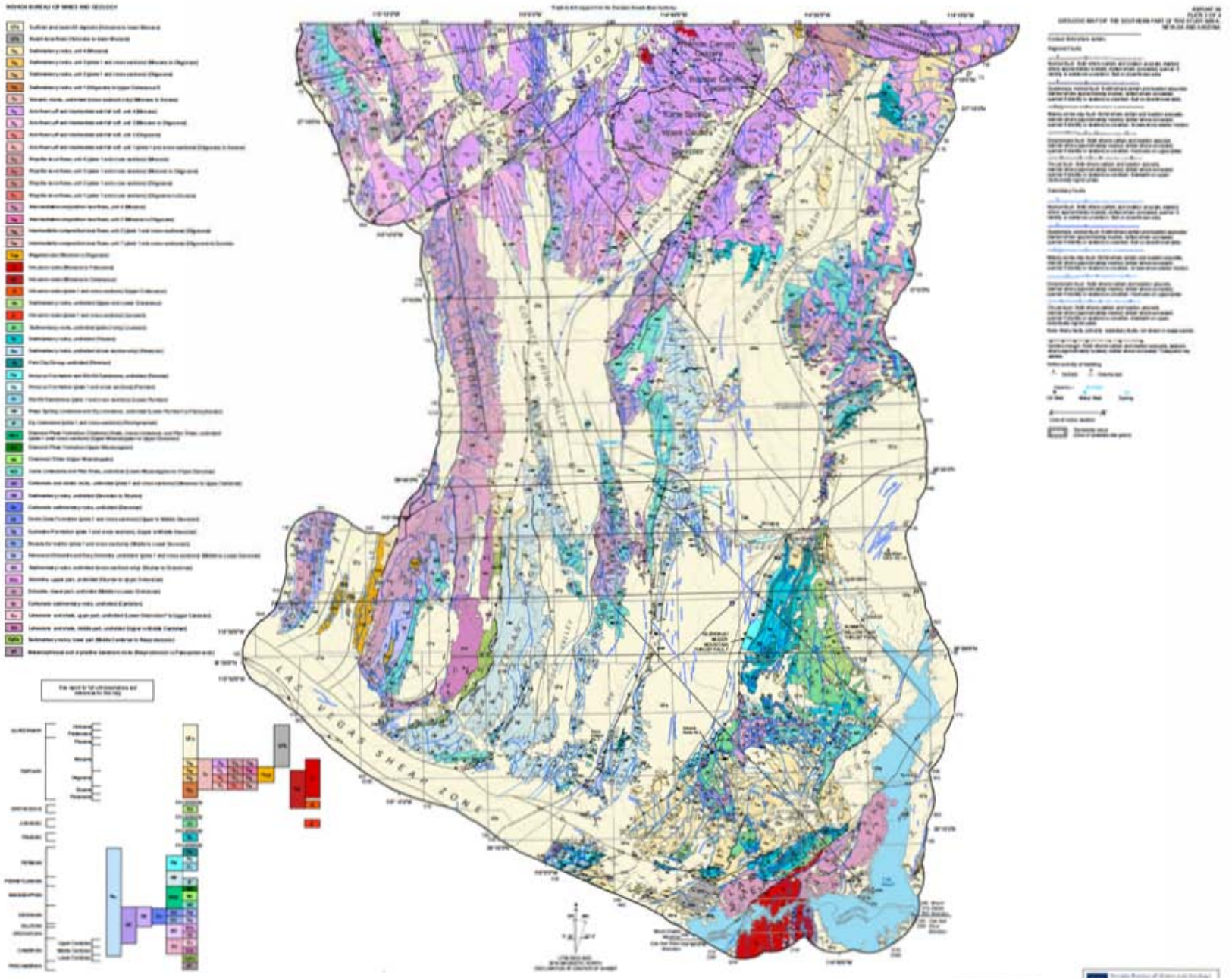

GEOLOGIC MAP OF THE SOUTHERN PART OF THE STUDY AREA, NEVADA AND ARIZONA
PLATE 2 of 4

Peter D. Rowley[1], Gary L. Dixon[2], Edward A. Mankinen[3], Keith T. Pari[4], Darcy K. McPhee[3], Edwin H. McKee[3], Andrew G. Burns[4], James M. Watrus[4], E. Bartlett Ekren[5], William G. Patrick[6], and Judith M. Brandt[7]

[1]Geologic Mapping, Inc., New Harmony, UT, [2]Southwest Geology LLC, Blackfoot, ID, [3]U.S. Geological Survey, Menlo Park, CA
[4]Southern Nevada Water Authority, Las Vegas, NV, [5]Private consultant, White Sulphur Springs, MT

2017

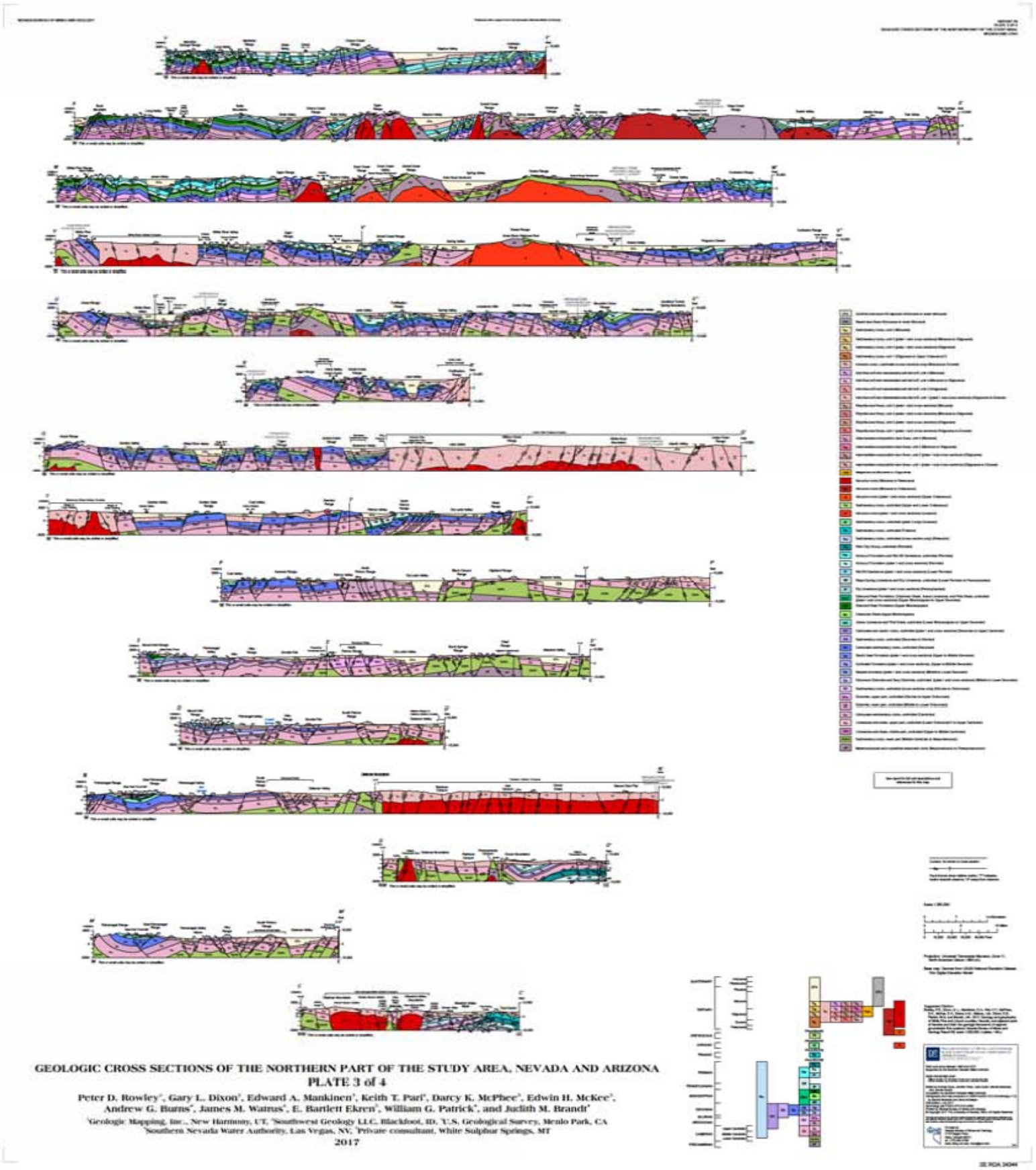

GEOLOGIC CROSS SECTIONS OF THE NORTHERN PART OF THE STUDY AREA, NEVADA AND ARIZONA
PLATE 3 of 4

Peter D. Rowley[1], Gary L. Dixon[2], Edward A. Mankinen[3], Keith T. Pari[4], Darcy K. McPhee[3], Edwin H. McKee[3], Andrew G. Burns[4], James M. Watrus[4], E. Bartlett Ekren[3], William G. Patrick[4], and Judith M. Brandt[4]

[1]Geologic Mapping, Inc., New Harmony, UT, [2]Southwest Geology LLC, Blackfoot, ID, [3]U.S. Geological Survey, Menlo Park, CA
[4]Southern Nevada Water Authority, Las Vegas, NV, [5]Private consultant, White Sulphur Springs, MT

2017

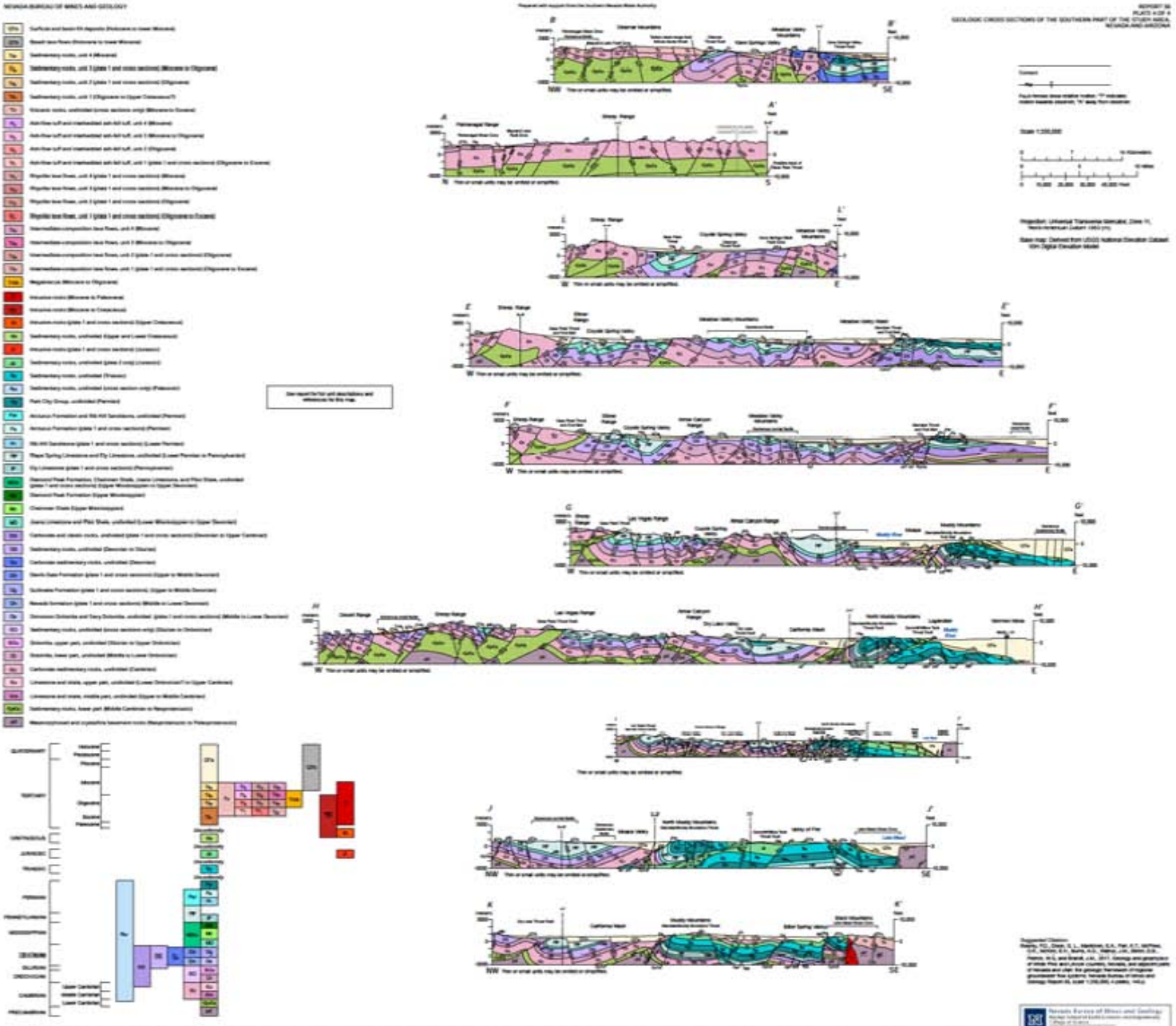

GEOLOGIC CROSS SECTIONS OF THE SOUTHERN PART OF THE STUDY AREA, NEVADA AND ARIZONA

PLATE 4 of 4

Peter D. Rowley[1], Gary L. Dixon[2], Edward A. Mankinen[3], Keith T. Pari[4], Darcy K. McPhee[3], Edwin H. McKee[3], Andrew G. Burns[4], James M. Watrus[4], E. Bartlett Ekren[3], William G. Patrick[4], and Judith M. Brandt[4]

[1]Geologic Mapping, Inc., New Harmony, UT, [2]Southwest Geology LLC, Blackfoot, ID, [3]U.S. Geological Survey, Menlo Park, CA
[4]Southern Nevada Water Authority, Las Vegas, NV, [5]Private consultant, White Sulphur Springs, MT

2017

Assessment of Lower White River Flow System Water Resource Conditions and Aquifer Response

PRESENTATION TO THE OFFICE OF THE NEVADA STATE ENGINEER

Prepared by

SOUTHERN NEVADA WATER AUTHORITY

LAS VEGAS VALLEY WATER DISTRICT

PEOPLE LEADING THE WAY

June 2019

Suggested citation:
Burns, A., Drici, W., Collins, C., and Watrus, J., 2019, Assessment of Lower White River Flow System Water Resource Conditions and Aquifer Response, Presentation to the Office of the Nevada State Engineer: Southern Nevada Water Authority, Las Vegas, Nevada.

Assessment of Lower White River Flow System Water Resource Conditions and Aquifer Response

Submitted to:
Timothy Wilson, P.E., Acting State Engineer
State of Nevada
Department of Conservation & Natural Resources
Division of Water Resources
901 S. Stewart Street, Suite 2002
Carson City, Nevada 89701

Pertaining to:
Nevada State Engineer
Interim Order 1303

June 2019

Prepared by:
Southern Nevada Water Authority and
Las Vegas Valley Water District
Water Resources Division
P.O. Box 99956
Las Vegas, Nevada 89193-9956

Andrew G. Burns, Water Resources Division Manager — Date: 6.27.2019

Warda Drici, Hydrologist — Date: 06/27/2019

Casey A. Collins, Hydrologist — Date: 6/27/2019

James M. Watrus, Sr. Hydrologist — Date: 6-27-2019

CONTENTS

CONTENTS (CONTINUED)

CONTENTS (CONTINUED)

FIGURES

FIGURES (CONTINUED)

TABLES

ACRONYMS

BLM	Bureau of Land Management
CSI	Coyote Springs Investment, LLC
CSV	Coyote Springs Valley
CSWR	Coyote Springs Water Resources
ET	Evapotranspiration
GID	General Improvement District
HA	Hydrographic Area
HRT	Hydrologic Review Team
ICS	Intentionally Created Surplus
LDS	The Church of Jesus Christ of Latter-day Saints
LIDAR	Light Detection and Ranging
LVVWD	Las Vegas Valley Water District
LVVSZ	Las Vegas Valley Shear Zone
LWRFS	Lower White River Flow System
MBOP	Moapa Band of Paiute Indians
METRIC	Mapping EvapoTranspiration at high Resolution with Internalized Calibration
MOA	Memorandum of Agreement
MRSA	Muddy River Springs Area
MR	Muddy River
MVIC	Muddy Valley Irrigation Company
MVWD	Moapa Valley Water District
NDWR	Nevada Division of Water Resources
NDVI	Normalized Difference Vegetation Index
NPS	National Park Service
NOAA	National Oceanic and Atmospheric Administration
NSE	Nevada State Engineer
NV	Nevada
NVE	Nevada Energy
NWIS	National Water Information System
PRISM	Parameter-elevation Regressions on Independent Slopes Model
PSZ	Pahranagat Shear Zone
SNWA	Southern Nevada Water Authority
USGS	U.S. Geological Survey
USFWS	U.S. Fish and Wildlife Service
WRCC	Western Region Climate Center
WRFS	White River Flow System

ABBREVIATIONS (CONTINUED)

°C	degrees Celsius
°F	degrees Fahrenheit
af	acre-foot
afy	acre-feet per year
cfs	cubic feet per second
ft	foot [feet]
ft amsl	feet above mean sea level
ft bgs	feet below ground surface
ft/yr	foot per year [feet per year]
gpm	gallons per minute
in.	inch [inches]
Ma	million years ago

ABSTRACT

In response to Nevada State Engineer (NSE) Interim Order 1303, the Las Vegas Valley Water District (LVVWD) and Southern Nevada Water Authority (SNWA) conducted an assessment of the current water-resource conditions of the Lower White River Flow System (LWRFS), an administrative unit of six conjoined basins designated by the NSE. The LVVWD and SNWA have significant interests in the administration of water rights and management of water resources within the LWRFS. The LVVWD is the management entity for the Coyote Springs Water Resources General Improvement District located in Coyote Spring Valley. This means LVVWD will, effectively, be the water purveyor responsible for providing water to any community that is developed. SNWA owns substantial groundwater rights and owns or leases 1920 Muddy River Decree surface-water rights. SNWA also controls over 51 percent of the Muddy Valley Irrigation Company shares through ownership and lease agreements. SNWA interests in the groundwater and surface-water resources of the LWRFS total over 31,863 afy, and include points of diversion located in five of the six basins composing the LWRFS. Of particular interest to this assessment are Muddy River Tributary Intentionally Created Surplus (ICS) credits created and managed by SNWA. ICS is a critical component of the SNWA water-resource portfolio which is relied upon to supply current and future water demands of over 2 million Nevada residents and 40 million annual visitors.

As part of the assessment, an analysis was completed to evaluate hydrologic responses to natural and anthropogenic stresses observed at various locations of interest. The analysis considered time-series data for several variables that describe the historical conditions of the hydrologic system over a period of decades. The analysis focused on the historical behavior of the carbonate aquifer composing the LWRFS, the hydrology of the Muddy River Springs Area (MRSA), and responses of Muddy River streamflow to groundwater production.

The assessment yielded the following conclusions: (1) the carbonate rocks underlying the LWRFS basins are contiguous and form a single aquifer that is the source of spring discharge, subsurface inflow to the MRSA alluvial reservoir, and perennial streamflow; (2) hydrologic responses are highly correlated amongst LWRFS wells and springs sourced by the carbonate aquifer; (3) carbonate-aquifer groundwater production has impacted spring discharges; (4) groundwater production has depleted Muddy River streamflow and conflicted with senior Muddy River water rights; (5) the long-term average annual groundwater production from the carbonate aquifer must be limited to maintain specified flows at the Warm Springs West gage; and (6) since 2006, Muddy River streamflow depletions have reduced the volume of SNWA's ICS by about 12,000 acre-feet at a replacement cost of almost $2.3 million.

Based on the findings of this assessment, responses to NSE Interim Order 1303 are as follows: (a) the geographic boundary of the LWRFS as defined by the NSE is appropriate; (b) the data gathered during and after the Order 1169 aquifer test indicate that recovery of the LWRFS had attained its maximum by late 2015 - early 2016; (c) the data indicate that groundwater production from the MRSA alluvial reservoir or the carbonate aquifer simply cannot occur over the long-term without depleting spring and streamflows and conflicting with senior surface-water rights; (d) changing points of diversion to move groundwater production from the MRSA alluvial reservoir to locations sourced by the carbonate aquifer will not mitigate these conflicts, only delay their inevitable occurrence; and (e) groundwater production should not be permitted to continue without strict regulatory oversight and appropriate mitigation to affected senior water-right holders and adequate protections to ensure the Moapa dace are protected. If the conflicts with senior water-right holders are adequately addressed, the annual groundwater production from the carbonate aquifer should be managed between 4,000 – 6,000 afy over the long-term.

1.0 INTRODUCTION

This report was prepared on behalf of the Las Vegas Valley Water District (LVVWD) and Southern Nevada Water Authority (SNWA) in response to the Nevada State Engineer's (NSE) Interim Order 1303 (Order 1303) (NSE, 2019) concerning the Lower White River Flow System (LWRFS). The NSE defines the LWRFS as the hydrographic areas (HA) of Coyote Spring Valley (HA 210), Hidden Valley (HA 217), Garnet Valley (HA 216), California Wash (HA 218), Muddy River Springs Area (HA 219), and the northwest portion of the Black Mountains Area (HA 215) (NSE, 2019). Figure 1-1 depicts the boundary of the LWRFS, as designated by the NSE, and the adjacent Kane Springs Valley which is included in this assessment because it is tributary to the LWRFS and contributes to the local recharge.

The LVVWD and SNWA have significant interests in the administration of water rights and management of water resources within the LWRFS. LVVWD is the management entity for the Coyote Springs Water Resources General Improvement District (CSWR GID) located in Coyote Spring Valley (CSV). Within the LWRFS, SNWA owns substantial groundwater rights (11,200 afy) and owns or leases Muddy River surface-water rights (10,663 afy). SNWA also controls over 51 percent of the Muddy Valley Irrigation Company (MVIC) shares through ownership and lease agreements which for 2018 equated to approximately 10,000 af. SNWA interests in the groundwater and surface-water resources of the LWRFS total over 31,863 afy and include points of diversion located in five of the six hydrographic areas designated by the NSE.

This report presents data, technical analyses, and results to address issues raised in NSE Order 1303 concerning water-resource conditions and responses to groundwater production within the LWRFS. SNWA and the LVVWD urge the NSE to consider this report in issuing any temporary or final order concerning the administration of water rights and management of groundwater development in the LWRFS.

1.1 Background

In 1920, all waters of the Muddy River were decreed. The Muddy River plays an important role in the LWRFS because (1) it is the sole source of perennial streamflow; and (2) its headwaters constitute the main regional discharge from the flow system. In 1989, the LVVWD filed applications with the Nevada Division of Water Resources (NDWR) to appropriate groundwater in Coyote Spring Valley. The NSE held administrative hearings on these applications and other applications filed by Coyote Springs Investment, LLC (CSI) during 2001. Subsequent to these hearings, several NSE orders, stakeholder agreements, and NSE rulings were issued. The pertinent details of the relevant documents are summarized in the following sections.

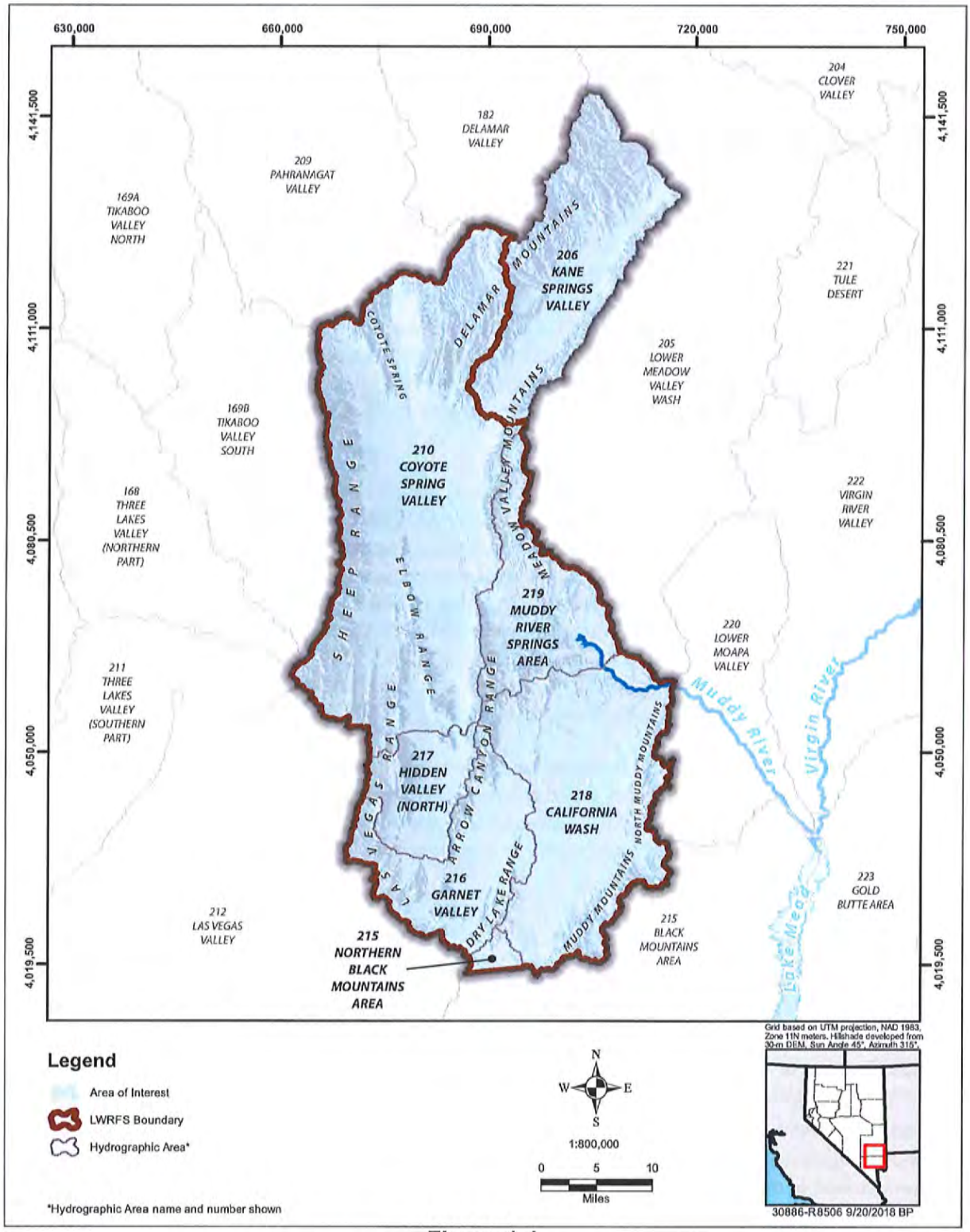

Figure 1-1
Boundary of the LWRFS

1.1.1 1920 Muddy River Decree

The Muddy River and the associated water rights were adjudicated and decreed in 1920 by the Tenth (now Eighth) Judicial District Court of the State of Nevada. The judgment and decree were in the case of Muddy Valley Irrigation Company et al. *v.* Moapa and Salt Lake Produce Company et al., *In the Matter of the Determination of the Relative Rights In and To the Waters of the Muddy River and its Tributaries in Clark County, State of Nevada*, dated March 12, 1920. The Muddy River Decree adjudicated the entire flow of the Muddy River including its tributaries, springs, headwaters, and other sources of supply. All of the decreed water rights are vested rights acquired by valid appropriation and beneficial use prior to March 1, 1905 and are considered as equal in rank without any party having any priority over another.

The decree specifies the entitlement to the waters of the Muddy River to several individuals and companies who were using the river prior to 1905 and maintained continuous use through the date of the decree. One of those companies is the Muddy Valley Irrigation Company (MVIC) who had certificated water rights in the Upper Muddy River but is, by the decree, entitled to the entire flow of the Muddy River except the flows granted to the other parties.

1.1.2 Order 1169

In 2002, the NSE issued Order 1169 holding in abeyance all pending and new applications for the appropriation of groundwater from the carbonate-rock aquifer (hereinafter referred to as the carbonate aquifer) underlying Coyote Spring, Hidden, Garnet, and Lower Moapa valleys, and the Muddy River Springs and Black Mountains areas. In addition, the NSE required a five-year study during which at least 50 percent of the existing groundwater rights in Coyote Spring Valley would be pumped for at least two consecutive years. The NSE stated the purpose of the study and aquifer test was to "*...determine if the pumping of those water rights will have any detrimental impacts on existing water rights or the environment.*" (NSE, 2002). The NSE directed the following entities to complete the study:

- LVVWD
- SNWA
- CSI
- Nevada Power Company (hereinafter referred to as Nevada Energy)
- Moapa Valley Water District (MVWD)

Order 1169 also instituted hydrologic monitoring and reporting requirements for the study participants and other water-right owners with points of diversion located in Garnet Valley and the Black Mountains Area. In April of 2002, the NSE granted requests by the Moapa Band of Paiutes (MBOP) and the U.S. Department of Interior to allow the Bureau of Indian Affairs, Fish and Wildlife Service (USFWS), and National Park Service (NPS) to participate in the study.

1.1.3 2006 Memorandum of Agreement

In 2006, to facilitate implementation of the Order 1169 study and aquifer test and to ensure protections of senior water rights and the endangered Moapa dace, the SNWA, CSI, USFWS, MBOP and MVWD entered into a Memorandum of Agreement (MOA) that instituted, among other things, Trigger Ranges associated with flows at the Warm Springs West near Moapa, Nevada gage under which pumping restrictions would apply (SNWA, 2006). These Trigger Ranges and the corresponding pumping restrictions are listed in Table 1-1.

Table 1-1
Trigger Ranges at Warm Springs West Gage and Corresponding Pumping Restrictions

	SNWA[1]	CSI[1]	MVWD[2]	MBOP[3]
Water Rights considered under MOA (afy)	9,000	4,600	--	2,500
Trigger Ranges (cfs)	**Pumping Restrictions (acre-feet per year [afy])**			
3.2 or less	Parties meet to discuss and interpret data and plan mitigation measures			
3.0 or less	SNWA & CSI take actions to redistribute pumping		--	--
3.0 to <2.9	< 8,050		--	--
2.9 to <2.8	< 6,000		--	< 2,000
2.8 to <2.7	< 4,000		--	< 1,700
≤2.7	< 724		--	< 1,250

[1] SNWA and CSI production from wells MX-5, RW-2, CSI-1, CSI-2 and other CSI wells in Coyote Spring Valley
[2] MVWD pumping restrictions were only for the duration of the NSE Order 1169 aquifer test
[3] MBOP pumping under permit no. 54075

In addition, the MOA established a Hydrologic Review Team (HRT) composed of representatives of each MOA signatory. The HRT is tasked with analyzing hydrologic data and determining, on an annual basis, whether the pumping restrictions under each Trigger Range should be modified.

1.1.4 Order 1169 Aquifer Test and Order 1169A

Pumping associated with the aquifer test began in accordance with Order 1169 on November 15, 2010. The aquifer test was completed on December 31, 2012; however, production from SNWA's MX-5 well continued into April 2013.

During the test, pumping rates of the SNWA MX-5 well ranged from 3,300 to 3,800 gpm and constituted the single largest stress on the carbonate aquifer in the LWRFS. Equipment issues associated with the water treatment facility connected to the well resulted in periods of non-pumping during the test. Production volumes from the MX-5 well totaled 4,131 af and 3,961 af for calendar years 2011 and 2012, respectively. Combined with CSI pumping from wells CSI-1 through CSI-4, a total of 5,331 and 5,102 af were pumped in Coyote Spring Valley during calendar years 2011 and 2012, respectively. Additional production from the carbonate aquifer occurred during the test by MVWD in the Muddy River Springs Area (MRSA) and by several entities in Garnet Valley. A

historical accounting of groundwater production in the LWRFS is presented in Section 4.0. Prior to and during the aquifer test, the study participants implemented a comprehensive hydrologic monitoring program under the direction of NDWR. Data collected under this program were submitted quarterly to NDWR in electronic form and made available to all study participants and the public.

The NSE issued amended Order 1169A on December 21, 2012 (NSE, 2012). In Order 1169A, the NSE declared the aquifer test completed as of December 31, 2012 and solicited information from the study participants regarding the test, impacts, and the availability of water pursuant to the pending applications held in abeyance by Order 1169. The reports submitted by the MOA signatories are summarized in Section 2.0.

1.1.5 NSE Rulings Nos. 6254 through 6261

In January 2014, the NSE issued Rulings 6254 through 6261 (NSE, 2014a through h). In these rulings the NSE denied all pending applications in the LWRFS and found that "*...the Order 1169 test measurably reduced flows in headwater springs of the Muddy River.*" The NSE also found that "*... the amount and location of groundwater that can be developed without capture of and conflict with senior water rights on the Muddy River and springs remains unclear, but the evidence is overwhelming that unappropriated water does not exist.*" Based on these findings, the NSE ruled that there is no unappropriated groundwater and that the applications would conflict with existing rights and threaten to prove detrimental to the public interest. The NSE also ruled that the basins composing the LWRFS would be jointly managed.

1.1.6 CSWR GID Letter to NSE

In a letter dated November 16, 2017, the LVVWD, acting in the capacity of the general manager of the CSWR GID, solicited an opinion from the NSE regarding whether Coyote Spring Valley groundwater could sustainably supply water for a project to develop 13,100 acres of land within Coyote Spring Valley. In the letter, LVVWD cited NSE Ruling 6255 in which the NSE concluded *"pumping under the Order 1169 test measurably reduced flows in the headwater Springs of the Muddy River...."* LVVWD further stated that while Ruling 6255 did not invalidate any existing water rights, LVVWD were not convinced that Coyote Spring Valley groundwater could sustainably support the project given the endangered species issues in the Muddy River and impacts to senior water rights. In addition, LVVWD solicited an opinion regarding the extent to which the NSE would be willing to execute subdivision maps for the project if the maps were predicated on the use of groundwater owned by the CSWR GID and developers of the project.

1.1.7 NSE Interim Order 1303

On January 11, 2019, the NSE issued Order 1303 designating the hydrographic areas composing the LWRFS as a joint administrative unit for the purpose of administering water rights. Order 1303 also held in abeyance any changes to existing groundwater rights and established a temporary moratorium on the review of final subdivision maps. In Order 1303, the NSE also requested input on the following issues from stakeholders with interests in the LWRFS that may be affected by water-rights development (NDWR, 2019):

(a) The geographic boundary of the hydrologically connected groundwater and surface-water systems comprising the Lower White River Flow System;

(b) The information obtained from the Order 1169 aquifer test and subsequent to the aquifer test and Muddy River headwater spring flow as it relates to aquifer recovery since the completion of the aquifer test;

(c) The long-term annual quantity of groundwater that may be pumped from the Lower White River Flow System, including the relationships between the location of pumping on discharge to the Muddy River Springs, and the capture of Muddy River flow;

(d) The effects of movement of water rights between alluvial wells and carbonate wells on deliveries of senior decreed rights to the Muddy River; and,

(e) Any other matter believed to be relevant to the State Engineer's analysis.

1.2 Purpose and Scope

The purpose of the work presented in this report is to summarize the current state of knowledge of the LWRFS, including spring discharge, the alluvial reservoir and perennial streamflow in the MRSA.

Specific objectives are to address the issues identified in Order 1303 by:

- evaluating hydrologic responses to the variable stress conditions affecting the LWRFS;
- evaluating the recovery responses associated with the cessation of the 2-year aquifer test;
- identifying trends in the behavior of key hydrologic variables;
- assessing the hydraulic connectivity between pumping centers and various points of interest;
- quantifying the average annual groundwater production from the carbonate aquifer that correspond to pre-selected spring discharge levels; and
- quantifying impacts to SNWA related to Muddy River streamflow depletions.

The scope of work includes a survey of the available information; compilation and analysis of time-series data; and the creation of various maps, tables, and charts to support the analyses and conclusions.

1.3 Approach

The objectives of this work were achieved by completing the following steps:

1. Performing a survey of the information available regarding the LWRFS, including hydrologic stress conditions and responses (Section 2.0).

2. Describing the flow system using the available information, including the interpretations derived from the data collected during the two-year aquifer test (Section 3.0).

3. Compiling and analyzing historical time-series data for natural and anthropogenic stresses affecting the hydrology of the LWRFS (Section 4.0).

4. Using historical time-series data to analyze the hydrologic responses of several variables that describe the historical conditions of the flow system over a period of decades (Section 5.0).

5. Qualitatively and quantitatively assessing the implications of changes in the hydraulic heads of the carbonate aquifer due to groundwater production in the LWRFS (Section 6.0).

6. Quantifying the impacts to SNWA related to Muddy River streamflow depletions caused by groundwater production in the LWRFS (Section 7.0)

7. Using the results of this assessment to respond to NSE requests for stakeholder input regarding several issues described in Order 1303 (Section 8.0).

2.0 SOURCES OF INFORMATION

This assessment required a review of the existing literature and the use of large quantities of data acquired from various sources. Depth to water measurements for wells and discharge measurements for the Muddy River and selected springs located in the LWRFS were assembled into an extensive database. These data were analyzed to evaluate current groundwater conditions, hydraulic gradients and flow directions, and aquifer responses to natural and anthropogenic stresses.

2.1 Previous Investigations

Previous investigations completed by SNWA, the LVVWD, and others that are relevant to this assessment are summarized in this section. Such investigations started with the reconnaissance studies initiated in the late 1940s and have continued since. Only relevant studies documented after the issuance of NSE's Order 1169A in December 2012 are summarized in this section.

2.1.1 Order 1169A Reports

In the months following the completion of the 2-year aquifer test mandated by NSE Order 1169, the various stakeholders, including the MOA signatories, evaluated the test results and documented their interpretations, conclusions, and recommendations in reports submitted to the NSE in June of 2013. These reports relied upon only a few months of recovery data that were influenced by the SNWA MX-5 well which continued pumping through mid-April 2013 (see Section 5.2.3 of this report for a more detailed explanation).

SNWA (2013b)

SNWA (2013b) presents the data collected before and during the test, as well as interpretations of aquifer responses and water availability. Based on their analysis of the pre-test and test data, the major conclusions made by SNWA (2013b) are as follows:

- Changes in groundwater levels are affected by both groundwater pumping from the carbonate aquifer and changes in prevailing hydrologic conditions before and after the aquifer test.

- The aquifer test confirmed that extensive hydraulic connectivity exists in the carbonate aquifer. However, the presence of boundaries and spatial variations in hydraulic conductivity affect the carbonate aquifer's response depending on location. For example, no discernible responses were observed north of the Kane Springs Fault and west of the MX-5 and CSI wells near the eastern front of the Las Vegas Range (note: the lack of responses cited in SNWA (2013b), referred to wells CSVM-3 and CSVM-5; see Sections 5.2.2 and 5.2.3 of this report for a more detailed explanation).

- Relatively minor declines in spring flow were observed at the highest elevation springs (Pederson and Pederson East springs) during the test. However, no changes were discerned in the flows of the Muddy River at the U.S. Geological Survey (USGS) Muddy River near Moapa, Nevada gage because the responses were relatively small compared to the large flows of the river and the impacts related to pumping within the MRSA.

- Pumping the existing groundwater rights in Coyote Spring Valley during the test did not result in an unreasonable lowering of the groundwater table. Furthermore, recovery began when pumping was reduced to pre-test levels.

- It remains unclear if additional resource development beyond existing permitted rights could take place in Coyote Spring Valley at selected locations.

USFWS, Bureau of Land Management (BLM), and NPS (2013)

The USFWS, BLM, and NPS prepared a similar report in 2013. Their analyses included a numerical groundwater flow model developed by Tetra Tech (2012a and b) and SeriesSEE analysis (Halford et al., 2012). They attempted to calibrate the model using the data from the 2-year aquifer test and used the resulting model to make predictions. The SeriesSEE analysis was conducted to segregate the drawdowns caused by the MX-5 pumping well from those caused by the other pumping wells. Their main conclusions are as follows:

- Pumping at MX-5 caused drawdowns of about the same magnitude in the portion of the carbonate aquifer underlying Coyote Spring Valley, the MRSA, Hidden and Garnet valleys, and California Wash at the end of the test.

- Using the results of the SeriesSEE analyses, USFWS et al. (2013) delineated the connected portion of the carbonate aquifer, which they state includes the source of the Muddy River Springs and majority source of the Muddy River.

- Based on these analyses, USFWS et al. (2013) concluded that pumping from the connected portion of the carbonate aquifer causes drawdowns of about the same magnitude throughout the delineated area.

- Based on previous information and the results of their analysis of the test data, they also concluded that no additional groundwater is available for appropriation.

Johnson and Mifflin (2013)

Johnson and Mifflin (2013) also prepared a report of the analysis of the 2-year aquifer test data. Based on their analysis, they found that (1) the portion of the WRFS located south of Pahranagat Valley consists of two separate flow fields, the northern and southern flow fields, that responded differently to the pumping in Coyote Spring Valley; and (2) the variations in the Muddy River baseflow caused by natural stresses are of the same order of magnitude as the pumping stresses in Coyote Spring Valley during the two-year aquifer test. Based on their analyses, they made the following four recommendations:

- At least four of the basins that include and extend upgradient from the MRSA should be combined into one water-management unit.

- The pending LVVWD water rights applications in this area should be denied on the grounds that they would impact senior rights by the full amount.

- The existing undeveloped permits located within the combined area must be mostly revoked, restricted, or very carefully managed to avoid periods of eliminated Muddy River base flows in the springs-area headwater reaches in the future.

- A large interim pumping test should be conducted in the northern portion of the Southern Flow Field to better evaluate the water-resource potential of this portion of the flow system.

CSI (2013)

CSI (2013) conducted a qualitative analysis of the 2-year aquifer test and concluded that the effects of pumping during the test generated a shallow drawdown cone that extends miles from the MX-5 well. Using the observations from the test and monitoring data collected by SNWA, CSI (2013) concluded the following:

- The Kane Spring fault acts as a groundwater barrier to groundwater flowing from north to south in Coyote Spring Valley and may also serve as a barrier to pumping from wells located north of the fault.

- Based on supporting information from SNWA's Annual Monitoring Reports, additional groundwater is available for appropriation in Coyote Spring Valley.

- Water-right applications submitted by CSI and SNWA should be fully or partly granted.

Myers (2013)

Myers (2013) describes an analysis of the 2-year aquifer test and a review of the groundwater flow model developed by Tetra Tech for the southern White River Flow System (WRFS) (Tetra Tech, 2012a and b). Myers (2013) concluded the following:

- The Order 1169 aquifer test data and the Tetra Tech groundwater flow model predictions indicate that pumping from existing groundwater rights in Coyote Springs Valley and the MRSA will cause the spring discharge to decrease to dangerous levels.

- Any additional water rights potentially granted in the future will cause the spring discharge to decrease further below the required target rates and may eventually dry up some or all of the springs in the MRSA.

2.1.2 Annual Data Reports (2013-2019)

This assessment relied upon the annual data reports prepared by the Order 1169 study participants and others who submit quarterly data to NDWR. Among these reports are the ones prepared by SNWA, MVWD, NVE and the HRT.

SNWA Annual Monitoring Reports

SNWA prepares and submits annual monitoring reports in satisfaction of water-right permit terms for groundwater and surface-water sites throughout the LWRFS. The reports of particular interest are the ones prepared after the completion of the aquifer test as they contain data characterizing the recovery responses to the pumping stresses imposed during the 2-year aquifer test (SNWA, 2013a; 2014; 2015a; 2016a; 2017a; 2018b and 2019).

HRT Annual Determination Reports

Also relevant to this assessment are the annual reports prepared by the HRT after the completion of the test (2013 through 2018). The MOA signatories collect and analyze data and share their findings to satisfy the objectives of the MOA. Since the MOA was signed in 2006, extensive data collection and analysis efforts have been performed, including those associated with the Order 1169 study. The HRT annual reports include descriptions of previous monitoring activities and interpretations prepared by the signatories and incorporated in the reports as appendices. Based on the findings of each year, the HRT makes recommendations about the action levels associated with the Trigger Ranges. As in all previous reports, HRT (2018) recommended that no changes be made to the existing pumping restrictions listed in the MOA (SNWA, 2006) and presented in Table 1-1.

2.1.3 Other Reports

A few other relevant reports have been issued since the completion of the Order 1169 aquifer test including the following:

Huntington et al. (2013)

Huntington et al. (2013) prepared a technical memorandum for SNWA containing estimates of evapotranspiration (ET) for the MRSA from 2001-2012. This work was part of a larger project designed to identify trends in ET over the period of 2001-2012 and the potential impacts that land management practices and vegetation changes may have on ET.

Rowley et al. (2017)

Rowley et al. (2017) published a comprehensive report describing the geology and geophysics of a large area including parts of eastern Nevada and western Utah, and the LWRFS. The report includes geologic maps at a scale of 1:250,000 based on various published and unpublished geologic maps, site studies and new local geologic maps. Their report includes 25 new geologic cross sections at the same scale and interpretations of new geophysical data collected by the USGS.

2.2 Data Sources

Data relevant to this assessment were obtained from many project-related sources as well as regional and national sources. Monitoring of hydrologic conditions and reporting of surface-water diversions and groundwater production has been on-going in the LWRFS for decades. Through the collective efforts of water-right owners, several monitoring programs have been implemented to comply with monitoring and reporting requirements associated with permit terms. In addition, the NDWR instituted comprehensive monitoring and reporting requirements associated with the Order 1169 study to ensure pertinent data were collected and reported in a timely manner. These data are summarized in annual data reports and are accessible on the NDWR website at http://water.nv.gov/Order1169Menu.aspx.

In addition, SNWA and NDWR participate in joint funding agreements with the USGS to fund operation and maintenance of several important surface-water and groundwater sites located within the LWRFS. These data are accessible through the USGS National Water Information System and Groundwater Site Inventory database (NWIS) (USGS, 2018). Additional data were compiled from the NDWR drillers log database (NDWR, 2018a), published reports documenting well completions or hydrologic studies. However, the majority of the data presented in this report were collected and reported by the 2006 MOA signatories and Order 1169 study participants.

Climate records spanning long periods were necessary for this assessment are not available for meteorological stations located within the LWRFS. Thus, climate data were obtained from the following agencies:

- Western Region Climate Center (WRCC) at https://wrcc.dri.edu/summary/Climsmnv.html
- National Oceanic and Atmospheric Administration (NOAA) at https://www.noaa.gov/climate
- Parameter-elevation Regressions on Independent Slopes Model (PRISM) at http://www.prism.oregonstate.edu/

3.0 LWRFS DESCRIPTION

The boundary of the LWRFS was initially described in NSE Rulings 6254 through 6261 (NSE, 2014a through h), inclusive, and a figure attached to the rulings that identified the Order 1169 basins. The boundary of the LWRFS is depicted in Figure 1-1. This section presents the physiography, climate, and hydrogeology of the LWRFS, and a description of the surface-water and groundwater hydrology.

3.1 Physiography

The LWRFS is within the Basin and Range physiographic province of the Great Basin, which is characterized by a series of parallel to sub-parallel, north-trending mountain ranges separated by elongated alluvial valleys (Fenneman, 1931). The western margin of the LWRFS is defined by the Sheep Range in the north and the Las Vegas Range in the south. The Sheep Range is the highest range in the LWRFS with peak elevations ranging from 7,000 to nearly 10,000 ft amsl. The eastern boundary of the LWRFS is defined by the Muddy and North Muddy mountains in the south and by the Meadow Valley and Delamar mountains in the north. Adjacent to the LWRFS, in Kane Springs Valley, elevations in the Delamar Mountains exceed 7,000 ft amsl. Included within the LWRFS are the Coyote Spring, Elbow, Arrow Canyon, and Dry Lake ranges all having elevations less than 6,000 ft amsl (Figure 1-1). During the Pleistocene Epoch, the White River flowed through Coyote Spring Valley entering the valley from southern Pahranagat Valley and traveling south and then southeast between the Arrow Canyon Range and the Meadow Valley Mountains where it continued along the present course of the Muddy River (Eakin, 1964). The elevations along this ancestral feature range from just above 3,000 ft amsl where it enters Coyote Spring Valley to 1,420 ft amsl where the river leaves California Wash near Glendale, Nevada.

3.2 Climate

The climate of the LWRFS is typical of southern Nevada ranging between arid and semi-arid conditions. This climate is characterized by small amounts of precipitation occurring mostly on the surrounding mountains, and high summer temperatures and evaporation rates. Winter-season precipitation occurs as snow at the higher elevations of the Sheep and Delamar Ranges and serves as the primary source of local recharge. During the summer months, precipitation occurs as a result of local storms. Air temperatures vary greatly on a daily and seasonal basis. Climate variations constitute natural stresses to the hydrologic system of the LWRFS and are discussed in more detail in Section 4.0.

3.3 Hydrogeology

The hydrogeology of the LWRFS is characterized by the complex geology of the area, which ranges in age from Precambrian siliciclastic rocks to Tertiary and Quaternary alluvial deposits that have been

structurally deformed during several tectonic episodes (Rowley et al., 2017). Three tectonic episodes as well as extensive volcanism have affected the region. The Antler deformation and Sevier deformation resulted in east-verging thrust sheets in which Paleozoic carbonate rocks were placed over the top of each other as well as over younger rocks producing thick sequences of carbonate rocks in the region. The third tectonic episode is the middle Miocene to Holocene basin-range deformation that shaped the current topography of the Great Basin. In this episode, basin-range faulting produced horst and graben topography resulting in typically deep basins and relatively high mountain ranges that are generally oriented north-south (Rowley et al., 2017).

The following sections summarize the structural setting and hydrogeology of the LWRFS, with reference to the 1:250,000 scale hydrogeologic map of Rowley et al. (2011) presented in Figure 3-1. The map is based on a geologic map and cross sections for a region including portions of White Pine, Lincoln, and Clark counties in Nevada, and adjacent areas.

3.3.1 Structural Setting

Major structural episodes have caused faulting within the LWRFS. These episodes have influenced the distribution and thickness of geologic units and the geometry of the basins and ranges. Major fault structures within the area are described in the following sections.

Thrust Faults

Thrust faults within the LWRFS include the Muddy Mountain thrust in the Muddy Mountains, the Dry Lake thrust in the Dry Lake Range, and the Gass Peak thrust in the eastern Sheep Range (Figure 3-1). The importance of these faults is that they create very thick carbonate-rock sequences that, as a result of compression and transport, have significant fracture development and therefore increased permeabilities (Heilweil and Brooks, 2011; Page et al., 2005). In addition, these faults have juxtaposed the carbonate-rock sequence with low permeability rocks that are older (e.g. Gass Peak Thrust in the southern Sheep Range) or younger (e.g. Muddy Mountain Thrust). In these areas, this juxtaposition effectively truncates the extent of LWRFS. The thrust faults themselves may also act as barriers to groundwater flow (Page et al., 2005).

Strike-Slip Faults

The left-lateral strike-slip fault of the Pahranagat Shear Zone (PSZ) and the right-lateral strike-slip fault of the Las Vegas Valley Shear Zone (LVVSZ) occur just to the north and south of the LWRFS, respectively. Faults of the PSZ, provide a partial barrier to southward flow from southern Pahranagat and Delamar valleys into the LWRFS (Rowley et al., 2011). Groundwater likely flows south through the barrier into Coyote Spring Valley along north-trending normal faults and fractures (Rowley et al., 2011). The LVVSZ has been interpreted to be a barrier to southward groundwater flow (Heilweil and Brooks, 2011).

The Kane Springs Wash fault zone is a left-lateral and normal down-to-the-west oblique fault that occurs in Kane Springs Valley and the northern portion of Coyote Spring Valley (Figure 3-1). The oblique fault along with the Kane Springs Wash caldera complex and thrust faults likely prevent groundwater flow between Kane Springs Valley and Meadow Valley Wash (Rowley et al., 2011). In

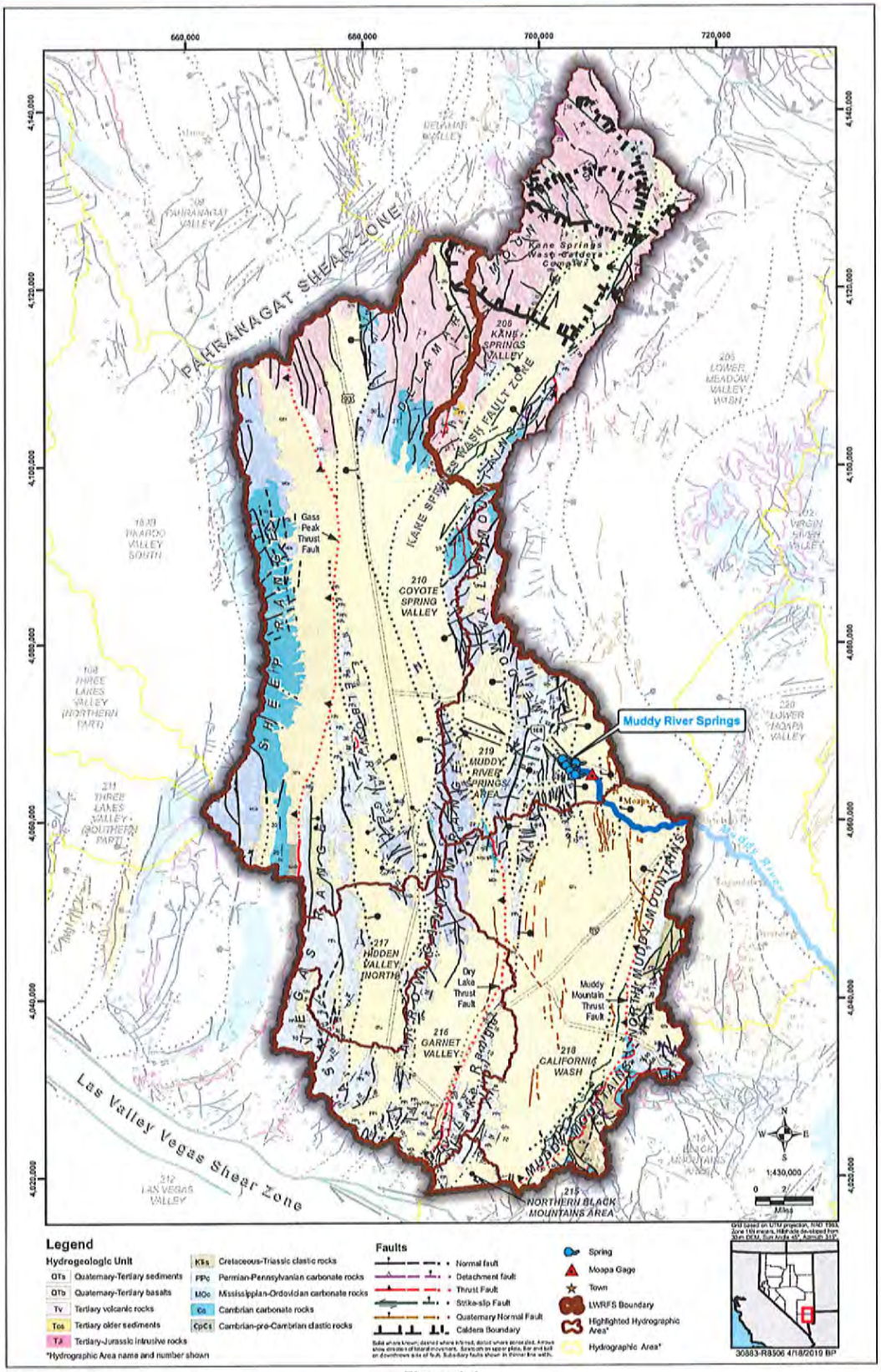

Figure 3-1
Hydrogeologic Map of the Lower White River Flow System

Coyote Spring Valley, the Kane Springs Wash fault zone may act as a partial barrier to flow, impeding flow across the fault from north to south.

Normal Faults

The main phase of Basin and Range deformation which began around 10 Ma, is characterized by steeply-dipping, north-striking, normal faulting (Rowley et al., 2017). This faulting is responsible for the formation of the present-day physiography of north-trending basins and ranges forming the LWRFS (Page et al., 2011). The many Basin and Range faults that underlie and define the sides of Coyote Spring Valley provide the pathways for southward groundwater flow (Harrill et al., 1988; Schmidt and Dixon, 1995). A major part of that groundwater flows southeast, between the northern end of the Arrow Canyon Range and the southwestern end of the Meadow Valley Mountains along what has been referred to as the east Arrow Canyon Range fault zone (Page et al., 2011; Rowley et al., 2011). East-striking faults intersect the north-striking faults likely increasing the permeability of carbonate rocks in the MRSA (Page et al., 2011; Rowley et al., 2017). The southeast-flowing groundwater is the principal source of many large springs in the MRSA, which currently create the perennial flow of the Muddy River (Schmidt and Dixon, 1995; Donovan et al., 2004; Buqo, 2007; Donovan, 2007; Johnson, 2007).

3.3.2 Hydrogeologic Setting

The hydrogeologic map presented in Figure 3-1 was constructed by grouping geologic units with similar hydrologic properties into hydrogeologic units. The following sections summarize the geology and hydrogeology of the mountain ranges within and at the boundaries of the LWRFS.

Delamar Mountains

The Delamar Mountains at the northern LWRFS boundary are dominated by Tertiary caldera complexes including the Kane Springs Wash caldera complex (Rowley et al., 1995; Scott and Swadley, 1995; Scott et al., 1996; Dixon et al., 2007). The main bounding fault of the Delamar Mountains is the down-to-the-west normal fault on the western side, which is joined from the southwest by several splays of the left-lateral and normal PSZ (Ekren et al., 1977). In Kane Springs Valley, the bounding fault is the oblique (left-lateral and normal down-to-the-west) Kane Springs Wash fault zone (Swadley et al., 1994). Tertiary caldera complexes forming the northern boundary of Kane Springs are effective barriers to groundwater flow. The calderas are barriers primarily because of their underlying intracaldera intrusions and both hydrothermal clays and contact-metamorphic rocks formed by emplacement of the intrusions into intracaldera tuffs (Rowley et al., 2011). Groundwater likely enters the LWRFS from southern Delamar Valley along the PSZ to Pahranagat Valley and then through the PSZ and along north-striking normal faults into Coyote Springs Valley (Figure 3-1).

Southern Sheep Range, Las Vegas Range, and Elbow Range

The southern Sheep Range is underlain by mostly Cambrian and Ordovician carbonate rocks that dip eastward (Guth, 1980). The range is a large tilt block uplifted along major north-striking, basin-range normal faults on its western side. The range is on the upthrown western side of the low-angle, west-dipping Gass Peak thrust. The thrust transported Neoproterozoic to Cambrian quartzite and

Cambrian to Devonian carbonate rocks eastward over Cambrian to Mississippian rocks (Dohrenwend et al., 1996).

The Las Vegas Range is defined by the Gass Peak thrust, which transported rocks as old as the Cambrian Wood Canyon Formation eastward over Mississippian, Pennsylvanian, and Permian carbonate rocks of the Bird Spring Formation (Maldonado and Schmidt, 1991). Most of the range is made up of folded Bird Spring limestone, with the Gass Peak thrust exposed along its western side (Maldonado and Schmidt, 1991; Page, 1998). The small Elbow Range, which bounds the Las Vegas Range on the northeast, is made up of thrusted and folded Bird Spring Formation that has been uplifted as a horst (Page and Pampeyan, 1996).

Meadow Valley Mountains

The Meadow Valley Mountains constitutes a narrow, generally low, north-northeast-trending range about 40-mi-long. The northern 30 mi of the range consists mostly of outflow ash-flow tuffs and part of the Kane Springs Wash caldera complex. The southern end of the Meadow Valley Mountains, just east of Coyote Spring Valley, is made up of mostly thrust-faulted and normally faulted Paleozoic rocks (Pampeyan, 1993; Swanson and Wernicke, 2017).

Arrow Canyon Range

The Arrow Canyon Range is a sharp, narrow, north-trending range consisting of a syncline of Cambrian to Mississippian carbonate rocks. It is uplifted along its western side by normal faults of the Arrow Canyon Range fault zone (Schmidt and Dixon, 1995; Page and Pampeyan, 1996; Page, 1998). The trace of the north-striking Dry Lake thrust, which carries Cambrian rocks over Silurian through Permian carbonate rocks, is exposed and projected north just east of the range (Page et al., 1992; Schmidt and Dixon, 1995; Beard et al., 2007).

North Muddy Mountains, Muddy Mountains, and Dry Lake Range

The southeastern corner of the LWRFS contains the Cretaceous-Triassic clastic rocks of the North Muddy Mountains and the Muddy Mountains (Bohannon, 1983). The Muddy Mountain thrust fault has placed the carbonate-rock sequence on top of these rocks, effectively truncating the LWRFS at this location. West of the Muddy Mountains and east of the Apex Industrial Park, is the small Dry Lake Range. This range is made up mostly of Bird Spring carbonate rocks. A narrow arm of bedrock extending west from Apex connects with the southern Arrow Canyon Range/Las Vegas Range. Basin-fill sediments to the northeast along the I-15 corridor (California Wash area) belong to an east-tilted half graben that reaches depths of 9,000 to 12,000 ft (Langenheim et al., 2001, 2010; Scheirer et al., 2006).

3.4 Hydrology

The hydrology of the LWRFS is presented in this section including descriptions of prominent surface-water features and associated time-series records of discharge; as well as descriptions of groundwater characteristics including aquifer types and conditions, and occurrence and movement. The sources of the data utilized in this section are described in Section 2.0.

3.4.1 Surface Water

The primary surface-water features of the LWRFS are located within the MRSA where five spring-complexes and numerous gaining stream reaches form the headwaters of the Muddy River, the only perennial stream within the LWRFS (Figure 3-2). There are additional small springs in Coyote Spring and Kane Springs valleys which discharge groundwater sourced from local recharge; however, these springs are not described in this report because their discharge is known to be minor (Eakin, 1964).

The regional carbonate aquifer is the source of water for the springs and the gaining stream reaches that form the headwaters of the Muddy River (Eakin, 1964; Rowley et al., 2017). Discharge from the springs coalesce with the gaining reaches to form the main channel of the Muddy River just above the USGS Muddy River near Moapa, Nevada (NV) gaging station. Figure 3-2 depicts the location of this gaging station and several other USGS gaging stations. Also depicted are the locations of metered surface-water diversions in the headwaters area. Table 3-1 lists the periods of record for each of the gaging stations.

Figure 3-2
Spring Complexes, Streams, Diversions, and Gaging Stations within the Headwaters of the Muddy River

There are three gaging stations that are critical to the analyses presented in this report. Two are associated with the Pederson Spring Complex: Pederson Spring near Moapa, NV and Warm Springs

West near Moapa, NV. The Pederson Spring near Moapa, NV gage is important because it measures flow from the highest elevation spring within the MRSA representing groundwater discharge from the regional carbonate aquifer. The Warm Springs West gage is important because flow triggers have been established at the gage as part of the 2006 MOA (see Table 1-1). The third gaging station is the Muddy River near Moapa gage, which is important because it (1) measures the streamflow at this location, (2) provides the only basis for estimating the total discharge from the carbonate aquifer to the springs area, and (3) has the longest period of record. Details for each are presented in the following sections.

Table 3-1
USGS Gaging Stations in the Headwaters of the Muddy River

USGS Station Number	Gaging Station Name	Period of Record for Daily Average flow
09415900	Muddy Springs at LDS Farm near Moapa, NV (LDS gage)	August 1985 to Present
09415908	Pederson East Spring near Moapa, NV (Pederson East gage)	May 2002 to Present
09415910	Pederson Spring near Moapa, NV (Pederson gage)	October 1986 to Present[1]
09415920	Warm Springs West near Moapa, NV (Warm Springs West gage)	August 1985 to September 1994 June 1996 to Present[2]
09415927	Warm Springs Confluence at Iverson Flume near Moapa, NV (Iverson Flume gage)	October 2001 to Present
09416000	Muddy River near Moapa, NV (Moapa gage)	July 1913 to September 1915 May 1916 to September 1918 October 1944 to Present

Note: [1]Flow data in the latter half of 2003 through April 2004 reflects flows bypassing the gage through a leak in the weir. The weir was replaced in April 2004.
[2]Flow records prior to October 1997 were influenced by an agricultural diversion above the gage.

Pederson Spring Complex

The Pederson Spring near Moapa, NV gage (09415910) measures spring discharge from the highest elevation spring in the Muddy River headwaters area. The gage record begins in 1986, but is missing data from 1994 to 1996. The aluminum weir was found to be severely warped and it is speculated this happened when a fire burned through the area in 1994 (SNWA, 2008). In addition, the record includes underreported values from 2003 until April 2004 during which time discharge was observed bypassing the gage. The record from 1994 to April 2004 when the gage was replaced is considered poor quality. Figure 3-3 presents the flow record for the gage for the period 1986 to present. As the highest-elevation spring, it is considered to be the most sensitive to changes in groundwater conditions associated with the regional carbonate aquifer, and, therefore, a good indicator of how these changes affect spring discharge in the MRSA.

Warm Springs West near Moapa, NV Gage (09415920)

The Warm Springs West near Moapa, NV gage (09415920) is a parshall flume that measures the total discharge from the Pederson Spring complex. The period of the continuous record ranges from 1985 to present. Continuous gage records prior to October 1997 are considered unreliable because the flows were influenced by an unmetered agricultural diversion above the gage. Discrete measurements such as those made by Eakin (1964) are also available. These measurements are important because they provide valuable information prior to significant development in the area. Figure 3-4 presents

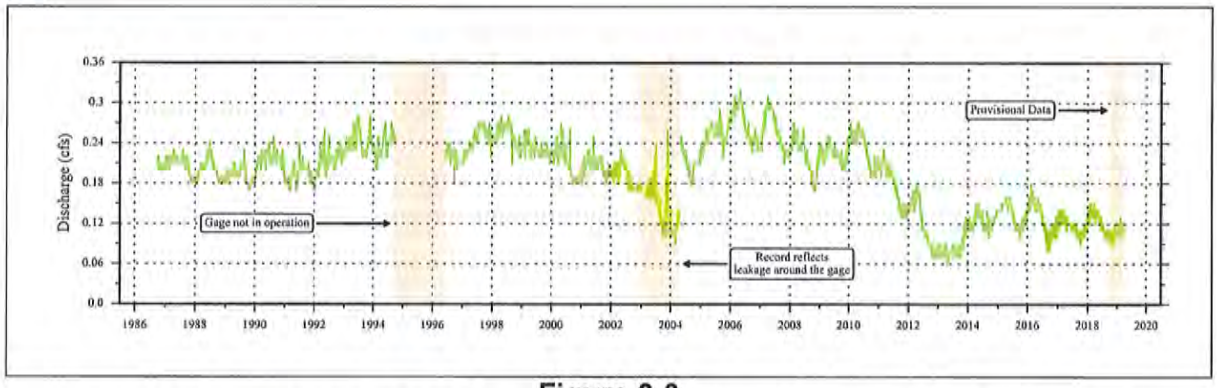

Figure 3-3
Pederson Spring near Moapa, NV - Daily Discharge Record (1986 to present)

the flow measured at the gage for the period of continuous record. The parties to the MOA established Trigger Ranges at various flow rates at the gage for the purpose of initiating water management actions to protect instream flow rights and habitat for the endangered Moapa dace. The first trigger has been established at 3.2 cfs.

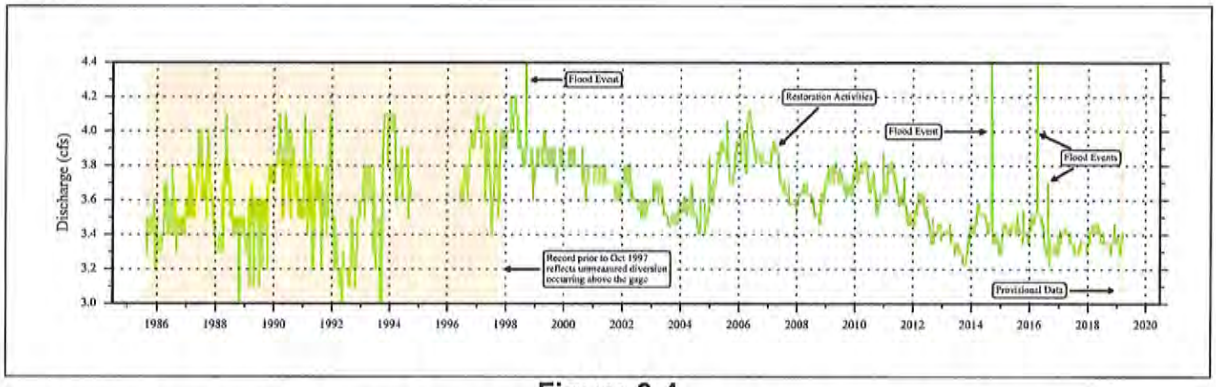

Figure 3-4
Warm Springs West near Moapa, NV - Daily Discharge Record (1985 to present)

Muddy River near Moapa, NV Gage (09416000)

The USGS Muddy River near Moapa, NV gage (Station No. 09416000; hereinafter referred to as the MR Moapa gage) measures the streamflow contributions from spring complexes, gaining reaches and intermittent flood flows. Streamflow is directly affected by surface-water diversions and ET occurring above the gage. Figure 3-5 presents a time-series chart of the annual streamflow measured at the MR Moapa gage for the period 1945 to 2018. Also presented on the chart is a record of these flows that has been adjusted to remove the influence of intermittent flood flows. These influences were removed from the mean daily flow record using a method that replaces the identified flood flow with the median monthly flow as described in Johnson (1999). The resulting flow record is more representative of actual baseflow conditions at the gage. The flood-adjusted flow record is used in the analyses presented in this report.

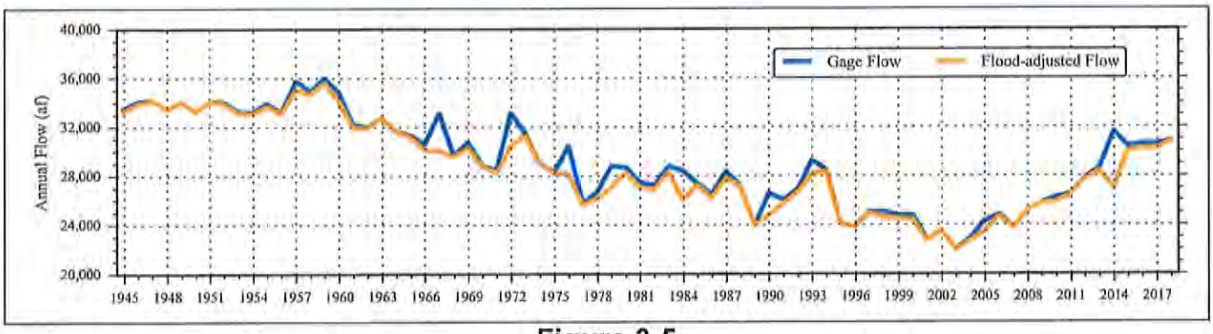

Figure 3-5
Muddy River near Moapa, NV (1945 to 2018)

The mean annual flow measured at the MR Moapa gage in 1946 was 46.8 cfs (33,900 af). This flow rate is considered the predevelopment baseflow because it predates municipal and industrial surface-water diversions and exports by NVE and MVWD, as well as groundwater development within the MRSA. This baseflow also matches the average mean annual flow when the gage was operated intermittently between 1913 and 1918. During two intervals covering 3-years (July 1, 1913 to June 30, 1915 and October 1, 1916 to September 30, 1917) the average flood-adjusted mean annual flow was 47.0 cfs (34,000 afy), a difference of 100 afy from the 1946 flow rate.

The 1946 pre-development baseflow also corresponds with information compiled by Eakin (1964). Eakin (1964) reported a 25-year average flood-adjusted mean annual flow of 46.4 cfs (33,600 afy) using intermittent data between 1914 and 1962. In addition, Eakin (1964) estimated that approximately 2,000 to 3,000 afy of spring flow was being consumed by phreatophytes between the spring orifices and the gage. Eakin and Moore (1964) examined the MRSA discharge in more detail and concluded that the January measurements of river flow at the MR Moapa gage are the most reliable estimates of discharge to the area as ET above the gage is practically zero during that month. They estimated the mean discharge to be 50.2 cfs, or about 36,000 afy, using data for a period spanning 1945 to 1962. As illustrated by Figure 3-5, the gage flow during pre-development conditions only varied by about 1,000 afy from 1945 to 1955. Starting in the early 1960s, Muddy River streamflow began to decline from the 33,900 afy pre-development baseflow. This decreasing trend continued, reaching a low of about 22,000 af in 2003. By this time, streamflow had declined by over one-third of the pre-development baseflow. Streamflow has since recovered, and by the end of 2018 the mean annual flood-adjusted flow was 30,800 af. The causes of this decline and subsequent recovery are analyzed in Section 5.0.

3.4.2 Groundwater

Descriptions of the groundwater characteristics of the LWRFS, including aquifer types and conditions and groundwater occurrence and movement are presented in this section.

3.4.2.1 Aquifer Types and Conditions

The hydrogeology described in Section 3.3 can be further simplified into a groundwater system composed of a regional carbonate aquifer interconnecting the basins of the LWRFS and one or more areas where saturated basin-fill is present. The regional carbonate aquifer is contiguous throughout the basins, while the saturated basin fill occurs primarily within the basin centers.

Regional Carbonate Aquifer

The identification of the regional carbonate aquifer was made by Eakin (1964, 1966) who noted that the large discharge from the springs located within the MRSA could not be supported by the relatively small local recharge. As a result, Eakin (1966) concluded that the springs were discharging groundwater originating from basins located upgradient. Eakin (1966) developed a water balance for thirteen basins located within south-eastern Nevada, ending with the MRSA. Based on the results, he concluded that recharge in these basins contributes to the discharge of the Muddy River springs and that the Paleozoic carbonate rocks must be the primary system that is transmitting water between these basins. Investigations conducted after Eakin (1966) revealed that the hydraulic connection of the carbonate aquifer extends to basins located south of the MRSA (SNWA, 2009; Burns and Drici, 2011; SNWA, 2013b).

The regional carbonate aquifer is predominantly composed of thick sequences of Paleozoic and Mesozoic carbonate rocks that have well-developed fracture networks (Heilweil and Brooks, 2011). As described in Section 3.3.2, thick sequences of carbonate rocks occur throughout the LWRFS as thrust faulting has placed carbonate-rock sequences on top of other carbonate rock sequences. The compressional and transport processes that are involved with thrusting may lead to significant fracture development (Heilweil and Brooks, 2011). Carbonate rocks typically have a low permeability but may have very high secondary permeabilities as result of fracturing and the dissolution of the carbonate minerals along faults, fractures, and bedding planes (Schaefer et al., 2005).

Basin-Fill Aquifers

Saturated basin fill may form aquifers in the LWRFS. Where they occur, these aquifers generally overlie the regional carbonate aquifer system and are typically separated from one another by mountain ranges composed of consolidated rocks (Schaefer et al., 2005). The aquifers are composed of Tertiary sediments consisting of eroded limestone, conglomerate, sandstones, as well as Quaternary alluvium, colluvium, playa deposits, and eolian deposits (Page et al., 2011). Basin fill can be composed of many sediment types with different grain sizes and levels of sorting, and, consequently, can have a large range of permeabilities (Heilweil and Brooks, 2011). Where present, basin-fill aquifers within the LWRFS occur at great depths above the carbonate aquifer, as perched, or as semi-perched systems.

MRSA Alluvial Reservoir

In the MRSA,the combination of permeable interbedded fine- and coarse-grained sediments on top of the low-permeability Muddy Creek Formation form a groundwater reservoir. Groundwater from the carbonate aquifer flows upwards through springs and seeps and recharges this reservoir. This

reservoir acts as a highly transmissive shallow, local alluvial aquifer that comprises at least the top 125 ft of basin fill based on well-driller's reports. The water table of this shallow alluvial reservoir is generally within a few feet of land surface. Discharge from this reservoir occurs as ET and outflow to the Muddy River.

3.4.2.2 Occurrence and Movement

Figure 3-6 is a map presenting the current conceptualization of groundwater occurrence and movement within the LWRFS. The map depicts areas of potential local recharge and primary groundwater discharge, boundary flow, and current aquifer conditions based on water-level observations collected in January, February, or March of 2019, a period when pumping is at its lowest during the year. The areas of potential recharge were approximated by areas where normal precipitation is greater than 8 in. The PRISM 800-meter normal precipitation grid was used for this purpose (Daly et al., 1994, 1997, 1998, 2008). Aquifer conditions are represented by measurements of static or near-static water-level elevations on the map (Figure 3-6). Depth-to-water and water-level elevation data are presented in Table A-1 (Appendix A). The existing well data are insufficient for the development of potentiometric contour maps. Thus, the discussion is based on the well data presented in this section, supplemented by information from previous interpretive reports.

As stated above, within the LWRFS, groundwater occurs in basin-fill and carbonate-rock aquifers. Within many of the LWRFS basins, groundwater in the basin fill occurs at great depths, or as perched systems as is the case in the extreme northern area of Coyote Spring Valley (Eakin, 1964). The alluvial reservoir of the MRSA constitutes an exception in the LWRFS. Depth to water within the basin fill ranges between about 7 ft bgs (03/19/2019) at well LDS-East in the MRSA to about 751 ft bgs (02/06/2019) at the CSV3011M well in Coyote Spring Valley (Appendix A). The shallower depths to water occur within the alluvial reservoir, downgradient from the Muddy River springs. The greater depths to water in the basin fill occur in northern and southern Coyote Spring Valley. Groundwater also occurs at substantial depths in other basins of the LWRFS. For example, the Byron Well completed in the basin fill within California Wash basin has a depth to water of about 238 ft bgs (03/06/2019) (Appendix A).

Depth to groundwater within the carbonate aquifer varies significantly. In general, depth to water is near the surface in the MRSA and much deeper in the other basins. A better understanding of the deeper groundwater that occurs in the carbonate aquifer was developed based on the water-level responses, which are discussed in greater detail in Section 5.0. The responses depend on the relative locations of the wells with respect to the range-front faults located at the base of the mountain ranges (Figure 3-1). These faults have created structural basins where most of the wells are located.

Within the Coyote Spring Valley structural basin, water-level elevations are higher in the northern portion of the valley and decrease to the south. Wells located within the structural blocks of the mountain ranges are significantly higher (e.g., CSVM-3 and CSVM-5). Well CSVM-3, which has a depth to water of 445 ft bgs (02/06/2019), is located to the far north of the valley and within a different structural block composing the southern Delamar Mountains. Water-level elevations in this structural block are greater than 320-ft higher than those observed in wells CSVM-4 and KMW-1 to the southeast that are completed within the Kane Spring Wash fault zone. Well CSVM-5 is located high off the valley floor and within the structural block of the Sheep Range and has a depth to water

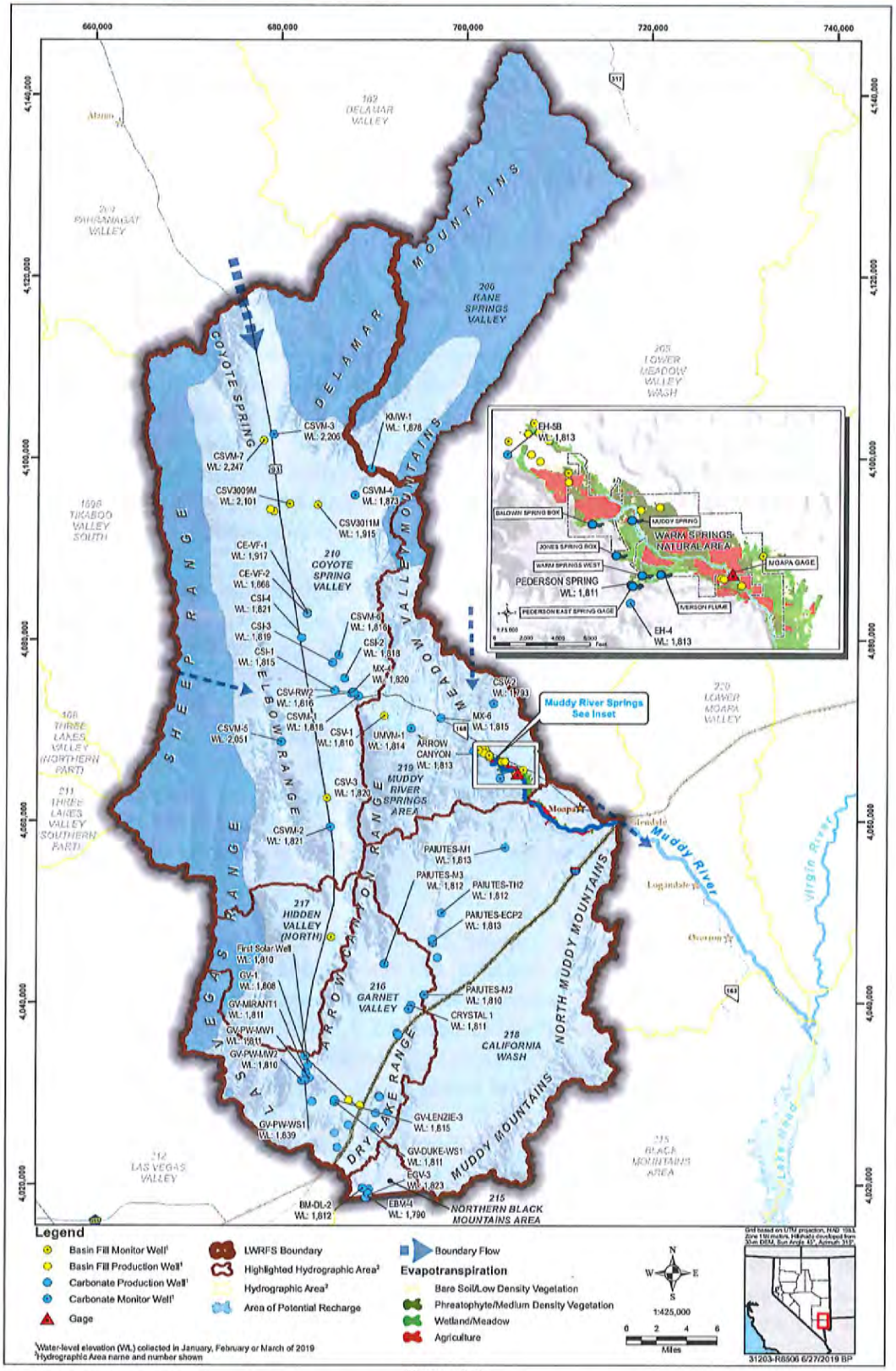

Figure 3-6
Conceptualization of the Lower White River Flow System

of 1,080 ft bgs (02/05/2019). At the CSVM-5 site, the Gass Peak thrust fault has influenced the geologic setting by causing the bedding orientation of the carbonate strata to be nearly vertical at the surface. Except for these two wells, water levels throughout the LWRFS respond in the same manner. This indicates a high-degree of hydraulic continuity between the structural basins of the LWRFS.

Based on the well data described in this section and presented in Figure 3-6 and Appendix A, the minimum depth to water measured within the connected portion of the carbonate aquifer was about 32 ft bgs (03/19/2019) measured at well EH-5B in the MRSA. The maximum depth to water of about 970 ft bgs (03/12/2019) was measured at well CSVM-4 in northern Coyote Springs Valley. Depth-to-water measurements in Garnet Valley range from about 261 to 884 ft bgs, all measured in early 2019. Despite the large differences in depth to water across the LWRFS, groundwater elevations in the carbonate aquifer near the center of the valleys only vary by approximately six feet between central Coyote Spring Valley, and Garnet Valley and Black Mountains Area to the south, and the MRSA and California Wash to the east. These minor differences in groundwater elevation across such a broad area are indicative of a high degree of hydraulic connection as demonstrated by the results of the NSE Order 1169 aquifer test.

In general, groundwater flows from areas of recharge at high elevations to discharge areas at lower elevations. The ssource of recharge to the carbonate aquifer underlying the LWRFS is a combination of regional groundwater inflow from the upper portion of the WRFS including Pahranagat, Delamar, and Kane Springs valleys; and from local recharge in the mountain ranges bounding the LWRFS (Figure 3-6). The potential areas of local recharge shown on the map are approximated by areas where annual precipitation is greater than 8 in. Such areas occur mainly on the higher elevations of the Delamar Mountains in Kane Springs Valley and northern Coyote Spring Valley, and the Sheep Range along the western boundary of Coyote Spring Valley. Within the LWRFS, natural groundwater discharge occurs through springs and seeps, ET from riparian and phreatophytic vegetation, leakage to gaining streams of the Muddy River, and by surface and subsurface outflow (Figure 3-6). Most of this natural discharge occurs within the MRSA where groundwater contributing to the headwaters of the Muddy River leaves the flow system in the form of surface water along this stream. A portion of the groundwater bypassing the MRSA rejoins the Muddy River below the MR Moapa Gage; whereas, any remainder likely flows to the Colorado River through the subsurface (SNWA, 2009a; Burns and Drici, 2011).

4.0 NATURAL AND ANTHROPOGENIC STRESSES

Groundwater levels, spring discharges, and perennial streamflow in the LWRFS are affected by many natural and anthropogenic stresses. The effects of these stresses depend on their magnitude, duration, and frequency, and can be classified as short- or long-term.

4.1 Natural Stresses

Natural stresses on a given hydrologic system include precipitation, air temperature, barometric pressure, earth tides, and earthquakes. Barometric pressure, earth tides, and earthquakes are short-term effects and are not given further consideration in this analysis. Air temperature, which is a controlling factor of ET, changes seasonally causing seasonal fluctuations in ET which may affect groundwater levels and discharge. In the LWRFS and its tributary basins, precipitation is the main source of recharge and is, therefore, the main driver of its hydrology. The LWRFS is within the Nevada Extreme Southern climate zone (Division 4) as defined by the National Oceanic and Atmospheric Administration's (NOAA) Climate Divisional Database (Figure 4-1).

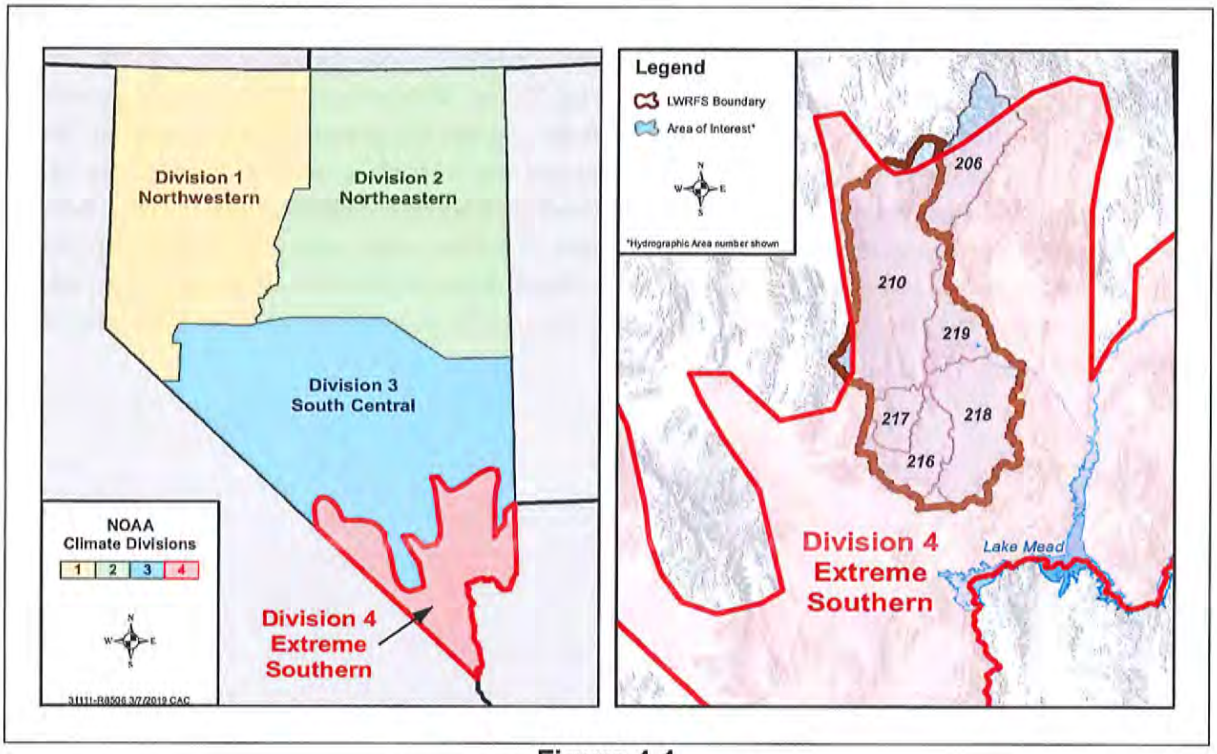

Figure 4-1
Nevada Division 4 Climate Zone

Divisional climate data are reported as average monthly values derived from daily climate observations within each climate division. Precipitation and air temperature data are of particular importance to the hydrology of the area of interest and were obtained from the on-line database (NOAA, 2019). Changes in precipitation can cause both short- and long-term effects in the groundwater levels and discharge from the area.

Annual precipitation data within Nevada Division 4 was compiled for the period 1895 to 2019. Winter precipitation in the LWRFS is understood to be the dominant source of local recharge. Winograd et al. (1998) demonstrated that winter precipitation (October through June) in the Spring Mountains of southern Nevada comprised two-thirds of the total precipitation for the area and was responsible for the majority of recharge to the hydrologic system, with summer precipitation comprising only a small fraction (perhaps 10 percent) of the recharge.

Division 4 winter-season precipitation, defined as the total precipitation occurring during the months of October through March, was used for the analyses presented in this report. These months were selected because most precipitation occurring during the warmer months (April through September) evaporates or is consumed by vegetation due to the high rates of potential ET, averaging 7.27 (ft/yr) from 2001 to 2012 at Overton, Nevada (Huntington et al., 2013). These rates are largely dependent upon air temperature. Based on the Division 4 period of record, the high temperatures for the months of April through September ranged from 64.1 to 104.4°F, averaging 89.9°F, while during the months of October through March, they ranged from 37.5 to 86.3°F, averaging 62.7°F. Figure 4-2 depicts the winter-season precipitation (October through March) from 1895 to 2019 with the data indicating a slight positive slope, or essentially no significant trend.

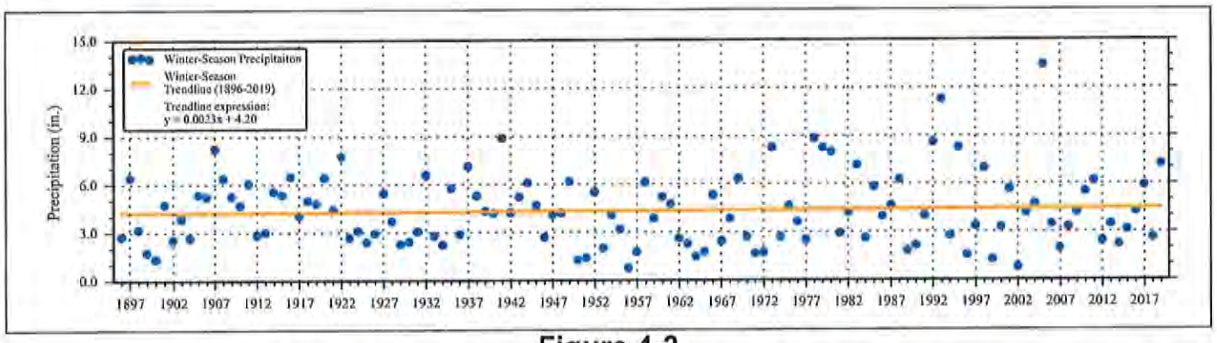

Figure 4-2
Climate Division 4 Precipitation with Trendline

Annual precipitation data were analyzed for the period 1990 to 2019, which is the period for which complete data sets are available for other LWRFS hydrologic and water-use records. Figure 4-3 presents the annual total precipitation as winter-season (October through March) and summer-season (April through September) totals. During this period, the winter- and summer-season precipitation averaged 4.60 and 2.58 in., respectively.

Precipitation data were evaluated by computing the annual percent of winter-season average for the period analyzed. These values are presented in Figure 4-3, with positive values (blue bars) representing above-average precipitation and negative values (red bars) representing below-average precipitation. There are several observations that can be made from Figure 4-3:

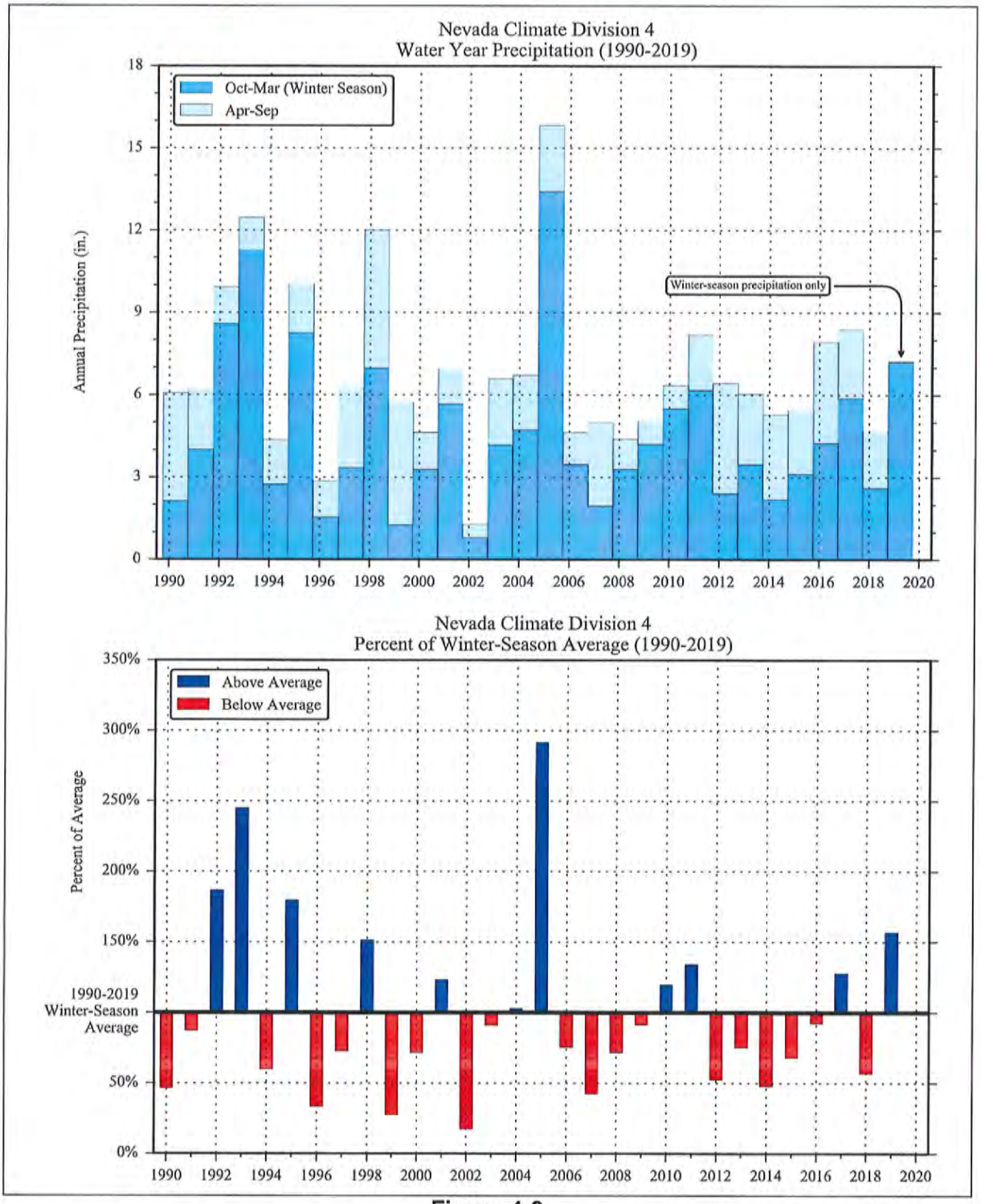

Figure 4-3
Nevada Climate Division 4 Precipitation

SE ROA 34385

JA_6983

- Winter seasons of 1992, 1993, 1995, and 2005 were extraordinarily high, with values of 190, 250, 183 and 297 percent of average, respectively.
- Winter seasons of 1996, 1999, and 2002 were extraordinarily low, with values of 34, 28, and 18 percent of average, respectively.
- The period from 2006 through 2019 was mostly below average, with 10 of the 14 seasons below average.

4.2 Anthropogenic Stresses

The primary anthropogenic stresses that have influenced surface-water and groundwater conditions within the LWRFS include surface-water diversions above the MR Moapa gage, groundwater production from both the regional carbonate aquifer and MRSA alluvial reservoir, and land use. These stresses have occurred over different time periods and durations. Records of surface-water diversions, groundwater production, and groundwater levels were compiled from all available sources for the entire LWRFS. Historical information on MRSA land use and water development was assembled from the literature. The following sections present time-series data for MRSA surface-water diversions (see Figure 3-2 for locations) and groundwater production from the regional carbonate aquifer and the MRSA alluvial reservoir. The sources of data were described in Section 2.0.

4.2.1 Surface-Water Diversions above Muddy River near Moapa, NV Gage

There are three primary surface-water diversions above the MR Moapa gage that are of significance to this assessment. These are the MVWD diversions at the Pipeline-Jones and Baldwin springs, and the NVE Muddy River diversion directly above the gage. The locations of the diversions are depicted in Figure 3-2. The MVWD has diverted spring flow from the Pipeline-Jones and Baldwin springs since 1959 and 1975, respectively. Diversions by NVE began in 1968 when the agency started leasing decreed Muddy River water rights from the MVIC. The MVWD diversions supply water to users within the MVWD service area, primarily outside the MRSA. The NVE diversions were historically exported out of the MRSA to supply industrial uses at the Reid Gardner Generating Station in the California Wash basin. In addition, SNWA owns and leases surface-water rights above the gage, but water associated with the majority of these rights is not diverted and eventually flows into the Colorado River and Lake Mead for Tributary Conservation Intentionally Created Surplus (ICS) credits as discussed in detail in Section 7.0.

Detailed records of surface-water diversions by NVE and MVWD began in 1978 and 1992, respectively, and are provided in Table B-1 of Appendix B. Historically, these two entities have been the principal surface-water diverters above the MR Moapa gage. With the gradual closure of the Reid Gardner Generating Station, which began in 2014 and was completed in March 2017, NVE has not diverted surface water since 2015. There have been, and still are, minor diversions and uses of surface water above the gage by other water users. However, these diversions are small and no records exist to determine their quantity; therefore, they are not accounted for in this analysis. Figure 4-4 presents the historical surface-water diversions above the MR Moapa gage for the period in which records are available.

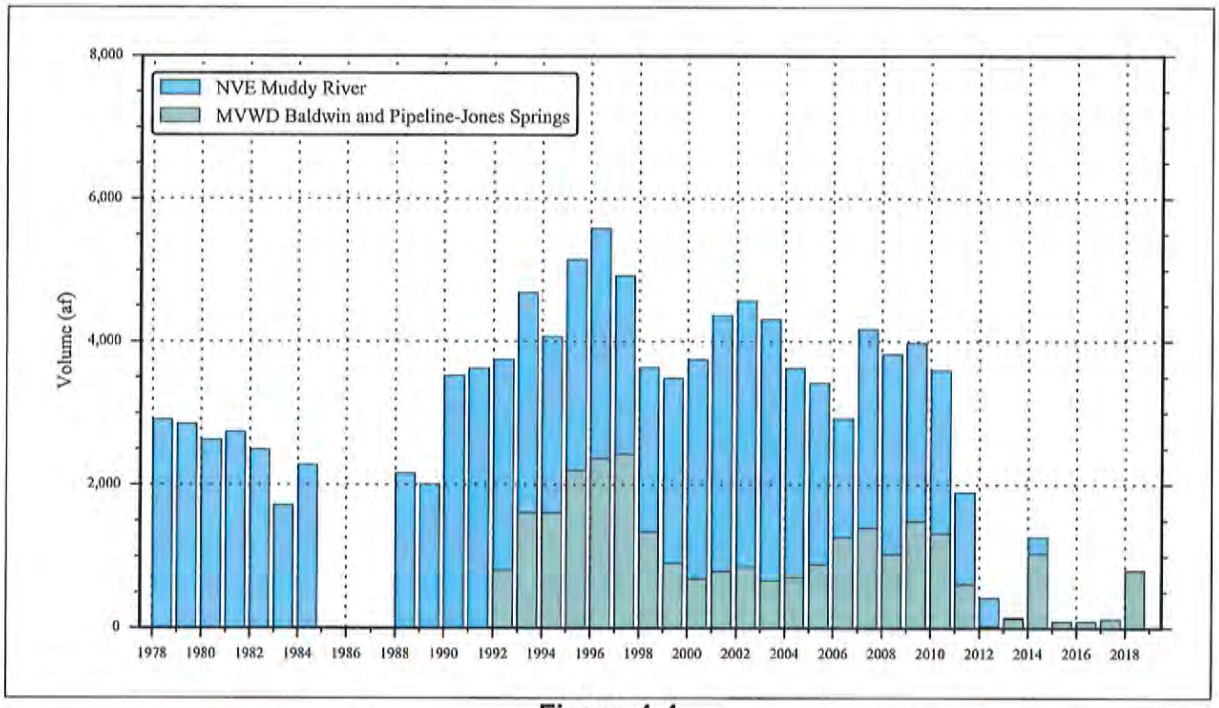

Figure 4-4
Surface-Water Diversions above the MR Moapa Gage

4.2.2 Groundwater Production

Groundwater is produced from two primary sources within the LWRFS: the MRSA alluvial reservoir and the regional carbonate aquifer underlying the six basins. As described in Section 3.4.2.2, the regional carbonate aquifer is also the source of water for the alluvial reservoir. Figure 4-5 depicts the locations of production wells within the LWRFS using symbology to differentiate between the sources (i.e., carbonate aquifer vs. basin fill). This section summarizes groundwater production from wells located within the MRSA and from wells located in the other LWRFS basins with completions in the carbonate aquifer.

4.2.2.1 Muddy River Springs Area

Groundwater production within the MRSA began around 1948 when the first well was constructed (Eakin, 1964; NDWR, 2018a). Eakin (1964) estimated groundwater production ranged from 2,000 to 3,000 af from about 12 wells completed in the alluvial reservoir as of 1964. The water was used for irrigation. Several of these wells (Lewis 1 through 5) were purchased by NVE and were used to supply water for the Reid Gardner Generating Station in the California Wash basin. NVE augmented the production from its Lewis well field using its Perkins and Behmer wells and by leasing water produced from three wells owned by the Corporation of the Presiding Bishop of the Church of Jesus Christ of Latter-Day Saints (LDS): LDS East, LDS Central, and LDS West. All of these production wells are completed to shallow depths in the alluvial reservoir ranging from 50 to 135 ft bgs. Well

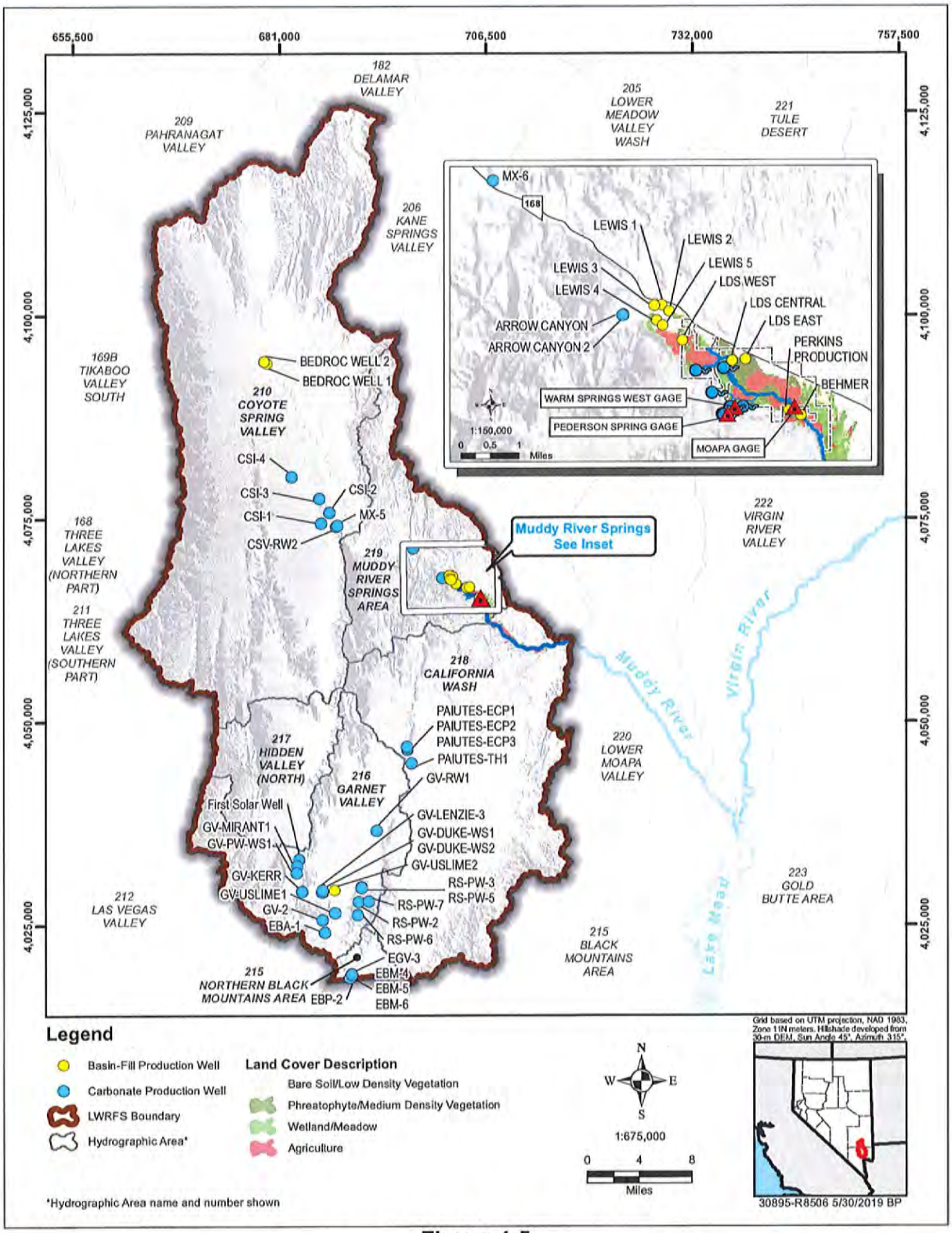

Figure 4-5
Locations of Production Wells in the LWRFS

construction details are provided in Table C-1 of Appendix C. NVE began reporting production data from these wells in 1987 (Table C-2 of Appendix C). Figure 4-6 presents the annual production from the wells grouped by well field (Lewis Wells, LDS Wells, and Perkins and Behmer wells).

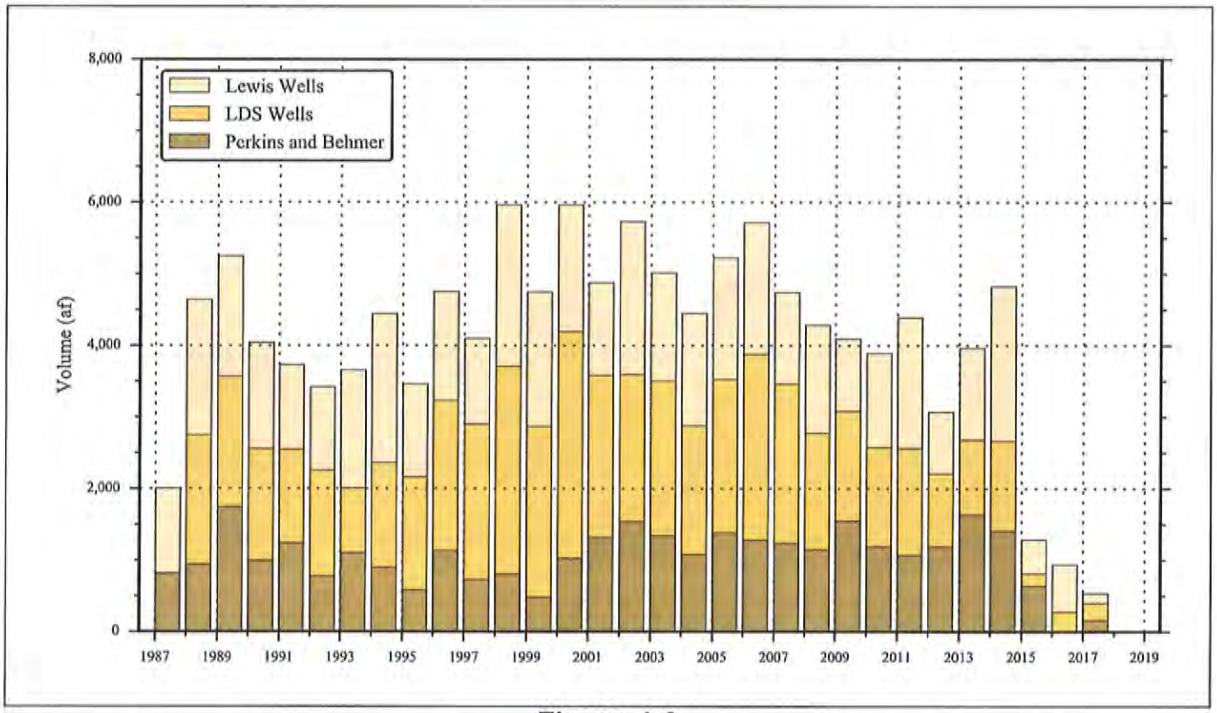

Figure 4-6
Annual Groundwater Production from the MRSA Alluvial Reservoir

Groundwater production by NVE constitutes the vast majority of production from the MRSA alluvial reservoir. However, there have been, and still are, other minor users within the area. These uses are small and no long-term records exist to determine their quantity; therefore, they were not accounted for in this analysis (2009c; 2011a and b; 2012a and b; 2013c; 2015b and c; 2016b; 2017b; 2018c; and NDWR, 2017; 2018b).

The MVWD produces groundwater from three wells completed in the regional carbonate aquifer within the MRSA. These wells, Arrow Canyon, Arrow Canyon 2, and MX-6, are located adjacent to and upgradient of the Muddy River headwaters (Figure 4-5). The wells are used to supply water for uses within the MVWD service area, primarily outside the MRSA. MVWD began reporting groundwater production totals from these wells in 1992 (Table C-2 of Appendix C). The groundwater production totals are presented in Figure 4-7 along with total production from the carbonate aquifer in the other LWRFS basins.

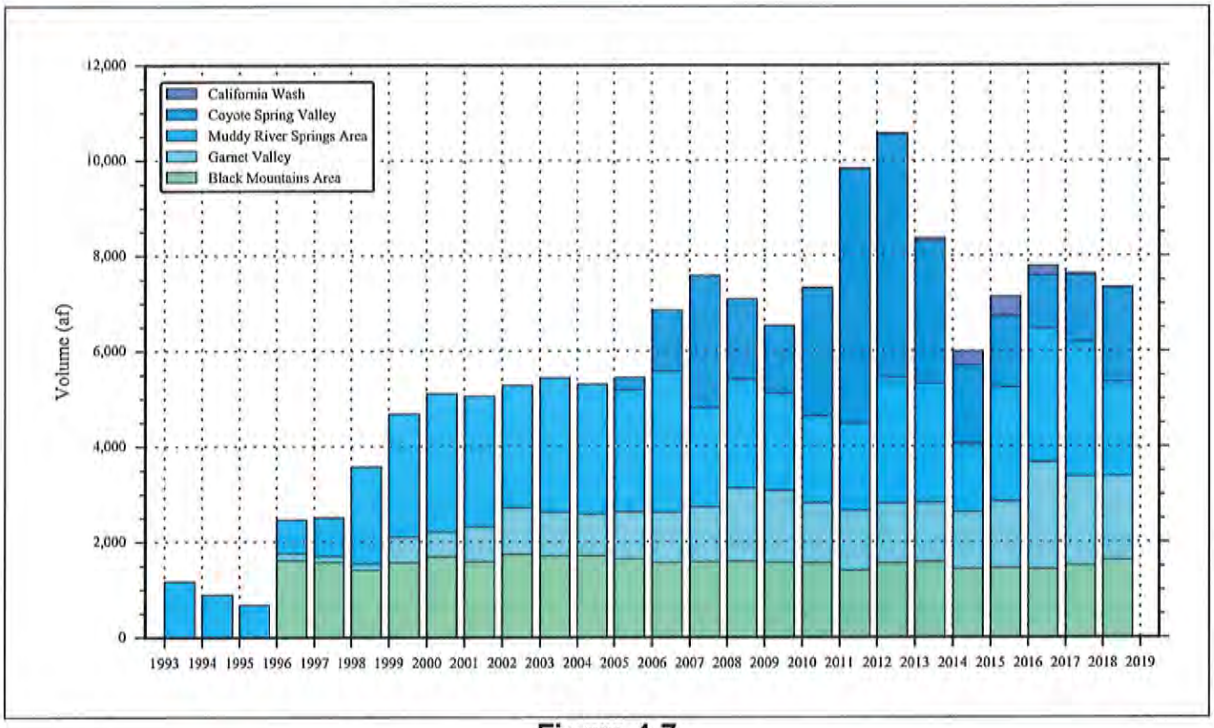

Figure 4-7
Carbonate-Aquifer Groundwater Production

4.2.2.2 *Carbonate Aquifer*

As described in Section 3.4.2.1, the LWRFS is defined by the interconnected nature of the underlying carbonate aquifer that provides hydraulic continuity between the basins. Production wells completed in the carbonate aquifer have some of the highest yields making it an attractive water-supply source. As a result, there has been significant development of the aquifer in various locations throughout the LWRFS. As stated in Section 1.0, one of the objectives of this assessment is to evaluate how the aquifer has responded to different stresses, in particular the long-term pumping stresses. This section summarizes annual groundwater production from the carbonate aquifer by LWRFS basin. The locations of the associated production wells are depicted in Figure 4-5. Site information and well construction data for these wells are provided in Table A-1 of Appendix A.

Coyote Spring Valley

Groundwater production started in 2005 when CSI began using water for construction purposes related to their Coyote Springs development. CSI has constructed four wells, CSI-1, CSI-2, CSI-3, and CSI-4, and has used them to support operation and maintenance of an 18-hole golf course and implementation of the NSE Order 1169 aquifer test. SNWA owns and operates the MX-5 well which was used as the primary production well during the NSE Order 1169 aquifer test. Annual production volumes for Coyote Spring Valley are provided in Table C-4 of Appendix C.

Garnet and Hidden Valleys

Groundwater production in Garnet Valley has predominantly been associated with mineral mining, electrical power generation, and industrial uses. There are several utility companies that lease groundwater rights owned by SNWA who have constructed production wells and operate them to supply water for industrial uses at their respective facilities. These entities report monthly production totals to SNWA who in turn reports them to NDWR on a quarterly basis. In addition, Republic Services operates several wells in support of their landfill operations in the southeast part of the valley, however, records are unavailable prior to 1999. Records for well EBA-1 are unverified for the period 1996 to 2000, and unavailable for wells GV-USLIME 1 and 2, Harvey, and GV-KERR prior to 1999. There has been no groundwater development in Hidden Valley. Annual production volumes for Garnet Valley are provided in Table C-4 of Appendix C.

Black Mountains Area

There are several wells completed in the carbonate aquifer in the northern portion of the Black Mountains Area that is a designated part of the LWRFS. Two of these wells, owned by Dry Lake Water, were constructed as production wells but have never been operational. The other wells, owned by Nevada Cogeneration Associates, have been used to supply water to a power generating station. Annual production volumes for the Black Mountains Area of the LWRFS are provided in Table C-4 of Appendix C.

California Wash

The MBOP has produced groundwater in the California Wash basin to supply municipal uses. Production has been relatively small as compared to other uses in the LWRFS. Annual production volumes for California Wash basin are provided in Table C-4 of Appendix C.

5.0 HYDROLOGIC RESPONSES

Using the time-series data compiled in Sections 3.0 and 4.0, hydrologic responses to natural and anthropogenic stresses were evaluated for the LWRFS. First, observed declines in Muddy River streamflow were evaluated. Second, responses to climate variability and carbonate-aquifer groundwater production were evaluated for representative wells in the LWRFS and high-elevation springs in the MRSA.

5.1 Evaluation of Muddy River Streamflow Declines

The Muddy River streamflow is measured near Moapa, NV as described in Section 3.4.1 and depicted in Figure 3-5. The flood-adjusted flow record was used in this analysis and compared to the average annual pre-development baseflow of 33,900 afy. By this comparison, a long-term trend of decreasing streamflow since the early 1960s was identified. The disparity between the pre-development baseflow and gage record indicates there have been factors impacting the flow over time. These may include one or more of the following: (1) climate variability, (2) changes in land use above the gage, (3) surface-water diversions above the gage, and (4) capture of spring and streamflows by production wells. These factors are evaluated in the following sections.

5.1.1 Climate Variability

To investigate the effects of climate variability on Muddy River streamflow, an evaluation of the historical precipitation record was performed. Only precipitation is considered in this analysis because it is the main climate variable affecting hydrology in the study area.

The winter-season precipitation record from 1895 to 2019 presented in Figure 4-2 was analyzed and a simple-linear regression indicated a positive slope, but essentially no trend. The precipitation record was also used to assess climate conditions before and after 1965. This year was selected to distinguish two periods of record for analysis that represented pre- and post-exports of water from the area, even though groundwater production in the MRSA had already been occurring since around 1947 (Eakin, 1964). Eakin (1964) reported that the groundwater production during this intervening period was relatively small, and had no discernible affect on the gage record.

The average annual winter-season precipitation was computed for each period and used as a metric to evaluate climate differences. The average annual winter-season precipitation was 4.17 and 4.50 in/yr, pre- and post-1965, respectively. Based on these values and because the post-1965 average is slightly higher, it is concluded that the historical trend in climate conditions have not been a primary factor causing the long-term trend of declining streamflow. The seasonal and annual variations in precipitation and temperature may, however, partly explain the short-term variability observed in the streamflow record.

5.1.2 Historical Land Use in the MRSA

Pre-development ET within the MRSA was estimated to be between 2,000 and 3,000 afy (Eakin, 1964). Land-use changes presumably have some impact on the consumptive use of water due to an increase or decrease in vegetative cover. An increase in vegetative cover would increase consumptive use, making less water available in the system. Conversely, if vegetative cover decreased, consumptive use would also decrease, and more water would be available. Examples of land-use change include:

- replacing natural vegetation with agriculture lands
- fallowing agricultural lands
- restoring natural landscapes (e.g., removal of palm trees and replacing with natural vegetation)
- fires
- stream restoration

To evaluate conditions in the MRSA and the influence of land-use changes in the early 2000s, SNWA funded the Desert Research Institute to compile and analyze satellite imagery and associated vegetation indices to estimate ET for the period 2001 through 2012 (Huntington et al., 2013). The main objectives of the study were "*to identify trends in ET over the study period of 2001-2012 to identify potential impact on ET due to land management and vegetation changes (Huntigton et al., 2013)*". The study area encompassed the spring complexes, agricultural lands, and phreatophytes within the Muddy River headwaters, where most of the changes have occurred.

The study applied two methods to derive ET estimates. The first method used Mapping EvapoTranspiration at high Resolution with Internalized Calibration (METRIC), and the second used the Normalized Difference Vegetation Index (NDVI). Both methods relied upon Landsat multispectral data. Precipitation was subtracted from the ET estimates to yield results that are more comparable from one year to the next, and also allow for the evaluation of changes independent of precipitation influences.

The study results for each method are presented in Figure 5-1 which depicts the annual ET reduced by annual precipitation for the study period. High and low values are observed in the estimates from both methods and correspond with observed conditions that would be expected to have an impact on ET rates in the area. The high estimate of 2005 is associated with increased vegetation density due to above normal precipitation. Even though the precipitation falling directly on the ET area was subtracted from the ET volume, the effects of the extraordinarily large precipitation of 2005 can be seen in Figure 5-1. These effects are due to the increased recharge resulting from the extraordinary precipitation that raised groundwater levels; thereby, increasing water availability to vegetation in the area. During 2004-2005, precipitation was about 300 percent of the 2001-2012 average. The low estimate of 2010 is associated with a major fire that burned more than 600 acres. During the years analyzed, other more gradual and subtle changes occurred involving landscape restoration and the removal of palm trees and weeds in the Warm Springs Natural Area. These changes may have contributed to the decline observed over the analysis period.

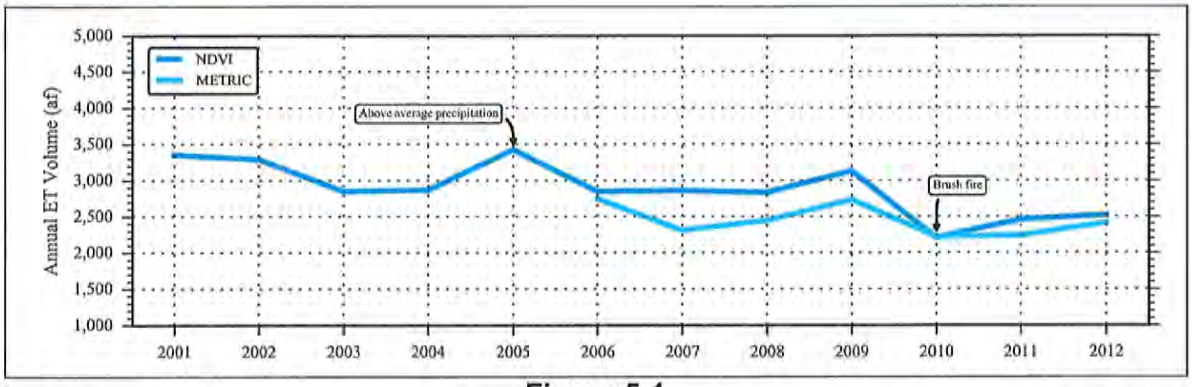

Figure 5-1
Annual ET Reduced by Precipitation for Muddy River Springs Area (2001 - 2012)

Although there were land-use changes observed during the years analyzed, the range of ET estimates closely aligns with the pre-development estimate of Eakin (1964). Estimates ranged from about 2,200 to 3,400 afy, and the estimates declined over the period of analysis by about 600 to 900 afy based on the METRIC and NDVI methods, respectively. These changes are relatively small compared to the measured flow of the Muddy River and appear to be within the range of seasonal variability observed during the period of pre-development baseflow from 1945 to 1955 (Figure 3-5).

5.1.3 MRSA Surface-Water Diversions

A natural-flow record was constructed for the period 1993 through 2018 by adding the total annual diversions above the MR Moapa gage to the flood-adjusted record (Figure 5-2). This period of record was selected because diversion data for the years prior to 1993 were incomplete or based on estimated values as opposed to metered records.

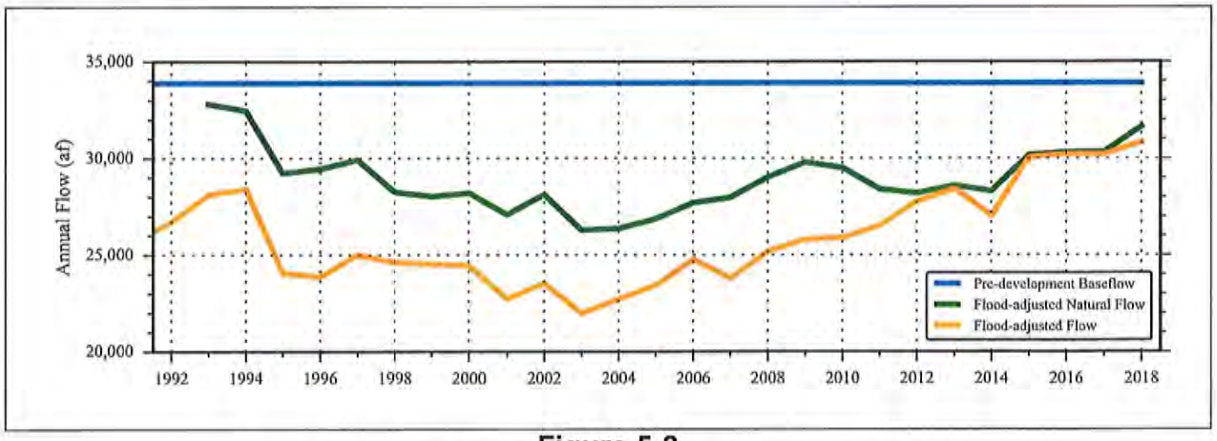

Figure 5-2
Natural Flow Record at MR Moapa Gage (1993 - 2018)

The diversion data used to construct the natural flow record include the MVWD diversions at Baldwin and Pipeline-Jones springs and the NVE diversion directly above the gage (Figure 4-4).

Water associated with these diversions was exported out of the basin to supply municipal uses within the MVWD service area and NVE industrial uses in California Wash basin. Figure 5-2 compares the natural flow record to the pre-development baseflow flow of 33,900 afy. Long-term climate variability and MRSA land-use were determined not to be primary factors causing the long-term trend of declining streamflow. Therefore, the difference between the pre-development baseflow and the natural flow record must be mostly associated with groundwater production within the MRSA.

5.1.4 MRSA Groundwater Production

MRSA groundwater production and its influence on Muddy River streamflow was evaluated by quantifying the difference between the pre-development baseflow, 33,900 afy, and the natural flow record (hereinafter referred to as the "MR Flow Deficit" depicted in Figure 5-3), and determining whether the difference and source of the deficit is equivalent to the annual groundwater production within the MRSA. Like the surface-water diversion data, groundwater-production records from 1993 through 2018 were used in the analysis.

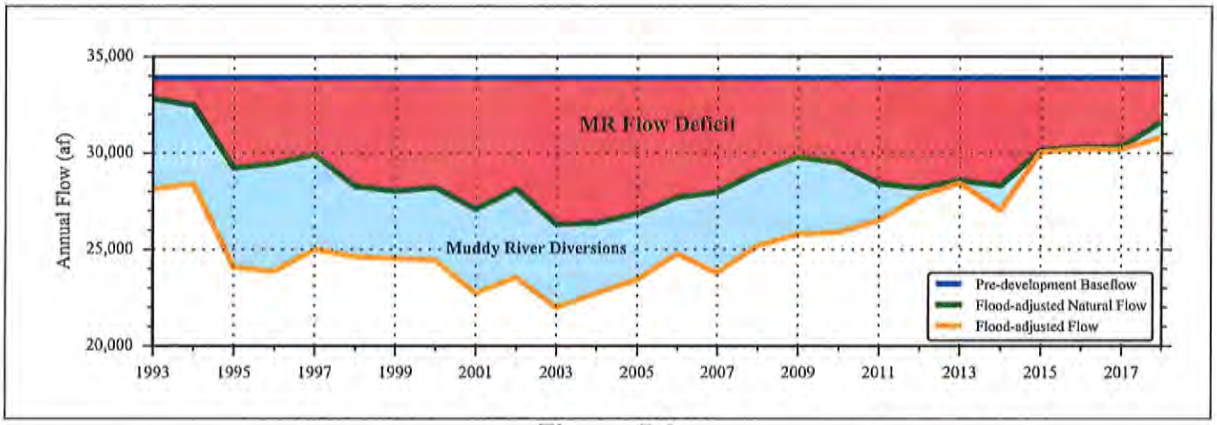

Figure 5-3
MR Flow Deficit (1993 - 2018)

As described in Section 4.2.2.1, there are several alluvial wells in the MRSA that are completed to shallow depths within the headwaters of the Muddy River. NVE has operated these wells to supply water for industrial uses in California Wash basin. Operation of the wells creates cones of depression that induce flow to the wells, capturing water from alluvial-reservoir storage, springs, and seeps on the valley floor, and gaining stream reaches above the gage. Conceptually, the wells capture water that would otherwise compose the flows measured at the gage during pre-development conditions. The locations of these wells and their historical production are presented in Figures 4-5 and 4-6, respectively.

In addition to the shallow alluvial wells operated by NVE, MVWD operates three municipal wells within the MRSA and northwest of the alluvial basin (i.e., Arrow Canyon, Arrow Canyon 2, and MX-6). These wells produce groundwater to supply municipal uses within the MVWD service area, but primarily to locations outside the MRSA. The locations of these wells and their historical production are presented in Figure 4-5 and 4-7, respectively.

Figure 5-4 presents a time-series chart of the annual MR Flow Deficit and MRSA groundwater production. Production from two wells, Perkins and Behmer, was excluded from the total because of their location in proximity to the MR Moapa gage. These wells are located downstream of the gage and are unlikely to influence the streamflow above the gage. As Figure 5-4 illustrates, groundwater production within the MRSA appears to fully account for the MR Flow Deficit observed for the period of analysis. Included on the chart is groundwater production by CSI and SNWA from production wells located farther away within Coyote Spring Valley and upgradient of the MRSA.

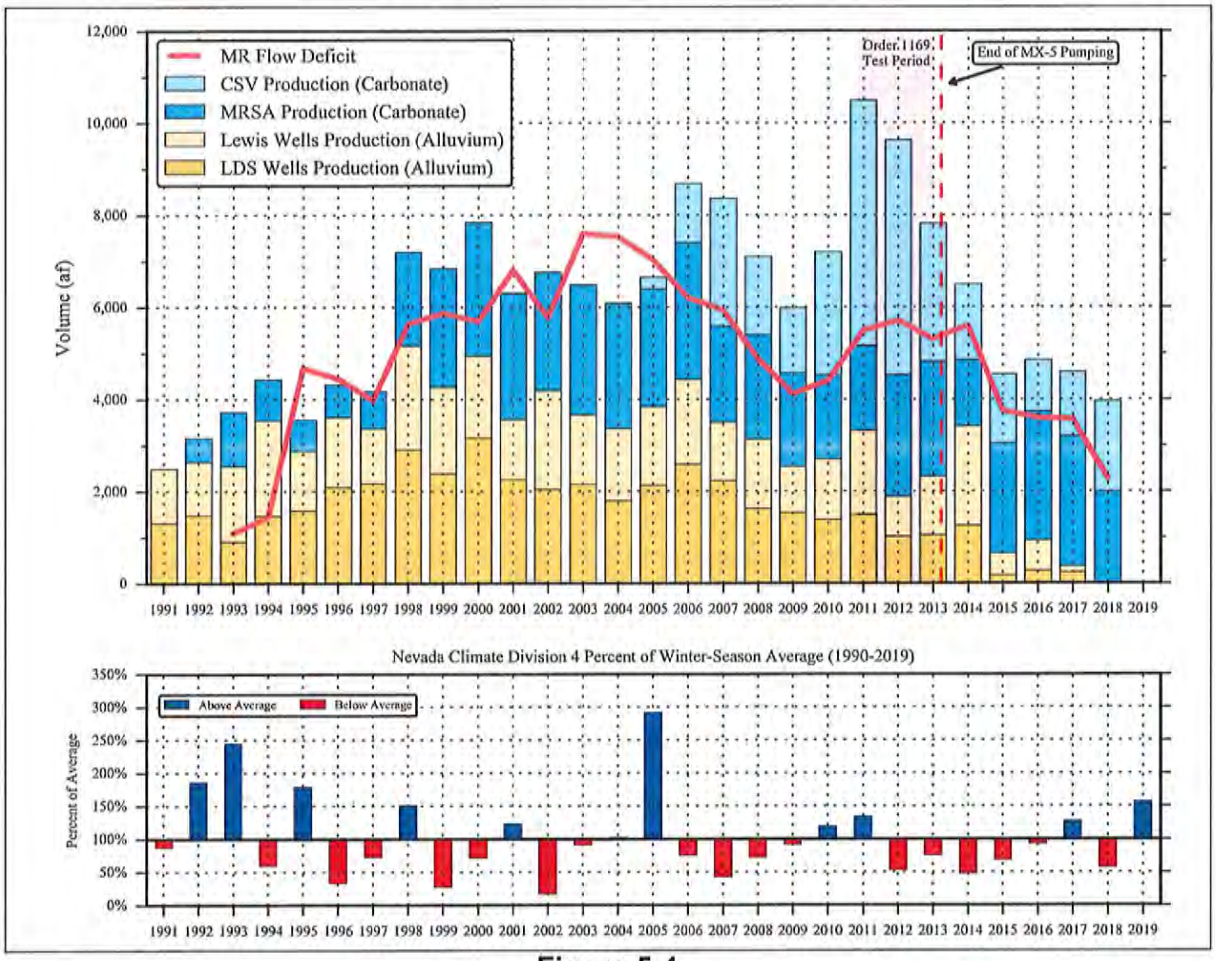

Figure 5-4
MR Flow Deficit and Coyote Spring Valley and MRSA Groundwater Production

There are certain years when the MR Flow Deficit appears to be too low (1993 and 1994) or too high (2003 and 2004) with respect to the annual groundwater production. This can be explained, in part, by the fluctuations in Muddy River streamflow caused by short-term variability in climate conditions as compared to the constant pre-development baseflow. During years of above average flow, the MR Deficit is apparently low because the difference between the pre-development baseflow and the above-average streamflow is smaller. Conversely, in years that the streamflow is below average, the MR Flow Deficit is apparently high because the difference is larger.

Regardless of the streamflow variability, the results of this analysis conclusively demonstrate the prominent impacts MRSA groundwater production has on MR streamflow. Groundwater production from the MRSA alluvial reservoir depletes MR streamflow on a 1:1 basis because the production wells are located within the MR headwaters and capture water that would otherwise flow into the river and past the MR Moapa gage. This is supported by the fact the production volumes fall beneath the MR Flow Deficit line as depicted in Figure 5-4. In similar fashion, MRSA production wells completed in the carbonate aquifer capture water that would otherwise replenish the alluvial reservoir through diffuse subsurface flow or contribute to MR streamflow via discrete springs. Capturing this groundwater ultimately depletes the source of supply to the alluvial reservoir and springs; thereby, depleting the MR streamflow. Based on the accounting depicted in Figure 5-4, the MRSA carbonate production wells have depleted MR streamflow approaching a 1:1 basis.

5.2 Carbonate-Aquifer Responses to Climate Variability and Pumping Stresses

Throughout the LWRFS, there are many groundwater sites that are monitored and provide information on groundwater conditions regarding the carbonate aquifer. These sites include production and monitor wells completed in the carbonate aquifer and various springs in the MRSA. In this section, a comparison of the hydrologic responses at selected wells and springs representative of the carbonate aquifer is presented. The comparison is followed by an analysis of the responses to climate variability and groundwater production.

5.2.1 Comparison of Hydrologic Responses

The comparison of the hydrologic responses at selected wells and springs representative of the carbonate aquifer was performed first by a visual examination of the hydrographs. Second, where correlations appear to exist, they were further analyzed, quantified and interpreted.

Time-series charts of water-level data for representative carbonate wells located in each of the basins composing the LWRFS were constructed and are presented in Figure 5-5 for wells CSVM-1, EH-4, PAIUTES-TH2, GV-1, and BM-DL-2. Based on a review of all of the data, most hydrographs exhibit very similar patterns. The only apparent exception is within Coyote Spring Valley for wells CSVM-3, CSVM-4, and CSVM-5, and within Kane Springs Valley for well KMW-1. Wells CSVM-3 and CSVM-5 are different because of their geologic setting and completion in the upthrown structural blocks of the southern Delamar Mountains and Sheep Range, respectively, as described in Section 3.4.2. Wells CSVM-4 and KMW-1 are completed within the Kane Springs fault zone. Time-series charts for these four wells are presented in Figure 5-6. The hydrograph for well CSVM-1 is included for comparison. As Figure 5-6 illustrates, the responses observed in CSVM-3 and CSVM-5 are distinctly different. The responses of wells CSVM-4 and KMW-1 are similar to those of other wells in the basin, but appear to be slightly attenuated by the Kane Springs fault.

Time-series charts of discharge data for springs located in the MRSA discharge area were constructed and evaluated. Records at the Pederson Spring and the Warm Springs West gage are used as indicators of how changes in aquifer conditions affect discharge from the regional springs in the area. These records are described in detail in Section 4.0 and are presented in Figure 5-7 with the percent of average winter-season precipitation and groundwater production from the carbonate aquifer. The

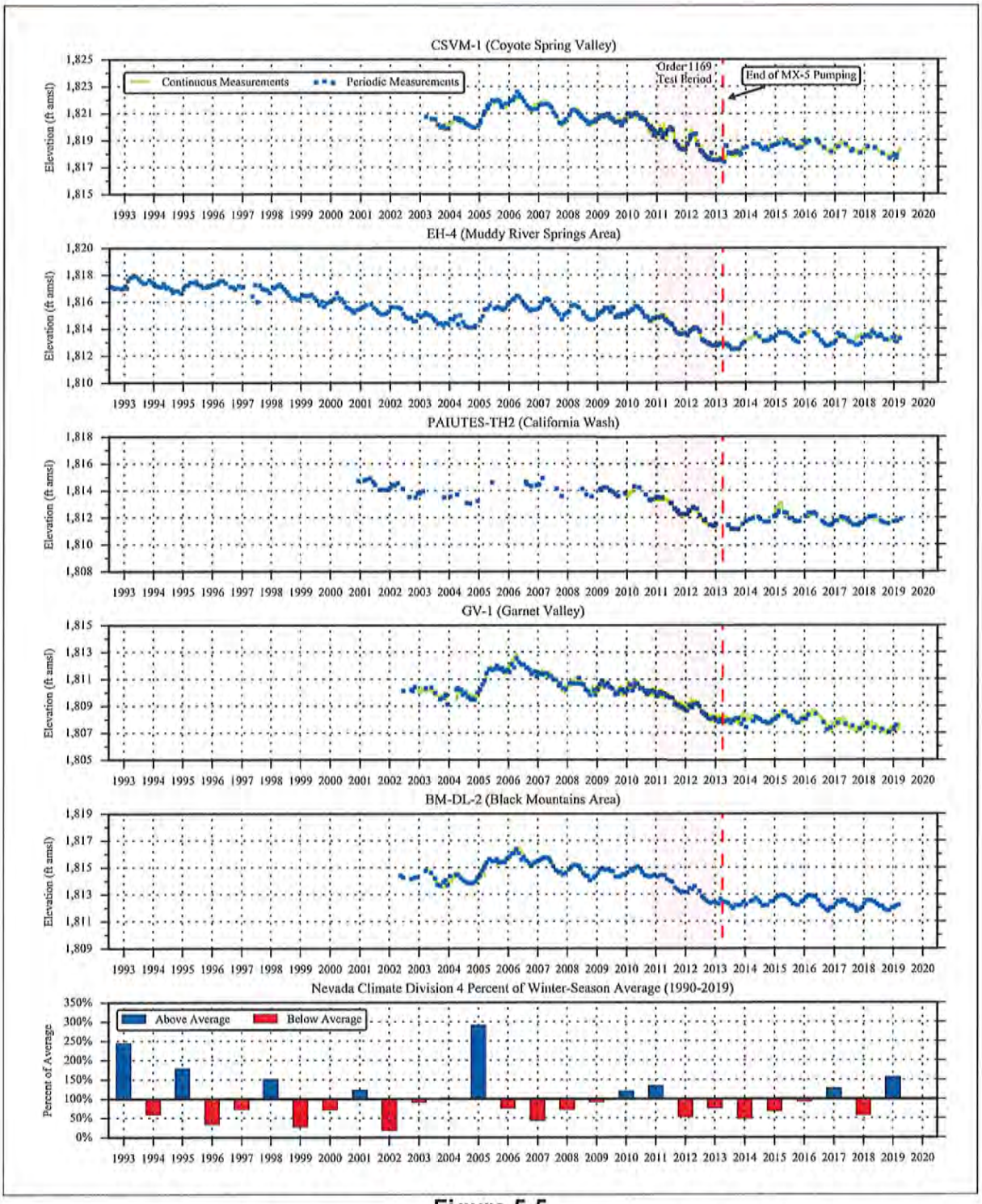

Figure 5-5
Water-Level Responses in Representative Carbonate Wells

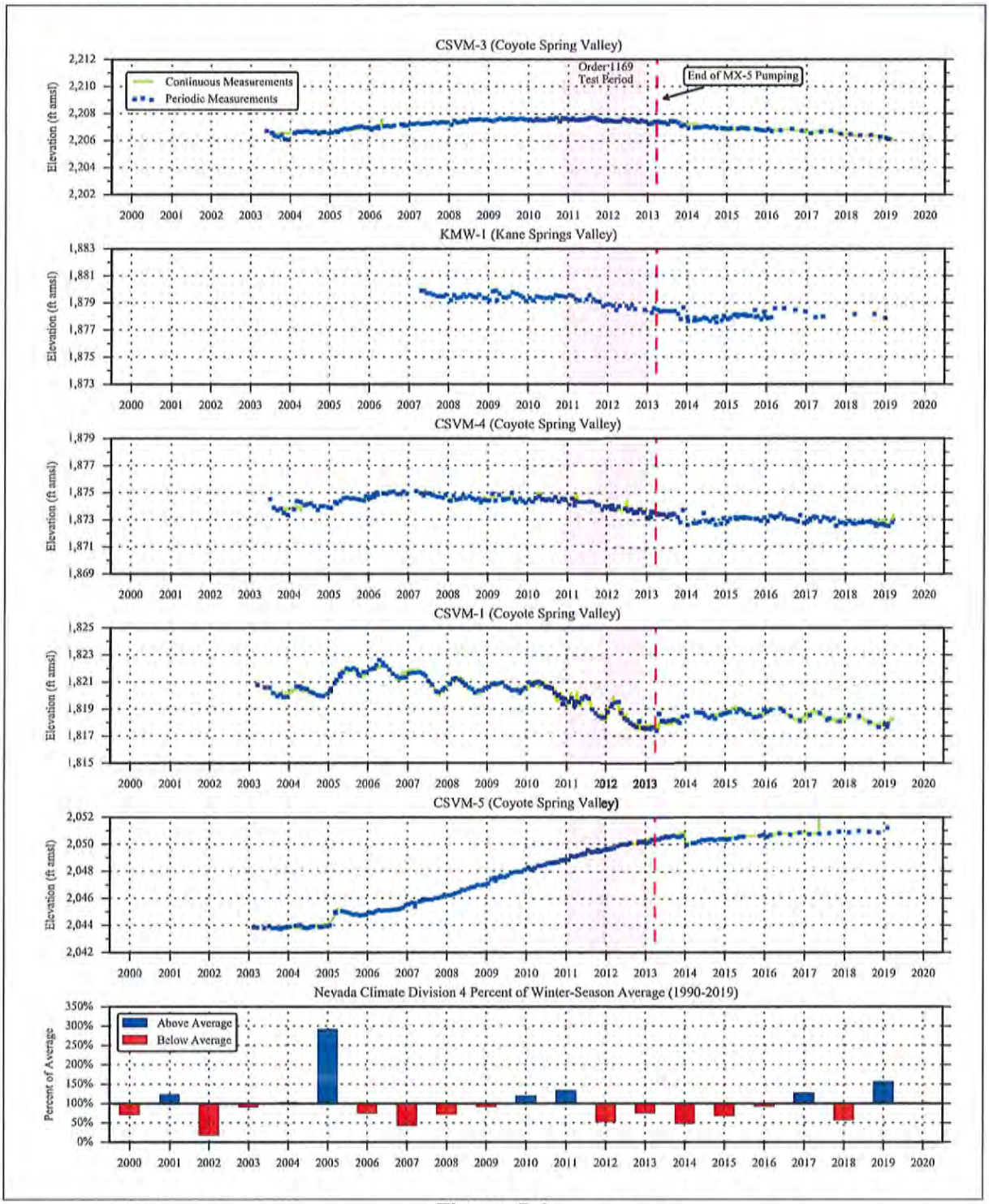

Figure 5-6
Water-Level Responses in Representative Carbonate Wells

SE ROA 34399

JA_6997

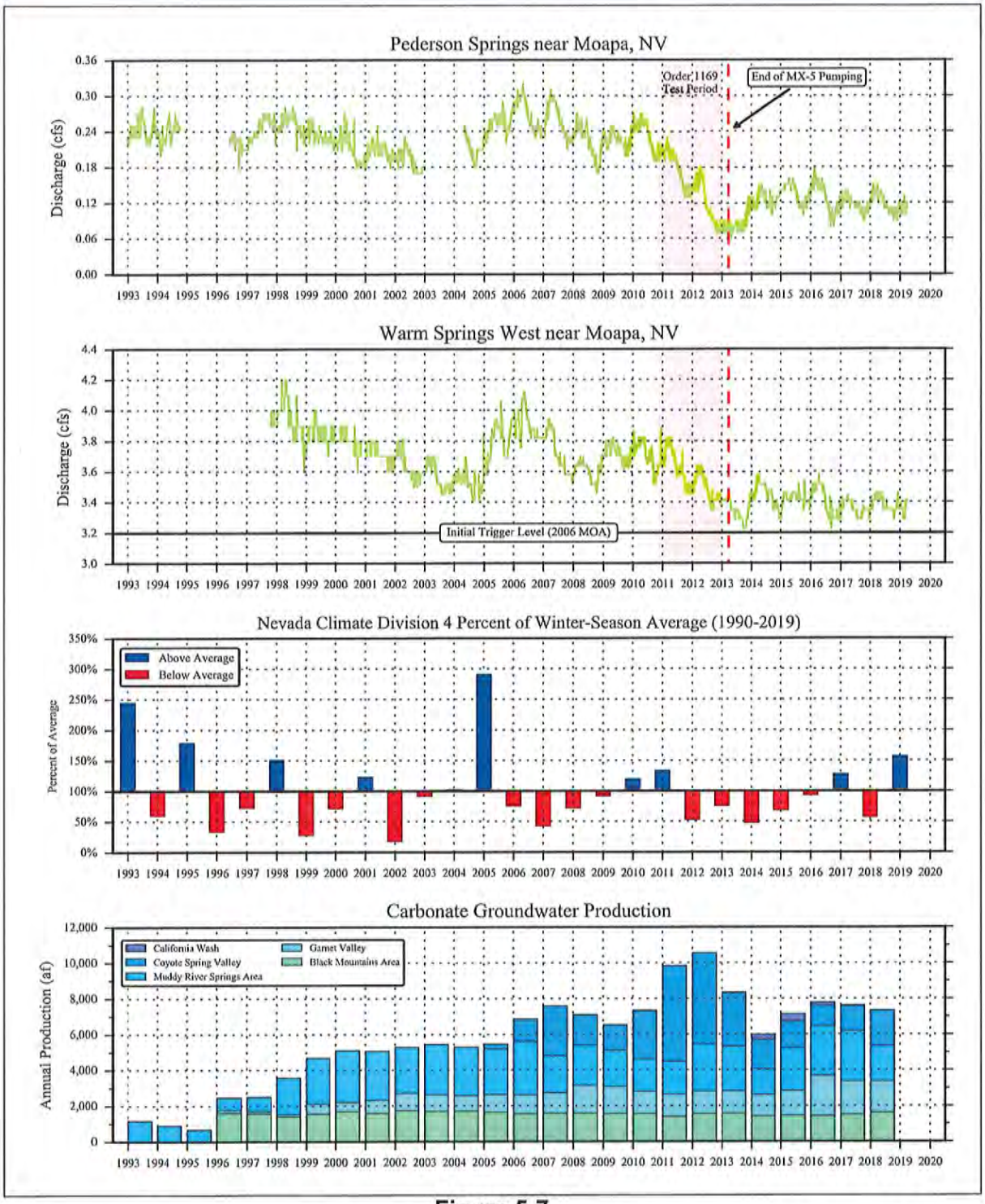

Figure 5-7
MRSA Spring Discharge and Carbonate-Aquifer Groundwater Production

SE ROA 34400

JA_6998

gage records respond in the same manner as the interconnected carbonate-aquifer water levels shown in Figure 5-5. A similar response was expected because it is known that the carbonate aquifer is the source of the spring discharge. The connection was further confirmed by a quantifying the correlation between aquifer levels and spring discharge.

The correlation between the hydraulic head in the carbonate aquifer and spring discharge can easily be derived using the data available for selected wells and springs. Carbonate well EH-4 located in the MRSA was selected to represent the hydraulic head in the carbonate aquifer. Correlations between EH-4 water-level elevations (i.e., hydraulic head) and the discharge records from the Pederson Spring and Warm Springs West gages were analyzed. Using the continuous data records, average monthly values were derived for both the hydraulic head and discharge. For Pederson Spring, the period from 2004 to 2018 was used, excluding previous years during which the record was compromised as described in Section 3.4.1. For the Warm Springs West gage, the period from 1997 to 2018 was used. The discharge data were plotted against the hydraulic head data and the results are presented in Figures 5-8 and 5-9 for Pederson Spring and Warm Springs West gages, respectively. As expected, the relationships between discharge and carbonate head are linear with very high correlations, R^2=0.97 for Pederson Spring and R^2=0.89 for the Warm Springs West gage. The high correlations also confirm that the hydraulic head in the carbonate aquifer is the main driver of spring discharge for the selected springs. The scatter is most likely caused by measurement errors particularly in the spring discharge. The slopes of the straight lines indicate the correspondence between changes in EH-4 levels and spring discharge. A one-foot change in EH-4 level causes changes in discharge of about 0.058 cfs for Pederson Spring and about 0.16 cfs for the Warm Springs West gage.

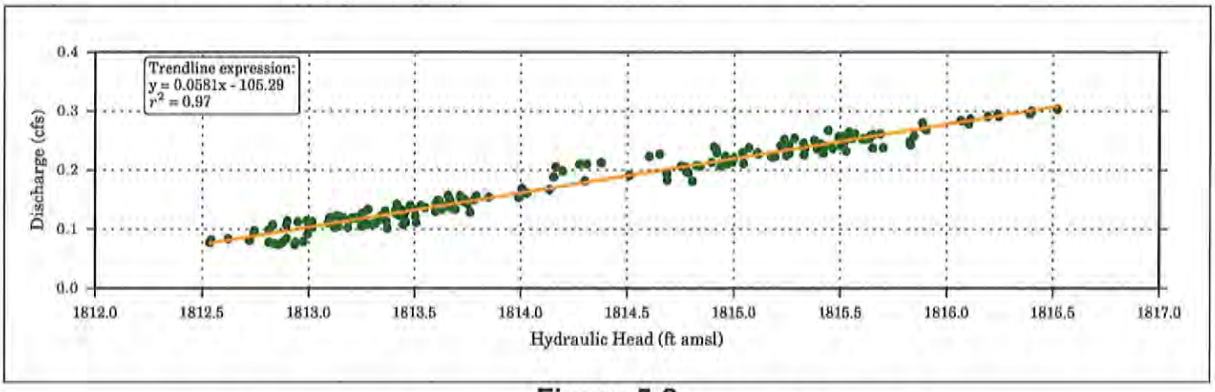

Figure 5-8
Correlation between Hydraulic Head at Well EH-4 and Discharge at Pederson Spring near Moapa, NV Gage

The USFWS developed the same relationships for Pederson Spring, Pederson East and the Warm Springs West gages using monthly data for 2002 to 2012 (USFWS et al., 2013). They separated the responses between 2 periods: 2002 to 2012 and the overlapping period of the 2-year aquifer test. The correlations they derived between spring discharge and the EH-4 hydraulic head were also very high, but also exhibited scatter most likely due to discharge measurement errors. The relationships developed using the 2-year aquifer test data had higher correlations because more accurate measurements of discharge were available for that time period (USFWS et al., 2013). These

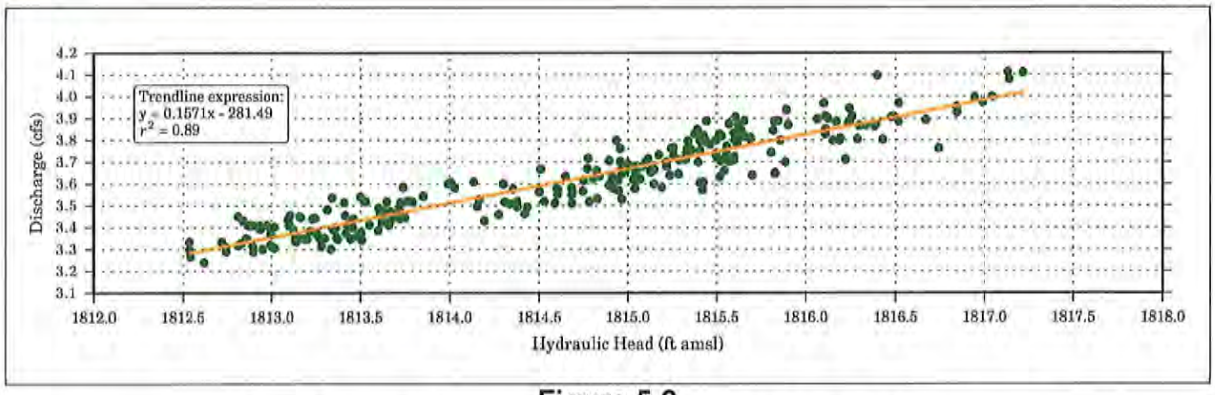

Figure 5-9
Correlation between Hydraulic Head at Well EH-4 and Discharge at Warm Springs West near Moapa Gage

relationships clearly demonstrate a direct connection between the carbonate head and spring flow for these specific sites.

Given that the EH-4/spring discharge correlations are high, it follows that the responses observed at carbonate wells could be correlated to that of EH-4 to assess if their responses are caused by the same stresses affecting the spring discharge. High correlation would also further confirm the hydraulic connectivity of the LWRFS. Correlations between water-level elevations of representative carbonate wells and well EH-4 were developed as follows. Average monthly values of hydraulic head were derived using water-level elevation records of the representative carbonate wells. The average monthly hydraulic heads of wells CSVM-1, BM-DL-2, PAIUTES-TH2, GV-1, CSVM-4 and MX-4 were plotted against EH-4 and the results are presented in Figure 5-10. EH-4 was selected as the focal carbonate well because of its long period of record, and its proximity to the MRSA discharge area. The periods used for the correlation analysis varied by well and were defined by the availability of data: PAIUTES-TH2 from 2000 to 2019, BM-DL-2 and GV-1 from 2002 to 2019, CSVM-1 from 2003 to 2019, CSVM-4 from 2003 to 2019, and MX-4 from 1987 to 2019. The relationships between the hydraulic head of carbonate wells in the LWRFS are linear and have very high correlations that range from R^2=0.82 to R^2=0.97. As these charts illustrate, groundwater levels respond in the same manner to natural and anthropogenic stresses throughout the LWRFS. The responses are indicative of a high degree of hydraulic connection within the aquifer and across all of the basins.

5.2.2 Responses to Climate Variability

Responses of selected wells and springs to climate variability were evaluated. As stated before, winter-season precipitation was the variable selected to represent climate because it is the main driver of natural recharge. The time-series charts shown in Figures 5-5, 5-6 and 5-7 are presented with precipitation data from the Nevada Division 4 as described in Section 4.1. In these figures, annual winter-season precipitation is represented as a percentage of average winter-season precipitation for the period 1990 through 2019.

The charts shown in Figures 5-5 and 5-6 illustrate the seasonal responses of groundwater levels to recharge pulses, with levels typically achieving their annual peak in April. The amplitudes of these

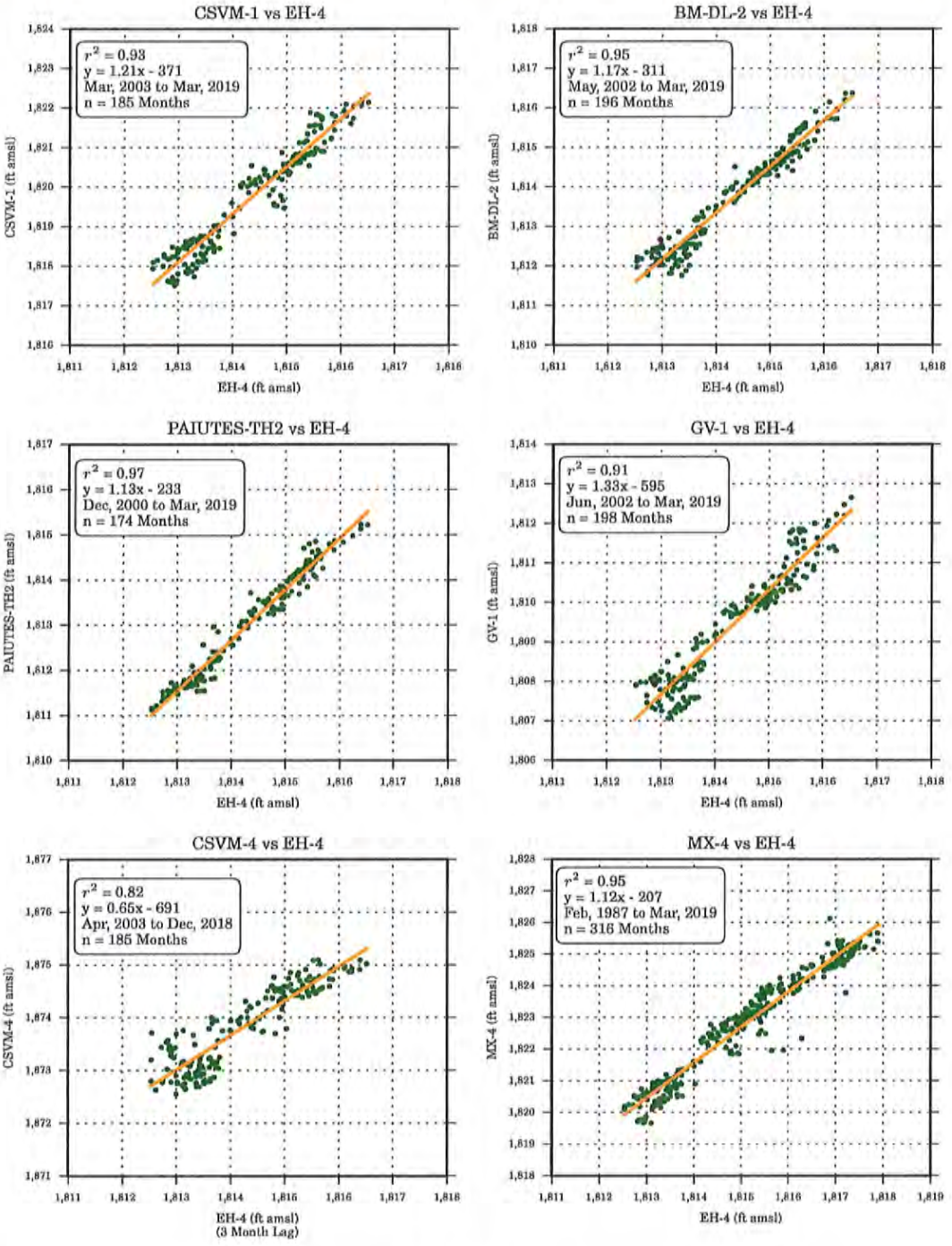

Figure 5-10
Correlation of Hydraulic Heads at Well EH-4 with Hydraulically Connected Carbonate Wells

SE ROA 34403

JA_7001

seasonal fluctuations are generally consistent except for years when the percent of average precipitation is extraordinary, like in 2004-2005. For the winter months spanning October 2004 through March 2005, winter-season precipitation was nearly 300 percent of average, the highest percentage for the 1990 to 2019 period of record. Water levels in all carbonate wells increased accordingly in 2005, and by the spring of 2006 most wells reached their period of record high. After 2006, water levels declined and appeared to stabilize from 2008 through 2010, prior to the start of the NSE Order 1169 aquifer test.

As shown in Figure 5-7, in the MRSA, the Pederson Spring and the Warm Springs West gage records respond similarly, reaching peak discharge levels in the spring of 2006 after the extraordinary precipitation during 2004-2005. Like the groundwater levels, after 2006 the spring discharge declined, then stabilized prior to the start of the NSE Order 1169 aquifer test.

5.2.3 Groundwater Production - NSE Order 1169 Aquifer Test and Recovery

The responses to pumping stresses within the LWRFS, including the 2-year aquifer test, were analyzed using the records of carbonate-aquifer groundwater production described in Section 4.2.2.2 and presented by basin in Figure 4-7. Evaluations of the LWRFS responses during the aquifer test production and recovery periods are presented in the following sections.

5.2.3.1 Production Period

In general, regional responses to local pumping stresses are difficult to discern from natural stresses in the water-level records, which typically only vary about 6 ft throughout the entire LWFRS over the various periods of record. On an annual basis, the typical seasonal fluctuations associated with recharge pulses are less than 2 ft. These seasonal responses and longer-term trends associated with climate variability mask the subtle effects of gradual changes in the relatively consistent pumping regime. Only abrupt and significant changes to the pumping regime, such as those implemented as part of the NSE Order 1169 aquifer test, cause responses that are discernible in the water-level and spring-discharge records (Figures 5-11 through 5-13). These responses and interpretations of the test results are documented in several reports that were submitted to the NSE in 2013 and summarized in Section 2.0. In summary, water-levels in the carbonate aquifer declined from 1.0 to 2.5 ft throughout the LWRFS as a result of the stresses imposed during the aquifer test.

In general, responses to groundwater production are even more difficult to discern in the spring discharge records. The measurement accuracy of the Pederson and Warm Springs West gages and the variability of discharge due to seasonal fluctuations and long-term trends associated with the carbonate aquifer make it difficult to identify responses to pumping stresses. However, responses to pumping stresses imposed during the Order 1169 aquifer test were very apparent in these records. As Figure 5-7 illustrates, by the end of the 2-year aquifer test, discharge from Pederson Spring was reduced to about one-third of its pre-test flow, from 0.21 to 0.07 cfs. Discharge measured at the Warm Springs West gage declined about 8 percent, from 3.70 to 3.41 cfs. After the test, discharge at the Warm Springs West gage continued to decline and, had the test or operation of the MX-5 well continued, the initial trigger of 3.2 cfs at the Warm Springs West gage would have been reached before the end of 2014.

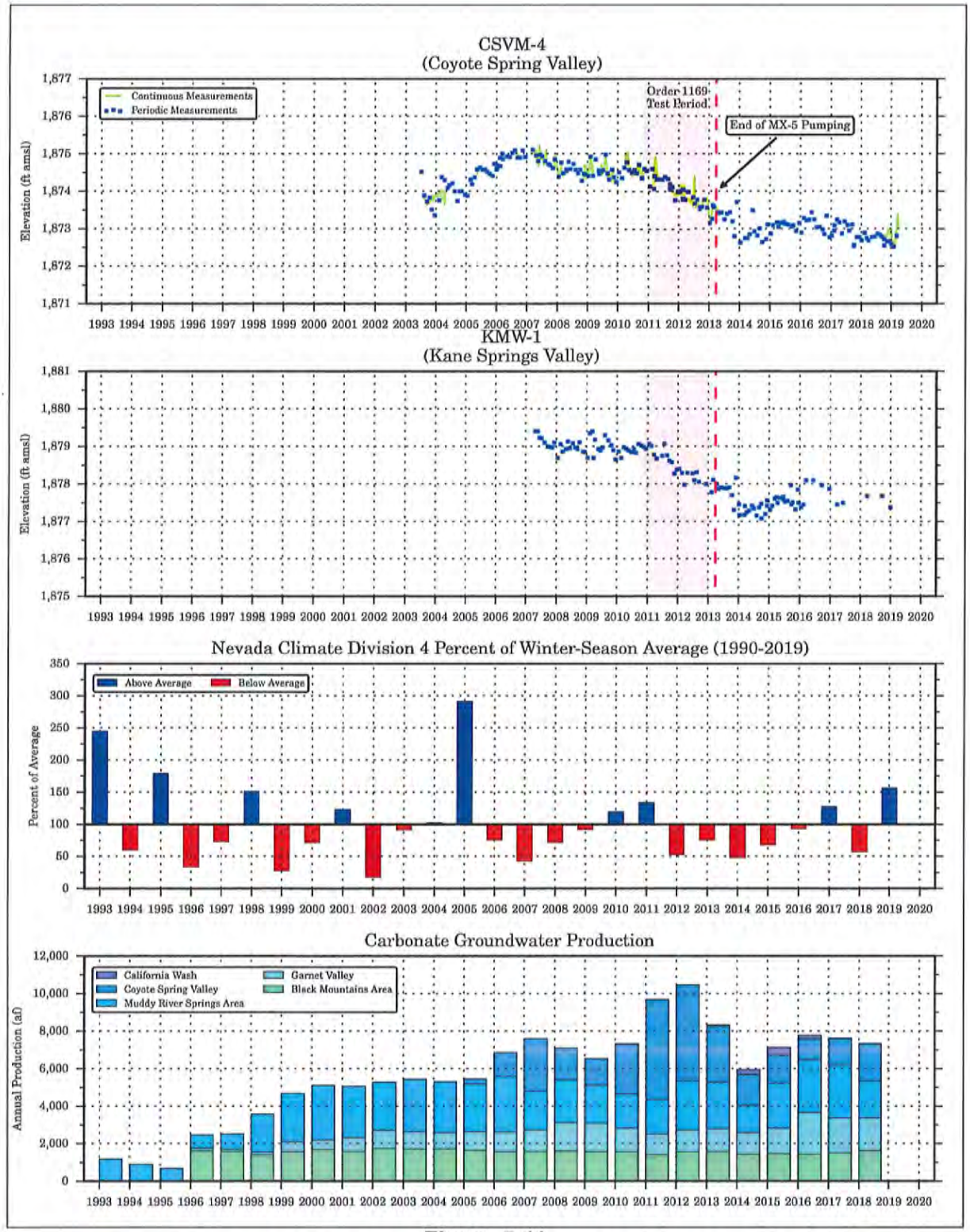

Figure 5-11
Carbonate-Aquifer Water Levels and Groundwater Production

SE ROA 34405

JA_7003

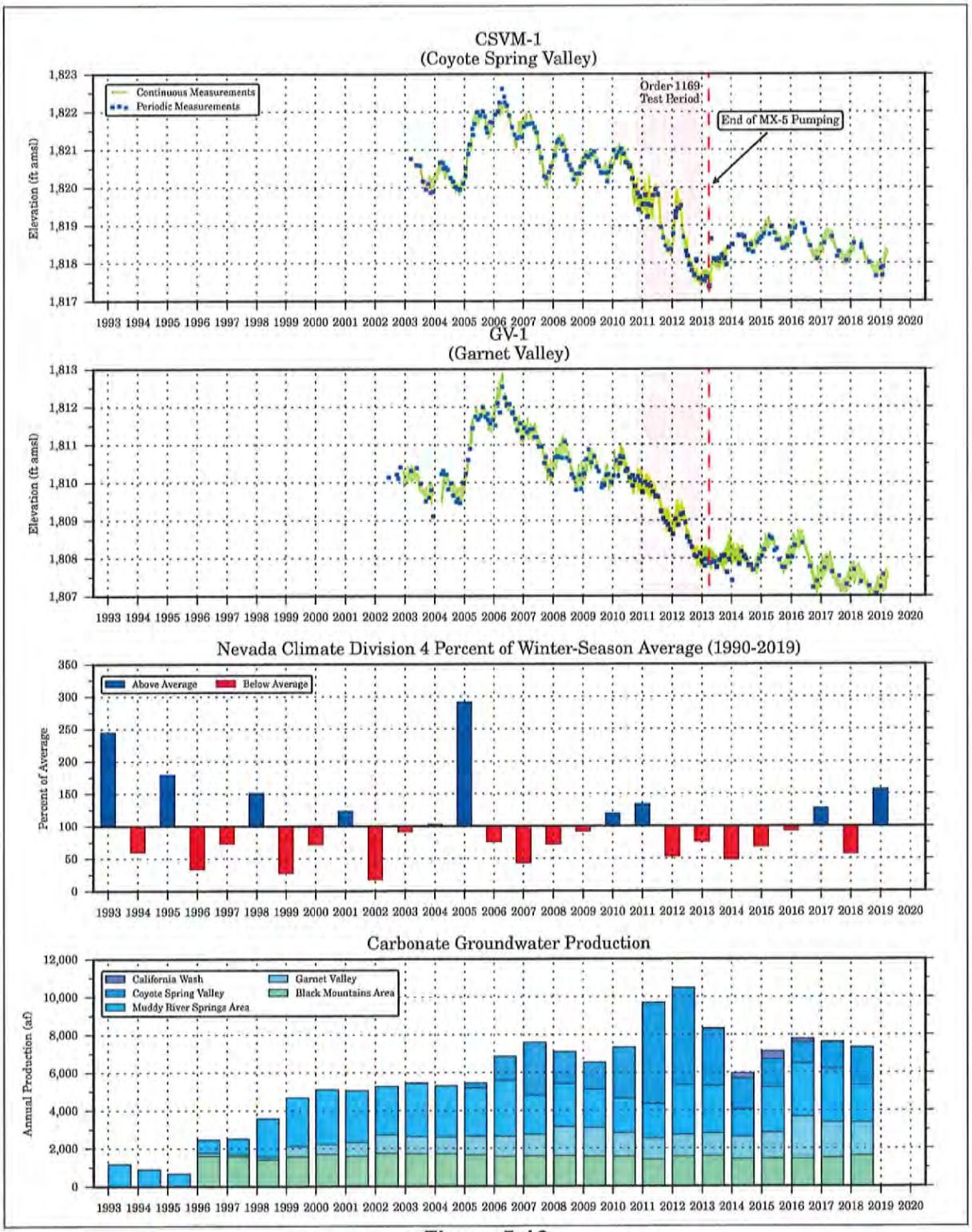

Figure 5-12
Carbonate-Aquifer Water Levels and Groundwater Production

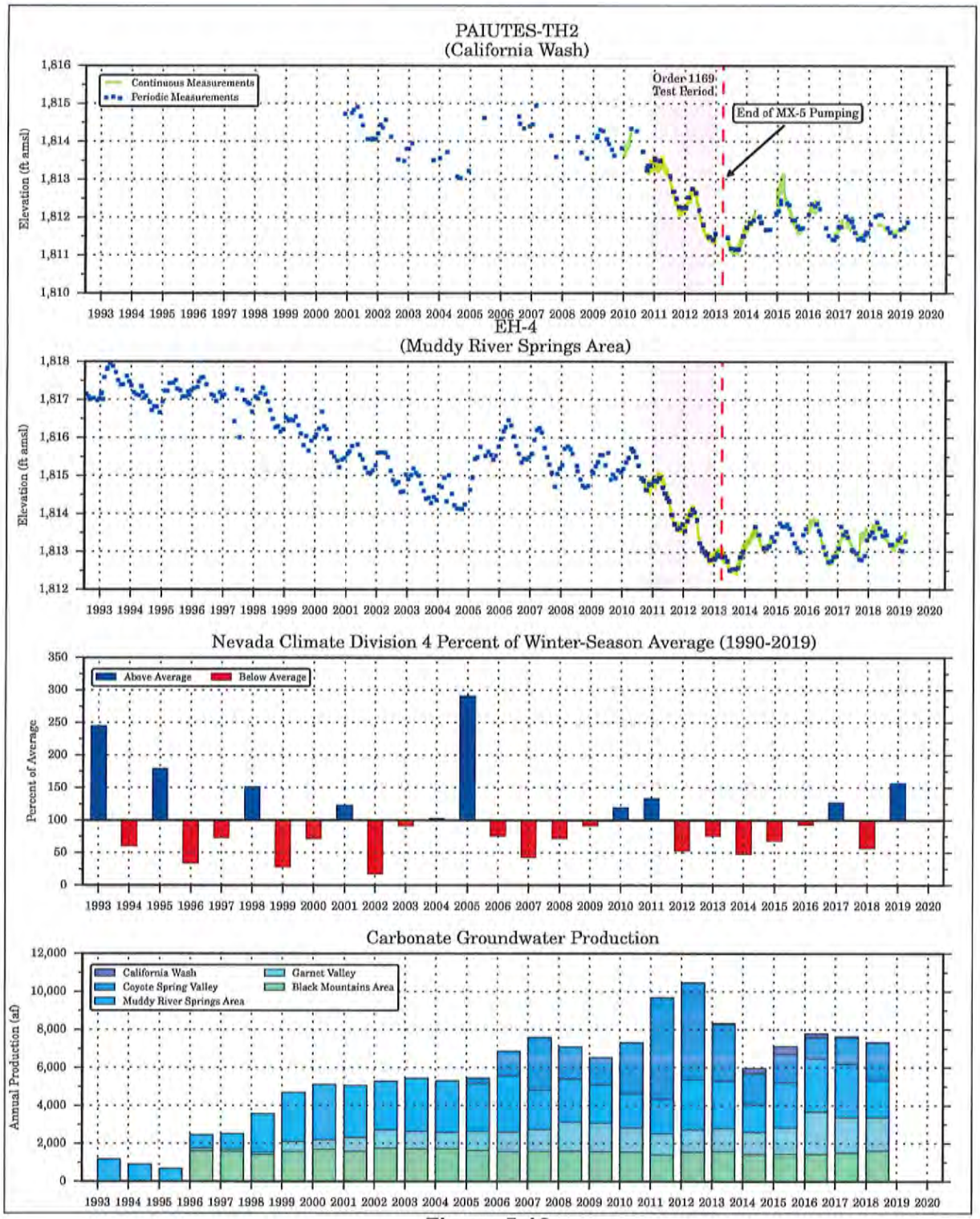

Figure 5-13
Carbonate-Aquifer Water Levels and Groundwater Production

SE ROA 34407

JA_7005

An analysis of the correlations of water-level elevations between well MX-4 and other representative carbonate wells located throughout the LWRFS was performed to confirm the widespread pumping responses observed during the 2-year aquifer test. Well MX-4 was selected because it is in close proximity to the primary production well, MX-5, and therefore, strongly reflected the resulting drawdown response. The correlations were developed using monthly data collected from November 2010 to April 2013, inclusive, and are presented as graphs in Figure 5-14. All relationships exhibit linear trends with very high R^2 values ranging from 0.78 to 0.99. As expected, the highest correlation is with well CSVM-1, which is located only 0.5 mile from well MX-4 in Coyote Spring Valley. The highest correlations indicate that most of the decreases in the groundwater levels at the wells during the test period were caused by pumping from well MX-5 and other nearby wells. Correlation with well CSVM-4 is the smallest at 0.78, but still indicates that changes in groundwater levels at this well are also mainly due to pumping associated with the aquifer test. The slopes of the straight lines provide estimates of the drawdown at the selected wells relative to the drawdown in well MX-4 and are indicative of the degree of connection between their respective locations and that of the MX-4/MX-5 wells. A one-foot drawdown in MX-4 corresponds to 0.92 ft drawdown in well CSVM-1, to about 0.76 ft in wells BM-DL-2 and EH-4, 0.75 ft in wells Paiutes-TH2 and GV-1, and 0.37 ft in well CSVM-4. This analysis provides undeniable evidence that (1) the selected wells were all impacted by the MX-5 pumping during the 2-year test, and (2) the basins of the LWRFS in which these wells are located are highly connected.

5.2.3.2 Recovery Period

Recovery from the pumping stresses imposed during the aquifer test was less than expected, and never reached pre-test levels. There were two primary factors that influenced the initial recovery record observed during 2013: (1) continued carbonate-well pumping, including the MX-5 well in Coyote Spring Valley and (2) the seasonal responses to recharge pulses. The drawdown associated with continued pumping of the MX-5 well muted the recovery response during a period in which water levels typically increase to their seasonal high in April. After the MX-5 well was shut down in mid-April 2013, the recovery response was attenuated by the seasonal water-level decline that starts in May and reaches a low in October. Although these factors complicated the 2013 record, the subsequent years of monitoring provided a clear picture of the recovery response and the following observations are made:

- Carbonate-aquifer water levels have not recovered to pre-test levels.
- Spring flows measured at the Pederson Spring and Warm Springs West gages have not recovered to pre-test levels.
- Recovery achieved its maximum levels between the first quarters of 2015 and 2016.

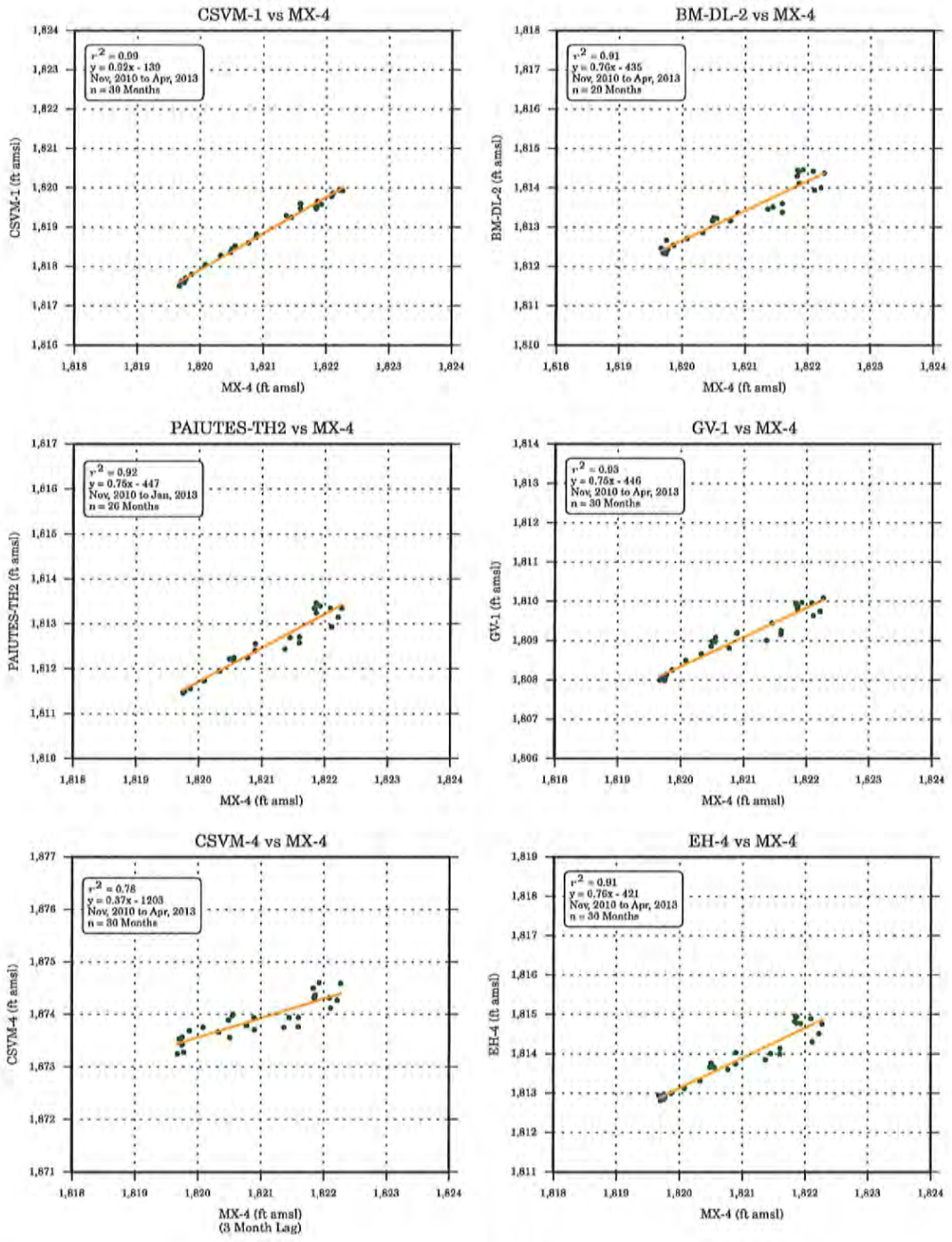

Figure 5-14
Correlation of Hydraulic Heads at Well MX-4 with Hydraulically Connected Carbonate Wells during the Order 1169 Aquifer Test

SE ROA 34409

JA_7007

6.0 IMPLICATIONS TO CHANGES IN HYDRAULIC HEAD OF THE CARBONATE AQUIFER

As previously discussed, the carbonate aquifer is the source of all perennial springs and seeps in the MRSA that sustain the Moapa dace habitat, recharge to the local alluvial reservoir, and discharge from the MRSA as a whole. Based on the hydrologic responses to climate variability and stresses imposed by groundwater production as described in Section 5.0, there are significant implications to the development of groundwater from the carbonate aquifer.

The observed responses indicate that to eliminate conflicts with Muddy River surface-water rights, which are the most senior water rights within the LWRFS and protect spring discharge relied upon by the endangered Moapa dace, groundwater production from the carbonate aquifer must be limited. This section presents a qualitative assessment of the LWRFS carbonate aquifer based on these responses, and quantitative analysis of the amount of carbonate groundwater that may be produced over the long term while still maintaining certain flow conditions at the Warm Springs West gage.

6.1 Qualitative Assessment of Historical Responses

The time-series data presented in Section 5.2 indicate that the carbonate aquifer responds uniformly to variable winter-season precipitation, and that responses to pumping stress are small in magnitude but widespread throughout the system. These responses are observed as changes in groundwater levels and spring discharge, particularly during the 2-year aquifer test, but cannot readily be discerned in Muddy River streamflow records.. The response of the Muddy River has been dominated by the changes in surface-water diversions and groundwater production above the MR Moapa gage.Small changes in the hydraulic heads (on the order of only 2-3 ft) have resulted in significant changes in the discharges from high-elevation springs. Additionally, the lack of any significant recovery response after the completion of the Order 1169 aquifer test and the fact that the system has yet to recover to pre-test levels are critical observations. These observations indicate that the aquifer has a very high transmissivity and low storage capacity (i.e., high aquifer diffusivity). As a result, the system is very sensitive to recharge and pumping stresses and is interpreted to effectively behave like a confined aquifer system. A significant withdrawal of water from a pumping center creates similar decreases in the hydraulic head throughout the system, and within relatively short time periods. Further, recharge pulses of local origin create similar increases in hydraulic head throughout the system and within relatively short time periods. This is demonstrated by the time-series data collected from representative wells completed in the carbonate aquifer at locations within the LWRFS basins (Figures 5-5 and 5-6). This behavior is also demonstrated by the discharge records from the Pederson Spring and Warm Spring West gages in the MRSA which have exhibited responses commensurate with changes in hydraulic heads (Figure 5-7).

Several high-elevation springs compose some of the most critical habitat for the Moapa dace (Marshall and Williams, 2019). These springs also happen to be the most sensitive to changes in hydraulic heads due to the elevation of their orifices. The elevation of the spring orifice controls the hydraulic potential (hydraulic head in the carbonate aquifer minus spring-orifice elevation) driving its discharge. The hydraulic potential driving spring discharge decreases with increasing spring elevation, resulting in increasing levels of sensitivity to natural and anthropogenic stresses affecting hydraulic heads in the carbonate aquifer.

Figure 6-1 presents the MRSA spring locations with Light Detection and Ranging (LIDAR) elevation data to illustrate the distribution of spring complexes and stream reaches with respect to ground-surface elevations. Spring orifices and gaining stream reaches occurring at higher elevations are more susceptible to changes in groundwater levels than lower elevations. For instance, discharge from high-elevation springs in the MRSA have been demonstrated to respond in a manner that is consistent with changes in the hydraulic heads of the carbonate aquifer (Figures 5-8 and 5-9). Small changes in hydraulic heads during the NSE Order 1169 aquifer test resulted in reduced discharge from the Pederson Spring Complex. Springs that occur at lower elevations have a greater hydraulic potential and are less sensitive to such changes.

Since 2016, hydraulic heads in the carbonate aquifer and discharge measured at Pederson Spring and Warm Springs West gages have declined. A significant increase in carbonate groundwater production, such as that which occurred during the NSE Order 1169 aquifer test, will increase the rate of decline so that the 2006 MOA trigger ranges are encountered much sooner. In this case, groundwater production would be restricted per the annual volumes listed in Table 1-1.

The observed declines since 2016 are likely caused by the on-going carbonate groundwater production coupled with a below average winter-season precipitation in 2018, but the respective contributions of each factor are unknown. Notably, the declines have occurred even though winter-season precipitation during 2017 and 2019 were above average. Precipitation can neither be predicted nor controlled; therefore, monitoring the response of the flow system and managing groundwater production is the only way to avoid reaching the protective triggers and impacting senior water rights. Based on this assessment, the following conclusions are made:

- Flow measured at the Warm Springs West gage will reach trigger ranges sooner and at lower production rates than contemplated in the 2006 MOA if pumping in Coyote Spring Valley resumed at levels commensurate with the Order 1169 aquifer test;

- Given the current rates of carbonate groundwater production, recovery of groundwater levels and spring discharge to pre-test levels is not possible without extraordinary hydrology such as the 2004-2005 winter-season precipitation; and

- Even with such extraordinary hydrology, subsequent years of lesser precipitation with similar groundwater production volumes will result in a resumption of declining trends as has been observed in the historical record.

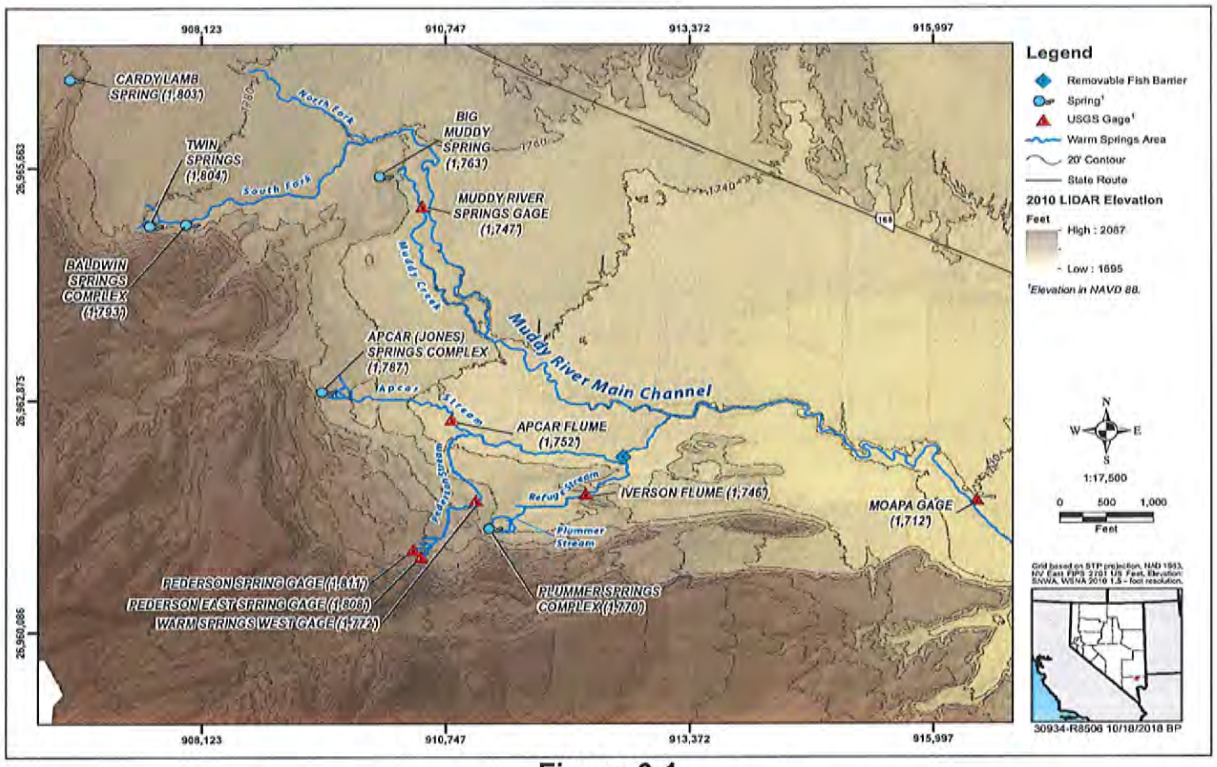

Figure 6-1
Elevation of Selected Springs and LIDAR Digital Elevation Model within the MRSA

6.1.1 *Implications of Continued Pumping*

Responses associated with the Order 1169 aquifer test demonstrate that the current pumping configuration within the LWRFS (i.e., pumping location, rates and duration) is not sustainable in the long-term without conflicting with senior Muddy River water rights and degrading the Moapa dace habitat in the high-elevation spring complexes. In the long-term, it is expected that any groundwater production from the carbonate system within the LWRFS will ultimately capture discharge to the MRSA (e.g., spring discharge, subsurface inflow to the alluvial reservoir and, consequently, Muddy River streamflow) because of the high aquifer diffusivity and hydraulic connectivity throughout the flow system and because the MRSA constitutes the majority, if not all, of the discharge from the flow systemThe results of the Order 1169 aquifer test indicate that for the areas directly upgradient of the MRSA (i.e., Arrow Canyon and Coyote Spring Valley), water-level responses to pumping stresses occur very quickly. As demonstrated in Figures 5-8 and 5-9, any reduction of the hydraulic head in the carbonate aquifer results in a proportional reduction in spring discharge.

The timing of impacts from groundwater production in pumping centers located farther from the MRSA, in Garnet Valley, California Wash and the Black Mountains Area, may take longer, but the properties of the aquifer are such that these impacts will eventually reach the MRSA. This is because, as the data indicate, the MRSA is hydraulically connected to the other LWRFS basins. Based on this assessment, the following conclusions are made:

- groundwater production from the carbonate aquifer in the LWRFS has impacted discharge to the MRSA and, consequently, senior surface-water rights associated with the 1920 Muddy River Decree

- impacts due to groundwater production within areas directly upgradient of the MRSA occur relatively quickly, and the magnitude of the impacts depends upon the pumping rates and durations

- additional appropriations that increase groundwater production from the carbonate aquifer within the LWRFS will accelerate the timing and magnitude of impacts

- changing the spatial distribution of pumping within the LWRFS will change the distribution of drawdown and the timing of impacts, but not the long-term outcome.

6.2 Quantitative Analysis

Many studies (Eakin, 1964; Eakin and Moore, 1964; Eakin, 1966) have shown that discharge in the MRSA is sourced by groundwater from the underlying carbonate aquifer. Some studies include complex equations or numerical groundwater flow models that are not easy to use to better understand the flow system (SNWA, 2009a and b; 2010; Tetra Tech, 2012a and b). A few studies have used the existing data to develop simpler mathematical relationships (USFWS et al., 2013). However, such studies concentrate on daily or monthly data, which clouds the interpretations of the flow system with effects of short-lived stresses. This analysis uses annual data and a simplified approach to characterize the relationship between the carbonate aquifer and discharge to the MRSA area (or MRSA discharge). The annual data are more representative of the system's response to longer-term stresses such as natural recharge and groundwater production from the carbonate aquifer.

6.2.1 Objective

The objective of this analysis is to derive simple methods quantifying the relationship between the carbonate aquifer and MRSA discharge at the annual scale. Such relationships can then be used to predict spring discharge based on measurements of hydraulic heads in the carbonate aquifer and estimate the quantities of groundwater production from the carbonate aquifer based on pre-selected rates of reduced MRSA spring discharge.

6.2.2 Approach

The available groundwater-production and hydrologic-response data were used to quantify the maximum amount of production from the carbonate aquifer that can occur over the long term while still maintaining selected flows at the Warm Springs West gage. This approach included the following:

- developing a relationship between the Warm Springs West gage records and total discharge to the MRSA

- applying the relationship to quantify the maximum allowable reduction in MRSA discharge from the predevelopment condition for each selected flow rate at the Warm Springs West gage.

6.2.3 Relationship between High-Elevation Spring Discharge and MRSA Discharge

The MRSA discharge occurs in the form of springs with measurable discharge rates and seeps that cannot be measured individually. The relationship between the hydraulic head in the carbonate aquifer and the MRSA discharge is governed by Darcy's law. The changes in the MRSA discharge are directly proportional to the changes in the hydraulic head in the carbonate aquifer. The relationships between discharge at selected spring gages, Pederson Spring and Warm Springs West gages, and the hydraulic head in the carbonate aquifer (Figures 5-8 and 5-9) demonstrate that spring discharge is directly proportional to hydraulic head as predicted by Darcy's law.

At time scales of one year or more, changes in the hydraulic head of the carbonate aquifer are mainly caused by changes in natural recharge and groundwater production from the carbonate aquifer. As demonstrated by the 2-year aquifer test, an essentially equal response spreads relatively quickly to carbonate monitor wells located within the six interconnected basins of the LWRFS. This indicates that the carbonate aquifer acts as a confined aquifer with a large average transmissivity and a low average storage coefficient. Thus, the following statements must hold true:

- a change in the hydraulic head of the carbonate aquifer causes a proportional change in the MRSA discharge throughout the springs area; and

- discharge from each spring and seep contributing to the MRSA discharge changes in a proportional manner relative to the hydraulic head change in the carbonate aquifer.

The following analysis demonstrates that these statements are true by showing that the relative contribution of a given spring to the MRSA discharge, or ratio of spring discharge to MRSA discharge, remains the same, independent of stress conditions (i.e., recharge and groundwater production). A constant ratio under variable stress conditions indicates that the relationship can be applied to estimate MRSA discharge under any flow condition based on the discharge record of the subject spring.

6.2.3.1 Ratio Calculations

Data needed to estimate the contribution of a selected spring or spring complex to the MRSA discharge are the discharge measurement record of the selected spring and estimates of the MRSA discharge for the same period of time. The Warm Springs West gage was selected to represent the flow from the Pederson Spring Complex.

MRSA discharge consists of the following components: (1) subsurface flow into the alluvial reservoir, (2) spring discharge, and (3) groundwater ET. Under pre-development conditions, this discharge can be estimated by adding the MR Moapa gage record to estimates of ET. Under transient conditions, surface-water diversions and alluvial groundwater production must be added to the gage

record and ET estimate to ensure a complete accounting. The period of time for which observations of all of these variables, including ET, are available is from 2001 to 2012.

All data used in this analysis for the 2001-2012 time period, along with the ratio of discharge measured at the West Springs West gage to MRSA discharge are presented in Table 6-1. Even though the discharge values for both components of the ratio vary from year to year, the ratio remains within a very narrow range. The average ratio is 0.078 with a narrow 95-percent confidence interval of 0.074 to 0.082. The variation in the ratio values are due to uncertainty in the data used to derive it (Sauer and Myer, 1992).

Table 6-1
Contribution of Warm Springs West Discharge to MRSA Discharge

Year	Flow at MR Moapa Gage		Losses above MR Moapa Gage			Total MRSA Discharge (af)	Flow at Warm Springs West Gage		Ratio
	Average Annual (cfs)	Annual Total (af)	Diversions (af)	MRSA Alluvial Groundwater Production (af)	ET above Gage (af)		Average Annual (cfs)	Annual Total (af)	
2001	31.37	22,726	4,363	3,560	3,359	34,008	3.72	2,694	0.079
2002	32.50	23,549	4,573	4,190	3,294	35,606	3.63	2,631	0.074
2003	30.34	21,982	4,313	3,673	2,855	32,822	3.56	2,580	0.079
2004	31.38	22,731	3,631	3,370	2,870	32,601	3.54	2,564	0.079
2005	32.34	23,432	3,425	3,837	3,426	34,121	3.80	2,752	0.081
2006	34.18	24,761	2,927	4,436	2,856	34,981	3.90	2,825	0.081
2007	32.83	23,784	4,176	3,506	2,864	34,329	3.72	2,694	0.078
2008	34.77	25,191	3,825	3,135	2,841	34,992	3.61	2,616	0.075
2009	35.61	25,799	3,985	2,539	3,134	35,456	3.71	2,690	0.076
2010	35.74	25,889	3,604	2,701	2,206	34,400	3.71	2,685	0.078
2011	36.59	26,510	1,895	3,322	2,462	34,189	3.63	2,628	0.077
2012	38.32	27,762	422	1,887	2,514	32,585	3.50	2,534	0.078

Ratios were also computed for Baldwin and Jones springs. These springs are located north and northwest of the Warm Springs West gage as depicted in Figure 6-1, and at slightly lower elevations than the Pederson Spring Complex. The ratios for each of the springs are presented with the corresponding data for the period of analysis in Figure 6-2. The average ratios are 0.061 and 0.034 for Baldwin and Jones springs, respectively. The 95-percent confidence intervals are very narrow at 0.055 to 0.068 for Baldwin spring and 0.032 to 0.036 for Jones spring. This is further proof that springs in the MRSA respond commensurately with the hydraulic head of the carbonate aquifer, regardless of the stress.

6.2.3.2 *Ratio Verification*

To verify that these ratios remain the same under any stress conditions, an additional estimate was made using predevelopment data reported by Eakin (1964). Data for this period reflect conditions preceding 1965, prior to the exportation of stream diversions above the MR Moapa gage. The LWRFS was practically under predevelopment conditions as Eakin (1964) reported a relatively small

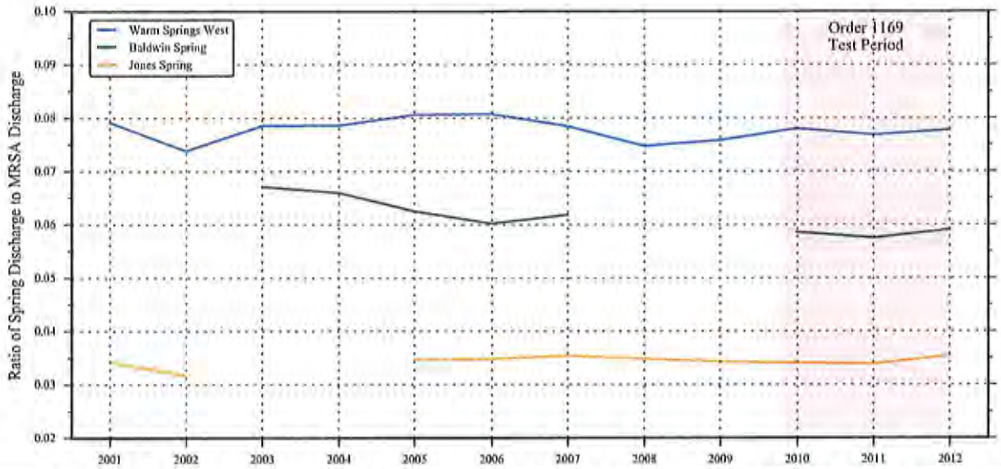

Year	2001	2002	2003	2004	2005	2006	2007	2008	2009	2010	2011	2012	Avg
Total MRSA Discharge (cfs)	4.6	4.5	3.9	4.0	4.7	3.9	4.0	3.9	4.3	3.0	3.4	3.5	4.0
Baldwin Spring (cfs/[ratio])	2.8 [0.059]	--	3.0 [0.067]	3.0 [0.066]	2.9 [0.063]	2.9 [0.060]	2.9 [0.062]	--	--	2.8 [0.059]	2.7 [0.058]	2.7 [0.059]	2.9 [0.061]
Jones Spring (cfs/[ratio])	1.6 [0.034]	1.6 [0.032]	--	--	1.6 [0.035]	1.7 [0.035]	1.7 [0.035]	1.7 [0.035]	1.7 [0.034]	1.6 [0.034]	1.6 [0.034]	1.6 [0.035]	1.6 [0.034]

Figure 6-2
Ratios of Spring Discharge to Total MRSA Discharge (2001 - 2012)

volume of groundwater withdrawal from the alluvial reservoir of the MRSA, which was used for local irrigation.

Eakin (1964) collected field measurements of individual spring discharge and Muddy River flow at Moapa from late 1963 to early 1964. Eakin (1964) found that discharge rates from the individual springs remain constant during this period, while the river flow at the MR Moapa gage fluctuated from month to month. The main cause of these fluctuations is ET, which Eakin (1964) estimated to be between 2,000 and 3,000 afy.

Eakin (1964) estimated the MRSA discharge at 49.8 cfs during the 1963-1964 study period and found that the sum of the individual spring discharges measured during that period constitutes 60 percent of this discharge. The data collected by Eakin (1964) may be used to calculate the contribution of individual springs to the total MRSA discharge. Only the Warm Springs West gage is used in this verification because the Eakin (1964) discharge measurement locations and values for Baldwin and Jones springs could not be matched with the current records. The discharge at the Warm Springs West gage was measured at 3.78 cfs during the investigation period. The ratio between the discharge at the Warm Springs West gage and the MRSA discharge is 0.076 (3.78 cfs/49.8 cfs), rounded to the nearest thousandth. In other words, the discharge from the Pederson Springs Complex above the Warm Springs West gage contributes 7.6 percent to the total discharge to the area.

This analysis demonstrates that the ratio between the discharge at the Warm Spring West gage and the MRSA discharge is constant at 0.076. This ratio is within the range calculated from the 2001-2012 data and actually constitutes the best estimate because the discharge values used were measured during the same short-time period, and less variables were used to calculate it. This analysis confirms the following:

- The change in hydraulic head in the carbonate aquifer is spatially the same across the area supplying the springs and seeps of the MRSA discharge area, under variable natural and anthropogenic stress conditions.
- The carbonate aquifer behaves as a confined system. Drawdown caused by pumping from the carbonate aquifer creates a wide and shallow cone of depression extending over the area supplying the MRSA springs and seeps above the MR Moapa gage.
- As long as the hydraulic head in the carbonate aquifer is maintained at a level high enough to keep all springs and seeps flowing, each spring and seep contributes a constant proportion to the MRSA discharge.

6.2.4 Quantification of Limits on Carbonate Groundwater Production

The relationships described in the previous section can be used to calculate reductions in the MRSA discharge that correspond to potential flow conditions at the Warm Springs West gage. This gage is important because it measures discharge from the most sensitive group of springs in the MRSA; therefore, it is deemed the best location to monitor the effects of carbonate-aquifer groundwater production on both decreed Muddy River water rights and Moapa dace habitat. It is for this reason that it was used to establish Trigger Ranges in the 2006 MOA. Knowing that a reduction in the MRSA discharge could only be caused by a lowering of the hydraulic head in the carbonate aquifer, limits on production from the carbonate aquifer could be set by calculating reductions in MRSA discharge that correspond to various discharge levels at the Warm Springs West gage. including the trigger ranges set in the 2006 MOA.

Reductions were calculated from discharge values estimated for predevelopment conditions. Eakin (1964) estimated the adjusted mean MRSA discharge at 50.2 cfs using flow measurements at the MR Moapa gage for the period 1945 to 1962. No predevelopment estimate of discharge at the Warm Springs West gage is available, but such an estimate can be derived by using the ratio calculated as described in Section 6.2.3. Thus, predevelopment average discharge at Warm Springs West gage is 7.6 percent of 50.2 cfs, or a flow rate of 3.82 cfs. Potential flow reductions at the Warm Springs West gage and corresponding reductions in MRSA discharge are listed in Table 6-2. The reductions in MRSA discharge from average predevelopment conditions can be used to represent limits on groundwater production from the carbonate aquifer for different discharge levels at the Warm Springs West gage.

Table 6-2
Limits on Carbonate-Aquifer Production Based on Selected Discharge Rates at Warm Springs West Gage

WSW Flow Condition (cfs)	Decrease from Predevelopment Discharge			
	Warm Springs West		MRSA Discharge	
	(cfs)	(afy)	(cfs)	(afy)
3.82	0.00	0	0.00	0
3.60	0.22	159	2.89	2,092
3.40	0.42	304	5.53	4,000
3.20	0.62	449	8.16	5,908
3.00	0.82	594	10.79	7,816
2.90	0.92	667	12.11	8,776
2.80	1.02	739	13.42	9,724
2.70	1.12	811	14.74	10,671

[1]Predevelopment discharge at WSW gage computed at 3.82 cfs (2,767 afy); predevelopment discharge from MRSA measured at 50.2 cfs (36,367 afy) (Eakin, 1964)

6.2.5 *Capture Analysis of Carbonate-Aquifer Production*

Using the available data and the analysis described above, an assessment of the approximate impacts of historical groundwater production from the carbonate aquifer was made. The objective of this assessment was to estimate the components of groundwater production in terms of the capture of aquifer storage and MRSA discharge.

Records of groundwater production from the carbonate aquifer are available starting in 1992, even though some minor and unrecorded production was initiated in the mid 1980s. Also, as described in Section 3.4.1, the Warm Spring West gage record is unreliable prior to October 1997. Therefore the period of analysis starts in 1992, when significant carbonate production was initiated and recorded, and ends in 2018, the last full year for which data are available. The following assumptions are made:

- production from the carbonate aquifer prior to 1992 was relatively small; and
- during the period of 1992 to 1998, the source of the production from the carbonate aquifer is assumed to be half from groundwater storage and half from the MRSA discharge.

The analysis approach consisted of the following steps.

1. Using the discharge record for the Warm Springs West gage, the change in average annual discharge from 1998 was calculated for each subsequent year.

2. Using the Eakin (1964) ratio of Warm Springs West discharge to MRSA discharge, 0.076, and the change in Warm Springs West discharge values (Step 1), the change from the 1998 MRSA discharge was calculated for each subsequent year. These values represent the approximate annual capture of MRSA discharge by groundwater production from the carbonate aquifer.

3. The volume of groundwater captured from aquifer storage for each year was computed by calculating the difference between total groundwater production and the volume of captured MRSA discharge (Step 2).

4. The cumulative volumes of groundwater production, aquifer-storage capture, and MRSA-discharge capture were calculated for each year of the 1992 through 2018 period of analysis.

The results are provided in Table D-1 of Appendix D and presented in Figure 6-3. In 2018, after 27 years of recorded production, a total of 148,241 af of groundwater were produced, with about 69,848 af captured from the MRSA discharge and 78,393 af from aquifer storage. As of 2018, about 47 and 53 percent of groundwater production is represented by the capture of MRSA discharge and aquifer storage, respectively.

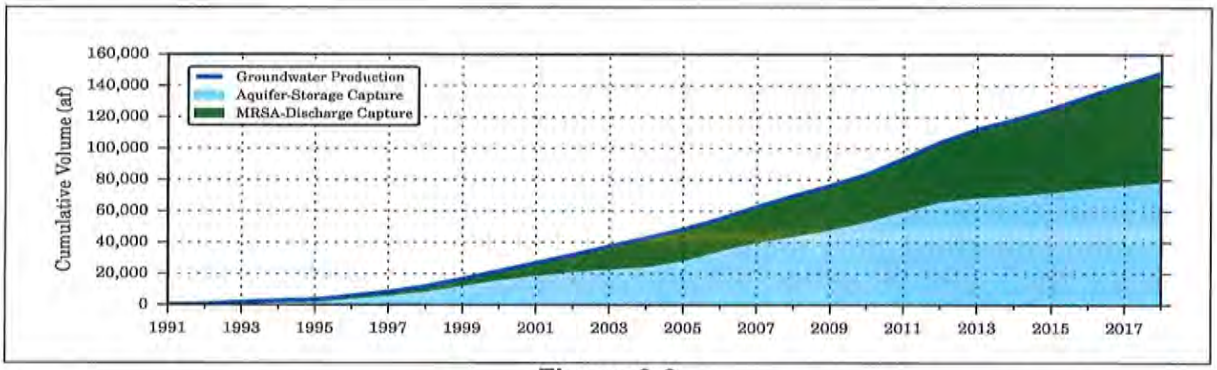

Figure 6-3
LWRFS Carbonate Groundwater Production Capture Analysis

Based on the method used to derive the MRSA capture limits in Table 6-2, the average discharge of 3.38 cfs observed at the Warm Springs West gage in 2018 corresponds to a reduction of about 4,200 afy in MRSA discharge. This value is comparable to the average capture of approximately 5,400 afy calculated for 2018 in the analysis described above.

The results of this analysis are approximate not only due to the uncertainty in the discharge and production data, but also because of the effects of recharge variability. Recharge to the LWRFS originates from local and regional sources located at different distances from the MRSA. Thus, changes in winter precipitation throughout the region create recharge pulses which arrive to the MRSA at different times, which are mostly unknown. Therefore, their effects on the spring discharge are difficult to quantify.

6.3 *Findings of Qualitative Assessment and Quantitative Analysis*

The analyses described in this section build on the relationships described in Section 5.0 and establish the following:

- The MRSA discharge varies with carbonate aquifer levels following a linear relationship.

- A linear relationship exists between individual spring discharge and the total MRSA discharge. Each spring contributes water to the MRSA discharge in the same proportion under any stress conditions.

- For purposes of estimating long-term limits on carbonate-aquifer production, a reduction in MRSA discharge from predevelopment conditions can be considered equivalent to a volume of groundwater withdrawn from the carbonate aquifer.

- Over the long-term, once capture of aquifer storage is reduced to levels approaching zero, production from the carbonate aquifer is expected to reduce MRSA discharge on a nearly 1:1 ratio.

7.0 DEPLETION OF MUDDY RIVER STREAMFLOW AND IMPACTS TO SNWA

Groundwater production from the MRSA alluvial reservoir and the LWRFS carbonate aquifer has depleted the flows of the Muddy River. Muddy River water rights were adjudicated in 1920 and the Muddy River Decree allocated the entire flow of the Muddy River. Therefore, groundwater production (whose associated rights are all junior in priority) that causes a depletion in streamflow also conflicts with the decreed rights on the river.

SNWA has significant assets associated with the Muddy River through its ownership and leases of water rights and MVIC shares, and uses these assets to create Tributary Conservation ICS credits in the Colorado River and Lake Mead. SNWA has spent over $80,000,000 on the acquisition of water rights on the Muddy River for the purpose of creating ICS credits. These credits compose a critical component of the SNWA water-resources portfolio that is needed to supply current and future water demands for a growing community with a population of over 2 million people and more than 40 million annual visitors (SNWA, 2018a).

This section describes SNWA's water-resource assets associated with the Muddy River, how they have been used to create ICS credits, and how SNWA has been impacted by Muddy River streamflow depletions caused by groundwater production within the LWRFS. The ensuing discussion describes these assets in relation to the Upper and Lower Muddy River reaches distinguished by the location of the USGS Muddy River near Glendale gaging station (MR Glendale gage) (Figure 7-1).

7.1 Upper Muddy River

Decreed water rights within the Upper Muddy River are individually owned with specific Places of Use to which water associated with the right is applied. Since 2006, SNWA has entered into lease agreements for some of these rights and has purchased others. Leased volumes may vary year to year as documented within the annual Muddy River ICS Certification reports (SNWA, 2009c; 2011a and b; 2012a and b; 2013c; 2015b and c; 2016b; 2017b; 2018c). Within the Upper Muddy River, SNWA leases or owns the following water rights;

- Up to 2,001 afy leased from the Church of Latter Day Saints (expires January 1, 2027)
- 111 afy of former Cox and Mitchell rights (SNWA-owned)
- 1,040 afy of former Hidden Valley rights (SNWA-owned)
- Up to 3,700 afy of rights held in a long-term lease by the Moapa Band of Paiutes and subleased to SNWA (expires December 31, 2026)
- 811 afy of former Knox and Holmes rights (SNWA-owned)
- Up to 3,000 afy of rights leased from MVIC (expires December 31, 2026).

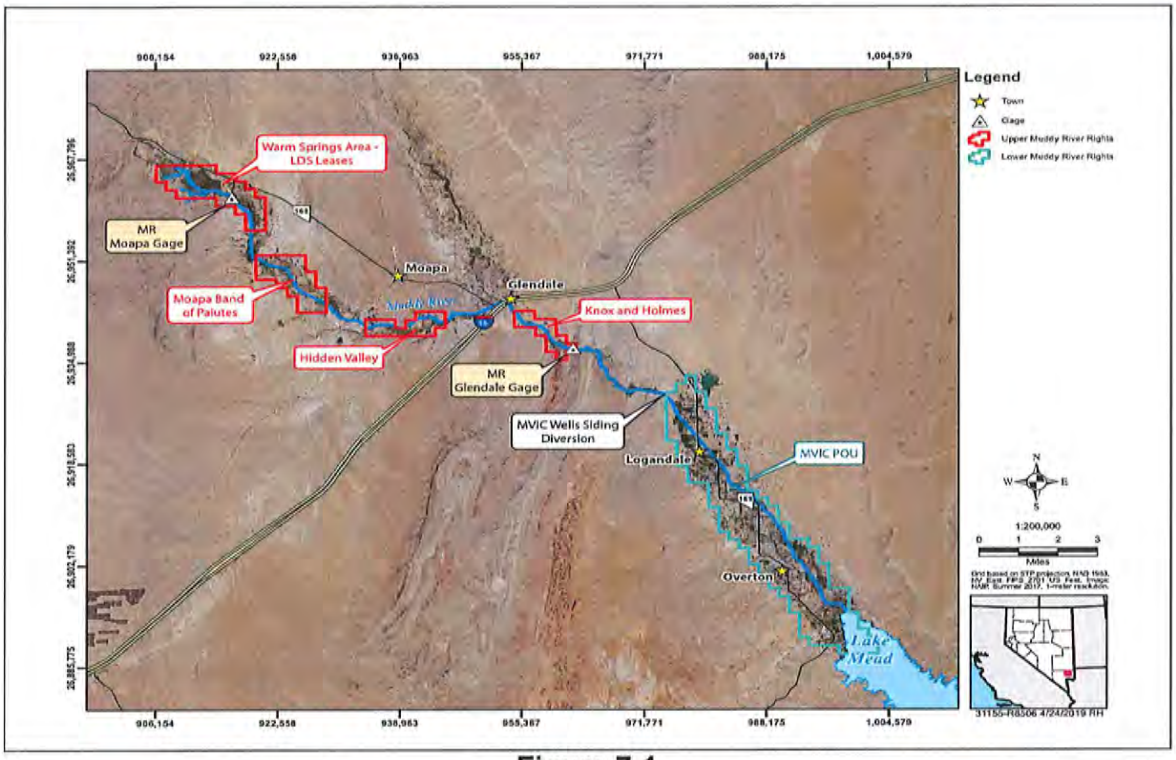

Figure 7-1
Upper and Lower Muddy River Reaches

7.2 *Lower Muddy River*

Decreed water rights within the Lower Muddy River are held by MVIC, which holds the largest quantity of decreed rights on the Muddy River. MVIC decreed Muddy River water rights are owned by MVIC shareholders through ownership of shares of preferred and common MVIC stock. There are 2,432 preferred shares and 5,044 common shares in MVIC. MVIC's operations and covenants define preferred shares as 100 percent of the Muddy River summer flow and 75 percent of the winter flow. Common shares represent the remaining 25 percent of the winter flow. In addition to their decreed and certificated rights, the 1920 Muddy River Decree states that MVIC can divert any additional unused Muddy River flows that reach their diversion structure on the Muddy River. Consequently, the actual water that MVIC splits among its shareholders varies from year to year based on the actual divertible flows that reach their diversion structure. MVIC delivers water to its shareholders through a network of concrete-lined ditches and pipes.

Currently, SNWA controls, through purchases and leases, 1,166 preferred shares and 3,208 common shares. The volume of water represented by these shares changes from year to year based on the flow of the river as measured at the MR Glendale gage. In 2018, SNWA shares represented approximately 10,000 af.

7.3 SNWA Tributary Conservation ICS Credits

SNWA relies upon Muddy River water rights and MVIC shares it owns and leases to create Tributary Conservation ICS credits. SNWA is allowed to store the water associated with these credits in Lake Mead, or divert it at its intakes in Lake Mead for delivery to water purveyors in the Las Vegas Valley.

The criteria for the development and delivery of ICS was established in the Record of Decision for Colorado River Interim Guidelines for Lower Basin Shortages and the Coordinated Operations for Lake Powell and Lake Mead, December 13, 2007 (USBR, 2007). Tributary Conservation ICS is one of several types of ICS and allows a Contractor, as defined in the Guidelines, to increase tributary flows into the mainstream of the Colorado River within its state for ICS credits. ICS credits are limited to flows associated with water rights that have been used for a significant period of years and were perfected prior to the effective date of the Boulder Canyon Project Act of June 25, 1929. ICS has been declared a beneficial use under Nevada Revised Statute 533.030.

To generate ICS credits, the Guidelines require a Contractor, SNWA in this case, to submit ICS plans of creation and certification reports. Plans of creation are written to demonstrate how the ICS will be created in the ensuing year, and certification reports are used to document the creation of ICS for the previous year. NSE Order 1194 requires the submittal of an annual report to the NSE that provides a full accounting of adjudicated Muddy River water rights, owned or controlled by the Contractor, that have been conveyed through the Muddy River to the Colorado River for the creation of ICS. The certification reports must comport with this order. SNWA has created 157,824 af of Muddy River Tributary Conservation ICS credits since the Guidelines were instituted in 2008 (SNWA, 2009c; 2011a and b; 2012a and b; 2013c; 2015b and c; 2016b; 2017b; 2018c). Annual ICS credits created by SNWA are presented in Table 7-1. The 2018 ICS data are not included here as the Certification Report has not yet been finalized and approved.

7.3.1 Impacts to SNWA as a Result of Muddy River Streamflow Depletions

As described in Section 5.1.4, Muddy River streamflow has been depleted by groundwater production from both the MRSA alluvial reservoir and LWRFS carbonate aquifer. Figure 5-4 demonstrates that groundwater production within the MRSA accounts for the MR Flow Deficit observed for the period of analysis. Production wells completed in the alluvial reservoir adjacent to the Muddy River capture groundwater that would otherwise discharge to the river. In addition, MRSA production wells completed in the carbonate aquifer capture water that would otherwise replenish the alluvial reservoir though diffuse subsurface flow or discharge from discrete springs. Capturing this groundwater depletes the source of supply to the alluvial reservoir and springs, thereby, depleting the streamflow. Groundwater production from other production wells located within the LWRFS also impact the MRSA discharge, and therefore the Muddy River flow. However, the impacts are not readily discernible in the streamflow record because of their relatively small magnitude compared to the flow of the river and the masking effect caused by recharge variability.

Muddy River streamflow depletions have had, and will continue to have, a direct impact on the volume of water associated with MVIC shares and, consequently, the water resources SWNA is able to secure through the creation of ICS credits. As previously described, the volume of water represented by MVIC shares is determined by the annual flows in the Muddy River. As the flows

Table 7-1
SNWA's Muddy River Tributary Conservation ICS Credits

Year	Tributary Conservation ICS Credits (af)		
	Upper Muddy River	Lower Muddy River	Annual Total
2008	2,112	4,983	7,095
2009	5,812	7,395	13,207
2010	8,622	8,161	16,783
2011	9,420	7,142	16,562
2012	9,929	7,384	17,313
2013	10,390	7,033	17,424[a]
2014	6,471	8,627	15,098
2015	9,963	8,509	18,472
2016	9,963	8,283	18,246
2017	9,963	7,660	17,624[a]
		GRAND TOTAL	157,824

[a]Differences in annual totals are the result of rounding.

have diminished as a result of groundwater production, so too has the volume of water associated with the shares that are owned by the individual MVIC shareholders, including SNWA. The impact to MVIC was estimated for the period 2008 through 2017 by summing the annual differences between the predevelopment baseflow and the natural flow as measured at the MR Moapa gage, which totaled over 46,000 af. The predevelopment baseflow was derived using streamflow records for a period of below-normal hydrology; therefore, using it as a reference point leads to conservatively low estimates of streamflow depletion. Table 7-2 presents the impacts these streamflow depletions have had on SNWA ICS credits. To quantify the impacts, the following steps were taken:

1. The natural flow as a percentage of the predevelopment baseflow was derived for each year of ICS creation using the annual flood-adjusted flow records of MR Moapa gage. The natural flow record was derived by accounting for all surface-water diversions above the gage as described in Section 5.1.3, and represents the water available for uses downstream of the gage, including the creation of ICS from MVIC shares. The computed percentage is less than 100 when the baseflow has been depleted by groundwater production, as was the case during the period of ICS creation. By using the MR Moapa gage, it is assumed that all gains/losses (i.e., diversions, ET) between the MR Moapa and MR Glendale gages remained essentially the same for the period of analysis.

2. The potential ICS credit that would have been created had the streamflow not been depleted was computed by dividing the ICS credit certified for each year by the percentage of natural flow computed in Step 1. The potential ICS is always greater than the certified ICS when the baseflow has been depleted by groundwater production.

3. The impacts were quantified by computing the difference between the potential and certified ICS volumes. The values are listed in Table 7-2 and presented in Figure 7-2. The total

estimated impact from 2008 through 2017 is 12,040 af. The cost to purchase additional water to replace the lost flows is estimated to be $2,288,746 using the annual value of leased shares.

Table 7-2
Impacts of MR Streamflow depletions on SNWA ICS Credits

Year	Certified ICS Credits (af)	Natural Flow at MR Moapa Gage[a] (af)	Natural Flow as Percentage of Predevelopment Baseflow[b] (%)	Potential ICS Credits (af)	Impact to SNWA ICS Credits (af)	Lease Cost per Acre-Foot	Replacement Water Costs
2008	4,983	29,016	86	5,794	(811)	$283.33	$229,781
2009	7,395	29,784	88	8,403	(1,008)	$283.33	$285,597
2010	8,161	29,493	87	9,380	(1,219)	$283.33	$345,379
2011	7,142	28,405	84	8,502	(1,360)	$184.17	$250,471
2012	7,384	28,184	83	8,896	(1,512)	$184.17	$278,465
2013	7,033	28,586	84	8,373	(1,340)	$184.17	$246,788
2014	8,627	28,302	83	10,394	(1,767)	$130.00	$229,710
2015	8,509	30,150	89	9,561	(1,052)	$130.00	$136,760
2016	8,283	30,302	89	9,307	(1,024)	$145.00	$148,480
2017	7,660	30,331	89	8,607	(947)	$145.00	$137,315
			TOTAL		**(12,040)**		**$2,288,746**

[a]MR Moapa Gage values are the Flood-Adjusted Natural Flow as shown in Figure 5-3
[b]Predevelopment baseflow estimate of 33,900 afy was used in calculation.

7.4 *Potential for Increased Damages due to Additional Carbonate Groundwater Production*

The MR Flow Deficit is, at this time, primarily the result of alluvial and carbonate groundwater production within the MRSA. However, as described in Section 6.1, any groundwater production from the carbonate system within the LWRFS will ultimately capture groundwater discharge to the MRSA and, consequently, deplete Muddy River streamflow. These impacts conflict with the senior water rights adjudicated in the 1920 Muddy River Decree and affect the ability of SNWA to create ICS credits for which significant investments have been made.

Changing points of diversion to move groundwater production out of the MRSA to locations sourced by the carbonate aquifer will not mitigate these conflicts, only delay their inevitable occurrence. Such changes would exacerbate issues associated with the already over-appropriated carbonate aquifer by accelerating the timing of impacts to sensitive springs due to the additional groundwater production. The timing of impacts will vary based on the magnitude, duration, and location of groundwater production. The impacts may occur relatively quickly, within weeks or months, if additional groundwater production were to occur in areas directly upgradient from the MRSA. Groundwater production in areas farther away, may take longer, but the properties of the aquifer are such that these impacts will eventually result in reduced spring discharge and depletions of Muddy River streamflow.

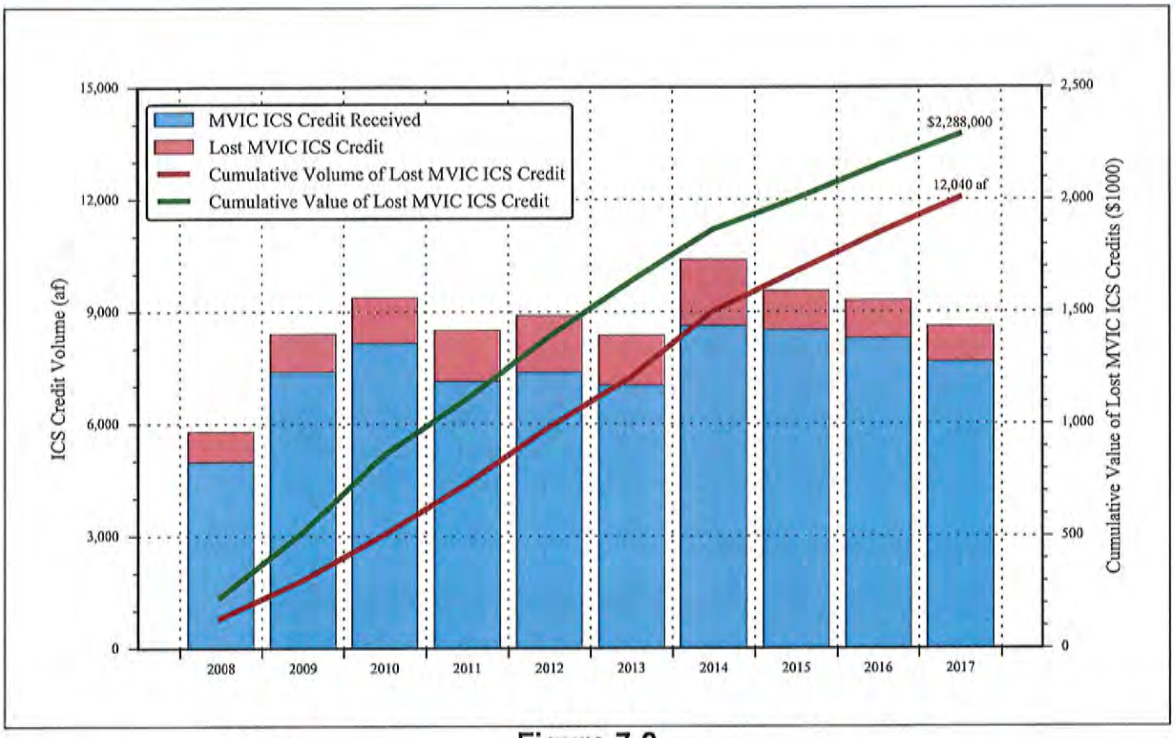

Figure 7-2
SNWA's Tributary ICS Credits and Credits Lost as a Result of Groundwater Production

8.0 RESPONSES TO NSE INTERIM ORDER 1303

An assessment of the current water-resource conditions for the LWRFS was performed and an analysis was completed to evaluate hydrologic responses to natural and anthropogenic stresses observed at various locations of interest. The analysis considered time-series data for several variables that describe the historical conditions of the hydrologic system over a period of decades. The analysis focused on the historical behavior of the Muddy River streamflow and the carbonate aquifer composing the LWRFS. The results and conclusions from this assessment are summarized in this section corresponding to the questions posed by the NSE in Order 1303.

A. Geographic Boundary of the LWRFS

The boundary of the LWRFS should be as defined by the NSE in Order 1303. The LWRFS is underlain by an interconnected distribution of carbonate rocks that constitute a laterally extensive and continuous aquifer extending beneath the basins and across the ranges. The data presented in Section 5.0 demonstrate that the aquifer responds similarly to changes in both groundwater production and recharge throughout the six basins composing the LWRFS. Observed trends are uniform across the system, with only slight variations in the magnitude of the responses. Drawdown responses to pumping stresses are small throughout the region; however, they are unequivocal and occur in very short time frames given the distances between the pumping centers and points of observation. This demonstrates the aquifer has a very high degree of hydraulic connection and should be treated as a single administrative unit.

B. Hydrologic responses to the cessation of the Order 1169 aquifer test

An analysis of the hydrologic responses to natural and anthropogenic stresses at wells and springs representative of the carbonate aquifer was performed for the LWRFS. Time-series charts of groundwater levels and gage records for the Pederson Spring and Warm Springs West gages were prepared for the period 1993 to 2018.

Small changes in the hydraulic heads (on the order of only 2-3 ft) have resulted in significant changes in the discharges from high-elevation springs. Additionally, the lack of any significant recovery response after the completion of the Order 1169 aquifer test and the fact that the system has yet to recover to pre-test levels are critical observations. These observations indicate that the aquifer has a very high transmissivity and low storage capacity (i.e., high aquifer diffusivity). As a result, the system is very sensitive to recharge and pumping stresses. The analysis observations and conclusions are listed below:

- Widespread responses to pumping stresses associated with the NSE Order 1169 aquifer test were observed in groundwater-level and spring-discharge records across all six basins of the LWRFS;

- High-elevation springs in the MRSA are highly sensitive to changes in carbonate groundwater levels and are most susceptible to impacts associated with carbonate groundwater production;
- By the end of the aquifer test, discharge from Pederson Spring decreased by about 0.15 cfs (to about 1/3 of baseflow).
- Spring discharge as measured at the Warm Springs West gage decreased about 0.3 cfs (< 10% of baseflow).
- Continuation of the aquifer test or pumping from the MX-5 well would have reduced flows at the Warm Springs West gage to the initial 2006 MOA trigger level (3.2 cfs), and lower depending on the duration.
- Groundwater levels and spring discharge rates have not recovered to pre-test levels.
- Recovery achieved its maximum levels between the first quarters of 2015 and 2016, or a period of time approximately equal to the duration of the pumping period.
- Carbonate groundwater levels and spring discharge-rates have declined since 2016.
- Flow measured at the Warm Springs West gage will reach Trigger Ranges sooner and at lower production rates than contemplated in the 2006 MOA if pumping in Coyote Spring Valley resumed at levels commensurate with the Order 1169 aquifer test.
- Given the current rates of carbonate groundwater production, recovery of groundwater levels and spring discharges to pre-test levels is not possible without extraordinary hydrology such as the 2004-2005 winter-season precipitation; and
- Even with such extraordinary hydrology, subsequent years of lesser precipitation with similar groundwater production volumes will result in a resumption of declining trends as has been observed in the historical record.

C. Groundwater production and the capture of the Muddy River (springs and river flows)

An evaluation of Muddy River streamflow was performed to identify the likely causes of a long-term trend of declining streamflow observed in the record of the MR Moapa gage since the early 1960s. Long-term climate variability and changes in land use were ruled out as major contributors to the decline. Annual records of winter-season precipitation, a reflection of climate conditions, indicate that the average annual precipitation during the period of declining streamflow (post-1965) is not substantively different than the average for the period prior to the decline (pre-1965). Land-use changes during this period may have had very short-term effects, but the incremental changes in consumptive uses above the gage have been minimal. Thus, the causes of the streamflow decline have been surface-water diversions above the MR Moapa gage and LWRFS groundwater production.

A period from 1993 to 2018, in which comprehensive records of Muddy River streamflow, surface-water diversions and groundwater production are available, were analyzed to estimate the

MR Flow Deficit. An average annual natural-flow record was constructed by adding annual surface-water diversions to the flood-adjusted flow record of the MR Moapa gage. The annual MR Flow Deficit was estimated by computing the difference between the average annual pre-development flow of the Muddy River and the natural-flow record. An analysis was performed to determine whether MRSA groundwater production could account for the MR Flow Deficit. The results of the analysis yielded the following observations and conclusions:

- Muddy River streamflow declined from a pre-development condition of 33,900 afy to a minimum of about 22,000 af in 2003.
- Since 2003, streamflow has steadily increased to its current rate of over 30,000 afy as a result of reduced surface-water diversions and MRSA groundwater production.
- The MR Flow Deficit peaked at about 7,500 af in 2003 and was about 2,300 af in 2018.
- MRSA groundwater production above the MR Moapa gage peaked in 2000 at 7,850 af, and was 1,990 af in 2018.
- Groundwater production from the MRSA alluvial reservoir depletes Muddy River streamflow on a 1:1 basis.
- Groundwater production from MRSA carbonate wells deplete Muddy River streamflow approaching a 1:1 basis. Groundwater production from other carbonate wells in the LWRFS deplete streamflow; however, their effect cannot be readily detected from the measurements.
- A significant increase in carbonate groundwater production, such as that which occurred during the NSE Order 1169 aquifer test, will cause sharp declines in carbonate-aquifer water levels and spring discharges.

An analysis was conducted to estimate the contribution of various springs to the total MRSA discharge over a period of several years and under different stress conditions. Ratios of spring discharge to total MRSA discharge were computed for the Pederson Spring Complex (as measured by the Warm Springs West gage), Baldwin Spring, and Jones Spring. Ratios were computed for the period 2001 to 2012 and were found to be relatively constant at 0.076, 0.061, and 0.034 (or 7.6, 6.1, and 3.4 percent of the total MRSA discharge), respectively. The fact that the ratios do not change under variable stress conditions indicates that the springs respond commensurately with the hydraulic head in the carbonate aquifer.

The ratio derived for the Warm Springs West gage was used to calculate reductions in the MRSA discharge that correspond to potential flow conditions at the Warm Springs West gage. Knowing that a reduction in the MRSA discharge could only be caused by a lowering of the hydraulic head in the carbonate aquifer, limits on production from the carbonate aquifer were quantified by calculating reductions in MRSA discharge (from predevelopment conditions) that correspond to selected discharge levels at the Warm Springs West gage, including trigger ranges set in the 2006 MOA. For example, a reduction of 0.62 cfs in the Warm Springs West discharge, from 3.82 to 3.20 cfs, corresponds to a decrease of approximately 8.16 cfs, or 5,908 afy in MRSA discharge. This value

represents the long-term average annual production from the carbonate aquifer that can occur while still maintaining an average flow rate of 3.20 cfs at the Warm Springs West gage.

The results of the Order 1169 aquifer test demonstrate that for the areas directly upgradient of the MRSA (i.e., Arrow Canyon and Coyote Spring Valley), impacts propagate to the high-elevation springs within a matter of weeks or months. In the long-term, the location of the production wells does not matter, groundwater withdrawn anywhere within the connected carbonate aquifer or the MRSA alluvial reservoir will impact the MRSA discharge and, consequently, deplete Muddy River streamflow. These impacts have already occurred, resulting in conflicts with senior water rights. In the short term, it is preferable to keep groundwater production away from the MRSA to protect flows in the high-elevations springs that are critical habitat for the Moapa dace while groundwater production is managed to a lower threshold.

The impacts of Muddy River streamflow depletions were analyzed and quantified. Groundwater production in the MRSA and, to a lesser extent, the rest of the LWRFS has depleted Muddy River streamflows and conflicted with senior surface-water rights adjudicated in the 1920 Muddy River Decree. Streamflow depletions between 2008 and 2017 have resulted in SNWA losing an estimated 12,040 af of potential Tributary Conservation ICS credits at a replacement cost of almost $2.3 million.

These data indicate that pumping simply cannot occur without conflicting with senior rights. While it is unreasonable to assume that all pumping in the LWRFS would be eliminated, it should not be permitted to continue without strict regulatory oversight and appropriate mitigation to affected senior water-right holders and adequate protections for the Moapa dace. If the conflicts with senior water-right holders are adequately addressed, the total annual groundwater production should be managed between 4,000 – 6,000 afy over the long-term.

D. The effects of moving water rights between alluvial wells and carbonate wells

Production wells completed in the alluvial reservoir adjacent to the Muddy River capture groundwater that would otherwise discharge to the river. In addition, MRSA production wells completed in the carbonate aquifer capture water that would otherwise replenish the alluvial reservoir through diffuse subsurface flow or discharge from discrete springs. Capturing this groundwater depletes the source of supply to the alluvial reservoir and springs, thereby, depleting the streamflow. In each case, this groundwater production conflicts with senior Muddy River water rights.

Changing points of diversion to move groundwater production from the MRSA alluvial reservoir to locations sourced by the carbonate aquifer will not mitigate these conflicts, only delay their inevitable occurrence. Such changes would exacerbate issues associated with the already over-appropriated carbonate aquifer by accelerating the timing of impacts to the high-elevation springs due to the additional groundwater production. The timing of impacts will vary based on the magnitude, duration, and location of groundwater production. The impacts may occur relatively quickly, within weeks or months, if additional groundwater production were to occur in areas directly upgradient from the MRSA. Groundwater production in areas farther away, may take longer, but the properties of the aquifer are such that these impacts will eventually result in reduced spring discharge and depletions of Muddy River streamflow.

E. Any other matter believed to be relevant to the NSE's analysis

In summary, all groundwater production within the LWRFS from the MRSA alluvial reservoir or carbonate aquifer will impact discharge to the MRSA and result in Muddy River streamflow depletions. Any streamflow depletion constitutes a conflict with senior-priority Muddy River water rights and must be mitigated. In addition, groundwater production from the carbonate aquifer has been shown to impact springs that provide critical habitat for the Moapa dace. The dramatic increase in Coyote Spring Valley groundwater production during the implementation of the Order 1169 aquifer test demonstrated that these impacts can occur in very short time frames.

9.0 REFERENCES

Beard, L.S., Anderson, R.E., Block, D.L., Bohannon, R.G., Brady, R.J., Castor, S.B., Duebendorfer, E.M., Faulds, J.E., Felger, T.J., Howard, K.A., Kuntz, M.A., and Williams, V.S., 2007, Preliminary geologic map of the Lake Mead 30' x 60' Quadrangle, Clark County, Nevada, and Mohave County, Arizona: U.S. Geological Survey Open-File Report 2007-1010, 109 p.

Bohannon, R.G., 1983, Geologic map, tectonic map and structure sections of the Muddy and northern Black Mountains, Clark County, Nevada: U.S. Geological Survey Miscellaneous Investigations Series Map I-1406, scale 1:62,500, two sheets.

Buqo, T., 2007, Carbonate development in the Muddy Springs area, in Coache, R., ed., Regional tour of the carbonate system guidebook: Nevada Water Resources Association, Clark County, Nevada, June 18-20, 2007, p. 5-6.

Burns, A.G., and Drici, W., 2011, Hydrology and water resources of Spring, Cave, Dry Lake, and Delamar valleys, Nevada and vicinity: Presentation to the Office of the Nevada State Engineer: Southern Nevada Water Authority, Las Vegas, Nevada.

Coyote Springs Land, 2013, Letter from Carl D. Savely to Jason King (Nevada State Engineer), regarding Report of Coyote Springs Investment LLC, Pursuant to Nevada State Engineer Order 1169A, dated June 14, 2013.

CSI, see Coyote Springs Land AKA Coyote Springs Investment, LLC.

Daly, C., Halbleib, M., Smith, J.I., Gibson, W.P., Doggett, M.K., Taylor, G.H., Curtis, J., and Pasteris, P.A., 2008, Physiographically sensitive mapping of climatological temperature and precipitation across the conterminous United States: International Journal of Climatology, Vol. 28, p. 2031-2064.

Daly, C., Neilson, R.P., and Phillips, D.L., 1994, A statistical-topographic model for mapping climatological precipitation over mountainous terrain: Journal of Applied Meteorology, Vol. 33, No. 2, p. 140-158.

Daly, C., Taylor, G., and Gibson, W., 1997, The PRISM approach to mapping precipitation and temperature: American Meteorological Society, Proceedings of the 10th AMS Conference on Applied Climatology, Reno, Nevada, October 20-23, 1997, p. 10-12.

Daly, C., Taylor, G.H., Gibson, W.P., and Parzybok, T., 1998, Development of high-quality spatial climate datasets for the United States: Proceedings of the First International Conference on Geospatial Information in Agriculture and Forestry, Lake Buena Vista, Florida, June 1-3, 1998, p. I-512-I-519.

Dixon, G.L., Donovan, D.J., and Rowley, P.D., 2007, Geology of Oak Springs Summit, in Coache, R., ed., Regional tour of the carbonate system guidebook: Nevada Water Resources Association, Clark County, Nevada, June 18-20, 2007, p. 71-72.

Dohrenwend, J.C., Schell, B.A., Menges, C.M., Moring, B.C., and McKittrick, M.A., 1996, Reconnaissance photogeologic map of young (Quaternary and late Tertiary) faults in Nevada, in Singer, D.A., ed., An analysis of Nevada's metal-bearing mineral resources: Nevada Bureau of Mines and Geology Open-File Report 96-2, p. 9-1-9-12.

Donovan, D.J., 2007, Geology of Muddy River Springs, in Coache, R., ed., Regional tour of the carbonate system guidebook: Nevada Water Resources Association, Clark County, Nevada, June 18-20, 2007, p. 1-2.

Donovan, D.J., Dixon, G.L., and Rowley, P.D., 2004, Detailed geologic mapping in the Muddy Springs area, Clark County, Nevada [abs.]: Nevada Water Resources Association Annual Conference, Mesquite, Nevada, February 24-26, 2004, p. 23.

Eakin, T. E., 1964, Ground-water appraisal of Coyote Spring and Kane Spring Valleys and Muddy River Springs area, Lincoln and Clark Counties, Nevada: Nevada Department of Conservation and Natural Resources, Ground-Water Resources Reconnaissance Series, Report 25, 40 p.

Eakin, T.E. and D.O. Moore, 1964, Uniformity of discharge of Muddy River Springs, Southeastern Nevada, and relation to interbasin movement of ground water, U.S. Geological Survey Professional Paper 50l-D, Pages Dl71-D176, Work done in cooperation with the Nevada Department of Conservation and Natural Resource, Carson City, Nev.

Eakin, T.E., 1966, A regional inter-basin ground-water system in the White River Area, Southeastern Nevada, published in Water Resources Research, Vol. 2, No. 2, pp. 251-271.

Ekren, E.B., Orkild, P.P., Sargent, K.A., and Dixon, G.L., 1977, Geologic map of Tertiary rocks, Lincoln County, Nevada: U.S. Geological Survey Miscellaneous Investigations Series Map -1041, scale 1:250,000.

Fenneman, N. M., 1931, Physiography of the western United States: Chapter 8: Basin and Range Province. First edition(?): New York, McGraw Hill Book Company, p. 326-395.

Guth, P.L., 1980, Geology of the Sheep Range, Clark County, Nevada: Massachusetts Institute of Technology, Cambridge, Massachusetts, unpublished Ph.D. dissertation, 189 p.

Halford, K., Garcia, C.A., Fenelon, J., and B. Mirus. 2012. Advanced methods for modeling water levels and estimating drawdowns with SeriesSEE, an Excel Add-in. USGS Techniques and Methods 4-F4. 30 pp.

Harrill, J.R., Gates, J.S., and Thomas, J.M., 1988, Major ground-water flow systems in the Great Basin region of Nevada, Utah, and adjacent states: U.S. Geological Survey Hydrologic Investigations Atlas HA-694-C, scale 1:1,000,000.

Heilweil, V.M., and Brooks, L.E., eds., 2011, Conceptual model of the Great Basin carbonate and alluvial aquifer system: U.S. Geological Survey Scientific Investigations Report 2010-5193, 191 p.

Huntington, J. Morton, C., Bromley, M. and Liebert, R., 2013, Analysis of evapotranspiration along the Muddy River and Warm Springs Natural Area, Desert Research Institute Technical memo prepared for Southern Nevada Water Authority.

Hydrologic Review Team, 2013, 2013 Annual Determination Report, prepared by the Hydrologic Review Team established under the Memorandum of Agreement dated April 20, 2006. Las Vegas, NV.

Hydrologic Review Team, 2014, 2014 Annual Determination Report, prepared by the Hydrologic Review Team established under the Memorandum of Agreement dated April 20, 2006. Las Vegas, NV.

Hydrologic Review Team, 2015, 2015 Annual Determination Report, prepared by the Hydrologic Review Team established under the Memorandum of Agreement dated April 20, 2006. Las Vegas, NV.

Hydrologic Review Team, 2016, 2016 Annual Determination Report, prepared by the Hydrologic Review Team established under the Memorandum of Agreement dated April 20, 2006. Las Vegas, NV.

Hydrologic Review Team, 2017, 2017 Annual Determination Report, prepared by the Hydrologic Review Team established under the Memorandum of Agreement dated April 20, 2006. Las Vegas, NV.

Hydrologic Review Team, 2018, 2018 Annual Determination Report, prepared by the Hydrologic Review Team established under the Memorandum of Agreement dated April 20, 2006. Las Vegas, NV.

Johnson, C., and M. Mifflin. 2013. Summary of Order 1169 testing impacts, per Order 1169A: a report prepared in cooperation with the Moapa Band of Paiutes. Submitted to Nevada Division Water Resources per Order 1169A, June 2013.

Johnson, J., 1999, Estimation of stormwater flows in Las Vegas Wash, Nevada and potential stormwater capture: In Las Vegas Wash Coordination Committee, (2000), Las Vegas Wash Comprehensive Adaptive Management Plan, Appendix 2.1, p. 1-31.

Johnson, J.A., 2007, Hydrology of Muddy River Springs, in Coache, R., ed., Regional tour of the carbonate system guidebook: Nevada Water Resources Association, Clark County, Nevada, June 18-20, 2007, p. 3-4.

Langenheim, V.E., Beard, L.S., and Faulds, J.E., 2010, Implications of geophysical analysis on basin geometry and fault offsets in the northern Colorado River extensional corridor and adjoining Lake Mead region, Nevada and Arizona, in Umhoefer, P.J., Beard, L.S., and Lamb, M.A., editors, Miocene tectonics of the Lake Mead region, central Basin and Range: Geological Society of America Special Paper 463, p. 39-59.

Langenheim, V.E., Miller, J.J., Page, W.R., and Grow, J.A., 2001, Thickness and geometry of Cenozoic deposits in California Wash area, Nevada, based on gravity and seismic-reflection data: U.S. Geological Survey Open-File Report 01-393, 26 p.

Maldonado, F., and Schmidt, D.L., 1991, Geologic map of the southern Sheep Range, Fossil Ridge, and Castle Rock area, Clark County, Nevada: U.S. Geological Survey Miscellaneous Investigations Series Map I-2086, scale 1:24,000.

Marshall, Z.L., and Williams, R.D., 2019, Assessment of Moapa dace and other groundwater-dependent special status species in the Lower White River Flow System, Presentation to the Office of the Nevada State Engineer: Southern Nevada Water Authority, Las Vegas, Nevada.

Myers, T., 2013, Comments on carbonate Order 1169 data and the groundwater flow system in Coyote Springs and Muddy River Springs Valley, Nevada; Technical memorandum dated June 12, 2013. Prepared for Great Basin Water Network, Baker, NV.

National Oceanic and Atmospheric Administration, 2018, Climate Division 4 monthly precipitation and temperature data for period of record (1895-2019), accessed multiple times between September 2018 and March 2019. Webpage: https://www.ncdc.noaa.gov/cag/divisional/time-series.

NDWR, See Nevada Division of Water Resources.

Nevada Division of Water Resources, 2018, Well log database [Internet], accessed multiple times between September 3 and September 14, 2018, available from http://water.nv.gov/welllogquery.aspx.

Nevada Division of Water Resources, 2018, Muddy River Springs Area (Upper Moapa Valley) Hydrographic Basin 13-219 Groundwater Pumpage Inventory Calendar Year 2017, Las Vegas, NV, 29 p.

Nevada Division of Water Resources, 2017, Muddy River Springs Area (Upper Moapa Valley) Hydrographic Basin 13-219 Groundwater Pumpage Inventory Calendar Year 2016, Las Vegas, NV, 30 p.

Nevada State Engineer, 2002, Order 1169, Holding in abeyance carbonate-rock aquifer system groundwater applications pending or to be filed in Coyote Springs Valley (Basin 210), Black Mountains Area (Basin 215), Garnet Valley (Basin 216), Hidden Valley (Casin 217), Muddy River Springs aka Upper Moapa Valley (Basin 219), Lower Moapa Valley (Basin 220), and for further study of the appropriation of water from the carbonate rock aquifer system, Lincoln and Clark Counties, Nevada. March 8, 2002. 11 p.

Nevada State Engineer, 2012, Order 1169A, Nevada State Engineer Order 1169A (1) Declaring the pumping test completed as of December 31,2012; (2) Rescinding the update of Exhibit No. 54; and (3) Stating that study participants may file a report addressing the information obtained from the study/pumping test and the availability of water, Carson City, NV, 3 p.

Nevada State Engineer, 2014a, Ruling 6254, In The Matter Of Applications 54055, 54056, 54057, 54058, 54059, 63272, 63273, 63274, 63275, 63276, 63867, 63868, 63869, 63870, 63871, 63872, 63873, 63874, 63875 and 63876 filed to appropriate the underground waters of the Coyote Spring Valley hydrographic basin (210), Clark County and Lincoln County, Nevada.

Nevada State Engineer, 2014b, Ruling 6255, In the matter of applications 64039, 64186, 64187, 64188, 64189, 64190, 64191, 64192, 67892, 71031, 72838, 72839, 72840, 72841, 79296, 79297, 79298, 79299, 79300, 79497, 79498 and 79518 filed to appropriate the underground waters of the Coyote Spring Valley hydrographic basin (210), Clark County And Lincoln) County, Nevada.

Nevada State Engineer, 2014c, Ruling 6256, In the matter of applications 54130, 54484, 62996, 62998, 64040, 64045, 64222, 64223, 67894, 79354, 79687, 79688, 79689, 79691 and 79903 filed to appropriate the underground waters of the Garnet Valley hydrographic basin (216), Clark County, Nevada.

Nevada State Engineer, 2014d, Ruling 6257, In the matter of applications 62997, 62999, 64038, 66162, 67895, 68501, 79355, 79692 and 79693 filed to appropriate the underground waters of the Hidden Valley hydrographic basin (217), Clark County, Nevada.

Nevada State Engineer, 2014e, Ruling 6258, In the matter of applications 54076, 54634, 64037, 65197, 65944, 65945, 65946, 65947, 65948, 65949, 65954, 65955, 66473, 66474, 66475, 66476, 67896 and 79690 filed to appropriate the underground waters of the California Wash hydrographic basin (218), Clark County, Nevada.

Nevada State Engineer, 2014f, Ruling 6259, In the matter of application 59369 filed to appropriate the underground waters) of the Muddy River Springs Area aka Upper Moapa Valley hydrographic basin (219), Clark County, Nevada.

Nevada State Engineer, 2014g, Ruling 6260, In the matter of applications 58592, 58593, 58594, 64041 and 67893 filed to appropriate) the underground waters of the Black Mountains Area hydrographic basin (215), Clark County, Nevada.

Nevada State Engineer, 2014h, Ruling 6261, In the matter of applications 59368, 59370, 59371, and 81019 filed to appropriate the underground waters of the Lower Moapa Valley hydrographic basin (220), Clark County, Nevada.

Nevada State Engineer, 2019, Interim Order 1303, Nevada State Engineer Interim Order 1303, Designating the administration of all water rights within Coyote Spring Valley hydrographic basin (210), a portion of Black Mountains Area basin (215), Garnet Valley basin (216), Hidden Valley basin (217), California Wash basin (218), And Muddy River Springs Area (Aka Upper Moapa Valley) basin (219) as a joint administrative unit, Holding in abeyance applications to change existing groundwater rights, and establishing a temporary moratorium, Carson City, NV, 15 pp.

NOAA, see National Oceanic and Atmospheric Administration.

NSE, see Nevada State Engineer.

Page, W.R., 1998, Geologic map of the Arrow Canyon NW quadrangle, Clark County, Nevada: U.S. Geological Survey Geologic Quadrangle Map GQ-1776, scale 1:24,000.

Page, W.R., and Pampeyan, E.H., 1996, Preliminary geologic map of the Paleozoic rocks in the Wildcat Wash SE and Wildcat Wash SW quadrangles, Lincoln and Clark Counties, Nevada: U.S. Geological Survey Open-File Report 96-26, 18 p., scale 1:24,000.

Page, W.R., Dixon, G.L., and Ash, S.R., 1992, Northern terminus of Mesozoic Dry Lake thrust fault, Arrow Canyon range, southeastern Nevada: Geological Society of America, Rocky Mountain Section, Abstracts with Programs, Vol. 24, No. 6, p. 56.

Page, W.R., Dixon, G.L., Rowley, P.D., and Brickey, D.W., 2005, Geologic map of parts of the Colorado, White River, and Death Valley groundwater flow systems-Nevada, Utah, and Arizona: Nevada Bureau of Mines and Geology Map 150, scale 1:250,000.

Page, W.R., Scheirer, D.S., Langenheim, V.E., and Berger, M.A., 2011, Revised geologic cross sections of parts of the Colorado, White River, and Death Valley regional groundwater flow systems, Nevada, Utah, and Arizona: U.S. Geological Survey Open-File Report 2006-1040.

Pampeyan, E.H., 1993, Geologic map of the Meadow Valley Mountains, Lincoln and Clark Counties, Nevada: U.S. Geological Survey Miscellaneous Investigations Series Map I-2173, scale 1:50,000.

Rowley, P.D., Dixon, G.L., Burns, A.G., Pari, K.T., Watrus, J.M., and Ekren, E.B., 2011, Geology and geophysics of Spring, Cave, Dry Lake, and Delamar valleys, White Pine and Lincoln Counties and adjacent areas, Nevada and Utah: The geologic framework of regional groundwater flow systems: Presentation to the Office of the Nevada State Engineer: Southern Nevada Water Authority, Las Vegas, Nevada.

Rowley, P.D., Dixon, G.L., Mankinen, E.A., Pari, K.T., McPhee, D.K., McKee, E.H., Burns, A.G., Watrus, J.M., Ekren, E.B., Patrick, W.G., and Brandt, J.M., 2017, Geology and Geophysics of White Pine and Lincoln Counties, Nevada, and adjacent parts of Nevada and Utah: The geologic framework of regional groundwater flow systems, Nevada Bureau of Mines and Geology Report 56, Prepared cooperatively by Geologic Mapping, Inc., New Harmony, Utah, U.S. Geological Survey, Menlo Park, California, Southern Nevada Water Authority, Las Vegas, Nevada and Private consultant, White Sulphur Springs, Montana.

Rowley, P.D., Nealey, L.D., Unruh, D.M., Snee, L.W., Mehnert, H.H., Anderson, R.E., and Grommé, C.S., 1995, Stratigraphy of Miocene ash-flow tuffs in and near the Caliente Caldera Complex, southeastern Nevada and southwestern Utah, in Scott, R.B., and Swadley, W.C., eds., Geologic studies in the Basin and Range-Colorado Plateau transition in southeastern Nevada, southwestern Utah, and northwestern Arizona: U.S. Geological Survey Bulletin 2056, p. 47-88.

Sauer, V.B. and R. W. Meyer, 1992, Determination of error in individual discharge measurements: U.S. Geological Survey Open-File Report 92-144, Norcross, Georgia.

Schaefer, D.H., Thiros, S.A., and Rosen, M.R., 2005; Ground-water quality in the Carbonate-Rock Aquifer of the Great Basin, Nevada and Utah, 2003: U.S. Geological Survey Scientific Investigations Report 2005-5232, 41 p.

Scheirer, D.S., Page, W.R., and Miller, J.J., 2006, Geophysical studies based on gravity and seismic data of Tule Desert, Meadow Valley Wash, and California Wash basins, southern Nevada,.U.S. Geological Survey Open-File Report 2006-1396, 44 p.

Schmidt, D.L., and Dixon, G.L., 1995, Geology and aquifer system of the Coyote Spring Valley area, southeastern Nevada: U.S. Geological Survey Open-File Report 95-579, 47 p.

Scott, R.B., and Swadley, W.C., eds., 1995, Geologic studies in the Basin and Range-Colorado Plateau transition in southeastern Nevada, southwestern Utah, and northwestern Arizona, 1992: U.S. Geological Survey Bulletin 2056, p. 5-42.

Scott, R.B., Rowley, P.D., Snee, L.W., Anderson, R.E., Harding, A.E., Unruh, D.M., Nealey, L.D., Hudson, M.R., Swadley, W.C., and Ferris, D.E., 1996, Synchronous Oligocene and Miocene extension and magmatism in the vicinity of caldera complexes in southeastern Nevada, in Thompson, R.A., Hudson, M.R., and Pillmore, C.L., eds., Geologic excursions to the Rocky Mountains and beyond-Field trip guidebook for the 1996 annual meeting, Geological Society of America, Denver, Colorado, October 28-31: Colorado Geological Survey Special Publication 44, (CD-ROM), 36 p.

SNWA, See Southern Nevada Water Authority.

Southern Nevada Water Authority, 2006, Memorandum of Agreement, dated April 20, 2006 for Muddy River: Las Vegas, NV: Southern Nevada Water Authority, 26 p.

Southern Nevada Water Authority, 2008, Volume 3: Physical settings of springs in Clark, Lincoln, and White Pine Counties Groundwater Development Project, 326 p.

Southern Nevada Water Authority, 2009a, Conceptual model of groundwater flow for the Central Carbonate-Rock Province-Clark, Lincoln, and White Pine Counties Groundwater Development Project: Southern Nevada Water Authority, Las Vegas, Nevada, 416 p.

Southern Nevada Water Authority, 2009b, Transient numerical model of groundwater flow for the Central Carbonate-Rock Province-Clark, Lincoln, and White Pine Counties Groundwater Development Project: Southern Nevada Water Authority, Las Vegas, Nevada, 394 p.

Southern Nevada Water Authority, 2009c, Muddy River tributary conservation intentionally created surplus certification report calendar year 2008: Southern Nevada Water Authority, Las Vegas, Nevada, 225 p.

Southern Nevada Water Authority, 2010, Addendum to the groundwater flow model for the Central Carbonate-Rock Province-Clark, Lincoln, and White Pine Counties Groundwater Development Project: Southern Nevada Water Authority, Las Vegas, Nevada, 48 p.

Southern Nevada Water Authority, 2011a, Muddy River tributary conservation intentionally created surplus certification report calendar year 2008: Southern Nevada Water Authority, Las Vegas, Nevada, 225 p.

Southern Nevada Water Authority, 2011b, Muddy River tributary conservation intentionally created surplus certification report calendar year 2009: Southern Nevada Water Authority, Las Vegas, Nevada, 274 p.

Southern Nevada Water Authority, 2012a, Muddy River tributary conservation intentionally created surplus certification report calendar year 2010: Southern Nevada Water Authority, Las Vegas, Nevada, 98 p.

Southern Nevada Water Authority, 2012b, Muddy River tributary conservation intentionally created surplus certification report calendar year 2011: Southern Nevada Water Authority, Las Vegas, Nevada, 104 p.

Southern Nevada Water Authority, 2013a, Monitoring report for Southern Nevada Water Authority and Las Vegas Valley Water District's groundwater right permits and applications in Coyote Spring Valley, Hidden Valley and Garnet Valley within Clark and Lincoln Counties, Nevada - calendar year 2012. Southern Nevada Water Authority, Las Vegas, Nevada.

Southern Nevada Water Authority, 2013b, Nevada State Engineer Order 1169 and 1169A study report: Southern Nevada Water Authority, Las Vegas, Nevada, Doc. No, WMP-ED-0001, 51 p.

Southern Nevada Water Authority, 2013c, Muddy River tributary conservation intentionally created surplus certification report calendar year 2012: Southern Nevada Water Authority, Las Vegas, Nevada, 93 p.

Southern Nevada Water Authority, 2014, 2013 Annual Monitoring Report for Southern Nevada Water Authority and Las Vegas Valley Water District groundwater permits in Coyote Spring, Garnet, and Hidden Valleys, Clark and Lincoln Counties, Nevada: Southern Nevada Water Authority, Las Vegas, Nevada, Doc. No. WMP-ED-0002, 67 p.

Southern Nevada Water Authority, 2015a, 2014 Annual monitoring report for Southern Nevada Water Authority groundwater permits in Coyote Spring, Garnet, and Hidden Valleys, Clark and Lincoln Counties, Nevada: Las Vegas, Nevada, Doc. No. WRD-ED-0029 72 p.

Southern Nevada Water Authority, 2015b, Muddy River tributary conservation intentionally created surplus certification report calendar year 2013: Southern Nevada Water Authority, Las Vegas, Nevada, 90 p.

Southern Nevada Water Authority, 2015c, Muddy River tributary conservation intentionally created surplus certification report calendar year 2014: Southern Nevada Water Authority, Las Vegas, Nevada, 84 p.

Southern Nevada Water Authority, 2016a: 2015 Annual SNWA monitoring report for Coyote Spring, Garnet, and Hidden Valleys, Clark and Lincoln Counties, Nevada: Las Vegas, Nevada, Doc. No. WRD-ED-0036, 72 p.

Southern Nevada Water Authority, 2016b, Muddy River tributary conservation intentionally created surplus certification report calendar year 2015: Southern Nevada Water Authority, Las Vegas, Nevada, 86 p.

Southern Nevada Water Authority, 2017a: 2016 Annual SNWA monitoring report for Coyote Spring, Garnet, and Hidden Valleys, Clark and Lincoln Counties, Nevada: Las Vegas, Nevada, Doc. No. WRD-ED-0042, 68 p.

Southern Nevada Water Authority, 2017b, Muddy river tributary conservation intentionally created surplus certification report calendar year 2016: Southern Nevada Water Authority, Las Vegas, Nevada, 87 p.

Southern Nevada Water Authority, 2018a, 2018 Water resource plan & water budget: Southern Nevada Water Authority, Las Vegas, Nevada, 82 p.

Southern Nevada Water Authority, 2018b, 2017 Annual monitoring report for SNWA groundwater permits in Coyote Spring, Garnet, and Hidden valleys, Clark and Lincoln counties, Nevada: Las Vegas, Nevada, Doc. No. WRD-ED-0048, 69 p.

Southern Nevada Water Authority, 2018c, Muddy River tributary conservation intentionally created surplus certification report calendar year 2017: Southern Nevada Water Authority, Las Vegas, Nevada, 86 p.

Southern Nevada Water Authority, 2019, 2018 Annual monitoring report for SNWA groundwater permits in Coyote Spring, Garnet, and Hidden valleys, Clark and Lincoln counties, Nevada: Las Vegas, Nevada, Doc. No. WRD-ED-0054, 72p.

Swadley, W.C., Page, W.R., Scott, R.B., and Pampeyan, E.H., 1994, Geologic map of the Delamar 3 SE quadrangle, Lincoln County, Nevada: U.S. Geological Survey Geologic Quadrangle Map-GQ-1754, scale 1:24,00.

Swanson, E., and Wernicke, B.P., 2017, Geologic map of the east-central Meadow Valley Mountains, and implications for reconstruction of the Mormon Peak detachment, Nevada: Geosphere, v. 13, no. 4, p. 1234-1253.

Tetra Tech, 2012a. Development of a numerical groundwater flow model of selected basins within the Colorado Regional Groundwater Flow System, Southeastern Nevada. Prepared for NPS, USFWS, and BLM. Prepared by Tetra Tech Inc., Louisville, CO.

Tetra Tech, 2012b. Predictions of the effects of groundwater pumping in the Colorado Regional Groundwater Flow System, Southeastern Nevada. Prepared for NPS, USFWS, and BLM. Prepared by Tetra Tech Inc., Louisville, CO.

United States Bureau of Reclamation, 2007, Record of Decision - Colorado river interim guidelines for Lower Basin shortages and the coordinated operations for Lake Powell and Lake Mead - Interim guidelines for the operation of Lake Powell and Lake Mead, December 2007, the Secretary of the Interior, Washington, D.C.

United States Fish and Wildlife Service, Bureau of Land Management, National Park Service, 2013, Test impacts and availability of water pursuant to applications pending under Order 1169, Presentation to the Office of the Nevada State Engineer, 92 p.

United States Geological Survey, 2018, National water information system, accessed multiple times between September 2018 and March 2019 at https://waterdata.usgs.gov/nwis

USFWS, see United States Fish and Wildlife Service.

USGS, see United States Geological Survey.

Winograd, I. J., Riggs, A. C., Coplen, T. B. 1998. The Relative Contributions of Summer and Cool-Season Precipitation to Groundwater Recharge, Spring Mountains, Nevada, USA, Hydrogeology Journal, Volume 6 p. 77-93, New York, NY: Published by Springer - Verlag.

Appendix A

Site Table for Wells

Table A-1
Site Table for Wells
(Page 1 of 3)

Site Name	UTM Northing (m)	UTM Easting (m)	Surface Elevation (ft amsl)	Drill Depth (ft bgs)	Well Depth (ft bgs)	Well Type[1]	Well Completion	Water Level Obs. Date	Depth to Water (ft-bgs)	Water Level Elevation (ft amsl)
KANE SPRINGS VALLEY (HA 206)										
KMW-1	4,098,863	689,882	2,870.60	—	—	M	Carbonate	1/3/2019	992.72	1,877.88
COYOTE SPRING VALLEY (HA 210)										
BEDROC 1	4,094,151	679,399	2,492.44	—	—	P	Basin Fill	—	—	—
BEDROC 2	4,094,374	679,009	2,529.00	—	—	P	Basin Fill	—	—	—
CE-VF-1	4,083,038	683,025	2,468.34	714	714	M	Basin Fill	2/6/2019	551.36	1,916.98
CE-VF-2	4,082,892	683,007	2,468.35	1,221	860	M	Carbonate	2/6/2019	600.08	1,868.27
CSI-1	4,074,459	686,044	2,278.05	935	920	P	Carbonate	2/4/2019	462.73	1,815.32
CSI-2	4,075,780	687,084	2,208.95	1,019	1,016	P	Carbonate	3/12/2019	391.41	1,817.54
CSI-3	4,077,518	685,809	2,334.51	1,156	1,152	P	Carbonate	3/12/2019	515.92	1,818.59
CSI-4	4,080,224	682,409	2,511.88	1,397	1,384	P	Carbonate	3/12/2019	691.04	1,820.84
CSV-3	4,062,583	685,222	2,415.93	780	756	M	Basin Fill	2/6/2019	595.48	1,820.45
CSV3009M	4,094,987	681,079	2,595.08	1,580	1,578	M	Basin Fill	2/20/2019	493.64	2,101.44
CSV3011M	4,094,873	684,075	2,665.72	1,580	1,555	M	Basin Fill	2/6/2019	751.00	1,914.72
CSVM-1	4,073,793	688,602	2,160.60	1,060	1,040	M	Carbonate	2/4/2019	342.70	1,817.90
CSVM-2	4,059,370	685,625	2,572.74	1,425	1,400	M	Carbonate	2/4/2019	752.11	1,820.63
CSVM-3	4,102,600	679,319	2,650.68	1,230	1,200	M	Carbonate	2/6/2019	444.56	2,206.12
CSVM-4	4,095,971	688,086	2,842.38	1,605	1,600	M	Carbonate	3/12/2019	969.57	1,872.81
CSVM-5	4,068,774	680,295	3,130.70	1,783	1,780	M	Carbonate	2/5/2019	1,079.51	2,051.19
CSVM-6	4,078,333	686,453	2,251.66	1,200	1,160	M	Carbonate	2/5/2019	436.13	1,815.53
CSVM-7	4,101,968	678,234	2,692.08	610	607	M	Basin Fill	2/6/2019	445.31	2,246.77
CSV-RW2	4,074,082	687,862	2,200.06	720	710	P	Carbonate	3/19/2019	384.54	1,815.52
MX-4	4,074,276	688,003	2,177.02	669	669	M	Carbonate	3/26/2019	356.36	1,820.66
MX-5	4,074,219	688,084	2,176.13	628	628	P	Carbonate	3/28/2019	357.56	1,818.57
BLACK MOUNTAINS AREA (HA 215)										
BM-DL-1	4,019,493	689,926	2,467.94	1,800	1,800	M	Carbonate	11/17/2011	650.74	1,817.20
BM-DL-2	4,019,591	689,270	2,487.56	1,400	1,400	M	Carbonate	3/11/2019	675.34	1,812.22
BM-ONCO-1	4,010,748	702,650	2,055.83	1,291	1,280	M	Clastic	2/4/2019	341.96	1,713.87
BM-ONCO-2	4,010,722	702,054	2,098.17	1,575	1,570	M	Clastic	2/4/2019	385.45	1,712.72
EBM-3	4,018,550	689,601	2,388.40	1,241	900	M	Carbonate	12/3/2017	579.00	1,809.40
EBM-4	4,018,828	689,782	2,391.14	1,134	1,128	M	Carbonate	3/1/2019	601.00	1,790.14
EBM-5	4,019,030	689,858	2,440.70	1,400	1,014	P	Carbonate	—	—	—
EBM-6	4,018,803	689,765	2,421.30	1,401	1,000	P	Carbonate	—	—	—
EBP-2	4,018,604	689,629	2,442.46	1,214	1,214	P	Carbonate	—	—	—
EGV-3	4,019,000	689,857	2,434.21	960	955	M	Carbonate	3/1/2019	611.00	1,823.21
GARNET VALLEY (HA 216)										
CRYSTAL 1	4,039,716	694,389	2,072.46	497	497	M	Carbonate	3/21/2019	261.44	1,811.02
CRYSTAL 2	4,039,284	694,146	2,069.91	565	565	M	Carbonate	—	—	—

Table A-1
Site Table for Wells
(Page 2 of 3)

Site Name	UTM Northing (m)	UTM Easting (m)	Surface Elevation (ft amsl)	Drill Depth (ft bgs)	Well Depth (ft bgs)	Well Type[1]	Well Completion	Water Level Obs. Date	Depth to Water (ft-bgs)	Water Level Elevation (ft amsl)
EBA-1	4,024,108	686,513	2,426.99	1,598	1,200	P	Carbonate	—	—	—
FIRST SOLAR	4,033,129	683,330	2,603.22	2,000	1,990	P	Carbonate	3/11/2019	792.90	1,810.32
GARNET	4,036,387	693,046	2,096.68	500	500	M	Basin Fill	—	—	—
GV-1	4,034,143	682,983	2,691.14	1,400	1,400	M	Carbonate	2/4/2019	883.58	1,807.56
GV-2	4,025,690	686,227	2,424.08	1,232	1,232	P	Carbonate	10/15/2018	610.63	1,813.45
GV-DUKE-WS1	4,029,104	686,286	2,243.50	685	685	P	Carbonate	3/11/2019	432.05	1,811.45
GV-DUKE-WS2	4,029,097	686,199	2,246.72	2,020	1,965	P	Carbonate	—	—	—
GV-KERR	4,029,147	683,738	2,404.60	1,145	1,145	P	Carbonate	—	—	—
GV-LENZIE-3[2]	4,029,329	686,247	2,247.00	1,960	1,920	P	Carbonate	3/11/2019	432.16	1,814.84
GV-MIRANT1	4,032,318	683,115	2,567.87	2,007	1,992	P	Carbonate	3/11/2019	756.92	1,810.95
GV-PW-MW1	4,031,730	683,460	2,502.27	1,500	1,500	M	Carbonate	2/5/2019	691.77	1,810.50
GV-PW-MW2	4,031,488	682,652	2,524.79	1,500	1,500	M	Carbonate	3/11/2019	715.02	1,809.77
GV-PW-WS1	4,031,435	683,005	2,532.29	2,020	2,000	P	Carbonate	3/13/2019	693.36	1,838.93
GV-RW1	4,036,645	692,928	2,069.20	870	833	P	Carbonate	12/13/2017	223.22	1,845.98
GV-USLIME1	4,026,564	687,748	2,286.48	860	860	P	Carbonate	—	—	—
GV-USLIME2	4,029,329	687,739	2,155.33	500	500	P	Basin Fill	—	—	—
HARVEY WELL	4,036,446	693,020	2,066.96	—	—	P	Carbonate	—	—	—
PAIUTES-M3	4,044,302	691,536	2,235	670	670	M	Carbonate	3/31/2019	423.19	1,811.81
RS-PW-1	4,028,841	690,787	2,240.00	860	860	P	Clastic	3/12/2019	511.63	1,728.37
RS-PW-2	4,027,890	690,674	2,412.00	—	—	P	Carbonate	—	—	—
RS-PW-3	4,029,719	691,026	2,162.00	720	720	P	Carbonate	—	—	—
RS-PW-5	4,029,626	691,053	2,076.94	—	—	P	Carbonate	—	—	—
RS-PW-6	4,026,318	690,552	2,471.00	—	—	P	Carbonate	—	—	—
RS-PW-7	4,027,940	691,938	2,420.00	940	940	P	Carbonate	—	—	—
Western Gypsum Well 1	4,028,739	688,924	2,197.00	725	725	P	Basin Fill	—	—	—
HIDDEN VALLEY (HA 217)										
SHV-1	4,047,256	685,751	2,650.32	920	—	M	Basin Fill	2/7/2019	834.38	1,815.94
CALIFORNIA WASH (HA 218)										
BYRON	4,051,282	710,993	1,903.06	1,095	1,095	M	Basin Fill	3/6/2019	238.32	1,664.74
PAIUTES-ECP1	4,046,590	696,729	2,230.05	1,170	1,125	P	Carbonate	3/13/2011	414.96	1,815.09
PAIUTES-ECP2	4,046,742	696,723	2,228.33	1,228	—	P	Carbonate	3/31/2019	414.86	1,813.47
PAIUTES-ECP3	4,046,984	696,714	2,243.08	1,500	—	P	Carbonate	—	—	—
PAIUTES-M1	4,057,109	704,517	1,895.69	400	400	M	Carbonate	3/31/2019	82.26	1,813.43
PAIUTES-M2	4,040,876	695,836	2,108.50	680	680	M	Carbonate	3/31/2019	298.17	1,810.33
PAIUTES-TH1	4,044,959	697,234	2,169.95	1,100	—	P	Carbonate	—	—	—
PAIUTES-TH2	4,049,916	697,684	2,338.09	1,198	—	M	Carbonate	3/31/2019	526.21	1,811.88

Table A-1
Site Table for Wells
(Page 3 of 3)

Site Name	UTM Northing (m)	UTM Easting (m)	Surface Elevation (ft amsl)	Drill Depth (ft bgs)	Well Depth (ft bgs)	Well Type[1]	Well Completion	Water Level Obs. Date	Depth to Water (ft-bgs)	Water Level Elevation (ft amsl)
MUDDY RIVER SPRINGS AREA (HA 219)										
ABBOTT	4,065,656	706,443	1,712.34	100	100	M	Basin Fill	3/19/2019	10.84	1,701.50
ARROW CANYON	4,067,763	701,108	1,861.45	565	565	P	Carbonate	2/28/2019	48.87	1,812.58
ARROW CANYON 2	4,067,750	701,083	1,863.29	746	742	P	Carbonate	11/6/2018	49.40	1,813.89
BEHMER MONITORIING	4,065,080	706,031	1,716.59	115	115	P	Basin Fill	7/25/2018	11.64	1,704.95
CSV-1	4,071,630	691,378	2,160.25	765	765	M	Basin Fill	3/6/2019	350.61	1,809.64
CSV-2	4,072,967	703,217	2,188.68	—	478	M	Carbonate	3/31/2019	395.52	1,793.16
EH-4	4,064,736	703,929	1,933.93	285	285	M	Carbonate	3/19/2019	120.65	1,813.28
EH-5B	4,067,619	701,569	1,844.80	265	264	M	Carbonate	3/19/2019	31.56	1,813.24
LDS CENTRAL	4,066,544	704,114	1,762.78	52	50	P	Basin Fill	11/20/2017	3.88	1,758.90
LDS EAST	4,066,594	704,479	1,753.13	77	77	P	Basin Fill	3/19/2019	7.27	1,745.86
LDS WEST	4,067,083	702,746	1,807.80	80	80	P	Basin Fill	3/19/2019	19.95	1,787.85
LEWIS 1	4,068,043	702,164	1,823.07	90	90	P	Basin Fill	—	—	—
LEWIS 1 OLD	4,068,229	702,077	1,828.71	58	58	M	Basin Fill	3/19/2019	29.86	1,798.85
LEWIS 2	4,067,886	702,365	1,826.04	100	100	P	Basin Fill	3/19/2019	28.92	1,797.12
LEWIS 3	4,068,022	701,963	1,825.08	100	100	P	Basin Fill	—	—	—
LEWIS 4	4,067,618	702,029	1,832.87	97	97	P	Basin Fill	—	—	—
LEWIS 5	4,067,484	702,195	1,828.11	93	93	P	Basin Fill	—	—	—
LEWIS NORTH	4,067,872	701,589	1,844.71	70	70	M	Basin Fill	3/19/2019	34.79	1,809.92
LEWIS SOUTH	4,067,266	702,737	1,808.10	90	90	M	Basin Fill	3/19/2019	14.74	1,793.36
MX-6	4,071,381	697,482	2,278.11	937	937	P	Carbonate	3/29/2019	463.30	1,814.81
PERKINS OLD	4,065,223	705,637	1,728.51	60	60	M	Basin Fill	3/19/2019	20.48	1,708.03
PERKINS PRODUCTION	4,065,206	705,693	1,734.86	135	135	P	Basin Fill	3/19/2019	21.33	1,713.53
UMVM-1	4,070,248	694,305	2,061.88	1,785	1,780	M	Carbonate	3/6/2019	247.46	1,814.42

[1] Well Type: M = Monitoring well, P = Production well
[2] GV-LENZIE-3 is the replacement well for GV-DUKE-WS2, which was plugged and abandoned in 2016

Appendix B

Surface Water Diversions above the MR Moapa Gage

Table B-1
Surface Water Diversions above the MR Moapa Gage in the MRSA

Year	Nevada Energy Muddy River Diversion (afy)	Moapa Valley Water District Diversions	
		Baldwin Spring Box (afy)	Pipeline-Jones Spring Box (afy)
1978	2,910	—	—
1979	2,850	—	—
1980	2,630	—	—
1981	2,740	—	—
1982	2,490	—	—
1983	1,720	—	—
1984	2,280	—	—
1985	—	—	—
1986	—	—	—
1987	—	—	—
1988	2,164	—	—
1989	2,012	—	—
1990	3,526	—	—
1991	3,625	—	—
1992	2,942	492[1]	318[1]
1993	3,083	922	684
1994	2,462	948	660
1995	2,950	1,449	750
1996	3,219	1,707	659
1997	2,494	1,771	656
1998	2,296	646	700
1999	2,585	250	656
2000	3,063	53	635
2001	3,573	101	690
2002	3,727	210	635
2003	3,651	9	653
2004	2,923	44	664
2005	2,535	248	642
2006	1,659	569	699
2007	2,776	719	681
2008	2,791	332	702
2009	2,496	1,166	322
2010	2,283	1,119	202
2011	1,287	605	3
2012	393	27	3
2013	17	131	1
2014	230	990	50
2015	0	92	0
2016	0	89	0
2017	0	126	0
2018	0	802	0

[1] Value reflects a partial year of production.

Appendix C

Groundwater Production Data

Table C-1
Shallow Alluvial Wells in the Muddy River Springs Area Pumped by Nevada Energy

Well Name	Well Log	Township	Range	Section	Section Quarter	Depth Cased[a]	Top of Perforation[a]	Bottom of Perforation[a]	Well Completion Date[b]
Lewis 1	27268	14S	65E	8	NW NE	90	30	90	3/7/1986
Lewis 2	62870	14S	65E	8	SE NE	100	35	100	6/22/1972
Lewis 3	12727	14S	65E	8	SW NE	100	35	100	6/22/1972
Lewis 4	10853	14S	65E	8	NW SE	97	38	88	4/12/1969
Lewis 5	10852	14S	65E	8	NW SE	93	38	88	5/6/1969
Perkins Production	31969	14S	65E	22	NE NE	135	25	125	6/16/1988
Behmer	15623	14S	65E	23	NW NW	115	30	115	5/20/1976
LDS East	102501	14S	65E	15	NW NW	77	17	77	6/15/1988
LDS Central	102500	14S	65E	16	NE NE	50	25	50	6/15/1988
LDS West	62880	14S	65E	9	SW SW	80	10	80	11/26/1968

[a]Depth cased, Top of Perforation and Bottom of Perforation depths are in feet below land surface.
[b]Well completion dates listed are the most recent well restoration/repair dates and may not reflect installation dates.

Table C-2
MRSA Annual Groundwater Production

Year	Alluvial Well Development (afy)			Carbonate Well Development (afy)
	Lewis Wells	LDS Wells	Perkins & Behmer Wells	
1987	1,188	0	816	---
1988	1,887	1,811	942	---
1989	1,682	1,820	1,746	---
1990	1,485	1,559	997	---
1991	1,182	1,310	1,240	---
1992	1,160	1,482	776	513[1]
1993	1,648	905	1,104	1,169
1994	2,074	1,468	899	894
1995	1,299	1,583	581	678
1996	1,522	2,097	1,134	705
1997	1,195	2,175	726	808
1998	2,259	2,903	804	2,039
1999	1,876	2,390	482	2,579
2000	1,773	3,169	1,024	2,908
2001	1,303	2,257	1,320	2,743
2002	2,139	2,051	1,545	2,573
2003	1,514	2,159	1,345	2,816
2004	1,568	1,802	1,080	2,718
2005	1,699	2,138	1,390	2,557
2006	1,846	2,591	1,285	2,966
2007	1,278	2,227	1,235	2,079
2008	1,509	1,626	1,150	2,272
2009	1,007	1,532	1,553	2,034
2010	1,315	1,386	1,194	1,826
2011	1,826	1,496	1,070	1,837
2012	869	1,018	1,189	2,638
2013	1,279	1,047	1,637	2,496
2014	2,160	1,255	1,411	1,442
2015	473	176	639	2,395
2016	661	276	0	2,798
2017	136	240	159	2,819
2018	13	0	0	1,979

[1] Value reflects a partial year of production.

Table C-3
LWRFS Carbonate-Aquifer Annual Groundwater Production

Year	Coyote Spring Valley (afy)	Black Mountains Area (afy)[1]	Garnet Valley (afy)	California Wash (afy)	Muddy River Springs Area (afy)	Total (afy)
1992	---	---	---	---	513[2]	513
1993	---	---	---	---	1,169	1,169
1994	---	---	---	---	894	894
1995	---	---	---	---	678	678
1996	---	1,613	145	---	705	2,463
1997	---	1,579	126	---	808	2,514
1998	---	1,408	131	---	2,039	3,578
1999	---	1,569	536	---	2,579	4,684
2000	---	1,693	509	---	2,908	5,110
2001	---	1,588	732	---	2,743	5,063
2002	---	1,744	967	---	2,573	5,284
2003	---	1,709	917	---	2,816	5,442
2004	---	1,710	878	---	2,718	5,306
2005	259	1,640	992	---	2,557	5,448
2006	1,277	1,569	1,050	---	2,966	6,861
2007	2,781	1,585	1,141	---	2,079	7,585
2008	1,690	1,591	1,538	---	2,272	7,091
2009	1,413	1,568	1,510	15	2,034	6,541
2010	2,672	1,561	1,257	19	1,826	7,336
2011	5,331	1,398	1,250	26	1,837	9,841
2012	5,101	1,556	1,253	21	2,638	10,568
2013	2,992	1,585	1,237	59	2,496	8,369
2014	1,643	1,430	1,191	288	1,442	5,994
2015	1,494	1,448	1,395	411	2,395	7,144
2016	1,117	1,434	2,242	200	2,798	7,791
2017	1,399	1,507	1,861	43	2,819	7,630
2018	1,967	1,623	1,751	24	1,979	7,344

[1] Values represent the combined production of NV Cogeneration Association wells EBM-4, EBM-5, EBM-6, EBP-2, and EGV-2

[2] Value reflects a partial year of production.

Table C-4
Groundwater Production
(Page 1 of 32)

Hydrographic Area	Well Name	Aquifer Material	Year	Production (gallons)	Production (af)	Comments	Source
210	BEDROC WELLS	Basin Fill	2012	209,512,417	642.97	Combined BEDROC wells 1-4	Western Elite, 2018
210	BEDROC WELLS	Basin Fill	2013	213,748,480	655.97	Combined BEDROC wells 1-4	Western Elite, 2018
210	BEDROC WELLS	Basin Fill	2014	189,977,650	583.02	Combined BEDROC wells 1-4	Western Elite, 2018
210	BEDROC WELLS	Basin Fill	2015	206,397,282	633.41	Combined BEDROC wells 1-6	Western Elite, 2018
210	BEDROC WELLS	Basin Fill	2016	200,632,978	615.72	Combined BEDROC wells 1-6	Western Elite, 2018
210	BEDROC WELLS	Basin Fill	2017	181,736,878	557.73	Combined BEDROC wells 1-7	Western Elite, 2018
210	CSI-1	Carbonate	2005	70,382,000	215.99		NDWR, 2018a
210	CSI-1	Carbonate	2006	235,338,000	722.23		NDWR, 2018a
210	CSI-1	Carbonate	2007	247,947,000	760.92		NDWR, 2018a
210	CSI-1	Carbonate	2008	14,273,000	43.80		NDWR, 2018a
210	CSI-1	Carbonate	2009	0	0.00		NDWR, 2018a
210	CSI-1	Carbonate	2010	0	0.00		NDWR, 2018a
210	CSI-1	Carbonate	2011	0	0.00		NDWR, 2018a
210	CSI-1	Carbonate	2012	6,885,242	21.13		NDWR, 2018a
210	CSI-1	Carbonate	2013	386,506,510	1,186.14		NDWR, 2018a
210	CSI-1	Carbonate	2014	294,814,000	904.75		NDWR, 2018a
210	CSI-1	Carbonate	2015	186,961,000	573.76		NDWR, 2018a
210	CSI-1	Carbonate	2016	233,857,000	717.68		NDWR, 2018a
210	CSI-1	Carbonate	2017	399,700,000	1,226.63		NDWR, 2018a
210	CSI-1	Carbonate	2018	131,660,000	404.05		NDWR, 2019a
210	CSI-2	Carbonate	2005	13,851,000	42.51		NDWR, 2018a
210	CSI-2	Carbonate	2006	170,586,000	523.51		NDWR, 2018a
210	CSI-2	Carbonate	2007	489,531,000	1,502.32		NDWR, 2018a
210	CSI-2	Carbonate	2008	313,515,000	962.14		NDWR, 2018a
210	CSI-2	Carbonate	2009	4,180,000	12.83		NDWR, 2018a
210	CSI-2	Carbonate	2010	0	0.00		NDWR, 2018a
210	CSI-2	Carbonate	2011	0	0.00		NDWR, 2018a

Table C-4
Groundwater Production
(Page 2 of 32)

Hydrographic Area	Well Name	Aquifer Material	Year	Production (gallons)	Production (af)	Comments	Source
210	CSI-2	Carbonate	2012	0	0.00		NDWR, 2018a
210	CSI-2	Carbonate	2013	0	0.00		NDWR, 2018a
210	CSI-2	Carbonate	2014	0	0.00		NDWR, 2018a
210	CSI-2	Carbonate	2015	0	0.00		NDWR, 2018a
210	CSI-2	Carbonate	2016	0	0.00		NDWR, 2018a
210	CSI-2	Carbonate	2017	0	0.00		NDWR, 2018a
210	CSI-2	Carbonate	2018	499,023,000	1531.45		NDWR, 2019a
210	CSI-3	Carbonate	2006	10,164,000	31.19		NDWR, 2018a
210	CSI-3	Carbonate	2007	160,672,000	493.08		NDWR, 2018a
210	CSI-3	Carbonate	2008	209,739,000	643.67		NDWR, 2018a
210	CSI-3	Carbonate	2009	263,978,000	810.12		NDWR, 2018a
210	CSI-3	Carbonate	2010	340,371,348	1,044.56		NDWR, 2018a
210	CSI-3	Carbonate	2011	233,891,372	717.79		NDWR, 2018a
210	CSI-3	Carbonate	2012	183,781,356	564.00		NDWR, 2018a
210	CSI-3	Carbonate	2013	11,779,752	36.15		NDWR, 2018a
210	CSI-3	Carbonate	2014	0	0.00		NDWR, 2018a
210	CSI-3	Carbonate	2015	0	0.00		NDWR, 2018a
210	CSI-3	Carbonate	2016	0	0.00		NDWR, 2018a
210	CSI-3	Carbonate	2017	0	0.00		NDWR, 2018a
210	CSI-3	Carbonate	2018	0	0.00		NDWR, 2019a
210	CSI-4	Carbonate	2007	7,898,000	24.24		NDWR, 2018a
210	CSI-4	Carbonate	2008	3,339,000	10.25		NDWR, 2018a
210	CSI-4	Carbonate	2009	187,369,000	575.01		NDWR, 2018a
210	CSI-4	Carbonate	2010	79,486,396	243.93		NDWR, 2018a
210	CSI-4	Carbonate	2011	156,854,000	481.37		NDWR, 2018a
210	CSI-4	Carbonate	2012	180,845,000	554.99		NDWR, 2018a
210	CSI-4	Carbonate	2013	0	0.00		NDWR, 2018a

Table C-4
Groundwater Production
(Page 3 of 32)

Hydrographic Area	Well Name	Aquifer Material	Year	Production (gallons)	Production (af)	Comments	Source
210	CSI-4	Carbonate	2014	101,517,000	311.54		NDWR, 2018a
210	CSI-4	Carbonate	2015	174,209,000	534.63		NDWR, 2018a
210	CSI-4	Carbonate	2016	130,213,000	399.61		NDWR, 2018a
210	CSI-4	Carbonate	2017	56,300,000	172.78		NDWR, 2018a
210	CSI-4	Carbonate	2018	9,116,000	27.98		NDWR, 2019a
210	CSV-RW2	Carbonate	2000	0	0.00		NDWR, 2018a
210	CSV-RW2	Carbonate	2001	0	0.00		NDWR, 2018a
210	CSV-RW2	Carbonate	2002	0	0.00		NDWR, 2018a
210	CSV-RW2	Carbonate	2003	0	0.00		NDWR, 2018a
210	CSV-RW2	Carbonate	2004	0	0.00		NDWR, 2018a
210	CSV-RW2	Carbonate	2005	0	0.00		NDWR, 2018a
210	CSV-RW2	Carbonate	2006	0	0.00		NDWR, 2018a
210	CSV-RW2	Carbonate	2007	0	0.00		NDWR, 2018a
210	CSV-RW2	Carbonate	2008	0	0.00		NDWR, 2018a
210	CSV-RW2	Carbonate	2009	0	0.00		NDWR, 2018a
210	CSV-RW2	Carbonate	2010	0	0.00		NDWR, 2018a
210	CSV-RW2	Carbonate	2011	0	0.00		NDWR, 2018a
210	CSV-RW2	Carbonate	2012	0	0.00		NDWR, 2018a
210	CSV-RW2	Carbonate	2013	0	0.00		NDWR, 2018a
210	CSV-RW2	Carbonate	2014	0	0.00		NDWR, 2018a
210	CSV-RW2	Carbonate	2015	0	0.00		NDWR, 2018a
210	CSV-RW2	Carbonate	2016	0	0.00		NDWR, 2018a
210	CSV-RW2	Carbonate	2017	0	0.00		NDWR, 2018a
210	CSV-RW2	Carbonate	2018	0	0.00		NDWR, 2019a
210	MX-5	Carbonate	2008	9,819,500	30.13		SNWA, 2010
210	MX-5	Carbonate	2009	5,017,300	15.40		SNWA, 2010
210	MX-5	Carbonate	2010	450,905,191	1,383.78		NDWR, 2018a

Table C-4
Groundwater Production
(Page 4 of 32)

Hydrographic Area	Well Name	Aquifer Material	Year	Production (gallons)	Production (af)	Comments	Source
210	MX-5	Carbonate	2011	1,346,243,737	4,131.47		NDWR, 2018a
210	MX-5	Carbonate	2012	1,290,557,441	3,960.58		NDWR, 2018a
210	MX-5	Carbonate	2013	576,659,399	1,769.70		NDWR, 2018a
210	MX-5	Carbonate	2014	138,903,080	426.28		NDWR, 2018a
210	MX-5	Carbonate	2015	125,583,895	385.40		NDWR, 2018a
210	MX-5	Carbonate	2016	0	0.00		NDWR, 2018a
210	MX-5	Carbonate	2017	0	0.00		NDWR, 2018a
210	MX-5	Carbonate	2018	1,265,648	3.88		NDWR, 2019a
215	EBM-4	Carbonate	1996	209,745,000	643.68		NDWR, 2018b
215	EBM-4	Carbonate	1997	252,361,100	774.47		NDWR, 2018b
215	EBM-4	Carbonate	1998	240,830,000	739.08		NDWR, 2018b
215	EBM-4	Carbonate	1999	243,225,000	746.43		NDWR, 2018b
215	EBM-4	Carbonate	2000	259,923,000	797.67		NDWR, 2018a
215	EBM-4	Carbonate	2001	277,466,000	851.51		NDWR, 2018a
215	EBM-4	Carbonate	2002	281,379,000	863.52		NDWR, 2018a
215	EBM-4	Carbonate	2003	176,807,000	542.60		NDWR, 2018a
215	EBM-4	Carbonate	2004	235,330,000	722.20		NDWR, 2018a
215	EBM-4	Carbonate	2005	250,208,000	767.86		NDWR, 2018a
215	EBM-4	Carbonate	2006	247,516,000	759.60		NDWR, 2018a
215	EBM-4	Carbonate	2007	253,668,000	778.48		NDWR, 2018a
215	EBM-4	Carbonate	2008	99,584,000	305.61		NDWR, 2018a
215	EBM-4	Carbonate	2009	208,401,000	639.56		NDWR, 2018a
215	EBM-4	Carbonate	2010	312,428,000	958.81		NDWR, 2018a
215	EBM-4	Carbonate	2011	253,605,000	778.29		NDWR, 2018a
215	EBM-4	Carbonate	2012	230,985,264	708.87		NDWR, 2018a
215	EBM-4	Carbonate	2013	218,728,708	671.25		NDWR, 2018a
215	EBM-4	Carbonate	2014	224,975,000	690.42		NDWR, 2018a

Table C-4
Groundwater Production
(Page 5 of 32)

Hydrographic Area	Well Name	Aquifer Material	Year	Production (gallons)	Production (af)	Comments	Source
215	EBM-4	Carbonate	2015	116,017,840	356.05	Converted to monitoring well and replaced with well EBM-6 as new production well.	NDWR, 2018a
215	EBM-5	Carbonate	2015	93,435,000	286.74		NDWR, 2018a
215	EBM-5	Carbonate	2016	244,061,013	749.00		NDWR, 2018a
215	EBM-5	Carbonate	2017	271,995,048	834.72		NDWR, 2018a
215	EBM-5	Carbonate	2018	167,309,392	513.45		NDWR, 2019a
215	EBM-6	Carbonate	2015	65,970,000	202.45		NDWR, 2018a
215	EBM-6	Carbonate	2016	194,914,456	598.17		NDWR, 2018a
215	EBM-6	Carbonate	2017	208,396,543	639.55		NDWR, 2018a
215	EBM-6	Carbonate	2018	261,318,592	801.96		NDWR, 2019a
215	EBP-2	Carbonate	1996	64,080,000	196.65		NDWR, 2018b
215	EBP-2	Carbonate	1997	33,070,000	101.49		NDWR, 2018b
215	EBP-2	Carbonate	1998	9,314,000	28.58		NDWR, 2018b
215	EBP-2	Carbonate	1999	36,840,000	113.06		NDWR, 2018b
215	EBP-2	Carbonate	2000	21,987,000	67.48		NDWR, 2018a
215	EBP-2	Carbonate	2001	1,179,000	3.62		NDWR, 2018a
215	EBP-2	Carbonate	2002	23,157,000	71.07		NDWR, 2018a
215	EBP-2	Carbonate	2003	166,841,000	512.02		NDWR, 2018a
215	EBP-2	Carbonate	2004	56,501,000	173.40		NDWR, 2018a
215	EBP-2	Carbonate	2005	483,000	1.48		NDWR, 2018a
215	EBP-2	Carbonate	2006	33,961,000	104.22		NDWR, 2018a
215	EBP-2	Carbonate	2007	171,000	0.52		NDWR, 2018a
215	EBP-2	Carbonate	2008	200,241,000	614.52		NDWR, 2018a
215	EBP-2	Carbonate	2009	23,172,000	71.11		NDWR, 2018a
215	EBP-2	Carbonate	2010	59,286,000	181.94		NDWR, 2018a
215	EBP-2	Carbonate	2011	795,000	2.44		NDWR, 2018a
215	EBP-2	Carbonate	2012	10,324,000	31.68		NDWR, 2018a
215	EBP-2	Carbonate	2013	41,058,893	126.01		NDWR, 2018a

Table C-4
Groundwater Production
(Page 6 of 32)

Hydrographic Area	Well Name	Aquifer Material	Year	Production (gallons)	Production (af)	Comments	Source
215	EBP-2	Carbonate	2014	1,954,000	6.00		NDWR, 2018a
215	EBP-2	Carbonate	2015	77,104,404	236.62		NDWR, 2018a
215	EBP-2	Carbonate	2016	28,249,904	86.70		NDWR, 2018a
215	EBP-2	Carbonate	2017	10,769,028	33.05		NDWR, 2018a
215	EBP-2	Carbonate	2018	100,124,568	307.27		NDWR, 2019a
215	EGV-3	Carbonate	1996	251,694,000	772.42		NDWR, 2018b
215	EGV-3	Carbonate	1997	228,981,000	702.72		NDWR, 2018b
215	EGV-3	Carbonate	1998	208,759,000	640.66		NDWR, 2018b
215	EGV-3	Carbonate	1999	231,181,000	709.47		NDWR, 2018b
215	EGV-3	Carbonate	2000	269,747,000	827.82		NDWR, 2018a
215	EGV-3	Carbonate	2001	238,938,000	733.27		NDWR, 2018a
215	EGV-3	Carbonate	2002	263,821,000	809.64		NDWR, 2018a
215	EGV-3	Carbonate	2003	213,277,000	654.52		NDWR, 2018a
215	EGV-3	Carbonate	2004	265,500,000	814.79		NDWR, 2018a
215	EGV-3	Carbonate	2005	283,714,000	870.69		NDWR, 2018a
215	EGV-3	Carbonate	2006	229,758,000	705.10		NDWR, 2018a
215	EGV-3	Carbonate	2007	262,651,000	806.05		NDWR, 2018a
215	EGV-3	Carbonate	2008	218,745,000	671.30		NDWR, 2018a
215	EGV-3	Carbonate	2009	279,226,000	856.91		NDWR, 2018a
215	EGV-3	Carbonate	2010	136,945,232	420.27		NDWR, 2018a
215	EGV-3	Carbonate	2011	201,293,696	617.75		NDWR, 2018a
215	EGV-3	Carbonate	2012	265,637,176	815.21		NDWR, 2018a
215	EGV-3	Carbonate	2013	256,576,104	787.40		NDWR, 2018a
215	EGV-3	Carbonate	2014	239,081,000	733.71		NDWR, 2018a
215	EGV-3	Carbonate	2015	119,275,720	366.04	Converted to a monitoring well and replaced by well EBM-5 as new production well.	NDWR, 2018a
216	EBA-1	Carbonate	1996	47,268,400	145.06		NDWR, 2019a

Table C-4
Groundwater Production
(Page 7 of 32)

Hydrographic Area	Well Name	Aquifer Material	Year	Production (gallons)	Production (af)	Comments	Source
216	EBA-1	Carbonate	1997	41,192,100	126.41		NDWR, 2019a
216	EBA-1	Carbonate	1998	42,663,100	130.93		NDWR, 2019a
216	EBA-1	Carbonate	1999	48,703,500	149.47		NDWR, 2019a
216	EBA-1	Carbonate	2000	12,835,500	39.39		NDWR, 2019a
216	EBA-1	Carbonate	2001	48,831,300	149.86		NDWR, 2019a
216	EBA-1	Carbonate	2002	45,366,300	139.22		NDWR, 2019a
216	EBA-1	Carbonate	2003	61,443,600	188.56		NDWR, 2019a
216	EBA-1	Carbonate	2004	60,837,000	186.70		NDWR, 2019a
216	EBA-1	Carbonate	2005	49,268,500	151.20		NDWR, 2019a
216	EBA-1	Carbonate	2006	45,460,300	139.51		NDWR, 2019a
216	EBA-1	Carbonate	2007	48,390,200	148.50		NDWR, 2019a
216	EBA-1	Carbonate	2008	47,455,000	145.63	Annual total of 145.63AF does not match 2008 Pumpage Report Total of 145.52AF.	NDWR, 2019a
216	EBA-1	Carbonate	2009	44,778,000	137.42	Annual total of 137.42AF does not match 2009 Pumpage Report Total of 112.45AF.	NDWR, 2019a
216	EBA-1	Carbonate	2010	40,540,300	124.41		NDWR, 2019a
216	EBA-1	Carbonate	2011	43,428,800	133.27		NDWR, 2019a
216	EBA-1	Carbonate	2012	35,922,000	110.24		NDWR, 2019a
216	EBA-1	Carbonate	2013	47,487,000	145.73		NDWR, 2019a
216	EBA-1	Carbonate	2014	22,665,000	69.56		NDWR, 2019a
216	EBA-1	Carbonate	2015	38,201,000	117.24		NDWR, 2019a
216	EBA-1	Carbonate	2016	37,062,000	113.74		NDWR, 2019a
216	EBA-1	Carbonate	2017	30,718,000	94.27		NDWR, 2019a
216	EBA-1	Carbonate	2018	31,814,000	97.63	Production data reported through Sep, 2018.	NDWR, 2019a
216	First Solar Well	Carbonate	2016	30,045,051	92.20	Well completed on Oct 8, 2016	NDWR, 2018a
216	First Solar Well	Carbonate	2017	70,833,966	217.38		NDWR, 2018a
216	First Solar Well	Carbonate	2018	58,136,000	178.41		NDWR, 2019a
216	GV-2	Carbonate	2007	10,883,423	33.40		NDWR,2007

Table C-4
Groundwater Production
(Page 8 of 32)

Hydrographic Area	Well Name	Aquifer Material	Year	Production (gallons)	Production (af)	Comments	Source
216	GV-2	Carbonate	2008	40,620,000	124.66		NDWR, 2018a
216	GV-2	Carbonate	2009	5,560,000	17.06		NDWR, 2018a
216	GV-2	Carbonate	2010	3,232,442	9.92		NDWR, 2010
216	GV-2	Carbonate	2011	4,077,300	12.51		NDWR, 2018a
216	GV-2	Carbonate	2012	13,170,000	40.42		NDWR, 2018a
216	GV-2	Carbonate	2013	4,307,750	13.22		NDWR, 2013
216	GV-2	Carbonate	2014	5,112,602	15.69		NDWR, 2014
216	GV-2	Carbonate	2015	9,667,999	29.67		NDWR, 2015
216	GV-2	Carbonate	2016	11,300,513	34.68		NDWR, 2016
216	GV-2	Carbonate	2017	9,765,754	29.97		NDWR, 2017
216	GV-2	Carbonate	2018	---	---	Garnet Valley 2018 Pumpage Inventory report not published prior to publication of this report.	
216	GV-DUKE-WS1	Carbonate	2002	36,984,037	113.50	Well completed on Dec 7, 2001	NDWR, 2018a
216	GV-DUKE-WS1	Carbonate	2003	0	0.00		NDWR, 2018a
216	GV-DUKE-WS1	Carbonate	2004	281,760	0.86		NDWR, 2018a
216	GV-DUKE-WS1	Carbonate	2005	27,866,150	85.52		NDWR, 2018a
216	GV-DUKE-WS1	Carbonate	2006	35,739,890	109.68		NDWR, 2018a
216	GV-DUKE-WS1	Carbonate	2007	75,670,000	232.22		NDWR, 2018a
216	GV-DUKE-WS1	Carbonate	2008	75,467,718	231.60		NDWR, 2018a
216	GV-DUKE-WS1	Carbonate	2009	48,129,840	147.71		NDWR, 2018a
216	GV-DUKE-WS1	Carbonate	2010	20,223,182	62.06		NDWR, 2018a
216	GV-DUKE-WS1	Carbonate	2011	18,432,325	56.57		NDWR, 2018a
216	GV-DUKE-WS1	Carbonate	2012	31,851,607	97.75		NDWR, 2018a
216	GV-DUKE-WS1	Carbonate	2013	43,496,700	133.49		NDWR, 2018a
216	GV-DUKE-WS1	Carbonate	2014	59,018,943	181.12		NDWR, 2018a
216	GV-DUKE-WS1	Carbonate	2015	23,200,200	71.20		NDWR, 2018a
216	GV-DUKE-WS1	Carbonate	2016	28,856,200	88.56		NDWR, 2018a

Table C-4
Groundwater Production
(Page 9 of 32)

Hydrographic Area	Well Name	Aquifer Material	Year	Production (gallons)	Production (af)	Comments	Source
216	GV-DUKE-WS1	Carbonate	2017	7,806,300	23.96		NDWR, 2018a
216	GV-DUKE-WS1	Carbonate	2018	6,594,600	20.24		NDWR, 2019a
216	GV-DUKE-WS2	Carbonate	2002	3,312,100	10.16	Well completed on May 23, 2002	NDWR, 2018a
216	GV-DUKE-WS2	Carbonate	2003	0	0.00		NDWR, 2018a
216	GV-DUKE-WS2	Carbonate	2004	0	0.00		NDWR, 2018a
216	GV-DUKE-WS2	Carbonate	2005	20,176,000	61.92		NDWR, 2018a
216	GV-DUKE-WS2	Carbonate	2006	52,927,802	162.43		NDWR, 2018a
216	GV-DUKE-WS2	Carbonate	2007	33,780,000	103.67		NDWR, 2018a
216	GV-DUKE-WS2	Carbonate	2008	54,572	0.17		NDWR, 2018a
216	GV-DUKE-WS2	Carbonate	2009	95,265,432	292.36		NDWR, 2018a
216	GV-DUKE-WS2	Carbonate	2010	101,809,227	312.44		NDWR, 2018a
216	GV-DUKE-WS2	Carbonate	2011	103,242,291	316.84		NDWR, 2018a
216	GV-DUKE-WS2	Carbonate	2012	102,565,323	314.76		NDWR, 2018a
216	GV-DUKE-WS2	Carbonate	2013	31,273,855	95.98		NDWR, 2018a
216	GV-DUKE-WS2	Carbonate	2014	1,767,473	5.42		NDWR, 2018a
216	GV-DUKE-WS2	Carbonate	2015	66,944,359	205.44		NDWR, 2018a
216	GV-DUKE-WS2	Carbonate	2016	43,864,896	134.62	Well plugged in Dec, 2016 and replaced with GV-LENZIE-3.	NDWR, 2018a
216	GV-KERR	Carbonate	2001	681,029	2.09		NDWR, 2001
216	GV-KERR	Carbonate	2002	1,029,689	3.16		NDWR, 2002
216	GV-KERR	Carbonate	2003	1,798,698	5.52		NDWR, 2003
216	GV-KERR	Carbonate	2004	3,287,837	10.09		NDWR, 2004
216	GV-KERR	Carbonate	2005	3,173,789	9.74		NDWR, 2005
216	GV-KERR	Carbonate	2006	1,358,799	4.17		NDWR, 2006
216	GV-KERR	Carbonate	2007	984,070	3.02		NDWR, 2007
216	GV-KERR	Carbonate	2008	1,309,921	4.02		NDWR, 2008
216	GV-KERR	Carbonate	2009	1,238,234	3.80		NDWR, 2009
216	GV-KERR	Carbonate	2010	2,078,929	6.38		NDWR, 2010

Table C-4
Groundwater Production
(Page 10 of 32)

Hydrographic Area	Well Name	Aquifer Material	Year	Production (gallons)	Production (af)	Comments	Source
216	GV-KERR	Carbonate	2011	2,078,929	6.38		NDWR, 2011
216	GV-KERR	Carbonate	2012	3,245,476	9.96		NDWR, 2012
216	GV-KERR	Carbonate	2013	3,196,598	9.81		NDWR, 2013
216	GV-KERR	Carbonate	2014	3,509,415	10.77		NDWR, 2014
216	GV-KERR	Carbonate	2015	5,774,080	17.72		NDWR, 2015
216	GV-KERR	Carbonate	2016	18,002,000	55.25		NDWR, 2018a
216	GV-KERR	Carbonate	2017	8,965,852	27.52		NDWR, 2018a
216	GV-KERR	Carbonate	2018	16,148,000	49.56		NDWR, 2019a
216	GV-LENZIE-3	Carbonate	2016	152,261,653	467.27	Replacement well for GV-DUKE-WS2. Well completed in Oct, 2016.	NDWR, 2018a
216	GV-LENZIE-3	Carbonate	2017	145,347,533	446.06		NDWR, 2018a
216	GV-LENZIE-3	Carbonate	2018	142,503,745	437.33		NDWR, 2019a
216	GV-MIRANT1	Carbonate	2002	24,939,000	76.53	Well completed on Mar 1, 2002.	NDWR, 2018a
216	GV-MIRANT1	Carbonate	2003	40,659,000	124.78		NDWR, 2018a
216	GV-MIRANT1	Carbonate	2004	14,411,400	44.23		NDWR, 2018a
216	GV-MIRANT1	Carbonate	2005	17,529,000	53.79		NDWR, 2018a
216	GV-MIRANT1	Carbonate	2006	20,102,000	61.69		NDWR, 2018a
216	GV-MIRANT1	Carbonate	2007	15,940,000	48.92		NDWR, 2018a
216	GV-MIRANT1	Carbonate	2008	20,270,000	62.21		NDWR, 2018a
216	GV-MIRANT1	Carbonate	2009	21,790,000	66.87		NDWR, 2018a
216	GV-MIRANT1	Carbonate	2010	11,780,000	36.15		NDWR, 2018a
216	GV-MIRANT1	Carbonate	2011	10,610,000	32.56		NDWR, 2018a
216	GV-MIRANT1	Carbonate	2012	5,160,000	15.84		NDWR, 2018a
216	GV-MIRANT1	Carbonate	2013	8,610,000	26.42		NDWR, 2018a
216	GV-MIRANT1	Carbonate	2014	13,850,000	42.50		NDWR, 2018a
216	GV-MIRANT1	Carbonate	2015	18,425,000	56.54		NDWR, 2018a
216	GV-MIRANT1	Carbonate	2016	25,815,000	79.22		NDWR, 2018a

Table C-4
Groundwater Production
(Page 11 of 32)

Hydrographic Area	Well Name	Aquifer Material	Year	Production (gallons)	Production (af)	Comments	Source
216	GV-MIRANT1	Carbonate	2017	30,400,000	93.29		NDWR, 2018a
216	GV-MIRANT1	Carbonate	2018	24,350,000	74.73		NDWR, 2019a
216	GV-PW-WS1	Carbonate	2002	24,628,280	75.58	Well completed on Jul 25, 2002	NDWR, 2018a
216	GV-PW-WS1	Carbonate	2003	15,721,736	48.25		NDWR, 2018a
216	GV-PW-WS1	Carbonate	2004	46,332,890	142.19		NDWR, 2018a
216	GV-PW-WS1	Carbonate	2005	43,064,719	132.16		NDWR, 2018a
216	GV-PW-WS1	Carbonate	2006	51,438,313	157.86		NDWR, 2018a
216	GV-PW-WS1	Carbonate	2007	54,400,000	166.95		NDWR, 2018a
216	GV-PW-WS1	Carbonate	2008	45,994,581	141.15		NDWR, 2018a
216	GV-PW-WS1	Carbonate	2009	48,684,769	149.41		NDWR, 2018a
216	GV-PW-WS1	Carbonate	2010	52,966,620	162.55		NDWR, 2018a
216	GV-PW-WS1	Carbonate	2011	43,557,511	133.67		NDWR, 2018a
216	GV-PW-WS1	Carbonate	2012	45,994,240	141.15		NDWR, 2018a
216	GV-PW-WS1	Carbonate	2013	45,222,054	138.78		NDWR, 2018a
216	GV-PW-WS1	Carbonate	2014	37,660,958	115.58		NDWR, 2018a
216	GV-PW-WS1	Carbonate	2015	50,122,548	153.82		NDWR, 2018a
216	GV-PW-WS1	Carbonate	2016	56,162,212	172.36		NDWR, 2018a
216	GV-PW-WS1	Carbonate	2017	62,814,431	192.77		NDWR, 2018a
216	GV-PW-WS1	Carbonate	2018	41,625,450	127.74		NDWR, 2019a
216	GV-RW1	Carbonate	2001	0	0.00	Well completed Jul 3, 2001. NVE production assigned to Harvey Well for accounting purposes.	NDWR, 2019a
216	GV-RW1	Carbonate	2002	0	0.00		NDWR, 2019a
216	GV-RW1	Carbonate	2003	0	0.00		NDWR, 2019a
216	GV-RW1	Carbonate	2004	0	0.00		NDWR, 2019a
216	GV-RW1	Carbonate	2005	0	0.00		NDWR, 2018a
216	GV-RW1	Carbonate	2006	0	0.00		NDWR, 2019a
216	GV-RW1	Carbonate	2007	0	0.00		NDWR, 2019a
216	GV-RW1	Carbonate	2008	0	0.00		NDWR, 2019a

Table C-4
Groundwater Production
(Page 12 of 32)

Hydrographic Area	Well Name	Aquifer Material	Year	Production (gallons)	Production (af)	Comments	Source
216	GV-RW1	Carbonate	2009	0	0.00		NDWR, 2019a
216	GV-RW1	Carbonate	2010	8,932,164	27.41	Total GV-RW1 production is 90.46 af: 27.41 af charged to SNWA (GV-RW1) and the remaining 63.06 af charged to NVE (Harvey Well).	NDWR, 2019a; and SNWA, 2011
216	GV-RW1	Carbonate	2011	12,156,162	37.31	Total GV-RW1 production is 123.97 af: 37.31 af charged to SNWA and the remaining 86.66 af charged to NVE.	NDWR, 2019a; and SNWA, 2012
216	GV-RW1	Carbonate	2012	4,240,979	13.02	Total GV-RW1 production is 87.63 af: 13.02 af is charged to SNWA (GV-RW1) and the remaining 74.60 af is charged to NVE (Harvey Well)	NDWR, 2019a; and SNWA, 2013
216	GV-RW1	Carbonate	2013	58,618,055	179.89		NDWR, 2019a
216	GV-RW1	Carbonate	2014	92,696,464	284.47		NDWR, 2019a
216	GV-RW1	Carbonate	2015	88,709,326	272.24		NDWR, 2019a
216	GV-RW1	Carbonate	2016	168,729,541	517.81		NDWR, 2019a
216	GV-RW1	Carbonate	2017	18,762,364	57.58		NDWR, 2019a
216	GV-RW1	Carbonate	2018	42,343,784	129.95		NDWR, 2019a
216	GV-USLIME1	Carbonate	2000	0	0.00	Well completed Jun 1, 1999 (75351)	NDWR, 2018a
216	GV-USLIME1	Carbonate	2001	33,388,170	102.46		NDWR, 2018a
216	GV-USLIME1	Carbonate	2002	35,554,390	109.11		NDWR, 2018a
216	GV-USLIME1	Carbonate	2003	33,117,643	101.63		NDWR, 2018a
216	GV-USLIME1	Carbonate	2004	38,606,818	118.48		NDWR, 2018a
216	GV-USLIME1	Carbonate	2005	36,171,110	111.01		NDWR, 2018a
216	GV-USLIME1	Carbonate	2006	42,614,870	130.78		NDWR, 2018a
216	GV-USLIME1	Carbonate	2007	41,089,881	126.10		NDWR, 2018a
216	GV-USLIME1	Carbonate	2008	32,559,872	99.92		NDWR, 2018a
216	GV-USLIME1	Carbonate	2009	27,974,570	85.85		NDWR, 2018a
216	GV-USLIME1	Carbonate	2010	24,452,529	75.04		NDWR, 2018a
216	GV-USLIME1	Carbonate	2011	23,470,206	72.03		NDWR, 2018a
216	GV-USLIME1	Carbonate	2012	19,097,000	58.61		NDWR, 2018a
216	GV-USLIME1	Carbonate	2013	26,117,000	80.15		NDWR, 2018a

Table C-4
Groundwater Production
(Page 13 of 32)

Hydrographic Area	Well Name	Aquifer Material	Year	Production (gallons)	Production (af)	Comments	Source
216	GV-USLIME1	Carbonate	2014	19,720,000	60.52		NDWR, 2018a
216	GV-USLIME1	Carbonate	2015	23,665,000	72.63		NDWR, 2018a
216	GV-USLIME1	Carbonate	2016	17,327,967	53.18		NDWR, 2018a
216	GV-USLIME1	Carbonate	2017	18,111,927	55.58		NDWR, 2018a
216	GV-USLIME1	Carbonate	2018	23,574,739	72.35		NDWR, 2019a
216	GV-USLIME2	Basin Fill	2000	0	0.00		NDWR, 2018a
216	GV-USLIME2	Basin Fill	2001	41,921,670	128.65		NDWR, 2018a
216	GV-USLIME2	Basin Fill	2002	47,303,000	145.17		NDWR, 2018a
216	GV-USLIME2	Basin Fill	2003	43,273,269	132.80		NDWR, 2018a
216	GV-USLIME2	Basin Fill	2004	41,337,821	126.86		NDWR, 2018a
216	GV-USLIME2	Basin Fill	2005	35,416,070	108.69		NDWR, 2018a
216	GV-USLIME2	Basin Fill	2006	39,206,320	120.32		NDWR, 2018a
216	GV-USLIME2	Basin Fill	2007	51,732,669	158.76		NDWR, 2018a
216	GV-USLIME2	Basin Fill	2008	43,563,740	133.69		NDWR, 2018a
216	GV-USLIME2	Basin Fill	2009	26,844,677	82.38		NDWR, 2018a
216	GV-USLIME2	Basin Fill	2010	27,664,227	84.90		NDWR, 2018a
216	GV-USLIME2	Basin Fill	2011	32,362,077	99.32		NDWR, 2018a
216	GV-USLIME2	Basin Fill	2012	36,961,000	113.43		NDWR, 2018a
216	GV-USLIME2	Basin Fill	2013	20,719,000	63.58		NDWR, 2018a
216	GV-USLIME2	Basin Fill	2014	23,136,000	71.00		NDWR, 2018a
216	GV-USLIME2	Basin Fill	2015	39,594,000	121.51		NDWR, 2018a
216	GV-USLIME2	Basin Fill	2016	29,348,314	90.07		NDWR, 2018a
216	GV-USLIME2	Basin Fill	2017	38,183,670	117.18		NDWR, 2018a
216	GV-USLIME2	Basin Fill	2018	30,855,521	94.69		NDWR, 2019a
216	HARVEY WELL	Carbonate	2001	15,779,600	48.43	NVE's portion of GV-RW1 production has been assigned to Harvey Well for accounting purposes.	NDWR, 2019a
216	HARVEY WELL	Carbonate	2002	27,656,500	84.87		NDWR, 2019a
216	HARVEY WELL	Carbonate	2003	379,900	1.17		NDWR, 2019a

Table C-4
Groundwater Production
(Page 14 of 32)

Hydrographic Area	Well Name	Aquifer Material	Year	Production (gallons)	Production (af)	Comments	Source
216	HARVEY WELL	Carbonate	2004	228,650	0.70		NDWR, 2019a
216	HARVEY WELL	Carbonate	2005	355,830	1.09		NDWR, 2019a
216	HARVEY WELL	Carbonate	2006	12,440,900	38.18		NDWR, 2019a
216	HARVEY WELL	Carbonate	2007	0	0.00		NDWR, 2019a
216	HARVEY WELL	Carbonate	2008	61,017,090	187.25	All GV-RW1 production charged to NVE (74399).	NDWR, 2019a
216	HARVEY WELL	Carbonate	2009	55,146,664	169.24	All GV-RW1 production charged to NVE (74399).	NDWR, 2019a
216	HARVEY WELL	Carbonate	2010	20,544,736	63.06	Total GV-RW1 production is 90.46 af; 27.41 af charged to SNWA (GV-RW1) and the remaining 63.06 af charged to NVE (Harvey Well).	NDWR, 2019a; and SNWA, 2011
216	HARVEY WELL	Carbonate	2011	40,395,469	86.66	Total GV-RW1 production is 123.97 af; 37.31 af charged to SNWA (GV-RW1) and the remaining 86.66 af charged to NVE (Harvey Well).	NDWR, 2019a; and SNWA, 2012
216	HARVEY WELL	Carbonate	2012	24,308,485	74.60	Total GV-RW1 production is 87.63 af; 13.02 af is charged to SNWA (GV-RW1) and the remaining 74.60 af is charged to NVE (Harvey Well)	NDWR, 2019a; and SNWA, 2013
216	HARVEY WELL	Carbonate	2013	24,308,485	74.60	First 74.57 af from 74399 pumped from GV-RW1 is reported as NVE production.	NDWR, 2019a
216	HARVEY WELL	Carbonate	2014	24,308,912	74.60	First 74.57 af from 74399 pumped from GV-RW1 is reported as NVE production.	NDWR, 2019a
216	HARVEY WELL	Carbonate	2015	24,298,709	74.57	First 74.57 af from 74399 pumped from GV-RW1 is reported as NVE production.	NDWR, 2019a
216	HARVEY WELL	Carbonate	2016	24,298,709	74.57	First 74.57 af from 74399 pumped from GV-RW1 is reported as NVE production.	NDWR, 2019a
216	HARVEY WELL	Carbonate	2017	24,300,000	74.57	First 74.57 af from 74399 pumped from GV-RW1 is reported as NVE production.	NDWR, 2019a
216	HARVEY WELL	Carbonate	2018	---	---	Garnet Valley 2018 Pumpage Inventory report not published prior to publication of this report.	
216	RS-PW-1	Clastic	1999	528,600	1.62		NDWR, 2018b
216	RS-PW-1	Clastic	2000	0	0.00		NDWR, 2018a
216	RS-PW-1	Clastic	2001	0	0.00		NDWR, 2018a
216	RS-PW-1	Clastic	2002	0	0.00		NDWR, 2018a
216	RS-PW-1	Clastic	2003	0	0.00		NDWR, 2018a
216	RS-PW-1	Clastic	2004	0	0.00		NDWR, 2018a

Table C-4
Groundwater Production
(Page 15 of 32)

Hydrographic Area	Well Name	Aquifer Material	Year	Production (gallons)	Production (af)	Comments	Source
216	RS-PW-1	Clastic	2005	0	0.00		NDWR, 2018a
216	RS-PW-1	Clastic	2006	0	0.00		NDWR, 2018a
216	RS-PW-1	Clastic	2007	0	0.00		NDWR, 2018a
216	RS-PW-1	Clastic	2008	0	0.00		NDWR, 2018a
216	RS-PW-1	Clastic	2009	0	0.00		NDWR, 2018a
216	RS-PW-1	Clastic	2010	0	0.00		NDWR, 2018a
216	RS-PW-1	Clastic	2011	46,502,300	142.71		NDWR, 2018a
216	RS-PW-1	Clastic	2012	30,563,900	93.80		NDWR, 2018a
216	RS-PW-1	Clastic	2013	9,566,000	29.36		NDWR, 2018a
216	RS-PW-1	Clastic	2014	8,560,074	26.27		NDWR, 2018a
216	RS-PW-1	Clastic	2015	6,572,526	20.17		NDWR, 2018a
216	RS-PW-1	Clastic	2016	1,450,728	4.45		NDWR, 2018a
216	RS-PW-1	Clastic	2017	0	0.00		NDWR, 2018a
216	RS-PW-1	Clastic	2018	0	0.00		NDWR, 2019a
216	RS-PW-2	Carbonate	1999	46,625,400	143.09		NDWR, 2018b
216	RS-PW-2	Carbonate	2000	29,818,300	91.51		NDWR, 2018a
216	RS-PW-2	Carbonate	2001	22,497,650	69.04		NDWR, 2018a
216	RS-PW-2	Carbonate	2002	33,203,350	101.90		NDWR, 2018a
216	RS-PW-2	Carbonate	2003	52,891,600	162.32		NDWR, 2018a
216	RS-PW-2	Carbonate	2004	44,666,500	137.08		NDWR, 2018a
216	RS-PW-2	Carbonate	2005	8,323,200	25.54		NDWR, 2018a
216	RS-PW-2	Carbonate	2006	16,073,000	49.33		NDWR, 2018a
216	RS-PW-2	Carbonate	2007	20,714,700	63.57		NDWR, 2018a
216	RS-PW-2	Carbonate	2008	39,794,700	122.13		NDWR, 2018a
216	RS-PW-2	Carbonate	2009	39,974,400	122.68		NDWR, 2018a
216	RS-PW-2	Carbonate	2010	37,954,200	116.48		NDWR, 2018a
216	RS-PW-2	Carbonate	2011	40,543,400	124.42		NDWR, 2018a

Table C-4
Groundwater Production
(Page 16 of 32)

Hydrographic Area	Well Name	Aquifer Material	Year	Production (gallons)	Production (af)	Comments	Source
216	RS-PW-2	Carbonate	2012	41,012,700	125.86		NDWR, 2018a
216	RS-PW-2	Carbonate	2013	34,236,700	105.07		NDWR, 2018a
216	RS-PW-2	Carbonate	2014	33,442,918	102.63		NDWR, 2018a
216	RS-PW-2	Carbonate	2015	11,947,708	36.67		NDWR, 2018a
216	RS-PW-2	Carbonate	2016	0	0.00		NDWR, 2018a
216	RS-PW-2	Carbonate	2017	0	0.00		NDWR, 2018a
216	RS-PW-2	Carbonate	2018	0	0.00		NDWR, 2019a
216	RS-PW-3	Carbonate	1999	0	0.00		NDWR, 2018b
216	RS-PW-3	Carbonate	2000	0	0.00		NDWR, 2018a
216	RS-PW-3	Carbonate	2001	0	0.00		NDWR, 2018a
216	RS-PW-3	Carbonate	2002	0	0.00		NDWR, 2018a
216	RS-PW-3	Carbonate	2003	0	0.00		NDWR, 2018a
216	RS-PW-3	Carbonate	2004	0	0.00		NDWR, 2018a
216	RS-PW-3	Carbonate	2005	0	0.00		NDWR, 2018a
216	RS-PW-3	Carbonate	2006	0	0.00		NDWR, 2018a
216	RS-PW-3	Carbonate	2007	0	0.00		NDWR, 2018a
216	RS-PW-3	Carbonate	2008	0	0.00		NDWR, 2018a
216	RS-PW-3	Carbonate	2009	0	0.00		NDWR, 2018a
216	RS-PW-3	Carbonate	2010	0	0.00		NDWR, 2018a
216	RS-PW-3	Carbonate	2011	0	0.00		NDWR, 2018a
216	RS-PW-3	Carbonate	2012	0	0.00		NDWR, 2018a
216	RS-PW-3	Carbonate	2013	0	0.00		NDWR, 2018a
216	RS-PW-3	Carbonate	2014	0	0.00		NDWR, 2018a
216	RS-PW-3	Carbonate	2015	0	0.00		NDWR, 2018a
216	RS-PW-3	Carbonate	2016	0	0.00		NDWR, 2018a
216	RS-PW-3	Carbonate	2017	0	0.00		NDWR, 2018a
216	RS-PW-3	Carbonate	2018	0	0.00		NDWR, 2019a

Table C-4
Groundwater Production
(Page 17 of 32)

Hydrographic Area	Well Name	Aquifer Material	Year	Production (gallons)	Production (af)	Comments	Source
216	RS-PW-5	Carbonate	1999	17,869,200	54.84		NDWR, 2018b
216	RS-PW-5	Carbonate	2000	83,063,400	254.91		NDWR, 2018a
216	RS-PW-5	Carbonate	2001	58,488,000	179.49		NDWR, 2018a
216	RS-PW-5	Carbonate	2002	39,610,100	121.56		NDWR, 2018a
216	RS-PW-5	Carbonate	2003	55,826,300	171.32		NDWR, 2018a
216	RS-PW-5	Carbonate	2004	44,048,100	135.18		NDWR, 2018a
216	RS-PW-5	Carbonate	2005	70,927,700	217.67		NDWR, 2018a
216	RS-PW-5	Carbonate	2006	37,547,900	115.23		NDWR, 2018a
216	RS-PW-5	Carbonate	2007	29,339,400	90.04		NDWR, 2018a
216	RS-PW-5	Carbonate	2008	78,452,840	240.76		NDWR, 2018a
216	RS-PW-5	Carbonate	2009	58,241,500	178.74		NDWR, 2018a
216	RS-PW-5	Carbonate	2010	45,005,000	138.12		NDWR, 2018a
216	RS-PW-5	Carbonate	2011	6,445,500	19.78		NDWR, 2018a
216	RS-PW-5	Carbonate	2012	11,561,900	35.48		NDWR, 2018a
216	RS-PW-5	Carbonate	2013	23,462,900	72.00		NDWR, 2018a
216	RS-PW-5	Carbonate	2014	33,141,107	101.71		NDWR, 2018a
216	RS-PW-5	Carbonate	2015	39,001,222	119.69		NDWR, 2018a
216	RS-PW-5	Carbonate	2016	31,413,123	96.40		NDWR, 2018a
216	RS-PW-5	Carbonate	2017	88,328,611	271.07		NDWR, 2018a
216	RS-PW-5	Carbonate	2018	79,141,056	242.87		NDWR, 2019a
216	RS-PW-6	Carbonate	1999	60,764,900	186.48		NDWR, 2018b
216	RS-PW-6	Carbonate	2000	40,254,200	123.54		NDWR, 2018a
216	RS-PW-6	Carbonate	2001	58,762,200	180.33		NDWR, 2018a
216	RS-PW-6	Carbonate	2002	42,952,100	131.82		NDWR, 2018a
216	RS-PW-6	Carbonate	2003	37,063,000	113.74		NDWR, 2018a
216	RS-PW-6	Carbonate	2004	33,310,199	102.23		NDWR, 2018a
216	RS-PW-6	Carbonate	2005	46,520,700	142.77		NDWR, 2018a

Table C-4
Groundwater Production
(Page 18 of 32)

Hydrographic Area	Well Name	Aquifer Material	Year	Production (gallons)	Production (af)	Comments	Source
216	RS-PW-6	Carbonate	2006	26,403,000	81.03		NDWR, 2018a
216	RS-PW-6	Carbonate	2007	40,707,000	124.93		NDWR, 2018a
216	RS-PW-6	Carbonate	2008	58,169,300	178.52		NDWR, 2018a
216	RS-PW-6	Carbonate	2009	45,197,400	138.71		NDWR, 2018a
216	RS-PW-6	Carbonate	2010	39,948,000	122.60		NDWR, 2018a
216	RS-PW-6	Carbonate	2011	24,497,000	75.18		NDWR, 2018a
216	RS-PW-6	Carbonate	2012	39,346,900	120.75		NDWR, 2018a
216	RS-PW-6	Carbonate	2013	42,697,000	131.03		NDWR, 2018a
216	RS-PW-6	Carbonate	2014	32,231,721	98.92		NDWR, 2018a
216	RS-PW-6	Carbonate	2015	42,679,916	130.98		NDWR, 2018a
216	RS-PW-6	Carbonate	2016	55,796,378	171.23		NDWR, 2018a
216	RS-PW-6	Carbonate	2017	68,200,752	209.30		NDWR, 2018a
216	RS-PW-6	Carbonate	2018	54,024,640	165.80		NDWR, 2019a
216	RS-PW-7	Carbonate	1999	39,430	0.12		NDWR, 2018b
216	RS-PW-7	Carbonate	2000	0	0.00		NDWR, 2018a
216	RS-PW-7	Carbonate	2001	0	0.00		NDWR, 2018a
216	RS-PW-7	Carbonate	2002	0	0.00		NDWR, 2018a
216	RS-PW-7	Carbonate	2003	0	0.00		NDWR, 2018a
216	RS-PW-7	Carbonate	2004	0	0.00		NDWR, 2018a
216	RS-PW-7	Carbonate	2005	0	0.00		NDWR, 2018a
216	RS-PW-7	Carbonate	2006	0	0.00		NDWR, 2018a
216	RS-PW-7	Carbonate	2007	0	0.00		NDWR, 2018a
216	RS-PW-7	Carbonate	2008	0	0.00		NDWR, 2018a
216	RS-PW-7	Carbonate	2009	0	0.00		NDWR, 2018a
216	RS-PW-7	Carbonate	2010	27,310	0.08		NDWR, 2018a
216	RS-PW-7	Carbonate	2011	7,850	0.02		NDWR, 2018a
216	RS-PW-7	Carbonate	2012	152,300	0.47		NDWR, 2018a

Table C-4
Groundwater Production
(Page 19 of 32)

Hydrographic Area	Well Name	Aquifer Material	Year	Production (gallons)	Production (af)	Comments	Source
216	RS-PW-7	Carbonate	2013	541,800	1.66		NDWR, 2018a
216	RS-PW-7	Carbonate	2014	432,500	1.33		NDWR, 2018a
216	RS-PW-7	Carbonate	2015	5,390,581	16.54		NDWR, 2018a
216	RS-PW-7	Carbonate	2016	27,925,361	85.70		NDWR, 2018a
216	RS-PW-7	Carbonate	2017	22,153,234	67.99		NDWR, 2018a
216	RS-PW-7	Carbonate	2018	50,193,066	154.04		NDWR, 2019a
216	Western Gypsum Well 1	Basin Fill	2001	1,471,600	4.52		NDWR, 2019a
216	Western Gypsum Well 1	Basin Fill	2002	2,184,700	6.70		NDWR, 2019a
216	Western Gypsum Well 1	Basin Fill	2003	2,544,400	7.81		NDWR, 2019a
216	Western Gypsum Well 1	Basin Fill	2004	755,974	2.32		NDWR, 2006
216	Western Gypsum Well 1	Basin Fill	2005	971,036	2.98		NDWR, 2006
216	Western Gypsum Well 1	Basin Fill	2006	1,000,000	3.07		NDWR, 2019a
216	Western Gypsum Well 1	Basin Fill	2007	1,127,444	3.46		NDWR, 2007
216	Western Gypsum Well 1	Basin Fill	2008	1,652,065	5.07		NDWR, 2008
216	Western Gypsum Well 1	Basin Fill	2009	1,329,472	4.08		NDWR, 2009
216	Western Gypsum Well 1	Basin Fill	2010	1,189,356	3.65		NDWR, 2010
216	Western Gypsum Well 1	Basin Fill	2011	1,202,390	3.69		NDWR, 2011
216	Western Gypsum Well 1	Basin Fill	2012	1,274,077	3.91		NDWR, 2012
216	Western Gypsum Well 1	Basin Fill	2013	1,238,234	3.80		NDWR, 2013
216	Western Gypsum Well 1	Basin Fill	2014	840,696	2.58		NDWR, 2014
216	Western Gypsum Well 1	Basin Fill	2015	1,114,410	3.42		NDWR, 2015
216	Western Gypsum Well 1	Basin Fill	2016	1,075,308	3.30		NDWR, 2016
216	Western Gypsum Well 1	Basin Fill	2017	883,056	2.71		NDWR, 2017
216	Western Gypsum Well 1	Basin Fill	2018	---	---	Garnet Valley 2018 Pumpage Inventory report not published prior to publication of this report.	
218	PAIUTES-ECP1	Carbonate	2011	1,928,600	5.92		NDWR, 2018a
218	PAIUTES-ECP1	Carbonate	2012	0	0.00		NDWR, 2018a
218	PAIUTES-ECP1	Carbonate	2013	7,610,000	23.35		NDWR, 2018a

Table C-4
Groundwater Production
(Page 20 of 32)

Hydrographic Area	Well Name	Aquifer Material	Year	Production (gallons)	Production (af)	Comments	Source
218	PAIUTES-ECP1	Carbonate	2014	57,130,000	175.33		NDWR, 2018a
218	PAIUTES-ECP1	Carbonate	2015	95,700,000	293.69		NDWR, 2018a
218	PAIUTES-ECP1	Carbonate	2016	44,510,000	136.60		NDWR, 2018a
218	PAIUTES-ECP1	Carbonate	2017	4,190,000	12.86		NDWR, 2018a
218	PAIUTES-ECP1	Carbonate	2018	0	0.00		NDWR, 2019a
218	PAIUTES-ECP3	Carbonate	2015	28,360,000	87.03		NDWR, 2018a
218	PAIUTES-ECP3	Carbonate	2016	9,620,000	29.52		NDWR, 2018a
218	PAIUTES-ECP3	Carbonate	2017	0	0.00		NDWR, 2018a
218	PAIUTES-ECP3	Carbonate	2018	0	0.00		NDWR, 2019a
218	PAIUTES-TH1	Carbonate	2009	5,000,000	15.34		NDWR, 2018a
218	PAIUTES-TH1	Carbonate	2010	6,300,000	19.33		NDWR, 2018a
218	PAIUTES-TH1	Carbonate	2011	6,470,000	19.86		NDWR, 2018a
218	PAIUTES-TH1	Carbonate	2012	6,790,000	20.84		NDWR, 2018a
218	PAIUTES-TH1	Carbonate	2013	11,670,000	35.81		NDWR, 2018a
218	PAIUTES-TH1	Carbonate	2014	36,830,000	113.03		NDWR, 2018a
218	PAIUTES-TH1	Carbonate	2015	10,020,000	30.75		NDWR, 2018a
218	PAIUTES-TH1	Carbonate	2016	11,040,000	33.88		NDWR, 2018a
218	PAIUTES-TH1	Carbonate	2017	9,806,313	30.09		NDWR, 2018a
218	PAIUTES-TH1	Carbonate	2018	7,870,000	24.15		NDWR, 2019a
219	ARROW_CANYON	Carbonate	1992	167,289,000	513.39		MVWD, 2018
219	ARROW_CANYON	Carbonate	1993	335,084,000	1,028.34		MVWD, 2018
219	ARROW_CANYON	Carbonate	1994	164,219,000	503.97		MVWD, 2018
219	ARROW_CANYON	Carbonate	1995	99,050,000	303.97		MVWD, 2018
219	ARROW_CANYON	Carbonate	1996	89,388,000	274.32		MVWD, 2018
219	ARROW_CANYON	Carbonate	1997	163,354,000	501.32		MVWD, 2018
219	ARROW_CANYON	Carbonate	1998	641,596,000	1,968.99		MVWD, 2018
219	ARROW_CANYON	Carbonate	1999	793,268,000	2,434.45		MVWD, 2018

Table C-4
Groundwater Production
(Page 21 of 32)

Hydrographic Area	Well Name	Aquifer Material	Year	Production (gallons)	Production (af)	Comments	Source
219	ARROW_CANYON	Carbonate	2000	904,935,000	2,777.14		MVWD, 2018
219	ARROW_CANYON	Carbonate	2001	793,065,000	2,433.83		MVWD, 2018
219	ARROW_CANYON	Carbonate	2002	737,673,750	2,263.84		MVWD, 2018
219	ARROW_CANYON	Carbonate	2003	804,304,520	2,468.32		MVWD, 2018
219	ARROW_CANYON	Carbonate	2004	816,215,000	2,504.87		MVWD, 2018
219	ARROW_CANYON	Carbonate	2005	679,303,000	2,084.70		MVWD, 2018
219	ARROW_CANYON	Carbonate	2006	641,990,508	1,970.20		MVWD, 2018
219	ARROW_CANYON	Carbonate	2007	416,343,000	1,277.71		MVWD, 2018
219	ARROW_CANYON	Carbonate	2008	583,101,000	1,789.47		MVWD, 2018
219	ARROW_CANYON	Carbonate	2009	461,027,733	1,414.84		MVWD, 2018
219	ARROW_CANYON	Carbonate	2010	375,264,540	1,151.64		MVWD, 2018
219	ARROW_CANYON	Carbonate	2011	547,436,576	1,680.02		MVWD, 2018
219	ARROW_CANYON	Carbonate	2012	641,920,168	1,969.98		MVWD, 2018
219	ARROW_CANYON	Carbonate	2013	613,093,890	1,881.52		MVWD, 2018
219	ARROW_CANYON	Carbonate	2014	379,141,924	1,163.54		MVWD, 2018
219	ARROW_CANYON	Carbonate	2015	655,291,990	2,011.02		MVWD, 2018
219	ARROW_CANYON	Carbonate	2016	736,378,979	2,259.86		MVWD, 2018
219	ARROW_CANYON	Carbonate	2017	748,223,000	2,296.21		MVWD, 2018
219	ARROW_CANYON	Carbonate	2018	367,593,000	1,128.10		MVWD, 2019
219	ARROW_CANYON_2	Carbonate	2005	66,440,000	203.90		MVWD, 2018
219	ARROW_CANYON_2	Carbonate	2006	261,000	0.80		MVWD, 2018
219	ARROW_CANYON_2	Carbonate	2007	184,622,000	566.58		MVWD, 2018
219	ARROW_CANYON_2	Carbonate	2008	32,129,000	98.60		MVWD, 2018
219	ARROW_CANYON_2	Carbonate	2009	201,394,403	618.06		MVWD, 2018
219	ARROW_CANYON_2	Carbonate	2010	216,208,406	663.52		MVWD, 2018
219	ARROW_CANYON_2	Carbonate	2011	50,554,746	155.15		MVWD, 2018
219	ARROW_CANYON_2	Carbonate	2012	159,785,076	490.36		MVWD, 2018

Table C-4
Groundwater Production
(Page 22 of 32)

Hydrographic Area	Well Name	Aquifer Material	Year	Production (gallons)	Production (af)	Comments	Source
219	ARROW_CANYON_2	Carbonate	2013	117,203,061	359.68		MVWD, 2018
219	ARROW_CANYON_2	Carbonate	2014	90,609,576	278.07		MVWD, 2018
219	ARROW_CANYON_2	Carbonate	2015	125,232,959	384.33		MVWD, 2018
219	ARROW_CANYON_2	Carbonate	2016	175,395,278	538.27		MVWD, 2018
219	ARROW_CANYON_2	Carbonate	2017	170,436,287	523.05		MVWD, 2018
219	ARROW_CANYON_2	Carbonate	2018	277,158,869	850.57		MVWD, 2019
219	BEHMER	Basin Fill	1993	200,429,800	615.10	Combined Behmer 14" and 8" production.	Mifflin and Adenle, 1994
219	BEHMER	Basin Fill	1994	75,445,300	231.53	Combined Behmer 14" and 8" production.	Mifflin and Adenle, 1995
219	BEHMER	Basin Fill	1995	139,805,760	429.05	Combined Behmer 14" and 8" production.	Pohlmann, 1996
219	BEHMER	Basin Fill	1996	222,068,000	681.50	Combined Behmer 14" and 8" production.	Pohlmann and Russell, 1997
219	BEHMER	Basin Fill	1999	78,801,740	241.83	Combined Behmer 14" and 8" production.	Kleinfelder, 2000
219	BEHMER	Basin Fill	2000	180,081,000	552.65	Production from Behmer 14".	NDWR, 2018a
219	BEHMER	Basin Fill	2001	270,722,000	830.82	Combined Behmer 14" and 8" production.	Converse, 2002
219	BEHMER	Basin Fill	2002	267,153,000	819.86	Production from Behmer 14".	Converse, 2003
219	BEHMER	Basin Fill	2003	209,306,000	642.34	Production from Behmer 14".	Converse, 2004
219	BEHMER	Basin Fill	2004	181,153,440	555.94	Production from Behmer 14".	Converse, 2005
219	BEHMER	Basin Fill	2005	214,128,000	657.13	Production from Behmer 14".	NDWR, 2018a
219	BEHMER	Basin Fill	2006	166,359,000	510.54	Production from Behmer 14".	NDWR, 2018a
219	BEHMER	Basin Fill	2007	170,896,000	524.46	Production from Behmer 14".	NDWR, 2018a
219	BEHMER	Basin Fill	2008	156,091,000	479.03	Production from Behmer 14".	NDWR, 2018a
219	BEHMER	Basin Fill	2009	295,797,000	907.77		NDWR, 2018a
219	BEHMER	Basin Fill	2010	199,527,000	612.33		NDWR, 2018a
219	BEHMER	Basin Fill	2011	141,521,000	434.31		NDWR, 2018a
219	BEHMER	Basin Fill	2012	141,012,500	432.75		NDWR, 2018a
219	BEHMER	Basin Fill	2013	202,634,000	621.86		NDWR, 2018a
219	BEHMER	Basin Fill	2014	200,741,453	616.05		NDWR, 2018a
219	BEHMER	Basin Fill	2015	94,933,000	291.34		NDWR, 2018a

Table C-4
Groundwater Production
(Page 23 of 32)

Hydrographic Area	Well Name	Aquifer Material	Year	Production (gallons)	Production (af)	Comments	Source
219	BEHMER	Basin Fill	2016	20,000	0.06		NDWR, 2018a
219	BEHMER	Basin Fill	2017	28,760,000	88.26		NDWR, 2018a
219	BEHMER	Basin Fill	2018	0	0.00		NDWR, 2019a
219	LDS CENTRAL	Basin Fill	1990	172,457,000	529.25		Mifflin, Adenle, and Johnson, 1991
219	LDS CENTRAL	Basin Fill	1993	67,889,000	208.28		Mifflin and Adenle, 1994
219	LDS CENTRAL	Basin Fill	1994	98,137,000	301.17		Mifflin and Adenle, 1995
219	LDS CENTRAL	Basin Fill	1995	159,600,000	489.79		Pohlmann, 1996
219	LDS CENTRAL	Basin Fill	1996	180,549,000	554.08		Pohlmann and Russell, 1997
219	LDS CENTRAL	Basin Fill	1999	238,859,000	733.03		Kleinfelder, 2000
219	LDS CENTRAL	Basin Fill	2000	315,045,000	966.84		NDWR, 2018a
219	LDS CENTRAL	Basin Fill	2001	310,055,000	951.52		NDWR, 2018a
219	LDS CENTRAL	Basin Fill	2002	296,357,000	909.49		NDWR, 2018a
219	LDS CENTRAL	Basin Fill	2003	317,365,000	973.96		NDWR, 2018a
219	LDS CENTRAL	Basin Fill	2004	237,541,000	728.99		NDWR, 2018a
219	LDS CENTRAL	Basin Fill	2005	252,015,000	773.41		NDWR, 2018a
219	LDS CENTRAL	Basin Fill	2006	287,471,000	882.22		NDWR, 2018a
219	LDS CENTRAL	Basin Fill	2007	230,442,000	707.20		NDWR, 2018a
219	LDS CENTRAL	Basin Fill	2008	198,628,000	609.57		NDWR, 2018a
219	LDS CENTRAL	Basin Fill	2009	267,394,000	820.60		NDWR, 2018a
219	LDS CENTRAL	Basin Fill	2010	231,525,000	710.52		NDWR, 2018a
219	LDS CENTRAL	Basin Fill	2011	161,742,000	496.37		NDWR, 2018a
219	LDS CENTRAL	Basin Fill	2012	77,824,000	238.83		NDWR, 2018a
219	LDS CENTRAL	Basin Fill	2013	128,674,000	394.89		NDWR, 2018a
219	LDS CENTRAL	Basin Fill	2014	68,333,661	209.71		NDWR, 2018a
219	LDS CENTRAL	Basin Fill	2015	5,190,000	15.93		NDWR, 2018a
219	LDS CENTRAL	Basin Fill	2016	19,670,000	60.37		NDWR, 2018a
219	LDS CENTRAL	Basin Fill	2017	0	0.00		NDWR, 2018a

Table C-4
Groundwater Production
(Page 24 of 32)

Hydrographic Area	Well Name	Aquifer Material	Year	Production (gallons)	Production (af)	Comments	Source
219	LDS CENTRAL	Basin Fill	2018	0	0.00		NDWR, 2019a
219	LDS EAST	Basin Fill	1990	137,505,000	421.99		Mifflin, Adenle, and Johnson, 1991
219	LDS EAST	Basin Fill	1993	92,336,000	283.37		Mifflin and Adenle, 1994
219	LDS EAST	Basin Fill	1994	100,962,000	309.84		Mifflin and Adenle, 1995
219	LDS EAST	Basin Fill	1995	175,869,000	539.72		Pohlmann, 1996
219	LDS EAST	Basin Fill	1996	171,100,000	525.09		Pohlmann and Russell, 1997
219	LDS EAST	Basin Fill	1999	191,588,000	587.96		Kleinfelder, 2000
219	LDS EAST	Basin Fill	2000	363,754,000	1,116.32		NDWR, 2018a
219	LDS EAST	Basin Fill	2001	197,351,000	605.65		NDWR, 2018a
219	LDS EAST	Basin Fill	2002	124,970,000	383.52		NDWR, 2018a
219	LDS EAST	Basin Fill	2003	213,657,000	655.69		NDWR, 2018a
219	LDS EAST	Basin Fill	2004	183,984,500	564.63		NDWR, 2018a
219	LDS EAST	Basin Fill	2005	140,928,000	432.49		NDWR, 2018a
219	LDS EAST	Basin Fill	2006	127,973,000	392.73		NDWR, 2018a
219	LDS EAST	Basin Fill	2007	207,036,000	635.37		NDWR, 2018a
219	LDS EAST	Basin Fill	2008	165,261,000	507.17		NDWR, 2018a
219	LDS EAST	Basin Fill	2009	63,551,000	195.03		NDWR, 2018a
219	LDS EAST	Basin Fill	2010	52,720,000	161.79		NDWR, 2018a
219	LDS EAST	Basin Fill	2011	196,639,000	603.46		NDWR, 2018a
219	LDS EAST	Basin Fill	2012	188,436,000	578.29		NDWR, 2018a
219	LDS EAST	Basin Fill	2013	177,234,000	543.91		NDWR, 2018a
219	LDS EAST	Basin Fill	2014	195,257,868	599.22		NDWR, 2018a
219	LDS EAST	Basin Fill	2015	13,710,000	42.07		NDWR, 2018a
219	LDS EAST	Basin Fill	2016	0	0.00		NDWR, 2018a
219	LDS EAST	Basin Fill	2017	60,100,000	184.44		NDWR, 2018a
219	LDS EAST	Basin Fill	2018	0	0.00		NDWR, 2019a
219	LDS WEST	Basin Fill	1990	198,115,000	607.99		Mifflin, Adenle, and Johnson, 1991

Table C-4
Groundwater Production
(Page 25 of 32)

Hydrographic Area	Well Name	Aquifer Material	Year	Production (gallons)	Production (af)	Comments	Source
219	LDS WEST	Basin Fill	1993	134,620,000	413.13		Mifflin and Adenle, 1994
219	LDS WEST	Basin Fill	1994	279,092,000	856.50		Mifflin and Adenle, 1995
219	LDS WEST	Basin Fill	1995	180,481,000	553.88		Pohlmann, 1996
219	LDS WEST	Basin Fill	1996	331,528,000	1,017.42		Pohlmann and Russell, 1997
219	LDS WEST	Basin Fill	1999	348,289,000	1,068.86		Kleinfelder, 2000
219	LDS WEST	Basin Fill	2000	353,827,000	1,085.86		NDWR, 2018a
219	LDS WEST	Basin Fill	2001	228,110,000	700.04		NDWR, 2018a
219	LDS WEST	Basin Fill	2002	246,938,000	757.82		NDWR, 2018a
219	LDS WEST	Basin Fill	2003	172,354,000	528.94		NDWR, 2018a
219	LDS WEST	Basin Fill	2004	165,522,000	507.97		NDWR, 2018a
219	LDS WEST	Basin Fill	2005	303,863,000	932.52		NDWR, 2018a
219	LDS WEST	Basin Fill	2006	428,686,000	1,315.59		NDWR, 2018a
219	LDS WEST	Basin Fill	2007	288,217,000	884.51		NDWR, 2018a
219	LDS WEST	Basin Fill	2008	166,099,000	509.74		NDWR, 2018a
219	LDS WEST	Basin Fill	2009	168,098,000	515.87		NDWR, 2018a
219	LDS WEST	Basin Fill	2010	167,529,000	514.13		NDWR, 2018a
219	LDS WEST	Basin Fill	2011	129,219,000	396.56		NDWR, 2018a
219	LDS WEST	Basin Fill	2012	65,323,000	200.47		NDWR, 2018a
219	LDS WEST	Basin Fill	2013	35,166,000	107.92		NDWR, 2018a
219	LDS WEST	Basin Fill	2014	145,313,981	445.95		NDWR, 2018a
219	LDS WEST	Basin Fill	2015	38,379,000	117.78		NDWR, 2018a
219	LDS WEST	Basin Fill	2016	70,410,000	216.08		NDWR, 2018a
219	LDS WEST	Basin Fill	2017	17,970,000	55.15		NDWR, 2018a
219	LDS WEST	Basin Fill	2018	0	0.00		NDWR, 2019a
219	LEWIS 1	Basin Fill	1993	135,885,000	417.02		Mifflin and Adenle, 1994
219	LEWIS 1	Basin Fill	1994	185,686,000	569.85		Mifflin and Adenle, 1995
219	LEWIS 1	Basin Fill	1995	59,146,000	181.51		Pohlmann, 1996

Table C-4
Groundwater Production
(Page 26 of 32)

Hydrographic Area	Well Name	Aquifer Material	Year	Production (gallons)	Production (af)	Comments	Source
219	LEWIS 1	Basin Fill	1996	79,882,000	245.15		Pohlmann and Russell, 1997
219	LEWIS 1	Basin Fill	1999	117,567,000	360.80		Kleinfelder, 2000
219	LEWIS 1	Basin Fill	2000	101,913,332	312.76		NDWR, 2018a
219	LEWIS 1	Basin Fill	2001	35,630,000	109.34		NDWR, 2018a
219	LEWIS 1	Basin Fill	2002	123,094,000	377.76		NDWR, 2018a
219	LEWIS 1	Basin Fill	2003	93,257,000	286.20		NDWR, 2018a
219	LEWIS 1	Basin Fill	2004	100,527,000	308.51		NDWR, 2018a
219	LEWIS 1	Basin Fill	2005	92,664,000	284.38		NDWR, 2018a
219	LEWIS 1	Basin Fill	2006	86,734,000	266.18		NDWR, 2018a
219	LEWIS 1	Basin Fill	2007	77,139,000	236.73		NDWR, 2018a
219	LEWIS 1	Basin Fill	2008	103,418,000	317.38		NDWR, 2018a
219	LEWIS 1	Basin Fill	2009	17,407,000	53.42		NDWR, 2018a
219	LEWIS 1	Basin Fill	2010	44,258,000	135.82		NDWR, 2018a
219	LEWIS 1	Basin Fill	2011	133,139,200	408.59		NDWR, 2018a
219	LEWIS 1	Basin Fill	2012	71,765,700	220.24		NDWR, 2018a
219	LEWIS 1	Basin Fill	2013	64,453,800	197.80		NDWR, 2018a
219	LEWIS 1	Basin Fill	2014	89,944,300	276.03		NDWR, 2018a
219	LEWIS 1	Basin Fill	2015	0	0.00		NDWR, 2018a
219	LEWIS 1	Basin Fill	2016	0	0.00		NDWR, 2018a
219	LEWIS 1	Basin Fill	2017	0	0.00		NDWR, 2018a
219	LEWIS 1	Basin Fill	2018	0	0.00		NDWR, 2019a
219	LEWIS 2	Basin Fill	1993	76,466,000	234.67		Mifflin and Adenle, 1994
219	LEWIS 2	Basin Fill	1994	70,949,000	217.73		Mifflin and Adenle, 1995
219	LEWIS 2	Basin Fill	1995	73,164,000	224.53		Pohlmann, 1996
219	LEWIS 2	Basin Fill	1996	64,856,000	199.04		Pohlmann and Russell, 1997
219	LEWIS 2	Basin Fill	1999	72,835,000	223.52		Kleinfelder, 2000
219	LEWIS 2	Basin Fill	2000	103,158,000	316.58		NDWR, 2018a

Table C-4
Groundwater Production
(Page 27 of 32)

Hydrographic Area	Well Name	Aquifer Material	Year	Production (gallons)	Production (af)	Comments	Source
219	LEWIS 2	Basin Fill	2001	6,180,000	18.97		NDWR, 2018a
219	LEWIS 2	Basin Fill	2002	78,513,000	240.95		NDWR, 2018a
219	LEWIS 2	Basin Fill	2003	68,188,000	209.26		NDWR, 2018a
219	LEWIS 2	Basin Fill	2004	102,914,000	315.83		NDWR, 2018a
219	LEWIS 2	Basin Fill	2005	100,377,000	308.05		NDWR, 2018a
219	LEWIS 2	Basin Fill	2006	74,216,000	227.76		NDWR, 2018a
219	LEWIS 2	Basin Fill	2007	116,889,000	358.72		NDWR, 2018a
219	LEWIS 2	Basin Fill	2008	108,228,000	332.14		NDWR, 2018a
219	LEWIS 2	Basin Fill	2009	97,690,000	299.80		NDWR, 2018a
219	LEWIS 2	Basin Fill	2010	113,247,000	347.54		NDWR, 2018a
219	LEWIS 2	Basin Fill	2011	127,704,000	391.91		NDWR, 2018a
219	LEWIS 2	Basin Fill	2012	35,537,000	109.06		NDWR, 2018a
219	LEWIS 2	Basin Fill	2013	26,465,000	81.22		NDWR, 2018a
219	LEWIS 2	Basin Fill	2014	44,022,000	135.10		NDWR, 2018a
219	LEWIS 2	Basin Fill	2015	0	0.00		NDWR, 2018a
219	LEWIS 2	Basin Fill	2016	0	0.00		NDWR, 2018a
219	LEWIS 2	Basin Fill	2017	0	0.00		NDWR, 2018a
219	LEWIS 2	Basin Fill	2018	0	0.00		NDWR, 2019a
219	LEWIS 3	Basin Fill	1993	129,001,000	395.89		Mifflin and Adenle, 1994
219	LEWIS 3	Basin Fill	1994	256,934,000	788.50		Mifflin and Adenle, 1995
219	LEWIS 3	Basin Fill	1995	118,406,000	363.37		Pohlmann, 1996
219	LEWIS 3	Basin Fill	1996	81,207,000	249.22		Pohlmann and Russell, 1997
219	LEWIS 3	Basin Fill	1999	205,279,000	629.98		Kleinfelder, 2000
219	LEWIS 3	Basin Fill	2000	152,499,000	468.00		NDWR, 2018a
219	LEWIS 3	Basin Fill	2001	141,026,000	432.79		NDWR, 2018a
219	LEWIS 3	Basin Fill	2002	238,372,000	731.54		NDWR, 2018a
219	LEWIS 3	Basin Fill	2003	136,780,000	419.76		NDWR, 2018a

Table C-4
Groundwater Production
(Page 28 of 32)

Hydrographic Area	Well Name	Aquifer Material	Year	Production (gallons)	Production (af)	Comments	Source
219	LEWIS 3	Basin Fill	2004	121,044,000	371.47		NDWR, 2018a
219	LEWIS 3	Basin Fill	2005	101,789,000	312.38		NDWR, 2018a
219	LEWIS 3	Basin Fill	2006	145,098,000	445.29		NDWR, 2018a
219	LEWIS 3	Basin Fill	2007	105,172,300	322.76		NDWR, 2018a
219	LEWIS 3	Basin Fill	2008	52,951,600	162.50		NDWR, 2018a
219	LEWIS 3	Basin Fill	2009	53,981,600	165.66		NDWR, 2018a
219	LEWIS 3	Basin Fill	2010	60,061,000	184.32		NDWR, 2018a
219	LEWIS 3	Basin Fill	2011	114,042,000	349.98		NDWR, 2018a
219	LEWIS 3	Basin Fill	2012	75,691,000	232.29		NDWR, 2018a
219	LEWIS 3	Basin Fill	2013	111,242,000	341.39		NDWR, 2018a
219	LEWIS 3	Basin Fill	2014	173,058,834	531.10		NDWR, 2018a
219	LEWIS 3	Basin Fill	2015	3,830,000	11.75		NDWR, 2018a
219	LEWIS 3	Basin Fill	2016	63,890,000	196.07		NDWR, 2018a
219	LEWIS 3	Basin Fill	2017	0	0.00		NDWR, 2018a
219	LEWIS 3	Basin Fill	2018	0	0.00		NDWR, 2019a
219	LEWIS 4	Basin Fill	1993	144,441,000	443.27		Mifflin and Adente, 1994
219	LEWIS 4	Basin Fill	1994	89,080,000	273.38		Mifflin and Adente, 1995
219	LEWIS 4	Basin Fill	1995	107,707,000	330.54		Pohlmann, 1996
219	LEWIS 4	Basin Fill	1996	175,769,000	539.42		Pohlmann and Russell, 1997
219	LEWIS 4	Basin Fill	1999	78,307,000	240.32		Kleinfelder, 2000
219	LEWIS 4	Basin Fill	2000	81,103,000	248.90		NDWR, 2018a
219	LEWIS 4	Basin Fill	2001	111,354,000	341.73		NDWR, 2018a
219	LEWIS 4	Basin Fill	2002	203,322,400	623.97		NDWR, 2018a
219	LEWIS 4	Basin Fill	2003	88,076,400	270.30		NDWR, 2018a
219	LEWIS 4	Basin Fill	2004	107,038,100	328.49		NDWR, 2018a
219	LEWIS 4	Basin Fill	2005	130,254,900	399.74		NDWR, 2018a
219	LEWIS 4	Basin Fill	2006	133,886,400	410.88		NDWR, 2018a

Table C-4
Groundwater Production
(Page 29 of 32)

Hydrographic Area	Well Name	Aquifer Material	Year	Production (gallons)	Production (af)	Comments	Source
219	LEWIS 4	Basin Fill	2007	103,962,300	319.05		NDWR, 2018a
219	LEWIS 4	Basin Fill	2008	108,001,400	331.44		NDWR, 2018a
219	LEWIS 4	Basin Fill	2009	67,665,100	207.66		NDWR, 2018a
219	LEWIS 4	Basin Fill	2010	89,094,000	273.42		NDWR, 2018a
219	LEWIS 4	Basin Fill	2011	87,828,000	269.53		NDWR, 2018a
219	LEWIS 4	Basin Fill	2012	45,697,000	140.24		NDWR, 2018a
219	LEWIS 4	Basin Fill	2013	61,536,000	188.85		NDWR, 2018a
219	LEWIS 4	Basin Fill	2014	154,217,229	473.28		NDWR, 2018a
219	LEWIS 4	Basin Fill	2015	15,250,000	46.80		NDWR, 2018a
219	LEWIS 4	Basin Fill	2016	17,310,000	53.12		NDWR, 2018a
219	LEWIS 4	Basin Fill	2017	680,000	2.09		NDWR, 2018a
219	LEWIS 4	Basin Fill	2018	0	0.00		NDWR, 2018a
219	LEWIS 5	Basin Fill	1993	51,249,000	157.28		Mifflin and Adenle, 1994
219	LEWIS 5	Basin Fill	1994	73,265,000	224.84		Mifflin and Adenle, 1995
219	LEWIS 5	Basin Fill	1995	64,863,000	199.06		Pohlmann, 1996
219	LEWIS 5	Basin Fill	1996	94,302,000	289.40		Pohlmann and Russell, 1997
219	LEWIS 5	Basin Fill	1999	137,169,000	420.96		Kleinfelder, 2000
219	LEWIS 5	Basin Fill	2000	139,206,000	427.21		NDWR, 2018a
219	LEWIS 5	Basin Fill	2001	130,284,000	399.83		NDWR, 2018a
219	LEWIS 5	Basin Fill	2002	53,624,000	164.57		NDWR, 2018a
219	LEWIS 5	Basin Fill	2003	107,017,000	328.42		NDWR, 2018a
219	LEWIS 5	Basin Fill	2004	79,409,000	243.70		NDWR, 2018a
219	LEWIS 5	Basin Fill	2005	128,429,000	394.13		NDWR, 2018a
219	LEWIS 5	Basin Fill	2006	161,538,500	495.74		NDWR, 2018a
219	LEWIS 5	Basin Fill	2007	13,424,600	41.20		NDWR, 2018a
219	LEWIS 5	Basin Fill	2008	119,084,000	365.46		NDWR, 2018a
219	LEWIS 5	Basin Fill	2009	91,462,000	280.69		NDWR, 2018a

Table C-4
Groundwater Production
(Page 30 of 32)

Hydrographic Area	Well Name	Aquifer Material	Year	Production (gallons)	Production (af)	Comments	Source
219	LEWIS 5	Basin Fill	2010	121,690,000	373.45		NDWR, 2018a
219	LEWIS 5	Basin Fill	2011	132,237,000	405.82		NDWR, 2018a
219	LEWIS 5	Basin Fill	2012	54,629,000	167.65		NDWR, 2018a
219	LEWIS 5	Basin Fill	2013	153,055,672	469.71		NDWR, 2018a
219	LEWIS 5	Basin Fill	2014	242,481,080	744.15		NDWR, 2018a
219	LEWIS 5	Basin Fill	2015	135,082,000	414.55		NDWR, 2018a
219	LEWIS 5	Basin Fill	2016	134,160,000	411.72		NDWR, 2018a
219	LEWIS 5	Basin Fill	2017	43,690,000	134.08		NDWR, 2018a
219	LEWIS 5	Basin Fill	2018	4,320,000	13.26		NDWR, 2019a
219	MX-6	Carbonate	1993	45,945,000	141.00		MVWD, 2018
219	MX-6	Carbonate	1994	127,033,000	389.85		MVWD, 2018
219	MX-6	Carbonate	1995	122,008,000	374.43		MVWD, 2018
219	MX-6	Carbonate	1996	140,352,000	430.72		MVWD, 2018
219	MX-6	Carbonate	1997	100,087,000	307.16		MVWD, 2018
219	MX-6	Carbonate	1998	22,782,800	69.92		MVWD, 2018
219	MX-6	Carbonate	1999	47,099,500	144.54		MVWD, 2018
219	MX-6	Carbonate	2000	42,504,600	130.44		MVWD, 2018
219	MX-6	Carbonate	2001	100,855,300	309.51		MVWD, 2018
219	MX-6	Carbonate	2002	100,644,540	308.87		MVWD, 2018
219	MX-6	Carbonate	2003	113,150,568	347.25		MVWD, 2018
219	MX-6	Carbonate	2004	69,423,000	213.05		MVWD, 2018
219	MX-6	Carbonate	2005	87,378,000	268.15		MVWD, 2018
219	MX-6	Carbonate	2006	324,073,000	994.54		MVWD, 2018
219	MX-6	Carbonate	2007	76,330,000	234.25		MVWD, 2018
219	MX-6	Carbonate	2008	125,056,000	383.78		MVWD, 2018
219	MX-6	Carbonate	2009	507,102	1.56		MVWD, 2018
219	MX-6	Carbonate	2010	3,645,192	11.19		MVWD, 2018

Table C-4
Groundwater Production
(Page 31 of 32)

Hydrographic Area	Well Name	Aquifer Material	Year	Production (gallons)	Production (af)	Comments	Source
219	MX-6	Carbonate	2011	460,864	1.41		MVWD, 2018
219	MX-6	Carbonate	2012	57,878,530	177.62		MVWD, 2018
219	MX-6	Carbonate	2013	82,912,071	254.45		MVWD, 2018
219	MX-6	Carbonate	2014	0	0.00		MVWD, 2018
219	MX-6	Carbonate	2015	0	0.00		MVWD, 2018
219	MX-6	Carbonate	2016	0	0.00		MVWD, 2018
219	MX-6	Carbonate	2017	0	0.00		MVWD, 2018
219	MX-6	Carbonate	2018	0	0.00		MVWD, 2019
219	PERKINS PRODUCTION	Basin Fill	1993	159,155,000	488.43		Mifflin and Adenle, 1994
219	PERKINS PRODUCTION	Basin Fill	1994	217,349,000	667.02		Mifflin and Adenle, 1995
219	PERKINS PRODUCTION	Basin Fill	1995	49,595,000	152.20		Pohlmann, 1996
219	PERKINS PRODUCTION	Basin Fill	1996	147,494,000	452.64		Pohlmann and Russell, 1997
219	PERKINS PRODUCTION	Basin Fill	1999	78,396,000	240.59		Kleinfelder, 2000
219	PERKINS PRODUCTION	Basin Fill	2000	153,475,000	471.00		NDWR, 2018a
219	PERKINS PRODUCTION	Basin Fill	2001	159,530,000	489.58		NDWR, 2018a
219	PERKINS PRODUCTION	Basin Fill	2002	236,304,000	725.19		NDWR, 2018a
219	PERKINS PRODUCTION	Basin Fill	2003	228,829,000	702.25		NDWR, 2018a
219	PERKINS PRODUCTION	Basin Fill	2004	170,913,000	524.51		NDWR, 2018a
219	PERKINS PRODUCTION	Basin Fill	2005	238,755,000	732.71		NDWR, 2018a
219	PERKINS PRODUCTION	Basin Fill	2006	252,270,000	774.19		NDWR, 2018a
219	PERKINS PRODUCTION	Basin Fill	2007	231,534,000	710.55		NDWR, 2018a
219	PERKINS PRODUCTION	Basin Fill	2008	218,774,000	671.39		NDWR, 2018a
219	PERKINS PRODUCTION	Basin Fill	2009	210,205,000	645.10		NDWR, 2018a
219	PERKINS PRODUCTION	Basin Fill	2010	189,468,000	581.46		NDWR, 2018a
219	PERKINS PRODUCTION	Basin Fill	2011	207,057,000	635.43		NDWR, 2018a
219	PERKINS PRODUCTION	Basin Fill	2012	246,502,000	756.49		NDWR, 2018a
219	PERKINS PRODUCTION	Basin Fill	2013	330,911,000	1,015.53		NDWR, 2018a

Table C-4
Groundwater Production
(Page 32 of 32)

Hydrographic Area	Well Name	Aquifer Material	Year	Production (gallons)	Production (af)	Comments	Source
219	PERKINS PRODUCTION	Basin Fill	2014	258,918,323	794.59		NDWR, 2018a
219	PERKINS PRODUCTION	Basin Fill	2015	113,142,000	347.22		NDWR, 2018a
219	PERKINS PRODUCTION	Basin Fill	2016	0	0.00		NDWR, 2018a
219	PERKINS PRODUCTION	Basin Fill	2017	23,170,000	71.11		NDWR, 2018a
219	PERKINS PRODUCTION	Basin Fill	2018	0	0.00		NDWR, 2019a

References

Converse Consultants, 2000, Groundwater level monitoring program 1999 annual report Moapa, Nevada, Prepared for Nevada Power Company, 14 p.

Converse Consultants, 2001, Groundwater level monitoring program 2000 annual report Moapa, Nevada, Prepared for Nevada Power Company, 24 p.

Converse Consultants, 2002, Production Well Construction and Testing, RW-2 Well, Coyote Spring Valley, Clark County, Nevada, Prepared for Nevada Power Company, June 2002.

Converse Consultants, 2004, Groundwater level monitoring program 2003 annual report Moapa, Nevada, Prepared for Nevada Power Company, 26 p.

Converse Consultants, 2005, Groundwater level monitoring program 2004 annual report Moapa, Nevada, Prepared for Nevada Power Company, 27 p.

Kleinfelder, 2000, 1999 Hydrologic Impacts from Groundwater Withdrawals in the Upper Muddy River Valley, Nevada, February 2000, 22 p.

Mifflin, M.D., Adenle, O.A., and Johnson, R.J., 1991, Effects of 1989 and 1990 Ground-Water Withdrawals on Muddy River Flows, Upper Muddy River Valley, Nevada, for Nevada Power Company, Las Vegas, Nevada, 160 p.

Mifflin, M.D., and Adenle, O.A., 1994, 1993 Hydrologic Impacts from Groundwater Withdrawals in the Upper Muddy River Valley, Nevada.

Mifflin, M.D., and Adenle, O.A., 1995, 1994 Hydrologic Impacts from Groundwater Withdrawals in the Upper Muddy River Valley, Nevada.

Moapa Valley Water District, 2018, Personal communication of September 14 to J. Johnson (Southern Nevada Water Authority) regarding pumpage data, Overton, Nevada.

Moapa Valley Water District, 2019, Personal communication of February 21 to D. Johnson (Southern Nevada Water Authority) regarding 2018 Monitoring Data, Overton, Nevada.

MVVWD, see Moapa Valley Water District.

NDWR, see Nevada Division of Water Resources.

Nevada Division of Water Resources, 2001-2017, Nevada Division of Water Resources Pumpage Inventories as accessed at http://water.nv.gov/PumpageInventoryFiles.aspx during October, 2018.

Nevada Division of Water Resources, 2018a, Nevada Division of Water Resources Pumpage Records as accessed at http://water.nv.gov/Order1169Menu.aspx during October, 2018.

Nevada Divison of Water Resources, 2018b, Personal communication of September, 19 from M. Dillon to J. Johnson (Southern Nevada Water Authority) regarding pumpage data, Carson City, Nevada.

Nevada Division of Water Resources, 2019a, Nevada Division of Water Resources Pumpage Records as accessed at http://water.nv.gov/news.aspx?news=LWRFS during March, 2018.

Pohlmann, K.F., 1996, Moapa Valley Ground-water Level Monitoring Program 1995 Annual Report: Desert Research Institute, Water Resources Center, Prepared for the Nevada Power Company, 48 p.

Pohlmann, K.F., Russell, C.E., 1997, Moapa Valley Ground-water Level Monitoring Program 1996 Annual Report: Desert Research Institute, Water Resources Center, Prepared for the Nevada Power Company, 55 p.

Pohlmann, K.F., Wert, B.L., 1992, Moapa Valley Ground-water Level Monitoring Program 1991 Annual Report: Desert Research Institute, Water Resources Center, Prepared for the Nevada Power Company, 72 p.

Pohlmann, K.F., Wert, B.L., 1993, Moapa Valley Ground-water Level Monitoring Program 1992 Annual Report: Desert Research Institute, Water Resources Center, Prepared for the Nevada Power Company, 72 p.

SNWA, see Southern Nevada Water Authority.

Southern Nevada Water Authority, 2010, Monitoring Report for Southern Nevada Water Authority and Las Vegas Valley Water District's Groundwater Right Permits and Applications in Coyote Spring Valley, Hidden Valley, and Garnet Valley within Clark and Lincoln Counties, Nevada, 79 p.

Southern Nevada Water Authority, 2011, Personal communication of January 27 to J. King, P.E., State Engineer (Nevada Department of Conservation and Natural Resources) regarding Garnet and Hidden Valleys Year End Water Production For Permit Nos. 79001-79010, Las Vegas, NV.

Southern Nevada Water Authority, 2012, Personal communication of January 31 to J. King, P.E., State Engineer (Nevada Department of Conservation and Natural Resources) regarding Garnet and Hidden Valleys Fourth Quarter Water Production For Permit Nos. 79001-79010, Las Vegas, NV.

Southern Nevada Water Authority, 2013, Personal communication of January 28 to J. King, P.E., State Engineer (Nevada Department of Conservation and Natural Resources) regarding Garnet and Hidden Valleys Fourth Quarter Water Production For Permit Nos. 79001-79010, Las Vegas, NV.

Western Elite, 2018, Personal communication of March 15, 2018 from D. Muaina to J. Watrus (Southern Nevada Water Authority) regarding details of BEDROC, LLC, Las Vegas, Nevada.

Appendix D

Carbonate Production Capture Analysis

D.1.0 CARBONATE PRODUCTION CAPTURE ANALYSIS

This appendix contains a table detailing the calculations performed to identify the sources of groundwater production from the carbonate aquifer of the LWRFS.

Table D-1
Capture Analysis of Carbonate Groundwater Production from the LWRFS

Year	MRSA Carbonate Production (1)	Total Carbonate Production (af) (2)	Warm Springs West Average Discharge (cfs) (3)	Warm Springs West Discharge Capture (cfs) (4)	MRSA Discharge Capture (cfs) (5)	MRSA Discharge Capture (afy) (6)	Aquifer Storage Capture (afy) (7)	Cumulative Groundwater Production (af) (8)	Cumulative MRSA Capture (af) (9)	Cumulative Storage Capture (af) (10)
1991	0	0	—	0.00	0.00	0	0	0	0	0
1992	513	513	—	0.00	0.35	256	257	513	256	257
1993	1,169	1,169	—	0.00	0.81	584	585	1,682	840	842
1994	894	894	—	0.00	0.62	447	447	2,576	1,287	1,289
1995	678	678	—	0.00	0.47	339	339	3,254	1,626	1,628
1996	705	2,463	—	0.00	0.49	352	2,111	5,717	1,978	3,739
1997	808	2,514	—	0.00	0.56	404	2,110	8,231	2,382	5,849
1998	2,039	3,578	3.95	0.00	1.41	1,020	2,558	11,809	3,402	8,407
1999	2,579	4,684	3.85	0.10	1.32	956	3,728	16,493	4,358	12,135
2000	2,908	5,110	3.80	0.15	1.97	1,427	3,683	21,603	5,785	15,818
2001	2,743	5,063	3.72	0.23	3.03	2,195	2,868	26,666	7,980	18,686
2002	2,573	5,284	3.64	0.31	4.08	2,956	2,328	31,950	10,936	21,014
2003	2,816	5,442	3.56	0.39	5.13	3,716	1,726	37,392	14,652	22,740
2004	2,718	5,306	3.53	0.42	5.53	4,006	1,300	42,698	18,658	24,040
2005	2,557	5,448	3.80	0.15	1.97	1,427	4,021	48,146	20,085	28,061
2006	2,966	6,861	3.90	0.05	0.66	478	6,383	55,007	20,563	34,444
2007	2,079	7,585	3.72	0.23	3.03	2,195	5,390	62,592	22,758	39,834
2008	2,272	7,091	3.60	0.35	4.61	3,340	3,751	69,683	26,098	43,585
2009	2,034	6,541	3.72	0.23	3.03	2,195	4,346	76,224	28,293	47,931
2010	1,826	7,336	3.71	0.24	3.16	2,289	5,047	83,560	30,582	52,978
2011	1,837	9,841	3.63	0.32	4.21	3,050	6,791	93,401	33,632	59,769
2012	2,638	10,568	3.49	0.46	6.05	4,383	6,185	103,969	38,015	65,954
2013	2,496	8,369	3.35	0.60	7.89	5,716	2,653	112,339	43,731	68,607
2014	1,442	5,994	3.45	0.50	6.58	4,767	1,227	118,332	48,498	69,834
2015	2,395	7,144	3.42	0.53	6.97	5,050	2,094	125,476	53,548	71,928
2016	2,798	7,791	3.40	0.55	7.24	5,245	2,546	133,267	58,793	74,474
2017	2,819	7,630	3.36	0.59	7.76	5,622	2,008	140,897	64,415	76,482
2018	1,979	7,344	3.38	0.57	7.50	5,433	1,911	148,241	69,848	78,393

Notes:
Column number shown inside parenthesis.
(4) = 3.95 - (3)
(5) = (6) / 724.4628 [1992 - 1998]; (5) = (4) / 0.076 [1999 - 2016]
(6) = 0.50 * (1) [1992 - 1998]; (6) = (5) * 724.4628 [1999-2018]
(7) = (2) - (6)